CENTRAL RESEARCH LIBRARY

LOCKHEED MARTIN ENERGY RESEARCH LIBRARIES

3 4456 0515484 6

ORNL-4976

Cy 3

Chemistry Division

ANNUAL PROGRESS REPORT

Period Ending May 20, 1974

OAK RIDGE NATIONAL LABORATORY
CENTRAL RESEARCH LIBRARY
DOCUMENT COLLECTION
LIBRARY LOAN COPY
DO NOT TRANSFER TO ANOTHER PERSON
If you wish someone else to see this document, send in name with document and the library will arrange a loan.

OAK RIDGE NATIONAL LABORATORY
OPERATED BY UNION CARBIDE CORPORATION • FOR THE U.S. ATOMIC ENERGY COMMISSION

Printed in the United States of America. Available from
National Technical Information Service
U.S. Department of Commerce
5285 Port Royal Road, Springfield, Virginia 22151
Price: Printed Copy $7.60; Microfiche $1.45

This report was prepared as an account of work sponsored by the United States Government. Neither the United States nor the United States Atomic Energy Commission, nor any of their employees, nor any of their contractors, subcontractors, or their employees, makes any warranty, express or implied, or assumes any legal liability or responsibility for the accuracy, completeness or usefulness of any information, apparatus, product or process disclosed, or represents that its use would not infringe privately owned rights.

ORNL-4976
UC-4 – Chemistry

Contract No. W-7405-eng-26

CHEMISTRY DIVISION ANNUAL PROGRESS REPORT

for Period Ending May 20, 1974

E. H. Taylor, Director
Sheldon Datz, Associate Director
Ralph Livingston, Associate Director
B. H. Ketelle, Assistant Director
G. E. Moore, Editor of Annual Report

OCTOBER 1974

OAK RIDGE NATIONAL LABORATORY
Oak Ridge, Tennessee 37830
operated by
UNION CARBIDE CORPORATION
for the
U.S. ATOMIC ENERGY COMMISSION

LOCKHEED MARTIN ENERGY RESEARCH LIBRARIES
3 4456 0515484 6

Reports previously issued in this series are as follows:

ORNL-2386	Period Ending June 20, 1957
ORNL-2584	Period Ending June 20, 1958
ORNL-2782	Period Ending June 20, 1959
ORNL-2983	Period Ending June 20, 1960
ORNL-3176	Period Ending June 20, 1961
ORNL-3320	Period Ending June 20, 1962
ORNL-3488	Period Ending June 20, 1963
ORNL-3679	Period Ending June 20, 1964
ORNL-3832	Period Ending May 20, 1965
ORNL-3994	Period Ending May 20, 1966
ORNL-4164	Period Ending May 20, 1967
ORNL-4306	Period Ending May 20, 1968
ORNL-4437	Period Ending May 20, 1969
ORNL-4581	Period Ending May 20, 1970
ORNL-4706	Period Ending May 20, 1971
ORNL-4791	Period Ending May 20, 1972
ORNL-4891	Period Ending May 20, 1973

Contents

INTRODUCTION ix

1. NUCLEAR CHEMISTRY

Delayed Neutron Emission from the Decay of Neutron-Rich Alkali Isotopes 1

Neutron Capture in Sulfur to 1100 keV 4

Decay of ^{59}Fe to Levels of ^{59}Co 5

Evaporation Residue Cross Section in the Reaction ^{107}Ag + ^{20}Ne 6

Angular Momentum Effects in the Fission of the ^{153}Tb Compound Nucleus 8

Precession of Gamma-Gamma Correlation in ^{126}Xe 9

Heavy-Ion Fusion Reactions 9

Excitation Functions and Alpha Decay from Compound Nuclei in Argon-Induced Reactions on ^{144}Sm and ^{166}Er 11

Multinucleon Transfer Reactions 13

Direct Determination of the Electron-Capture Branching Ratio, ^{149}Dy → ^{149g}Tb 14

Observed Differences Between Argon- and Krypton-Induced Reactions Leading to the Same Compound Nuclei, ^{158}Er and ^{156}Er 15

A Doppler-Shift Plunger Device for Measurement of Picosecond Lifetimes 18

A Computer Program for the Correction of Doppler-Shift Recoil-Distance Data 20

Lifetimes of Rotational States in ^{232}Th by the Doppler-Shift Recoil-Distance Technique 21

Lifetimes of Rotational States in ^{236}U by the Doppler-Shift Recoil-Distance Technique 23

Coulomb Excitation of Ground Bands in ^{160,162,164}Dy with ^{20}Ne and ^{35}Cl Ions 24

Lifetimes of Rotational States in ^{164}Dy by the Doppler-Shift Recoil-Distance Method 25

Anomalous Nuclear Rotational Behavior in the Rare-Earth Region 26

Cosmogenic Radionuclides in Samples from Taurus-Littrow: Effects of the Solar Flare of August 1972 29

Primordial Radioelement Concentrations in Rocks and Soils from Taurus-Littrow 29

2. CHEMISTRY AND PHYSICS OF TRANSURANIUM ELEMENTS

Coulomb Excitation of Vibrational-Like States in the Even-*A* Actinide Nuclei 32

Attempted Coulomb Excitation of the 8.5-μsec Spontaneous Fission Isomeric State in ^{239}Pu 33

Transfer and Compound-Nucleus Reactions That Lead to the Nuclei ^{245}Cf and ^{244}Cf: Interactions of ^{12}C with ^{239}Pu and ^{238}U . . . 33
Reactions of Heavy Elements with Very Heavy Ions . . . 35
Analyses of Neutron-Induced Fission Cross Sections for ^{249}Cf . . . 36
Comparative Solution Chemistry, Ionic Radius, and Single-Ion Hydration Energy of Nobelium . . . 36
Decay Properties and X-Ray Identification of ^{257}104 . . . 37
Properties of ^{259}Rf . . . 39
Predicted Properties of Superheavy Element 115, Ekabismuth . . . 40
Search for Superheavy Elements in Lead Irradiated at SLAC . . . 42
Search for Superheavy Elements in Uranium Target from SLAC after Processing . . . 42
Search for Superheavy Elements in Thorium Target at Super HILAC . . . 43
Additional Natural Samples Investigated for Neutron Emission . . . 43
Radiohalos . . . 44
Systematics in the Relative Energies of Some Low-lying Electron Configurations in the Gaseous Atoms and Free Ions of the Lanthanide and Actinide Series . . . 47
Ionization Energies of Doubly and Triply Ionized Lanthanides by a Linearization Technique . . . 47
On the Electronic Configuration in the Ground State of Atomic Lawrencium . . . 47
Spectroscopy of Lanthanide and Actinide (Lanact) Compounds at Elevated Temperatures . . . 47
The Uranium *M* X-Ray Emission Spectrum . . . 48
Nonaqueous Chemistry of Lanthanides and Actinides . . . 50
Crystallographic Studies with Lanthanide and Transuranic Tricyclopentadienides . . . 51
An NMR Study of the Configuration of the Cyclohexyl Ring in the Adduct of Praseodymium Tricyclopentadienide with Cyclohexyl Isonitrile . . . 51
Crystal Structure of Curium Tribromide . . . 52
Crystallographic Studies of the Trifluorides and the Tribromides of Cm-248 and Cm-244 . . . 53
Preparation of Elemental ^{248}Cm and ^{249}Cf and the Nitrides of ^{248}Cm and ^{249}Bk . . . 54
Electrochemical and Spectroscopic Studies of Transuranic Species in Nonaqueous Inorganic Media . . . 55
The First Experimental Determination of the Heat of Solution of Berkelium Metal . . . 55

3. ISOTOPE CHEMISTRY

Laser Photochemical Isotope Separation . . . 57
Chromatographic Separation of Isotopes . . . 60
Chemical Fractionation of Uranium Isotopes . . . 61
Search for a New Sulfur-Isotope Separation System . . . 61

4. RADIATION CHEMISTRY

Pulse Radiolysis of N_2 + CO Mixtures: The Formation and Decay of the CN and NCO Radicals . . . 63
Pulse Radiolysis of Nitrogen and Argon in the Presence of Ammonia . . . 64
Absorption Spectrum and Reaction Kinetics of the Methylperoxy Radical . . . 65
Photooxidation and Fluorescence of Cerium(III) in Aqueous Sulfuric Acid Solutions . . . 66
On the Dissociation of HSO_4^- . . . 67

5. ORGANIC CHEMISTRY

Combinatorial Chemistry 69
Preparation of Charge-Transfer Complexes 70
^{14}C Isotope Effects During the Addition of Diphenylketene to Styrene 71
3,2-Hydride Shift in Bicyclic Compounds 72
Do S_N2 Reactions Go Through Ion Pairs? The Isotope Effect Criterion 72
Preparation of Butyl Nitrate 74

6. PHYSICAL CHEMISTRY

AQUEOUS SYSTEMS

Problems Encountered in Deriving Activity Coefficient Values from Data on Mixed Electrolyte Systems 75
The Standard Potential of the Ag, AgBr Electrode in DBr Solutions 76
The Hydrolysis of Cations: A Critical Review of Hydrolysis Species and Their Stability Constants in Aqueous Solution 77
Phosphoric Acid Dissociation Equilibria in Aqueous Solutions to 300°C 80
High-Temperature Equilibria in Light and Heavy Water 82
Fluorine-19 Nuclear Magnetic Resonance Studies on Fluoroborate Species in Aqueous Solution 83
Studies on the Vaporization of Methylmercury Compounds and Their Halogen Decomposition Using Gas Chromatography with a Microwave Detector 85
Liquid-Vapor Critical Temperatures of Aqueous Electrolyte Solutions 86
Liquid-Vapor Critical Temperatures of Several Aqueous-Organic and Organic-Organic Solution Systems 87
Effect of Pressure on Liquid-Liquid Immiscibility of High-Temperature Aqueous Solution Mixtures of Uranyl Sulfate and Sulfuric Acid, 280–450°C, 75–1800 Bars 88
Debye-Hückel Correlated Solubilities of Calcium Sulfate in Water and in Aqueous Sodium Nitrate and Lithium Nitrate Solutions 89
Calcium Sulfate Solubility in Brackish Water Concentrates and Applications to Hyperfiltration (Reverse Osmosis), Polyphosphate Additives 90
Advanced Filtration of Waste Waters 91
Adsorption of Inorganic Materials on Uncharged Polystyrene-DVB Copolymers 98
Adsorption of Inorganic Materials on Activated Carbon 99
Extraction of Lithium from Neutral Salt Solutions with Fluorinated β-Diketones 101

ELECTROCHEMISTRY

Twenty-Year Inhibition of Corrosion by the Pertechnetate Ion 102
Effect of Ti(IV) on the Electrochemical Behavior of Titanium and Its Relevance to Pitting and Crevice Corrosion 102
Separation and Analysis of Ions with a Packed-Bed Electrode 105
Sensor for Dissolved Oxygen 108
Electroanalysis of Small Solution Volumes with a Packed-Bed Electrode Using Linear Potential-Sweep Coulometry 109

Porous Electrode Studies in Molten Salts 111
Electrochemical Recovery of Reducible Inorganic Pollutants from Aqueous Streams 111
Effect of Solvent on the Electrochemistry of Iron 112

CALORIMETRY

Heat of Immersion of Thorium Oxide at Elevated Temperatures 113

INTERFACIAL PHENOMENA

Theory of Thermodiffusiophoresis of Spherical Aerosol Particles 115
Ion Microprobe Investigation of the Surface Migration of Molecular Oxides on NaCl 116
Sorption by Sol-Gel Thoria 118
Some Surface Properties of Apollo 17 Soils 120

MOLTEN SALTS

Temperature and Solvent Effects on the Equilibrium of Dilute Uranium Trifluoride Solutions Contained in Graphite 121
Effect of Oxygen on the Equilibrium of UF_3-UF_4 Molten Fluoride Solutions Contained in Graphite 122
Synthesis and Ligand-Field Spectrum of Potassium Heptafluoroniobate(IV) 122
Coordination Behavior of Nb(IV) in Molten LiF-BeF_2 Mixtures 123
Phase Relations in Fluoroborate Systems. The System RbF-$RbBF_4$ 123
Phase Equilibria in the Systems BeF_2-CeF_3, LiF-CeF_3, and LiF-BeF_2-CeF_3 124
Oxide Chemistry of Niobium(V) in Molten LiF-BeF_2 Mixtures 126
The Chemistry and Thermodynamics of Molten-Salt Reactor Fuels 128
Competitive Hydration and Association Equilibria in Hydrous Melts 130
Transport Behavior of Concentrated Aqueous Electrolyte Solutions 132
Anodic Chronopotentiometry of Beryllium Electrodes in Molten Mixtures of Beryllium Fluoride with Alkali Fluorides 134
Irreversible Thermodynamics of Electromigrational Depletion Chronopotentiometry 135
Electrochemical Study of Mass Transport in Molten LiF-BeF_2 Mixtures 139
Application of the Quasi-Lattice Model in Dilute Reciprocal Molten Salt Mixtures. The System Silver Sulfate—Potassium Nitrate 143
Thermodynamics of Lithium-Bismuth Alloys from EMF Measurements with Molten LiF-BeF_2 Mixtures 145

7. CHEMICAL PHYSICS

NEUTRON AND X-RAY DIFFRACTION

X-Ray and Neutron Crystal-Structure Analysis of Phosphotungstic Acid Hexahydrate, $H_3PW_{12}O_{40}\cdot 6H_2O$ 146
Crystal Structure of the 1:1 Adduct Between Chlorpromazine and 7,7,8,8-Tetracyanoquinodimethane 149
Numerical Experiments to Facilitate the Direct Solution of the Crystallographic Phase Problem 150

ORTRAN: A Computer Program for Determining the Orientation of a Known Molecular Fragment in an Unknown Crystal Structure . . . 151

Utilizing Molecular Structure Information in Direct Methods of Crystal Structure Determination via a Modified Tangent Formula . . . 152

Calculation of Electrostatic Crystal Potentials for Use in the Interpretation of ESCA Measurements . . . 154

Neutron Diffraction Structural Studies of Two TCNQ-Complex Crystals, A Bifluoride Crystal, and a Norbornanone Crystal . . . 155

The Representation Problem in Combinatorial Chemistry . . . 159

Mean Spherical Model for the Structure of Lennard-Jones Fluids . . . 161

Correlations in Molecular Liquids . . . 162

Diffraction by Molecular Liquids . . . 163

Molecular Scattering Factors . . . 165

Amorphous Water . . . 166

Diffraction Pattern and Structure of Ionic Solutions . . . 167

Dibarium Chromate(IV), Isotypic with Rubidium Chromate(VI) and Dibarium Titanate(IV) . . . 169

INFRARED AND RAMAN SPECTROSCOPY

Molecular Spectroscopy . . . 169

Infrared Study of Adsorption Species of Water on Monoclinic and Tetragonal Zirconium Oxide as a Function of Temperature . . . 172

MICROWAVE AND RADIO-FREQUENCY SPECTROSCOPY

Electron Spin Resonance Studies of Liquids during Photolysis: Peptides . . . 177

Electron Spin Resonance Studies of Liquids during Photolysis: Heterocyclic Compounds Containing Nitrogen . . . 179

Electron Spin Resonance Study of the Hydroxyl Radical in Single Crystals of Potassium Hydroxylamine Disulfonate . . . 179

ELECTRON SPECTROSCOPY

Photoionization of Neon Between 100 and 2000 eV; Single and Multiple Processes, Angular Distributions, and Subshell Cross Sections . . . 180

Total and Partial Atomic Level Widths . . . 180

ATOMIC AND MOLECULAR COLLISIONS

Crossed-Molecular-Beam Study of Excited-Atom Reactions: Hg(6^3P_2) with Chlorine and Chlorinated Methane Molecules . . . 181

Crossed-Molecular-Beam Study of Electron Transfer Reactions at Thermal Collision Energies . . . 184

Influence of Ionic Charge State on the Stopping Power of 27.8- and 40-MeV Oxygen Ions in the [011] Channel of Silver . . . 185

Velocity Dependence of the Stopping Power of Channeled Iodine Ions . . . 186

Hyperchanneling: Investigations for High-Energy Heavy Ions in Silver 187
Characterization of Charge States of Energetic Ions in Solids 188

PUBLICATIONS 192
PAPERS PRESENTED AT SCIENTIFIC AND TECHNICAL MEETINGS 200
LECTURES 205
SUPPLEMENTARY ACTIVITIES 208

Introduction

Once again it has been possible to fit the year's results into the seven sections (Nuclear Chemistry to Chemical Physics) used for some time. And, again, brief introductory paragraphs preface each of those to point out unifying themes and relations to the overall interests of the AEC and other sponsors.

By a year from now, the new directions of research in support of broader AEC missions – directions of research we have worked so hard during the year to identify, describe, and justify – may require a reorganization of our Annual Report. But for one more time, at least, constant readers will find topics where they expect them, and a generally similar table of contents.

1. Nuclear Chemistry

In spite of recent emphasis on nonnuclear energy, it is almost certain that nuclear fission will be a major source of energy for some period of time. Therefore they study of nuclear properties, both for specific pieces of information of practical importance and for general understanding, is still of special importance. Further impetus to such work here has been given by the decision of the AEC to locate a major nuclear research facility, an advanced heavy-ion accelerator, at ORNL.

The work reported this year represents a continuing evolution of the program of recent years. The trend already in evidence a year ago toward on-line experiments, particularly with heavy ions, has continued, and, because such experiments tend to cut across the interests of many groups, most of the reports show collaboration with persons in other divisions or other institutions. Reports involving Orsay, Darmstadt, and other European institutions reflect foreign assignments for some of our nuclear chemists, undertaken principally to obtain experience in research with heavy ions in anticipation of our new accelerator.

Our capabilities for low-level gamma spectroscopy continued to be demonstrated on lunar samples. It is likely that this source of material is about dried up, but we are actively seeking other applications, particularly in connection with the monitoring of reactor effluents.

Some other nuclear work is reported in the following section, "Chemistry and Physics of Transuranium Elements;" the dividing point is $Z = 93 + \delta$.

DELAYED NEUTRON EMISSION FROM THE DECAY OF NEUTRON-RICH ALKALI ISOTOPES[1]

P. F. Dittner C. Thibault[3]
E. Roeckl[2] C. Rigaud[3]
R. Klapisch[3] C. Detraz[3]
R. Prieels[4]

The need for more and better experimental data on delayed neutron emission in the fission product mass region has been stressed during the past few years. Due to the importance of the understanding of the delayed particle emission itself and its astrophysical implication in the r process, the delayed neutron emission probabilities P_n of individual isotopes and their neutron spectra are of primary interest. Experiments along this line, however, are difficult because of the low production cross sections and the short half-lives of delayed-neutron precursors and by the inherent difficulty of neutron detection and spectroscopy.

We undertook a systematic study of the delayed neutron emission probabilities for the decays of neutron-rich alkali isotopes. Two series of experiments were carried out: The first one at the "Cyclone" isochronous cyclotron of the University of Louvain-la-Neuve, using the 1- to 5-μA, 100-MeV external alpha beam, which was pulsed for typically 0.1-sec beam pulses at a 10% duty cycle, and the second one with the 24-GeV proton beam of the CERN proton synchrotron, giving 2.1-μsec pulses every 10 sec. In both experiments an on-line mass spectrometer[5] was used. Essentially, the reaction recoils from the ^{238}U target are caught in heated graphite, from which alkali isotopes diffuse very quickly. Ions produced by surface ionization are accelerated and analyzed in a magnetic prism. The mass-separated ion beam is refocused onto a thin stainless steel catcher in a shielded area several meters away from

the target. The catcher is located at the center of a beta-neutron detector array. A 5-cm-diam, 0.3-mm-thick NE 102A plastic scintillator faces the catcher with the beta detection probability ϵ_β limited by solid angle to about 20%. It is surrounded by eight ^{3}He proportional counters embedded in a paraffin moderator and shielded by a cadmium sheet and an additional paraffin layer. The neutron detector has been designed to give a high efficiency and a relatively fast response to enable observation of beta-neutron coincidence. Its absolute detection probability ϵ_n for neutrons, measured with an americium-lithium standard source, was approximately 10%.

The target was bombarded by short beam pulses, while the mass spectrometer was set to a fixed mass. After a suitable collection time the ion beam was switched off by a fast electrostatic deflector in order to observe the radioactive decay of the collected activity regardless of the time dependence (due to diffusion) of the supply of ions on the collector. The signals from both detectors were simultaneously multiscaled; thus the P_n value can be determined from the ratio of the two rates. In this direct P_n determination the dependence on the production cross section is circumvented.

The final multiscaling curves are the result of the activity of the sum of many ion bursts having a period determined by the primary beam. Thus activities produced by earlier bursts will contribute to the counting rate of later multiscaling sweeps. This effect tends to enhance the relative intensities of longer-lived components and was accounted for in our analysis. All but one of the neutron multiscaling curves (NMC) had only one component (the alkali), since the decay daughters do not emit neutrons. The exception occurred at mass 98, where a weak, longer-lived neutron activity from ^{98}Sr and/or ^{98}Y was found. The beta multiscaling curves (BMC), however, are more complex due to the daughter activities from beta and neutron decays. We assumed time dependences for the number of precursor nuclei arriving at our detector, consistent with the respective target bombardment times and diffusion time characteristics. These, together with the appropriate differential equations, enabled us to calculate the contribution of the daughter activities to the BMC's. The calculated BMC's were fitted to the experimental points using a previously measured or

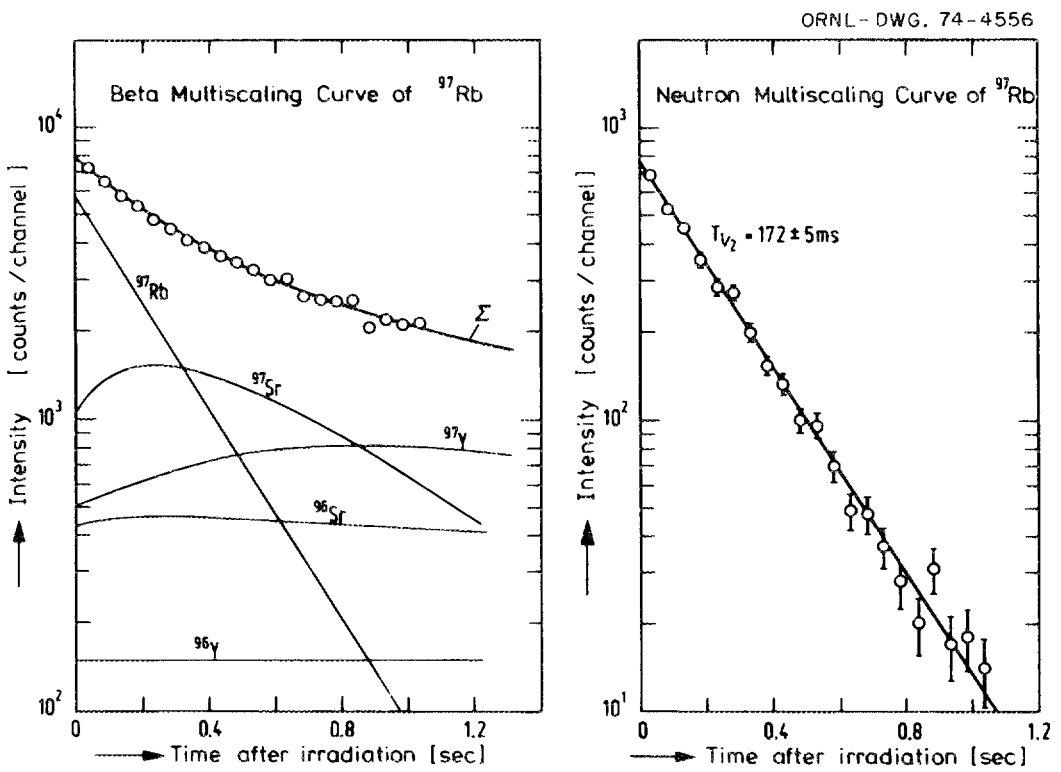

Fig. 1.1. Beta and neutron multiscaling curves for ^{97}Rb, obtained from 139 collection-counting cycles with a timing of 0.2-sec beam pulses every 1.3 sec. The neutron decay curve (*b*) consists of one component only, whereas the beta curve (*a*) is complex due to daughter activities from beta and neutron decay.

Table 1.1. Half-lives and delayed neutron emission probabilities

Precursor	Mass	$\tau_{1/2}$(msec)		$P_n(T)$	
		This work	Others	This work[a]	Others
Li	9	180.56 ± 0.65	177 ± 3[b]	35.0 ± 3.5	35.0 ± 3.5[b]
	11	9.71 ± 0.55		60.8 ± 7.2	
Na	27		295 ± 10[c]	0.08 ± 0.03	
	28	30.3 ± 1.1	35.7 ± 1[c]	0.58 ± 0.12	
	29	42.3 ± 2.3	48.6 ± 2[c]	15.1 ± 1.8	
	30	54.5 ± 2.4	55 ± 3[c]	33.1 ± 3.8	
	31		17.7 ± 1[c]	30 ± 8	
Rb	93	6390 ± 350	5890 ± 40[d]	1.24 ± 0.14	2.6 ± 0.4[e] 1.65 ± 0.30[f] 1.43 ± 0.18[g] 2.1 ± 0.6[h]
	94	2755 ± 80	2670 ± 40[d]	8.46 ± 0.92	11.1 ± 1.1[g] 11 ± 2[h]
	95	383.2 ± 6.0	360 ± 20[d]	8.54 ± 0.91	7.10 ± 0.93[g]
	96	199.0 ± 3.5	207 ± 3[i]	13.0 ± 1.4	12.7 ± 1.5[g]
	97	172.2 ± 5.0	176 ± 5[i]	27.2 ± 3.0	>20[g]
	98	106.1 ± 5.6	136 ± 8[i]	13.3 ± 2.1	
Cs	145	611 ± 21	563 ± 27[i]	12.1 ± 1.4	
	146	352 ± 42	189 ± 11[i]	14.2 ± 1.7	

[a]Normalization of P_n values and error calculation; see text.
[b]Y. S. Chen, T. A. Tombrello, and R. W. Kavanagh, *Nucl. Phys. A* **146**, 136 (1970).
[c]R. Klapisch et al., *Phys. Rev. Lett.* **29**, 1254 (1972).
[d]I. Amaral et al., *Phys. Lett. B* **24**, 402 (1967).
[e]S. Amiel et al., p. 115 in *Delayed Fission Neutrons*, Proc. of IAEA Panel, Vienna, 1967.
[f]W. L. Talbert, A. B. Tucker, and G. M. Day, *Phys. Rev.* **177**, 1805 (1969).
[g]I. Amarel, H. Gauvin, and A. Johnson, *J. Inorg. Nucl. Chem.* **31**, 577 (1969).
[h]H. D. Schüssler and G. Herrmann, *Radiochim. Acta* **18**, 123 (1972).
[i]B. L. Tracy et al., *Phys. Lett. B* **34**, 277 (1971).

estimated value of P_n as a trial value. Iteration of the P_n was then begun, and the intensity of the precursor component of the BMC's was obtained. Figure 1.1 shows as an example the BMC and the NMC for mass 97, for a data set from Louvain. The NMC is a single-component exponential giving a half-life for ^{97}Rb of 172 ± 5 msec. In the BMC the beta activities of ^{97}Rb, of the beta-decay daughters, ^{97}Sr and ^{97}Y, and of the neutron-decay daughters, ^{96}Sr and ^{96}Y, have been adjusted to reflect the neutron branching.

The values of P_n can now be calculated from the relation

$$P_n = (I_n/I_\beta) \quad (\epsilon_\beta/\epsilon_n) \,, \tag{1}$$

where I_n and I_β are the intensities of the neutrons and betas respectively. We used the previously measured[6] P_n of ^{9}Li and our value of I_n/I_β for ^{9}Li to determine the ratio of $\epsilon_\beta/\epsilon_n$ in situ.

In Table 1.1, our results for the half-lives and P_n values are listed and compared with previous measurements. The error of a particular P_n value (Table 1.1) includes the statistical uncertainty of the intensities I_n and I_β of that nuclide and the error of the efficiency calibration [see Eq. (1)]. The latter was assumed to be equal to the uncertainty of the $\epsilon_\beta/\epsilon_n$ for ^{9}Li, which results almost entirely from the 10% uncertainty of the P_n value, since the value of I_n/I_β for ^{9}Li was determined to better than 1% in our experiment.

1. Expanded abstract of paper, *Nucl. Phys. A* **222**, 621 (1974).
2. Gesellschaft für Schwerionenforschung mbH., Darmstadt, Germany.
3. Laboratoire René-Bernas du Centre de Spectrométrie Nucléaire et de Spectrométrie de Masse, Orsay, France.
4. Institut de Physique Corpusculaire, Louvain-la-Neuve, Belgium.
5. C. Rigaud, Thèse de 3e Cycle, Orsay (1972), unpublished.
6. Y. S. Chen, T. A. Tombrello, and R. W. Kavanagh, *Nucl. Phys. A* **146**, 136 (1970).

NEUTRON CAPTURE IN SULFUR TO 1100 keV

J. Halperin R. L. Macklin[1]
R. R. Winters[2]

Neutron time-of-flight radiative capture data for a sample of natural sulfur (95% ^{32}S, 0.026 atoms/b) have been taken at ORELA and have been analyzed for single-level resonance parameters. Detailed descriptions of the experimental arrangement and data handling have been given previously.[3] Figure 1.2 illustrates the structure discernible in a plot of capture cross section (mb) vs laboratory neutron energy (keV) and the adequacy of the background corrections. More than 50 resonances to 1100 keV have been identified and listed in Table 1.2, of which more than half had not previously been reported.[4] Resonances appear not to have been missed up to about 500 keV as judged by a plot of the cumulative number of observed resonances vs energy.

On the basis of ten identified s-wave resonances, an upper limit may be placed for the average level spacing $D(l = 0) \leqslant 110$ keV. The average reduced s-wave neutron width and strength function are found to be $\langle g\Gamma_n^0 \rangle = 10.3 \pm 4$ eV and $S_0 = (0.94 \pm 0.42) \times 10^{-4}$. Of some 44 resonances assigned to p-wave neutron capture, we obtain an average level spacing $D(l = 1) = 25$ keV. Of the 14 identified p-wave resonances, 6 were found to be $J = 3/2$ resonances from analyses of total cross-section measurements.[5,6] The $J = 3/2$ p-wave strength function was found to be $S_1 = (0.57 \pm 0.3) \times 10^{-4}$, whereas the $J = 1/2$ p-wave strength function is $S_1 = (0.16 \pm 0.05) \times$

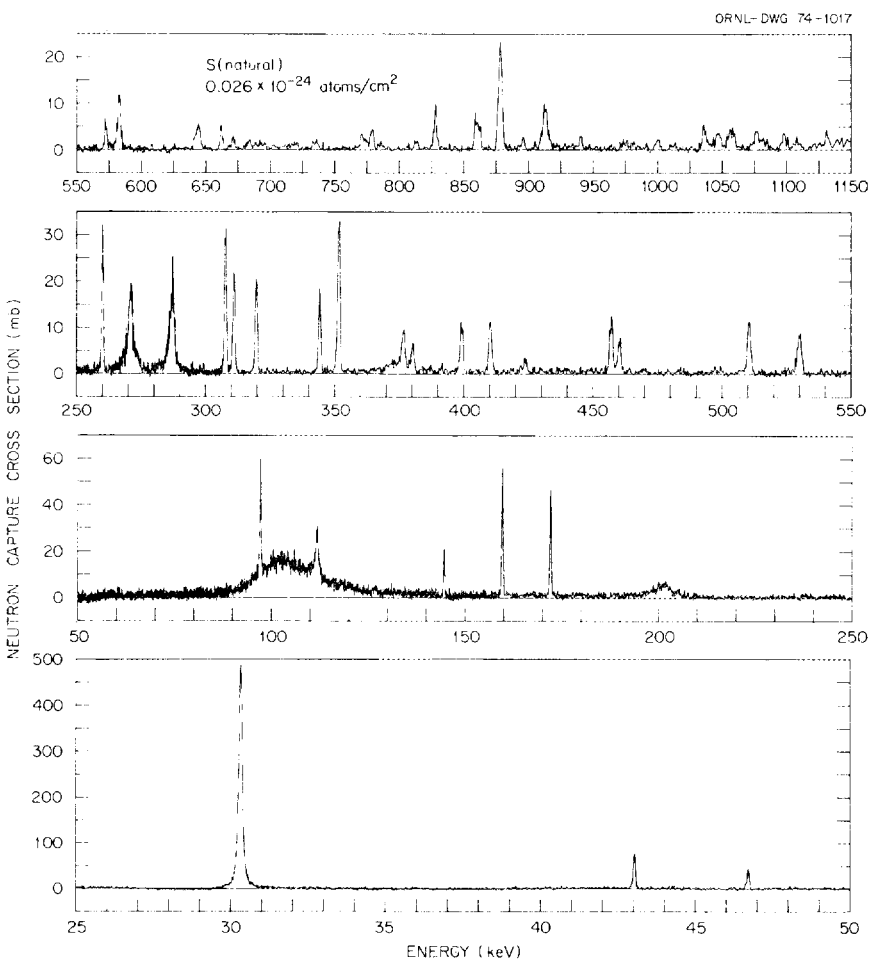

Fig. 1.2. Radiative capture yield of ^{32}S (95%). No resonances were seen below 25 keV except for two resonances at 17.6 and 23.9 keV attributable to the minor (0.75%) isotope ^{33}S. Resolution worsens from $1.7 \times 10^{-3} E_n$ (FWHM) at the lower energies to $4 \times 10^{-3} E_n$ at 1000 keV.

10^{-4}. Further, the average *s*- and *p*-wave radiation widths can be similarly estimated as 4.1 ± 2 eV and 2.33 ± 0.6 eV respectively. Interestingly, the six resolved $J = 3/2$ resonances give a mean radiation width of 0.91 eV.

Table 1.2. Resonance parameters for $^{32}S(n,\gamma)^{33}S$

E_0 (keV)	l	J	$g\Gamma_\gamma\Gamma_n/\Gamma$ (eV)	$g\Gamma_n$ (eV)	$g\Gamma_\gamma$ (eV)	$g\Gamma_n^0$ (eV)	$g\Gamma_n^1$ (eV)
30.36	1	3/2	1.26	80	0.64		18.6
43.12			0.075	<4	0.076		(<0.6)
46.8			0.050	<4	0.51		(<0.6)
97.4	1	3/2	0.52	200	0.52		8.6
102.9	0	1/2		17000	7.5	53.0	
112.1	1	3/2	0.62	1000	0.62		35.2
145.2			0.25	<22	0.26		(<0.5)
160.3			0.87	27	0.89		(0.6)
172.8			0.82	<26	0.85		(<0.5)
203.0	1	3/2	0.34	3100	0.34		48.
261.3			1.42	<23	1.5		(<0.3)
272.3	1	1/2	2.23	1700	2.2		17.7
288.7	1	3/2	3.62	5000	3.6		48.4
309.4			2.29	<41	2.4		(<0.4)
312.8			1.73	<42	1.8		(<0.4)
321.4			1.58	<35	1.7		(<0.3)
346.1			1.56	72	1.6		(0.6)
353.6			3.20	<43	3.5		(<0.3)
377	0	1/2	0.47	5000	0.47	8.2	
378.9			1.32	<49	1.35		(<0.4)
382.6			0.66	95	0.66		(0.6)
401.6			1.27	<56	1.3		(<0.40)
412.8			1.52	176	1.5		(1.1)
426.2			0.42	<50	0.42		(<0.4)
460.2			1.91	177	1.9		(1.0)
463.3			1.13	184	1.1		(1.0)
514.0			2.23	136	2.3		(0.6)
533.9			2.20	147	2.2		(0.6)
576.5			1.82	<115	1.85		(<0.5)
587.2	1	3/2	4.55	3000	4.6		12.7
649.5	1	1/2	3.76	1000	3.8		3.8
668.6			1.89	90	1.9		(0.4)
675.7	1	1/2	1.31	500	1.3		1.7
688			1.00	<30	1.1		(<0.4)
699.5	0	1/2	1.36	10000	1.4	12.0	
725.5	0	1/2	1.41	6000	1.4	7.0	
741.5	1	1/2	1.62	2000	1.6		6.4
779.3	0	1/2	2.05	4000	2.1	4.5	
784.5			2.39	150	2.4		(0.5)
819.1	1	1/2	0.87	1200	0.87		3.4
835			3.74	300	3.8		(0.9)
869			5.81	<60	6.2		(<0.3)
886			16.6	150	18.3		(0.4)
904			1.27	<40	1.3		(<0.2)
921	0	1/2	5.0	3000	5.0	3.1	
921	1	1/2	5.0	2000	5.0		5.1
948	1	1/2	1.2	2200	1.2		5.4
986	0	1/2	3.6	9000	3.6	9.1	
1008	0	1/2	2.0	2000	2.0	2.0	
1048	0	1/2	15.0	3000	15.4	2.9	
1056	1	1/2	5.1	2100	5.1		4.6
1067			7.6	250	7.9		(0.5)
1084			3.0	250	3.		(0.5)
1091	0	1/2	2.0	1200	2.	1.1	

The current evaluation of the capture gamma area for the 30.88-keV resonance is about 50% greater than reported earlier.[4] The effect of this resonance is relevant to the theory of weak *s*-process element formation since ^{32}S serves as a seed nucleus and Maxwellian averages for $kT \simeq 30$ keV neutrons are of course sensitive to this resonance.[7] The 30-keV Maxwellian average cross section is computed as 4.95 ± 0.50 mb.

1. Physics Division.
2. Denison University, Granville, Ohio.
3. B. J. Allen, R. L. Macklin, R. R. Winters, and C. Y. Fu, *Phys. Rev. C* 8, 1504 (1973).
4. S. F. Mughabghab and D. I. Garber, *Neutron Cross Sections*, vol. 1, *Resonance Parameters*, BNL-325, 3d ed. (June 1973).
5. S. Cierjacks et al., "High Resolution Total Neutron Cross Sections between 0.5 and 30 MeV," Gesellschaft für Kernforschung mbH., Karlsruhe, June 1968.
6. We are indebted to J. A. Harvey for permitting us to examine preliminary and unpublished data of the total cross section of sulfur from 10 to 1000 keV.
7. J. G. Peters, W. A. Fowler, and D. D. Clayton, *Astrophys. J.* **173**, 637 (1972).

DECAY OF ^{59}Fe TO LEVELS OF ^{59}Co[1]

S. C. Pancholi[2] S. K. Soni[4]
J. J. Pinajian[3] M. M. Bajaj[4]
N. R. Johnson S. L. Gupta[4]
Ashok Kumar[4] N. K. Saha[4]

The decay of 45.1-day ^{59}Fe has been studied with a 40-cm^3 Ge(Li) detector, a Ge(Li) low-energy photon detector, and a Ge(Li)-NaI(Tl) coincidence system. The measured gamma-ray energies in keV (intensities in parentheses) are as follows: 142.648 (1.02% ± 0.04%), 192.344 (3.08% ± 0.10%), 334.8 ± 0.2 (0.27% ± 0.01%), 382.0 ± 0.4 (0.018% ± 0.003%), 1099.224 (56.5% ± 1.5%), 1291.564 (43.2% ± 1.1%), and 1481.7 ± 0.2 (0.059% ± 0.006%). Gamma-gamma coincidence measurements show that the 382.0-keV gamma ray is in coincidence with the 1099.22-keV gamma ray and that the 1481.7-keV gamma ray is a ground-state transition, thereby establishing a ^{59}Co level at 1481.7 ± 0.2 keV. We also measured gamma-gamma directional correlations for the following cascades, and the expansion coefficients obtained are: 142.65-1291.56 keV, A_2 = −0.070 ± 0.005; 334.8-1099.22 keV, A_2 = 0.099 ± 0.012; and 192.34-1099.22 keV, A_2 = +0.008 ± 0.004. The mixing parameters δ for the 142.65-, 192.34-, and 334.8-keV gamma rays are −0.015 to 0.026, −0.12 ± 0.06, and −0.22 ± 0.02 respectively.

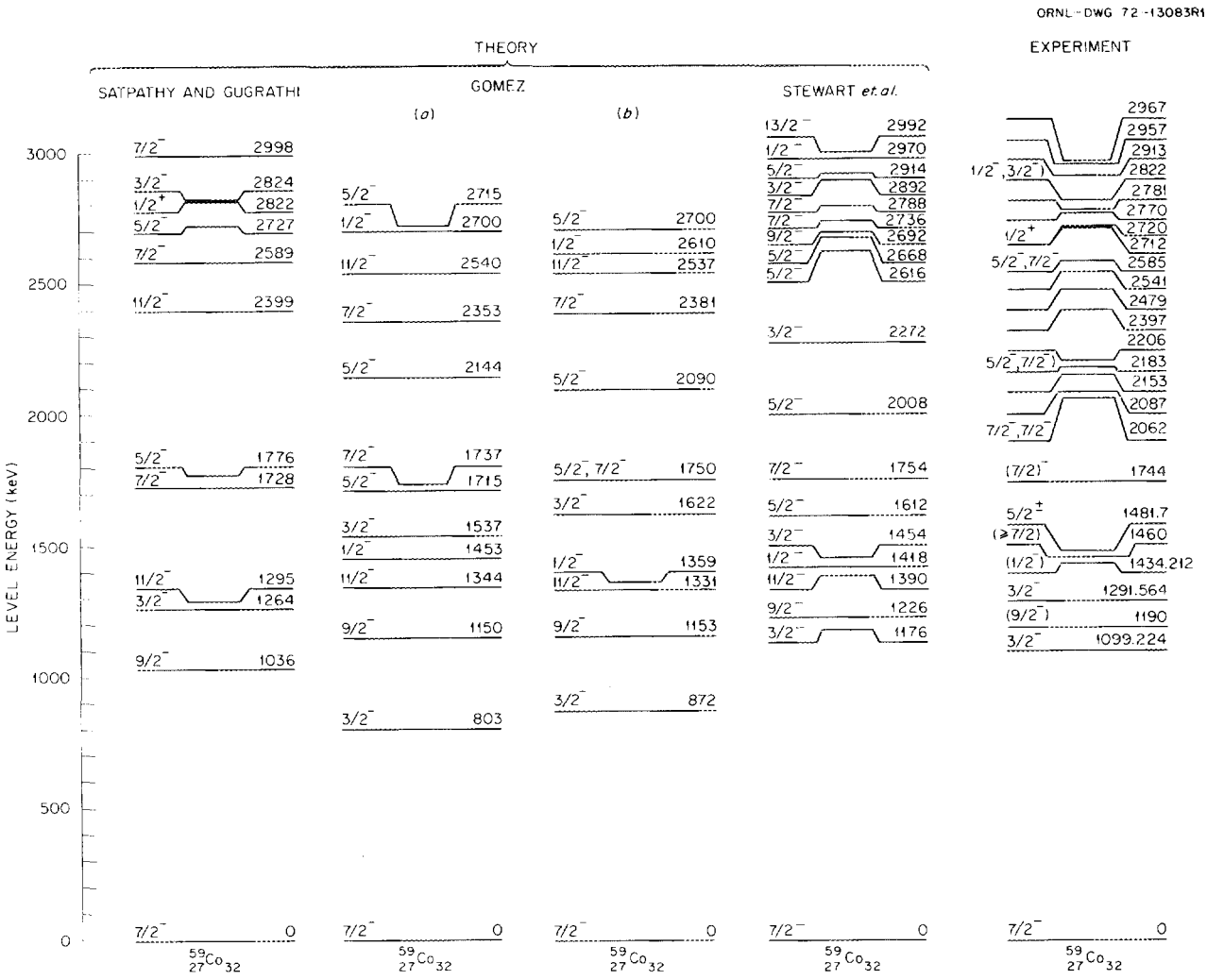

Fig. 1.3. Comparison of experimental and theoretically calculated energy levels of ^{59}Co below 3 MeV.

Numerous theoretical attempts have been made in an effort to explain the low-lying level structure in the odd-mass cobalt nuclei. The premise of most of these calculations is that the odd particle or odd hole state couples to the quadrupole vibrations of the neighboring even nickel core. The approaches differ in such aspects as a variation in the coupling strength, the inclusion of pairing effects, and the introduction of quasi-hole states. In Fig. 1.3 we show a summary of the best energy data available on the levels of ^{59}Co up to 3 MeV including the results of the present measurements. These data are compared with the theoretical calculations of Satpathy and Gugrathi,[5] Gómez,[6] and Stewart et al.[7] As seen in Fig. 1.3, all of the calculations show general agreement with experiment, but those of Stewart, Castel, and Singh[7] give the best overall fit.

1. Expanded abstract of published paper, *Phys. Rev. C* **8**, 2277 (1973).

2. Physics Division and University of Delhi, Delhi, India.
3. Isotopes Division.
4. University of Delhi, India.
5. L. Satpathy and S. G. Gugrathi, *Nucl. Phys. A* **110**, 400 (1968).
6. G. M. G. Gómez, *Phys. Rev. C* **6**, 149 (1972).
7. K. W. C. Stewart, B. Castel, and B. P. Singh, *Phys. Rev. C* **4**, 2131 (1971).

EVAPORATION RESIDUE CROSS SECTION IN THE REACTION ^{107}Ag + ^{20}Ne

R. L. Ferguson R. L. Hahn
F. Pleasonton[1] F. Plasil[1]

The excitation function for ^{20}Ne-induced fission of ^{107}Ag has been reported recently.[2] In that work, attempts to fit the experimental results with calculated excitation functions[3] were unsuccessful when it was assumed that the cross section for compound-nucleus

formation σ_{CN} was equal to the calculated total reaction cross section σ_R, at all bombarding energies. For $\sigma_{CN} < \sigma_R$, however, it was shown to be possible to fit the experimental results using a wide range of parameters. These parameters were σ_{CN}/σ_R, B_f, the fission barrier for a nonrotating system, and a_f/a_ν, the ratio of the level density parameter for fission to that for particle evaporation. Thus, in order to extract an unambiguous value for the fission barrier from such data, it is necessary to determine the value of σ_{CN}/σ_R. We have begun a series of measurements of the excitation function for formation of evaporation residues σ_{ER} in the $^{107}Ag + {}^{20}Ne$ reaction, which, together with results on the fission cross section σ_f, will yield the required values of σ_{CN}. Evaporation residues are those products resulting from the fusion of target and projectile nuclei, followed by the emission of a few nucleons.

In this report we present results of a measurement performed at a bombarding energy E_L of 163.5 MeV. Angular distributions of reaction products were determined at laboratory angles between 3° and 30° with a ΔE-E counter telescope similar to one described by Hildebrand et al.[4] A telescope of this type was first applied to the measurement of evaporation residue cross sections by Gutbrod, Winn, and Blann.[5]

From ΔE-vs-E arrays for each angle, events corresponding to detection of evaporation residues (high ΔE, low E) were extracted and summed. Events corresponding to detection of neon ions elastically scattered by the target (low ΔE, high E) were also extracted from the telescope data. Values of σ_{ER} were then calculated relative to the known cross section for Rutherford scattering, as measured by the elastic-scatter events. At those angles where the elastic scattering is no longer Rutherford, normalization via beam monitor detectors was performed. The resulting distribution in σ_{ER}, corrected for geometrical effects, was then extrapolated to 0° and integrated over all angles to yield the total cross section.

Our value of σ_{ER} was combined with the appropriate value[2] of σ_f to give a value of σ_{CN} at E_L = 166 MeV, and this result is shown in Fig. 1.4 as the triangular point. The circular point is the result of a track detector experiment by Natowitz[6] and is in good agreement with our present result. The curves shown in Fig. 1.4 represent interpretations of the fission results[2] based on the assumption that only at the lowest E_L does $\sigma_{CN} = \sigma_R$ and that, at higher energies, the highest partial waves lead to incomplete fusion of projectile and target and thus to values of $\sigma_{CN}/\sigma_R < 1$. For the lower curve, σ_{CN}/σ_R was determined, as a function of E_L, by

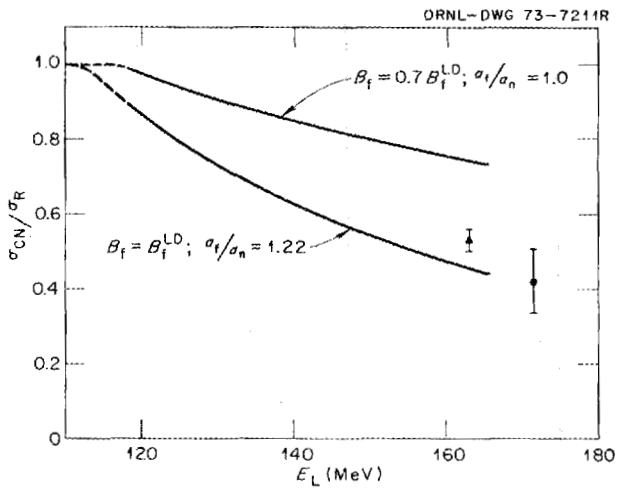

Fig. 1.4. Ratio of compound-nucleus cross section to total reaction cross section for two sets of B_f and a_f/a_ν values as functions of bombarding energy. Both curves were arbitrarily required to pass through σ_{CN}/σ_R = 1 at E_L = 110.4 MeV. The dashed portions of the curves represent extrapolations. The triangular data point is the result of the present work and the circular point is due to Natowitz, *Phys. Rev. C* **1**, 623 (1970).

setting B_f equal to the predicted[7] nonrotating liquid-drop barrier B_f^{LD}; calculating the value of a_f/a_ν required to fit the experimental σ_f value at E_L = 110.4 MeV (with the assumption that σ_{CN}/σ_R = 1); and fitting, with these parameters, to the σ_f data[2] at higher energies. The upper curve was derived similarly, beginning with a choice of $B_f = 0.7B_f^{LD}$.

We are currently measuring σ_{ER} at enough other energies in this system to enable us to determine unambiguous values of B_f and a_f/a_ν, as well as to remove the necessity for assuming that $\sigma_{CN} = \sigma_R$ at the lowest energy. This will allow us to make valid comparisons with theory and should lead to a better understanding of the nuclear macrophysics[8] of heavy-ion-induced reactions.

---

1. Physics Division.
2. F. Plasil, R. L. Ferguson, and F. Pleasonton, "Neon-Induced Fission of Silver," paper IAEA/SM-174/71 in *Proc. Third IAEA Symposium on the Physics and Chemistry of Fission, Rochester, N.Y., August 1973*; also CONF-730823-8 (1972).
3. M. Blann and F. Plasil, *ALICE: A Nuclear Evaporation Code*, USAEC report COO-3494-10 (Nov. 1, 1973).
4. K. D. Hildebrand et al., *Nucl. Phys. A* **157**, 297 (1970).
5. H. H. Gutbrod, W. G. Winn, and M. Blann, *Nucl. Phys. A* **213**, 267 (1973).
6. J. B. Natowitz, *Phys. Rev. C* **1**, 623 (1970).
7. S. Cohen, F. Plasil, and W. J. Swiatecki, *Ann. Phys.* (New York) **82**, 557 (1974).
8. W. J. Swiatecki, *J. Phys.* (Paris) **33**, C5-45 (1972).

ANGULAR MOMENTUM EFFECTS IN THE FISSION OF THE ^{153}Tb COMPOUND NUCLEUS[1]

R. L. Ferguson F. Plasil[2]
F. Pleasonton[2]

There is experimental[3,4] as well as theoretical[5] evidence that high angular momenta can lower the fission barrier drastically. This effect not only influences the decay properties of compound nuclei[6] but may also play a role in determining the compound-nucleus formation probability.[6,7] Calculations indicate[5] that for angular momenta greater than about 100ħ the fission barrier vanishes for all nuclei.

We have attempted to isolate angular momentum effects on fission barriers and thus to check the validity of liquid-drop predictions.[5] To accomplish this, we have investigated two reactions in which angular momentum effects are substantially different, in particular, the reactions ^{133}Cs + ^{20}Ne → [^{153}Tb*] → fission and ^{141}Pr + ^{12}C → [^{153}Tb*] → fission. Here we report our results on the fission excitation functions for these reactions.

The compound-nucleus excitation energy ranged from 70 MeV to 120 MeV in the ^{20}Ne case and from 70 MeV to about 100 MeV in the ^{12}C case. Over an identical range in excitation energy, the difference in cross section between the two fissioning systems is very probably due to the different values of angular momentum involved. Thus, at a comparable excitation energy, we would expect the fission cross section σ_f from the ^{20}Ne-induced fission of ^{133}Cs to be higher than that from the ^{12}C-induced fission of ^{141}Pr since the higher angular momentum brought in by the ^{20}Ne ion results in a greater lowering of the fission barrier. The results are shown in Fig. 1.5. The experimental values of the fission cross section are given by the closed circles and triangles. It can be seen that at a given excitation energy, σ_f is higher for the ^{20}Ne than for the ^{12}C case. At an excitation energy of 90 MeV, for example, $\sigma_f \simeq 0.7$ mb for the ^{12}C bombardment, compared with $\sigma_f \simeq 10$ mb for the ^{20}Ne reaction.

The curves of Fig. 1.5 represent fits to the experimental data obtained from the compound-nucleus de-excitation program ALICE,[8] which allows for multiple neutron, proton, and ^{4}He evaporation in competition with fission and which includes angular-momentum-dependent fission barriers. The absolute magnitude of the nonrotating fission barrier, B_f, and the ratio of the level density parameter for fission, a_f, to the level density parameter for particle emission, a_ν, were treated as adjustable parameters. The angular momentum dependence of B_f, however, was taken from liquid-drop-model calculations,[5] and the variation of B_f was made by varying k in the expression $B_f = kB_f^{LD}$, where B_f^{LD} is the liquid-drop value of B_f.

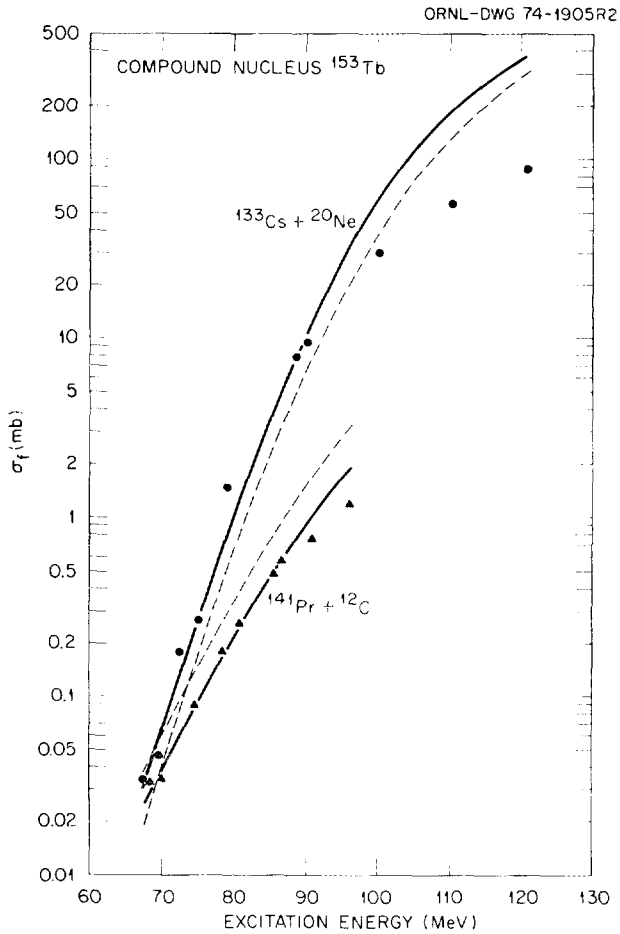

Fig. 1.5. Fission excitation functions for fission of the ^{153}Tb compound nucleus. Circles, ^{20}Ne bombardments of ^{133}Cs; triangles, ^{12}C bombardments of ^{141}Pr. The curves are calculated excitation functions (see text); $B_f = 0.8B_f^{LD}$ for both curves, and $a_f/a_\nu = 1.0$ for the upper curve and 0.965 for the lower curve.

The fission barriers associated with the curves are given by $B_f = 0.8B_f^{LD}$ in both cases, while a_f/a_ν is 0.965 in the ^{12}C case and 1.0 in the ^{20}Ne case. It can be seen that the fit to the steep part of the excitation function is good in both cases up to an excitation energy of about 90 MeV. These are "best fits" in the sense that they follow the experimental data over the greatest range of excitation energies. They are, however, based on the assumption that the compound-nucleus cross section σ_{CN} is equal to the estimated total reaction cross section σ_R; that is, $\sigma_{CN}/\sigma_R = 1$. This assumption almost certainly does not hold over the

entire range of excitation energies studied in this work, and thus the fission barrier is not uniquely determined from our fit. The deviation of the solid curve from the data points at higher excitation energies is most apparent in the ^{20}Ne case and can, very probably, be accounted for by a decreasing σ_{CN}/σ_R ratio with increasing excitation energy. Thus, while adequate fits to our data can be obtained, the unambiguous determination of B_f can only by made if σ_{CN}/σ_R is known. For this purpose, measurements of evaporation residue cross sections are required.

We conclude that angular momentum effects in fission can be understood reasonably well in terms of the rotating-liquid-drop model[5] and that the variation of fission barriers with angular momentum given by the model is probably adequate. We also emphasize that unambiguous extraction of fission barriers from fission excitation functions is only possible when the evaporation residue excitation functions are also known. We are presently in the process of measuring the required evaporation residue cross sections.

1. A similar report has appeared in *Phys. Div. Annu. Progr. Rep. Dec. 31, 1973,* ORNL-4937, p. 28.
2. Physics Division.
3. J. Gilmore, S. G. Thompson, and I. Perlman, *Phys. Rev.* **128**, 2276 (1962).
4. T. Sikkeland, *Phys. Rev.* **135**, B669 (1964).
5. S. Cohen, F. Plasil, and W. J. Swiatecki, *Ann. Phys.* (New York) **82**, 557 (1974).
6. M. Blann and F. Plasil, *Phys. Rev. Lett.* **29**, 303 (1972); M. Blann and F. Plasil, to be published.
7. H. H. Gutbrod, F. Plasil, H. C. Britt, B. H. Erkkila, R. H. Stokes, and M. Blann, "Fission and Complete Fusion Measurements in ^{40}Ar Bombardments of ^{58}Ni and ^{109}Ag," paper IAEA-SM-174/59 in *Third IAEA Symposium on the Physics and Chemistry of Fission Rochester, N.Y., August 1973.*
8. M. Blann and F. Plasil, *ALICE: A Nuclear Evaporation Code,* USAEC report COO-3494-10 (Nov. 1, 1973).

PRECESSION OF GAMMA-GAMMA CORRELATION IN ^{126}Xe[1,2]

K. S. R. Sastry[3] J. H. Hamilton[4]
A. V. Ramayya[4] R. Mlekodaj[5]
R. S. Lee[4] N. R. Johnson

The g factor of the first 2^+ level ($T_{1/2}$ = 40 psec) in ^{126}Xe is being investigated by measuring the precession of the gamma-gamma directional correlation involving the $2^+ \rightarrow 2^+ \rightarrow 0^+$ cascade in ^{126}Xe populated by the decay of ^{126}I. The ^{126}I atoms were implanted as a dilute impurity in an iron foil using the UNISOR facility to utilize the strong internal field (about 1 megagauss) felt by the ^{126}Xe nucleus in iron. A NaI-Ge(Li) coincidence system was used. Preliminary results indicate that the asymmetry $R = (N_+ - N_-)/(N_+ + N_-)$ is about 3%, corresponding to a precession angle of about 50 milliradians. The g factor is positive, and it is less than Z/A.

1. Abstract of paper presented at the American Physical Society Meeting, Bloomington, Ind., Nov. 3, 1973; *Bull. Amer. Phys. Soc.* **18**, 1425 (1973).
2. Research supported in part by the National Science Foundation.
3. University of Massachusetts, Amherst.
4. Vanderbilt University, Nashville, Tenn.
5. UNISOR – a consortium of 14 institutions supported in part by the U.S. Atomic Energy Commission.

HEAVY-ION FUSION REACTIONS[1]

H. G. Bingham[2] R. L. Hahn
C. R. Bingham[3] M. J. Saltmarsh[2]
E. E. Gross[2] A. Zucker[4]

The question of the interaction of heavy ions and target nuclei to form compound systems (complete fusion) has received considerable interest, both experimentally and theoretically, in recent years,[5–11] especially since beams of very heavy ions such as ^{84}Kr and ^{129}Xe have become available. Consideration of the interaction mechanism for such reactions gives rise to specific questions about barrier heights, interaction radii, channel effects, and limiting angular momentum effects on cross-section systematics for fusion reactions.

How does one effectively and efficiently measure integrated cross sections for heavy systems where the fusion product angular distribution is spread only a few degrees from the beam direction? Two methods of detection have been developed which have enjoyed some degree of success – gas proportional counters[6] with thin entrance windows, and track detectors.[7] But proportional counters have one distinct disadvantage in measuring fusion products, and that is their inability because of size and count-rate limitations to go forward of 3°. That is not to say track detectors are faultless. Registration efficiency, radiation damage levels, and etch rates for optimum track exposure plague the reliability factor for most track-detector measurements. However, glass or quartz track detectors appear to have complete registration efficiency under normal conditions and optimum damage sensitivity for intermediate and heavy masses.[12]

Using quartz track detectors at ORIC, we have measured cross sections for argon-induced fusion on targets of titanium, nickel, copper, and silver at incident energies from 115 to 189 MeV. Targets were of the

order of 70 $\mu g/cm^2$ thick and were prepared by vacuum evaporation of the metal onto 40-$\mu g/cm^2$ carbon backings, except for the nickel target, which was self-supporting. Beam intensities were monitored by silicon surface-barrier detectors placed at ±15° with respect to the beam, assuming that the yields from each target were given by the Rutherford law. Beam intensities for the track detector in-beam measurements were obtained by comparison of $K\alpha$ yields from a Si(Li) detector at 135° to $K\alpha$ yields associated with the Rutherford yields of the ±15° surface-barrier detectors.

The quartz track detectors exposed to fusion products were etched in a 26% hydrofluoric acid bath (at about 21°C) for 5 min to reveal etch pits, the signature of a heavy charged particle. Figure 1.6 is a scanning electron micrograph (SEM) taken at 10,000X of a region on a quartz disk that was exposed to argon-plus-copper fusion products and then etched. These disks were then automatically scanned in the region of the beam spot at a magnification of 1600X using an image-analyzing computer. The scanning procedure consisted of a sizing of each etch pit encountered and the increment of a storage register representing its average size. The resultant measurement appears as the number of etch pits scanned having diameters which fall between predetermined limits as in Fig. 1.7. The fusion products appear as the largest etch pits encountered. The smaller pits represent fission, inelastic scattering, and few-nucleon transfer reactions. These conclusions are based on SEM calibrations of etch pit diameters obtained by directly irradiating quartz wafers with beams of ^{32}S (101 MeV), ^{40}Ar (115, 150, 190 MeV), ^{56}Fe (60 MeV), ^{65}Cu (50 MeV), ^{83}Kr (87 MeV), ^{93}Nb (78 MeV), and ^{129}Xe (101 MeV). These beams were selected because they correspond to average fission and fusion products of the systems studied.

The fusion cross-section results are given in Table 1.3. The errors associated with each measurement represent the cumulative experimental uncertainties and are typically 10%. The largest single uncertainty

PHOTO 0459-74

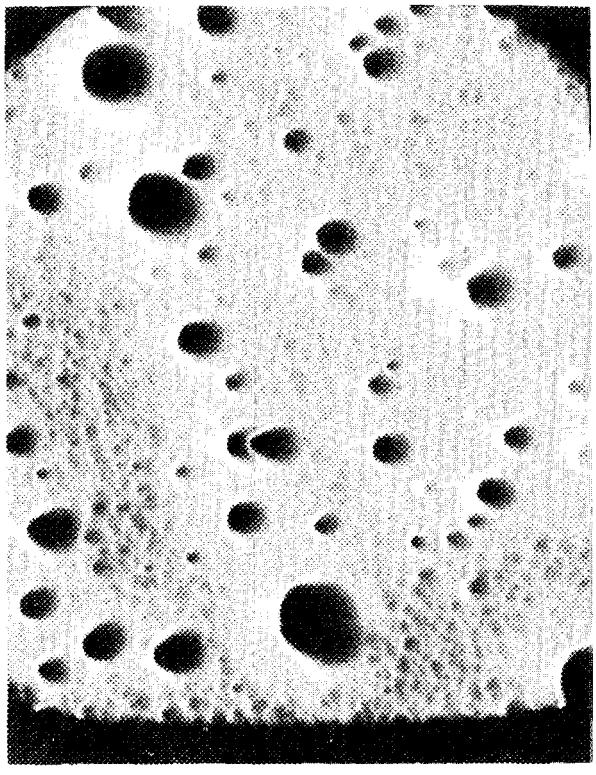

Fig. 1.6. Scanning electron micrograph taken at 10,000X of a region on a quartz track detector that has been exposed to fusion products from 190-MeV argon plus copper and etched in a 26% hydrofluoric acid bath for 5 min. The large holes correspond to fusion or "heavy" products, and the smaller holes are fission, inelastic scattering, etc. Reduced 59%.

ORNL-DWG 74-1719

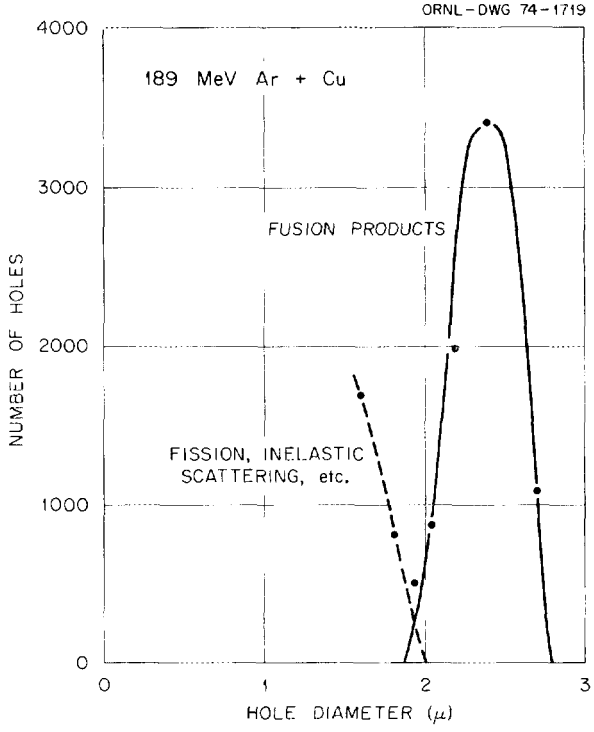

Fig. 1.7. Sample of raw data output from a beam spot scan by an image-analyzing computer. It shows the number of holes within a given diameter limit encountered in a complete scan.

Table 1.3 Fusion cross section for argon on titanium, nickel, copper, and silver

^{40}Ar energy (MeV)	Cross section (mb)			
	Ti	Ni	Cu	Ag
115	98^{+30}_{-50}	192^{+65}_{-130}		
151	804 ± 80	892 ± 90		
189	1065 ± 100	928 ± 93	1634 ± 160	(0)

Table 1.4. Radius and barrier-height parameters extracted from fusion cross sections for argon on targets of titanium, nickel, and copper

Target	r_e (fm)	Approximate barrier height (MeV)
Ti	1.35	110
Ni	1.50	112
Cu	1.50	112

is that associated with distinguishing fusion tracks from those of fission, inelastic scattering, etc., but that uncertainty is generally 5% or less.

The total reaction cross section σ_R for the interaction of nuclei with masses A_1 and A_2 and atomic numbers Z_1 and Z_2 can be approximately expressed as

$$\sigma_R = \pi D^2(1 - B/E) , \quad (1)$$

where D is the radius of the compound nucleus, taken to be

$$D = r_e(A_1^{1/3} + A_2^{1/3}) , \quad (2)$$

B is the Coulomb barrier,

$$B = Z_1 Z_2 e^2/D , \quad (3)$$

E is the kinetic energy in the center-of-mass system, and r_e is the effective nuclear radius parameter.[11] Using Eqs. (1)–(3), one can extract values of r_e and B from the data; these are listed in Table 1.4.

For argon on nickel, the fusion cross section was found to increase rapidly above the barrier up to some critical energy and then level off. By combining these results with those of Gutbrod and Plasil,[13] it appears that the limiting angular momentum[7] for this system is not constant but increases slowly with energy. This conclusion would appear to be consistent with the argon-plus-titanium results, but additional data on this and other systems are necessary for a complete analysis.

1. A similar account of this work has appeared in *Phys. Div. Annu. Progr. Rep. Dec. 31, 1973*, ORNL-4937, p. 31.
2. Physics Division.
3. Consultant, University of Tennessee, Knoxville.
4. Director's Division.
5. For example, see L. Kowalski, J. C. Jodogne, and J. Miller, *Phys. Rev.* **169**, 894 (1968).
6. H. H. Gutbrod, W. G. Winn, and M. Blann, *Nucl. Phys. A* **213**, 267 (1973).
7. J. B. Natowitz, *Phys. Rev. C* **1**, 623 (1970).
8. M. Blann and F. Plasil, *Phys. Rev. Lett.* **29**, 303 (1972).
9. J. Galin et al., *Phys. Rev. C* **9**, 1018 (1974).
10. A. J. Sierk and J. R. Nix, Los Alamos Scientific Laboratory report LA-UR-73-981 (1973).
11. C. Y. Wong, *Phys. Lett. B* **42**, 186 (1972).
12. M. Lecerf and J. Péter, *Nucl. Instrum. Methods* **104**, 189 (1972).
13. H. H. Gutbrod and F. Plasil, to be published.

EXCITATION FUNCTIONS AND ALPHA DECAY FROM COMPOUND NUCLEI IN ARGON-INDUCED REACTIONS ON ^{144}Sm AND ^{166}Er[1]

H. Gauvin[2] B. Lagarde[2]
R. L. Hahn Y. LeBeyec[2]
M. Lefort[2]

As part of a program to study the mechanisms of nuclear reactions induced by very heavy ions, excitation functions for the reactions ^{40}Ar + ^{144}Sm → Pt and ^{40}Ar + ^{166}Er → Po, in which the observed radioactive nuclei have two protons less than the product of the complete fusion of projectile and target, were measured at the accelerator ALICE in Orsay and found to be characterized by two peaks (Figs. 1.8 and 1.9). This double-peaked structure was shown not to be due to isotopic impurities in the targets nor to radioactive decay from other reaction products but to be the result of nuclear reactions on ^{144}Sm and ^{166}Er that lead to the observed platinum and polonium nuclides.

Similar two-peaked excitation functions for reactions leading to products with two protons less than the composite nucleus (agglomeration of projectile and target) have been previously reported in studies[3–9] involving projectiles much lighter than ^{40}Ar. All of these investigations, with ions such as protons, ^{10}B, or ^{12}C, ascribed at least one of the two peaks to a

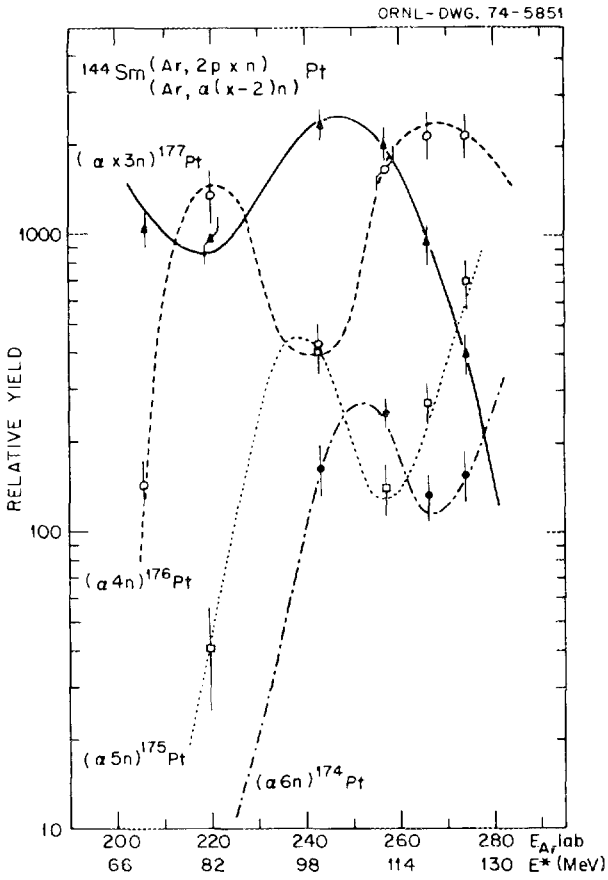

Fig. 1.8. Excitation functions for the production of platinum isotopes by bombardment of ^{144}Sm with argon ions, for x = 3 to 6.

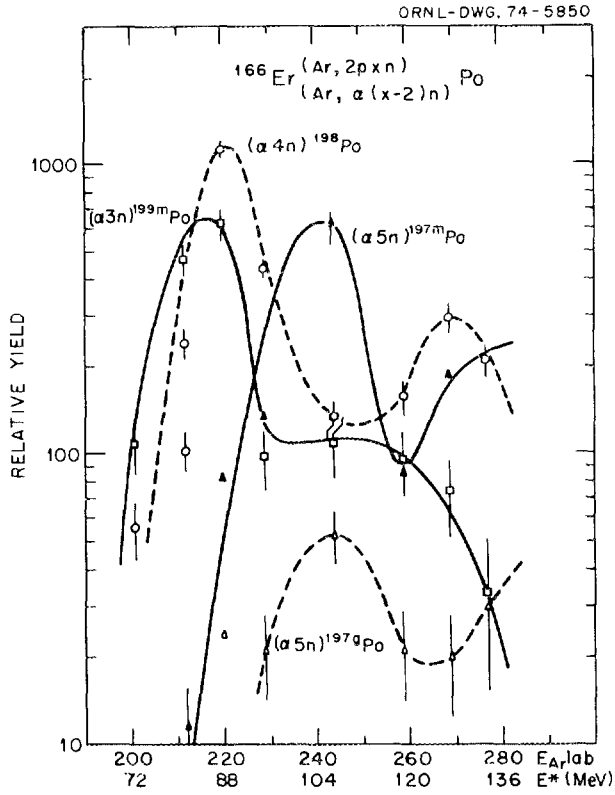

Fig. 1.9. Excitation functions for the production of polonium isotopes by bombardment of ^{166}Er with argon ions, for x = 3, 4, and 5.

direct nuclear process, such as alpha-particle knockout or a transfer reaction. However, it is difficult to admit such possibilities in the present work. Studies of other nuclear reactions induced by ^{40}Ar indicate that (1) the emitted protons and alpha particles are products of compound-nucleus reactions, with almost no contribution from direct reactions,[10] and (2) that the transfer of a large aggregate such as ^{32}S from ^{40}Ar to the target (leaving an alpha particle as a product of the reaction) is very improbable.[11]

We thus conclude that the observed two-peaked excitation functions must arise from compound-nuclear processes. To interpret these results further, we note that the two peaks are consistently found to be separated by about 40 MeV of excitation energy, independent of whether the target was samarium or erbium and independent of the mass of the product. Then, since the binding energy of the alpha particle is 28 MeV, it seems reasonable to assign the first peak in the excitation function to the evaporation of an alpha particle from the compound nucleus, that is, the (Ar,αxn) reaction, and the second peak to the successive evaporation of the $2n$ + $2p$ that would constitute an alpha particle, the [Ar,$2p(x+2)n$] reaction. The enhanced probability for alpha-particle emission observed here, relative to results obtained with lighter ions, would appear to be due to the large angular momentum values brought to the compound nucleus by ^{40}Ar.

1. Expanded abstract of published paper, *Nucl. Phys. A* **220**, 84 (1974).
2. Institut de Physique Nucléaire, Orsay, France.
3. J. W. Meadows and R. B. Holt, *Phys. Rev.* **83**, 47 (1951).
4. F. O. Bartell and S. Softky, *Phys. Rev.* **84**, 453 (1951).
5. R. A. Sharp, R. M. Diamond, and G. Wilkinson, *Phys. Rev.* **101**, 1493 (1956).
6. H. Gauvin, M. Lefort, and X. Tarrago, *Nucl. Phys.* **39**, 447 (1962).
7. R. Bimbot and M. Lefort, *J. Phys.* (Paris) **27**, 385 (1966).
8. Iu. Oganescian et al., Dubna preprint P7-5912 (1971).
9. F. Hubert, thesis No. 408, University of Bordeaux, 1973.
10. J. Galin et al., *Phys. Rev.* (in press).
11. A. G. Artukh et al., *Nucl. Phys. A* **176**, 284 (1971).

MULTINUCLEON TRANSFER REACTIONS[1]

R. Bimbot[2] R. L. Hahn
D. Gardes[2] Y. de Moras[2]
M. F. Rivet[2]

Two classes of reactions induced by heavy ions have been extensively studied: complete-fusion reactions, in which the projectile and target completely merge, and transfer reactions, in which a small number of nucleons are exchanged between projectile and target. A third type of reaction that is beginning to receive attention, especially now that beams of very heavy ions are becoming available, involves multinucleon transfers, wherein a large number of nucleons are exchanged by the colliding partners.

A systematic study of such complex transfer reactions is being carried out at the accelerator ALICE in Orsay, by determining the recoil properties of selected radioactive products. The nuclides ^{151}Dy, ^{150}Dy, and ^{149g}Tb have properties such as reasonably large alpha branching ratios and long half-lives (18 min, 7.1 min, and 4.1 hr respectively) that are especially suited for such experiments, and so were used in the work reported here. To survey a wide variety of transfer reactions, the production of these three nuclides was followed for the reactions of ^{40}Ar at 282 MeV with many different target nuclei, from cesium to gadolinium.

The most complete set of results has been obtained to date for reactions of ^{40}Ar with enriched targets of each of the stable isotopes of neodymium (mass numbers 142, 143, 144, 145, 146, 148, and 150). The experimental technique involved the measurement of the cross sections, angular distributions, and recoil ranges (or energies) at each recoil angle, of the heavy product nuclei.

Measuring the (relative) yields as a function of both recoil energy and angle represents a significant improvement in such studies because one then has sufficient information to transform the data to the center-of-mass system (c.m.s.). The c.m.s. angular distributions so obtained, as illustrated in Fig. 1.10 for ^{151}Dy produced with the ^{142}Nd target, are peaked at large angles, close to 180°. This observation suggests that the present reactions are of the same type as the multinucleon transfer reactions recently studied by other authors,[3,4] where the angular distribution of the light fragment was found to be peaked forward in the c.m.s. (in a two-body breakup in the c.m.s., the angles defining the trajectories of the resulting nuclei are supplementary).

The experimental energy distributions in the c.m.s. were used to test the feasibility of various assumed

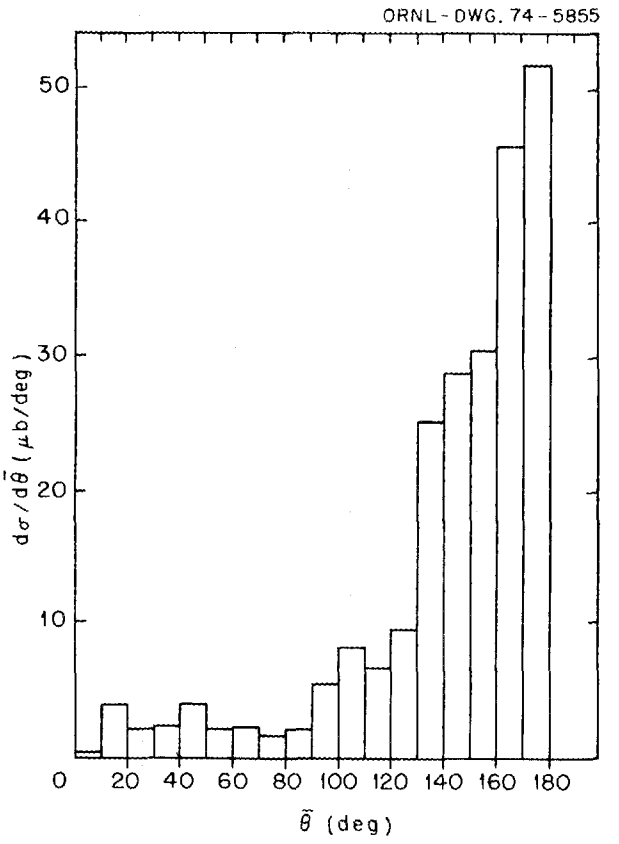

Fig. 1.10. Angular distribution in the center-of-mass system of ^{151}Dy from the reaction of 282-MeV ^{40}Ar + ^{142}Nd.

reaction paths which could lead to the production of the observed isotopes. Each path was assumed to involve a two-step process: the first step was the transfer, from the projectile to the target, of some number of nucleons, leading to an excited intermediate nucleus, and the second step, the deexcitation of the intermediate nucleus by nuclear evaporation to reach the final product. This testing procedure is illustrated in Fig. 1.11, which shows the measured c.m.s. energy distribution for ^{151}Dy from ^{40}Ar + ^{142}Nd (note that a net transfer of six protons and three neutrons is required to reach ^{151}Dy from ^{142}Nd). Each horizontal line above the energy distribution represents the calculated span of allowable kinetic energies for a particular two-step path. On the right side of the figure, each postulated transfer path is identified by the first step of the process; thus, there may be the transfer of six protons and from three to ten neutrons, to be followed by the evaporation of the appropriate number (xn) of neutrons. For possible reactions involving transfer of seven or eight protons, multiple paths are indicated,

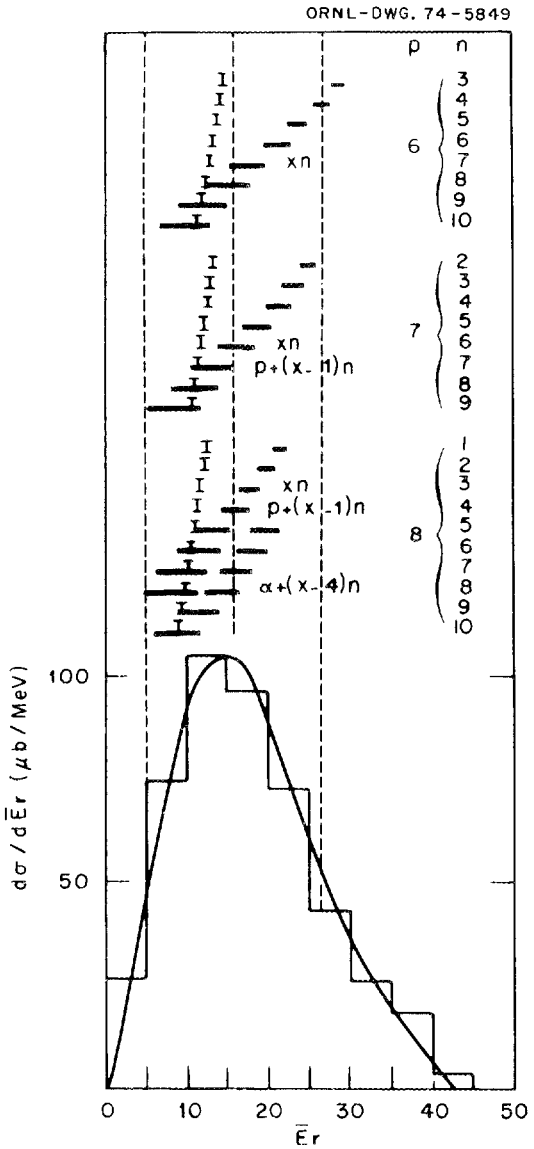

Fig. 1.11. Kinetic energy distribution in the center-of-mass system of ^{151}Dy produced from 282-MeV ^{40}Ar + ^{142}Nd. Dotted vertical lines show the maximum and half-width values of the distribution. The horizontal lines give the calculated spans of kinetic energies for the various assumed transfer paths indicated; the vertical bars show the kinetic energies expected from Coulomb repulsion of the two nuclei resulting from the transfer.

since, for example, one can reach ^{151}Dy by the transfer of seven protons and $2 + x$ neutrons followed either by evaporation of a proton and $x - 1$ neutrons or by evaporation of x neutrons succeeded by radioactive (electron-capture) decay.

Several conclusions can be readily drawn from the comparison in Fig. 1.11. First, the large width of the energy distribution is evidence for several different reaction paths contributing to the observed product ^{151}Dy. Second, all of the assumed reaction paths lead to kinetic energies that fall within the span of the measured values. Third, the peak of the distribution, at about 15 MeV, indicates that the most likely reaction path involves the transfer of six protons and seven or eight neutrons (our cross-section data show that the transfer probability decreases as the number of transferred protons increases, so that transfer of six protons is more likely than transfer of seven or eight).

In summary, measurements of the energy and angular distributions of transfer products such as have been described here allow us to draw conclusions about, and perhaps even to choose among, the mechanisms involved in complex transfer processes.

---

1. Summary of a paper to be published in *Nuclear Physics.*
2. Institut de Physique Nucléaire, Orsay, France.
3. A. G. Artukh et al., *Nucl. Phys. A* **215**, 91 (1973).
4. L. G. Moretto, *Bull. Amer. Phys. Soc.* **19**, 465 (1974).

DIRECT DETERMINATION OF THE ELECTRON-CAPTURE BRANCHING RATIO, ^{149}Dy → ^{149g}Tb[1]

H. Gauvin[2] B. Lagarde[2]
R. L. Hahn Y. LeBeyec[2]
M. Lefort[2]

The radioactive nuclei ^{151}Dy, ^{150}Dy, and ^{149}Dy have been used in many studies of nuclear-reaction mechanisms (see, e.g., refs. 3–5). Unlike the alpha-emitting nuclides ^{151}Dy and ^{150}Dy, ^{149}Dy is difficult to detect directly because it decays by electron capture. Its radioactive daughter, ^{149g}Tb, which decays by alpha-particle emission, has usually served as a measure of the number of ^{149}Dy atoms produced in a given nuclear reaction. However, no direct measurement had previously been made of the decay probability, x, for the transition

$$^{149}\mathrm{Dy} \xrightarrow[\mathrm{EC}]{} {}^{149g}\mathrm{Tb}\ ;$$

Alexander and Simonoff,[3] by comparing the yields of nuclear reactions leading to ^{151}Dy and ^{150}Dy with those for ^{149g}Tb (produced by decay of ^{149}Dy) had obtained an estimate of $x = 0.22$.

In the present work, we determined x directly by producing ^{153}Er in the reaction ^{118}Sn(^{40}Ar,5n) at the accelerator ALICE, and observing the alpha-active products in the decay chain

Table 1.5. Radioactive decay properties

Nuclide	Half-life	Decay mode	Branching ratio
^{153}Er	36 sec	α (4.67 MeV)	0.95
^{149}Dy	15 min	EC (to ^{149g}Tb) EC (to ^{149m}Tb)	
^{149g}Tb	4.1 hr	α (3.97 MeV)	0.16
^{149m}Tb	4.3 min	EC	1.0

$$^{153}\mathrm{Er} \xrightarrow[\alpha]{} {}^{149}\mathrm{Dy} \xrightarrow[\mathrm{EC}]{} {}^{149g}\mathrm{Tb} \xrightarrow[\alpha]{} {}^{145}\mathrm{Eu}\,.$$

(^{149}Dy also decays by electron capture to an isomeric level, ^{149m}Tb). Pertinent decay properties of these nuclides are listed in Table 1.5. By determining the number of alpha particles emitted *from the same sample* by ^{153}Er and ^{149g}Tb, we measured x, independent of such experimental conditions as target thickness, beam intensity, efficiency of collection of the product nuclei, and efficiency of the counting system. To ensure that no ^{149}Dy or ^{149}Tb could be directly produced in nuclear reactions such as (Ar,$\alpha 5n$) or (Ar,$\alpha p5n$), the irradiation was done at 180 MeV, below the thresholds of these reactions. Thus all of the detected ^{149g}Tb came from the decay of ^{153}Er. The value of $x = 0.475 \pm 0.050$ measured in this work is much larger than the previous estimate of 0.22 used in refs. 3 and 4.

1. Summary of published paper, *C. R. Acad. Sci., Ser. B* **277**, 107 (1973).
2. Institut de Physique Nucléaire, Orsay, France.
3. J. M. Alexander and G. N. Simonoff, *Phys. Rev. B* **133**, 93 (1964).
4. J. M. Alexander and G. N. Simonoff, *Phys. Rev. B* **133**, 104 (1964).
5. R. Bimbot, D. Gardes, R. L. Hahn, Y. de Moras, and M. F. Rivet, "Multinucleon Transfer Reactions," the preceding contribution, this report.

OBSERVED DIFFERENCES BETWEEN ARGON- AND KRYPTON-INDUCED REACTIONS LEADING TO THE SAME COMPOUND NUCLEI, ^{158}Er AND ^{156}Er[1]

H. Gauvin[2] M. Lefort[2]
Y. LeBeyec[2] R. L. Hahn

There have been a great number of experiments done to verify the independence hypothesis of compound-nucleus formation and decay, with identical compound nuclei being produced by different entrance channels. In principle, when the excitation energy and the angular momentum are specified, the decay processes should be entirely determined, independent of the manner in which the compound system was formed. Cross-bombardment experiments, so called Ghoshal-type tests,[3] have been carried out by many authors who have particularly compared the excitation functions for the production of the same evaporation residues in different reactions. A typical example is shown in the work of Alexander and Simonoff,[4] who found that excitation functions of the reactions ^{144}Nd(^{12}C,$6n$)^{150}Dy and ^{136}Ba(^{20}Ne,$6n$)^{150}Dy had the same threshold energy, the same maximum energy, and the same width. Until recently the heaviest projectiles used in cross bombardments were neon and argon ions.

In order to explore how much heavier projectiles fuse with target nuclei and to obtain information on the compound system which might be formed, a comparison has been made, using beams from the accelerator ALICE, between (^{40}Ar,xn) and (^{84}Kr,xn) reactions leading to the same compound nuclei, ^{158}Er and ^{156}Er. Excitation functions were constructed for two evaporation residues, ^{152}Er and ^{153}Er, for excitation energies between 50 and 110 MeV. These two isotopes are very convenient for such measurements because they are well-characterized alpha emitters with short half-lives. The (H.I.,xn) and, to a lesser extent, the (H.I.,pxn) reactions (where H.I. = heavy ion) were studied for the interactions of ^{40}Ar with ^{116}Sn and ^{118}Sn and of ^{84}Kr with ^{70}Ge, ^{72}Ge, and ^{74}Ge, with x varying from 1 to 6 for the germanium targets, and from 3 to 6 for the tin targets.

To obtain precisely the same compound nucleus by different entrance channels, it is necessary to produce it at the same excitation energy and the same angular momentum. The maximum values of the orbital angular momentum brought into the compound system by the projectile have been calculated for a large range of excitation energies E^* with the simple relationship

$$l_{\max}\hbar = (R_1 + R_2)[2\mu(\bar{E} - \bar{E}_0)]^{1/2}\,, \qquad (1)$$

where R_1 and R_2 are the radii of the partners, μ the reduced mass, $\bar{E}$ the center-of-mass kinetic energy, and $\bar{E}_0$ the energy at the total reaction threshold, taken to be the Coulomb barrier. Also, $E^* = \bar{E} + Q$, where Q is the mass balance for compound-nucleus formation. These results are presented in Fig. 1.12, and it is seen that in the energy range under consideration, 50 to 110 MeV, the maximum l values are always a little higher

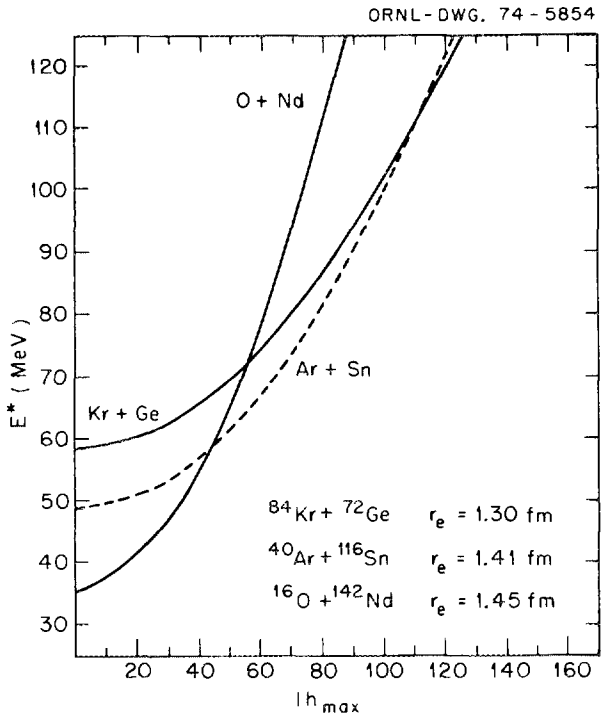

Fig. 1.12. Excitation energies vs calculated maximum orbital angular momenta [Eq. (1)] for the systems $^{16}O + ^{142}Nd$, $^{40}Ar + ^{116}Sn$, and $^{84}Kr + ^{72}Ge$. Values of $l\hbar$ were calculated by taking radius parameters r_e = 1.30 fm for ^{84}Kr, r_e = 1.41 fm for ^{40}Ar, and r_e = 1.45 fm for ^{16}O.

for argon projectiles than for krypton, since the kinetic energies for argon relative to krypton are much farther above the barrier. However, they are never very different, and one might assume that the compound nuclei are formed with very similar angular-momentum populations. The situation is quite different for the case of oxygen, where l_{max} is always much lower than for the very heavy ions (the reaction $^{16}O + ^{142}Nd$, ref. 5, leads to ^{158}Er, while the curves for argon and krypton are for compound nucleus ^{156}Er).

Several interesting and unexpected results were found in this comparison of argon- and krypton-induced reactions.

1. A comparison of the absolute cross sections shows that complete fusion is more severely limited in the case of krypton ions than for argon ions, at the same values of excitation energy and of maximum orbital angular momentum. The argon-induced reactions [i.e., the (Ar,xn) and (Ar,pxn) reactions] have probabilities for compound-nucleus formation that are approximately double those for the corresponding krypton-induced reactions. Relating this fact to the notion of a critical angular momentum l_{cr} for compound-nucleus formation (see, e.g., ref. 6), we find that since $l_{cr} \approx 70\hbar$ for argon ions[7] at an excitation energy of 80 MeV, $l_{cr} \approx 45\hbar$ for krypton ions.

2. A measurable probability of emitting only two neutrons is still observed when a compound nucleus is formed by $^{84}Kr + ^{70}Ge$ at 70 MeV of excitation energy. This energy is much above the threshold for emission of three neutrons and corresponds to a very large energy available per neutron (around 25 MeV), an unexpected result.

3. The most striking result found in these experiments is that the excitation function for a given reaction induced by krypton ions, (Kr,xn), exhibits a threshold energy about 15 MeV higher than for the same reaction induced by argon ions, (Ar,xn), for the evaporation of the same number of neutrons. Such a shift is not due to any Coulomb barrier effects, since both thresholds are well above the interaction barrier, and is observed for any value of x where the comparison can be made, for x = 4, 5, or 6. This behavior is illustrated in Fig. 1.13, where σ/σ_R, the ratio of the observed xn cross section to the calculated total reaction cross section, is shown vs E^* for x = 4, 5, and 6. It is striking to observe exactly the same behavior for the three cases. The krypton-induced excitation functions are narrower, due to the larger values of the reaction thresholds. For example, if one takes $\sigma(4n)/\sigma_R = 5 \times 10^{-3}$ as a reference for the rising part of the curve, this value is found at 48 MeV for (Ar,4n) and at 64 MeV for (Kr,4n). The same ratio for $\sigma(5n)/\sigma_R$ is observed at 60 MeV for (Ar,5n) and at 75 MeV for (Kr,5n). *There is a shift of about 15 MeV toward higher excitation energies with krypton ions, which is not at all predicted by any theoretical aspect of the compound-nuclear deexcitation process.* Such a difference was so unexpected that the measurements of the energies of the argon and krypton beams were carefully rechecked, and the observed energy shifts were verified.

A useful way[4] of seeing the effect of angular momentum on neutron-evaporation chains is to calculate the "available energy per emitted neutron,"

$$\langle E_{xn} \rangle = (\bar{E} + Q)/x \ ,$$

where Q is the mass balance. In the case of compound nuclei formed with high angular momenta in the rare-earth region by carbon, nitrogen, and oxygen ions, it was previously found[4] that $\langle E_{xn} \rangle$ was around 5 to 6 MeV, as compared with a value of about 3 MeV per neutron when low angular momenta were involved.

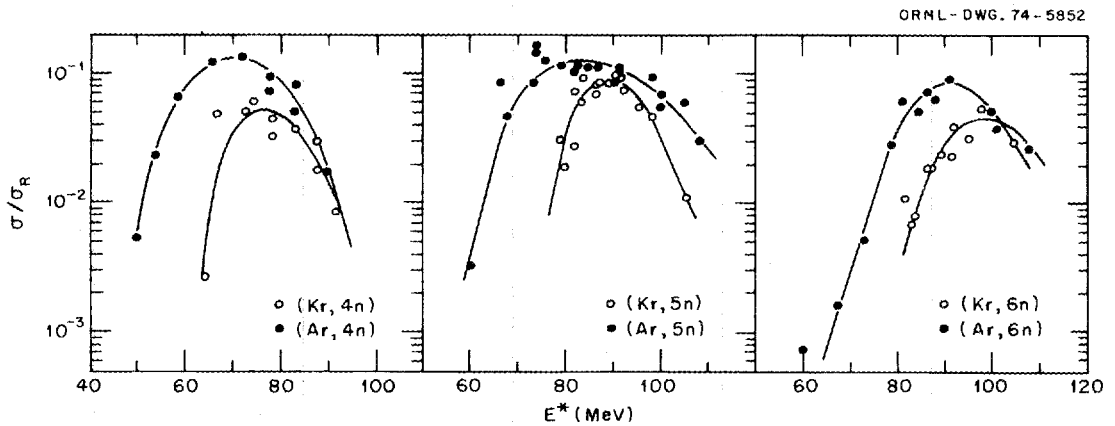

Fig. 1.13. σ(H.I.,xn)/σ_R **as a function of excitation energy for** x **= 4, 5, and 6.**

Using this concept of $\langle E_{xn} \rangle$, Fig. 1.14 presents our results on ^{40}Ar + ^{118}Sn and ^{84}Kr + ^{74}Ge and those of ref. 5 for ^{16}O + ^{142}Nd for emission of five neutrons from compound nucleus ^{158}Er. The maximum of the ratio σ_{5n}/σ_R is located at a higher energy (about 7.3 MeV per neutron) for argon than for ^{16}O (about 5.2 MeV per neutron), as expected, since large angular momenta occur in the compound nucleus ^{158}Er formed by argon projectiles. Similar results have been obtained by Natowitz and Alexander[8] for the reaction ^{114}Cd(Ar,5n). The fact that excitation functions are broader when high angular momenta are involved can be predicted from consideration of the angular momentum population of the compound nucleus. For low angular momentum (l) values, the minimum excitation energy at which a given xn reaction occurs should be essentially independent of the way the compound nucleus was formed. But when high angular momenta are reached, a large part of the excitation energy becomes rotational energy, reducing the energy available for neutron emission. Therefore a given xn excitation function is broadened toward higher energies, and the maximum is shifted. This change in shape and centroid of the excitation function also causes an apparent shift in the reaction threshold, for the relative number of low-l waves decreases as l_{max} becomes larger.

Now if one considers the curve for the (Kr,5n) reaction in Fig. 1.14, a puzzling result is observed. While the probability for $\langle E_{5n} \rangle$ rises from 10^{-3} at about 1 MeV up to 10^{-1} at 7.3 MeV in the case of (Ar,5n), the probability of 10^{-3} for (Kr,5n) is observed only at about 5 MeV. This result arises from the energy shifts of about 15 MeV observed in the krypton excitation functions. It is difficult to find any explanation for this difference based on angular momentum effects. First of all, the maximum l values (Fig. 1.12) are lower for krypton than for argon ions, and therefore the excitation function for the (Kr,5n) reaction should be in between the (O,5n) and (Ar,5n) curves. Moreover, there is no reason why low angular momenta would not exist *at all* when a compound nucleus is formed by the

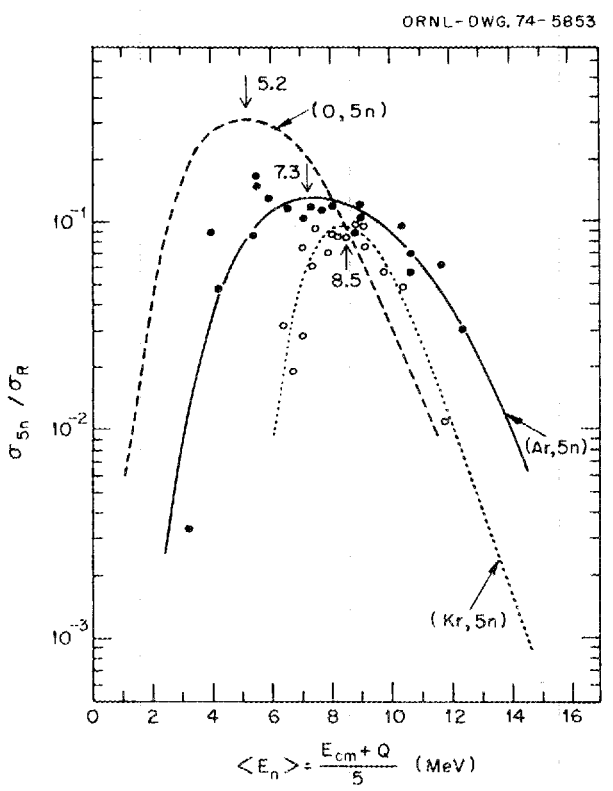

Fig. 1.14. σ(H.I.,5n)/σ_R **vs the available energy per neutron** $\langle E_{5n} \rangle = (\bar{E} + Q)/5$, **where** $\bar{E}$ **is the center-of-mass energy of the bombarding projectile and** Q **the mass balance.**

entrance channel Kr + Ge. And finally, it is not likely that this result is an effect of some special fusion barrier, since at energies lower than the threshold for the (Kr,5*n*) reaction, we found large cross sections for the (Kr,4*n*) and (Kr,3*n*) reactions.

Our interpretation of these differences in the argon and krypton excitation functions is that they do not result from differences in the way the compound nuclei decay (i.e., exit-channel effects), but from the fact that the compound nuclei formed by argon and krypton are not identical (entrance-channel effects). More specifically, it appears that there is some special effect which inhibits the evaporation of nucleons from the compound system formed with krypton ions, affecting all of the reactions observed, namely, (Kr,4*n*), (Kr,5*n*), (Kr,6*n*), and (Kr,*p*3*n*) and (Kr,*p*4*n*). We conclude that a fairly large amount of energy is somehow dissipated in the interaction of krypton with germanium, so that the compound nucleus which is formed does not share all of the excitation energy which is deduced from the $\bar{E} + Q$ balance.

Further investigation of these interesting questions is planned, both experimentally, where other compound systems formed by argon and krypton beams will be compared, and theoretically, where ideas such as "pre-compound emission"[9] and "special barriers to fusion"[10] will be considered.

1. Summary of paper to be published in *Physical Review*.
2. Institut de Physique Nucléaire, Orsay, France.
3. N. T. Porile, chap. 2 in *Nuclear Chemistry*, vol. 1, ed. L. Yaffe, Academic Press, New York, 1968.
4. J. M. Alexander and G. N. Simonoff, *Phys. Rev. B* **133**, 93 (1964).
5. R. D. Macfarlane and R. D. Griffioen, *Phys. Rev.* **131**, 2176 (1963).
6. L. Kowalski, J. Jodogne, and J. M. Miller, *Phys. Rev.* **169**, 894 (1968).
7. Y. LeBeyec, M. Lefort, and J. Peter, *Riv. Nuovo Cimento Ser. 2*, **4**, 1 (1974).
8. J. B. Natowitz and J. M. Alexander, *Phys. Rev.* **188**, 1734 (1969).
9. M. Blann, personal communication.
10. A. J. Sierk and J. R. Nix, Los Alamos Scientific Laboratory report LA-UR-73-981 (1973).

A DOPPLER-SHIFT PLUNGER DEVICE FOR MEASUREMENT OF PICOSECOND LIFETIMES

E. Eichler R. J. Sturm[1]
N. R. Johnson E. W. Chandler[2]

Even though energy-level systematics have been the basis of many nuclear models, lifetimes of the nuclear states provide much more stringent tests of these models. A great body of lifetime data has been accumulated using electronic methods; however, the shortest measurable half-life with these techniques is about 0.1 nsec. The Doppler-shift recoil-distance method opens up a new range of lifetime possibilities in that it is capable of determining nuclear lifetimes as short as 1 psec (10^{-12} sec). The "hardware" for applying the method requires three components: (1) a target holder, (2) a plunger whose end adjacent to the target serves as a beam "stopper," and (3) a distance-measuring system. The target holder must hold the target rigid and perpendicular to the beam and must include a device to stretch the thin target foil flat. The stopper must also be flat, parallel to the target, and capable of changes in position from tens of micrometers to several millimeters. Finally, the measuring system should be able to measure the relative target-stopper separation to better than 2.5 μm. The principle of the method is outlined in the following contribution[3] as well as in last year's annual report.[4]

For some time the "standard" system in the field was that designed by Alexander and Bell.[5] They placed the stretched target on a 9-cm-high support to intercept the beam. Since the stopper requires careful adjustment to establish accurate coplanarity with the target, it is mounted on a multiply articulated mount which rides on a slide. The position of the slide, and hence the separation of target and stopper, is changed by means of a micrometer screw acting through a high-vacuum seal.

The advent of the Heidelberg[6] design marked a new departure in the design of plunger apparatus since it utilized a hollow micrometer with the beam axis corresponding to the centerline of the double cylinder: the target was mounted on the stationary cylinder and the stopper on the rotor. In a variant due to Brandolini, Signorini, and Kusstatscher[7] the screw aspect of the Heidelberg system is replaced by smooth cylinders with a slot guide to prevent rotation and depth gages to give relative separation.

We chose to construct a modified version of the plunger of Brandolini et al.[7] for two basic reasons: (1) It avoids the elaborate setting up and alignment procedure required with the Alexander-Bell system.[5] (2) There is no danger of the target destruction that can occur at zero separation with a rotating device such as the Heidelberg[6] apparatus.

Figures 1.15 and 1.16 present a schematic and photographic rendering of our plunger design. We used brass for the outer (movable) cylinder, while the inner cylinder is a composite of brass and stainless steel. A

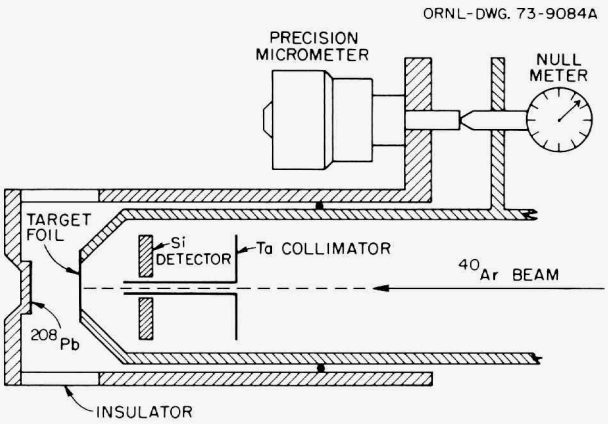

Fig. 1.15. Schematic drawing of the Doppler-shift recoil-distance device.

tab and groove guide prevents rotation of the outer cylinder, and an O-ring maintains high vacuum. The large knurled brass ring propels the outer cylinder, and the inclusion of a thrust bearing (barely visible in the photograph) is of great assistance in reducing friction. This is vital, since under vacuum the system supports an approximately 10-kg force due to atmospheric pressure.

The Lucite ring which joins the stopper to the outer cylinder has two roles. It insulates the stopper electrically, permitting beam-current measurement, and also allows visual inspection of target and stopper. A layer of metallic lead about 25 μm thick is evaporated onto the copper stopper, which was previously lapped to a surface-finish tolerance of 3 μm.

Separation measurements involve adjusting the Boeckler precision micrometer until the null meter indicates + 1.0 mil, an arbitrary reading. The zero point

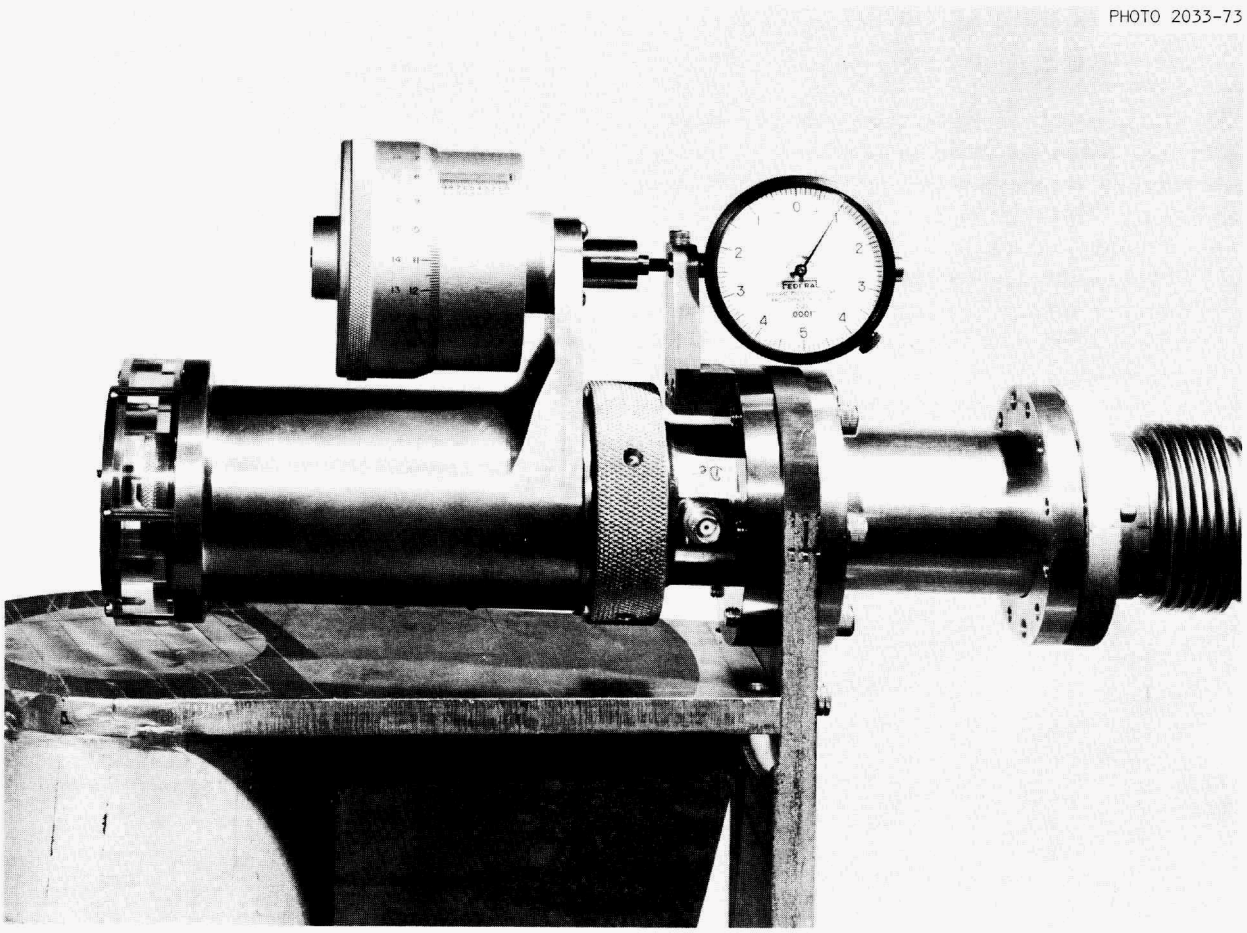

Fig. 1.16. Photograph of the Doppler-shift apparatus attached to the cyclotron beam line.

of the micrometer scale in an actual experiment is established by measuring electrical resistance. With this system we can measure relative target-stopper separations to an accuracy af about 1 μm.

1. Max Kade Foundation Fellow, University of Marburg, Marburg, Germany.
2. Plant and Equipment Division.
3. M. W. Guidry and R. J. Sturm, "A Computer Program for the Correction of Doppler-Shift Recoil-Distance Data," the following contribution, this report.
4. N. R. Johnson, R. Sturm, M. W. Guidry, E. Eichler, R. O. Sayer, N. C. Singhal, and D. C. Hensley, *Chem. Div. Annu. Progr. Rep. May 20, 1973,* ORNL-4891, p. 5.
5. T. K. Alexander and A. Bell, *Nucl. Instrum. Methods* **81**, 22 (1970).
6. H. Saun et al., vol. 2 in *Proc. Int. Conf. on Properties of Nuclei Far from the Region of Beta-Stability,* CERN-70-30 (Nov. 23, 1970).
7. F. Brandolini, C. Signorini, and P. Kusstatscher, *Nucl. Instrum. Methods* **91**, 341 (1971).

A COMPUTER PROGRAM FOR THE CORRECTION OF DOPPLER-SHIFT RECOIL-DISTANCE DATA

M. W. Guidry[1] R. J. Sturm[2]

The Doppler-shift recoil-distance technique is currently regarded as the most favorable method for the determination of lifetimes for nuclear states in the range of 10^{-9} to 10^{-12} sec. In the major portion of our work at ORIC, we utilize this technique to measure half-lives of excited states in deformed nuclei. As a part of this project, we have developed a detailed method of extracting lifetimes from the recoil-distance data which is implemented in the computer code ORACLE. The mathematical details of this procedure will be described in a forthcoming publication. In this contribution we will limit ourselves to a qualitative discussion only.

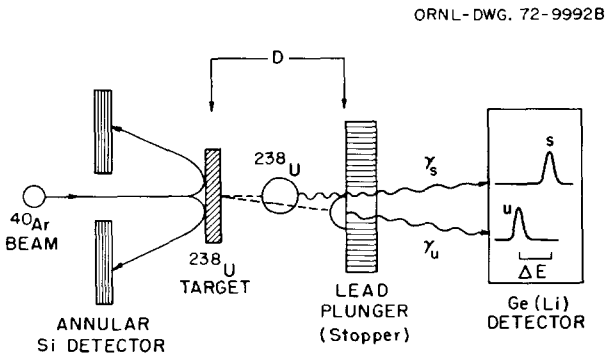

Fig. 1.17. Illustration of the recoil-distance method for measurement of lifetimes of nuclear states.

Figure 1.17 illustrates the basic principle of the recoil-distance method. The nuclei in a thin target foil are Coulomb-excited with a beam of heavy ions. The excited target nuclei recoil from the target until halted by a movable lead stopper (plunger). The deexcitation gamma rays emitted by the ensemble of recoiling nuclei are divided into two subsets by the movable stopper: (1) the gamma rays that are emitted after the recoiling nuclei strike the stopper – these have the characteristic energy E of the transition – and (2) the gamma rays that are emitted in flight with an energy shifted to a higher value $E + \Delta E$ due to the Doppler effect.

With sufficient gamma-ray energy resolution the peak in the spectrum characterizing the transition is split into a doublet – a lower-energy "unshifted" peak and a higher-energy "shifted" one. Typically one defines a ratio R of the unshifted intensity I_u to the total intensity $(I_u + I_s)$:

$$R = \frac{I_u}{I_u + I_s} . \tag{1}$$

As a first approximation it is a simple matter to show that R is related exponentially to the mean life τ:

$$R = \exp(-D/v\tau) , \tag{2}$$

$$\ln R = -D/v\tau , \tag{3}$$

where D is the target-stopper distance and v is the recoil velocity. The mean life τ is then obtained from the slope of a linear fit of $\ln R$ as a function of D.

In practice the simple exponential relation between R and τ is altered by several perturbing effects, which include:

1. Different detection efficiencies for the shifted and unshifted gamma rays.
2. Different detector solid angles presented to the shifted and unshifted gamma rays due to
   a) the emission of unshifted and shifted gamma rays from different average positions relative to the detector,
   b) the relativistic transformation of the angular distribution of gamma rays between the moving and stopped reference frames.
3. Attenuation of nuclear alignment as the nucleus recoils in vacuum through interaction with the electronic hyperfine field. This reduces the angular distribution correction by a varying amount for the two members of the doublet.

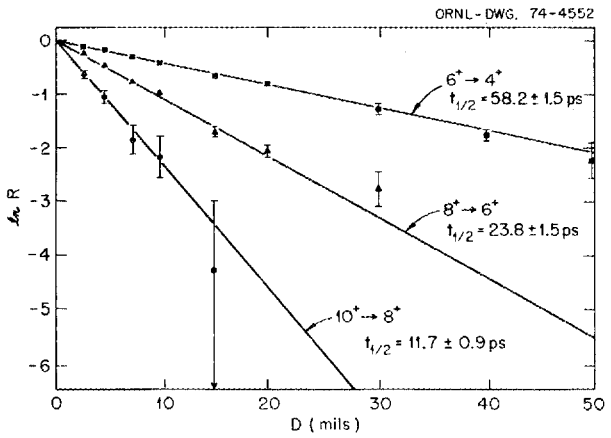

Fig. 1.18. Illustration of recoil-distance data corrected and fitted by the program ORACLE.

4. Cascade feeding of the level in question by other levels having comparable lifetimes, which alters in a time-dependent manner both the population and alignment of the state being analyzed.

These effects cause deviations from the linear behavior of ln R predicted by Eq. (3). The theoretical considerations embodied in the code ORACLE correct the experimental data for these perturbing effects by a self-consistent iterative process. The corrected data then exhibit the linear behavior predicted by Eq. (3), and the mean life follows from a weighted least-squares (linear) fit to the corrected data. As an example, Fig. 1.18 illustrates the effect of the corrections on the experimental data for a case where the perturbing effects (most notably cascade feeding) were quite large.

1. Oak Ridge Graduate Fellow from the University of Tennessee under appointment with the Oak Ridge Associated Universities.

2. Max Kade Foundation Fellow, University of Marburg, Marburg, Germany.

LIFETIMES OF ROTATIONAL STATES IN ^{232}Th BY THE DOPPLER-SHIFT RECOIL-DISTANCE TECHNIQUE[1]

N. R. Johnson R. O. Sayer[4]
R. J. Sturm[2] N. C. Singhal[5]
E. Eichler G. D. O'Kelley
M. W. Guidry[3] D. C. Hensley[4]
J. H. Hamilton[6]

One main aspect of our Coulomb-excitation program at ORIC is a continuing investigation of the behavior of deformed actinide nuclei at high spins. For example, in

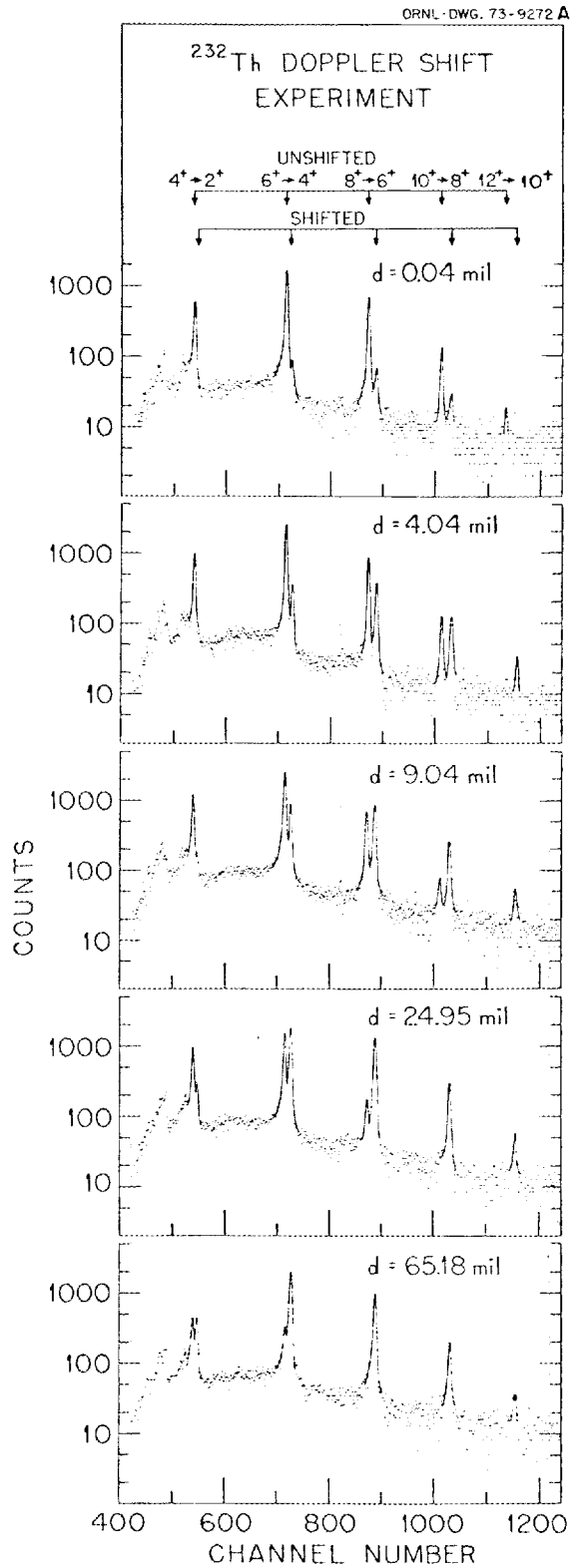

Fig. 1.19. Spectra of shifted and unshifted gamma rays in ^{232}Th at several target-stopper separations.

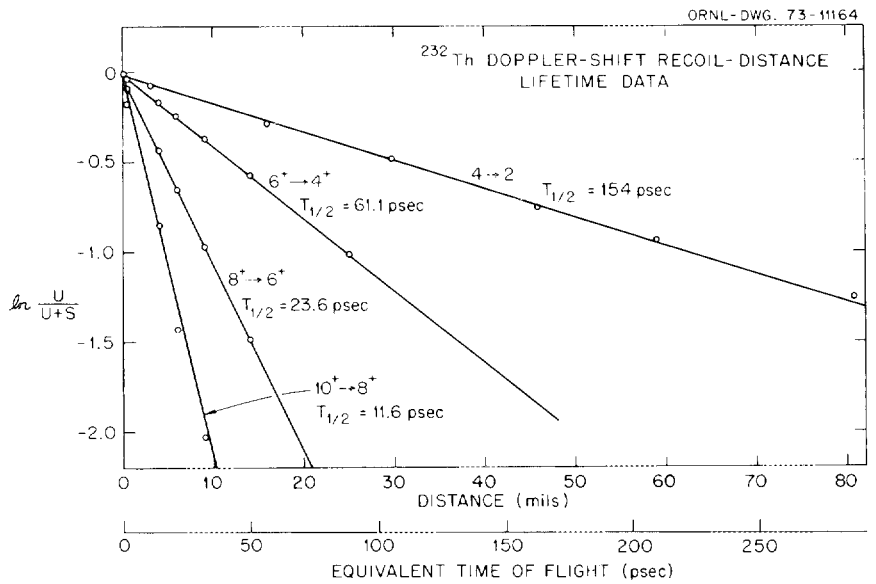

Fig. 1.20. Plot of ratios of unshifted to sum of unshifted and shifted gamma-ray peak intensities as a function of target-stopper separation for ^{232}Th.

a study of the multiple Coulomb-excitation process in ^{232}Th and ^{238}U with ^{40}Ar projectiles, we[7] were able to establish that the shapes of the nuclei are characteristic of large positive rather than negative hexadecapole moments. Some reservation is introduced into such a conclusion since it is necessary to rely on the rotational model for the required $E2$ and $E4$ matrix elements in the Winther–de Boer computer program.

Since the emission of $E4$ radiation cannot compete with the $E2$ process in the deexcitation of these rotational states, a direct measurement of their lifetimes provides the $E2$ matrix elements in a model-free manner. These matrix elements are a measure of the overlap of the wave functions of the connecting states in a rotational band. Information about them is necessary to the ultimate understanding of such nuclear phenomena as multiple Coulomb excitation and the apparent drastic change in the nuclear moment of inertia at high spins. Thus a major objective now is to obtain such lifetime data for the actinide nuclei.

We have used the Doppler-shift recoil-distance technique to measure the lifetimes of members of the ground-state band in ^{232}Th up through a spin of 10^+. A beam of 152-MeV ^{40}Ar projectiles from ORIC was used to Coulomb-excite the states in 1.5-mg/cm^2 metallic thorium foils. The experimental details were described previously.[8]

The type of data obtained in these experiments is illustrated in Fig. 1.19, which shows the spectra of shifted and unshifted gamma-ray peaks at several target-stopper separations. In Fig. 1.20 we show for each transition a plot of the ratio of the unshifted gamma-ray peak to the sum of the shifted and the unshifted peaks as a function of both the target-stopper separation and the equivalent time of flight of the recoiling thorium nuclei. These data have been corrected for several small perturbing effects described previously.[9] A summary of the half-lives determined here is given in column 3 of Table 1.6.

For each half-life, we have computed the corresponding reduced electric quadrupole transition probability, $B(E2)$, and compared it with the prediction of the rotational model. As seen in column 5 of Table 1.6, there is good agreement between experiment and

Table 1.6. Summary of half-life and $B(E2)$ data for ^{232}Th

Transition	E (keV)	$T_{1/2}$ (psec)	Exptl $B(E2)$ (e^2b^2)	$B(E2)$, expt/theory
2 → 0	49.37		1.84[a]	1.00[b]
4 → 2	112.75	154 ± 9	2.56	0.97 ± 0.05
6 → 4	171.00	61.1 ± 3.8	2.87	0.99 ± 0.06
8 → 6	223.84	23.6 ± 1.7	2.94	0.97 ± 0.07
10 → 8	270.47	11.6 ± 1.9	2.72	0.88 ± 0.14

[a]C. E. Bemis, Jr., F. K. McGowan, J. L. C. Ford, W. T. Milner, P. H. Stelson, and R. L. Robinson, *Phys. Rev. C* 6, 1466 (1973).

[b]Normalized to unity.

theory for all states. Not only does this result agree with the rotational model, but in addition it lends support to our earlier conclusion that the sign of the $E4$ moment in ^{232}Th is positive.

1. A similar account of this work appeared in the *Phys. Div. Annu. Progr. Rep. Dec. 31, 1973,* ORNL-4937, p. 42.

2. Max Kade Foundation Fellow, University of Marburg, Marburg, Germany.

3. Oak Ridge Graduate Fellow from the University of Tennessee under appointment with the Oak Ridge Associated Universities.

4. Physics Division.

5. Vanderbilt University Postdoctoral Fellow assigned to ORNL.

6. Vanderbilt University, Nashville, Tenn.

7. E. Eichler, N. R. Johnson, R. O. Sayer, D. C. Hensley, and L. L. Riedinger, *Phys. Rev. Lett.* **30,** 568 (1973).

8. N. R. Johnson, R. Sturm, M. W. Guidry, E. Eichler, R. O. Sayer, N. C. Singhal, and D. C. Hensley, *Chem. Div. Annu. Prog. Rep. May 20, 1973,* ORNL-4891, p. 5.

9. M. W. Guidry and R. J. Sturm, "A Computer Program for the Correction of Doppler-Shift Recoil-Distance Data," the preceeding contribution, this report.

LIFETIMES OF ROTATIONAL STATES IN ^{236}U BY THE DOPPLER-SHIFT RECOIL-DISTANCE TECHNIQUE[1]

M. W. Guidry[2] N. R. Johnson
R. J. Sturm[3] E. Eichler
G. D. O'Kelley R. O. Sayer[4]
N. C. Singhal[5]

Half-lives for the 4^+, 6^+, 8^+, and 10^+ members of the ^{236}U ground-state rotational band have been determined by the recoil-distance technique following Coulomb excitation produced by 152-MeV $^{40}Ar^{8+}$ projectiles at ORIC. Corrections for (1) energy dependence of detection efficiency, (2) positional and velocity dependence of solid angle, (3) multistage cascade feeding, and (4) alignment attenuation due to hyperfine perturbation have been applied by a computer program described previously.[6]

Figure 1.21 is a plot of ln R vs target-stopper separation D for the $6^+ \rightarrow 4^+$, $8^+ \rightarrow 6^+$, and $10^+ \rightarrow 8^+$ transitions. Here R is the experimentally determined ratio of intensity in the unshifted gamma-ray peak to the total of unshifted plus shifted intensity (suitably corrected for the perturbing effects mentioned above).

The half-lives extracted from these data and a comparison of corresponding $B(E2)$ values with rotational predictions are shown in Table 1.7. The constancy (through spin 8^+) of the $B(E2)$ ratios as a function of spin is indicative of rotational behavior for these states, in support of previous assumptions made in Coulomb-excitation studies on this nucleus.[7] The approximately 10% deviation of our data from the $B(E2)$ values predicted by applying the rotational model to

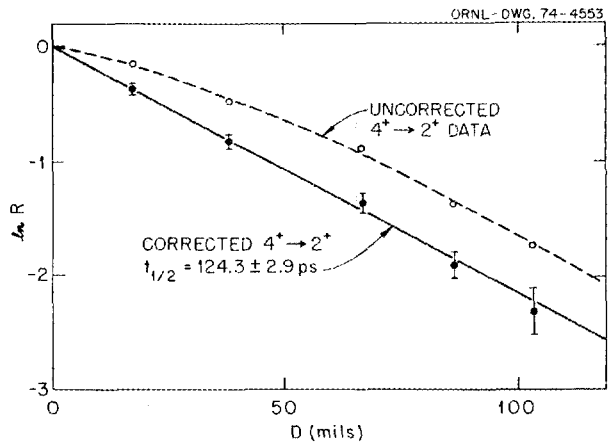

Fig. 1.21. Plot of ln R vs D for 10^+, 8^+, and 6^+ members of ^{236}U ground-state rotational band.

Table 1.7. Summary of half-life and $B(E2)$ data for ^{236}U

Transition	$T_{1/2}$[a] (psec)	Exptl $B(E2)$ (e^2b^2)	$B(E2)$, expt/theory[b]
$10^+ \rightarrow 8^+$	11.4 ± 0.9	3.21 ± 0.26	0.82 ± 0.07
$8^+ \rightarrow 6^+$	23.9 ± 1.5	3.42 ± 0.22	0.90 ± 0.06
$6^+ \rightarrow 4^+$	58.2 ± 1.5	3.28 ± 0.09	0.90 ± 0.04
$4^+ \rightarrow 2^+$	124.0 ± 2.9	3.03 ± 0.11	0.92 ± 0.05

[a]Extracted using Abragam-Pound theory and spin-independent alignment relaxation constants (τ_2 = 20 psec, τ_4 = 6 psec).

[b]Rotational values based on alpha-scattering work of Bemis et al., *Phys. Rev. C* 8, 1466 (1973).

the $B(E2,\ 0^+ \rightarrow 2^+)$ value of Bemis et al.[8] is not completely understood and is the object of continued investigation.

1. A similar account of this work appeared recently in the *Phys. Div. Annu. Progr. Rep. Dec. 31, 1973,* ORNL-4937, p. 46.
2. Oak Ridge Graduate Fellow from the University of Tennessee, Knoxville, under appointment from Oak Ridge Associated Universities.
3. Max Kade Foundation Fellow, University of Marburg, Marburg, Germany.
4. Physics Department.
5. Vanderbilt University Postdoctoral Fellow assigned to ORNL.
6. M. W. Guidry and R. J. Sturm, "A Computer Program for the Correction of Doppler-Shift Recoil-Distance Data," a preceding contribution, this report.
7. M. W. Guidry, R. J. Sturm, N. R. Johnson, E. Eichler, G. D. O'Kelley, R. O. Sayer, G. B. Hagemann, D. C. Hensley, and L. L. Riedinger, *Bull. Amer. Phys. Soc.* **18**, 1405 (1973).
8. C. E. Bemis, Jr., F. K. McGowan, J. L. C. Ford, Jr., W. T. Milner, P. H. Stelson, and R. L. Robinson, *Phys. Rev. C* 8, 1466 (1973).

COULOMB EXCITATION OF GROUND BANDS IN ^{160,162,164}Dy WITH ^{20}Ne and ^{35}Cl IONS[1]

R. O. Sayer[2] N. R. Johnson
E. Eichler D. C. Hensley[3]
L. L. Riedinger[4]

Even those nuclei which obey the rotational model at low spins deviate in energy from the strict $I(I+1)$ rule at higher spin values, presumably due to such effects as centrifugal stretching and Coriolis antipairing. These factors should also cause the intraband $B(E2)$ values to deviate from the rotational-model predictions.

To explore the trends in such deviations as a function of neutron number, we have made multiple Coulomb-excitation measurements on a series of dysprosium nuclei. Previously we reported results[5] on the multiple Coulomb excitation of ^{162}Dy and ^{164}Dy with ^{35}Cl ions. We have extended this study to ^{160}Dy and have utilized both ^{20}Ne and ^{35}Cl projectiles at ORIC to test the rigid-rotor prediction for intraband $B(E2)$ ratios. A complete account of this work was published[6] recently.

Multiple Coulomb excitation of states up to $J^\pi = 12^+$ in the ground band of ^{160,162,164}Dy was measured. The deexcitation gamma rays were observed in singles and in the particle-gamma coincident mode following excitation by ^{20}Ne or ^{35}Cl ions. Values of $B(E2)$ were extracted by comparing experimental excitation probabilities with theoretical values calculated with the Winther–de Boer computer code. Vibrational states, $E4$ Coulomb excitation, and quantal corrections were included in the calculations. To check for Coulomb-nuclear interference, we set a narrow digital window, 127.6 to 120.9 MeV, and a wide digital window, 127.6 to 108.7 MeV, on the heavy-ion energy for one of the ^{35}Cl-gamma runs. If $R_0 = 1.2A^{1/3}$ fm, the corresponding separation distances between surfaces were 5.0 to 5.8 fm for the narrow window and 5.0 to 7.7 fm for the wide window. Since the experimental probabilities extracted with the two windows were in good agreement, we doubt that Coulomb-nuclear interference is significant in the present work.

A sample spectrum of the gamma rays from ^{162}Dy in coincidence with backscattered ^{35}Cl ions is shown in Fig. 1.22. Our best $B(E2)$ values are compared graphically in Fig. 1.23 with recent Notre Dame[7] results from Coulomb excitation with ^{16}O ions. There is excellent agreement between the two sets of data for the $2 \rightarrow 4$ and $4 \rightarrow 6$ transitions and a slight systematic discrepancy for the $6 \rightarrow 8$ transitions.

Two surprising features can be seen in Fig. 1.23. One is the 10 to 15% dip in $B(E2;\ 4 \rightarrow 6)$ below the rotational prediction, and the other is a jump in $B(E2)$ values at the 10^+ state. If other perturbing factors are ignored, centrifugal stretching is implied by the $B(E2;\ 8 \rightarrow 10)$ values, whereas the dip in $B(E2;\ 4 \rightarrow 6)$ could be explained by a reduction in the nuclear deformation, that is, shrinking. The following contribution[8] describes our Doppler-shift recoil-distance measurements of states in ^{164}Dy and compares the results with the Coulomb-excitation data.

1. A similar account of this work appeared in the *Phys. Div. Annu. Progr. Rep. Dec. 31, 1973,* ORNL-4937, p. 38.
2. Jointly supported by Vanderbilt University, Nashville, Tenn. and by the ORNL Physics Division; on leave from Furman University, Greenville, S.C.
3. Physics Division.
4. Consultant, University of Tennessee, Knoxville.
5. R. O. Sayer, E. Eichler, N. R. Johnson, D. C. Hensley, and L. L. Riedinger, *Chem. Div. Annu. Progr. Rep. May 20, 1972,* ORNL-4791, p. 6.
6. R. O. Sayer, E. Eichler, N. R. Johnson, D. C. Hensley, and L. L. Riedinger, *Phys. Rev. C* 9, 1103 (1974).
7. R. N. Oehlberg, L. L. Riedinger, et al., *Nucl. Phys. A* **219**, 543 (1974).
8. R. O. Sayer, R. J. Sturm, N. R. Johnson, E. Eichler, N. C. Singhal, M. W. Guidry, and G. D. O'Kelley, "Lifetimes of Rotational States in ^{164}Dy by the Doppler-Shift Recoil-Distance Method," the following contribution, this report.

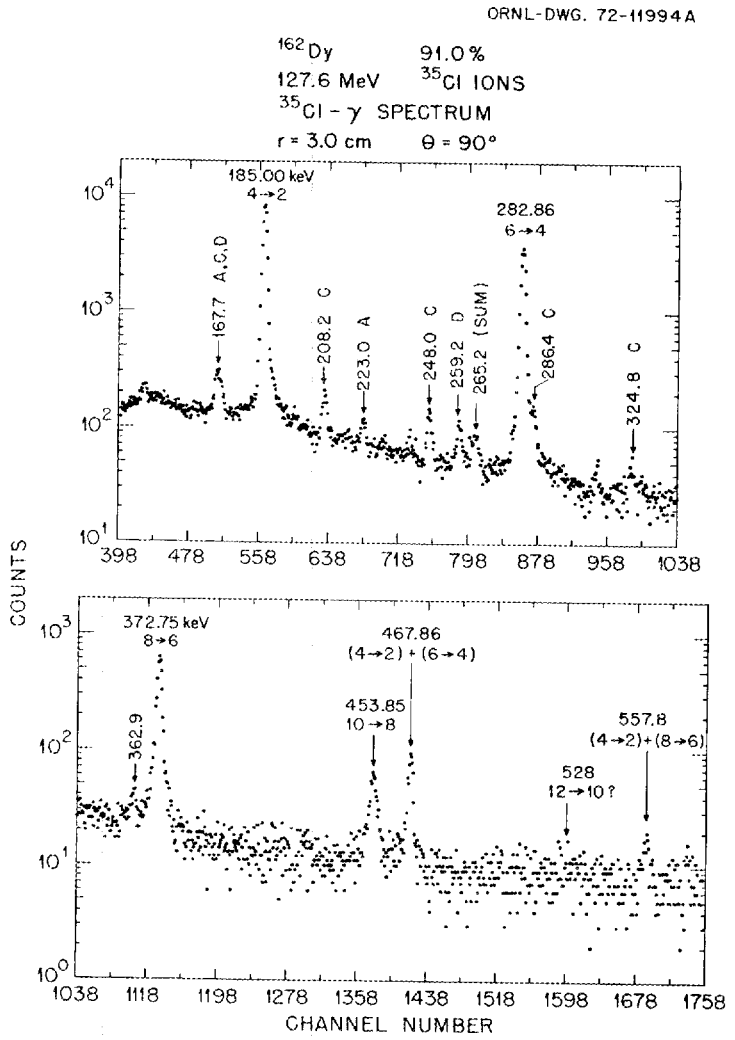

Fig. 1.22. Ge(Li)-detector spectrum of gamma rays in coincidence with ^{35}Cl ions backscattered from a ^{162}Dy target. Peaks labeled *A*, *C*, and *D* are attributed to the isotopic impurities ^{161,163,164}Dy respectively.

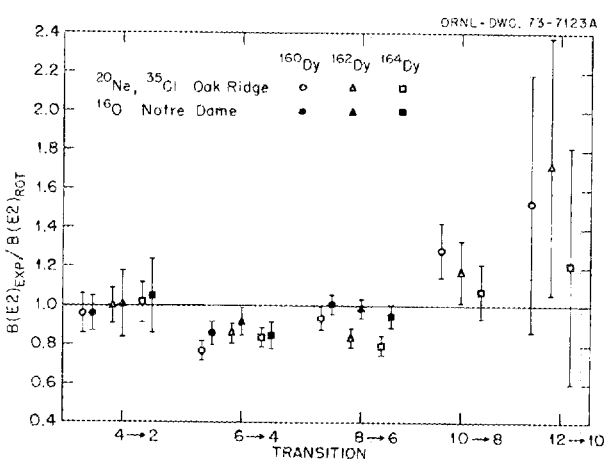

Fig. 1.23. Comparison of *B*(*E*2) values derived from Coulomb-excitation measurements with rigid-rotor predictions.

LIFETIMES OF ROTATIONAL STATES IN ^{164}Dy BY THE DOPPLER-SHIFT RECOIL-DISTANCE METHOD

R. O. Sayer[1] E. Eichler
R. J. Sturm[2] N. C. Singhal[3]
N. R. Johnson M. W. Guidry[4]
G. D. O'Kelley

Coulomb-excitation measurements described in the preceding contribution indicate significant deviations from the rotational-model predictions for rates of transitions between members of the ground-state band in three even-mass, dysprosium nuclei. We decided to use the Doppler-shift recoil-distance method in an attempt to verify these intriguing anomalies. We used 153-MeV ^{40}Ar ions to bombard a 1.0-mg/cm^2 foil enriched to

98.6% ^{164}Dy. The apparatus, data analysis, and correction methods are discussed in several preceding contributions. In Fig. 1.24 we show the "decay" curves for three of the transitions studied. These results are compared in Fig. 1.25 with the multiple Coulomb-excitation results from ORNL[5] and Notre Dame,[6] as well as the DSAM (Doppler-shift attenuation, or line-broadening) results of Kearns et al.[7]

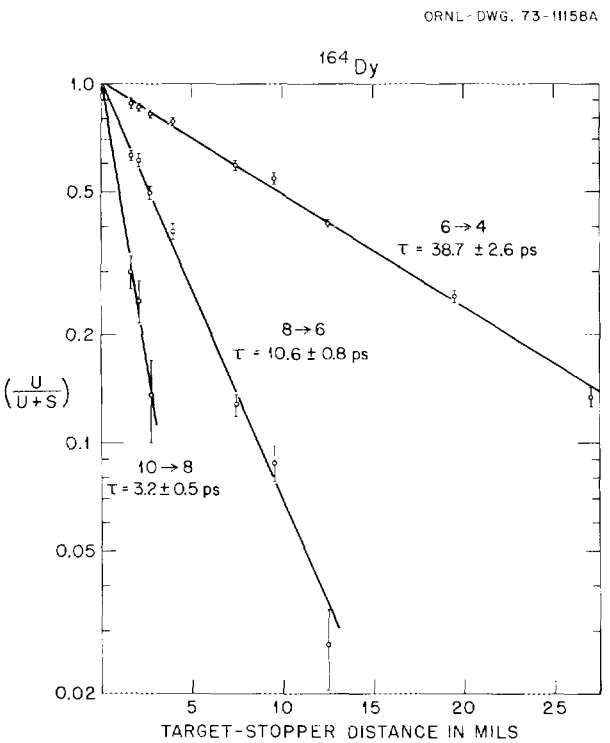

Fig. 1.24. Semilogarithmic plot of R vs separation distance for ^{164}Dy. $R = u/(u + s)$.

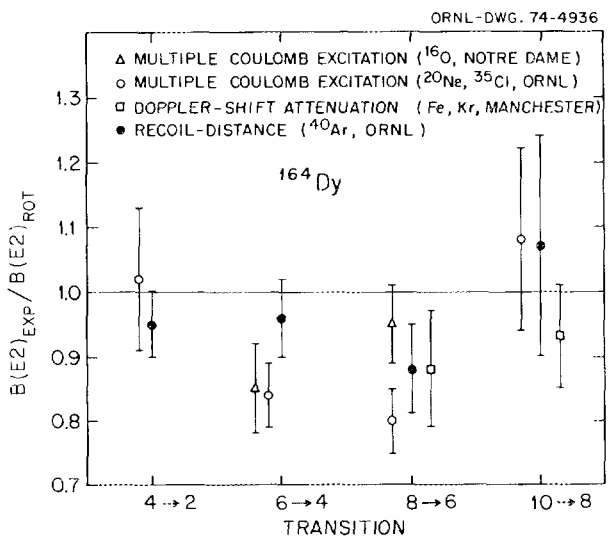

Fig. 1.25. A comparison of $B(E2)$ values with the rotational-model predictions for 4^+, 6^+, 8^+, and 10^+ states in ^{164}Dy as measured by various methods.

Within uncertainties, the $B(E2; 4 \rightarrow 2)$ and $B(E2; 10 \rightarrow 8)$ values are consistent with the rigid-rotor predictions. The plunger data suggest a much smaller dip in $B(E2; 6 \rightarrow 4)$ than the Coulomb-excitation data. However, we used a relaxation time $\tau_2 = 25$ psec to compute the dealignment correction; $\tau_2 = 40$ psec would reduce the plunger $B(E2)$ value by 5%. In the case of the $8 \rightarrow 6$ transition, four independent measurements using three techniques indicate significant retardation in $B(E2)$ relative to the rigid-rotor value. The unweighted average retardation for $B(E2; 8 \rightarrow 6)$ is (12 ± 4)%.

1. Jointly supported by Vanderbilt University, Nashville, Tenn., and by the ORNL Physics Division; on leave from Furman University, Greenville, S.C.
2. Max Kade Foundation Fellow, University of Marburg, Marburg, Germany.
3. Vanderbilt University Postdoctoral Fellow assigned to ORNL.
4. Oak Ridge Graduate Fellow from University of Tennessee under appointment with the Oak Ridge Associated Universities.
5. R. O. Sayer, E. Eichler, N. R. Johnson, D. C. Hensley, and L. L. Riedinger, *Phys. Rev. C* **9**, 1103 (1974).
6. R. N. Oehlberg, L. L. Riedinger et al., *Nucl. Phys. A* **219**, 543 (1974).
7. F. Kearns et al., *J. Phys. A* **7**, L11 (1974).

ANOMALOUS NUCLEAR ROTATIONAL BEHAVIOR IN THE RARE-EARTH REGION[1]

L. L. Riedinger[2] D. C. Hensley[3]
P. H. Stelson[3] N. R. Johnson
G. B. Hagemann[4] R. L. Robinson[3]
E. Eichler R. O. Sayer[5]
G. J. Smith[6]

In the early 1950's the collective model of Bohr and Mottelson succeeded in describing the rotational-like bands in deformed nuclei; these bands consisted mostly of 2^+ and 4^+ states populated by alpha decay. The ensuing years saw a gradual development as higher spin states began to be reached by in-beam spectroscopic methods. At higher spins the level energies sagged slightly below the values predicted by the $I(I + 1)$ rule for a pure rotor, but the deviations could be encompassed readily by a myriad of correctional models.

In the winter of 1971 came a report that would make rotational studies at once exciting and perplexing.

Johnson, Ryde, and Starkier[7] found an abrupt discontinuity at spin 14^+ in the rotational-level energies of the nucleus ^{160}Dy. Since 1971, examples of this phenomenon have multiplied — mostly confined to the neutron-deficient gadolinium, dysprosium, and erbium nuclei. When the rotational data are portrayed on a plot of **I**, the moment of inertia, vs ω^2 (ω is angular velocity), the anomalous bands reveal a "backbending" S-shaped curve.

The goals of our efforts (a collaboration of University of Tennessee, Chemistry Division, and Physics Division personnel) have been (1) to try to reach higher spins in previously discovered backbenders, (2) to find new backbenders, and (3) to try to aid in the understanding of these strange anomalies.

By taking advantage of heavy-ion beams from ORIC, we have been able to push the ground-state bands in the nuclei ^{160}Er and ^{164}Yb to spin 22^+, whereas the Jülich[8] group, using alpha particles, could observe at most the 18^+ level.

We discovered a new backbending nucleus ^{170}W in the course of a survey of the upper end of the rare-earth deformed region. Backbending plots for all of these nuclei can be seen in Fig. 1.26 along with the plot for

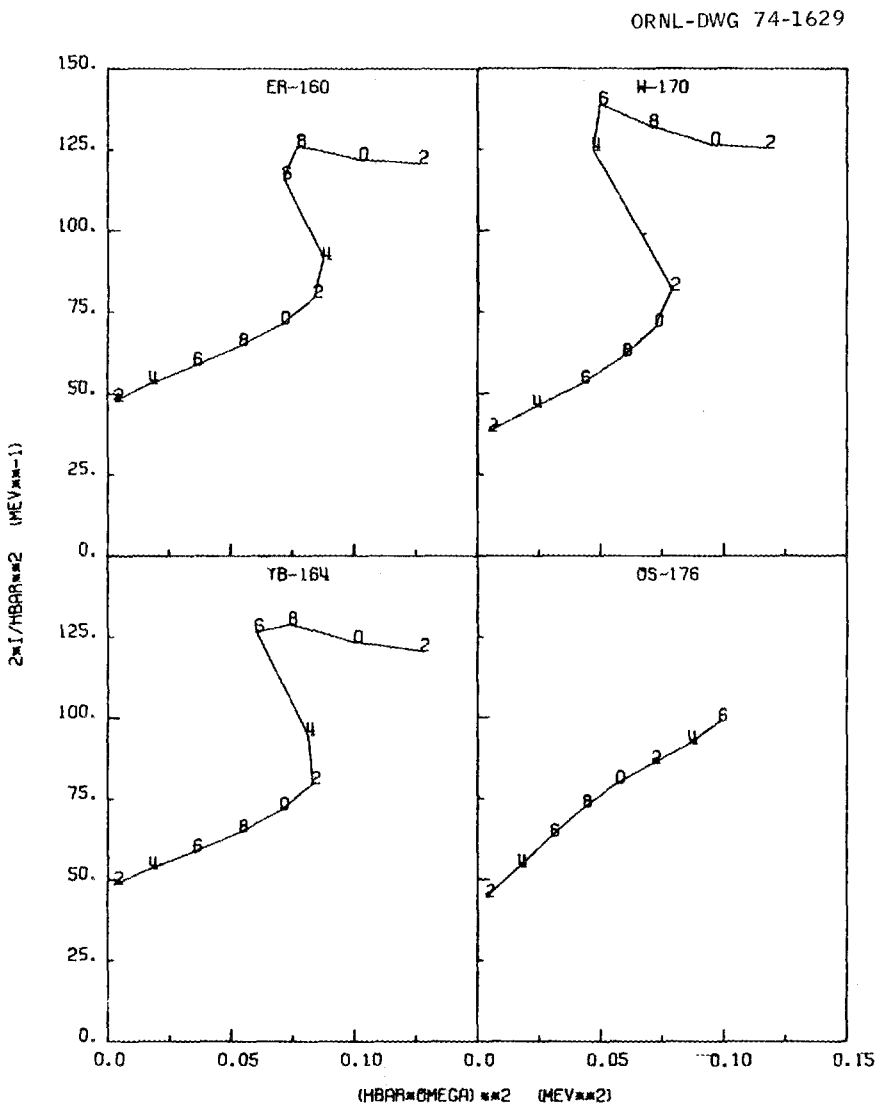

Fig. 1.26. "Backbending" plots [$2I/\hbar^2$ vs $(\hbar\omega)^2$] for ^{160}Er, ^{164}Yb, ^{170}W, and ^{176}Os. The numbers on the curves refer to the spins of the members of the rotational band. For spins 10 and higher the numeral "1" is understood.

ORNL-DWG 74-1628

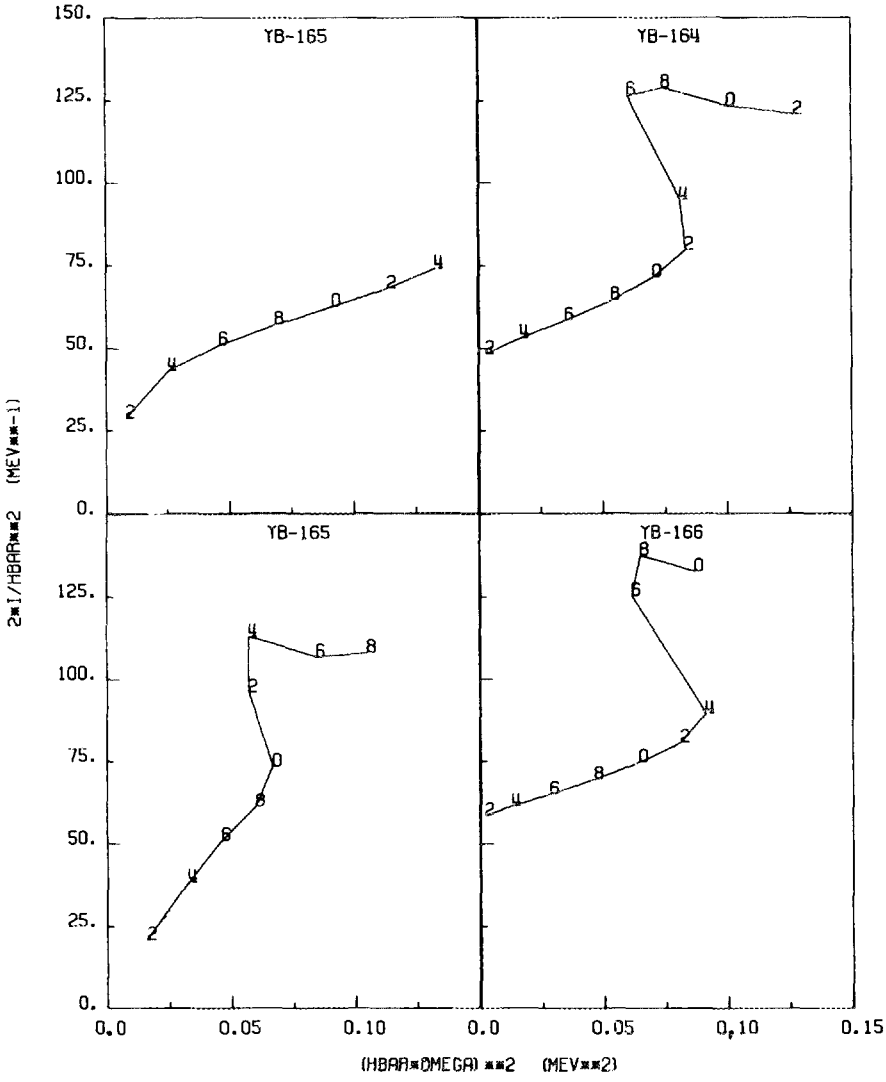

Fig. 1.27. A graph of $2I/\hbar^2$ vs $(\hbar\omega)^2$ for the ground-state bands in ^{164}Yb and ^{166}Yb and two decoupled bands in ^{165}Yb. For the odd-A bands the spins on the curves correspond to $I = 13/2$ for the $i_{13/2}$ band (upper left) and $I = 9/2$ for the $h_{9/2}$ band (lower left).

the nucleus ^{176}Os, which exhibits no backbending but instead is inclined "forward," suggestive of a transition of the nucleus between two static shapes.

Although several models have been proposed to explain backbending, they fall into two distinct groups: the pairing-collapse model and the decoupling model. In the first approach, as proposed, for example, by Kumar,[9] there is a complete collapse of neutron pairing at the backbending point, leading to an abrupt increase in the moment of inertia. By contrast, in the decoupling model,[10] two $i_{13/2}$ neutrons decouple from the rotating core at the backbending point, recoupling to spin 12^+. The rotating core then effectively slows down, leading to much smaller level spacing. Decoupling should occur also in odd-A nuclei — here only a single nucleon would become a spectator. Such decoupled bands have been observed in odd-A neighbors of many of the even-mass backbenders. We have searched for and identified decoupled bands in both ^{163}Yb and ^{165}Yb. In the latter case, we excited the bands up to spin $^{41}/_2{}^+$ ($^{13}/_2{}^+ + 14^+$); however, this highest state maintains a normal rotational-energy spacing, even though the rotating core (in ^{164}Yb) does backbend without the extra neutron. This can be understood since the already decoupled $i_{13/2}$ neutron blocks the alignment of further $i_{13/2}$ neutrons needed for backbending. We

found yet another piece of evidence to support this view, namely, an additional decoupled band — this one involving an $h_{9/2}$ neutron. This band does exhibit backbending since no $i_{13/2}$ particles are involved in the original decoupling. The backbending curves in Fig. 1.27 should clarify these differences.

A similar deduction was made by Grosse et al.[11] when they found that the decoupled $h_{11/2}$ proton in the odd holmium isotopes did not prevent backbending. If our tentative conclusions are correct, the presence of two decoupled bands in ^{165}Yb, one which backbends and one which does not, would be even more striking proof that the decoupling of $i_{13/2}$ neutrons is the prime cause of backbending for these nuclei.

We have begun a further test of the decoupling model using the Doppler-shift recoil-distance method to measure lifetimes of transitions in the odd-A decoupled bands. It would be very interesting to measure with good accuracy the lifetimes of states beyond the backbending point, but unfortunately these states are only weakly populated, making the measurements very difficult. Further, all the competing models project only a modest decrease in transition rates [or $B(E2)$ values] at the backbending point. By contrast a determination of low-lying and strongly populated members of a decoupled band would prove a stringent test of that picture. Preliminary analysis of our first attempt with 154-MeV ^{40}Ar on ^{130}Te indicates that the method should yield accurate lifetimes.

1. Similar accounts of this work appeared recently in the *Phys. Div. Annu. Progr. Rep. Dec. 31, 1973,* ORNL-4937, pp. 33 and 35.
2. Consultant, University of Tennessee, Knoxville.
3. Physics Division.
4. Niels Bohr Institute, Copenhagen.
5. Vanderbilt University, Nashville, Tenn., and ORNL.
6. Oak Ridge Associated Universities Postdoctoral Fellow.
7. A. Johnson, H. Ryde, and J. Starkier, *Phys. Lett.* B **34**, 605 (1971).
8. R. M. Lieder et al., *Z. Phys.* **257**, 147 (1972).
9. K. Kumar, *Phys. Scr.* **6**, 270 (1972).
10. F. S. Stephens et al., *Phys. Rev. Lett.* **29**, 438 (1972).
11. E. Grosse, F. S. Stephens, and R. M. Diamond, *Phys. Rev. Lett.* **31**, 840 (1973).

COSMOGENIC RADIONUCLIDES IN SAMPLES FROM TAURUS-LITTROW: EFFECTS OF THE SOLAR FLARE OF AUGUST 1972[1,2]

G. D. O'Kelley J. S. Eldridge[3] K. J. Northcutt[3]

Cosmogenic radionuclide concentrations in a suite of Apollo 17 samples were determined nondestructively by use of gamma-ray spectrometers with high sensitivity and low background. Measurements were made on 12 rock samples, which included 2 thin chips from a boulder, and 13 soil samples, which included 1 skim soil and 2 rather shallow surface samples from trenching operations. Cosmogenic radionuclides determined were ^{22}Na, ^{26}Al, ^{46}Sc, ^{48}V, ^{54}Mn, ^{56}Co, and ^{7}Be.

The general pattern of radionuclide concentrations in these Taurus-Littrow samples is profoundly different from that observed for samples from previous Apollo missions since, prior to collection, the Taurus-Littrow samples had been subjected to bombardment by the intense series of solar flares of August 4–9, 1972, which caused large enhancements in the yields of ^{22}Na, ^{46}Sc, ^{54}Mn, and ^{56}Co. The high energy and intensity of this proton flare made it possible for us to identify ^{7}Be in a lunar sample for the first time. Except for the Fra Mauro materials, which had a different chemical composition, surface samples from previous Apollo sites typically showed ^{26}Al/^{22}Na concentration ratios of 2 or more for samples in which the ^{26}Al had reached its saturation value. However, the ratio ^{26}Al/^{22}Na in most Apollo 17 samples was close to unity, because the intense solar-flare bombardment in August 1972 more than doubled the amount of ^{22}Na present when the flare occurred.

Data on the ^{56}Co and ^{54}Mn contents of thin surface samples were used to calculate the proton flux and rigidity of the August 1972 solar event. We determined the integrated proton flux J_i (>10 MeV) = 1.9×10^{10} cm^{-2}. For a differential energy spectrum expressed as the function $kE^{-\alpha}$, the shape parameter α was found to be $1.9^{+0.2}_{-0.1}$ if the energy E is in MeV. Thus the solar cosmic-ray event of August 1972 exhibited a much higher average proton energy than other flares of solar cycle 20, which had characteristic values of $\alpha \cong 3.0$.

1. Research carried out under Union Carbide's contract with the U.S. Atomic Energy Commission through interagency agreements with the National Aeronautics and Space Administration.
2. Summary of a paper submitted for publication in the *Proceedings of the Fifth Lunar Science Conference, Geochimica et Cosmochimica Acta,* Supplement 5, vol. 2. A preliminary account of some of this work was reported in *Chem. Div. Annu. Progr. Rep. May 20, 1973,* ORNL-4891, pp. 16–17.
3. Analytical Chemistry Division.

PRIMORDIAL RADIOELEMENT CONCENTRATIONS IN ROCKS AND SOILS FROM TAURUS-LITTROW[1,2]

J. S. Eldridge[3] G. D. O'Kelley K. J. Northcutt[3]

The concentrations of the primordial radioelements potassium, thorium, and uranium were determined nondestructively by gamma-ray spectrometry in 9

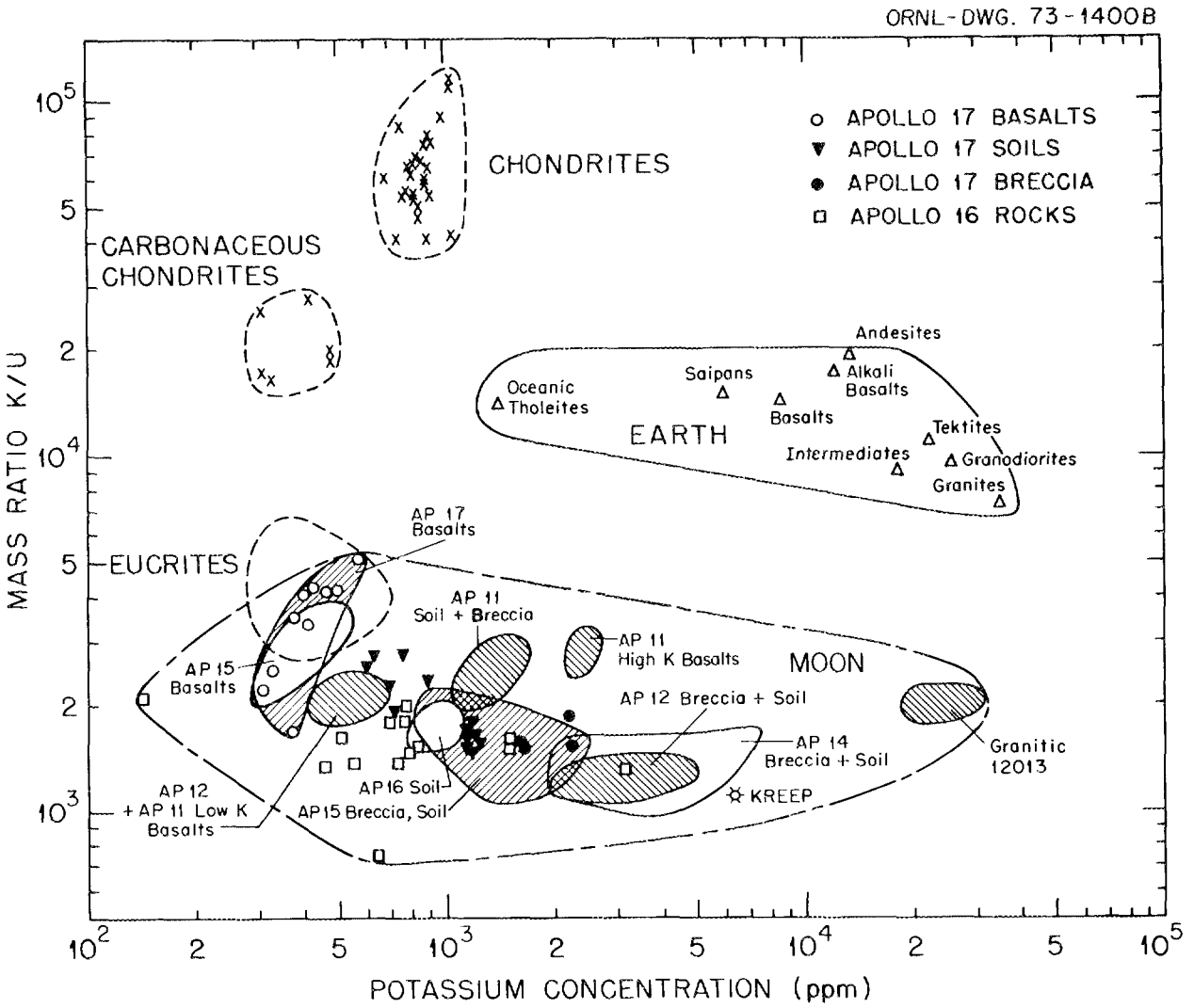

Fig. 1.28. Values of the mass ratio K/U as a function of the concentration of potassium. The Apollo 17 basalts, soils, and breccias appear to fall on a line with the basalts and KREEP as end members.

basalts, 4 breccias, and 13 soil samples of the Apollo 17 sample collection returned from the valley of Taurus-Littrow.

Variations in concentration ratios of Th/U and K/U were observed in three classes of basaltic rocks. These observations lend geochemical support to geological speculations that two or three separate subfloor basalt units were sampled at the Taurus-Littrow site. Grouping of the Apollo 17 basalts, soils, and breccias in the potassium-uranium systematics of Fig. 1.28 suggests that the soils and breccias are situated along a two-component mixing line with coarse basalts and KREEP as end members. Elevated values of primordial radioelement concentrations in breccia samples compared with the soils of Taurus-Littrow indicate that the breccias could not have been formed by simple impact induration of the local regolith. On the other hand, similarities of the potassium, thorium, and uranium contents of the soils and basaltic rocks indicate that the dark regolith in the Taurus-Littrow valley may be the comminuted product of the underlying subflow unit.

Concentrations of potassium, thorium, and uranium in the Apollo 17 soil samples were found to lie in two narrow ranges. Compositions of seven light mantle soils were distinctly different from those of six dark regolith soils. The average thorium content of the light soils is the same as that determined for the lunar highlands near Taurus-Littrow by the orbiting gamma-ray spec-

trometer.[4] Little or no variation in primordial radioelement concentration was observed in trench samples as a function of depth, color, or texture.

1. Research carried out under Union Carbide's contract with the U.S. Atomic Energy Commission through interagency agreements with the National Aeronautics and Space Administration.

2. Summary of a paper submitted for publication in the *Proceedings of the Fifth Lunar Science Conference, Geochimica et Cosmochimica Acta,* suppl. 5, vol. 2. A preliminary account of some of this work was reported in *Chem. Div. Annu. Progr. Rep. May 20, 1973,* ORNL-4891, pp. 16–17.

3. Analytical Chemistry Division.

4. J. I. Trombka et al., "Some Correlations between Measurements by the Apollo Gamma-Ray Spectrometer and Other Lunar Observations," *Proc. Fourth Lunar Sci. Conf., Geochim. Cosmochim. Acta,* suppl. 4, vol. 3, pp. 2847–53 (1973).

2. Chemistry and Physics of Transuranium Elements

The nuclides beyond those of uranium continue to hold a special interest for a variety of scientific and practical reasons, and experiments to produce and study them continued along lines previously established. The identification of element 104 (through 5-sec ^{257}104) was fully confirmed by the final analysis of the x-ray–alpha coincidence data. A very fast tape transport system was developed and built for extending such experiments (and others) to nuclides of shorter half-life. Newer, high-spatial-resolution techniques like ion microprobe analysis and x-ray analysis with scanning electron microscopy began to be applied to the inclusions in radiohalos.

From the beginning of this program, we have recognized the desirability of doing more than identifying those elements produced only to the extent of a few atoms per day on an accelerator. Now our first results of studying chemical properties one atom at a time are available, a comparison of the chemistry of divalent nobelium in solution with that of other divalent metals. More conventional chemical studies continued on elements available in macro quantities, including preparation of compounds, crystallography, and electron spectroscopy. New directions included the first measurement of the heat of solution of berkelium metal and a start on spectroscopy of actinides in molten salts.

COULOMB EXCITATION OF VIBRATIONAL-LIKE STATES IN THE EVEN-*A* ACTINIDE NUCLEI[1]

F. K. McGowan[2] J. L. C. Ford, Jr.[2]
C. E. Bemis, Jr. R. L. Robinson[2]
W. T. Milner[2] P. H. Stelson[2]

Coulomb excitation of vibrational-like states in the even-A actinide nuclei ($230 \leqslant A \leqslant 248$) was measured using ^{4}He ions in order to test nuclear models describing these states. In particular, the one-phonon octupole vibrational interpretation of the low-lying negative-parity states provides an interesting theoretical framework with which to compare experimental information. The excitation probabilities were determined relative to the elastic scattering by the observation of elastically and inelastically scattered ^{4}He ions using a split-pole magnetic spectrometer equipped with a position-sensitive proportional detector. The details of the experimental procedure have been discussed in an earlier publication.[3] The values of $B(E\lambda,0_g \rightarrow J = \lambda)$ range from 0.5 to 4-single-particle units for $\lambda = 2$ and from 10 to 30 single-particle units for $\lambda = 3$. For those cases where the K, J^π assignments are known, the agreement between the experimental results and the microscopic calculations by Neegard and Vogel[4] and Vogel[5] of the $B(E3,0 \rightarrow 3)$ for the 3^- members of the one-phonon octupole quadruplet is good when the Coriolis coupling between the states with K and $K \pm 1$ is taken into account. The values of the reduced $E0$ nuclear matrix element, $\rho(E0,2' \rightarrow 2_g)$, extracted from the $E0$ transition probabilities $T(E0,2' \rightarrow 2_g)$, for decay of the β-vibrational-like $2'^+$ state are 0.37 ± 0.06 and 0.43 ± 0.06 for ^{232}Th and ^{238}U respectively. Several 2^+ states observed in this Coulomb excitation reaction survey are presumed to be 2^+ members of rotational bands based on 0^+ excited states which are strongly populated in the (p,t) reaction. Our results have been submitted for publication in *Phys. Rev. C.*

1. A similar report has also appeared in the *Phys. Div. Annu. Progr. Rep. Dec. 31, 1973,* ORNL-4937, p. 129.
2. Physics Division.
3. C. E. Bemis, Jr., F. K. McGowan, J. L. C. Ford, Jr., W. T. Milner, P. H. Stelson, and R. L. Robinson, *Phys. Rev. C* 8, 1466 (1973).

4. K. Neegard and P. Vogel, *Nucl. Phys. A* **145**, 33 (1970).
5. P. Vogel, private communication of Coriolis matrix elements and wave functions, 1971.

ATTEMPTED COULOMB EXCITATION OF THE 8.5-μsec SPONTANEOUS FISSION ISOMERIC STATE IN ^{239}Pu[1]

C. E. Bemis, Jr. R. L. Ferguson
F. Plasil[2] E. E. Gross[2]
A. Zucker[3]

Fission induced by the time-dependent electromagnetic field of a passing ion is an intriguing possibility that has been investigated theoretically by several authors.[4,5] The related case of spontaneous fission isomer excitation has also been theoretically investigated.[5] As the observation of spontaneous fission isomeric states is inherently easier to perform experimentally than the pure Coulomb-induced fission process because the fission events are delayed relative to the time of excitation, we have chosen to investigate the isomer excitation as a prelude to investigating pure Coulomb fission, which may become possible with the proposed newer heavy-ion facilities at ORNL.

We have attempted the Coulomb excitation and subsequent observation of the 8.5-μsec spontaneous fission isomeric state in ^{239}Pu using 100- and 117-MeV ^{20}Ne ions at ORIC. A beam pulsing system, based on the use of 1-m-long parallel deflection plates with a 2-cm spacing, was developed for these experiments. A high-power pulse generator using an Eimac 4 CW-25000A radial-beam power tetrode in the switch-tube mode was used to produce 6.5-kV square-wave high-voltage pulses which were applied to one of the deflection plates. The deflected beam was intercepted on a water-cooled plate while the undeflected beam was transmitted to the target station. Recoil ^{239}Pu atoms, resulting from elastic and inelastic scattering, were stopped in a thin nickel catcher foil located downstream from a 120-μg/cm^2 isotopically pure ^{239}Pu target, also on nickel foil. The catcher foil was viewed by two large-area surface-barrier detectors, operated in coincidence, for the observation of delayed fission events during the time the beam was deflected from the target.

Only one delayed fission event was observed in these experiments, which corresponds to a production cross section of about 3.2×10^{-34} cm^2 integrated over ^{20}Ne scattering angles in the range 90° to 180°$_{lab}$ as dictated by our experimental arrangement. We conclude that further attempts to Coulomb excite fission isomers will have to await the production of ions much heavier than neon, particularly in light of recent negative results[6] using 60-MeV ^{12}C ions and 740-MeV ^{136}Xe ions in similar experiments for the 200-nsec isomer in ^{238}U.

A full account of our work has been prepared for publication.

1. A similar report has appeared in *Phys. Div. Annu. Progr. Rep. Dec. 31, 1973*, ORNL-4937, p. 26.
2. Physics Division.
3. Director's Division.
4. E. Guth and L. Wilets, *Phys. Rev. Lett.* **16**, 30 (1966); L. Wilets, E. Guth, and J. S. Tenn, *Phys. Rev.* **156**, 1349 (1967); P. W. Riesenfeldt and T. D. Thomas, *Phys. Rev. C* **2**, 711 (1970); H. Holm and W. Greiner, *Nucl. Phys. A* **195**, 333 (1972).
5. K. Beyer and A. Winther, *Phys. Lett. B* **30**, 296 (1969); K. Beyer, A. Winther, and U. Smilansky, in *Nuclear Reactions Induced by Heavy Ions*, R. Bock and W. Herring, ed., North-Holland Publ. Co., Amsterdam, 1970, p. 804.
6. Yu. P. Gangrsky et al., Joint Institute of Nuclear Research preprint P7-7022, Dubna, U.S.S.R. (1973).

TRANSFER AND COMPOUND-NUCLEUS REACTIONS THAT LEAD TO THE NUCLEI ^{245}Cf AND ^{244}Cf: INTERACTIONS OF ^{12}C WITH ^{239}Pu AND ^{238}U[1]

R. L. Hahn K. S. Toth[2]
P. F. Dittner O. L. Keller, Jr.

As part of our continuing program of studying nuclear reaction mechanisms in the actinide elements, we have investigated several heavy-ion transfer reactions leading to the same product nuclei, ^{245}Cf and ^{244}Cf; the systems surveyed were ^{239}Pu + ^{12}C, ^{242}Pu + ^{12}C, ^{237}Np + ^{14}N, and ^{235}U + ^{16}O. To learn more about the details of such transfers, we determined recoil properties for the reactions ^{239}Pu + ^{12}C.

In particular, the nuclear reactions ^{239}Pu(^{12}C,$\alpha 2n$-$\alpha 3n$) and ^{238}U(^{12}C,$5n$-$6n$) leading to ^{245}Cf and ^{244}Cf were studied by measuring excitation functions and recoil range and angular distributions. As expected, the uranium plus carbon data are consistent with predictions for complete-fusion (CF) reactions; for example, the range distributions are Gaussian with mean values that increase with increasing bombarding energy, and the angular distributions are forward peaked in the laboratory system. Figure 2.1 shows $\bar{R}$, the experimental mean range (centroid), as a function of ^{12}C bombarding energy. The straight lines are ranges calculated by assuming complete fusion of projectile and target nucleus and using the range-energy values of either Steward[3] or Northcliffe and Schilling.[4] The measured angular distributions are shown in Fig. 2.2. The results for the plutonium plus carbon reactions differ markedly from those for uranium plus carbon. The range distributions are asymmetric, with

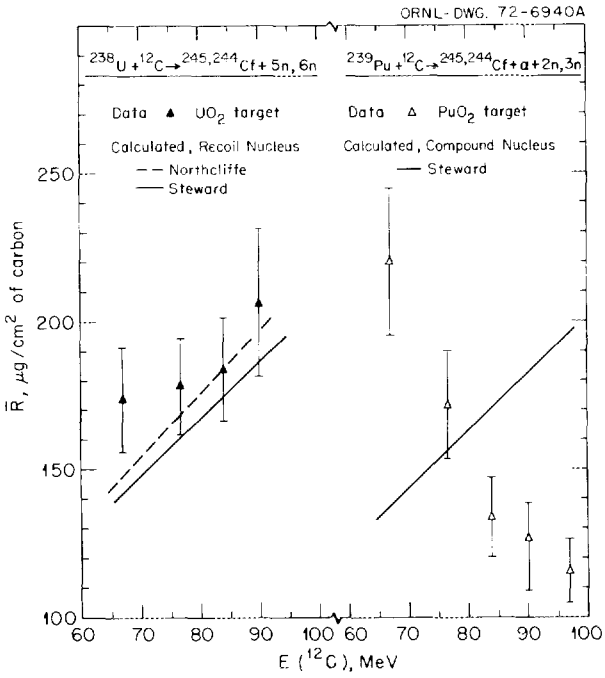

Fig. 2.1. Average ranges, $\bar{R}$, in carbon (over the angular interval from 0 to 10.7°) of the recoil nuclei ^{245}Cf and ^{244}Cf from the reactions ^{238}U + ^{12}C and ^{239}Pu + ^{12}C. Each datum point has been obtained from the measured range distribution, appropriately corrected for stopping in the targets. The lines are ranges calculated by assuming full momentum transfer in the reactions and using the range-energy relations of either Steward (ref. 3) or Northcliffe and Schilling (ref. 4).

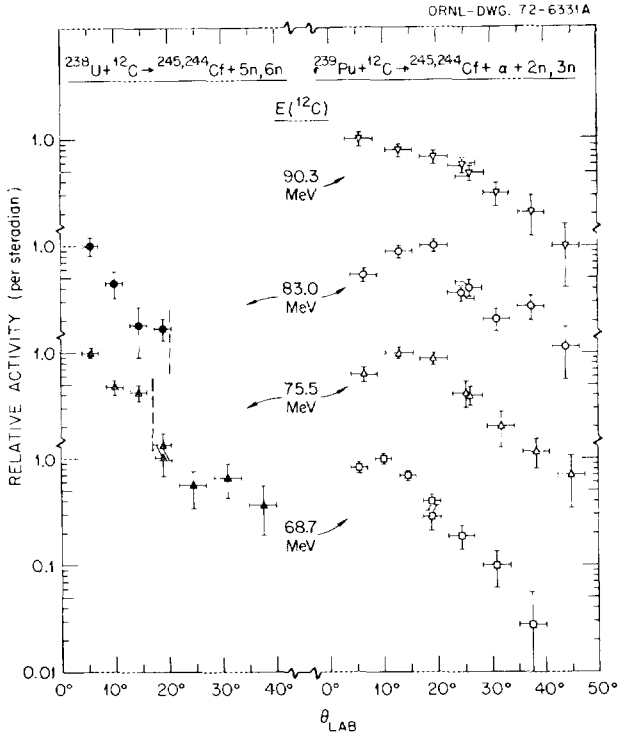

Fig. 2.2. Relative angular distributions of ^{245}Cf and ^{244}Cf from the reactions ^{238}U + ^{12}C and ^{239}Pu + ^{12}C. The distributions are proportional to $d\sigma/d\Omega$. For the ^{238}U + ^{12}C reactions, the dashed vertical lines represent the maximum angles in the laboratory system at which the californium products should be observed, as calculated from reaction kinematics. Data beyond these angles are indicative of scattering in the uranium target.

high-energy tails, and have centroids that decrease monotonically with increasing ^{12}C energy, from 1.6 times the expected CF value at 67 MeV to 0.6 times the CF value at 97 MeV (Fig. 2.1); the angular distributions are characterized by a maximum at about 17° (laboratory) at energies well above the Coulomb barrier (Fig. 2.2). The cross sections for the ^{239}Pu(^{12}C,$\alpha 2n$ and $\alpha 3n$) reactions are much larger than those of the ^{239}Pu(^{12}C,$2n$ to $4n$) reactions, indicating that noncompound processes are involved in the production of the californium nuclides, since evaporation of charged particles is negligible in such heavy nuclei.

All of these results for the (C,αxn) reactions are consistent with models of transfer reactions in which an aggregate is transferred from the projectile to the target nucleus, followed by evaporation of neutrons from the resulting heavy nucleus. Figure 2.3 shows the recoil data for the Pu(C,αxn) reactions, compared with calculated curves obtained with two different models of the transfer process. The recoil energies, E_R, were derived from the $\bar{R}$ values of Fig. 2.1 with the aid of Steward's range-energy values.[3] The average angle θ_R associated with the trajectories of the recoil nuclei was evaluated in two different ways: the filled circles show the centroids, and the filled triangles, the maximum values, of the angular distributions.

Part *a* of Fig. 2.3 shows calculated values of E_R and θ_R obtained with a model first proposed by Strudler et al.[5] The model deals with the reaction ^{239}Pu(^{12}C,X)R in which an aggregate ^{12}C-X is transferred from projectile to target. In the model, the residual nucleus R receives a velocity in the forward direction as a result of this transfer process; an additional velocity is then imparted to R by Coulombic scattering between R and the remaining light nucleus X (in the figure, the calculated curves are for reactions in which particle X is either ^{3}He, ^{4}He, or ^{5}He). Figure 3(*b*) shows curves calculated with the model of Galin et al.,[6] in which the trajectories of the incoming and outgoing particles are determined by Rutherford scattering, with the additional requirement that

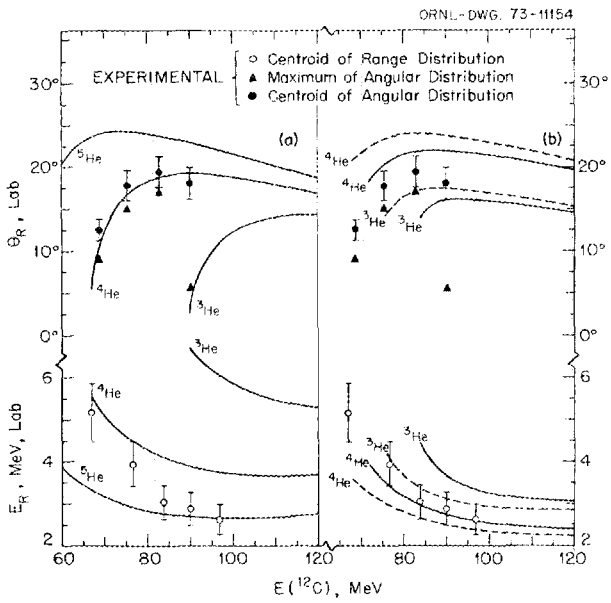

Fig. 2.3. Results derived from the range and angular distributions measured for ^{245}Cf and ^{244}Cf (from ^{239}Pu + ^{12}C), compared with calculations based on two different kinematic models. The experimental recoil energies E_R were obtained from the range values of Fig. 2.1 and Steward's range-energy values (ref. 3). Lab angles θ_R were obtained from the distributions of Fig. 2.2. The circles represent the centroids and the triangles, the maxima, of the angular distributions. Part *a* shows calculations with the model of Strudler et al. (ref. 5), and *b*, with the model of Galin et al. (ref. 6). The curves are identified by the helium nuclide remaining after the transfer. In part *b*, the dashed curves are for the cases where sufficient excitation energy remains in the respective intermediate nucleus to evaporate neutrons and reach ^{245}Cf; the solid curves, to reach ^{244}Cf.

sufficient energy remains in the heavy product of the transfer to evaporate neutrons and reach either ^{245}Cf (dashed curves) or ^{244}Cf (solid curves). Although the details of the models presented in Figs. 3*a* and *b* are not the same, their predictions for E_R and θ_R are similar. Clearly, Coulombic interactions are important in such transfer reactions. The calculations also indicate that a beryllium aggregate is probably transferred from ^{12}C to the target.

Investigations such as these can also have application to experimental searches for new isotopes and elements: knowledge of differences in the yields of compound-nucleus and transfer reactions can be very important in optimizing the conditions of such experiments.

An interesting by-product of such recoil studies is that range and angular distributions can be used as aids in identifying new isotopes by distinguishing between compound-nucleus and transfer reactions. Such arguments have been put forth as support (e.g., ref. 7) for discovery claims of elements 104 and 105. The present data and calculations indicate that the products of transfer reactions, although not very far removed from the compound nucleus (californium rather than fermium), can still be distinguished from compound-nucleus products. However, there are some intervals of bombarding energy where the recoil properties of both the transfer and complete-fusion reactions are rather similar, so that one must choose the experimental conditions carefully if recoil energies or angles are to be used to characterize new isotopes.

---

1. Expanded abstract of paper submitted to the *Physical Review*.
2. Physics Division.
3. P. G. Steward, University of California report, UCRL-18127 (1968).
4. L. C. Northcliffe and R. F. Schilling, *Nucl. Data, Sect. A* **7**, 233 (1970).
5. P. M. Strudler, I. L. Preiss, and R. Wolfgang, *Phys. Rev.* **154**, 1126 (1967).
6. J. Galin et al., *Phys. Rev.* **182**, 1267 (1969).
7. G. N. Flerov et al., *Nucl. Phys. A* **160**, 181 (1971).

REACTIONS OF HEAVY ELEMENTS WITH VERY HEAVY IONS

R. L. Hahn Y. LeBeyec[1]
H. Gauvin[1] M. Lefort[1]

To begin some studies of the interactions of very heavy ions with heavy-element nuclei, preliminary irradiations of ^{209}Bi and ^{248}Cm (borrowed from the Transuranium Research Laboratory at ORNL) were done at the accelerator ALICE in Orsay. The ^{209}Bi was bombarded with ^{40}Ar at several different energies, and the ^{248}Cm, by 280-MeV ^{40}Ar and 520-MeV ^{84}Kr. Radioactive products of these nuclear reactions were collected by a gas-jet system[2] and transported about 2 m through a capillary tube for assay with an annular Si(Au) detector. The growth of alpha radioactivity during the irradiations was measured. Delayed fission activities were also sought.

Typical beam intensities (electrical units) were about 100 nA for $^{40}Ar^{13+}$ and about 0.5 nA for $^{84}Kr^{25+}$. Only alpha-active products ascribable to incomplete-fusion reactions were detected; no delayed fissions were seen. For ^{209}Bi, transfer reactions leading to nuclei with $Z \leqslant 90$, (i.e., transfers of less than about seven protons) were much more probable than reactions leading to nuclides in the vicinity of compound nucleus ^{249}Md. For ^{248}Cm, most of the products were

apparently associated with nuclides lighter than the target nucleus. Conservative upper limits of about 0.8 μb for argon and about 0.3 mb for krypton were estimated for the complete-fusion cross sections that would lead to $^{288}114$ and $^{332}132$.

1. Institut de Physique Nucléaire, Orsay, France.
2. Y. LeBeyec, M. Lefort, and M. Sarda, *Nucl. Phys. A* **192**, 405 (1972).

ANALYSES OF NEUTRON-INDUCED FISSION CROSS SECTIONS FOR ^{249}Cf[1]

C. E. Bemis, Jr. N. W. Hill[4]
J. W. T. Dabbs[2] M. S. Moore[5]
G. D. James[3] A. N. Ellis[5]

The analysis of measurements of the neutron-induced fission cross sections for ^{249}Cf in the energy range 0.3 eV to 2 MeV has been completed. These measurements were made using ORELA as a pulsed neutron source and have been reported previously.[6] Eleven resonances below the approximately 20-eV cutoff of the Physics-8 underground nuclear explosion data of Silbert[7] have been found. A multilevel analysis of the data up to 70 eV was performed and, for the energy interval 20 eV to 70 eV, is in substantial agreement with Silbert.[7] The results for the resonances below 20 eV are listed in Table 2.1.

A direct integration of our results has also yielded the standard fission resonance integral, R.I.:

$$\text{R.I.} = \int_{0.55\ \text{eV}}^{2\ \text{MeV}} \sigma_f \, dE/E = 1630\ \text{b},$$

Table 2.1. Summary of ^{249}Cf resonances below 20 eV

Γ_γ = 40 meV assumed

E_0 (eV)	Γ_n^0 (meV)	Γ_f (meV)
0.708	0.741	119.6
3.90	0.115	44.9
5.08	0.268	154.3
7.52	0.063	83.4
8.66	0.115	146.0
9.52	0.362	97.1
10.35	0.078	252.2
11.90	0.037	242.4
13.63	0.403	205.1
16.06	0.159	325.4
16.82	0.420	162.9

which may be compared with the earlier value of 2940 ± 280 b by Halperin, Oliver, and Stoughton.[8]

The presence of the large fission resonance at 0.708 eV and the assumption of a 1/v cross section in this energy region in the cadmium-shielded determination by Halperin et al. would presumably account for the large discrepancy in the fission resonance integral. This work is being prepared for publication.

1. A similar report has appeared in *Phys. Div. Annu. Progr. Rep. Dec. 31, 1973,* ORNL-4937, p. 181.
2. Physics Division.
3. Present address: AERE, Harwell, England.
4. Instrumentation and Controls Division.
5. Los Alamos Scientific Laboratory, Los Alamos, N.M.
6. C. E. Bemis, Jr., J. W. T. Dabbs, N. W. Hill, M. S. Moore, and A. N. Ellis, *Chem. Div. Annu. Progr. Rep. May 20, 1972,* ORNL-4791, p. 27.
7. M. G. Silbert, *Nucl. Sci. Eng.* **51**, 376 (1973).
8. J. Halperin, J. H. Oliver, and R. W. Stoughton, *Chem. Div. Annu. Progr. Rep. May 20, 1970,* ORNL-4581, p. 37.

COMPARATIVE SOLUTION CHEMISTRY, IONIC RADIUS, AND SINGLE-ION HYDRATION ENERGY OF NOBELIUM[1]

R. J. Silva O. L. Keller, Jr.
W. J. McDowell[2] J. R. Tarrant

We are currently examining the chemistry of the elements at the end of the actinide series with the intent of continuing to the transactinides. This area of the periodic table is particularly interesting in that the heaviest actinides have a far greater tendency than expected to assume positive oxidation states lower than III. In fact, nobelium, element 102, is the only one of the 28 rare earths (actinide and lanthanide) to be most stable in the positive oxidation state of II in acid aqueous solution. This added stability is undoubtedly connected with the $5f^{14}$ filled shell predicted by the actinide concept for the next to the last member of the series in the divalent state. But that this is not the whole story is shown by the fact that the lanthanide analog of nobelium, ytterbium, is most stable in the trivalent state and forms only a somewhat stable divalent state. The correlation technique of Nugent, Baybarz, Burnett, and Ryan[3] allows an understanding of the (II-III) redox behavior of the actinides and the lanthanides in terms of the electrostatic and spin-orbit interaction energies of their *f*-orbital configuration as developed by Griffith,[4] Jørgensen,[5] and Vander Sluis and Nugent.[6] The purpose of our work is to establish the descriptive chemistry of nobelium by comparing its behavior with other divalent elements and to take the first steps in developing an understanding of nobelium's

behavior in terms of ionic radius and thermodynamic quantities.

Nobelium-255 ($T_{1/2}$ = 223 sec) was produced at the ORIC cyclotron at the rate of about 500 atoms per bombardment using a ^{249}Cf target and a ^{12}C beam in (^{12}C,$\alpha 2n$) reaction. Nobelium was first placed in general perspective by comparing its chloride-complexing ability with the divalent ions Hg^{2+}, Cd^{2+}, Cu^{2+}, Co^{2+}, and the alkaline earths. The extraction behavior of No^{2+} from aqueous HCl (0.2 to 10 *M*) into tri-*n*-octylamine in toluene showed that it is relatively noncomplexing, like an alkaline earth. Further experiments with the Dowex 50–4 *M* HCl and di(2-ethylhexyl)phosphoric acid (HDEHP)–0.025 *M* HCl systems showed that No^{2+} is similar in behavior to the alkaline earths Ca^{2+} and Sr^{2+} (Fig. 2.4). This was further confirmed by extraction of No^{2+} from dilute nitric acid into HDEHP in *n*-octane.

Since the logarithms of the distribution coefficients in both the ion exchange and solvent extraction experiments are found to be linear in ionic radius for the alkaline earths, an experimental value of the ionic radius of No^{2+} could be obtained (1.0 to 1.1 Å). Furthermore, by the use of relativistic Hartree-Fock-Slater calculations, a theoretical correlation between the ionic radius of No^{2+} and the alkaline earths was obtained. This theoretical value was found to be

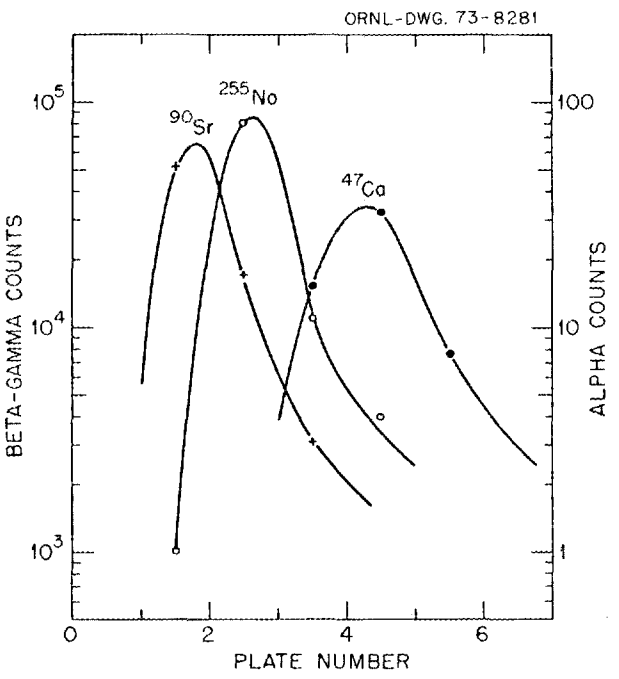

Fig. 2.4. Elution with 0.025 *M* HCl of No^{2+} relative to Ca^{2+} and Sr^{2+} from a column using di(2-ethylhexyl)phosphoric acid on an inert support.

1.1 Å, in good agreement with the experimental value. The six-coordinate ionic radius of Yb^{2+}, the lanthanide analog of No^{2+}, is 1.03 Å as found by Beck and Bärnighausen.[7] The $5f^{14}$ electronic shell must shield the $6p$ outer shell of No^{2+} in much the same way as the $4f^{14}$ shell shields the $5p$ outer shell of Yb^{2+} since the contraction from Ba^{2+} to Yb^{2+} is nearly the same as the contraction from Ra^{2+} to No^{2+}.

A modified form of the Born equation was used to calculate the single-ion heat of hydration of No^{2+} as −355 kcal/g-atom, compared with −373 for Ca^{2+}.

1. To be published in *Inorganic Chemistry*.
2. Chemical Technology Division.
3. L. J. Nugent, R. D. Baybarz, J. L. Burnett, and J. L. Ryan, *J. Phys. Chem.* 77, 1528 (1973).
4. J. S. Griffith, *The Theory of Transition Metal Ions*, Cambridge University Press, Cambridge, England, 1961, pp. 99–101.
5. C. K. Jørgensen, *Mol. Phys.* 5, 271 (1962).
6. K. L. Vander Sluis and L. J. Nugent, *Phys. Rev. A* 6, 86 (1972).
7. H. P. Beck and H. Bärnighausen, *Z. anorg. allg. Chem.* 386, 221 (1971).

DECAY PROPERTIES AND X-RAY IDENTIFICATION OF ^{257}104[1]

C. E. Bemis, Jr. J. R. Tarrant
R. J. Silva L. D. Hunt
D. C. Hensley[2] P. F. Dittner
O. L. Keller, Jr. R. L. Hahn
C. D. Goodman[2]

A preliminary evaluation of our experiments on the x-ray identification of element 104, was reported last year,[3] and the completed identification studies were the subject of a formal publication.[4] The alpha-particle spectrum representing a portion of our data is shown in Fig. 2.5, and the alpha groups from the decay of ^{257}104 are indicated. The photon spectrum in coincidence with these ^{257}104 alpha particles is shown in Fig. 2.6. The observation of the *K*-series x-ray spectrum of element 102 in coincidence with alpha particles constitutes a conclusive identification of element 104.

In addition to the x-ray identification, described in ref. 4 and briefly above, other information about the decay properties of ^{257}104 was derived from our experiments. From the decay of alpha events in the energy range 8.50 to 9.20 MeV, a half-life value of 4.76 ± 0.28 sec was derived for ^{257}104. Our value supports the earlier value of 4.8 ± 0.5 sec of Ghiorso[5] and Ghiorso et al.[6] Our decay curve is shown in Fig. 2.7.

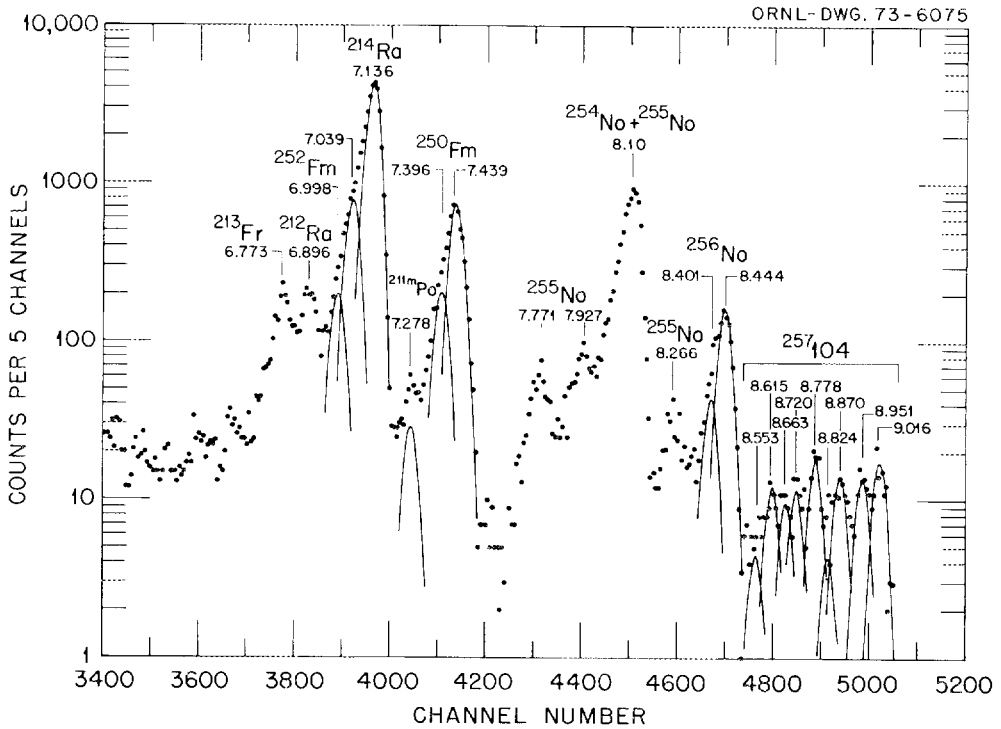

Fig. 2.5. **Alpha-particle energy spectrum for activities produced in the bombardment of ^{249}Cf with 73.0-MeV ^{12}C ions for a total of 31.3 pμA-hr.** Counting time is 11 sec, and the energy range expected for alpha events from the decay of ^{257}104 is indicated.

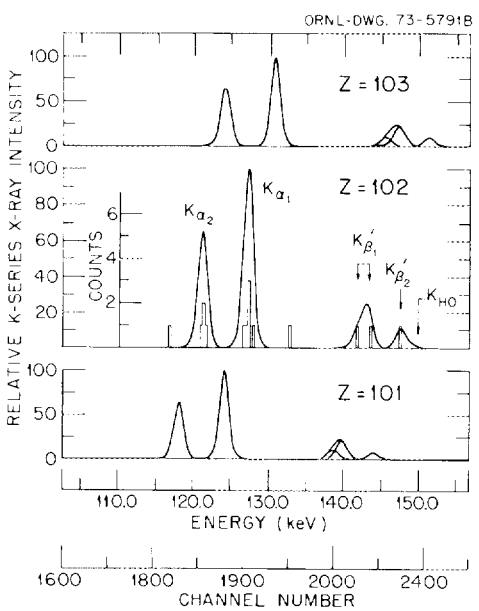

Fig. 2.6. **Characteristic K-series x-ray spectra expected for the elements with Z = 100 through Z = 103.** The experimental photon spectrum coincident with alpha particles in the energy range 8.5 to 9.1 MeV is shown in histogram fashion under the curve labeled Z = 102 and forms the basis of a conclusive identification of element 104.

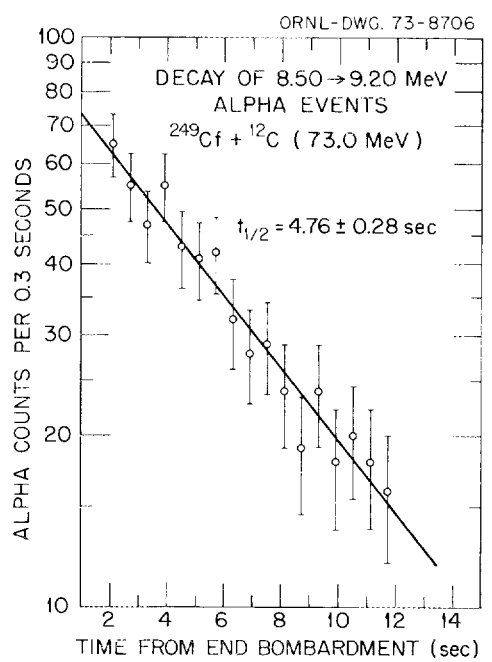

Fig. 2.7. **Decay curve for alpha events in the energy range 8.50 to 9.20 MeV and the derived half-life for ^{257}104.**

A decay scheme for $^{257}104$ based on alpha-particle energies and intensities, coincident gamma rays, and alpha–gamma-ray (x-ray) delayed coincidence information was also derived from our multiparameter data. This decay scheme is shown in Fig. 2.8 and includes an 18% electron-capture decay branch to 0.6-sec ^{257}Lr which was derived from the presence of the 8.870- and 8.824-MeV alpha groups in equilibrium decay with the alpha groups of $^{257}104$.

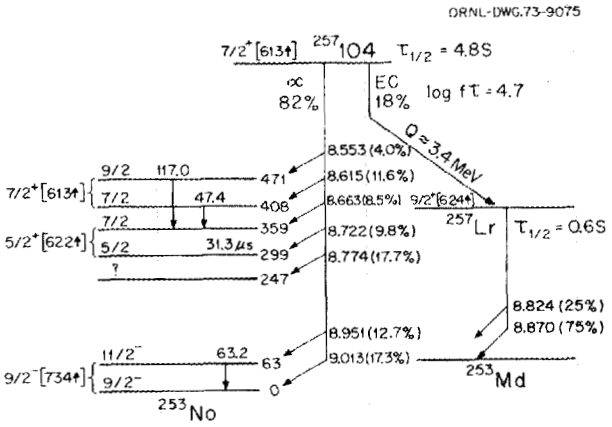

Fig. 2.8. Decay scheme for $^{257}104$ showing the level scheme for ^{253}No and the 18% electron-capture branching decay of $^{257}104$.

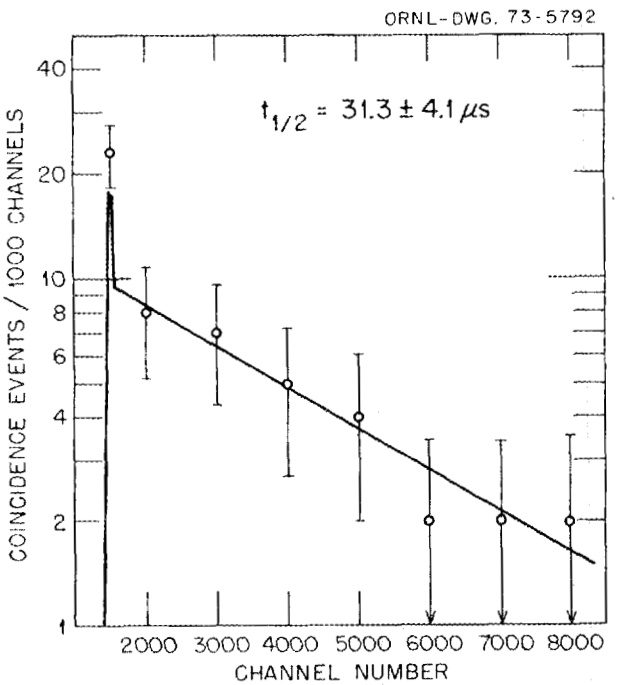

Fig. 2.9. Delayed alpha–x-ray coincidence curve for the approximately 300-keV state in ^{253}No.

An analysis of our alpha–x-ray delayed coincidence data, shown in Fig. 2.9, has led to the determination of the half-life of the approximately 300-keV state in ^{253}No. This half-life, 31.3 ± 4.1 μsec, is in accord with the state assignment of $5/2^+[622\uparrow]$. The $M2$ transition to the ^{253}No ground state, $5/2^+[622\uparrow] \rightarrow 9/2^-[734\uparrow]$, is similar to the other cases of $M2$ isomerism in the $N = 151$ nuclides previously discussed.[7] Our state assignment of $7/2^+[613\uparrow]$ for the ground state of $^{257}104$ is unlike that for the other $N = 153$ nuclides ($1/2^+[620\uparrow]$) and was deduced from the alpha-decay intensity pattern and the log ft value for the electron-capture decay. Our results are being prepared for publication.

1. A report dealing with this subject has also appeared in the *Phys. Div. Annu. Progr. Rep. Dec. 31, 1973,* ORNL-4937, p. 47.
2. Physics Division.
3. C. E. Bemis, Jr., R. J. Silva, D. C. Hensley, O. L. Keller, J. R. Tarrant, L. D. Hunt, P. F. Dittner, and R. L. Hahn, *Chem. Div. Annu. Progr. Rep. May 20, 1973,* ORNL-4891, p. 29.
4. C. E. Bemis, Jr., R. J. Silva, D. C. Hensley, O. L. Keller, Jr., J. R. Tarrant, L. D. Hunt, P. F. Dittner, R. L. Hahn, and C. D. Goodman, *Phys. Rev. Lett.* **31**, 647 (1973).
5. A. Ghiorso, "The Berkeley HILAC Heaviest Element Research Program," p. 107 in *Proceedings of Robert A. Welch Foundation Conference on Chemical Research XIII. The Transuranium Elements – The Mendeleev Centennial,* W. O. Milligan, ed., Houston, Tex., 1970.
6. A. Ghiorso et al., *Nature* (London) **229**, 603 (1971).
7. C. E. Bemis, Jr., P. F. Dittner, C. D. Goodman, D. C. Hensley, K. Kumar, and R. J. Silva, *Chem. Div. Annu. Progr. Rep. May 20, 1971,* ORNL-4706, p. 64.

PROPERTIES OF ^{259}Rf

P. F. Dittner — F. Plasil[1]
C. E. Bemis, Jr. — F. Pleasonton[1]
R. L. Ferguson — D. C. Hensley[1]

As part of our continuing study of the identification and properties of transfermium elements, we carried out an experiment to observe the decay of approximately 3-sec ^{259}Rf. We produced ^{259}Rf in the ^{249}Cf(^{13}C,3n) reaction using 86.5-MeV $^{13}C^{4+}$ ions accelerated in the Oak Ridge Isochronous Cyclotron (ORIC). The $^{13}C^{4+}$ ion beam was modulated at 1 kHz with a 50% duty cycle by passing the beam between a pair of 1-m-long parallel deflection plates driven by a 6-kV square-wave modulated supply. After an energy loss of about 15 MeV in the beryllium target chamber window and target backing, the ^{13}C ions had an energy optimized for the ^{249}Cf(^{13}C,3n) reaction. Our measured production cross section for ^{259}Rf was about 6×10^{-33} cm^2. The reaction products recoiling out of the

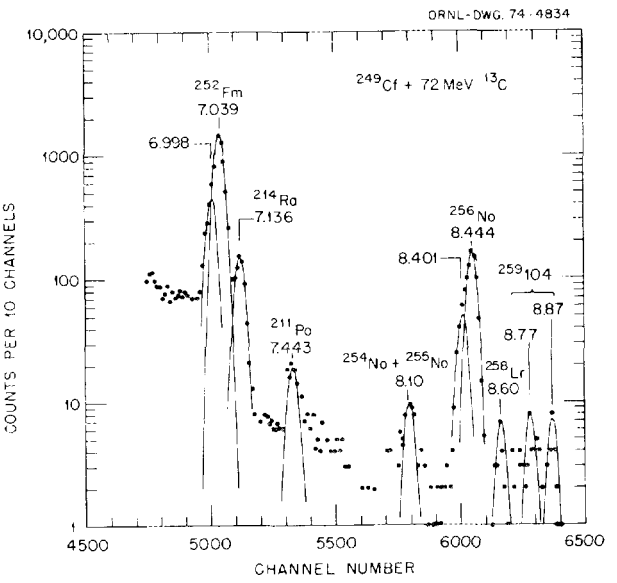

Fig. 2.10. Alpha energy spectrum resulting from the decay of nuclides produced in the interactions of approximately 72-MeV ^{13}C with ^{249}Cf.

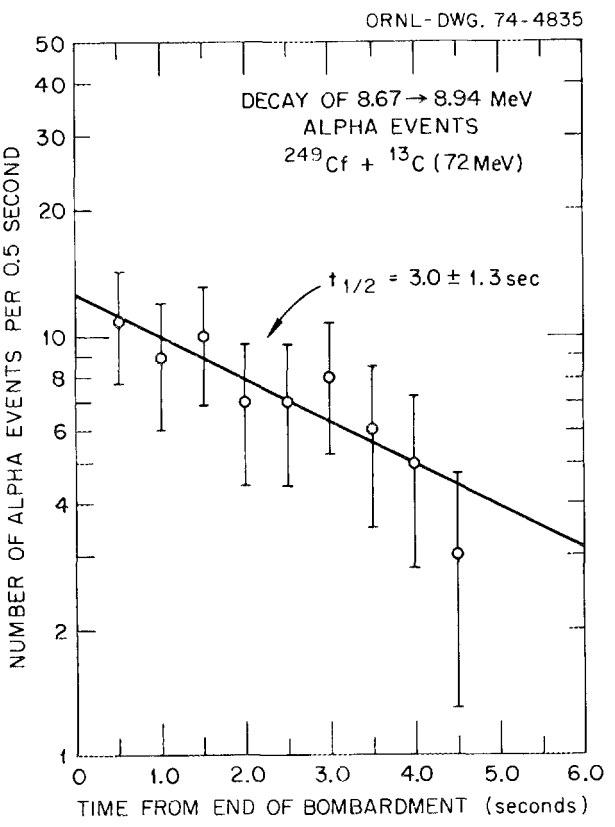

Fig. 2.11. Time dependence of the alpha events in the energy range containing the two peaks of ^{259}Rf.

^{249}Cf target were thermalized in helium gas and pumped through a small orifice into an evacuated (0.04 torr) chamber. The gas stream containing the reaction products then impinged on an aluminum wheel located about 5 mm from the orifice. The wheel was periodically (about 6 sec) rotated through about 100° so that the spot of collected activity faced the first, and on the next rotation a second, Si(Au) surface-barrier alpha and fission detector. Each detector responded to alpha or fission events with the same geometry, and thus the spontaneous-fission to alpha-decay ratio was determined directly.

Our electronics allowed us to measure the energy of the emitted alpha particles and fission fragments and the time from the end of the irradiation associated with each event. The output from the detectors was stored and analyzed in the 50% of the time during which the beam did not strike our target, that is, when the deflecting plates were energized. During about 24,000 irradiation-counting cycles, we observed 68 alpha events and 13 spontaneous fission events. Two prominent alpha groups roughly equal in intensity were seen at 8.87 and 8.77 MeV (see Fig. 2.10), in agreement with the previous measurement of Ghiorso.[2] The alpha events having energies above 8.67 MeV and below 8.94 MeV decay with a half-life of 3.0 ± 1.3 sec (see Fig. 2.11). The fission events decayed with a half-life compatible with that derived from the alpha-decay data.

The spontaneous-fission branching, based on rather poor statistics and a significant correction due to the fission events coming from the decay of ^{256}No, was determined to be 10 ± 7%. The nuclide ^{256}No ($t_{1/2}$ = 3.04 ± 0.15 sec) is also produced in the bombardment of ^{249}Cf with ^{13}C ions via the ^{249}Cf(^{13}C,$\alpha 2n$) reaction with a production cross section of about 1 × 10^{-31} cm^2 as determined from our data.

1. Physics Division.

2. A. Ghiorso, "The Berkeley HILAC Heaviest Element Research Program," p. 107 in *Proceedings of the Robert A. Welch Foundation Conference on Chemical Research. XIII. The Transuranium Elements – The Mendeleev Centennial,*" W. O. Milligan, ed., Houston, Tex., 1970.

PREDICTED PROPERTIES OF SUPERHEAVY ELEMENT 115, EKABISMUTH[1]

O. L. Keller, Jr. C. W. Nestor, Jr.[2]
Burkhard Fricke[3]

It was thought that the reaction of an accelerated $^{76}_{32}$Ge beam with a $^{232}_{90}$Th target would be a favorable one for the production of a superheavy element.[4] The

recent attempt by the heavy-ion accelerator group at Dubna (U.S.S.R.) was unfortunately unsuccessful.[5] This suggests that the discovery of superheavy elements may be even more difficult than was previously supposed. Chemical separations methods, which offer high selectivity and sensitivity, may therefore once again hold the key to discovery, as they did for fission.[6] For this reason we have predicted the chemical properties of elements 111, 113, and 114[7,8] as a guide for the experimenter in these very difficult investigations. We have now predicted the properties of element 115, ekabismuth.

Element 115 is a particularly interesting case since its properties will be strongly and unmistakably altered by relativistic effects. No element like 115 is known at present; so we have taken an approach involving careful comparisons within the periodic table and analogies based on relativistic Hartree-Fock and relativistic Hartree-Fock-Slater calculations. We first calculated electronic energy levels, ionization potentials, promotion energies to excited states, and atomic and ionic radii. Further properties were estimated by combining these calculated properties with valence-bond theory or other general theories and by extrapolations in the periodic system.

Element 115 is expected to be in group V-A of the periodic table and have most stable (positive) oxidation states of I and III. The oxidation state I, which plays a minor role in bismuth chemistry, should be a major factor in element 115 chemistry. This change will arise because of the large relativistic splitting of the spherically symmetric $7p_{1/2}$ shell from the $7p_{3/2}$ shell. Element 115 will therefore have a single $7p_{3/2}$ electron outside a $7p^2_{1/2}$ closed shell. The magnitudes of the first ionization energy and ionic radius suggest a chemistry similar to Tl^+. Similar considerations suggest that 115^{3+} will have a chemistry similar to Bi^{3+}. Hydrolysis will therefore be easy, and relatively strongly complexing anions of strong acids will be needed in general to effect studies of complexation chemistry. Some other predicted properties of element 115 are given in Table 2.2 and Fig. 2.12.

1. Submitted to *J. Phys. Chem.*
2. Mathematics Division.
3. Gesellschaft für Schwerionenforschung, Darmstadt, BRD/Germany.
4. W. J. Swiatecki and C. F. Tsang, "Possible Heavy-Ion Reactions Leading to Superheavy Nucleus Formation," *Nucl. Chem. Annu. Rep.*, LBL-666 Lawrence Berkeley Laboratory (1971).
5. Yu. Ts. Oganessian, "Synthesis of Superheavy Elements," *Proceedings of International Conference on Nuclear Physics, Munich, Aug. 27–Sept. 1, 1973.*
6. O. R. Frisch and J. A. Wheeler, *Phys. Today* **20**(11), 43 (1967).

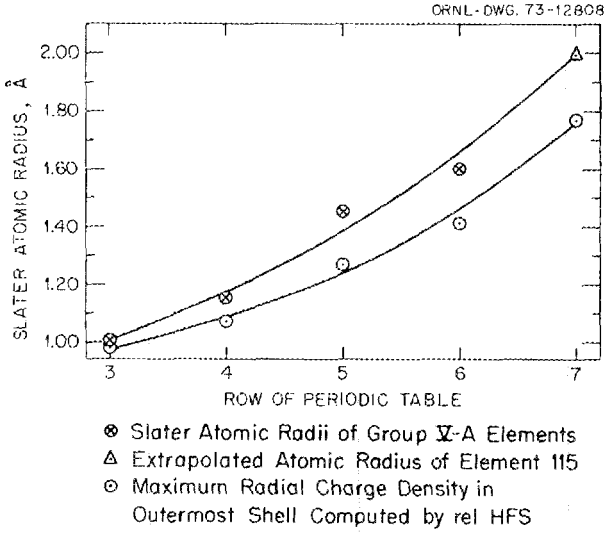

Fig. 2.12. Atomic radius of element 115, ekabismuth.

Table 2.2. Predicted properties of element 115

Ionization potential, eV	
I	5.2
II	18.1
III	27.4
IV	48.5
$0 \rightarrow 5^+$	159
Heat of sublimation, kcal/g-atom	34
Atomic radius, Å	2.0
Ionic radius, Å	
115^+	1.5
115^{3+}	1.0
Entropy, cal deg^{-1} $(g\text{-atom})^{-1}$ (at 25°)	16
Standard electrode potential ($115^+/115$), V	−1.5
Melting and boiling points	Similar to element 113

7. O. L. Keller, J. L. Burnett, T. A. Carlson, and C. W. Nestor, Jr., *J. Phys. Chem.* **74**, 1127 (1970).
8. O. L. Keller, Jr., C. W. Nestor, Jr., T. A. Carlson, and Burkhard Fricke, *J. Phys. Chem.* **77**, 1806 (1973).

SEARCH FOR SUPERHEAVY ELEMENTS IN LEAD IRRADIATED AT SLAC[1]

J. Malý[2] Dieter Waltz[1]
R. W. Stoughton Donald Busick[1]
J. Halperin

A sample of lead in which fission-fragment tracks were observed by the Lexan technique[3] before and especially after an intermediate-energy electron irradiation (250 to 1250 MeV) at Orsay was rolled into thin sheets about 0.3 mm thick. Forty-five 5 X 5 cm plates were cut from this sheet (about 366 g total) and sent to SLAC for irradiation by high-energy electrons. These were irradiated with about 4×10^{19} to 5×10^{19} electrons of 1.5 to 20 GeV over a several-month period. Before the irradiation, they were put into two assemblies, with the plates separated with aluminum spacers so that they could be water-cooled. After the irradiation the two assemblies (assembly I, which first "saw" the electrons, and assembly II, which was placed farther "downstream" in the irradiation path) were sent to ORNL for examination in our neutron multiplicity counter.[4]

Table 2.3 shows the results of our counts. We conclude there is no evidence for high multiplicities. The apparent decrease of the rates of the 3's and ≥4's with counting time is very likely not significant in view of the low number of counts and in view of the long time after irradiation compared with the relatively short times between counts. We do not understand the apparent excess of 2's and in some cases of 3's in the irradiated samples. Such an effect was observed in our previous ORELA irradiations, especially with gold-mercury targets.[5] In all cases the targets were radioactive. This fact may have caused some unknown electronic effects; however, the observed excess low multiplicities cannot be due to statistical pile-up of singles. Another possible contributing effect is the presence of aluminum spacers and steel bolts, which held the assemblies together; however, this effect is thought to be of insufficient magnitude to explain the results.

1. Stanford Linear Accelerator Center.
2. Institut de Physique Nucléaire, Orsay, France.
3. J. Malý, *Phys. Lett. B* **35**, 148 (1971).
4. R. L. Macklin et al., *Nucl. Instrum. Methods* **102**, 181 (1972).
5. J. Malý et al., *Chem. Div. Annu. Progr. Rep. May 20, 1973*, ORNL-4891, p. 30.

SEARCH FOR SUPERHEAVY ELEMENTS IN URANIUM TARGET FROM SLAC[1] AFTER PROCESSING

Dieter Waltz[1] Ruth Sjoblom[2]
Donald Busick[1] K. L. Wolf[2]
J. Halperin J. P. Unik[2]
R. W. Stoughton

Last year[3] we reported examining in our neutron multiplicity counter[4] a uranium sheet (5 X 10 X 0.1 cm) which had been irradiated at SLAC with about 4.7×10^{18} electrons of about 19 GeV. We saw no multiplicities which could not be attributed to spontaneous fission of the uranium itself. The uranium was then sent to ANL for determining the production of actinides in the irradiation. A fraction which should have contained essentially all elements except actinides was returned to ORNL for measuring neutron multiplicities. In a ten-day count and eight-day background

Table 2.3. Neutron multiplicities in lead irradiated at SLAC with 19-GeV electrons

Sample	Time after end of irradiation (days)	Time of count (days)	Observed count			Corrected count (day^{-1})		
			2's	3's	≥4's	2's	3's	≥4's
Assembly I	110	6.92	177	14	8	7.0	0.45	0.44
Assembly I	118	5.36	131	9	4	4.8	0.11	0.04
Assembly I	127	5.97	164	9	1	6.9	−0.06	−0.54
Assembly I, total count		18.25	472	32	13	6.3	0.18	0
200 g Pb (background)		7.01	137	11	5	19.6[a]	1.57[a]	0.71[a]
Assembly II	140	4.79	207	15	3	23.7	1.55	−0.08

[a]These are the corrections; the corrected counts would be zero.

count we observed 23.3 ± 2.3 and 3.8 ± 0.8 for 2's and 3's, respectively, with higher multiplicities showing zero within statistical error. Semiquantitative analyses indicated too little ^{238}U, ^{240}Pu, and ^{242}Pu to explain more than about half of the observed counts. Somewhat similar low multiplicities apparently were observed in lead irradiated by high-energy electrons.[5]

1. Stanford Linear Accelerator Center.
2. Argonne National Laboratory.
3. J. Halperin et al., *Chem. Div. Annu. Progr. Rep. May 20, 1973,* ORNL-4891, p. 30.
4. R. L. Macklin et al., *Nucl. Instrum. Methods* **102**, 181 (1972).
5. J. Malý et al., "Search for Superheavy Elements in Lead Irradiated at SLAC," the preceding contribution, this report.

SEARCH FOR SUPERHEAVY ELEMENTS IN THORIUM TARGET AT SUPER HILAC

R. W. Stoughton A. Ghiorso[1]
J. Halperin R. E. Eppley[1]
F. Plasil[2]

We irradiated a 1.25-in.-diam, 0.035-in.-thick thorium plate with 604-MeV Kr^{22+} ions at the Super HILAC for two 8-hr shifts. The thorium plate had been cleaned with an HNO_3-HF acid mixture, and the back of the plate had a 200-$\mu g/cm^2$ layer of gold sputtered onto it to improve thermal and electrical conductivities to the brass holder.[3] The plate was fastened securely to the holder with three screws. After the irradiation the plate was shipped to ORNL by plane and inserted into our neutron multiplicity counter[4] 13 hr after irradiation ceased. In 87 hr of counting, we observed no multiplicities of ≥3's and 35 total counts of 2's. Since these values are less than our average background, we conclude we have observed no evidence for superheavy elements.

Our irradiation involved about 0.021 C (about 5.7×10^{15}) Kr^{22+} ions. A simple calculation indicates a "Coulomb barrier" of about 405 MeV. Since we expect some 40 to 50 MeV more than this to be required for any significant barrier penetration, we calculated an upper limit to a reaction cross section based on the thickness of thorium to reduce the Kr^{22+} energy to about 450 MeV (about 12 mg/cm^2)[5] and on an optimum half-life (about one to three days). This calculation indicated an upper limit of about 10^{-2} nb for superheavy element formation.

A similar previous irradiation in a parasitic position also gave negative results; however, in that case the beam appeared to have been severely dissipated before it hit our target.

1. Lawrence Berkeley Laboratory.
2. Physics Division.
3. We thank R. E. Druschel for cleaning the thorium plate and L. D. Hulett of the Analytical Chemistry Division for covering one side with gold.
4. R. L. Macklin et al., *Nucl. Instrum. Methods* **102**, 181 (1972).
5. L. C. Northcliffe and R. F. Schilling, *Nucl. Data, Sect. A* **7**, 324 (1970).

ADDITIONAL NATURAL SAMPLES INVESTIGATED FOR NEUTRON EMISSION

R. W. Stoughton S. Fried[1]
J. Halperin G. J. Nihart[2]

As we obtain additional natural samples[3] which might contain elements 110 through about 124, we examine them for spontaneous multiple neutron events in our counter[4] as a possible indication of the presence of superheavy elements. Since element 114 (ekalead) is thought to be a likely candidate (if superheavy elements exist), we obtained about 1 kg each of matte, slag, and flue dust from a smelter of the St. Joseph Lead Co., Herculaneum, Missouri. We noted that some heavy elements tended to concentrate in the bones of ocean fish and water animals; accordingly, we counted a whale's tooth, some walrus ivory carvings, and some coral which were available. Some possible superheavy elements (if they exist) are postulated to be at least somewhat volatile: ekalead,[5] ekapolonium, ekaastatine, and ekaradon; hence we obtained about 13 kg of silica gel which had been used for sorbing and desorbing gases in air at a Union Carbide Corporation Linde Division plant in Kansas City. Because the unknown heavy "island of stability" may run into a "third rare-earth series," we obtained about 20 kg each of monazite sand from Australia, Malaysia, South Africa, and the State of Georgia.[6] The results of our multiplicity counts are shown in Table 2.4.

The first three samples obviously show negative results. Additional and more accurate corrections or chemical separations will have to be made in the case of the monazite sands before anything definitive can be reported. The biggest single correction is due to the uranium content: mainly spontaneous fission but also effects of cosmic-ray muons. The uranium content was determined by neutron activation in which delayed neutrons from ^{235}U fission were measured[7] and both the uranium and thorium were determined by counting gamma rays of members of their decay series.[8] Both methods are much more accurate than the 50% or so the differences might indicate. We attribute the large differences to our method of sampling, as the samples

Table 2.4. Neutron multiplicities in natural samples

Sample	Counting time (days)	Weight (kg)	Observed neutron multiplicities		Corrected neutron multiplicities (counts kg^{-1} day^{-1})	
			3's	≥4's	3's	≥4's
Matte, slag, flue dust (lead smelter)	6.1	3.0	4	0	−0.3	−0.2
Whale's tooth, ivory, coral	3.9	1.2	2	0	−0.5	0
Silica gel	16.5	13.0	7	2	−0.2	0
Monazite sand						
Australia	1.93	22.0	585	63	2.8[a] (−4.8)[b]	0.12[a] (−0.65)[b]
Malaysia	2.87	22.7	986	87	5.2[a] (−0.7)[b]	0.01[a] (−0.57)[b]
South Africa	2.07	20.4	292	40	−0.1[a] (−2.8)[b]	−0.04[a] (−0.30)[b]
Georgia	2.06	23.2	1083	85	5.9[a] (−7.0)[b]	−0.13[a] (−1.42)[b]

[a]Corrected for empty counter background and spontaneous fission of uranium and thorium present; not corrected for cosmic-ray muon effects on other elements present nor neutron absorption by the samples.

[b]Same corrections based on different uranium analyses.

were obviously not homogeneous. Without accurate uranium analyses, accurate corrections cannot be made. There seem to be more higher multiplicities (≥5's) than can be explained by the uranium present. Such multiplicities are seen, however, with large amounts of materials of high Z; our samples contained between 0.8 and 1.4 kg of thorium as well as high percentages of cerium rare earths. Two other effects which are difficult to estimate are neutron moderation and neutron absorption by the samples (the former would tend to increase and the latter to decrease the counting efficiency).

1. Argonne National Laboratory.
2. Linde Division, Union Carbide Corporation, Tonawanda, N.Y.
3. R. W. Stoughton et al., *Nature* (London), *Phys. Sci.* **246**, 26 (1973).
4. R. L. Macklin et al., *Nucl. Instrum. Methods* **102**, 181 (1972).
5. O. L. Keller et al., *J. Phys. Chem.* 74, 1127 (1970).
6. We thank Messrs. W. R. Fort of Kerr-McGee Chemical Corp., Oklahoma City, and Bruce Bennett of Kerr-McGee Chemical Corp., West Chicago, for sending us the four monazite samples.
7. Courtesy of J. F. Emery, ORNL Analytical Chemistry Division.
8. Courtesy of G. D. O'Kelley, J. S. Eldridge, and K. J. Northcutt, the latter two of the ORNL Analytical Chemistry Division.

RADIOHALOS

R. V. Gentry[1]

In some thin samples of certain minerals, such as mica, there can be observed tiny aureoles of discoloration which, on microscopic examination, prove to be concentric dark and light circles with diameters between about 10 and 40 μm and centered on a tiny inclusion. The origin of these halos was a mystery until the discovery of radioactivity and its powers of coloration; in 1907 it was suggested that the central inclusion was radioactive and that the alpha emissions from it produced the concentric shells of coloration (the circular patterns observed in cross section are, of course, simply plane sections through concentric spheres).

Aside from their interest as attractive mineralogical oddities, halos command attention because they are an integral record of radioactive decay in minerals that constitute the most ancient rocks. Most importantly, this thermal-resistant record is detailed enough to allow estimation of the decay energies involved and to identify the nuclides decaying through the energies and through genetic connections. As might be expected, halos are found with ring structure consistent with alpha decay of the uranium and thorium chains; somewhat unexpectedly, halos with ring structure

consistent with alpha decay of ^{218}Po, ^{214}Po, and ^{210}Po are also found. However, because of the rather short half-lives of the polonium isotopes involved in halo formation, it is important to establish the identity of polonium halos using analytical methods other than ring-structure analysis.

I estimate that the total number of uranium and thorium halos in crustal rocks with $\geqslant$3-μm-diam radiocenters exceeds those with 1 to 2 μm diameters by a factor of about 10^5. Between 10^{15} and 10^{20} uranium, thorium, and polonium radiohalos of the latter type (i.e., with pointlike radiocenters) are extant in Precambrian granites and pegmatites alone in the approximate ratio of U : Th : Po = 10^3 : 75 : 8×10^3.

Despite this availability of evidence (admittedly some polonium halo types are scarce), it is recognized that a general unfamiliarity of the scientific community both with polonium halos and the associated analytical techniques has perhaps made evaluation difficult. For example, Gentry[2] has reported that polonium halo radiocenters in biotite contain ten to several thousand times less uranium than do uranium halo radiocenters as deduced from (1) the absence of halo rings from ^{238}U-chain alpha emitters above ^{218}Po and (2) the absence or near absence of fossil (from ^{238}U spontaneous fission) and neutron-induced (from ^{235}U) fission tracks. Ordinarily the above results would have been considered confirmed by later ion-microprobe studies that showed this deficiency of uranium directly. However, the simultaneous observation that polonium halo radiocenters exhibited abnormally high mass 206/207 ratios (12 to 80) compared with the much lower ratios in uranium halo radiocenters[3,4] apparently changed the picture considerably. Although evidence in hand indicated the polonium halo radiocenter mass ratios were indeed lead isotope ratios resulting from polonium alpha decay to ^{206}Pb, such unusual lead isotope ratios had never been previously reported, and it was understandable that lead isotope geochronologists might view all ion-microprobe data on halos as suspect. It was imperative, therefore, to analyze uranium and polonium halo radiocenters with more familiar analytical methods. Therefore the widely accepted scanning electron microscope (SEM) x-ray fluorescence techniques were combined with halo ring structure and ion-microprobe analyses in directly confirming one of the most important differences between uranium and polonium halo types, namely, that lead exists without supporting uranium in polonium halo radiocenters.

Ordinarily halos are seen in thin section around individual pointlike radiocenters singly or randomly spaced in clusters or along conduits. Figure 2.13 shows, however, a spectacular arrangement of halo radiocenters in a Precambrian biotite (from Silver Crater mine, Faraday Township, Ontario) that is unlike any group of halo radiocenters previously observed. Identification of this halo assemblage as arising from ^{210}Po alpha decay was first made by the standard criterion of halo radius (r = 18.5 μm). It possesses a true halo characteristic: when cleaved, the noncentral section faithfully matched, minus the radiocenters themselves, the "spectacle" coloration pattern seen in Fig. 2.13. While other polonium halos exist in this biotite specimen, no other unusual structures were seen nearby. Fortunately this specimen was cleaved so that the radiocenters, which all lie in the same plane, were at exactly the right location for both ion-microprobe and SEM x-ray fluorescence investigation. Having a number of polonium halo radiocenters so closely spaced afforded opportunity to analyze several of these radiocenters with the ion microprobe and still have a representative group for future experiments of this type. No attempt is made to explain how this assemblage was formed.

Ion-microprobe analysis by J. A. McHugh, Knolls Atomic Power Laboratory, showed that the mass spectra of the radiocenters possessed prominent peaks at the 206, 207, 208, and 209 mass positions (lead and bismuth), which were absent in the spectra from the surrounding biotite. The ion-microprobe detection efficiency for uranium and thorium is equal to or greater than lead. In these polonium radiocenters, no significant ion signals were detected at the prominent uranium and thorium mass positions — 238 (U^+), 254 (UO^+), 232 (Th^+), and 248 (ThO^+). No mass 204 was detected above background (1 count/sec), and the

Fig. 2.13. Unusual assemblage of ^{210}Po halo radiocenters so closely spaced that the halo coloration patterns overlap, thus simulating the appearance of a pair of spectacles. Halo radius about 18.5 μm.

Y-123154
ORNL-DWG. 73-6399R

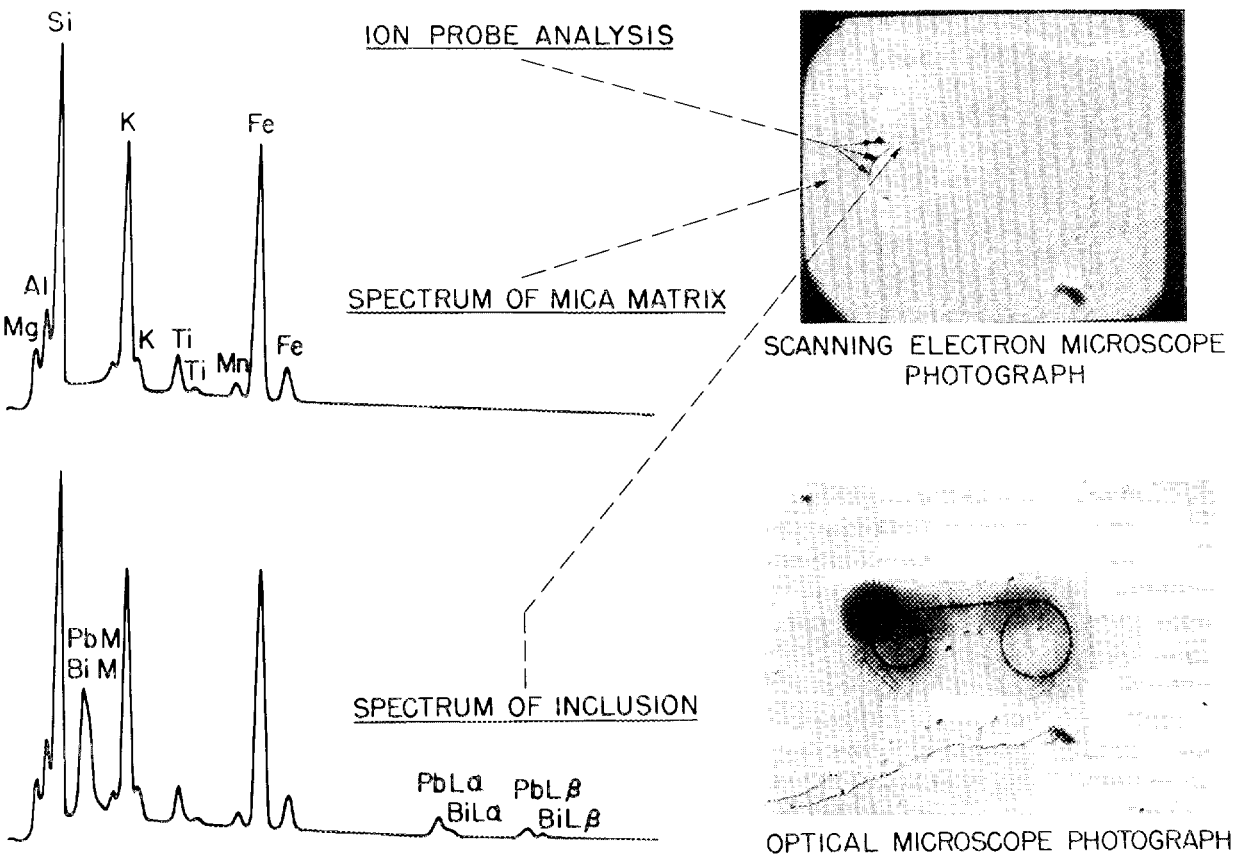

Fig. 2.14. SEM x-ray fluorescence spectra of mica matrix and polonium halo radiocenters.

206/207 ratio was about 20 (mass 206 signal about 2000 counts/sec). The above data were previously interpreted[3] as showing Pb/U and Pb/Th ratios greater than 4000 and a $^{206}Pb/^{207}Pb$ ratio of about 20, which, considering the absence of ^{204}Pb, uranium, and thorium, cannot be fitted into any known type of common, primordial, or uranium-derived (no uranium present!) radiogenic lead. The mass 209 signal was interpreted as ^{209}Bi.

SEM x-ray analysis by L. D. Hulett, Analytical Chemistry Division, confirmed the above interpretation. Figure 2.14 illustrates the SEM x-ray fluorescence spectrum of the surrounding biotite as contrasted with the x-ray spectrum of one of the polonium halo radiocenters in Fig. 2.13. The lead and to a lesser extent bismuth x-ray lines are the only elements detectable in this radiocenter that are not in the biotite. Later many of the other adjacent polonium halo radiocenters were analyzed by Gentry, and they all showed similar spectra. It is noted that the Pb/Bi ratio is variable in different radiocenters. At present it is not clear how, or in fact if, this or any assemblage of polonium halos can be explained by known physical and geological processes because of the short half-lives of the polonium isotopes responsible for the polonium halos.

Differentiation of uranium and polonium halos by SEM x-ray analysis is not limited to halos in biotite. Gentry[5] recently showed this technique is applicable for characterizing uranium and polonium halos in fluorite as well. A general review article describing all known types of radiohalos was also published.[6]

SEM x-ray techniques are also being combined with ion-microprobe studies of giant and dwarf halos. Preliminary results indicate the presence of yttrium in the

dwarf-halo radiocenter. Further, either the halo region itself or the radiocenter contains significant amounts of calcium, while potassium is depleted.

1. Visiting scientist from Columbia Union College, Takoma Park, Md.
2. R. V. Gentry, *Science* **160**, 1228 (1968).
3. R. V. Gentry, *Science* **173**, 727 (1971).
4. R. V. Gentry, S. S. Cristy, J. F. McLaughlin, and J. A. McHugh, *Nature* (London) **244**, 282 (1973).
5. R. V. Gentry, *Science* **184**, 62 (1974).
6. R. V. Gentry, *Annu. Rev. Nucl. Sci.* **23**, 347 (1973).

SYSTEMATICS IN THE RELATIVE ENERGIES OF SOME LOW-LYING ELECTRON CONFIGURATIONS IN THE GASEOUS ATOMS AND FREE IONS OF THE LANTHANIDE AND ACTINIDE SERIES[1]

K. L. Vander Sluis[2] L. J. Nugent

We observe a linear characteristic and a common nonlinear characteristic in the energy differences associated with many lanthanide and actinide electronic configurations involving a change in the number of f electrons by 1. The differences in energy, $\Delta_d E(q)$, between the lowest energy levels of the two principal electron configurations in the gaseous atoms of the lanthanide and actinide series exemplify these characteristics. By assuming that the common nonlinear characteristic involves only electrostatic and spin-orbit interaction energy differences between the parent f-electron core configurations, we obtain linearization functions — one for the lanthanide series and one for the actinide series — which linearize the $\Delta_d E(q)$ data. These same linearization functions are found to be applicable to the energy differences between most electronic configurations involving the same number of f electrons, including the neutral, the singly, the doubly, and the triply ionized gaseous lanthanides and actinides, independent of the nature or number of valence electrons.

1. Accepted for publication in *J. Opt. Soc. Amer.*
2. Thermonuclear Division.

IONIZATION ENERGIES OF DOUBLY AND TRIPLY IONIZED LANTHANIDES BY A LINEARIZATION TECHNIQUE[1]

K. L. Vander Sluis[2] L. J. Nugent

Linear intraseries correlations of the ionization energies I_3 and I_4 have been developed for the gaseous lanthanides. Good agreement was found between our results and previous results[3] for those cases where these ionization energies are more precisely known. For those cases where these ionization energies are less well known, we have interpolated more precise values. Our values for I_3 and I_4 in these cases are slightly smaller through the center of the series than the values of Sugar and Reader,[3] probably because of the different method chosen to interpolate the difference in term values between the $4f^q6s$ and $4f^q7s$ configurations.

1. Expanded abstract of published paper, *J. Chem. Phys.* **60**, 1927 (1974).
2. Thermonuclear Division.
3. J. Sugar and J. Reader, *J. Chem. Phys.* **59**, 2083 (1973).

ON THE ELECTRONIC CONFIGURATION IN THE GROUND STATE OF ATOMIC LAWRENCIUM[1]

L. J. Nugent Burkhard Fricke[3]
K. L. Vander Sluis[2] J. B. Mann[4]

Self-consistent relativistic Dirac-Hartree-Fock calculations have been made of some low-lying electronic energies for the atoms of all elements in ground-state ds^2 electron configurations. The results indicate that, contrary to some previous estimates, the ground electronic state of atomic lawrencium could be in either the $5f^{14}6d7s^2$ electron configuration or the $5f^{14}7p7s^2$ electron configuration. The separation between the lowest energy level of the $5f^{14}6d7s^2$ configuration and the lowest energy level of the $5f^{14}7p7s^2$ configuration is estimated to be $(0 \pm 3) \times 10^3$ cm^{-1} for atomic lawrencium.

1. Accepted for publication in *Phys. Rev.*
2. Thermonuclear Division.
3. Gesellschaft für Schwerionenforschung, Darmstadt, Germany.
4. Los Alamos Scientific Laboratory.

SPECTROSCOPY OF LANTHANIDE AND ACTINIDE (LANACT) COMPOUNDS AT ELEVATED TEMPERATURES[1]

J. P. Young[2] K. L. Vander Sluis[4]
J. R. Peterson[3] G. K. Werner[5]

There is a need for suitable techniques which would permit the spectral study of microgram samples of lanthanide and actinide (lanact) compounds at elevated temperature. Such spectral studies would be useful in establishing coordination number or oxidation state of these compounds as a function of temperature and would be a powerful allied tool to other high-temperature structure-determining techniques.

We have fabricated a platinum heating coil approximately 1.5 mm in diameter and 5 mm long from 3-mil platinum wire to be used in conjunction with a microscope-spectrophotometer system of local design. The heating coil is positioned between two facing objective lenses of horizontally inclined microscopes, mounted on an optical bench. The lanact compound, sealed in a silica capillary, is positioned within the coil. Both coil and capillary are independently movable by means of separate micromanipulators.

Light from a suitable source is concentrated by the first microscope and directed onto the sample. After passage through the sample, the light is viewed by the second microscope, which directs it to a Jarrell-Ash monochromator, model 82-020. The dispersed light is seen by a suitable detector and electronically amplified and recorded. We have demonstrated the applicability of this apparatus for spectral studies of microsamples held at temperatures up to 700°C. With the heater in place in the microspectrophotometer, no degradation of the optical quality of the instrument has been observed after repeated use of the heater at these temperatures, even though the heating coil is within several millimeters of the microscope lenses.

With this system we have obtained spectral data from an approximately 5-μg $CfBr_3$ sample at temperatures from ambient to about 700°C. The results verify the proposed thermal decomposition of $CfBr_3$ to $CfBr_2$.[6]

The Cf(II) is characterized by a strong absorption band near 500 nm, arising from an $f \rightarrow d$ transition.[7] As this peak grows in with increasing temperature, a corresponding reduction in the intensity of the $f \rightarrow f$ transition absorption bands of Cf(III) is observed. Of particular note is the fact that at temperatures as low as 150°C one clearly observes these changes, suggesting that Cf(III) is relatively unstable with respect to Cf(II) in a bromide matrix. Another interesting observation is the rapidity with which equilibrium is reached at each temperature, being essentially instantaneous with the application or removal of power to the heating coil.

1. Supported in part by AEC Contract AT-(40-1)-4447 with the University of Tennessee, Knoxville.
2. Analytical Chemistry Division.
3. Consultant, Department of Chemistry, University of Tennessee, Knoxville.
4. A member of the Physics Division when work was carried out; now with the Thermonuclear Division.
5. Physics Division.
6. J. R. Peterson and R. D. Baybarz, *Inorg. Nucl. Chem. Lett.* 8, 423 (1972).
7. L. J. Nugent, R. D. Baybarz, J. L. Burnett, and J. L. Ryan, *J. Phys. Chem.* 77, 1528 (1973).

THE URANIUM *M* X-RAY EMISSION SPECTRUM

O. Keski-Rahkonen[1] M. O. Krause

As part of a program aimed at determining the soft x-ray emission spectra of the actinides, the *M* x-ray lines of uranium were measured. Energies of *M* x rays have been determined previously for thorium, protactinium, uranium, and plutonium but not for the other elements of the actinide series; widths and intensities of *M* x-ray lines, on the other hand, have not been reported so far for any actinide. The *M* series is of interest in several ways: (1) for establishing a complete level diagram, it provides an important link between the lightly bound levels that are accessible to photoelectron spectrometric determinations and the tightly bound levels that are accessible to internal conversion measurements and interconnecting hard *K* and *L* series x rays; (2) besides the more energetic *K* and *L* x rays, *M* x rays provide a fingerprint in analytical applications; (3) lifetimes of inner-shell vacancies can be obtained from, and theoretical predictions of rates of inner atomic decay processes can be tested by, a measurement of the level widths and x-ray intensities; and (4) accurate knowledge of *M* x-ray energies and intensities of known elements provides a basis for reliably predicting properties of *M* x rays from superheavy elements.

We used the PAX technique (photoelectron spectrometry for analysis of x rays) to investigate the uranium *M* x rays. Although these x rays have energies between 2500 and 3500 eV that lie somewhat above the most useful range of the PAX technique, a more accurate energy determination could be made than previously possible, and data on line widths and line intensities could be obtained for the first time. The experimental setup and operational mode were the same as previously reported;[2,3] however, because of the higher energies of the x rays, other converter levels (such as argon 1*s* and sulfur 1*s* of H_2S) were used besides the neon 1*s* level. This afforded us an excellent effective resolution, since the photoelectrons could be analyzed at low kinetic energy. For example, the uranium $M\beta$ line, $h\nu = 3336.7$ eV, converted by the argon 1*s* level, $E_B = 3206.0$ eV, yields a photoelectron with $E_{kin} = 130.7$ eV, resulting in a negligible instrumental contribution, 0.2 eV with $\Delta E/E = 0.15\%$, to the line width.

Figure 2.15 shows the shape of the uranium $M\beta$ line as seen through the argon 1*s* (uranium $M\beta$) photoelectron line. As indicated by the inset of Fig. 2.15, the natural line width of uranium $M\beta$ is obtained directly from $\Gamma(U\ M\beta) \approx \Gamma(\text{measured}) - \Gamma(\text{Ar } 1s)$. Data on the other *M* lines are summarized in Table 2.5 and compared with theoretical predictions.[4]

Figure 2.16 shows a survey of the prominent M x rays, recorded with neon 1s as converter level. From this type of spectrum the relative intensities were deduced that are listed in Table 2.5. This table also compares experimental branching ratios with theoretical branching ratios;[5] satisfactory agreement is found.

Finally, energy values are tabulated in Table 2.5 and compared with the evaluation by Bearden.[6] While agreement between the two sets is good, the present results have a smaller uncertainty. The energies are referred to silver $L\beta_1$ = 3150.97(3) eV, which served as the calibration line. Since the only measurement needed for an energy determination is the energy difference (ΔE) between the calibration line ($h\nu_0$) and the line under study ($h\nu$), $h\nu = h\nu_0 + \Delta E$, the energy of the converter level need not be known.

A detailed final account of this study is in preparation, and a study of the M series of neptunium and curium is being planned. Other contributions on electron spectroscopy appear in Chap. 7 of this report.

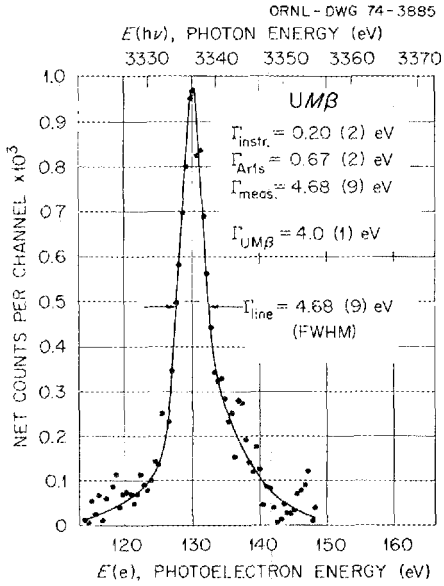

Fig. 2.15. The uranium $M\beta$ line recorded with a PAX spectrometer. Converter level is argon 1s. Observed line width is essentially the sum of the widths of the argon 1s level and the uranium $M\beta$ line.

1. Graduate student, Helsinki University of Technology, Otaniemi, Finland.
2. M. O. Krause, *Chem. Div. Annu. Progr. Rep. May 20, 1973*, ORNL-4891, p. 144.
3. M. O. Krause, *Advan. X-Ray Anal.* **16**, 74 (1972).
4. E. J. McGuire, "L- and M-Shell Yields and Electron

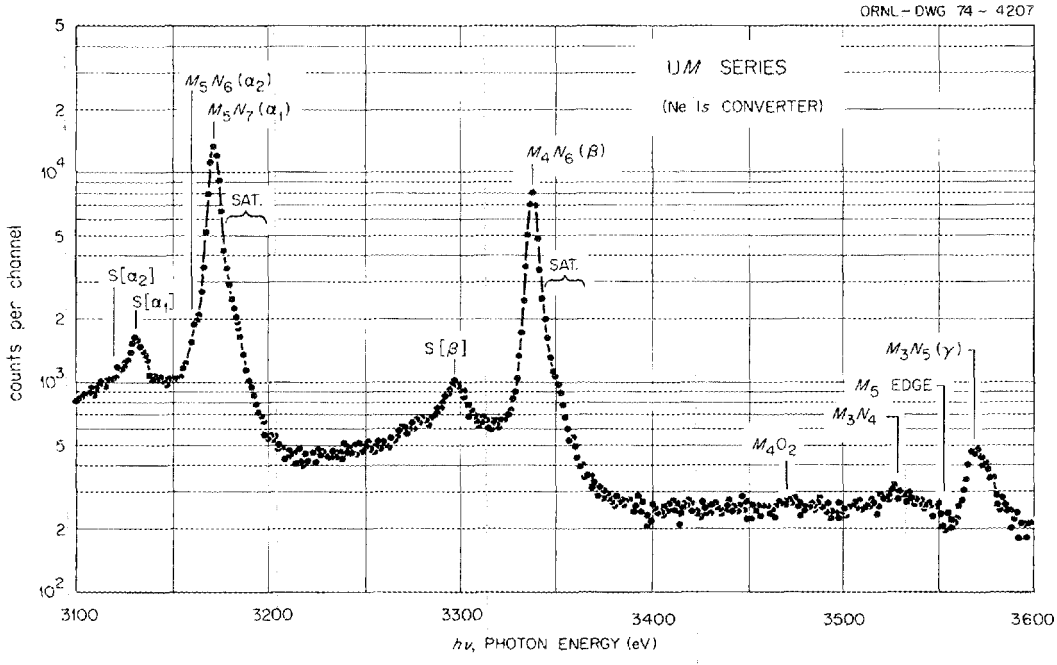

Fig. 2.16. Spectrum of prominent M x-ray emission lines of uranium. Lines designated by S are due to shakeoff and shakeup processes, a peculiarity of the converter in the PAX technique The broad multiple excitation satellite bands on the high-energy sides of uranium $M\alpha$ and β are denoted by SAT.

Table 2.5. Energies, widths, relative intensities, and branching ratios of uranium *M* x rays (preliminary analysis)

Line	Energy (eV)		FWHM (eV)		Relative intensity, expt.	Branching ratio	
	Expt.[a]	Bearden[b]	Expt.	Theory[c]		Expt.	Theory[d]
M_3N_4	3524(3)	3521(2)		16.8	1.1	29	13.3
$M_3N_5\gamma$	3563(1)	3563.7(1.0)	11(1)	16.8	3.8	100	100
$M_4N_2\zeta_2$	2455.8(4)	2455.1(1.0)	12.9(5)	11.9	2.3	4.1	4.56
$M_4N_6\beta$	3336.6(2)	3336.4(9)	4.0(1)	4.7	59	100	100
$M_5N_3\zeta_1$	2506.6(4)	2506.7(1.0)	11.7(5)	10.8	2.9	2.9	3.26
$M_5N_6\alpha_2$	3160.7(6)	3159.6(8)		4.5	4.6	4.6	5.12
$M_5N_7\alpha_1$	3171.3(1)	3170.9(8)	3.8(3)	4.5	100	100	100

[a]Silver $L\beta_1$ = 3150.97(3) eV.
[b]J. A. Bearden, *Rev. Mod. Phys.* 39, 78 (1967).
[c]E. J. McGuire, "*L*- and *M*-Shell Yields and Electron Spectra for the Transuranic Elements," USAEC CONF-720404-4 (1972).
[d]C. P. Bhalla, *J. Phys. B* 3, 916 (1970).

Spectra for the Transuranic Elements," USAEC CONF-720404-4 (1972).
5. C. P. Bhalla, *J. Phys. B* 3, 916 (1970).
6. J. A. Bearden, *Rev. Mod. Phys.* 39, 78 (1967).

NONAQUEOUS CHEMISTRY OF LANTHANIDES AND ACTINIDES

W. H. Baldwin C. E. Higgins[1]
J. H. Burns

Several more anhydrous lanthanide compounds, surrogates for actinide salts, have been prepared. Dehydration of rare-earth salt hydrates by heating at elevated temperatures has not always proven a satisfactory method for preparing the anhydrous salt; ligand exchange has been a more reliable method.[2] Anhydrous lanthanide, and especially actinide, compounds are desired in order to determine their chemical and physical properties, including structure, and make possible comparisons among and between such compounds of the lanthanide and actinide series.

$CeCl_2$(*d*-10-camphorsulfonate)·bis-dimethylformamide. Earlier work on the preparation of $CeCl_2(OAc)\cdot HOAc$,[3] where Ac stands for CH_3CO and HOAc is acetic acid, was used as the model for this reaction. Hydrated cerium chloride was heated with *d*-10-camphorsulfonic acid at 100°C under a pressure of 1 torr to displace HCl with a molecule of the sulfonic acid; water was replaced with dimethylformamide. Attempts are now being made to grow large single crystals of this compound that contains an asymmetric carbon atom.

Oxidation of Metal Ions with Ozone in Acetic Acid Solution. Uranous hydroxide, wet with water, was mixed with a solution of acetic acid and an excess (over that required for the reaction with water) of acetic anhydride. Ozone was bubbled through the mixture to produce a yellow solid $UO_2(CH_3COO)_2\cdot CH_3COOH$. The same compound was prepared from uranyl acetate dihydrate by reaction with a solution of acetic anhydride in acetic acid. Uranyl acetate·acetic acid is unstable in moist air, emitting quantities of acetic acid, whose odor can be detected. When the ozone treatment of uranous hydroxide was repeated with solutions that contained potassium ion or pyridine, the corresponding complexes $UO_2(OAc)_2\cdot KOAc$ and $UO_2(OAc)_2\cdot C_5H_5NHOAc$ were obtained.

$CeCl_3\cdot 2$(2-methoxyethanol). This compound resulted from the displacement of water from the heptahydrate by evaporation of a solution in 2-methoxyethanol at 60°C and 1 torr. This ligand (2-methoxyethanol) replaces water from the hydrate under conditions where neither ethanol nor isopropyl alcohol did. Therefore, it appears that 2-methoxyethanol must be acting as a bidentate ligand.

$Ce(OCH_2CH_2OCH_3)_3$. The above-mentioned solvated chloride [$CeCl_3\cdot 2$(2-methoxyethanol)] was reacted with $NaOCH_2CH_2OCH_3$ to prepare the substituted alkoxide, $Ce(OCH_2CH_2OCH_3)_3$; its properties are now being studied.

1. Now of the Analytical Chemistry Division.
2. C. E. Higgins and W. H. Baldwin, *Chem. Div. Annu. Progr. Rep. May 20, 1972*, ORNL-4791, p. 46.

3. C. E. Higgins and W. H. Baldwin, *Chem. Div. Annu. Progr. Rep. May 20, 1973*, ORNL-4891, p. 40.

CRYSTALLOGRAPHIC STUDIES WITH LANTHANIDE AND TRANSURANIC TRICYCLOPENTADIENIDES

J. H. Burns

All of the trivalent lanthanide and transuranic elements (studied for $Z \leqslant 98$) are known to form tricyclopentadienides.[1] These organometallic compounds crystallize in either of two modifications. For the lanthanides from lanthanum to terbium and for all the transuranides studied, the structure is orthorhombic with space group *Pbcm*. For smaller trivalent lanthanide ions a different orthorhombic structure is observed; it has space group symmetry $Pna2_1$. As prototypes of these two structures, crystals of $Pu(C_5H_5)_3$ and $Ho(C_5H_5)_3$ are under investigation by x-ray diffraction methods. Unit-cell dimensions for the two are as follows:

$Pu(C_5H_5)_3$ at 21.5°C	$Ho(C_5H_5)_3$ at 24°C
a = 14.183(4) Å	a = 19.30(2)Å
b = 17.593(3) Å	b = 13.96(2) Å
c = 9.726(3) Å	c = 8.74(1) Å

Intensity data have been collected and processed. Structure determinations are in progress by Patterson and Fourier methods but neither is completed yet. Although the crystal symmetries are different, the molecular structures appear quite similar and involve pentahapto bonding of some, if not all, the C_5H_5 rings to the metal atoms.

1. P. G. Laubereau and J. H. Burns, *Inorg. Chem.* 9, 1091 (1970); *Inorg. Nucl. Chem. Lett.* 6, 59 (1970).

AN NMR STUDY OF THE CONFIGURATION OF THE CYCLOHEXYL RING IN THE ADDUCT OF PRASEODYMIUM TRICYCLOPENTADIENIDE WITH CYCLOHEXYL ISONITRILE

B. M. Benjamin J. H. Burns
W. H. Baldwin

A determination[1] of the crystal structure of $Pr(C_5H_5)_3 \cdot CNC_6H_{11}$ showed the cyclohexyl isonitrile molecule to have the shape and thermal motions shown in Fig. 2.17. The cyclohexyl ring appears considerably flattened from its normal chair form, with two carbon atoms having especially large thermal amplitudes perpendicular to the ring. In addition to the possibility

ORNL-DWG 74-2718

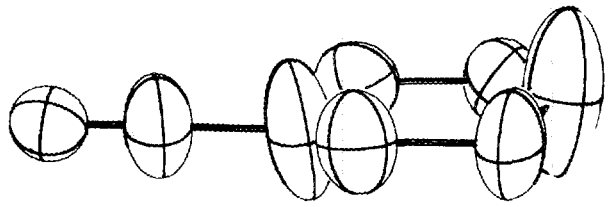

Fig. 2.17. The cyclohexyl isonitrile molecule as determined in the crystal structure of $Pr(C_5H_5)_3 \cdot CNC_6H_{11}$. Atoms are represented by thermal ellipsoids, and hydrogens are omitted.

that the ring is actually flattened in the solid, models involving dynamic inversion of the chair and static disorder of a mixture of two conformers were considered. We examined the compound by NMR in order to help distinguish between the first and the latter two possibilities.

In an earlier NMR study[2] of the proton chemical shifts of the complex in toluene-d_8, it was shown that the cyclohexyl ring undergoes rapid inversion at room temperature and slow inversion at lower temperatures; at −70°C, separate spectra were observed for the axial and equatorial conformers. The conformational free energy difference was 282 ± 15 cal/mole. No distortions of the chair were suggested.

Using high-resolution NMR spectroscopy, we measured the proton coupling constants to obtain more information about the cyclohexyl ring configuration. The proton chemical shifts of the complex dissolved in benzene-d_6 are approximately the same as those reported.[2] All axial proton signals and the equatorial-4 proton signal appeared as well-resolved multiplets with individual components having a half-width of about 2 Hz. Analysis of the spectra was aided by use of the double resonance method to effect spin decoupling. Experimental coupling constants are recorded in Table 2.6; these were confirmed by spectral simulation using the computer program LAOCN3.[3] Line-width studies showed that a small long-range coupling occurred between equatorial hydrogens, which therefore have the 1,4-W relationship.[4] Long-range coupling probably accounts for the lack of resolution of the 2- and 3-equatorial signals.

The magnitude of the coupling between adjacent axial and equatorial hydrogens, $J_{ae} \cong 3.5$ Hz, is the value expected[5–7] for hydrogens subtending an angle ϕ of 60°. For cyclohexyl rings held rigidly in the chair form, the coupling between adjacent equatorial hydrogens, J_{ee} for $\phi = 60°$, is also expected to be about 3.5 Hz; for adjacent axial hydrogen, J_{aa} for $\phi = 180°$, it is expected

to be 10 to 12 Hz. Measured values, $J_{a_4a_3}$ = 8.6 Hz and $J_{e_4e_3}$ = 7 Hz, indicate that the axial and equatorial hydrogens are exchanging positions and that their absolute values are averaged.

By assuming that J_{ee} for a rigid conformer is 3.5 Hz, as explained above, it was calculated that J_{aa} for the same is 12.1 Hz and that the equilibrium constant $K = N_a/(1 - N_a)$ is 0.686, which slightly favors the conformer with the equatorial isonitrile substituent. The corresponding $-\Delta G$ is about 230 cal/mole. We interpret these results to mean that the cyclohexyl moiety is not distorted from its normal chair configuration at the potential minimum of the inversion process in benzene solution at room temperature. These findings plus the previous low-temperature study favor the static disorder model for the C_6H_{11} rings in the crystal structure.

1. J. H. Burns, W. H. Baldwin, and P. G. Laubereau, *Chem. Div. Annu. Progr. Rep. May 20, 1973*, ORNL-4891, p. 42; Paper 14, American Crystallographic Association Meeting, Berkeley, Calif., Mar. 24, 1974.

Table 2.6. Coupling constants for the cyclohexyl protons in $Pr(C_5H_5)_3 \cdot CNC_6H_{11}$ in benzene-d_6 solution at 36°C

Couple proton positions[a]	J (Hz)
a_4e_4	13.5
a_4e_3	3.5
a_4a_3	8.6
e_4a_3	3.6
e_4e_3	7.0
a_3e_3	13.5
a_3a_2	9.0
a_3e_2	4.0
a_2e_2	13.3
a_2a_1	8.0
a_2e_3	3.5
a_1e_2	3.5

[a] a ≡ axial hydrogen, e ≡ equatorial hydrogen. Numbers refer to ring positions with the isonitrile substituent at position 1.

2. R. v. Ammon, R. D. Fischer, and B. Kanellakopulos, *Chem. Ber.* **104**, 1172 (1971).
3. A. A. Bothner-By and S. Castellano, *J. Chem. Phys.* **41**, 3863 (1964).
4. J. Meinwold and Y. C. Meinwold, *J. Amer. Chem. Soc.* **85**, 2514 (1963).
5. H. Conroy, p. 311 in *Advances in Organic Chemistry*, vol. 2, R. A. Raphael, E. C. Taylor, and H. Wynberg, eds., Interscience Publishers, New York, 1960.
6. E. L. Eliel et al., *Conformational Analysis*, Interscience Publishers, New York, 1965, p. 152.
7. N. S. Bhacca and D. H. Williams, *Applications of NMR Spectroscopy in Organic Chemistry*, Holden-Day, Inc., San Francisco, 1964, pp. 49, 135.

CRYSTAL STRUCTURE OF CURIUM TRIBROMIDE

J. H. Burns J. N. Stevenson[1]
J. R. Peterson[2]

The structure of $CmBr_3$ was found previously[3] by powder x-ray diffraction to be of the orthorhombic $PuBr_3$ type, but no atomic positions or bond lengths were determined. In order to obtain these structural details, we have used single-crystal methods with a specimen of $^{244}CmBr_3$ grown by slow cooling of a melt. Some 334 x-ray reflections were measured and used in a least-squares refinement of positional and thermal parameters.

We verified the space-group symmetry of $CmBr_3$ as *Cmcm* and obtained the following unit-cell dimensions: a = 4.041(2) Å, b = 12.70(2) Å, and c = 9.135(3) Å. Four formula units per cell yields a calculated density of 5.85 g/cm^3. Table 2.7 lists the refined parameters.

Qualitatively the structure has the appearance of orthorhombic $CfCl_3$, which is pictured elsewhere.[4] Figure 2.18 shows the Cm-Br bond lengths and the 75% probability ellipsoids of thermal motion for each kind of atom. Figure 2.18 also portrays coordination polyhedra of two other recently determined[5] structures, $PuCl_3$ and $CfBr_3$, to illustrate the decreasing number of neighbors which the trivalent actinide ions have as the cation : anion radius ratio decreases.

1. Graduate student, University of Tennessee, Knoxville. Present address: Nuclear Power School, U.S. Navy, Bainbridge, Md.

Table 2.7. Positional and thermal parameters for $CmBr_3$

Atom	Site	x	y	z	β_{11}	β_{22}	β_{33}	β_{12}	β_{13}	β_{23}
Cm	4(*c*)	0	0.2431(2)	¼	0.0099(9)	0.0029(2)	0.0021(2)	0	0	0
Br(1)	4(*c*)	0	0.5831(6)	¼	0.0151(30)	0.0038(5)	0.0032(5)	0	0	0
Br(2)	8(*f*)	0	0.1461(4)	0.5658(4)	0.0166(22)	0.0034(3)	0.0020(3)	0	0	−0.0002(3)

Table 2.8. Heat of solution of berkelium metal in 1 *M* HCl at 25°C

Sample No.	Sample weight (μg)	Heat of solution (kcal/mole)
I	251.6	−134.2
II	443.3	−137.0
III	405.4	−139.1
IV	499.7	−138.7
V	386.2	

2. Consultant, Department of Chemistry, University of Tennessee, Knoxville.

3. L. B. Asprey, T. K. Keenan, and F. H. Kruse, *Inorg. Chem.* **4**, 985 (1965).

4. J. H. Burns, J. R. Peterson, and R. D. Baybarz, *Chem. Div. Annu. Progr. Rep. May 20, 1972,* ORNL-4791, p. 50; *J. Inorg. Nucl. Chem.* **35**, 1171 (1973).

5. J. H. Burns and J. R. Peterson, *Chem. Div. Annu. Progr. Rep. May 20, 1972,* ORNL-4791, p. 51; ibid., *May 20, 1973,* ORNL-4891, p. 43.

CRYSTALLOGRAPHIC STUDIES OF THE TRIFLUORIDES AND THE TRIBROMIDES OF Cm-248 AND Cm-244[1]

J. N. Stevenson[2] J. R. Peterson[3]

As part of the continuing program to study the properties of curium in the absence of intense self-irradiation by making use of the long-lived isotope of mass number 248,[4–6] several samples of $^{248}CmF_3$ and $^{248}CmBr_3$ were prepared and studied by x-ray diffraction. For comparison purposes, several samples of $^{244}CmF_3$ and $^{244}CmBr_3$ were prepared.

All halide samples were prepared on the microgram scale utilizing the standard single cation exchange resin bead technique. Calcination of the saturated resin beads to the oxide was followed by treatment with anhydrous HBr or HF at elevated temperature to produce the halide compounds. X-ray diffraction and annealing studies were carried out on these samples contained in quartz capillaries.

The average lattice parameters found for $^{248}CmF_3$ are $a_0 = 7.014(3)$ and $c_0 = 7.194(3)$ Å. These values were found to be larger than those reported in the literature for $^{244}CmF_3$ [a_0 = 6.999(2) Å, c_0 = 7.179(4) Å].[7] As such behavior would be contrary to all previous observations, we held the literature values suspect and prepared our own samples of $^{244}CmF_3$. A first batch of ^{244}Cm proved to contain significant cationic impurities, so a second batch was

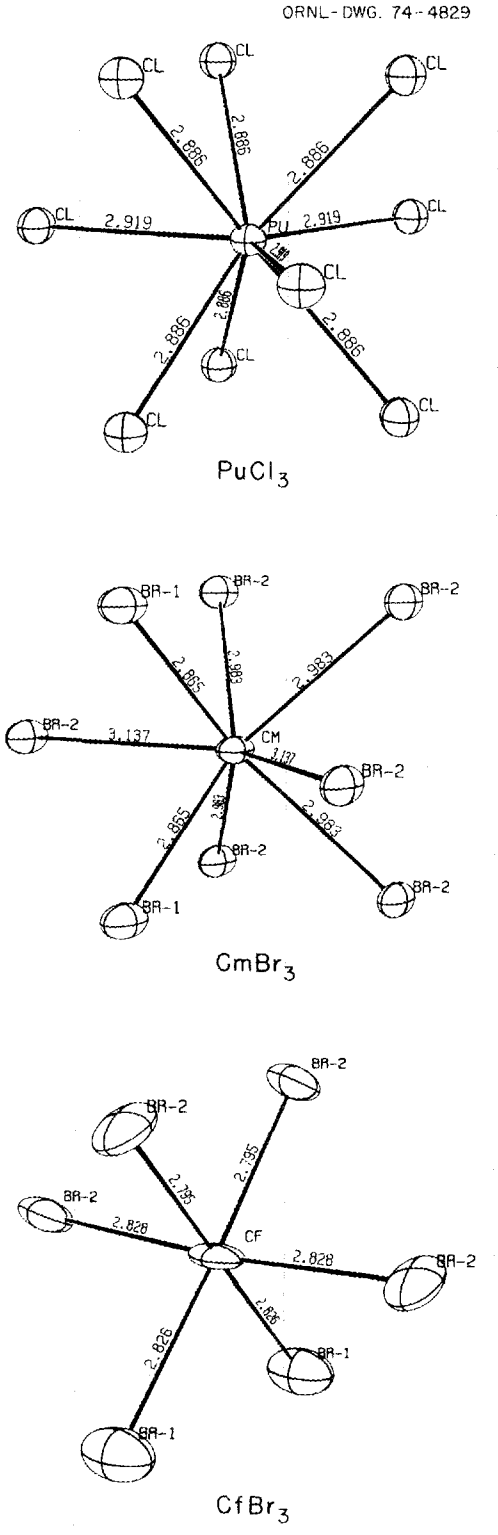

Fig. 2.18. Coordination polyhedra for actinide trihalides with different cation:anion radius ratios.

obtained from which the trifluoride samples, freshly prepared, yielded lattice parameters comparable with ours for $^{248}CmF_3$. Radiation damage was apparent in the $^{244}CmF_3$ samples after several days at room temperature; however, it could be annealed out rapidly by heating at about 800°C.

The lattice parameters determined for the orthorhombic $^{248}CmBr_3$ and $^{244}CmBr_3$ samples were also comparable, indicating lack of significant expansion in $^{244}CmBr_3$ as a result of the intense self-irradiation. This supports the suggestion that the rapid lattice expansion observed in $^{244}CmO_2$ is in large part due to the radiation-induced reduction of Cm(IV) to Cm(III).[6]

1. Supported in part by AEC Contract AT-(40-1)-4447 with the University of Tennessee, Knoxville.
2. Graduate student, University of Tennessee, Knoxville. Present address: Nuclear Power School, U.S. Navy, Bainbridge, Md.
3. Consultant, Department of Chemistry, University of Tennessee, Knoxville.
4. J. R. Peterson and J. Fuger, *J. Inorg. Nucl. Chem.* **33**, 4111 (1971).
5. M. Noé and J. R. Peterson, *Inorg. Nucl. Chem. Lett.* **8**, 897 (1972).
6. J. R. Peterson and J. H. Burns, *J. Inorg. Nucl. Chem.* **35**, 1525 (1973).
7. L. B. Asprey, T. K. Keenan, and F. H. Kruse, *Inorg. Chem.* **4**, 985 (1965).

PREPARATION OF ELEMENTAL ^{248}Cm AND ^{249}Cf AND THE NITRIDES OF ^{248}Cm AND ^{249}Bk[1]

J. N. Stevenson[2] J. R. Peterson[3]

As part of a continuing program to investigate the properties of the transuranium elements in the metallic state, a detailed study of elemental ^{248}Cm was undertaken and an initial attempt made to prepare bulk ^{249}Cf metal samples. The work with ^{248}Cm provided additional data for our interest in the self-irradiation effects on the properties of curium. The nitride work extended the series of known actinide nitrides through berkelium.

The elemental curium, berkelium, and californium samples were prepared by reduction of their trifluorides with lithium metal vapor in a low total heat capacity crucible and heating system. The product metals were recovered in bulk form adhering to the tungsten wire of the spiral used to contain the trifluoride in the reaction crucible. Two synthetic routes were employed to prepare the nitrides. The direct route was reaction of the metal with nitrogen at very high temperatures. The indirect route involved the initial reaction of the metal with hydrogen at about 250°C and subsequent treatment of the hydride with nitrogen at about 600°C.

Ten samples of ^{248}Cm metal were prepared for structural studies, phase-transformation studies, and use as starting material for the preparation of CmN. Two structural forms of ^{248}Cm metal were identified, the double hexagonal close packed (dhcp), characterized by $a_0 = 3.500(3)$ Å and $c_0 = 11.34(1)$ Å, and the face-centered cubic (fcc), characterized by $a_0 = 5.070(8)$ Å. These structure types are the same as those reported for ^{244}Cm.[4,5] Our lattice parameters for both modifications of ^{248}Cm give no evidence for radiation-induced expansion in ^{244}Cm.

Through study of the results of cold working, annealing, and quenching various ^{248}Cm samples, we have demonstrated for the first time the complete reversibility of the phase transformation and have confirmed that the fcc phase is the high-temperature modification.

Three samples of ^{249}Cf metal were prepared. In one case, however, the product metal was found to be coated with LiF. All three samples exhibited the fcc structure, with the lattice constants for the two samples not coated with LiF being 4.995(4) and 4.993(2) Å. Of particular note is the fact that this fcc phase, whose cell dimension is just slightly smaller than that for fcc berkelium metal, has not been observed previously.

Both ^{248}Cm and ^{249}Bk nitrides were found to crystallize in the cubic NaCl-type structure with unit-cell edges equal to 5.027 Å for CmN and 5.010 Å for BkN. No efforts were made to ascertain the precise compound stoichiometry. A plot of unit-cell edge vs actinide atomic number did not give the usual smooth curve, in marked contrast to a similar plot of lanthanide nitride data.

1. Supported in part by AEC Contract AT-(40-1)-4447 with the University of Tennessee, Knoxville.
2. Graduate student, University of Tennessee, Knoxville. Present address: Nuclear Power School, U.S. Navy, Bainbridge, Md.
3. Consultant, Department of Chemistry, University of Tennessee, Knoxville.
4. B. B. Cunningham and J. C. Wallmann, *J. Inorg. Nucl. Chem.* **26**, 271 (1964).
5. R. D. Baybarz and H. L. Adair, *J. Inorg. Nucl. Chem.* **34**, 3127 (1972).

ELECTROCHEMICAL AND SPECTROSCOPIC STUDIES OF TRANSURANIC SPECIES IN NONAQUEOUS INORGANIC MEDIA[1]

J. P. Young[2] R. L. Fellows[3]
J. R. Peterson[4]

Molten salts offer wide versatility as solvent media for the generation and characterization of unusual oxidation states of lanthanides and actinides (lanacts). This became experimentally obvious with the generation of Np(VII) in aqueous hydroxide[5] and the subsequent simple preparation of Np(VII) in molten hydroxide media.[6] Molten salts as a solvent medium offer advantages in the area of transuranic ion redox studies. Certain molten salts exhibit much greater thermodynamic stability than, for example, water. Further, molten salts can be self-annealing to radiation damage, as was demonstrated in molten-salt reactor experience, and therefore offer an inert solvent with respect to radiation effects. For these reasons, coupled with the wide range of spectral transparency exhibited by many molten salt mixtures, we are investigating the electrochemical generation and spectral characterization of transuranic ions in molten salt media. Earlier work has shown that U(III)/U(IV) redox could be followed by a combination electrochemical-spectrophotometric study when this couple was present in molten $LiF\text{-}BeF_2$.[7,8] We are presently designing and fabricating apparatus to be used in similar combination studies of unusual oxidation states of lanacts in molten KF-HF solvent. Preliminary work has shown that trivalent lanacts are soluble in this melt, that an isothermal environment promotes stability of a specified melt composition, and that a suitable cell can be made from Teflon or Kel-F and equipped with Al_2O_3 windows. We have fabricated a three-compartment electrochemical cell in which spectral studies can be carried out simultaneously on the products electrochemically generated at the working electrode, without interference from the separate reference and counterelectrodes. In addition, a furnace to heat this cell system has been designed and is being fabricated. We are also modifying a 3-ft gloved box so that it will include an appendage which fits into the sample space of a Cary spectrophotometer, model 14H. With this gloved-box facility we will be able to carry out electrochemical and spectral studies of solutions — aqueous, nonaqueous, or molten salt — without risking radioactive contamination of the Cary spectrophotometer. We have fabricated and operated a fluorination apparatus to purify and store HF for use in this and other projects. The purification system was built along the lines of that described by Asprey,[9] and the product anhydrous HF has been checked for purity by its nonreactivity with K_3NiF_7.[9]

1. Supported in part by AEC Contract AT-(40-1)-4447 with the University of Tennessee, Knoxville.

2. Analytical Chemistry Division.

3. Postdoctoral research associate, University of Tennessee, Knoxville.

4. Consultant, Department of Chemistry, University of Tennessee, Knoxville.

5. V. I. Spitsyn et al., *J. Inorg. Nucl. Chem.* **31**, 2733 (1969).

6. D. Cohen and S. Fried, *Inorg. Nucl. Chem. Lett.* **5**, 653 (1967).

7. J. P. Young, F. L. Whiting, and G. Mamantov, *J. Phys. Chem.* **71**, 782 (1967).

8. H. W. Jenkins, G. Mamantov, D. L. Manning, and J. P. Young, *J. Electrochem. Soc.* **116**, 1712 (1969).

9. L. B. Asprey, Los Alamos Scientific Laboratory, personal communication, 1973.

THE FIRST EXPERIMENTAL DETERMINATION OF THE HEAT OF SOLUTION OF BERKELIUM METAL[1]

J. R. Peterson[2] J. N. Stevenson[4]
J. Fuger[3] R. G. Haire[5]

Until recently the small sample sizes of berkelium metal have precluded the direct measurement of its heat of solution, which leads to the determination of the heat of formation of the aqueous Bk(III) ion. This latter quantity is a key unknown in the thermodynamic systematics of the members of the actinide series.[6] Berkelium is the first member of the second half of the actinide series, and knowledge of its thermodynamic properties is essential for a more accurate extrapolation to the thermodynamic properties of the heavier actinides, for which experimental measurements are at present not feasible.

Five bulk metal samples were prepared on the 250- to 500-μg scale by the lithium metal vapor reduction of BkF_3 at about 1000°C. Losses due to volatilization of the product metal were minimized by using a tantalum crucible and heating system of minimal heat capacity such that attainment of thermal equilibrium was rapid.[7] These metal samples were transported to Liège (Belgium), where they were prepared for solution microcalorimetry. Small pieces of two metal samples were cut off for examination by x-ray powder diffraction and spark-source mass spectrometric analysis.

A brief summary of the experimental data is presented in Table 2.8. All five metal samples were thought to exhibit the room-temperature-stable double hexagonal close packed (dhcp) structure[8] as a result of

the x-ray identification of only this phase in the two pieces examined and in consideration of the preparative method employed. No heat of solution value for sample V was calculated following observation of its slow dissolution, probably caused by oxide contamination as a result of loss of integrity of the quartz capillary in which it was shipped. All the metal samples were dissolved in the 1 *M* HCl calorimeter solution within 16 days of their preparation, so their californium contents were less than 3.5%.

The mass analyses indicated that samples I and II contained 1.5 wt % cationic impurities or less, whereas samples III, IV, and V (from a second batch of purified berkelium) contained 3 wt % cationic impurities or less. Our best experimental value for the heat of solution of dhcp berkelium metal in 1 *M* HCl at 25°C is -138^{-6}_{+3} kcal/mole (-578^{-25}_{+13} kJ/mole) from the average of the values obtained with samples II, III, and IV, where the empirical error limits are set in accord with a detailed analysis of the effects of the impurities found in the samples. Sample I was inadvertently exposed to a partial atmosphere of laboratory air prior to its encapsulation for shipping, so its result is held suspect.

Since the level of purity of the berkelium metal samples was not as high as it could have been, it is suggested that the value reported be considered preliminary until additional experimental determinations can be made.

---

1. Supported in part by North Atlantic Treaty Organization Research Grant No. 585 and by AEC contract AT-(40-1)-4447 with the University of Tennessee, Knoxville.

2. Consultant, Department of Chemistry, University of Tennessee, Knoxville.

3. Radiochemistry Institute, University of Liège, Sart Tilman, 4000 Liège, Belgium.

4. Graduate student, University of Tennessee, Knoxville. Present address: Nuclear Power School, U.S. Navy, Bainbridge, Md.

5. Chemical Technology Division.

6. L. J. Nugent, J. L. Burnett, and L. R. Morss, *J. Chem. Thermodyn.* **5**, 665 (1973).

7. J. N. Stevenson, USAEC document TID-26453 (1973).

8. J. R. Peterson, J. A. Fahey, and R. D. Baybarz, *J. Inorg. Nucl. Chem.* **33**, 3345 (1971).

3. Isotope Chemistry

This work continues to be directed at those aspects of the chemistry underlying isotope separation which seem most likely to yield useful results for a small but continuous effort. Search for an improved chemical exchange method for sulfur is proceeding systematically, so far with no breakthrough, but with increasing confidence that, if there is a right track, we are closing in on it. Further work on uranium is being done to help the AEC cover all bets, and in particular to demonstrate to an even higher degree of certainty that a viable chemical exchange scheme does not exist. Photochemical separation by laser excitation is currently of great interest for possible application to uranium; at our level of manpower we intend to study lighter elements to establish more about the fundamental reasons for failure or success, and, of course, with the hope that such information may lead to attractive schemes for the lighter elements as well as to some useful contributions to the understanding of the uranium problem.

LASER PHOTOCHEMICAL ISOTOPE SEPARATION

G. M. Begun W. H. Fletcher[1]

With the rapid development of laser technology during recent years the interest in possible photochemical separation of isotopes has been revived. A large number of proposals have been made, and much speculation concerning possible economic separation of isotopes with lasers has resulted. Several experiments[2-4] have actually demonstrated laser-photochemical enrichment of small quantities of isotopes. There is at present general agreement that isotopic effects can be obtained by the use of laser-induced photoreactions, but no economically practical systems have been demonstrated. Our program is aimed at defining the necessary criteria for the successful photochemical separation of isotopes and evaluating the economic feasibility of such separations.

Two of the proposed methods for isotopic enrichment using laser excitation are the single-photon and double-photon methods. These are illustrated in Fig. 3.1. In the single-photon method (Fig. 3.1, I) a laser is tuned to a frequency that results in dissociation or reaction of a single isotopic species. In order to obtain isotopic selectivity, it is necessary that the molecule be one in which predissociation takes place. That is, the molecule must have an upper energy state with discrete levels from which spontaneous dissociation or reaction will take place. The majority of molecules dissociate into a continuum and thus are not amenable to this approach. In addition, a tunable laser with considerable energy in the short-wavelength region is necessary. Such

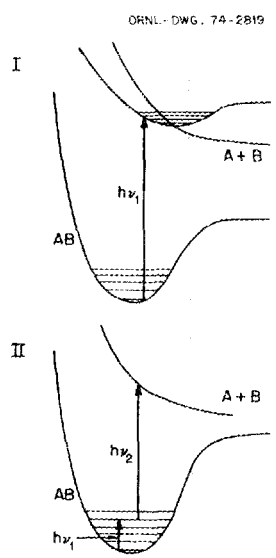

Fig. 3.1. Isotope separation diagrams. (I) Single-photon excitation, (II) double-photon excitation.

a laser is not yet commercially available. The argon-ion laser, however, does have the capability of exciting the halogen molecules (Cl_2, Br_2, and I_2) to an upper electronic state from which dissociation or reaction can take place. We have studied this idea previously and are currently considering it in the case of Cl_2. The two problems to be surmounted here are: (1) the argon-ion laser is not tunable except over about six different discrete lasing frequencies, and (2) excitation of Cl_2 is usually followed by a chain reaction which destroys any isotope effect.

Figure 3.2 shows the computer-calculated spectra of the various Cl_2 isotopic molecules for the 18-0 band of the $^3\Pi^+_{0u} \leftarrow \Sigma^+_g$ state. This band is in the region of the 488.0-nm argon-ion laser line. As can be seen in Fig. 3.2, there are quite a number of regions where a fairly strong line of a single species (^{35}Cl-^{35}Cl, ^{35}Cl-^{37}Cl, or ^{37}Cl-^{37}Cl) is well separated from the other lines. With proper tunability provided by a dye laser attachment or the use of pressure broadening and an etalon, we believe that Cl_2 can be selectively excited to the $^3\Pi^+_{0u}$ state. In order to prevent a chain reaction, we intend to surround each Cl_2 molecule with excess HI molecules so that Cl atoms cannot react with Cl_2 molecules. Initial experiments indicate that Cl_2 and HI react spontaneously, but this may not be the case if all reagents are purified and kept in the dark.

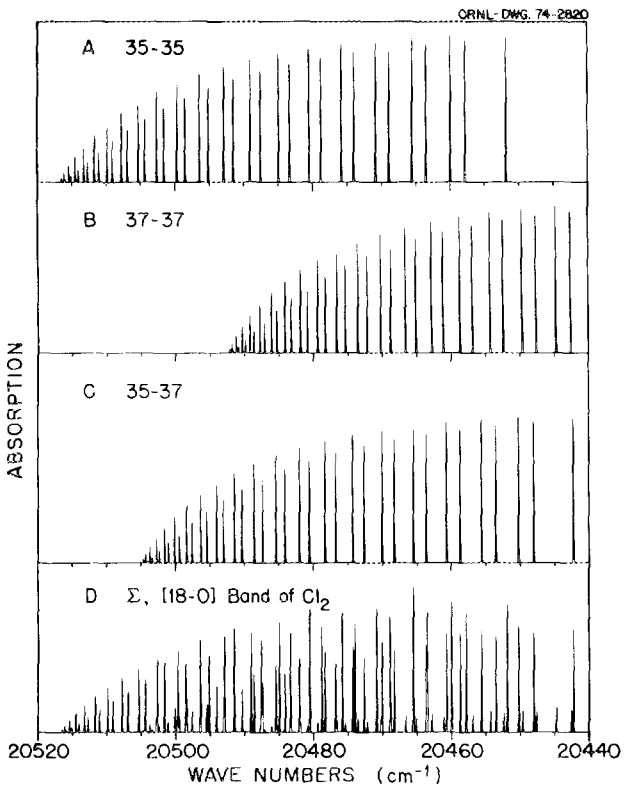

Fig. 3.2. Computer-calculated Cl_2 spectra 18-0 absorption band. *A*, ^{35}Cl-^{35}Cl; *B*, ^{37}Cl-^{37}Cl; *C*, ^{35}Cl-^{37}Cl; *D*, normal composite.

Another approach to laser isotope separation is the two-photon method illustrated in Fig. 3.1, II. In this method the gaseous compound is first illuminated with a tunable infrared laser to excite a specific isotopic vibrational-rotational state. Simultaneously a photon of higher energy then causes dissociation or reaction of the excited molecule. In this case the second photon need not be tuned so carefully, but should not have enough energy to dissociate unexcited molecules.

This method offers greater flexibility than the single-photon method. Since it is not possible to buy a tunable laser that will cover the complete infrared region desired, we have centered our program around the CO_2 laser. This laser is widely available commercially and, at present, can be tuned over some 80 lines in the region 920–1080 cm^{-1}. This does not give us continuous coverage of the region, but it appears that higher-pressure CO_2 lasers will soon be developed which may make it possible to tune continuously over this spectral region.

Tunable ultraviolet lasers to furnish the second photon are not yet available below 260 nm, and those with longer wavelengths are still very weak. Our plan at present is to use high-energy flash lamps with a filter or broadband monochromator to limit the wavelength region. We have ordered a pulsed TEA CO_2 laser and flash equipment. Currently we are studying by infrared spectroscopy and computer calculations the vibrational-rotational spectra of molecules that have infrared absorption bands in the 920–1080 cm^{-1} region.

In most cases of interest the vibrational-rotational spectra have been previously observed to some degree, but the fine structure and isotopic detail necessary for laser separation have not been studied. The molecules we have under consideration include COS, H_2S, NH_3, BCl_3, and CH_4. In order to establish which of the available laser lines may be useful, we have initiated a program of computer calculations of isotopic vibrational-rotational spectral bands for molecules of interest. In the calculated spectra we can clearly see in what regions the isotopic bands coincide and where they are separated distinctly. Figure 3.3 shows the calculated spectra of the $2\nu_2$ band for various isotopic mixtures of COS molecules. Figure 3.4 is an actual spectrum of this band as observed on the FTS-20 Fourier transform spectrometer belonging to the Solid State Division. We

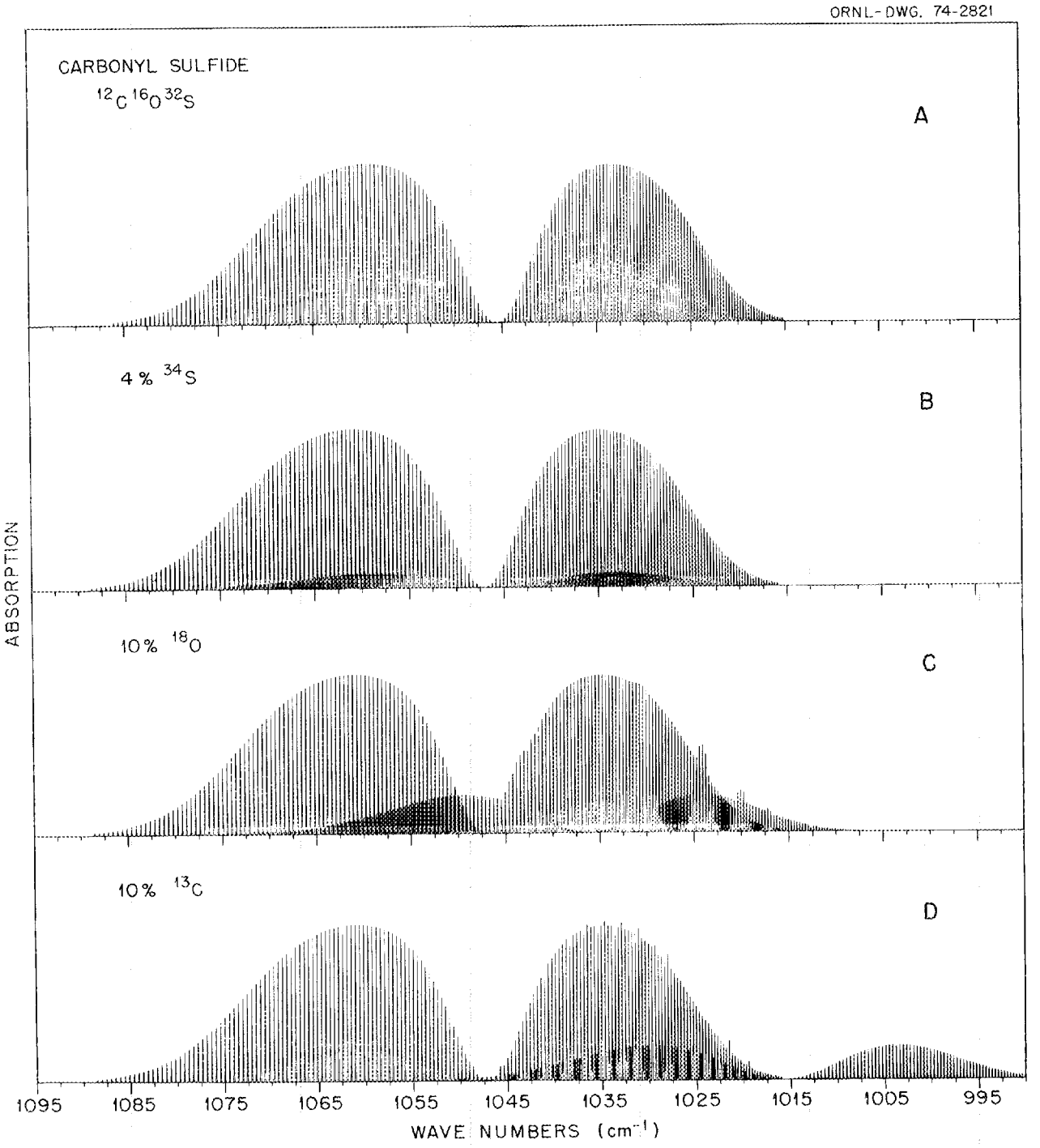

Fig. 3.3. Computer-calculated vibrational-rotational bands of isotopic COS molecules ($2\nu_2$). *A*, $^{12}C^{16}O^{32}S$; *B*, 4% ^{34}S; *C*, 10% ^{18}O; *D*, 10%, ^{13}C.

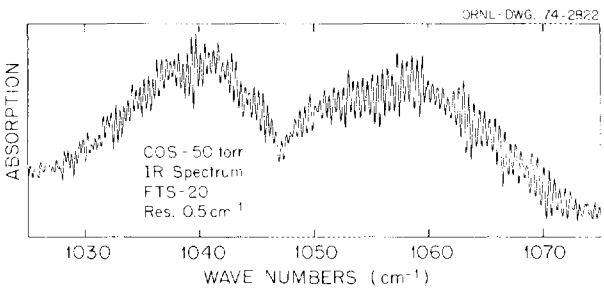

Fig. 3.4. Infrared spectrum of gaseous COS taken on the FTS-20 Fourier transform spectrometer. 50 mm pressure, 0.5 cm^{-1} resolution.

are proceeding with a complete analysis of this band. Regions for study of the CO_2-laser excitation of COS will be selected from these spectra. It appears that the ^{34}S species can be selectively excited by tuning one of the CO_2 emission lines with an intracavity etalon. The isotope shift for the ^{13}C species is very large, and the *P* branch of ^{13}C is almost entirely free of interfering absorption by the normal isotopic species. Broad-beam laser lines in the region below 1015 cm^{-1} should selectively excite this species.

Related Raman spectroscopy is the subject of another contribution in this report.[5]

1. Consultant, Department of Chemistry, University of Tennessee, Knoxville.
2. R. V. Ambartsumyan et al., *Zh. Eksp. Teor. Fiz. Pisma Red.* **17**, 91 (1973).
3. E. S. Yeung and C. B. Moore, *Appl. Phys. Lett.* **21**, 109 (1972).
4. S. W. Mayer et al., *Appl. Phys. Lett.* **17**, 516 (1970).
5. G. M. Begun, "Molecular Spectroscopy," a contribution in chap. 7, this report.

CHROMATOGRAPHIC SEPARATION OF ISOTOPES

D. A. Lee

Studies of isotopic fractionation by the chromatographic method continued. Single-stage separation factors (α) for cobalt and calcium isotopes were determined by band elution on ion exchange columns. Factors which affect column performance and the magnitude of the separation factor were observed. The radioassay technique for cobalt and calcium isotopes was further developed.

Several experiments to separate cobalt isotopes ^{59}Co and ^{60}Co were carried out. The octahedral cobalt cation $[Co{\cdot}6H_2O]^{2+}$ was equilibrated between several different aqueous salt solutions and the cation exchange resin Dowex 50. The nature of the eluent had a profound effect upon column performance. Of all the eluent salt solutions tried, ammonium sulfate solutions produced elution curves which were most nearly Gaussian. The concentrations of $(NH_4)_2SO_4$ in the eluent determined the width of the band eluted. Very narrow, concentrated bands were obtained with 1 *M* $(NH_4)_2SO_4$, and the resulting number of theoretical plates calculated from the elution curves was large ($\sim 10^6$). With ≤ 0.5 *M* $(NH_4)_2SO_4$ the bands were more diffuse and the number of plates much less ($\sim 10^4$). Although the sharp, narrow bands produced more plates, the resulting isotopic separation factors were erroneously small because of isotopic mixing as the samples were withdrawn from the column. The separation factors for cobalt isotopes eluted from Dowex 50 with 0.50 to 0.25 *M* $(NH_4)_2SO_4$ ranged from 1.00005 to 1.00010. Cobalt-60 was concentrated in the resin phase.

Some chromatographic experiments were performed under high pressure in an effort to eliminate isotopic mixing and obtain better performance. Cobalt isotope separation experiments were done on Dowex 50 packed in stainless steel columns ¼ to ½ in. in diameter and 5 to 47 ft long. The eluents were pumped with a Milton Roy minipump with pressures up to 1000 psi. There was no improvement in performance as far as isotopic separation was concerned. Generally, the height equivalent of a theoretical plate was too large to be practical for isotope separation.

Calcium isotopes were separated on Dowex 50. A mixture of natural calcium, 97% ^{40}Ca, and ^{47}Ca, a 4.5-day-half-life gamma emitter, was eluted in a band with 0.5 *M* ammonium lactate. The isotopic ratios were determined by counting ^{47}Ca and titrating the total $^{40}Ca + {}^{47}Ca$ ions in each sample. The titration method was a modification of the method of Vorlicek et al.[1] The local enrichment factors were plotted against the fraction of isotopes eluted according to the method of Glueckauf,[2] and α was determined to be 1.00026. Calcium-47 concentrated in the resin phase.

Since the last report,[3] some improvements have been made in the microtitration procedure used for the radioisotope assay of cobalt isotopes. The accuracy has been enhanced by the use of an ultraprecision microburet and an automatic dc digital voltmeter. A paper, "Potentiometric Microtitration of Cobalt," describing the method, has been submitted to the *Microchemical Journal* for publication.

1. J. Vorlicek, M. Fara, and F. Vydra, *Microchem. J.* **12**, 409 (1967).

2. E. Glueckauf, *Trans. Faraday Soc.* **54**, 1203 (1958).
3. D. A. Lee, *Chem. Div. Annu. Progr. Rep. May 20, 1973*, ORNL-4891, p. 53.

CHEMICAL FRACTIONATION OF URANIUM ISOTOPES

L. L. Brown

We continued our efforts to place chemical methods of fractionating uranium isotopes in perspective relative to other isotopic separation techniques. In response to the recommendations of the AEC Uranium Isotope Separation Review Ad Hoc Committee, we examined the isotopic separation obtainable by fractionally desorbing UF_6 from several of the alkali fluorides with which this molecule forms complexes.[1] The LiF complex appeared not to form; however, characteristic yellow compounds, M_2UF_8, were obtained with NaF, KF, and CsF.

The Na_2UF_8 complex was prepared from pelletized NaF obtained by thermally dehydrofluorinating $NaHF_2$. A bed of NaF pellets (37.4 g) was preconditioned by heating under vacuum to 350°C, followed by a preliminary loading (90°C) and desorption (310°C) of UF_6. Finally, 3.6 g of UF_6 was similarly deposited and stripped from the conditioned NaF. The first 11% of this UF_6 was desorbed at temperatures up to 290°C. An additional 13% was subsequently removed by further heating to 305°C. The two fractions of UF_6 were collected separately and converted to U_3O_8 prior to isotopic analysis by mass spectroscopy. An isotope effect, k_{235}/k_{238}, equal to $\sim 1.000_5$ was computed from these samples, an effect too small for practical application.

Potassium fluoride was prepared by heating KHF_2 to 500°C. The ground product was treated with UF_6 in dry CCl_4 at 70°C for 16 hr, after which the liquid phase was removed by distillation. The resulting complex had a molar composition $KF/UF_6 = 2.45$. Three fractions of UF_6 (12.7, 18.4, and 3.6%) were desorbed from this complex at <100°, 100–105°, and 105°C respectively. No appreciable isotopic fractionation was observed in these samples.

Cesium fluoride was prepared by drying some wet material first at 105° then at 250°C. The dried product was slurried with 48% HF and redried at 250°C to constant weight. Cs_2UF_8 was made by the process described for K_2UF_8 except that the milling operation was omitted to minimize exposure and handling of the hygroscopic CsF. The product had a molar composition $CsF/UF_6 = 1.79$. It was very stable, losing no UF_6 even after heating in vacuo for several hours at 285°C. This extreme stability of Cs_2UF_8 rendered it unattractive for our purpose, and no further examination of its properties was made.

The results noted above appear to eliminate any possibility that fractional desorption of UF_6 from alkali fluorides can serve as a viable process for separating uranium isotopes.

1. J. G. Malm, H. Selig, and S. Siegel, *Inorg. Chem.* **5**, 130 (1966).

SEARCH FOR A NEW SULFUR-ISOTOPE SEPARATION SYSTEM

J. S. Drury

The search for an economical chemical exchange process for separating sulfur isotopes continued during this report period.[1] The search was aimed at discovering an isotopic exchange reaction of the type

$$R^{34}S(g) + R^{32}S\cdot A(l) \rightleftharpoons R^{32}S(g) + R^{34}S\cdot A(l)\,, \qquad (1)$$

where RS is a sulfur-containing compound and RS·A is a thermally dissociable molecular-addition complex of RS. An isotopic separation process based on such a reaction could be refluxed thermally and thus should be more economical than the existing chemical-exchange process, which requires costly chemical refluxing. Earlier studies of reaction (1), in which RS was dimethyl sulfide and A was triethylaluminum or tributylaluminum, revealed little isotopic fractionation, presumably because the S–Al bond was too strong to permit rapid exchange to occur during the period of equilibration. This thesis was tested by replacing the R_3Al compounds, above, with $(C_2H_5)_2AlF$, in which the halogen weakens the S–Al bond in the molecular-addition complex. Significantly, a separation factor of 1.01 was measured for reaction (1) under these conditions, compared with 1.001 when A was $(C_2H_5)_3Al$ and 1.004 when A was $(C_4H_9)_3Al$. This is the largest separation factor observed for reaction (1) thus far.

Since the work reported above suggested that the aluminum alkyl complexes of dimethyl sulfide were too strong to permit ready exchange of the isotopic species in reaction (1), we examined the feasibility of using a gallium alkyl as the complexing agent for dimethyl sulfide. $(CH_3)_3Ga$ was prepared and found to have physical characteristics ideal for the implementation of reaction (1) as a countercurrent gas-liquid system which could be thermally refluxed. Unfortunately, however, the isotopic equilibrium constant for the gallium alkyl

exchange reaction was found to be identically 1 to four decimal places.

Other Lewis acids were also used in forming molecular-addition complexes of dimethyl sulfide. Solutions of $Cu_2Cl_2 \cdot 8NH_4Cl$, which complex CO very well, were not useful with dimethyl sulfide. The latter precipitated copious quantities of NH_4Cl from such solutions. AgCN was found to complex dimethyl sulfide very well, but the resulting solutions resembled molten salts rather than a molecular-addition complex and were physically unsuitable for use as a thermally refluxable system. At this point in the screening process it appeared prudent to consider sulfur donors other than dimethyl sulfide, such as SO_2. This molecule can act as a Lewis base by donating electrons from either sulfur or oxygen. For our purposes, it was essential that bonding should occur through the sulfur atom. A reaction meeting this and certain other requirements for an isotope separation system is shown in reaction (2):

$$^{34}SO_2Cl_2 \overset{cat}{\rightleftharpoons} {}^{32}SO_2 + Cl_2 \ . \qquad (2)$$

We measured a large isotopic fractionation factor for reaction (2) at 57°C, but subsequent investigation revealed it to be caused, at least in part, by analytical interference from SO_2Cl_2. Resolution of this analytical problem has not yet been achieved.

1. L. Landau and J. S. Drury, *Chem. Div. Annu. Progr. Rep. May 20, 1973*, ORNL-4891, p. 53.

4. Radiation Chemistry

Like nuclear chemistry, radiation chemistry has been pursued, here and elsewhere, because it underlies technological problems of nuclear energy. However, many of the reactions and intermediates of radiation chemistry are common to other kinds of chemistry, and studies or techniques originated for their bearing on radiation chemistry have value in other areas. In particular, many of the intermediates formed by irradiation of simple atmospheric gases are the same as those produced photochemically in the atmosphere. The identities and quantitative reactivities of those substances are vital to an understanding of atmospheric chemistry and the evaluation of the effects of pollutants on ozone, smog, and other good or bad features of the upper and lower atmosphere.

Most of the work reported here is in just this area and can be considered supportive both of nuclear energy and of those other kinds which supply pollutants to the atmosphere. A smaller portion of the program continues to be in the radiation chemistry of liquid water and solutions, but this work, too, is closely connected to (and often includes) photochemical studies that relate to various schemes for solar energy storage.

PULSE RADIOLYSIS OF N_2 + CO MIXTURES: THE FORMATION AND DECAY OF THE CN AND NCO RADICALS

C. J. Hochanadel J. W. Boyle
J. A. Ghormley M. S. Wolfe[1]

In a continuing effort to learn about the primary species produced in the pulse radiolysis of N_2, we employed CO as scavenger and observed as products the free radicals CN and NCO. Relative yields were measured as a function of N_2-CO composition, and the kinetics of formation and decay were studied in order to establish mechanisms.

It had previously been shown[2,3] that a few percent of O_2 added to N_2 scavenges the primary N_2 species, thereby leading to the formation of O_3. By measuring O_3 yields in O_2 + N_2 mixtures with and without the electron scavenger SF_6 present, we had found[4] the total yield of O_3 originating from N_2 precursors to be about 9.7 molecules per 100 eV, of which about 6.6 was attributed to ionic precursors and about 3.1 to neutral precursors. The neutral species are thought to be electronically excited states of N_2 or N, since the formation of O_3 via slow reactions of ground-state N atoms such as $N + O_2 \rightarrow NO + O$ is ruled out by the short time scale for O_3 formation.

It had also been observed[4] that a small amount of the positive ion scavenger NH_3 added to the N_2 + O_2 system competes favorably for the primary N_2 species and completely inhibits the sensitized formation of O_3. Likewise, the NH_3 scavenges most, but not all, of the primary O_2 species and reduces the yield of O_3 originating from energy absorbed by the O_2 from 13.8 to about 3. We have now studied the sensitized decomposition of NH_3 in the pulse radiolysis of N_2 + NH_3 mixtures (also Ar with NH_3), and the results are described below.[5] Our goal is to establish consistent relationships among the yields observed in the three scavenger systems (O_2 yielding O_3, NH_3 yielding NH and NH_2, and CO yielding CN and NCO) and the yields of specific primary species produced in the N_2.

In the N_2 + CO system the CN was formed after the pulse at a rate which increased with increasing CO concentration; the formation time varied from 3 μsec at 0.25% CO to 0.05 μsec at 75% CO. The yield of CN (measured by absorption at 3883 Å) increased with CO concentration, reaching a maximum at about 10% CO, above which the yield decreased nearly linearly to zero

in pure CO. For low concentrations of CO, a plot of 1/[CN] vs 1/[CO] was linear, indicating typical scavenger behavior in which CN is produced by competition of CO for a primary species produced in the N_2. The drop in CN yield with further increase in CO concentration indicates that the energy absorbed by the CO leads only to the normal radiolysis products of CO, namely, CO_2 and C_3O_2. The behavior of NCO (measured at 4403 Å) was somewhat similar, with the yield reaching a maximum at about 20% CO, above which it declined nearly linearly to zero in pure CO.

The decay kinetics of CN in the N_2 + CO system are complex, and a mechanism has not yet been established. With O_2 added to the system the decay rate of CN increased, and the decay became first order due to the reaction $CN + O_2 \rightarrow NCO + O$. Our value for the rate constant was $(5 \pm 1) \times 10^9\ M^{-1}\ sec^{-1}$, which agrees well with recent literature values.[6] The added O_2 also decreases the amount of CN formed since O_2 and CO compete for the primary N_2 species.

In the N_2 + CO system, part of the NCO was formed during the pulse, but most of it was formed after, with a formation time (e.g., for 3% CO) of about 15 μsec. The decay of NCO was second order and insensitive to the composition of the system. The decay reaction is probably $2NCO \rightarrow N_2 + 2CO$. The time scales were such that part of the NCO may have formed from the CN. We found no absorption by NCN (3290 Å), indicating that the reaction $CN + NCO \rightarrow NCN + CO$ is not important. Positive N_2 ions react rapidly with CO by charge exchange[7] and probably lead to normal radiolysis products of CO. The CN and most of the NCO apparently originate from reaction of CO with electronically excited states of N_2. Light emission measurements showed that CO quenches emission by N_2 very efficiently. Quantitative kinetic analysis has not been completed and requires accurate extinction coefficients for CN and NCO for our conditions. The accuracy of the analysis may suffer the usual uncertainty concerning nonadherence to the Lambert-Beer law for measurements on these sharp lines, and, for reactions higher than first order, there is also the additional uncertainty caused by nonuniform concentration throughout the optical path. However, these limitations may not be too serious since we found that: (1) The exponent n is equal to 1 for both CN and NCO in the modified Lambert-Beer expression $O.D. = \epsilon(cl)^n$, indicating that this law is obeyed. The value of n was obtained from a plot of log O.D. vs log c, where c was varied by changing the pulse energy and relative values of c were determined using O_3 formation in O_2 as dosimeter. (2) For this dosimeter, the ratio of optical densities for eight and four light passes was 2.1, indicating relatively uniform concentration throughout this volume of the cell.

1. Student participant in the Great Lakes Colleges Association Science Semester, fall 1973, from Earlham College, Richmond, Ind.

2. J. A. Ghormley, C. J. Hochanadel, and J. W. Boyle, *Chem. Div. Annu. Progr. Rep. May 20, 1967*, ORNL-4164, pp.40–41.

3. C. Willis, A. W. Boyd, and M. J. Young, *Can. J. Chem.* **48**, 1515 (1970).

4. J. A. Ghormley et al., *Chem. Div. Annu. Progr. Rep. May 20, 1971*, ORNL-4706, p. 100.

5. C. J. Hochanadel, J. A. Ghormley, and J. W. Boyle, "Pulse Radiolysis of Nitrogen and Argon in the Presence of Ammonia," the following contribution, this report.

6. See, for example, G. C. Bullock and R. Cooper, *Trans. Faraday Soc.* **68**, 2175 (1972).

7. F. C. Fehsenfeld, A. L. Schmeltekopf, and E. E. Ferguson, *J. Chem. Phys.* **44**, 4537 (1966); ibid., **46**, 2019 (1967).

PULSE RADIOLYSIS OF NITROGEN AND ARGON IN THE PRESENCE OF AMMONIA

C. J. Hochanadel J. A. Ghormley J. W. Boyle

We have previously shown[1] that a small amount of NH_3 inhibits the sensitized formation of O_3 by N_2 or Ar in the pulse radiolysis of $N_2 + O_2$ and $Ar + O_2$ systems. We have now studied the sensitized decomposition of NH_3 in the pulse radiolysis of both N_2-NH_3 and Ar-NH_3 mixtures. Yields of the transients NH_2 and NH (measured at 5976 and 3360 Å respectively) have been measured over the entire composition range, and we now attempt to relate these yields to yields of primary species in N_2 or Ar. Studies by others[2] of the radiolysis of pure NH_3 have been interpreted on the basis of the NH_2 intermediate produced in high yield from the ionic precursor NH_3^+ and the NH produced in relatively small yield from a neutral excited precursor. For the sensitized decomposition of NH_3, where M represents N_2 or Ar in our systems, the postulated reactions are:

$$M \rightsquigarrow M^+, M^*, e^- , \quad (1)$$

$$M^+ + NH_3 \rightarrow NH_3^+ + M , \quad (2)$$

$$NH_3^+ + NH_3 \rightarrow NH_4^+ + NH_2 , \quad (3)$$

$$NH_4^+ + e^- \rightarrow NH_3 + H , \quad (4)$$

$$M^* + NH_3 \rightarrow NH_3^* + M , \quad (5)$$

$$NH_3^* \rightarrow NH + H_2 \quad (6)$$

$$\rightarrow NH_2 + H .$$

For both the N_2 and Ar systems the yield of NH_2 increased linearly as the composition changed from 1% NH_3 to 100% NH_3. In both systems the intercept of this line with the 100% N_2 or Ar composition was 0.63 ± 0.03 times that for 100% NH_3. In the Ar system, the NH yield also increased linearly with composition in the range 1% to 100% NH_3. The extrapolated yield for 100% Ar was 0.26 ± 0.03 times that for 100% NH_3. The NH yield in the N_2 systems has not yet been measured.

The ratio of ions to neutral excited species is considerably higher for argon and the other rare gases than for molecular gases, and it might be expected that for the rare gases the formation of NH_2 would be favored over NH. On the basis of the proposed mechanism and the W values for NH_3 and Ar, a higher yield of NH_2 from an Ar ion precursor would have been expected. The NH results also suggest that excited Ar* atoms do not ionize NH_3 and that the yield of excited NH_3* is approximately four times the yield of excited Ar* (or the excitation transfer to NH_3 is inefficient).

Work is continuing in these systems with special attention being given to the kinetics of decay of the NH_2 and NH radicals. The NH_2 radical decays faster than NH, appearing to be gone in about 20 μsec, whereas NH lasts up to about 50 μsec. The kinetics are complicated in each case because the absorptions are sharp lines and the Beer-Lambert relationship is not applicable. As might be expected in such cases the raw data do not appear to follow either first- or second-order kinetics. A modified relationship O.D. = $\epsilon(cl)^n$ is sometimes used in such cases. In the case of NH, n was determined to be 0.625 for our experimental conditions. Neither the extinction coefficient nor the absolute concentration is known here, but relative concentrations may be determined in this way. Using this modified relationship the NH decay in 100% NH_3 seems to follow first-order kinetics until about 90% has decayed. As this suggests a mechanism different from the mechanism postulated by others, additional experiments are planned to disprove or verify these results.

1. J. A. Ghormley et al., *Chem. Div. Annu. Progr. Rep. May 20, 1971,* ORNL-4706, p. 100.

2. C. Willis, A. W. Boyd, and O. A. Miller, *Can. J. Chem.* 47, 3007 (1969).

ABSORPTION SPECTRUM AND REACTION KINETICS OF THE METHYLPEROXY RADICAL

C. J. Hochanadel J. A. Ghormley
P. J. Ogren[1] J. W. Boyle

Reactions of peroxy radicals are important in mechanisms of oxidation reactions. These reactions may be induced by heat, light, or high-energy radiation and, therefore, are of great interest in many aspects of radiation chemistry, environmental chemistry, combustion, etc. We are continuing our studies of peroxy radicals, which started with measurements of the HO_2 radical, by measuring the absorption spectrum of the CH_3O_2 radical and the rate constant for its formation from the reaction of the methyl radical with oxygen. We are also studying the combination of methylperoxy radicals and the combination of methyl radicals.

Methyl radicals are produced by photolysis of azomethane. The reactions are monitored by kinetic spectrophotometry of CH_3 absorption at 2164 Å and CH_3O_2 at 2380 Å. Extinction coefficients are evaluated from the loss of azomethane measured by means of a Cary model 15 spectrophotometer before and after the sample is subjected to flash photolysis. Loss of azomethane was measured not at the peak, 1849 Å, but at several longer wavelengths where oxygen absorbs less. For example, at 1849 Å, ϵ = 7257 M^{-1} cm^{-1} for azomethane and 8.2 M^{-1} cm^{-1} for O_2. At 1861 Å, ϵ = 6919 for azomethane (down 5%) but ϵ = 0.2 for oxygen (down a factor of 41). Methyl radical absorption could not be measured earlier than about 15 μsec after the start of the flash, and a computer calculation will be necessary in order to determine from the absorption measurements the total methyl produced by the flash. The determination of the extinction coefficient for methylperoxy does not require a computer calculation to extrapolate back to zero time because the decay is relatively slow.

Figure 4.1 shows a typical oscilloscope photograph and second-order plot of the data for the reaction

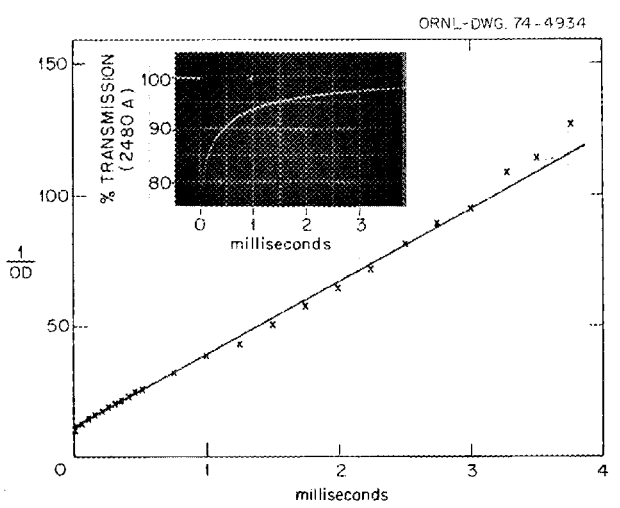

Fig. 4.1. Second-order decay of CH_3O_2 produced by flashing azomethane (6.3 × 10^{-5} M) in the presence of O_2 (1.4 × 10^{-3} M) in an atmosphere of N_2 (4 × 10^{-2} M).

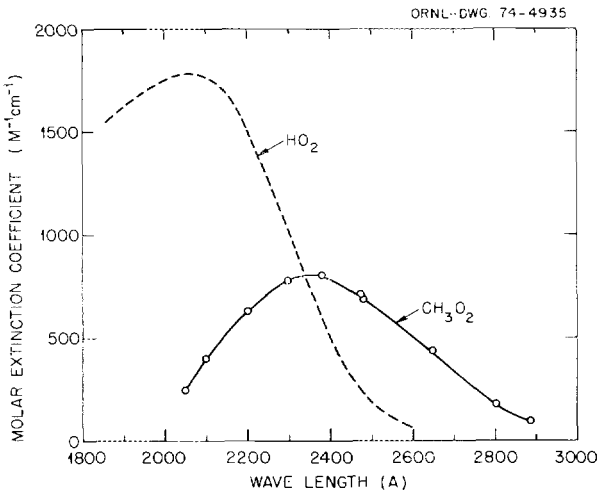

Fig. 4.2. Absorption spectra of CH_3O_2 with our published spectrum of HO_2.

$CH_3O_2 + CH_3O_2$. Our preliminary values for the second-order rate constants are:

$$k(CH_3 + O_2 + M \rightarrow CH_3O_2 + M) = 1.2 \times 10^9\ M^{-1}\ sec^{-1}\ ,$$

$$k(CH_3 + CH_3 + M \rightarrow C_2H_6 + M) = 3.4 \times 10^{10}\ M^{-1}\ sec^{-1}\ ,$$

$$k(CH_3O_2 + CH_3O_2 \rightarrow \text{products}) = 7.5 \times 10^8\ M^{-1}\ sec^{-1}\ .$$

The absorption spectrum of CH_3O_2 is shown in Fig. 4.2 along with the spectrum of HO_2 for comparison.

The absorption spectrum of the methylperoxy radical and the rate constant for its combination were recently measured by Parkes et al.,[2] using the method of molecular modulation spectrometry. They report an extinction coefficient equivalent to 1146 M^{-1} cm^{-1} at 2380 Å, compared with our preliminary value of 800 M^{-1} cm^{-1}, and a rate constant equivalent to 1.3 to 2.6 $\times$ 10^8 M^{-1} sec^{-1}, compared with our 7.5 $\times$ 10^8 M^{-1} sec^{-1}. They also report an increase in ϵ for methyl, methylperoxy, and ethylperoxy going down to wavelengths below 2100 Å, suggesting a second peak, but we see no rise in the methyl or methylperoxy radical spectra down to 2050 Å. At shorter wavelengths, azomethane absorption becomes important, perhaps more important in the molecular modulation method than in our more direct method.

1. Department of Chemistry, Central College, Pella, Iowa.
2. D. A. Parkes et al., *Chem. Phys. Lett.* **23,** 425 (1973).

PHOTOOXIDATION AND FLUORESCENCE OF CERIUM(III) IN AQUEOUS SULFURIC ACID SOLUTIONS[1]

R. W. Matthews[2] T. J. Sworski

Production of hydrogen by the photolysis of cerium(III) in aqueous perchloric acid solutions has been proposed[3] as a process for the chemical storage of solar energy. Three different reaction mechanisms have been proposed[4-6] for hydrogen production with either H_2^+, H, or e_{aq}^- as transitory intermediates. To evaluate these alternative reaction mechanisms, we studied the oxidation of cerium(III) by persulfate photosensitized by cerium(III) in aqueous sulfuric acid solutions. We previously evaluated[7] the role of H and e_{aq}^- in the radiolysis of cerium(III)-persulfate mixtures in aqueous sulfuric acid solutions.

The dependence of both the photooxidation and fluorescence of cerium(III) on persulfate concentration is quantitatively explicable by the following reaction mechanism:

$$Ce^{III} + h\nu \rightarrow (Ce^{III})^*\ , \qquad (1)$$

$$(Ce^{III})^* \rightarrow Ce^{III} + h\nu'\ , \qquad (2)$$

$$(Ce^{III})^* + H_3O^+ \rightarrow Ce^{III} + H_3O^+\ , \qquad (3)$$

$$(Ce^{III})^* + S_2O_8^{2-} \rightarrow Ce^{IV} + SO_4^{2-} + SO_4^-\ , \qquad (4)$$

$$Ce^{III} + SO_4^- \rightarrow Ce^{IV} + SO_4^{2-}\ . \qquad (5)$$

Our reaction mechanism requires that the dependence of fluorescence intensity F, on persulfate concentration adhere to Eq. (I):

$$F = F^0 \left(1 + \frac{k_4\,[S_2O_8^{2-}]}{k_2 + k_3\,[H^+]}\right)^{-1}\ . \qquad (I)$$

Our reaction mechanism also requires that the dependence of the photooxidation rate, R, on persulfate concentration adhere to Eq. (II):

$$R = R^0 \left(1 + \frac{k_2 + k_3\,[H^+]}{k_4\,[S_2O_8^{2-}]}\right)^{-1}\ . \qquad (II)$$

The experimental data were fitted to Eqs. (I) and (II) by the method of least squares using the computer program of Lietzke.[8] Stern-Volmer constants for the quenching of cerium(III) fluorescence {values for $k_4/(k_2 + k_3\,[H^+])$ of 98.9 $\pm$ 2.5 M^{-1} and 93.5 $\pm$ 2.0

M^{-1} for 0.03 and 0.003 M cerium(III) solutions in 0.4 M sulfuric acid respectively} are in good agreement with Stern-Volmer constants for the photooxidation of cerium(III) {values for $k_4/(k_2 + k_3[H^+])$ of 90.5 ± 3.4 M^{-1} and 102.7 ± 3.0 M^{-1} for aerated and deaerated 0.03 M cerium(III) solutions in 0.4 M sulfuric acid respectively}, conclusive evidence that photooxidation is induced by the quenching process.

Evidence was obtained to establish that the quenching of cerium(III) fluorescence by persulfate is not due either to complex formation or to energy transfer. We propose that the quenching of cerium(III) fluorescence by persulfate is an irreversible electron-transfer process[9] according to reaction (4).

No evidence was obtained for any significant quantum yield of either H or e_{aq}^-. This is convincing evidence that both photoionization[6] of cerium(III) and quenching of cerium(III) fluorescence by hydrogen ion with concomitant formation[5] of H atom, if they occur at all, are not major processes. We propose that hydrogen ion quenches cerium(III) fluorescence by a reversible electron-transfer process with H_3O as a transitory intermediate:

$$(Ce^{III})^* + H_3O^+ \rightarrow [Ce^{IV} + H_3O] \rightarrow Ce^{III} + H_3O^+ . \quad (6)$$

Our proposal that H_3O is an intermediate in the quenching of cerium(III) fluorescence by hydrogen ion requires consideration of H_3O as an intermediate in hydrogen production. Assume that some of the H_3O radicals escape geminate reaction with cerium(IV) by diffusion into the bulk of the solution with a quantum yield of 0.0007. An alternative mechanism for hydrogen production, quantitatively consistent with the kinetic study of Heidt and McMillan,[4] would be oxidation of cerium(III) by H_3O in competition with thermal dissociation[10] of H_3O:

$$Ce^{III} + H_3O \rightarrow Ce^{IV} + H_2 + OH^- , \quad (7)$$

$$H_3O \rightarrow H + H_2O , \quad (8)$$

$$H_3O \rightarrow e_{aq}^- + H_3O^+ . \quad (9)$$

We have no basis for rejecting the mechanism of Heidt and McMillan[4] for H_2 production. The precursor of H_2 may well be H_2^+. Our proposal that H_3O is an intermediate can be made consistent with the mechanism of Heidt and McMillan[4] by postulating that H_3O is a precursor of H_2^+:

$$H_3O \rightarrow H_2^+ + OH^- . \quad (10)$$

1. Expanded abstract of paper submitted to the *Journal of Physical Chemistry* and to the Eleventh Informal Conference on Photochemistry, Vanderbilt University, Nashville, Tenn., June 16–20, 1974. Research sponsored jointly by the U.S. Atomic Energy Commission and the Australian Atomic Energy Commission.
2. Australian Atomic Energy Commission Research Establishment, Lucas Heights, New South Wales.
3. L. J. Heidt and A. F. McMillan, *Science* **117**, 75 (1953).
4. L. J. Heidt and A. F. McMillan, *J. Amer. Chem. Soc.* **76**, 2135 (1954).
5. F. Hussain and R. G. W. Norrish, *Proc. Roy. Soc., Ser. A* **275**, 161 (1963).
6. A. W. Adamson et al., *Chem. Rev.* **68**, 541 (1968).
7. R. W. Matthews, H. A. Mahlman, and T. J. Sworski, *J. Phys. Chem.* **74**, 2475 (1970).
8. M. H. Lietzke, *A Generalized Least Squares Program for the IBM 7090 Computer*, ORNL-3259 (March 21, 1962).
9. K. H. Grellman, A. R. Watkins, and A. Weller, *J. Phys. Chem.* **76**, 469 (1972).
10. J. L. Magee, *Radiat. Res., Suppl.* **4**, 20 (1964).

ON THE DISSOCIATION OF HSO_4^-

T. J. Sworski

In our studies on the radiolysis of cerium(IV)–cerium(III)–formic acid mixtures in 4.0 M sulfuric acid solutions, we discovered[1] that the rate of reduction of cerium(IV) by hydrogen peroxide was markedly dependent on sulfuric acid concentration. The rate of reaction decreases markedly with increase in sulfuric acid concentration from 2.0 to 8.0 M and then increases markedly with further increase in sulfuric acid concentration.[2] The minimum in reaction rate occurs at about the same sulfuric acid concentration at which the sulfate ion concentration is a maximum. A search for a common cause indicated[3] that both the reaction rate and the sulfate ion concentration may depend on water activity.

The second dissociation quotient of sulfuric acid can be expressed[3] surprisingly well as a function of water activity for sulfuric acid concentrations up to 14.2 M, suggesting the importance of the complete equilibrium constant[4] that includes water as a reactant. Alternatively, the dependence of the second dissociation quotient on sulfuric acid concentration can be expressed[5] quite well up to 8.0 M by a conventional equilibrium constant, provided one accepts the contention of Stokes and Robinson[6] that the Debye-Hückel theory predicts the behavior of the rational activity coefficient of hydrated ions.

The significance of the two expressions for the second dissociation quotient is uncertain owing to the conflicting data, obtained by Raman spectroscopy, on the

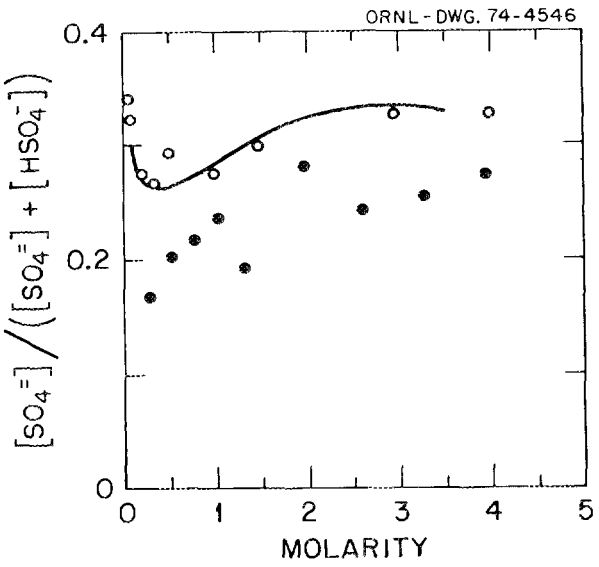

Fig. 4.3. The degree of dissociation of HSO_4^- as a function of sulfuric acid concentration according to the data of ○ Young et al.[7] and ● Chen and Irish.[8] The curve is theoretical and represents the degree of dissociation calculated from the mean activity coefficients for sulfuric acid of Covington et al.[9] using the theory for ion hydration of Stokes and Robinson.[6]

dependence of SO_4^{2-} and HSO_4^- concentrations on sulfuric acid concentration. Figure 4.3 shows that the values for the degree of dissociation of HSO_4^- reported by Young et al.[7] are significantly higher than those reported by Chen and Irish.[8]

An iterative procedure was developed to calculate the degree of dissociation of HSO_4^- from the mean activity coefficient of sulfuric acid. The relationship between the mean activity coefficient and the rational activity coefficients of the hydrated ions was obtained by the method of Stokes and Robinson.[6] This relationship expresses the degree of dissociation of HSO_4^- as a function of an ion size parameter B_f and the degree of ion hydration n. The *approximation* that anions are unhydrated was used, n being the degree of hydration of the hydrogen ion. Values for B_f and n were found which yielded those values for the degree of dissociation of HSO_4^- that gave the best fit by the method of least squares to our expression[5] of the second dissociation quotient of sulfuric acid by a conventional equilibrium constant. This least-squares fit yielded values also for the equilibrium constant K and an ion size parameter B_Q.

For values of $B_f = 0.713$ and $n = 4.78$, the mean activity coefficients of Covington et al.[9] for sulfuric acid from 0.1 to 4.0 M yielded $K = 0.0112 \pm 0.0001$, $B_Q = 0.393 \pm 0.002$, and values for the degree of dissociation of HSO_4^- that are represented by the curve in Fig. 4.3. The data of Covington et al.[9] are equal to the data of Robinson and Stokes[10] multiplied by a correction factor of 0.9228. A more commonly accepted value of $K = 0.0102$ can be obtained from the mean activity coefficients of Robinson and Stokes[10] multiplied by a correction factor of 0.899. The uncorrected data of Robinson and Stokes[10] yield $K = 0.0151$.

A tentative conclusion is that only the data of Young et al.[7] are consistent with the mean activity coefficients of sulfuric acid. The data of Chen and Irish[8] have been criticized by Turner.[11]

1. R. W. Matthews, H. A. Mahlman, and T. J. Sworski, *J. Phys. Chem.* 72, 3704 (1968); ibid., 76, 1265 (1972).
2. H. A. Mahlman, R. W. Matthews, and T. J. Sworski, *J. Phys. Chem.* **75**, 250 (1971).
3. T. J. Sworski, *Chem. Div. Annu. Progr. Rep. May 20, 1972*, ORNL-4791, p. 63.
4. W. L. Marshall and A. S. Quist, *Proc. Nat. Acad. Sci. U.S.* **58**, 901 (1967).
5. T. J. Sworski, *Chem. Div. Annu. Progr. Rep. May 20, 1973*, ORNL-4891, p. 59.
6. R. H. Stokes and R. A. Robinson, *J. Amer. Chem. Soc.* **70**, 1870 (1948).
7. T. F. Young, L. F. Maranville, and H. M. Smith, p. 35 in *The Structure of Electrolyte Solutions*, ed. by W. J. Hamer, Wiley, New York, 1959.
8. H. Chen and D. E. Irish, *J. Phys. Chem.* **75**, 2672 (1971).
9. A. K. Covington, J. V. Dobson, and Lord Wynne-Jones, *Trans. Faraday Soc.* **61**, 2050 (1965).
10. R. A. Robinson and R. H. Stokes, p. 477 in *Electrolyte Solutions*, 2d ed., Butterworths, London, 1959.
11. D. J. Turner, *J. Chem. Soc., Faraday Trans. 2* **68**, 643 (1972).

5. Organic Chemistry

Organic chemistry has had a small but significant role at the Laboratory over many years. In a practical way it provided various materials (e.g., solvents) for other programs, and in a fundamental way it made use of nuclear materials and techniques to further its own understanding. With broadened missions for the Laboratory, the responsibilities and opportunities for organic chemistry will increase manyfold.

An event signaling the new role expected for organic chemistry was the acquisition of a state-of-the-art, 100-MHz NMR instrument, which is expected to see heavy use in programs in biology and in coal research, as well as in ongoing basic organic research.

COMBINATORIAL CHEMISTRY

C. J. Collins C. K. Johnson
W. W. Schmidt[1]

In further application of the algebraic model and the coset graphs previously discussed,[2,3] the data of Sorensen and co-workers[4] were examined. Sorensen's results[4] for the rearrangements, in superacid, of the α-fenchyl cation are given in Chart I. An abbreviated coset graph[3] portraying the pertinent section of concern is shown in Chart II. The reactions[3] "allowed" were: Wagner-Meerwein (WM), 6,2-hydride shift (62H), *exo*-3,2-hydride shift (32H), Nametkin (32M), and double Wagner-Meerwein rearrangement (DWM). From Chart II we infer that (1) the cations whose spectra are observed are not formed one from the other in a series of discrete, irreversible steps, but rather are those cations which are thermodynamically most stable at the given temperatures, and (2) the double Wagner-Meerwein rearrangement[3] is not essential to provide a pathway between BJK and ABE. Since the coset graph (Chart II) was generated by use of the ORNOCARE program,[2] which also keeps track, for any given pathway between any two cations of Chart II, of every atom in the structure, the means are now available, with isotopic labels, to determine which pathway(s) contribute to the reaction BJK → ABE.

The rearrangement[5] of longifolene to isolongifolene was also examined, using the ORNOCARE[2] program and a technique previously described.[6] We found no new pathways between these two compounds, but

ORNL-DWG 73-6390

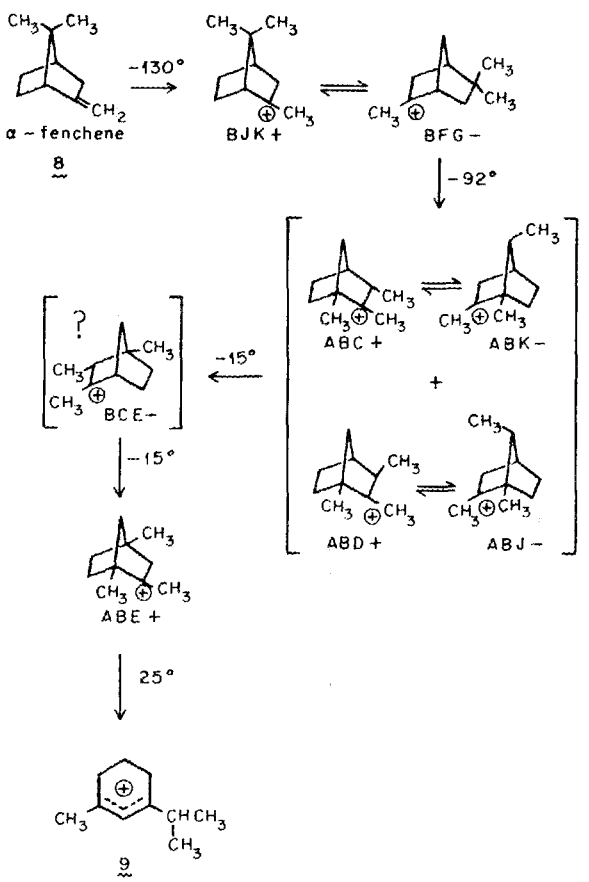

Chart I

ORNL-DWG. 73-6084

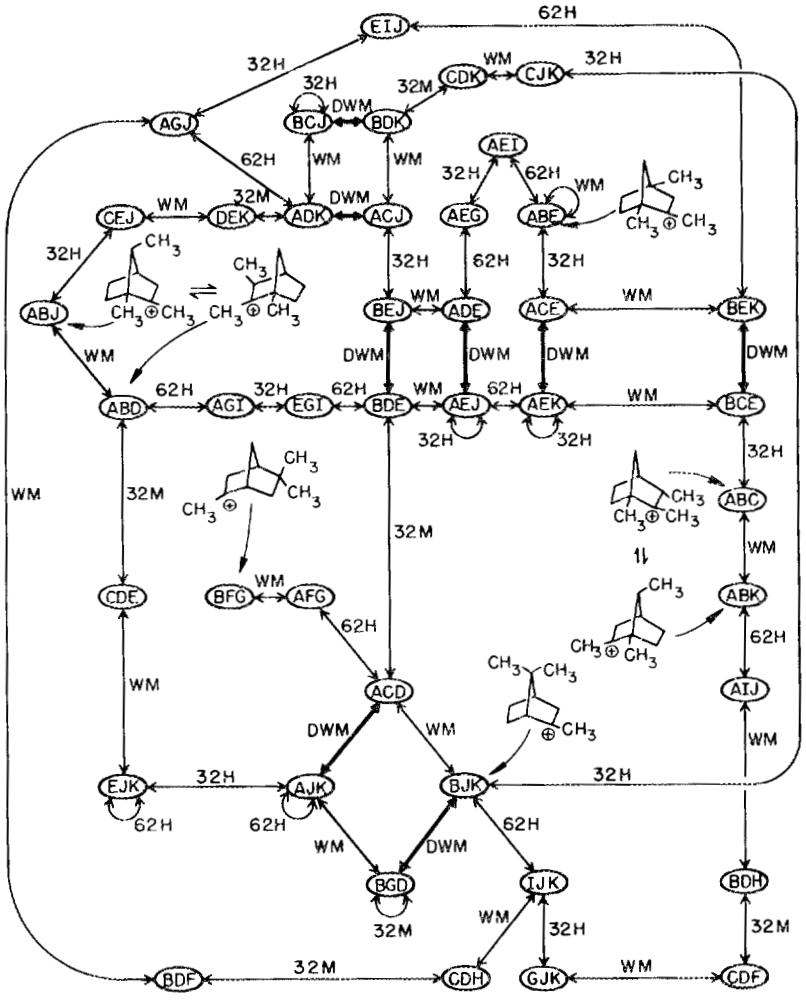

Chart II

confirmed[7] that WM, 62H; WM, 32M; WM; 62H; WM is the least-complicated series of interconversions not requiring *endo*-3,2 shifts.

Another contribution on combinatorial chemistry appears in Chap. 7 of this report.[8]

1. ORAU Predoctoral Fellow from the University of Tennessee, Knoxville.
2. C. K. Johnson, B. M. Benjamin, and C. J. Collins, *Chem. Div. Annu. Progr. Rep. May 20, 1972*, ORNL-4791, pp. 67–69; C. J. Collins and C. K. Johnson, *Chem. Div. Annu. Progr. Rep. May 20, 1973*, ORNL-4891, pp. 62–64.
3. C. J. Collins and C. K. Johnson, *J. Amer. Chem. Soc.* **95**, 4766 (1973); C. K. Johnson and C. J. Collins, *J. Amer. Chem. Soc.* **96**, 2514 (1974); C. J. Collins, C. K. Johnson, and V. F. Raaen, *J. Amer. Chem. Soc.* **96**, 2524 (1974).
4. H. Huang, K. Ranganayabula, and T. S. Sorensen, *J. Amer. Chem. Soc.* **94**, 1779, 1780 (1972).
5. R. Ranganathan et al., *Tetrahedron* **26**, 621 (1970).
6. C. K. Johnson and C. J. Collins, *J. Amer. Chem. Soc.* **96**, 2522 (1974).
7. J. A. Berson et al., *J. Amer. Chem. Soc.* 89, 2595 (1967).
8. C. K. Johnson, "The Representation Problem in Combinatorial Chemistry," chap. 7, this report.

PREPARATION OF CHARGE-TRANSFER COMPLEXES

V. F. Raaen Becky Wenzel[1]
C. R. Watson, Jr.[2]

As part of a study of conductivities and other physical properties of charge-transfer complexes (in collaboration with members of the ORNL Health Physics Division), we have synthesized the donor molecules heptafulvalene[3] and tetrathiafulvalene.[4] The complex of 1,3,1′,3′-tetrathiafulvalene (TTF) with 7,7,

8,8-tetracyanoquinodimethane (TCNQ)[5] was slowly recrystallized to provide crystals up to 1 cm in length, well suited to conductivity measurements. Similar complexes were formed between the acceptor molecule TCNQ and the donors 4,4′-diphenyltetrathiafulvalene and 4,4′,5,5′-tetraphenyltetrathiafulvalene.[6] TCNQ formed 1:1 complexes with benzene and with hexamethylbenzene; these adducts were given to C. K. Johnson for structure analysis by neutron spectroscopy.[7] Benzene and hexamethylbenzene also formed crystalline adducts with 1,3,5-trinitrobenzene; the complexes are stable in an atmosphere saturated with the hydrocarbon vapor.

Tetrathionaphthacene (TTN)[8] was synthesized, and the preparation or attempted preparation of charge-transfer complex crystals with the following electron acceptors is now under way: tetracyanoethylene (TCNE),[9] dichlorodicyanoquinone (DDQ),[5] chloranil,[10] and TCNQ.[5]

The synthesis of 7,7,8′,8′-tetracyanodiphenoquinodimethane[11] is nearly complete. Iodanil[12] and bromanil[12] have been prepared and will be tried, along with chloranil,[10] as electron acceptors in a variety of charge-transfer complexes.

1. ORAU Summer Student Trainee from the University of Northern Iowa, Cedar Falls.
2. Postdoctoral Fellow, University of Tennessee, Knoxville.
3. J. R. Mayer, Ph.D. dissertation, Yale University, New Haven, Conn., June 1955.
4. I. E. Klingsberg, *J. Amer. Chem. Soc.* **86**, 5290 (1964).
5. Aldrich Chemical Co.
6. These derivatives were kindly furnished by D. G. Doherty of the ORNL Biology Division.
7. See C. K. Johnson, H. L. Reed III, and R. F. Hall, "Neutron Diffraction Structural Studies of Two TCNQ-Complex Crystals, a Bifluoride Crystal, and a Norbornanone Crystal," chap. 7, this report.
8. C. Marschalk and C. Stumm, *Bull. Soc. Chim. Fr.* 427 (1948).
9. Eastman Kodak Co.
10. Matheson Coleman and Bell.
11. D. J. Sandman and A. F. Garito, *J. Org. Chem.* **39**, 1165 (1974).
12. C. L. Jackson and E. K. Bolton, *J. Amer. Chem. Soc.* **36**, 305 (1914).

^{14}C ISOTOPE EFFECTS DURING THE ADDITION OF DIPHENYLKETENE TO STYRENE

B. M. Benjamin John Zeigler[1]
C. J. Collins

The concerted nature of the addition of diphenylketene to styrene[2] to yield 2,2,3-triphenylcyclobutanone is indicated[3] by the fact that both styrene-α-d and styrene-β-d_2 undergo the reaction with sizable isotope effects [k_H/k_D = 1.23 (α) and 0.91 (β) per deuterium]. The perplexing result of Baldwin and Kapecki is that these two ratios, $(k_H/k_D)_\alpha$ and $(k_H/k_D)_\beta$, are in opposite directions.[4] The reaction is even more intriguing because it was at first believed[5] that the thermal ketone-olefin addition was disallowed by the orbital symmetry rules.[6]

For the foregoing reasons we have now studied the ^{14}C isotope effects in all four positions during the additions of styrene to diphenylketene. Styrene-α-^{14}C and styrene-β-^{14}C were prepared by standard methods,[7] as were diphenylketene-1-^{14}C and -2-^{14}C.[8] Three of the k/k^* ratios were determined by the method of competing reactions and the low-conversion approximation.[9] The results are shown in Fig. 5.1. The value k/k^* = 1.0055 ± 0.0005 for styrene-β-^{14}C was determined by examining the product at 93–100% reaction (r/r_0 = 1.062 ± 0.005), a procedure[10] associated with a much smaller error.

The theory of heavy-atom isotope effects has been discussed by Fry.[11] The Bigeleisen-Mayer expression[12] was invoked[11] to explain small, primary heavy-atom isotope effects, and the prediction that in favorable cases k/k^* could be less than unity was nicely confirmed by Kresge and his co-workers.[13] Three of the k/k^* ratios portrayed in Fig. 5.1 show that the labeled compounds react more slowly by 1% or less – values which are small for primary ^{14}C isotope effects.[11] In

ORNL-DWG. 74-4542

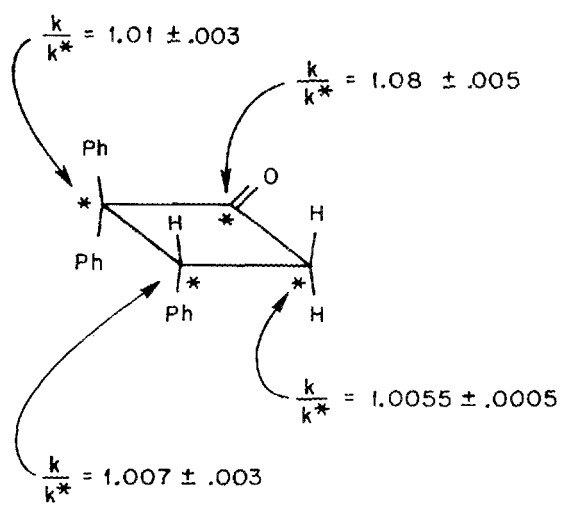

Fig. 5.1. Carbon-14 isotope effects in the addition of styrene to diphenylketene.

each case the hybridization change as the affected carbon proceeds from reactant to product is $sp^2 \rightarrow sp^3$. These three k/k^* ratios are all significantly smaller than those observed in the 1,3-dipolar additions of styrene to *N*,α-diphenylnitrone.[14,15]

The largest of the four ratios ($k/k^* = 1.081 \pm 0.005$) is for the carbonyl carbon of diphenylketene as its hybridization changes from *sp* to sp^2. It remains to be seen whether there is a general correlation between hybridization change and k/k^*.

1. Student participant in the Great Lakes Colleges Association Science Semester, fall 1973, from Wabash College, Crawfordsville, Ind.

2. H. Staudinger and E. Suter, *Ber. Deut. Chem. Ges.* **53**, 1092 (1920).

3. J. E. Baldwin and J. A. Kapecki, *J. Amer. Chem. Soc.* **92**, 4874 (1970).

4. A. Streitwieser, Jr., et al. [*J. Amer. Chem. Soc.* **80**, 232 (1958)] predicted that an inverse k_H/k_D ratio should result during an $sp^2 \rightarrow sp^3$ conversion from ground to transition state.

5. D. G. Fornum et al., *J. Amer. Chem. Soc.* **87**, 5191 (1965).

6. R. B. Woodward and R. Hoffman [*The Conservation of Orbital Symmetry*, pp. 163–68, Academic, 1970] point out that the *sp* hybridization of the carbonyl carbon in ketenes (and in vinyl cations) presents an additional factor not normally present in symmetry-disallowed thermal 2 + 2 additions.

7. G. A. Ropp, V. F. Raaen, and A. J. Weinberger, *J. Amer. Chem. Soc.* **75**, 3694 (1953).

8. The synthetic methods employed were: benzophenone-*carbonyl*-^{14}C ($LiAlH_4$) → benzhydrol-^{14}C ($SOCl_2$) → benzhydryl-^{14}C chloride [$Cu_2(CN)_2$] → diphenylaceto-2-^{14}C nitrile (aq H_2SO_4) → diphenylacetic-2-^{14}C acid ($SOCl_2$) → diphenylaceto-2-^{14}C chloride (Pr_3N) → diphenylketene-2-^{14}C. For the synthesis of diphenylketene-1-^{14}C, unlabeled benzhydryl chloride and $Cu_2(^{14}CN)_2$ were employed.

9. V. F. Raaen and C. J. Collins, *Pure Appl. Chem.* **8**, 347 (1964).

10. V. F. Raaen, G. A. Ropp, and H. P. Raaen, *Carbon-14*, pp. 56–57, McGraw-Hill, New York, 1968.

11. A. Fry, chap. 6 in *Isotope Effects in Chemical Reactions*, American Chemical Society Monograph No. 167, ed. by C. J. Collins and N. S. Bowman, Van Nostrand Reinhold Co., New York, 1971.

12. J. Bigeleisen and M. Goeppert-Mayer, *J. Chem. Phys.* **15**, 261 (1947).

13. A. J. Kresge, N. N. Lichtin, and K. N. Rao, *J. Amer. Chem. Soc.* **85**, 1210 (1963); A. J. Kresge et al., ibid. **87**, 437 (1965).

14. B. M. Benjamin and C. J. Collins, *J. Amer. Chem. Soc.* **95**, 6145 (1973).

15. R. Huisgen et al., *Chem. Ber.* **101**, 2548 (1968).

3,2-HYDRIDE SHIFT IN BICYCLIC COMPOUNDS

W. W. Schmidt[1] C. J. Collins

We reported earlier[2] on the relative rates of 6,2- and 3,2-hydride shifts in unsubstituted norbornyl cations during acetolysis. A puzzling observation in the course of that research[2] was that more ^{14}C originally in the 4 position of the cation finds its way to the 1 position (0.52%) than to the 2 position (0.33%). In an attempt to gain more information about this mechanistically important problem, we synthesized Δ^3-1-*d*-cyclopentenyl-2,2-dimethylethyl *p*-nitrobenzenesulfonate.[3] The ester was subjected to acetolysis conditions (acetic acid, 0.58 *m* in potassium acetate, 60°, 160 hr). In addition to the products isolated[3] by Chuit, the key product of 3,2-hydride shift, 6,6-dimethylbicyclo-[2.2.1]heptyl acetate must be searched for, found, and identified. It now remains to repeat the acetolysis on a larger scale, isolate the 6,6-dimethylbicyclo[2.2.1]-heptyl acetate, purify it, and determine (by NMR spectroscopy) the deuterium distribution in the compound.

1. ORAU Predoctoral Fellow from the University of Tennessee, Knoxville.

2. C. J. Collins and C. E. Harding, *J. Amer. Chem. Soc.* **92**, 1787 (1970); C. J. Collins and C. E. Harding, *Justus Liebigs Ann. Chem.* **745**, 124 (1971).

3. The method used was a modification, for deuterium incorporation, of the method of C. Chuit, *Tetrahedron* **28**, 4815 (1972).

DO S_N2 REACTIONS GO THROUGH ION PAIRS? THE ISOTOPE EFFECT CRITERION

V. F. Raaen F. J. Brown[1b]
Timothy Juhlke[1a] C. J. Collins

It has been suggested[2f] that all S_N2 reactions[3] proceed through ion pairs[2] and that borderline[3] solvolyses comprise competing S_N1 and S_N2 processes which occur through common intermediates. The experimental basis for this suggestion has been criticized by Schleyer and co-workers,[4] who failed to confirm the claim[2d,2f] that the rate of solvolysis of 2-octyl mesylate (25°, 25% dioxane, 75% water by volume) is "nearly independent of the concentration of sodium azide." Schleyer et al.[4] point out, additionally, that the Sneen-Larsen[2f] assumption of a positive salt effect is also open to question.

We have applied the isotope effect criterion[5-7] to the hydrolyses, in aqueous acetone solution, of ^{14}C-labeled benzyl chloride, *p*-methylbenzyl chloride, and 2-octyl brosylate. In addition, using modifications of the method previously reported by us,[6,7] in which ^{14}C was used as a tracer for determining the deuterium isotope effects by the low-conversion approximation,[8] we determined the α-deuterium isotope effects for the

Table 5.1. ^{14}C and α-deuterium isotope effects in the formation of carbinol and azide during hydrolyses in 80% aqueous acetone at 60°

Experiment	Reactant	Product	k/k^*	k_H/k_D[a]
1	$Ph\overset{*}{C}H_2Cl$	Benzyl alcohol	1.085 ± 0.007	
		Benzyl azide	1.130 ± 0.007	
2	$\overset{*}{Ph}CD_2Cl$[b]	Benzyl alcohol		1.003 ± 0.007
		Benzyl azide		1.033 ± 0.007
3	CH_3–⟨◯⟩–$\overset{*}{C}H_2Cl$	*p*-Methylbenzyl alcohol	1.061 ± 0.007	
		p-Methylbenzyl azide	1.096 ± 0.007	
4	CH_3–⟨◯⟩–$\overset{*}{C}D_2Cl$[c]	*p*-Methylbenzyl alcohol		0.996 ± 0.007
		p-Methylbenzyl azide		1.004 ± 0.007
5	$C_6H_{11}{}^*CH(OBs)CH_3$	2-Octanol	1.063 ± 0.007	
		2-Octyl azide	1.105 ± 0.007	
6	$C_6H_{11}CD(OBs)\overset{*}{C}H_3$[d]	2-Octanol		1.097 ± 0.007
		2-Octyl azide		1.106 ± 0.007

[a] k_H/k_D per atom of deuterium.
[b] Carbon-14 label, indiscriminate in ring.
[c] k_H/k_D corrected for k/k^*.
[d] Carbon-14 in methyl group. Secondary ^{14}C isotope effect assumed to be within experimental error.

conversions of these same reactants.[9] *Both primary ^{14}C and α-deuterium isotope effects were determined during formation of both carbinol and azide.* The results are displayed in Table 5.1, from which the following important conclusions are derivable: (1) The hydrolyses of benzyl and *p*-methylbenzyl chlorides exhibit high ^{14}C isotope effects and low α-deuterium isotope effects, results consistent with a classic S_N2 transition state. The extremely high k/k^* ratios require that carbon atom motion must be a strong feature of the reaction coordinate; they signify as well that the transition states must be nearly symmetrical.[10,11] Neither of these features is compatible with a mechanism in which nucleophilic attack on an ion pair occurs.[12] The higher k/k^* values for azide vs carbinol formation are also intelligible through the Fry[10,11] and Sims[11] calculations, the more nucleophilic azide ion increasing the bond order of the new bond and thus the ratio k/k^*. The extremely low α-D isotope effects strongly support the above picture of a classic S_N2 reaction[3,13] proceeding through a normal pentacoordinate transition state, *require* strong bonding in the transition state, and offer no support at all for the intervention of ion pairs.

Turning now to k/k^* and k_H/k_D for the 2-octyl brosylates (experiments 5 and 6 in Table 5.1), it is clear that the results are consistent with competing classical S_N1 and S_N2 processes.[14] The k_H/k_D values (Table 5.1, experiment 6) are considerably larger than the others in Table 5.1, but still far below the maximum[15] to be expected for an S_N1 process.[16] The k/k^* ratios are considerable and indicate a strong competing classic S_N2 component in the reaction. Such high primary ^{14}C isotope effects are unintelligible on the basis of the Sneen mechanism; for the calculations of Sims and Fry,[11] as well as the Bigeleisen-Mayer relation,[12] require that a highly unsymmetrical transition state,[11] or one stabilized by carbocation resonance[12] – that is, the type of transition state expected for ion-pair formation – should exhibit k/k^* values much closer to unity.[17]

1. Student participants in the Great Lakes Colleges Association Science Semester, fall 1972. (*a*) From Wabash College, Crawfordsville, Ind.; (*b*) from Kalamazoo College, Kalamazoo, Mich.

2. (*a*) A. Weiner and R. A. Sneen, *J. Amer. Chem. Soc.* **87**, 287, 292 (1965); (*b*) A. Streitwieser, Jr., T. D. Walsh, and J. R. Wolfe, Jr., ibid. **87**, 3682 (1965); (*c*) A. Streitwieser, Jr., and T. D. Walsh, ibid. **87**, 3686 (1965); (*d*) R. A. Sneen and J. W. Larsen, ibid. **88**, 2593 (1966); (*e*) R. A. Sneen, J. V. Carter, and P. S. Kay, ibid. **88**, 2594 (1966); (*f*) R. A. Sneen and J. W. Larsen, ibid. **91**, 362, 6031 (1969); (*g*) J. A. Cramer and J. G. Jewett, ibid. **94**, 1377 (1972).

3. C. K. Ingold, *Structure and Mechanism in Organic Chemistry*, Cornell University Press, Ithaca, N.Y., 1969.

4. D. J. Raber et al., *J. Amer. Chem. Soc.* **93**, 4821 (1971); D. J. Raber, J. M. Harris, and P. von R. Schleyer, ibid. **93**, 4829 (1971). See also D. Kovačević et al., *Tetrahedron* **28**, 2469 (1972).

5. (*a*) The prediction that heavy-atom isotope effects (^{13}C and ^{14}C) should be large in S_N2 reactions and small in S_N1, whereas α-deuterium isotope effects should be small in S_N2 and large in S_N1 reactions, was tentatively suggested by A. Streitwieser, Jr., *Solvolytic Displacement Reactions*, McGraw-Hill, New York, N.Y., 1962, pp. 172–74. (*b*) The subsequent validity of this prediction and the experimental and theoretical bases for the isotope effect criterion are to be found in *Isotope Effects in Chemical Reactions,* American Chemical Society Monograph No. 166, ed. by C. J. Collins and N. S. Bowman, Van Nostrand Reinhold Co., New York, N.Y., 1971, chap. 1, by A. W. Van Hook, pp. 23–27; chap. 2, by V. J. Shiner, Jr., pp. 104–35; and chap. 6, by A. Fry, pp. 377–86.

6. V. F. Raaen et al., *J. Amer. Chem. Soc.* **85**, 3497 (1963).

7. V. F. Raaen and C. J. Collins, *Pure Appl. Chem.* **8**, 347 (1964).

8. V. F. Raaen, G. A. Ropp, and H. P. Raaen, *Carbon-14,* p. 56, McGraw-Hill, New York, N.Y., 1968.

9. The benzyl-α-^{14}C and benzyl-*phenyl*-^{14}C chlorides, as well as the ^{14}C-labeled *p*-methylbenzyl chlorides, were prepared by standard methods (A. Murray III and D. L. Williams, *Organic Syntheses with Isotopes,* Part I, pp. 75, 94, Interscience, New York, 1958. Carbon-14-labeled 2-octanols were synthesized using *n*-hexylmagnesium bromide and acetyl-1-^{14}C or acetyl-2-^{14}C chloride, followed by reduction of the ketones so obtained with lithium aluminum hydride or deuteride. The azides were reduced to the amines with lithium aluminum hydride and assayed as the crystalline benzoates. All ^{14}C assays were performed by the Tolbert method (ref. 8).

10. A. Fry, *Pure Appl. Chem.* **8**, 409 (1964).

11. L. B. Sims et al., *J. Amer. Chem. Soc.* **94**, 1364 (1972).

12. The correspondence between experiment and theory for a heavy-atom (^{13}C) isotope effect during a reaction whose transition state closely resembles a highly resonance-stabilized carbonium ion has been successfully demonstrated by A. J. Kresge, N. N. Lichtin, and K. N. Rao, *J. Amer. Chem. Soc.* **85**, 1210 (1963), and A. J. Kresge et al., ibid. **87**, 437 (1965), who found $k/k^* < 1$ for the ionization of trityl chloride. According to the Bigeleisen-Mayer expression [J. Bigeleisen and M. Goeppert-Mayer, *J. Chem. Phys.* **15**, 261 (1947)], the additional bonding in the transition state caused by the strong resonance stabilization of the incipient triphenylmethyl cation shows up as a subtractive $G(u^{\ddagger})\ \Delta u^{\ddagger}$ term, thus reducing k/k^* below unity.[5b]

13. The data in Table 5.1 are completely consistent with the α-*d* isotope effects and the kinetic data of A. V. Willi, Chih-Kuo Ho, and A. Ghanbarpour, *J. Org. Chem.* **37**, 1185 (1972), for the hydrolyses of benzyl and *p*-methylbenzyl chlorides in 55% (by volume) aqueous methyl Cellosolve.

14. Because of experimental difficulties, we were unable to determine isotope effects under the exact conditions used by previous investigators.[2] For solvolysis of the 2-octyl brosylates we used 80% aqueous acetone (80% acetone, 20% water by volume) at 60°, 0.43 *M* in brosylate. Because of the generality of the Sneen-Larsen claim,[2f] however, this is not a serious problem.

15. J. M. Harris, R. E. Hall, and P. von R. Schleyer, *J. Amer. Chem. Soc.* **93**, 2251 (1971); V. J. Shiner, Jr., and R. D. Fisher, ibid. **93**, 2554 (1971).

16. It must be remembered that the magnitude of k_H/k_D for an α-deuterium label depends upon the nature of the leaving group [V. J. Shiner, Jr., and W. Dowd, *J. Amer. Chem. Soc.* **93**, 1029 (1971)]; see also V. J. Shiner, Jr., ref. 5, above.

17. They also exclude, in our opinion, Sneen's latest definition [R. A. Sneen, *Accounts Chem. Res.* **6**, 52–53 (1973)] of an ion pair:

"Considerable polarization of the electron density of the anionic component toward the cationic component must exist; this will be recognized as the essence of the covalent bond. An alternative to the name, 'ion pair,' might be 'extended covalent bond.' But this would tend to deemphasize too strongly the charge separation which undoubtedly exists.

"We will continue to use the term ion pair, but we would hope that the organic chemical public would recognize that the situation is perhaps better described as 'an extended bond with considerable ionic character.' "

PREPARATION OF BUTYL NITRATE

W. H. Baldwin W. E. Clark[1]

Butyl nitrate is required for studies associated with the processing of reactor fuels. We have developed a method of synthesis, based on earlier observations, that has definite advantages over the classical reaction of an alcohol with nitric acid.

It was found possible to confine the reactions between metal nitrates and tributyl phosphate to the endothermic reaction that liberates butyl nitrate. For example, the reaction between lithium nitrate and tributyl phosphate gives good yields (over 75%) of butyl nitrate of good purity. A minimum effort is being continued to define the scope and limitations of this reaction.

1. Chemical Technology Division.

6. Physical Chemistry

Our work in physical chemistry is greatly expanded over previous years because of the addition of many programs from the former Reactor Chemistry Division. The research is greatly augmented in the study of molten salts, especially fluoride systems because of continued effort on the molten-salt breeder reactor concept, and in aqueous solutions of electrolytes over wide ranges of temperature and pressure. The combined effort has strong representation in the areas of heterogeneous and homogeneous equilibria with systems ranging from those of applied interest to those that are models that permit development of a more fundamental understanding of underlying theory. Our electrochemical interests range from the analysis, removal, and recovery of a host of elements in solution to studies of transport phenomena and corrosion. Advanced filtration techniques continue to show great applicability to many pressing problems, while the more newly initiated studies of adsorption on activated carbon continue to demonstrate the fascinating properties of this material.

AQUEOUS SYSTEMS

PROBLEMS ENCOUNTERED IN DERIVING ACTIVITY COEFFICIENT VALUES FROM DATA ON MIXED ELECTROLYTE SYSTEMS[1]

M. H. Lietzke R. W. Stoughton

We have considered the various types of problems that may be encountered in deriving activity coefficient values from data on mixed electrolyte systems. The most serious of these problems, and one which may lead to very poor values of the activity coefficient of at least one component in a mixture, involves the degree of statistical correlation between the parameters of the mathematical representation (or model) used in fitting experimental activity coefficient data on mixed electrolyte systems. This problem is by no means specific to activity coefficients but may be encountered whenever members from two sets of correlated parameters are combined to compute some desired quantity and not all of the members from each set are used in the calculation. The problem is not encountered in the case of mixed electrolyte systems when osmotic coefficients are measured and fitted, since *all* the parameters estimated in fitting the osmotic coefficients are used in computing the activity coefficient of each component in the mixture.

Another problem that may be encountered in calculating activity coefficient values in mixed electrolyte systems is as follows: when several different treatments are used in fitting the data, it is often observed that the values of the activity coefficients are sensitive to the method of calculation used. For example, values of the activity coefficient of NaCl in HCl-NaCl mixtures may differ by as much as 1% or more, depending upon whether they were obtained by cross differentiation[2] or by application of the "neutral electrolyte" treatment[3] to HCl-NaCl mixture data.[4] This makes it impossible to state, for example, whether the activity coefficient of NaCl at 10°C in a 50:50 mixture at $I = 1.0$ is 0.700 or 0.709.[4] It has also been shown[5] that similar results are obtained when the "neutral electrolyte" treatment and an ion-component treatment[6] are applied to the same set of mixture data by the method of least squares. The differences may partly result from a difference in weighting when attention is focused on the ions as components or on the electrolytes themselves. In addition, any approximations made in the derivation of the various models may manifest themselves differently and result in slight differences in the predicted values of

the activity coefficients of the components of a mixture.

In view of the difficulties associated with treating thermodynamic data on mixed electrolyte systems, the following recommendations are made. Whenever possible, osmotic coefficient data should be used for calculating the activity coefficient values of each component in mixed electrolyte systems, because, as mentioned above, all the parameters obtained in the fit of the osmotic coefficients are used in calculating the activity coefficients, and the problem of statistical correlation between the parameters does not arise. If activity coefficient data must be used and parameters from two different least-squares fits must be combined, then activity coefficient values for each component in the mixtures should also be predicted using one of several proposed models[5-7] If much disparity is observed between the predicted values and values calculated from the parameters of the least-squares fits, then the matrix of correlation coefficients (calculated from the elements of the least-squares inverse matrix) should be examined. If large correlations between any of the parameters are observed, then the predicted values are to be preferred as estimates of the activity coefficients of the components of the mixture.

1. An abbreviated version of part of paper accepted for publication in the *Journal of the Tennessee Academy of Science.*

2. N. Bjerrum, *Z. Phys. Chem.* (Leipzig) **104**, 406 (1923).
3. G. Scatchard, *J. Amer. Chem. Soc.* **82**, 2636 (1961).
4. M. H. Lietzke and R. W. Stoughton, *J. Tenn. Acad. Sci.* **39**, 30 (1964).
5. M. H. Lietzke and R. W. Stoughton, *J. Solution Chem.* **1**, 299 (1972).
6. G. Scatchard, R. M. Rush, and J. S. Johnson, *J. Phys. Chem.* **74**, 3786 (1970).
7. P. J. Reilly, R. H. Wood, and R. A. Robinson, *J. Phys. Chem.* **75**, 1305 (1971).

THE STANDARD POTENTIAL OF THE Ag, AgBr ELECTRODE IN DBr SOLUTIONS[1]

M. H. Lietzke T. J. Lemmonds[2]

Although the standard potential of the Ag, AgBr electrode has been measured[3,4] over a wide range of temperature in HBr solution, it appears that the standard potential in the corresponding deuterated medium has not previously been determined. Accordingly, we have investigated the cell

$$\mathrm{Pt} - \mathrm{D_2}(p = 1)|\mathrm{DBr}(m) \text{ in } \mathrm{D_2O}|\mathrm{AgBr, Ag}$$

in the temperature range 20°–75° using DBr solutions whose composition varied between ca. 0.005 and 0.1 m. From these data the standard potential of the cell and the thermodynamic properties of the DBr solutions (in D_2O) have been computed.

Values of the standard potential E° of the cell are given in Table 6.1. Values calculated on a molal basis are shown in columns A and B, while values expressed on an equal-moles-of-solvent (aquamolal) basis are given in columns A′ and B′. For comparison, values of the standard potential of the corresponding protonated cell are shown in the last two columns of the table.

Table 6.1. The standard potential E° of the cell

$\mathrm{Pt} - \mathrm{D_2}(p = 1)|\mathrm{DBr}(m)|\mathrm{AgBr, Ag}$

t (°C)	A[a]	B[b]	A′[a]	B′[b]	HBr[c]	HBr[d]
20	0.06314	0.06313	0.06807	0.06824	0.07340	
25	0.06014	0.06014	0.06515	0.06534	0.07103	0.0712
30	0.05706	0.05707	0.06215	0.06235	0.06845	
35	0.05391	0.05391	0.05908	0.05928	0.06575	
40	0.05067	0.05067	0.05592	0.05612	0.06292	
45	0.04734	0.04735	0.05269	0.05289	0.05997	
50	0.04395	0.04395	0.04937	0.04957	0.05687	
55	0.04048	0.04048	0.04599	0.04618	0.05363	
60	0.03693	0.03692	0.04251	0.04271	0.05031	0.0499
65	0.03330	0.03329	0.03896	0.03916		
70	0.02959	0.02958	0.03533	0.03554		
75	0.02579	0.02580	0.03161	0.03184		

[a]Values obtained by extrapolation at each temperature separately.
[b]Values obtained by fitting all data at all temperatures and molalities simultaneously.
[c]Harned et al., ref. 3.
[d]Towns et al., ref. 4.

Table 6.2. Values of the logarithms of the activity coefficient of DBr on an equal-moles-of-solvent basis

t (°C)	$m = 0.005^a$	$m = 0.01$	$m = 0.02$	$m = 0.05$	$m = 0.1$
20	$\bar{1}.9658$	$\bar{1}.9536$	$\bar{1}.9378$	$\bar{1}.9109$	$\bar{1}.8863$
25	$\bar{1}.9655$	$\bar{1}.9532$	$\bar{1}.9373$	$\bar{1}.9102$	$\bar{1}.8855$
30	$\bar{1}.9653$	$\bar{1}.9528$	$\bar{1}.9368$	$\bar{1}.9096$	$\bar{1}.8849$
40	$\bar{1}.9647$	$\bar{1}.9521$	$\bar{1}.9359$	$\bar{1}.9086$	$\bar{1}.8841$
50	$\bar{1}.9641$	$\bar{1}.9513$	$\bar{1}.9350$	$\bar{1}.9078$	$\bar{1}.8838$
60	$\bar{1}.9635$	$\bar{1}.9506$	$\bar{1}.9342$	$\bar{1}.9072$	$\bar{1}.8840$
70	$\bar{1}.9628$	$\bar{1}.9498$	$\bar{1}.9334$	$\bar{1}.9067$	$\bar{1}.8845$

[a]Molality of DBr.

Representative values of the logarithm of the activity coefficient of DBr on an equal-moles-of-solvent basis are shown in Table 6.2. These values are all lower than the corresponding values in the protonated system, averaging 0.22% lower in 0.005 m solution, 0.40% lower in 0.01 m solution, 0.55% lower in 0.02 m solution, 1.0% lower in 0.05 m solution, and 1.5% lower in 0.1 m solution. Examination of the corresponding activity coefficient values in the chloride system reveals that the activity coefficient of the deuterated compound (DCl in D_2O) is in each case very nearly the same percent lower than that of the protonated compound (HCl in H_2O) at the same aquamolality value.

1. An abbreviated version of part of paper accepted for publication in the *Journal of Inorganic and Nuclear Chemistry.*
2. Graduate student, University of Tennessee, Knoxville.
3. H. S. Harned, A. S. Keston, and J. G. Donelson, *J. Amer. Chem. Soc.* 58, 989 (1936).
4. M. B. Townes, R. S. Greeley, and M. H. Lietzke, *J. Phys. Chem.* 64, 1861 (1960).

THE HYDROLYSIS OF CATIONS: A CRITICAL REVIEW OF HYDROLYSIS SPECIES AND THEIR STABILITY CONSTANTS IN AQUEOUS SOLUTION[1]

C. F. Baes, Jr. R. E. Mesmer

Hydrolysis reactions, which may generally be represented

$$xM^{z+} + yH_2O \rightleftharpoons M_x(OH)_y^{(xz-y)+} + yH^+ ; \quad (1)$$

$$Q_{xy} = \left[M_x(OH)_y^{(xz-y)+}\right] [H^+]^y / [M^{z+}]^x ,$$

are common to most cations. Because of the number and diversity of the hydroxide complexes which can be formed in solution, the resulting chemical behavior of a given metal in a given valence can be a complicated function of pH and concentration and – if the identity and stability of the hydrolysis products are not known – quite unpredictable. Consequently there is a general need for sound knowledge of hydrolysis reactions in order to deal with the chemical behavior of the metallic elements in aqueous solution; our particular concern is the necessity of such information which often arises in AEC-supported programs and in the NSF/RANN-supported programs at ORNL and elsewhere.

The variety and complexity of the hydrolysis products of metal cations have made reliable information difficult to obtain experimentally and have produced a rather large and conflicting literature in which the truth often lies hidden. We have undertaken to review this literature, first to bring together the reliable information concerning the identity and stability of the various hydrolysis products that are formed in solution, and then to gain therefrom some understanding of why cations produce such a variety of hydrolysis products. At this stage in the review, we feel the first objective can be accomplished satisfactorily, but the extent to which understanding can be gained remains to be seen.

The review is now approximately two-thirds complete. It includes reviews of the methods of measurement, the interpretation of the data, and the hydrolysis of the cations of the pre-transition and post-transition elements. The elements remaining to be reviewed include the lanthanides, the actinides, and the transition metals. For each hydrolyzing species an attempt has been made to determine those hydrolysis products which have been well established, to tabulate their formation quotients (Q_{xy}) in various media, and to estimate their formation constants (K_{xy}) at zero ionic strength. Included, as well, are similar data on the solubility of their hydroxides or oxides.

Mononuclear Hydrolysis Products

Almost without exception, metal ions (M^{z+}) produce mononuclear hydrolysis products in solution, usually a series of hydroxide complexes

$$MOH^{(z-1)+}, M(OH)_2^{(z-2)+}, M(OH)_3^{(z-3)+} \ldots .$$

In most cases this series includes at least one anionic species that causes the hydroxide or oxide precipitate to be at least slightly amphoteric (Fig. 6.1).

The stability of the initial hydrolysis product generally increases as the charge on the cation (z) increases and as the radius of the cation (r) decreases. Pre-transition-metal cations show a fairly smooth increase of log K_{11} with z^2/r. In general the post-transition-metal cations exhibit considerably higher values of K_{11}.

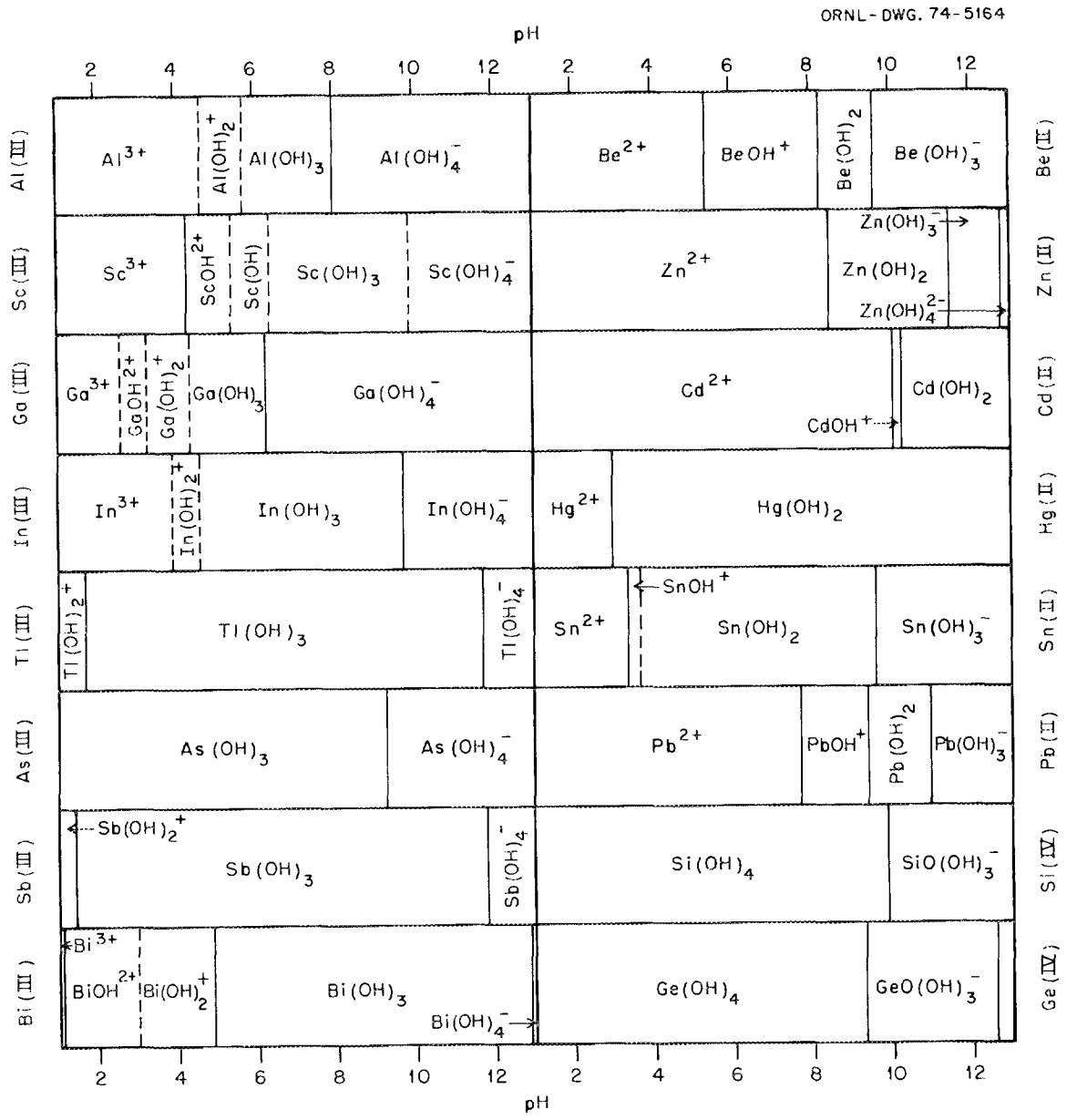

Fig. 6.1. Predominance diagrams for mononuclear hydrolysis products. The boundaries indicate pH values at which adjacent species occur at equal concentrations. In most cases the mononuclear species will dominate over polynuclear species only if the total metal concentration is quite low (e.g., less than 10^{-3} M).

The addition of successive OH^- ligands to a hydrolyzing cation generally is accompanied by a decrease in the stepwise equilibrium quotient

$$Q_y = \frac{Q_{1,y+1}}{Q_{1,y}} = \frac{\left[M(OH)_{y+1}{}^{(z-y-1)+}\right]\ [H^+]}{\left[M(OH)_y{}^{(z-y)+}\right]}, \quad (2)$$

typically by about one logarithm unit per step. There are numerous exceptions, however, again mostly among the post-transition-metal ions. The most notable exceptions are the unusually stable neutral species of certain post-transition elements: $Au(OH)_3$, $In(OH)_3$, $Tl(OH)_3$, $Sb(OH)_3$, $Bi(OH)_3$, $Hg(OH)_2$, $Sn(OH)_2$, which are stable over wide ranges of pH (typically 6 units) which usually include the neutral pH region (Fig. 6.1).

Polynuclear Hydrolysis Products

Among polyvalent cations, hydrolysis species containing more than one metal ion are the rule rather than the exception. Such species not only cause difficulty in characterizing hydrolysis reactions, they also restrict the stability of the mononuclear species to quite dilute solutions (typically less than 10^{-4} *M*) where the latter can be studied only by solubility or extraction techniques. The most commonly occurring polynuclear species are summarized in Table 6.3. It is noteworthy that Δz^2 for the corresponding formation reaction

$$\Delta z^2 = (xz - y)^2 + y^2 - xz^2$$

is a fairly small number. In addition to these species, a few larger species are formed; these include $Al_{13}O_4(OH)_{24}{}^{7+}$ and $Bi_6(OH)_{12}{}^{6+}$.

As the review proceeds, trends in the stabilities of the polynuclear hydrolysis products will perhaps become apparent. For the present, we note that, unlike the decreasing stability exhibited by successive mononuclear species, the stability of polynuclear species usually is such that they form readily from the initial hydrolysis product $MOH^{(z-1)+}$. Thus the equilibrium constant for the reaction

$$yMOH^{(z-1)+} \rightleftharpoons M_x(OH)_y{}^{(xz-y)+} + (y-x)M^{z+}, \quad (3)$$

$K_{xy}/K_{11}{}^y$, is almost always greater than unity (Fig. 6.2). All three species in this equilibrium can occur at equal concentrations when

$$[M^{z+}] = [MOH^{(z-1)+}]$$
$$= [M_x(OH)_y{}^{(xz-y)+}] \cong (K_{11}{}^y/K_{xy})^{1/(x-1)}.$$

(This is an approximation because we are neglecting activity coefficients.) With the exception of the relatively unstable M_2OH^{3+} species, all the polynuclear

Table 6.3. Polynuclear hydrolysis products

Species	Δz^2, reaction (1)	Cations
M_2OH^{3+}	2	Be^{2+}, Zn^{2+}, Cd^{2+}, Hg^{2+}, Pb^{2+}
$M_2(OH)_2{}^{2+}$	−2	Cu^{2+}, Sn^{2+}
$M_3(OH)_3{}^{3+}$	0	Be^{2+}, Hg^{2+}
$M_3(OH)_4{}^{2+}$	−4	Sn^{2+}, Pb^{2+}
$M_4(OH)_4{}^{4+}$	+4	Mg^{2+}, Cd^{2+}, Pb^{2+}
$M_6(OH)_8{}^{4+}$	0	(Be^{2+}), Pb^{2+}
$M_2(OH)_2{}^{4+}$	0	Al^{3+}, Sc^{3+}
$M_3(OH)_4{}^{5+}$	2	Al^{3+}, (In^{3+})

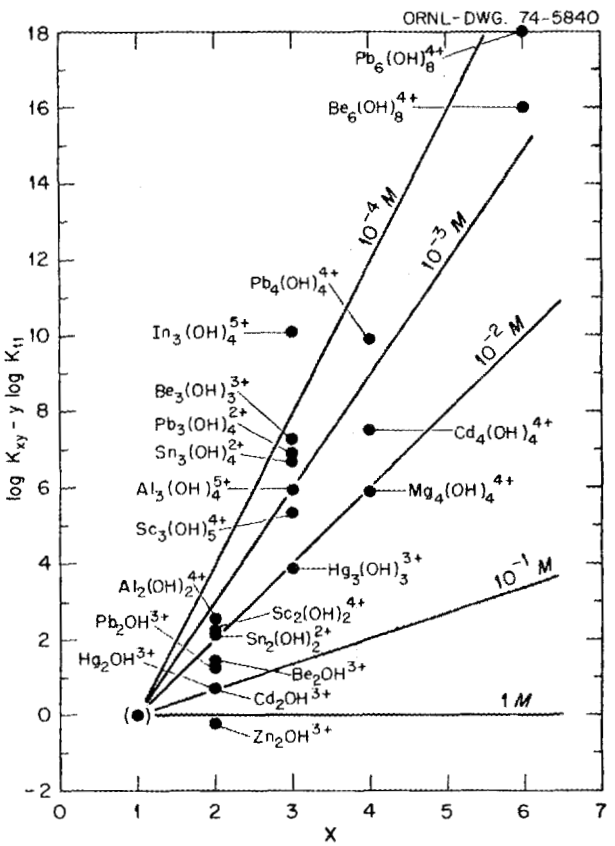

Fig. 6.2. The equilibrium constant for reaction (3) as a function of the degree of polymerization of the polynuclear hydrolysis product. The straight lines indicate minimum concentrations of the unhydrolyzed cation at which a polynuclear species can become the dominant hydrolysis product.

species for which $\log (K_{xy}/K_{11}{}^{y})$ is plotted vs x in Fig. 6.2 give $(K_{11}{}^{y}/K_{xy})^{1/(x-1)}$ values less than 0.01. From this it is evident that in these cases, polynuclear species can become dominant when the concentration of the unhydrolyzed cation is no more than 0.01 M.

1. This contribution is based on a review begun as a spare-time project of the authors. More recently, support has come in part from the National Science Foundation's RANN-EATC Program, the College of William and Mary, and the USAEC. This summary is based on two parts of a three-part report (ORNL-NSF-EATC-3: Part I, January 1973; Part II, in press). According to present plans, the completed review will be published as a book by John Wiley, Inc.–Interscience Publishers. The authors were formerly members of the Reactor Chemistry Division, now of the Chemistry Division.

PHOSPHORIC ACID DISSOCIATION EQUILIBRIA IN AQUEOUS SOLUTIONS TO 300°C[1]

R. E. Mesmer C. F. Baes, Jr.

The dissociation equilibria of phosphoric acid are important in many areas of chemistry and geochemistry, but these reactions have not been adequately determined at temperatures above 60°C. Using a recently developed potentiometric technique for precise acidity measurements, we have studied the dissociation equilibria in dilute phosphoric acid solutions in KCl media to 1 m and to 300°C. The utility and precision of this technique using a hydrogen electrode concentration cell have been previously demonstrated by measurements on the dissociation equilibria of water itself[2] and of boric acid[3] and also in the evaluation of transport numbers for hydrochloric acid to 200°C.[4]

A mathematical expression was fitted to the data in order to provide a means of smoothing and for interpolation and extrapolation to practical conditions. Also, this enables one to derive the thermodynamic data associated with the reactions analytically as well as to test the form of classical models which have served well for the analysis of data at low temperatures. The more accurate data which were previously reported over the 0 to 60°C temperature range at low ionic strengths were combined with the data of Fig. 6.3 for this purpose.

First neutralization. The following expression represents the data for $\log Q_1$ (Fig. 6.3*a*), including the data of Bates,[5] for the first neutralization reaction,

$$H_3PO_4 + OH^- \rightleftharpoons H_2PO_4^- + H_2O ,$$

with an agreement factor of 0.8:

$$\log Q_1 = 1.76558 \times 10^4/T + 39.4277 \ln_e T - 0.0325405T - 8.10134 \times 10^5/T^2 - 253.198 + 0.152147I + 0.00105195IT + 0.140119I^{3/2} - 0.0013143TI^{3/2} .$$

The reaction is accompanied by no change in the charges on the reactants and products, and therefore a small ionic strength effect is expected, just as in the case of boric acid. The change in $\log Q$ in going from infinite dilution to ionic strength of unity is only 0.2 at 25°C and 0.1 at 300°.

Second neutralization. The second neutralization reaction,

$$H_2PO_4^- + OH^- \rightleftharpoons HPO_4^{2-} + H_2O ,$$

is somewhat more accurately determined since the free hydrogen and hydroxide concentrations are small over most of the conditions studied. Using our data for $\log Q_2$ (Fig. 6.3*b*) along with the data of Bates and Acree,[6] the following expression was obtained:

$$\log Q_2 = \frac{1.71569 \times 10^4}{T} + 37.7345 \ln_e T - 3.22082 \times 10^{-2}T - 8.97579 \times 10^5/T^2 - 246.045 + \frac{2AI^{1/2}}{1 + (-0.110812 + 0.0113329T)A'I^{1/2}} - 0.525884I + 0.0019989IT + 0.453717I^{3/2} - 0.00140089TI^{3/2} ,$$

where

$$A = -2.97627 + 4.80688 \times 10^{-2}T - 2.69280 \times 10^{-4}T^2 + 7.49524 \times 10^{-7}T^3 - 1.02352 \times 10^{-9}T^4 + 5.58004 \times 10^{-13}T^5$$

and

$$A' = 0.4125A^{1/3} .$$

Here A is the Debye-Hückel coefficient expressed as a power series in T for convenience. In this treatment, 11 parameters have been evaluated by least squares, and the agreement factor obtained was 1.3. This is the same form as was previously employed to fit data on the

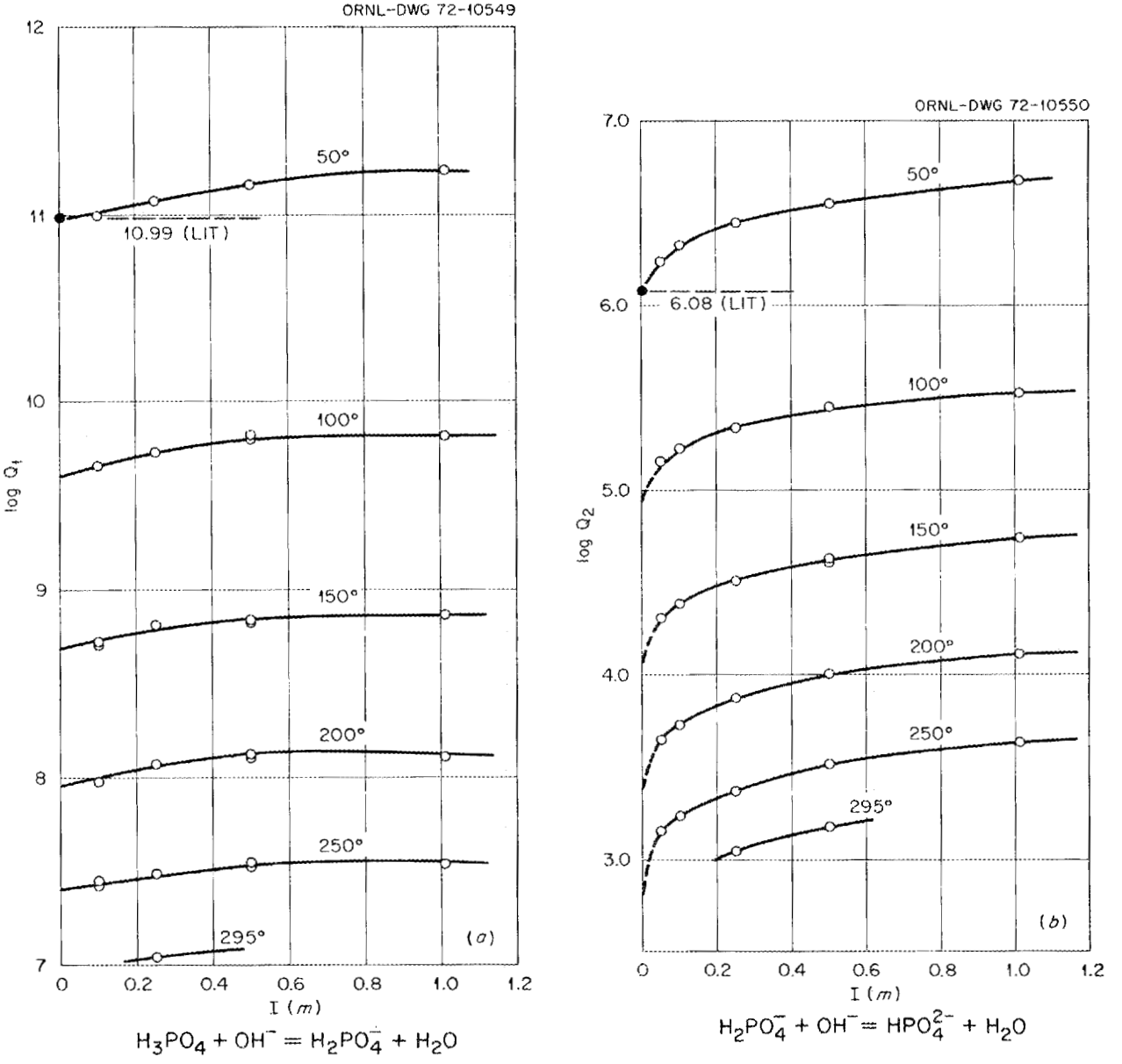

Fig. 6.3. Stepwise neutralization quotients for phosphoric acid. (*a*) The dependence of log Q_1 for the neutralization of the first proton of H_3PO_4 on ionic strength and temperature in KCl media. (*b*) The dependence of log Q_2 for the neutralization of the second proton of H_3PO_4 on ionic strength and temperature in KCl media.

dissociation of water, where Δz^2 was also equal to 2; Δz^2 is defined as the difference in value of the sum of nz^2 of the products and that of the reactants, where n is the number of moles of ionic species of valence z. The magnitude of the salt effect on this equilibrium is compared in Table 6.4 with that found for the dissociation of H_2O in KCl and also with that reported by Liu and Lindsay[7] for the square of the mean activity coefficient of NaCl in NaCl media. The quantity

$$\gamma_{HPO_4^{2-}} a_{H_2O} / \gamma_{H_2PO_4^-} \gamma_{OH^-}$$

was divided by a_{H_2O} and $\gamma_{H^+}\ \gamma_{OH^-}/a_{H_2O}$ was multiplied by a_{H_2O} to obtain the quantities tabulated. These data indicate that there is probably no significant difference at $I = 0.1$ in these values except possibly at 300°C, where their uncertainty is greatest (probably 0.04 unit). At an ionic strength of unity, more significant deviations are seen at 100° to 150°C and also at 300°C.

1. Abstracted from paper submitted for publication in *J. Solution Chemistry*. Work performed in the Reactor Chemistry Division.

Table 6.4. Values for activity coefficient ratios for three similar cases:

case A, $\log (\gamma_{H^+}\gamma_{OH^-})_{KCl}$;

case B, $\log [\gamma_{HPO_4^{2-}}/(\gamma_{H_2PO_4^-}\gamma_{OH^-})]_{KCl}$;

case C, $\log (\gamma^2_{\pm NaCl})_{NaCl}$

T (°C)	$I = 0.1$			$I = 1.0$		
	Case A	Case B	Case C	Case A	Case B	Case C
100	−0.26	−0.28	−0.25	−0.37	−0.62	−0.42
150	−0.31	−0.31	−0.30	−0.47	−0.68	−0.51
200	−0.37	−0.35	−0.36	−0.63	−0.74	−0.65
250	−0.48	−0.40	−0.44	−0.89	−0.81	−0.85
300	−0.65	−0.48	−0.59	−1.33	−0.90	−1.17

2. F. H. Sweeton, R. E. Mesmer, and C. F. Baes, Jr., *J. Solution Chem.* **3**, 191 (1974).
3. R. E. Mesmer, C. F. Baes, Jr., and F. H. Sweeton, *Inorg. Chem.* **11**, 537 (1972).
4. D. D. MacDonald and D. Owen, *Can. J. Chem.* **51**, 2747 (1973).
5. R. G. Bates, *J. Res. Nat. Bur. Stand.* **47**, 127 (1951).
6. R. G. Bates and S. F. Acree, *J. Res. Nat. Bur. Stand.* **30**, 129 (1943); **34**, 373 (1945).
7. C. Liu and W. T. Lindsay, *J. Solution Chem.* **1**, 45 (1972).

HIGH-TEMPERATURE EQUILIBRIA IN LIGHT AND HEAVY WATER[1]

R. E. Mesmer B. F. Hitch[2] D. Herting[3]

Experimental work has been completed on studies of the dissociation equilibria in several important buffering systems at high temperatures: NH_3 and amines (cyclohexylamine and morpholine) in light water, and D_2O itself and $D_2PO_4^-$ in heavy water.

Ammonia. Ammonia is used in nuclear-reactor and boiler applications for pH control at high temperatures. The dissociation equilibrium

$$NH_3 + H_2O \rightleftharpoons NH_4^+ + OH^- \qquad (1)$$

has been studied from 50° to 300°C at KCl concentrations from 0.04 to 3.3 *m* at pressures up to 100 bars with the flowing emf cell with the representation

$$H_2, Pt \left| \begin{array}{l} a\ m\ KCl \\ 0.02a\ m\ KOH \\ (\text{reference}) \end{array} \right\| \left. \begin{array}{l} a\ m\ KCl \\ 0.02a\ m\ NH_4OH \\ 0.02a\ m\ NH_4Cl \end{array} \right| Pt, H_2$$

Previously this equilibrium had been studied by potentiometric methods to 50°C and in dilute solutions by conductance to 343°C. Our results extrapolated to the saturation pressure of water are shown in Fig. 6.4, where the curves were calculated from a 15-parameter expression used for smoothing the data.

A comparison of the change in heat capacity for the dissociation of ammonia [reaction (1)] with that for the ionization of water shows the close similarity over the whole temperature range at infinite dilution. Sudden wide divergences occur at temperatures above 250°C and at high concentrations of KCl and suggest the association of HCl in these solutions. The change in volume for the dissociation of NH_3 is 35% greater than that for the ionization of water at low temperatures and about 15% greater at 250°C. It is also interesting to note that ammonia exhibits maximum buffering capacity on the acidic side of neutral at 300°C at infinite dilution. The transition from the basic character to acidic character at $(NH_4^+)/(NH_4OH) = 1$ occurs at about 220°C.

Amines. The use of volatile amines for the control of pH and for corrosion protection in the condensate of boilers is a common practice in the power industry. The most commonly used amines are piperidine, cyclohexylamine, and morpholine. The latter two were selected for our study at high temperatures because they represent two different classes of basicity, one (cyclohexylamine) more basic than ammonia and the other (morpholine) less basic at low temperatures. The quotients for the dissociation equilibria,

$$C_6H_{11}NH_2 + H_2O \rightleftharpoons C_6H_{11}NH_3^+ + OH^-$$

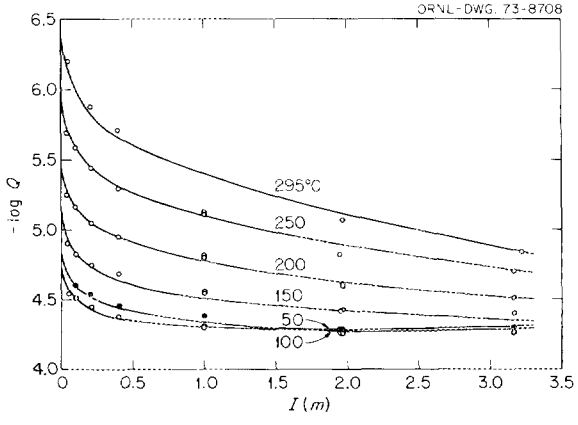

Fig. 6.4. The dissociation quotient for ammonia in aqueous KCl at the saturation pressure of water, as a function of the ionic strength (*I*).

and

$$(CH_2)_2O(CH_2)_2NH + H_2O \rightleftharpoons (CH_2)_2O(CH_2)_2NH_2^+ + OH^-,$$

are given in Table 6.5 along with the corresponding values for H_2O and NH_3. The measurements were made in 0.08 *m* KCl for both bases with the flowing emf cell. Estimates of log *K* values can be made with good reliability using the $\gamma_{NH_4^+}\gamma_{OH^-}/\gamma_{NH_3}$ ratio in the same medium. The results show very different temperature coefficients for these two amines and also that the log *Q* for morpholine is nearly equal to that for NH_3 at 250°C. At that temperature, cyclohexylamine remains a stronger base.

Table 6.5. Values of log *Q* for the aqueous dissociation equilibria

$$H_2O + H_2O \rightleftharpoons H_3O^+ + OH^-,$$
$$RNH_2 + H_2O \rightleftharpoons RNH_3^+ + OH^-$$

T (°C)	H_2O, $I = 0.10$	NH_3, $I = 0.10$	Cyclohexylamine, $I = 0.08$	Morpholine, $I = 0.08$
50	−13.05	−4.49	−3.27	−5.09
100	−12.00	−4.59	−3.51	−4.94
150	−11.33	−4.83	−3.86	−5.00
200	−10.93	−5.17	−4.28	−5.20
250	−10.72	−5.58	−4.75	−5.52
300	−10.65	−6.03		

Table 6.6. Deuterium isotope effects in 0.2 *M* KCl

T (°C)	Log Q_H	Log Q_D	$\frac{\log (Q_H/Q_D)}{\log Q_H}$
	Dissociation of water		
	$H_2O + H_2O \rightleftharpoons H_3O^+ + OH^-$,	Q_H	
	$D_2O + D_2O \rightleftharpoons D_3O^+ + OD^-$,	Q_D	
50	−13.003	−13.934	−0.072
100	−11.950	−12.811	−0.072
150	−11.265	−12.077	−0.072
200	−10.837	−11.598	−0.070
250	−10.579	−11.293	−0.067
293	−10.482	−11.099	−0.059
	Dissociation of $H_2PO_4^-$		
	$H_2PO_4^- + H_2O \rightleftharpoons H_3O^+ + HPO_4^{2-}$,	Q_H	
	$D_2PO_4^- + D_2O \rightleftharpoons D_3O^+ + DPO_4^{2-}$,	Q_D	
50	−6.587	−7.100	−0.078
100	−6.651	−7.112	−0.069
150	−6.795	−7.245	−0.066
200	−7.000	−7.439	−0.063
250	−7.238	−7.663	−0.059
293	−7.483	−7.842	−0.048

D_2O and $D_2PO_4^-$. The dissociation equilibria of D_2O and $D_2PO_4^-$ were studied from 50° to 293°C in 0.2 *m* KCl using the titration-emf assembly. These represent the first measurements of the deuterium isotope effect on such equilibria at high temperatures. At 50°C the dissociation quotient (Table 6.6) for light water is about 8.5 times that for heavy water, and this effect decreases to 4 times at 293°C. At 50°C the dissociation quotient for $H_2PO_4^-$ is 3.3 times that for $D_2PO_4^-$, and at 293°C this becomes 2.2 times. The comparison in Table 6.6 shows a slight variation with temperature in both cases for the fractional change in the quotients, log (Q_H/Q_D)/log Q_H. There is an approximate proportionality of log (Q_H/Q_D) with $1/T$ for both cases. From these results and the known magnitude of $\gamma_{H^+}\gamma_{OH^-}/a_{H_2O}$ and $\gamma_{HPO_4^{2-}}\gamma_{H^+}/\gamma_{H_2PO_4^-}$, good estimates can be made for log Q_D at other ionic strengths after correcting the Debye-Hückel limiting slope for the difference in densities and conversion to an equal-moles-of-solvent basis.

1. Work performed in the Reactor Chemistry Division.
2. Chemical Technology Division.
3. ORAU Summer Student Trainee from the University of South Dakota, Vermillion, 1973.

FLUORINE-19 NUCLEAR MAGNETIC RESONANCE STUDIES ON FLUOROBORATE SPECIES IN AQUEOUS SOLUTION[1]

R. E. Mesmer A. C. Rutenberg[2]

The behavior of fluoroborates in water has been recently studied potentiometrically[3] to determine the composition of species which are present in metastable amounts with respect to equilibrium with BF_4^-. Because the BF_4^- ion is kinetically slow to form except in highly acidic media, only the species BF_3OH^-, $BF_2(OH)_2^-$, and $BF(OH)_3^-$ are present after short times when adding fluoride to boric acid solutions.

Kuhlmann and Grant[4] have shown that the ^{19}F resonance of BF_4^- produces a quartet of equivalent lines with a coupling constant for the B-F interactions to 1 to 4 Hz depending on the concentration and nature of the cations. Also, the ^{11}B spectra for 7 *M* $NaBF_4$ solutions exhibit the sharp 1:4:6:4:1 quintet expected for the ^{11}B coupled to four equivalent F nuclei with a coupling constant of 4.6 Hz. By boiling solutions containing $NaBF_4$ in the presence of calcium carbonate, a small amount of hydrolysis was effected, and the ^{19}F and ^{11}B spectra were observed for what was believed to

be BF_3OH^-. A weak ^{19}F quartet was observed 6.2 ppm downfield from the BF_4^- quartet. The ^{11}B resonance spectrum consisted of a partially resolved quartet with a coupling constant of 12.7 Hz. The wider resonance lines of BF_3OH^- compared with BF_4^- are attributed to the quadrupolar broadening in the unsymmetrical BF_3OH^-.

We have examined the ^{19}F spectra of solutions expected to contain BF_3OH^-, $BF_2(OH)_2^-$, and $BF(OH)_3^-$ in different amounts. Estimates of equilibrium quotients were made from these data along with potentiometric measurements of hydrogen ion and fluoride ion concentrations.

Figure 6.5 shows spectra of a solution containing 1 *m* $NaBF_3OH$ and 1 *m* $NaB(OH)_4$ (i.e., an F:B ratio of 1.5 and a boron concentration of 2 *m*) at temperatures from 0° to 65°C. The peaks (27°C) at about −16, −23, −30, and −44 ppm are assigned, respectively, to BF_4^-, BF_3OH^-, $BF_2(OH)_2^-$, and a combination of free fluoride and $BF(OH)_3^-$. The assignments of the BF_4^-, $BF_3(OH)^-$, and F^- peaks were made by addition of these ions under conditions where they persist at equilibrium and by comparison with spectra reported in the literature.[5,6] At 0° the resonance peaks for the free fluoride and the $BF_2(OH)_2^-$ are well resolved but devoid of fine structure. At 27° these two peaks are partially overlapping, and at 65° they are completely coalesced at the mean position, as expected for exchange between equally populated sites. The lifetime for fluorine on $BF_2(OH)_2^-$ was estimated at 27° to be 0.6 msec, but a detailed analysis of this reaction in terms of the rate law was not attempted. This lifetime is shorter than that reported by Connick and Poulson[7] for AlF_2^+ (16 msec). The activation energy estimated from the peak separation at 27° and the peak width at 65° is 14 kcal/mole. This quantity does not correspond to the exchange process alone, however, since the

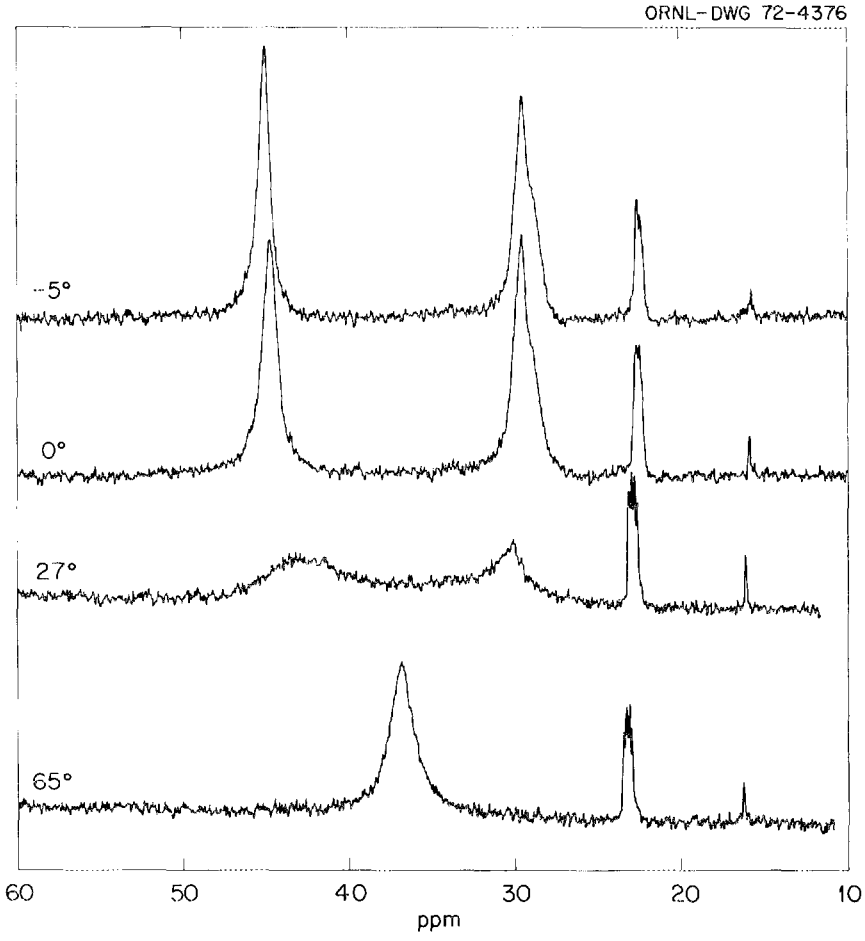

Fig. 6.5. ^{19}F spectra of a solution with the composition 1 *m* $NaBF_3OH$ and 1 *m* $NaB(OH)_4$ (F:B ratio of 1.5) as a function of temperature (C_6F_6 reference).

equilibrium is also expected to shift with temperature.

These direct observations of the fluoroborate species, along with potentiometric data for the H^+ and F^- concentrations, enable us to obtain estimates of the equilibrium quotients for the reactions

$$B(OH)_3 + xF^- + (x-1)H^+ \rightleftharpoons BF_x(OH)_{4-x}^- + (x-1)H_2O .$$

Nmr peaks cannot be integrated with great accuracy, especially for the species with broad signals resulting from exchange. Calculations were made from measurements at 27° and 0°, where signals for the composite of $F^- + BF(OH)_3^-$ were observed. The agreement with the previous data[3] is satisfactory and gives semiquantitative evidence for the validity of the assignments made here.

1. Abstracted from paper, *Inorg. Chem.* **12**, 699 (1973). Work performed in the Reactor Chemistry Division.
2. Now of the Product Certification Division, Y-12.
3. R. E. Mesmer, K. M. Palen, and C. F. Baes, Jr., *Inorg. Chem.* **12**, 89 (1973).
4. K. Kuhlmann and D. M. Grant, *J. Phys. Chem.* **68**, 3208 (1964).
5. I. G. Ryss and M. M. Slutskaya, *J. Gen. Chem. USSR* **22**, 451 (1952).
6. M. Noshiro and Y. Jitsugiri, *Bunseki Kagaku* **18**, 1200 (1969).
7. R. E. Connick and R. E. Poulson, *J. Amer. Chem. Soc.* **79**, 5153 (1957).

STUDIES ON THE VAPORIZATION OF METHYLMERCURY COMPOUNDS AND THEIR HALOGEN DECOMPOSITION USING GAS CHROMATOGRAPHY WITH A MICROWAVE DETECTOR[1]

Y. Talmi[2] R. E. Mesmer

Organic mercury compounds, primarily $(CH_3)_2Hg$ and CH_3HgX, are known to play an important role in the toxicological behavior of mercury. Knowledge of the factors affecting the movement and transformations of these substances is of obvious importance in understanding and controlling the hazard. Biological transformations of inorganic to organic or methylated mercury have been reported under both aerobic and anaerobic conditions for several years,[3,4] and yet many of the physical and chemical properties of the methylated forms of mercury are unknown.

The volatility of the CH_3HgX salts and their solutions is unknown, and an estimate of the solubility of $(CH_3)_2Hg$ in water has only recently been reported.[5] Our work is addressed to some of the properties of organomercury compounds which have significance in their environmental behavior as well as in their analytical determination. To obtain such data in dilute solutions, highly efficient separation techniques as well as very sensitive detection is required. The combination of gas chromatographic separation with a microwave plasma emission spectrometric detector (GC-MES) has proven capable of meeting these demands. Two methods have been applied in the determination of the distribution coefficient, K_D (dimensionless), for the partition of $(CH_3)_2Hg$ between a gas phase (air) and a water phase: (1) analysis of both phases and (2) successive analyses of the gas phase. There is excellent agreement between the results of the two methods. The value for the distribution coefficient is 0.31 at 25° and 0.15 at 0°C, which leads to a value of −4.5 kcal/mole for the heat of dissolution of $(CH_3)_2Hg$ gas:

$$(CH_3)_2\ Hg(g) \rightleftharpoons (CH_3)_2Hg(aq) .$$

Although $(CH_3)_2Hg$ is distributed toward the vapor phase, one might expect a much greater tendency for a nonpolar linear molecule such as this. The relatively polar CO_2 molecule, in contrast, has a distribution coefficient greater than $(CH_3)_2Hg$; the K_D for CO_2 from the data of Helgeson[6] is 1.19.

The solubility of CH_3HgCl calculated from the equilibrium data in the literature is 0.0200 *M* (5020 ppm). We have obtained a value for the solubility of CH_3HgCl of 0.0236 *M* (5930 ± 115 ppm) in water and 0.0230 *M* (5780 ± 180 ppm) in 1 *M* NaCl at 25°C.

Table 6.7 summarizes data on the vapor pressure of CH_3HgX above the solids CH_3HgCl and CH_3HgOH.

Table 6.7. Vapor pressures of CH_3HgX

Sample	N^a	T (°C)	CH_3HgX concentration in vapor phase (ng/ml)	Vapor pressure (μ Hg)
$CH_3HgCl(s)$	15	22	154 ± 11.4	11.1 ± 0.8
$CH_3HgCl(s)$	3	0	12.1 ± 2.3	0.80 ± 0.2
$CH_3HgOH(s)$	2	22	77.4 ± 7.6	5.6 ± 0.6
$CH_3HgCl(aq)$, 1000 ppm)	12	22	27.8 ± 4.1	2.0 ± 0.3

[a]Number of determinations.

Since the chromatographic retention times for both CH_3HgCl and CH_3HgOH are indistinguishable, the species in the gas phase could not be specifically identified. Figure 6.6 shows the effect on the vapor concentration above a solution of 0.004 *M* CH_3HgCl with varying pH due to additions of NaOH at 22°C. Plotted on the same graph is the distribution of methylmercury as $CH_3HgCl(aq)$. At these concentrations, CH_3Hg^+ is a very minor species (less than 2% of the mercury), and $CH_3HgOH(aq)$ forms at high pH. When the two curves are superimposed at low pH values, the failure of the vapor concentration curve to approach the axis at the same rate as the distribution plot of $CH_3HgCl(aq)$ indicates that $CH_3HgOH(aq)$ probably contributes to the vapor composition in the high-pH region.

It was discovered that very rapid photochemical reactions of CH_3HgX with I_2 or Br_2 at very low concentrations take place in water at room temperature. Such reactions offer a potential means for the destruction of CH_3HgX from laboratory or industrial discharges. In addition, the reaction with I_2 is an important potential source of error in analytical procedures utilizing the high extractability of the CH_3HgI species. This reaction produces CH_3I and $HgI_2(s)$ as follows:

$$CH_3HgCl(aq) + I_2 \rightleftharpoons CH_3I + \tfrac{1}{2}HgI_2(s) + \tfrac{1}{2}HgCl_2(aq) .$$

The dependence of the slopes in Fig. 6.7 on the I_2 concentration shows that the reaction is bimolecular. Actinometry was not conducted on this system, but the observation was made that fluorescent lighting with a continuous spectrum over the range 380 to 750 nm with superimposed mercury lines was sufficient to induce the reaction; the experiments were conducted in the laboratory, where the light intensity was about average (80 ft-c). The reaction essentially stops when the I_2 hydrolyzes at high pH.

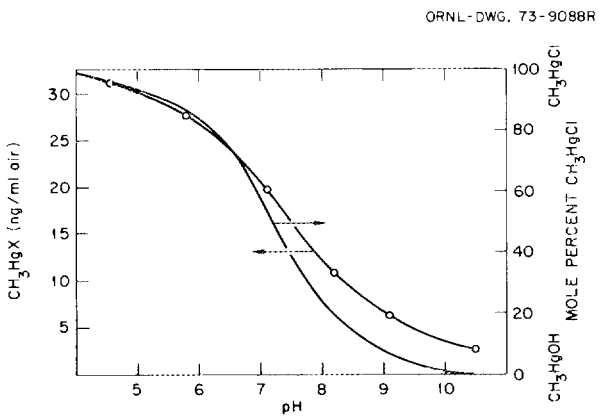

Fig. 6.6. Effect of pH on the vapor concentration (left coordinate) and the distribution of mercury species in the aqueous phase (right coordinate) at 22°C.

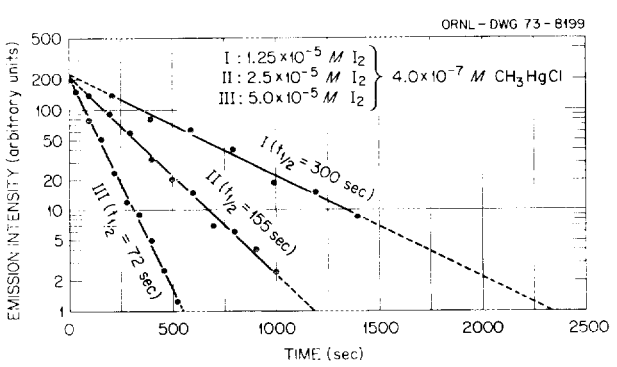

Fig. 6.7. The first-order disappearance of CH_3HgCl in the presence of excess I_2 under constant illumination.

1. Abstracted from paper submitted to *Water Research*. Research carried out under the ORNL-NSF Ecology and Analysis of Trace Contaminants program, sponsored by NSF/RANN, under Union Carbide Corporation's contract with the U.S. Atomic Energy Commission.
2. Analytical Chemistry Division.

3. A. Jensen and A. Jernelöv, *Biocidinformation* **10**, 3 (1967); **14**, 3 (1968); *Nature* (London) **223**, 753 (1969).
4. J. M. Wood, F. S. Kennedy, and C. G. Rosen, *Nature* (London) **220**, 173 (1968).
5. G. A. Parks, Stanford University, private communication (1973).
6. H. C. Helgeson, *J. Phys. Chem.* **71**, 3121 (1967).

LIQUID-VAPOR CRITICAL TEMPERATURES OF AQUEOUS ELECTROLYTE SOLUTIONS[1]

W. L. Marshall E. V. Jones[2]

Liquid-vapor critical temperatures (t_c) of 21 separate sets of single electrolyte aqueous solutions, determined earlier in this program, were evaluated on the basis of relative ion association, hydration, ion size, and reversible and irreversible decomposition. The dissolved electrolytes considered at molalities up to 1.5–2.5 were LiCl, NaCl, KCl, KBr, KI, $CsNO_3$, $KHSO_4$, NH_4Cl, NH_4HCO_3 $(NH_4)_2CO_3$, $(NH_4)_2SO_4$, $CaCl_2$, $MgCl_2$, $Mg(NO_3)_2$, HCl, $HClO_4$, HNO_3, CH_3COOH, H_2SO_4, H_3PO_4, and H_3BO_3.

The alkali halide solutions produced the greatest increase in t_c from that of pure water (t_c = 374.2°C), where at 2 *m* all values of t_c were in the range of 450° to 480°C, providing an increase of +80° to +110°C.

Several of the acids (H_2SO_4, H_3PO_4, H_3BO_3) and divalent salts [$CaCl_2$, $MgCl_2$, $Mg(NO_3)_2$, $(NH_4)_2SO_4$] showed intermediate increases, while particular solutes [HCl, $HClO_4$, $(NH_4)_2CO_3$, NH_4HCO_3, CH_3COOH] gave very little change from t_c for water.

Critical temperatures of aqueous solutions are important in establishing the presence or absence of liquid-vapor heterogeneity of multicomponent geothermal solutions. This knowledge is of fundamental interest and is also directly applicable to geothermal power prospecting.

1. Summary of paper to appear in *J. Inorg. Nucl. Chem.* (1974). Work performed in the Reactor Chemistry Division.
2. Deceased.

LIQUID-VAPOR CRITICAL TEMPERATURES OF SEVERAL AQUEOUS-ORGANIC AND ORGANIC-ORGANIC SOLUTION SYSTEMS[1]

W. L. Marshall E. V. Jones[2]

Liquid-vapor critical temperatures (t_c) of several two-component aqueous-organic and organic-organic solution systems, studied earlier in this program, were interpreted on the basis of concentration (moles per liter) of the components, rather than composition (weight percent, mole fraction). The systems considered were methanol-water, ethanol-water, acetone-water, tetrahydrofuran-water, dioxane-water, benzene-toluene, and acetone-ethanol.

When t_c was plotted against the molarity of water, the values of t_c for the systems methanol-water, ethanol-water, acetone-water, and tetrahydrofuran-water fell on one curve from moderately low $M(H_2O)$ [$t_c \simeq 270°C$] to pure water ($t_c = 374°C$), as shown in Fig. 6.8. This superposition of the four curves simplified the description of the systems and may reflect a common hydrogen bonding characteristic of these two-component solutions. The critical temperatures for the system dioxane-water failed to superimpose even at moderately high $M(H_2O)$ (Fig. 6.8). Dioxane, however, would not be expected to exhibit much hydrogen bonding.

The study of the two organic-organic systems benzene-toluene and acetone-ethanol produced smoothly varying critical curves between values of t_c for the pure components (t_c: benzene, 290°C, toluene, 320°C; acetone, 238°C; ethanol, 243°C), as shown in Fig. 6.9. Use of a molarity scale for describing these

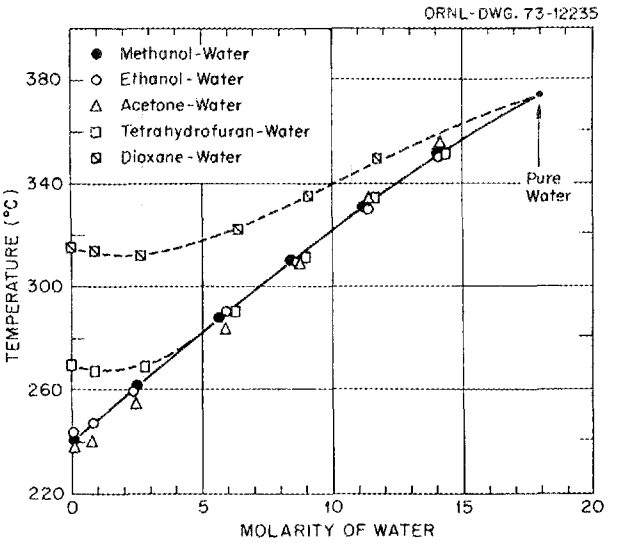

Fig. 6.8. Liquid-vapor critical temperatures of the systems methanol-water, ethanol-water, acetone-water, tetrahydrofuran-water, and dioxane-water plotted against molarity of water.

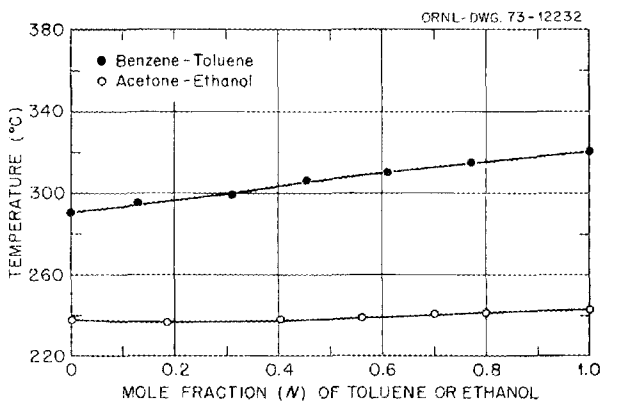

Fig. 6.9. Liquid-vapor critical temperatures of the systems benzene-toluene and acetone-ethanol plotted against mole fraction.

two organic-organic systems produced approximately the same type of symmetry.

These studies complement the analogous studies of t_c for aqueous electrolyte solutions[3] and may lead to greater understanding of liquid-vapor critical phenomena of solutions. Future applications to predictions of high-temperature aqueous behavior are anticipated.

1. Summary of paper to appear in *J. Inorg. Nucl. Chem.* (1974). Work performed in the Reactor Chemistry Division.
2. Deceased.
3. W. L. Marshall and E. V. Jones, "Liquid-Vapor Critical Temperatures of Aqueous Electrolyte Solutions," the preceding contribution, this report.

EFFECT OF PRESSURE ON LIQUID-LIQUID IMMISCIBILITY OF HIGH-TEMPERATURE AQUEOUS SOLUTION MIXTURES OF URANYL SULFATE AND SULFURIC ACID, 280–450°C, 75–1800 BARS[1]

W. L. Marshall J. S. Gill[2]

An important variable in the study of aqueous solutions at high temperature is hydrostatic pressure. In earlier investigations under this program, the effect of pressure to 330 bars on two-liquid-phase formation of UO_2SO_4-H_2O solutions was studied.[3] In later work, an optical cell for withstanding much higher pressures at high temperatures was developed, and similar studies on UO_2SO_4-H_2O solutions were performed to 2000 bars.

It has been shown that the temperature of appearance of liquid-liquid immiscibility in these systems is an approximate function of the product of dielectric constant times the absolute temperature (*DT*), a highly important quantity in electrostatic theory of electrolyte solution behavior. The results show that the temperature of first appearance of two liquid phases in the above systems may be raised by as much as 135°C through application of hydrostatic pressures up to 1800 bars, the initial immiscibility temperature at saturation vapor pressure being in the vicinity of 300°C.

1. Summary of paper to appear in *J. Inorg. and Nucl. Chem.* (1974). Work performed in the Reactor Chemistry Division.

2. Present address: Department of Public Health, State of Tennessee, Nashville.

3. W. L. Marshall and J. S. Gill, *J. Inorg. Nucl. Chem.* **25**, 1033 (1963).

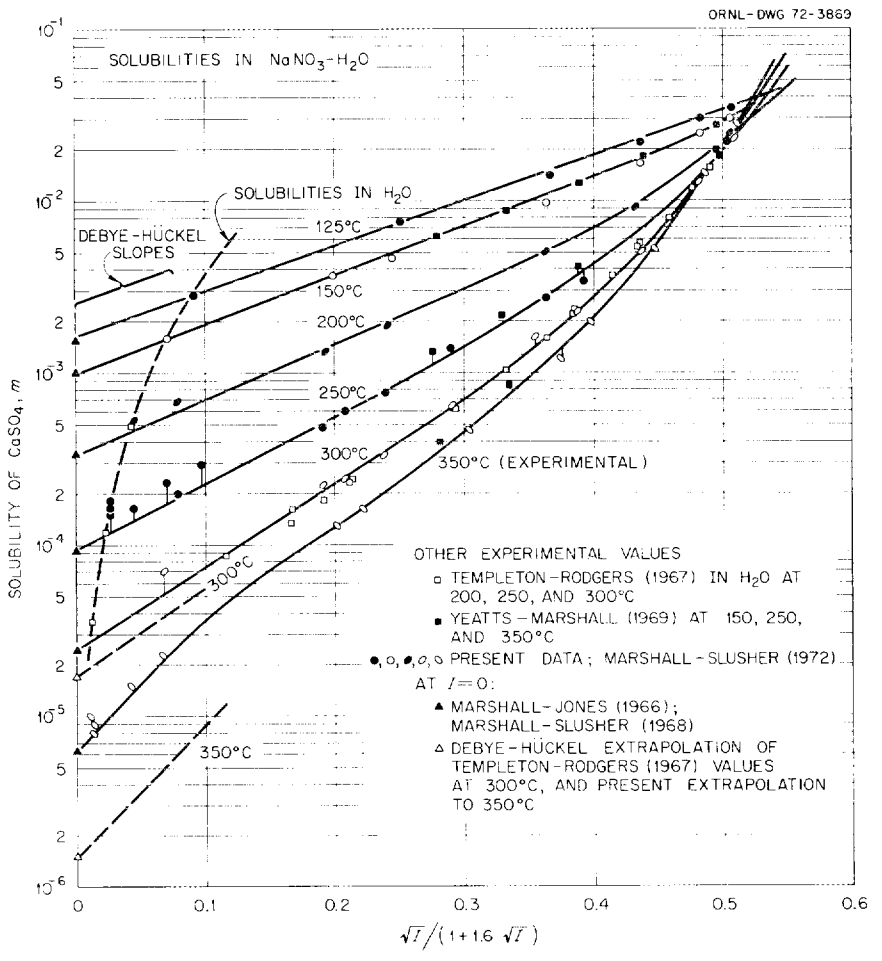

Fig. 6.10. The solubility of $CaSO_4$ (anhydrous) in $NaNO_3$-H_2O solutions as a function of the ionic strength (*I*, molal units), 125–350°C.

DEBYE-HÜCKEL CORRELATED SOLUBILITIES OF CALCIUM SULFATE IN WATER AND IN AQUEOUS SODIUM NITRATE AND LITHIUM NITRATE SOLUTIONS[1]

W. L. Marshall Ruth Slusher[2]

In order to test further the application of the Debye-Hückel theory in describing solubility behavior at high temperatures, the solubility of calcium sulfate was determined in aqueous sodium nitrate and lithium nitrate solutions to 350°C. Figures 6.10 and 6.11 show the solubilities obtained together with other published values, where the logarithm of the molal solubility is plotted against an extended Debye-Hückel function, $\sqrt{I}/(1 + 1.5\sqrt{I})$, and where I is the ionic strength in units of molality. The solubilities are observed to adhere reasonably well to the extended Debye-Hückel theory at the experimental temperatures of 125 to 350°C to ionic strengths of 1 m, but show divergences at higher ionic strengths.

Solubilities of calcium sulfate in water over the temperature range 125° to 350°C obtained in this study are compared in Fig. 6.12 with earlier published values. While there is still some uncertainty in the values for the solubility of calcium sulfate above 250°C, the present values and those of Templeton and Rodgers[3] are believed to best approximate the true solubilities to the highest temperature. Fundamental knowledge of calcium sulfate solubilities in high-temperature water and its electrolyte solutions is of direct application in predicting scale formation for water desalination, geothermal power, and other high-temperature water technologies.

1. Summary of paper, *J. Chem. Thermodyn.* **5**, 189 (1973). Work performed in the Reactor Chemistry Division.
2. Now of the Computer Sciences Division.
3. C. C. Templeton and J. C. Rodgers, *J. Chem. Eng. Data* **12**, 536 (1967).

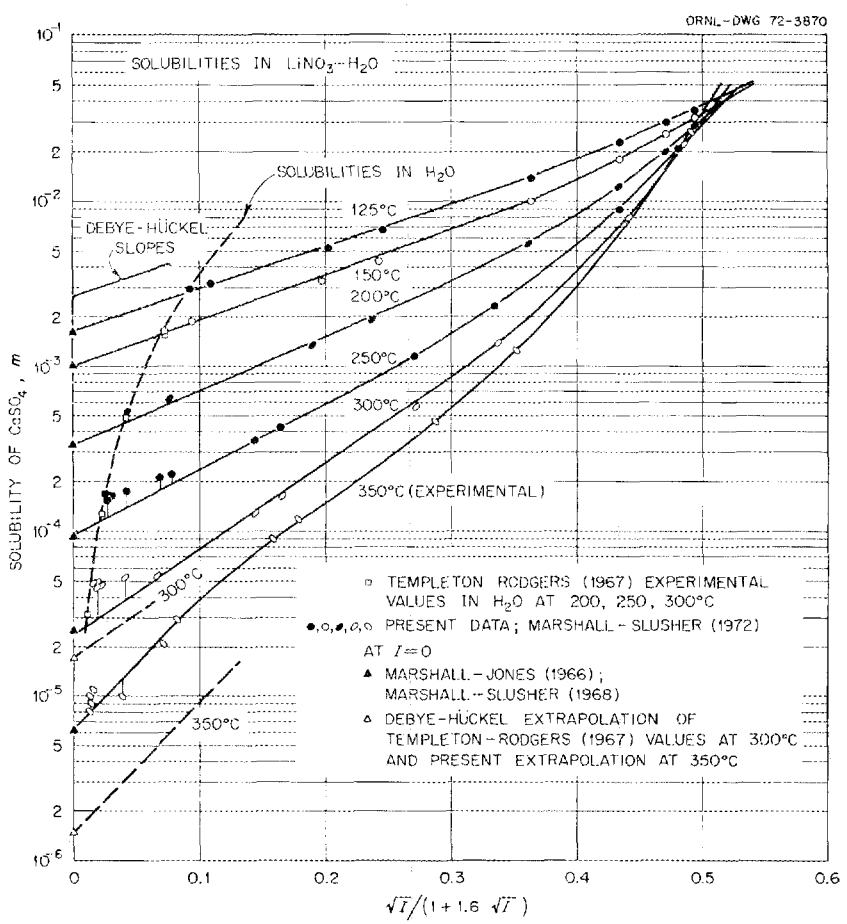

Fig. 6.11. The solubility of $CaSO_4$ (anhydrous) in $LiNO_3$-H_2O solutions as a function of the ionic strength (I, molal units), 125–350°C.

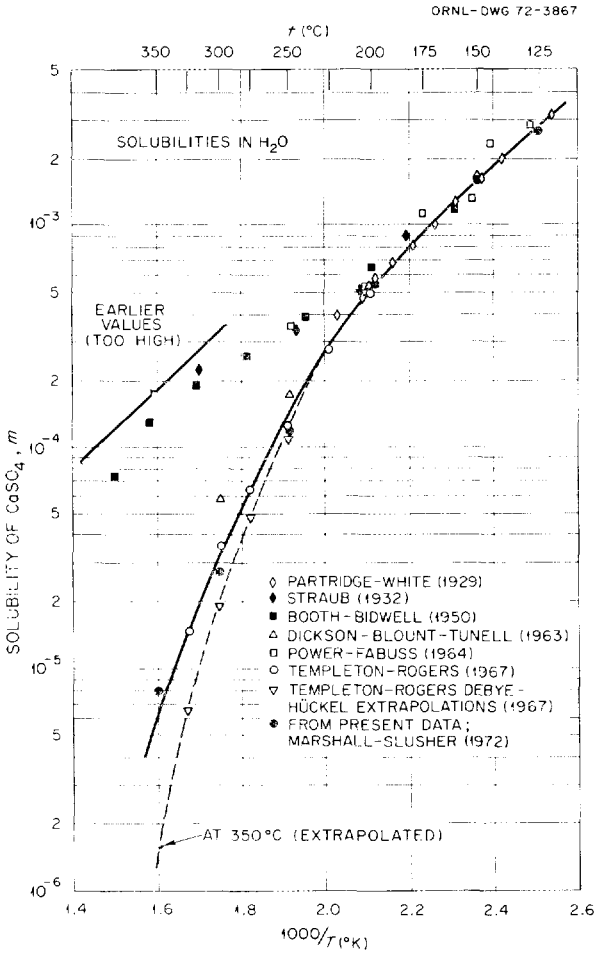

Fig. 6.12. The molal solubility of $CaSO_4$ (anhydrous) in H_2O, 125–350°C.

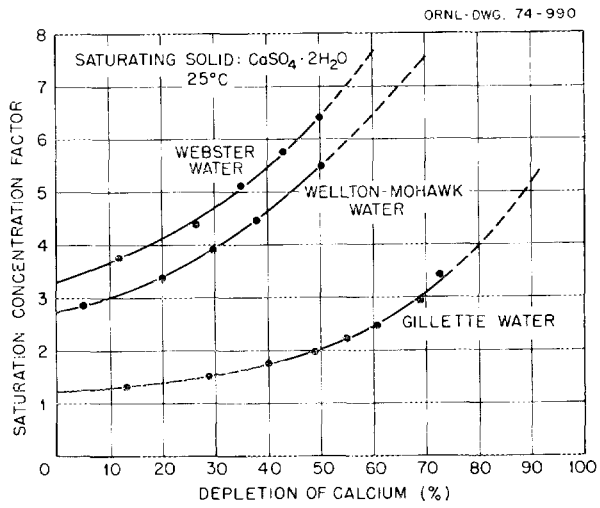

Fig. 6.13. Effect of calcium depletion upon the experimentally derived saturation concentration factors for brackish waters from Gillette, Wyoming, Webster, South Dakota, and Wellton-Mohawk, Arizona, at 25°C. Saturating solid is $CaSO_4 \cdot 2H_2O$.

CALCIUM SULFATE SOLUBILITY IN BRACKISH WATER CONCENTRATES AND APPLICATIONS TO HYPERFILTRATION (REVERSE OSMOSIS), POLYPHOSPHATE ADDITIVES[1,2]

L. B. Yeatts[3] P. M. Lantz[4]
W. L. Marshall

The solubility of calcium sulfate dihydrate, a substance which can impede hyperfiltration [reverse osmosis (RO)] by saturation precipitation in RO membrane pores, was determined at 25°C in three typical brackish water compositions and their concentrates. These waters were synthetically prepared and corresponded to compositions and concentrates of well waters used by the Office of Saline Water RO plants at Gillette, Wyoming, and Webster, South Dakota, and to those of a post-irrigation water from the Wellton-Mohawk Canal in Arizona. In this study, a commercial solid polyphosphate preparation, Calgon, was shown, when added in small amounts (5 to 40 ppm in unconcentrated solutions), initially to produce an apparent increase in the saturation concentration of $CaSO_4 \cdot 2H_2O$ (the solid phase). Later (two to six days), the solution concentration of $CaSO_4$ decreased to near the expected solubilities in the absence of Calgon.

Figure 6.13 shows experimentally obtained saturation concentration factors for the three representative waters, plotted as a function of initial depletions of calcium. Our successful method of calculation of the solubility of $CaSO_4$ and its hydrates in various saline waters is found to apply equally well to the calculation of saturation limits of $CaSO_4 \cdot 2H_2O$ in the present waters and concentrates. Calculations of maximum possible water recoveries and of other parameters that are of direct application to RO processes have been made; the method should be useful in predicting properties of other waters.

1. Research sponsored by the Office of Saline Water, U.S. Department of the Interior, under Union Carbide Corporations contract with the U.S. Atomic Energy Commission.
2. Summary of paper to appear in *Desalination* (1974).
3. Now of the Health Physics Division.
4. Now of the Analytical Chemistry Division.

ADVANCED FILTRATION OF WASTE WATERS

J. S. Johnson, Jr.

The Water Research Program's work on advanced filtration techniques during this year was directly or indirectly almost entirely aimed at pollution abatement problems. Support came from the AEC and the National Science Foundation/RANN, along with a minor contribution specifically for dye wastes from the Environmental Protection Agency (EPA). Included at a low level has been membrane development for specific purposes, and somewhat more attention to assembling and testing of porous supports in practical modules.

With respect to types of waste streams, we have directed significant effort to food wastes and herbicide effluents, in addition to those classes for which we give examples of tests below.

Kraft Wastes

R. E. Minturn C. G. Westmoreland
N. E. Harrison

Work with kraft effluents, in cooperation with International Paper Company (IPCo), has focused primarily on two points in the process.[1,2] In one, discussed last year,[3] we have attempted by hyperfiltration to concentrate the sulfur-containing solutes, along with impurities, in pulp-washing effluents enough for introduction into the chemical recovery system and, at the same time, to produce purified hot filtrate for recycling in the operation. In the other, lower pressure operation[4] is used to filter colored substances, largely lignin derivatives, and other organic material from effluents generated in the bleaching of the pulp, the concentrate going to the recovery system for disposal; in order to avoid building up chloride salts in the recovery system, the membrane used should have low salt rejection. For wash liquors, dual-layer hydrous oxide–polycarboxylate membranes appear at present a strong first choice. For bleach plant wastes, membranes of polyvinylpyrrolidone, a neutral organic polymer, and single-layer hydrous Zr(IV) oxide, operated at neutral pH's, have appeared promising, but our survey of dynamic ultrafiltration membranes for any application has been far less complete than with hyperfiltration membranes. Consequently, we have tested a number of other materials.

The results are summarized in Table 6.8. Except for the Zr(IV)-Si(IV), the membranes were formed dynamically on zirconia-coated Ferro 600p ceramic tubes[5] at about 500 psig, 25°C, and 6-7 fps from 0.05 *M* NaCl. The Zr(IV)-sodium silicate membrane was formed in two steps on a 0.27-μ Selas ceramic filter element at 500 psig, 25°C, and 15 fps. Tests were made at the formation velocity and at elevated temperature with a number of different samples of combined bleach-plant effluent from IPCo's Mobile, Alabama, installation.

Of these additives, three look at least as good as and possibly better than polyvinylpyrrolidone and hydrous Zr(IV) oxide. The membrane from Pluronic 98, a 80% polyoxyethylene–20% polyoxypropylene polymer manufactured by Wyandotte Chemicals Corporation, had good organic carbon and color rejection, reasonably low chloride rejection, and fair fluxes. The sodium silicate membrane had similar properties, and separation between organic materials and dissolved salt remained fairly good at high water-recovery levels, indicated by total organic carbon in the solution being filtered (Fig.

Table 6.8. Summary of results for ultrafiltration of bleach plant effluents by dynamic membranes of various additives

Ferro 600p ceramic tube supports, 185–225 psig, 50–58°C, 6–7 fps, pH 8–9

Additive	Duration of run (hr)	Flux range (gal ft^{-2} day^{-1})	Observed rejection (%), range		
			Total organic carbon	Color	Chloride
Polyvinylpyrrolidone	175	46–41	89–87	97–95	36–9
Poly(vinyl methyl ether)	22	126–62	87–84	94–98	40–41
Pluronic 98	64	90–73	90–91	97–98	28–25
Poly(ethylene glycol)	15	135–92	54–82	64–93	3–2
Sodium silicate	291	174–44	85–93	95–99	28–4
Hydrous Zr(IV) oxide	24	54–33	82	99	16
Hydroxyethyl cellulose	20	101–30	69–78	85–96	(–1)–(–3)
Hydrous Zr(IV)-Si(IV) oxide[a]	243	60–94	84–89	98–99	33–5

[a]Dual-layer membrane on a 0.27-μ Selas ceramic support, tested at 15 fps.

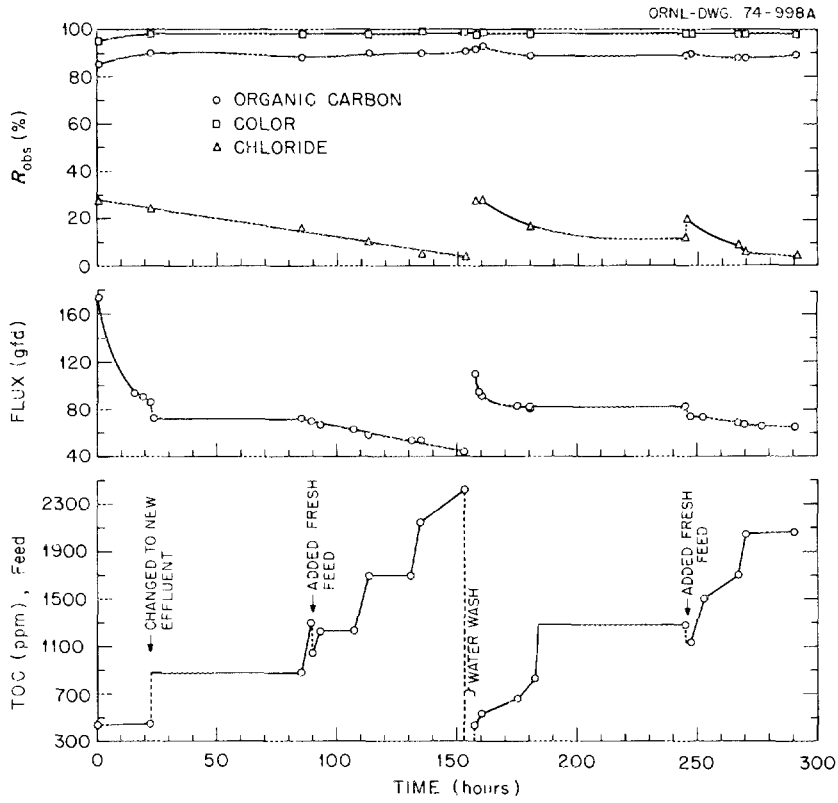

Fig. 6.14. Ultrafiltration of bleach plant effluent by dynamic sodium silicate membrane on zirconia-coated Ferro 600p tube. Conditions: about 200 psig, 52 to 56°C, 6 fps, pH about 8.4. Abbreviation: gfd = gal ft^{-2} day^{-1}.

6.14). There was also substantial flux recovery from a water wash. Since silicate is somewhat soluble in water, we tested a membrane stabilized against anticipated (though not so far observed) deterioration by first depositing a hydrous Zr(IV) oxide layer, before forming the silicate membrane. This dual-layer ultrafiltration membrane also looked promising (Table 6.8), and the separation of organics and salt improved with time during the test. At the end of the 240-hr run, flux was 94 gal ft^{-2} day^{-1}, organic carbon rejection was 88%, color rejection 99%, and chloride rejection only 5%, all at zero percent water recovery.

Pilot tests at the IPCo Mobile site, referred to in last year's report,[3] were not funded by NSF/RANN, but EPA appears to be interested at present.

Hyperfiltration of Textile Wastes

R. E. Minturn C. G. Westmoreland
N. E. Harrison

Our earlier work with dyeing wastes,[6,7] in collaboration with Professors C. A. Brandon and J. J. Porter of Clemson University, has led to an EPA-supported test program at the La France Mills of the Riegel Corporation and to a proposal, recently funded by EPA, for tests utilizing a Water Research Program mobile unit at six plants, the prime contractor being the South Carolina Textile Manufacturers' Association.

In support of these programs, we have looked more closely at the effect of several process variables on the hyperfiltration of dye wastes by dynamic membranes. These tests were made with the help of an MIT Practice School team, and the results have appeared as an ORNL-MIT report.[8] The variables studied were circulation velocity, porous support, temperature, pressure, concentration, and time. The effect of regeneration procedures was also investigated.

The effects of circulation velocity, water-recovery level, and time are illustrated in Fig. 6.15. Formation of all three dual-layer hydrous Zr(IV) oxide-poly(acrylic acid) [Zr(IV)-PAA] membranes had been at 15 fps on three similar zirconia-coated Ferro 600p ceramic tubes,[5] though they had been subsequently exposed to a PAA-containing solution at the velocities cited in Fig. 6.15 to restore rejection after a move to another test loop.

Figure 6.15 shows that the fluxes in the hyperfiltration of a composite dye waste supplied by La France had higher values at higher circulation velocities. Although there was a decrease in flux with time at all velocities tried, the relative rate of decrease was about the same for the membranes at 15 and 10 fps, and somewhat greater for the membrane at 6 fps; through the first 45 hr of the run of Fig. 6.15 the flux-decline parameter, b, which is the negative of the slope of a log flux vs log time plot, was 0.11 for 15 and 10 fps, and 0.15 for 6 fps. In addition, fluxes appeared to be relatively independent of feed concentration over the range tested. The addition of fresh increments of feed to the feed tank during the run appeared to have only a small adverse effect on flux, in comparison with the larger effect sometimes observed (see, for example, Fig. 6.14). Percentage removal of solutes in the circulating solution was insensitive to circulation velocity; percentage removal of color and organic carbon was insensitive to concentration as well (top, Fig. 6.15). Salt rejection declined with concentration, as one would expect of an ion exchange membrane.

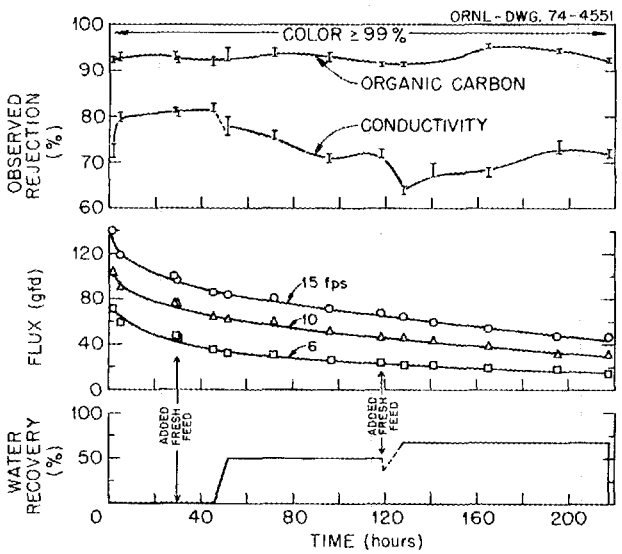

Fig. 6.15. Hyperfiltration of effluent from textile dyeing mill (La France Industries) by dynamic dual-layer Zr(IV)-PAA membranes on zirconia-coated Ferro 600p ceramic tubes. Conditions: 950 psig, 57 to 63°C. Data by MIT Practice School Team.

In other experiments the MIT team showed that, as expected, fluxes increased with temperature and pressure, and carbon tubes and Selas ceramic tubes were also promising as membrane supports. Following 300-hr and 150-hr exposures to the dye wastes, a wash with a 0.1 M solution of Na_2CO_3, adjusted to pH 10, restored fluxes to as much as 80% of their original values.

Figure 6.16 gives the results of a hyperfiltration run with different dye wastes, indigo and indigo–sulfur black, both supplied by Mr. Cranston Gray of Canton Textile Mills, Canton, Georgia. Dual-layer Zr(IV)-PAA membranes were formed in a Selas Flotronics protomodule which contained two bundles of ceramic tubes with about 2.4 ft^2 total area. Formation was at 800

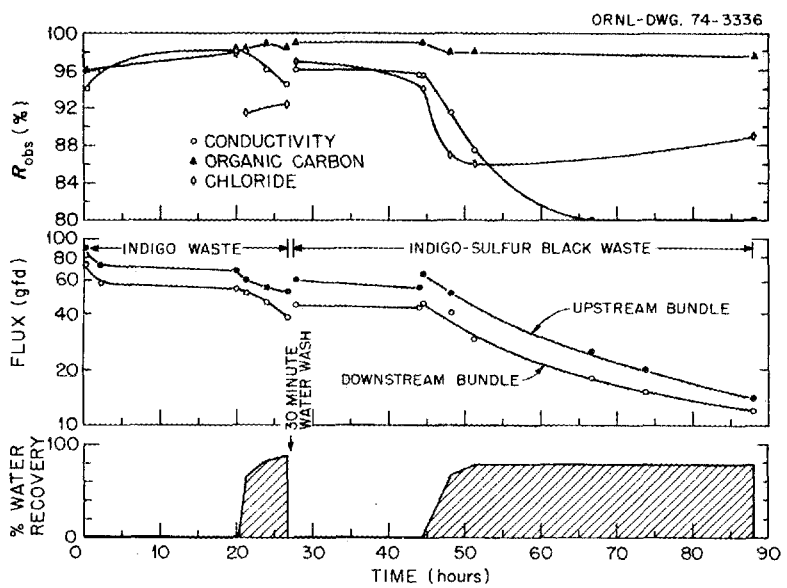

Fig. 6.16. Hyperfiltration of dyeing wastes by dual-layer hydrous Zr(IV) oxide–PAA membranes on Selas-tube module. Conditions: 800 psig, 15 fps, 45°C, pH about 7.3.

psig, 25°, and 15 fps; operation was under the same conditions except that the temperature was raised to 45°C. Before hyperfiltration, the dye wastes were neutralized with concentrated sulfuric acid. During the run, as indicated at the bottom of Fig. 6.16, the indigo waste was concentrated to about 88% water recovery by discarding product; the indigo–sulfur black waste was concentrated to 78% water recovery.

The rejections indicated in Fig. 6.16 are averages of those for the two tube bundles, which generally differed by no more than a percentage point. Rejection of organic carbon was good with both wastes, with carbon concentration in the product ranging from about 2 to 3 ppm at low recovery levels to about 10 ppm at 88% recovery with the indigo waste. With the more concentrated indigo–sulfur black waste, organic carbon concentration was about 100 ppm at the 78% water-recovery level. Product samples had the appearance of tap water up to the point at which the indigo–sulfur black dye waste had been concentrated to about 67% water recovery (at about 48 hr), at which time they assumed a bluish hue, the shade becoming darker at higher recovery levels. The product at all levels appeared satisfactory for reuse in the textile washing process from which the waste was generated.

Fluxes were generally encouraging during the run, especially for this pressure and temperature, except at high recovery levels with sulfur black. Here fluxes fell to less than 15 gal ft^{-2} day^{-1}. At high recovery level, the waste is thick, and a post-run examination of the module indicated heavy solid deposits in the interstices of the tube bundles. It is likely that these deposits reduced the membrane area available for filtration, resulting in loss in flux. A somewhat more open arrangement of tubes in the bundles might ameliorate this problem.

Lead Electroplating Wastes

G. E. Moore

In filtration of particulates and colloids, circulation of the feed solution past the filtering surface slows the thickening of filter cake and thus allows operation with a cake tight enough for good separations without prohibitive sacrifice of flux.[9] If substances which must be removed occur as solids or can be precipitated, cross-flow filtration may provide a better decontamination with lower space requirements than conventional settling or filtration techniques. If the solutes are in low concentrations, they often can be removed on adsorbents in particulate form, without the severe constraints imposed by necessity of chromatographic column operation; removal of toxic ions by this approach has been demonstrated.[10]

An opportunity for a test of purifying a real effluent before discharge into receiving waters arose recently, in the form of an electroplating rinse effluent from a $Pb\text{-}PbO_2$ plating plant. Electrochemical removal and solvent extraction to reduce the Pb(II) content from an original 20 ppm to the commonly accepted discharge standard of 0.05 ppm were evaluated by others in the Laboratory, but neither method showed much potential for success.[11]

Preliminary experiments with synthetic solutions using axial filtration[12] (a variant, developed by K. A. Kraus and F. Nelson, of cross-flow filtration in which the filtering surface is mounted on a rotor and filtrate is withdrawn from the inside) to remove precipitates or solid adsorbents were carried out to determine solution compositions which reduced the Pb(II) concentration from an original 20 ppm to less than 0.05 ppm in the filtrate. Demonstration of removal is necessary, since predictions from the solubility products of $Pb(OH)_2$ and $PbCO_3$ that Pb(II) concentration in aqueous systems at pH > 8 should be in the range 0.001 to 0.010 ppm[13] may be incorrect because of formation of soluble hydroxo and carbonato complexes;[14] even if the solubility is low, removal of colloidal dispersions from aqueous solutions may require very efficient filtration. Table 6.9 summarizes some tests with synthetic solutions which indicate that cross-flow or axial filtration, under appropriate solution conditions, indeed removes Pb(II) to concentrations less than 0.05 ppm.

Two effluent samples were received from our industrial battery collaborators: one was directly from the

Table 6.9. Removal of Pb(II) from aqueous solutions using cross-flow or axial filtration

Original Pb(II) concentration: about 20 ppm

Solution composition	pH	Pb(II) in filtrate (ppm)
Synthetic solutions		
1.5×10^{-3} *M* Fe(III)	10.3	0.01
3.0×10^{-3} *M* Na_2CO_3, 6.0×10^{-4} *M* Fe(III)	8.3	0.02
0.83×10^{-3} *M* Mg(II), 2.5×10^{-3} *M* Ca(II), 3.0×10^{-3} *M* Na_2CO_3[a]	11.2	0.01
$Pb\text{-}PbO_2$ Electroplating rinse water		
1.5×10^{-3} *M* Fe(III)	7.6	0.01

[a]Treatment essentially soda-lime softening.

process, untreated; the other had had Na_3PO_4 added to precipitate lead. (Phosphate addition, followed by settling, is their present waste treatment method.) Presumably because of variations in settling efficiency, unacceptably high concentrations of lead have on occasion been discharged to the city sewer system. Carry-over of solids containing lead seems a likely explanation, since axial filtration of the phosphate-treated waste yielded a filtrate containing only about 0.01 ppm Pb. Even if control of conditions were improved so that reliable removal were attained, however, this treatment might in the future be unacceptable if restrictions on phosphate discharge were imposed.

A characteristic of these electroplating wastes is the presence of Fe(III) solids [probably Fe(III) oxide] which most likely arise in plating Pb and PbO_2 on a steel substrate. The cation exchange properties of hydrous oxides in alkaline medium are well established,[15] so that the removal of Pb(II) by Fe(III) oxide at pH ~7 is to be expected; even if Fe(III) oxide is not present already, the addition of Fe(III) and its subsequent precipitation should be just as effective. About 0.43 mole of lead was associated with a kilogram of the (dried) suspended solids, a capacity that is not unusual for hydrous oxides.[15] However, effective separation of solids from liquid is required to assure low levels of Pb(II) in the effluent.

Filtration of the untreated rinse wastewater [originally about 20 ppm Pb(II), pH about 7, about 250 ppm suspended solids, probably Fe(III) oxide] from the electroplating plant was also carried out. Axial filtration through 0.45-μ Acropor AN or fire-hose jackets gave clear, colorless filtrates containing less than 0.02 ppm of lead; fluxes at about 20 psi were more than 500 gal ft^{-2} day^{-1} for 3-hr tests (extrapolated, about 350 gal ft^{-2} day^{-1} at 7 hr), and rejuvenation of the Acropor filter was easily accomplished by increased rotor velocity or mild backwashing. Filtration in the cross-flow loop confirmed these results: filtrate contained less than 0.04 ppm of lead (most likely about 0.01 ppm); turbidity was 0.25 JTU (distilled water, 0.10 JTU), and Fe(III) was undetectable. Fluxes were encouraging (Fig. 6.17).

Confirmation of these results with fresh solutions to higher water recoveries is desirable, especially since the shipped-in effluents used had aged considerably before our runs. It appears likely that cross-flow filtration, without further chemical additions to the industrial waste studied [or in other cases, if necessary, the addition of Fe(III) and the removal of Pb(II) by the Fe(III) oxide solids] will remove most of the water with a Pb(II) impurity (and, predictably, many other

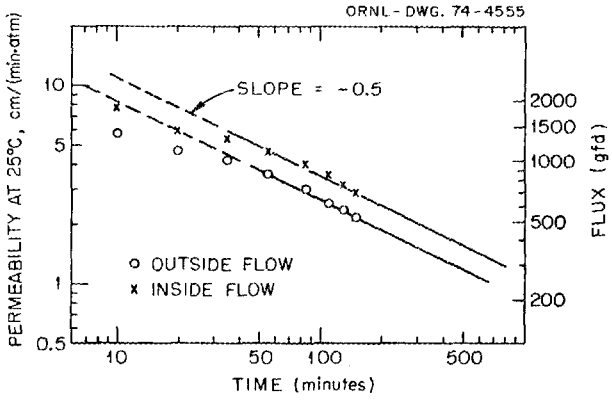

Fig. 6.17. Cross-flow filtration of lead-plating rinse wastewater. Conditions: about 10 psig, about 5 fps, about 25°C, fire-hose jacket filter.

toxic ion impurities as well) adequately low for discharge or reuse.

Cross-Flow Filtration of Sewage: ORNL Pilot Plant

N. E. Harrison J. J. Perona[17]
J. D. Hutchins[16] W. G. Sisson[18]

For a number of years we have been investigating the treatment of the effluent from the primary settling of municipal sewage with "physical-chemical" additives – powdered activated carbon or Al(III) or Fe(III) salts – followed by cross-flow filtration to remove the bulk of the water. This treatment usually produces product of higher quality than standard biochemical secondary treatment, should be more reliable, and should require much less space. In comparison with standard physical-chemical treatment, in which solid-liquid separation is achieved by settling, the product from cross-flow filtration usually appears better, and space requirements are also less. These advantages may in some situations overbalance the higher energy requirements. For further development of the concept, the Chemical Technology Division and Operations Division have built a pilot plant, comprising approximately 70 ft^2 of membrane surface, with a nominal capacity of 10,000 gal/day, at the ORNL sewage plant. The Water Research Program has cooperated in the initial operation of this unit.

In the pilot plant, Fe(II) is added as sulfate and oxidized to Fe(III) by air sparging; additional H_2SO_4 is added to reach a preset controlled acidity (usually pH about 4); the pH is then adjusted to neutral, and the slurry is pumped past the filtering surface. The filtering surfaces consist of approximately 3-in.-diam fire-hose jackets, supported on the inside by perforated metal tubes and contained in another metal jacket. There are

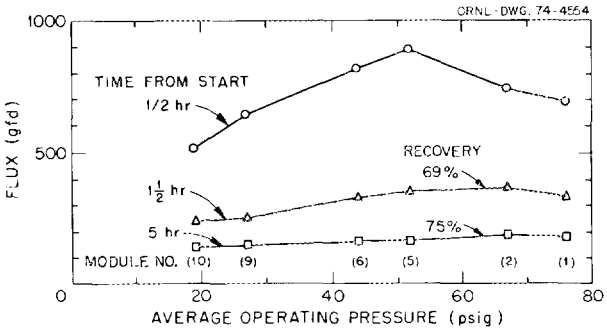

Fig. 6.18. Flux vs average pressure in cross-flow filtration of ORNL sewage.

ten modules, each about 10 ft long, pressurized slurry being circulated in the annulus.

The results so far have confirmed in general the observations we had made earlier in our mobile unit at the Oak Ridge Municipal East Sewage Plant. Average fluxes (with backwashes at 24-hr intervals) of about 150 gal ft^{-2} day^{-1} appear attainable. Product quality is usually good – typical values are about 15 ppm organic carbon, about 0.5 ppm phosphate, and about 1 JTU turbidity.

One question which the pilot plant is settling fairly definitively is the effect of pressure on flux rate. Earlier results at the city plant had suggested that, within the limits of our operating range, pressure, after relatively short initial transients, had relatively little effect on flux. It appeared that the higher the pressure, the thicker or the more compacted the filter-cake layer. However, since only one pressure could be tested at a time, our earlier results were somewhat ambiguous, because of the rapid changes which frequently occur in sewage composition. With the ORNL pilot plant, there is a rather large pressure drop through the system from the first to the last modules. Since only a small fraction of the water is removed in a single pass of feed through the module bank, fluxes are obtained in which conditions are essentially identical, except for pressure. Figure 6.18, obtained by a team from the MIT School of Chemical Engineering Practice, confirms that flux is clearly not directly proportional to pressure and, in time, becomes almost independent of pressure.[19]

Removal of Low-Level Radioactivity from Aqueous Solutions

A. J. Shor R. E. Minturn
C. G. Westmoreland

We have been interested for some time in developing filtration techniques for decontamination of solutions containing low-level radioactivity. As an example of a practical feed, we have used ORNL process water. Plans for construction of a new treatment plant have provided further motivation.

In earlier laboratory tests,[4] cross-flow filtration of process water, softened by precipitation of $CaCO_3$ and $Mg(OH)_2$ in the presence of a few ppm of Fe(III), removed 99% of ^{90}Sr. This can be compared with the 80% removal typical of the present plant, which utilizes softening and clay addition, with solid-liquid separation by settling. Attempts during the period of this report to confirm these results with a field cross-flow unit utilizing fire-hose jackets, located at the present processing plant, were not very successful, either with Fe(III) or clay addition; 97% was the highest removal, and values were frequently less. However, hyperfiltration of filtered water from one of the tests confirmed that removal of over 99.9% ^{90}Sr was attained by a two-stage process.

A rough correlation was noted between the hardness reduction and ^{90}Sr removal in cross-flow filtration. Good removal of Ca(II) and Mg(II) is also important for a second-stage hyperfiltration, since fluxes through dual-layer Zr(IV)-PAA membranes are sensitive to hardness above 10 ppm,[5] expressed as $CaCO_3$ (about 10^{-4} *M*). In the run of Table 6.10, when the cross-flow product was added to the loop, fluxes fell to 15–30 gal ft^{-2} day^{-1}, less than a third of their value with feed containing no divalent cations. Further, the design of the new processing plant[20] calls for softening to less than 10 ppm in a step preliminary to ion exchange treatment, a value which may prove difficult to attain consistently with settling.

The importance of efficient softening, plus a desire to identify factors affecting performance in cross-flow filtration, led us to resume laboratory tests with synthetic feeds under better controlled conditions. A typical run is summarized in Fig. 6.19; the numbers in the points indicate the order in which they were taken. The pH range from 10.5 to 12 was scanned repetitively. Concentration of Mg(II) in the filtrate was in all cases somewhat higher than that calculated (solid line) from a literature value of the solubility product,[21] even when adjusted by estimate[22] of the effect of the ionic strength contribution of other solutes at the maximum level in which they occurred during the run (dotted line). Whether the difference arises from passage of small particles through the filter, slow precipitation, or inaccurate solubility data is not yet clear.

In any case, softening at pH above 11, in the presence of adequate carbonate to precipitate Ca(II), combined with cross-flow filtration, should give a filtrate below

Table 6.10. Hyperfiltration of product from cross-flow filtration of ORNL process waste[a]

Cross-flow filtration at pH 10 with clay added, hyperfiltration with dual-layer hydrous Zr(IV) oxide–PAA dynamic membranes, 950 psig, 25°C

Nuclide	Process waste	Cross-flow product	Hyperfiltration product	
			Zero recovery	90% recovery
Gross beta, counts min^{-1} ml^{-1}	97	8.6	<0.056	0.26
^{90}Sr, dis min^{-1} ml^{-1}	104	12.9	<0.053	<0.064
^{137}Cs, dis min^{-1} ml^{-1}	170	16.2	<0.02	1.3

[a]The analyses for radioactivity were made by M. E. Pruitt and associates of the Analytical Chemistry Division.

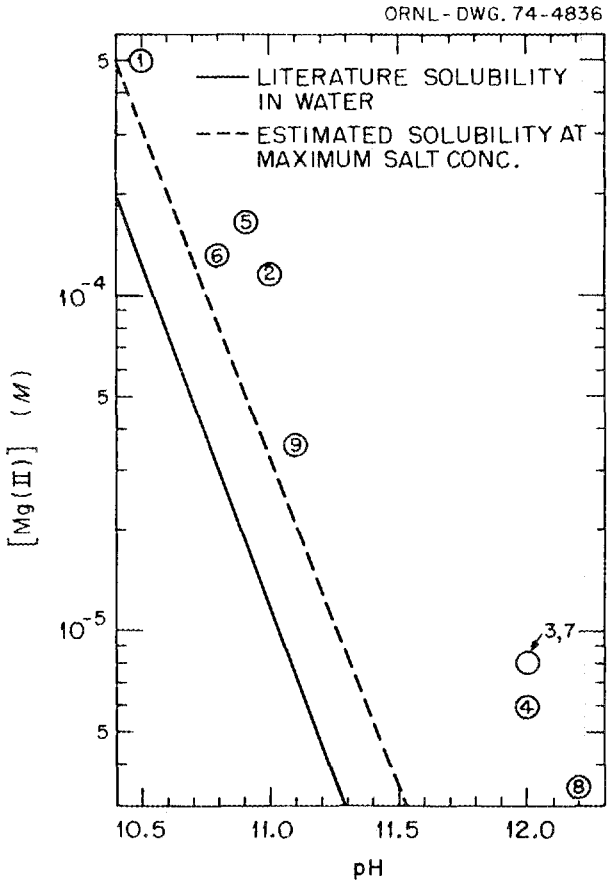

Fig. 6.19. Mg(II) concentration in cross-flow filtration product vs feed pH. Conditions: inside pressure, fire-hose jacket, 5 fps, 10 psi.

10 ppm hardness. It also appears that even with the less-than-optimum performance reported here, cross-flow filtration and hyperfiltration may eventually provide a cheaper[5] alternative to the softening–ion exchange approach[20] for removal of low-level radioactivity.

1. G. E. Moore, R. E. Minturn, et al., *Hyperfiltration and Cross-Flow Filtration of Kraft Pulp Mill and Bleach Plant Wastes,"* ORNL-NSF-EP-14 (May 1972).
2. J. S. Johnson, R. E. Minturn, and G. E. Moore, *Tappi* 57, 134 (1974).
3. *Chem. Div. Annu. Progr. Rep. May 20, 1973,* ORNL-4891, pp. 81–85.
4. *Chem. Div. Annu. Progr. Rep. May 20, 1972,* ORNL-4791, pp. 94–98.
5. D. G. Thomas, "Application of Dynamic Membranes to Desalination of Brackish Water," *Proceedings of the 4th International Symposium on Fresh Water from the Sea, Heidelberg, Germany, September 1973,* A. Delyannis, ed., Work. Party Fresh Water Sea: Amaroussion, Greece, 1973, vol. 4, pp. 407–416.
6. C. Aurich, C. A. Brandon, J. S. Johnson, Jr., R. E. Minturn, K. Turner, and P. H. Wadia, *J. Water Pollut. Contr. Fed.* **44**, 1545 (1972).
7. C. A. Brandon, J. S. Johnson, R. E. Minturn, and J. J. Porter, *Text. Chem. Color.* **5**, 35 (1973).
8. T. W. Bush, E. M. Suuberg, J. J. Toman, and M. Yonezawa, "Performance Characteristics of Dynamically Formed Hydrous Zr(IV) Oxide–Polyacrylic Acid Membranes in Treating Textile Dyeing Effluents," ORNL-MIT-182 (October 1973). (J. W. Tester was the Director of the Massachusetts Institute of Technology School of Chemical Engineering Practice, Oak Ridge Station, and R. M. Mayer the Assistant Director during this period.)
9. J. A. Dahlheimer, D. G. Thomas, and K. A. Kraus, *Ind. Eng. Chem., Process Des. Develop.* **9**, 565 (1970).

10. *The Environment and Technology Assessment Progr. Rep. June–December 1970,* ORNL-NSF-EP-3 (February 1971), p. 231.

11. W. Fulkerson, W. D. Shults, and R. I. Van Hook, eds., *Ecology and Analysis of Trace Contaminants, Progr. Rep. January 1973–September 1973,* ORNL-NSF-EATC-6 (January 1974), p. 32.

12. F. Nelson, H. O. Phillips, and K. A. Kraus, *Chem. Div. Annu. Progr. Rep. May 20, 1972,* ORNL-4791, p. 88.

13. J. G. Dean, F. L. Bosqui, and K. H. Lanouette, *Environ. Sci. Technol.* 6, 519 (1972); J. D. Hem and W. H. Durum, *J. Amer. Water Works Ass.* 65, 562 (1973).

14. W. Stumm and H. Bilinski, "Trace Metals in Natural Waters," p. 39 in *Advances in Water Pollution Research,* Proceedings of 6th International Conference, Jerusalem, June 18–23, 1972, S. H. Jenkins, ed., Pergamon Press, New York, 1972.

15. K. A. Kraus et al., "Ion Exchange Properties of Hydrous Oxides," p. 73 in *Progress in Nuclear Energy,* series IV, vol. 2, Pergamon Press, New York, 1960.

16. Operations Division.

17. Consultant to the Chemical Technology Division; Professor of Chemical Engineering, University of Tennessee, Knoxville.

18. Chemical Technology Division.

19. S. A. Murtha, R. Filiba, J. S. Newman, and R. D. Orlandi, "Characterization of ORNL's Cross-Flow Filtration Plant for Treating Primary Sewage Effluent," ORNL-MIT-189 (Apr. 26, 1974). (J. W. Tester, Director, and R. M. Mayer, Asst. Director, of the Oak Ridge Station, MIT School of Chemical Engineering Practice.)

20. J. M. Holmes and F. E. Harrington, *AIChE Symposium Series* 69 (No. 129), 183 (1973).

21. Handbook of Chemistry and Physics, 50th ed., The Chemical Rubber Co., Cleveland, Ohio, p. B252.

22. W. L. Marshall and R. Slusher, *J. Chem. Eng. Data* 13, 83 (1968).

ADSORPTION OF INORGANIC MATERIALS ON UNCHARGED POLYSTYRENE-DVB COPOLYMERS

F. Nelson K. A. Kraus

From a comparison of adsorption reactions of activated carbons and of ion exchange resins of the polystyrene-DVB type, it became obvious that many of them do not depend on the presence of fixed charges on the network. The concentration of such fixed charges on activated carbon immersed in acidic solutions is at least an order of magnitude less than for the anion exchanger Dowex 1. In many instances – for example, acid adsorption and complex-ion adsorption – the similarities between these two types of adsorbents probably result from similarities in the solvent properties of the imbibed water. On the basis of these considerations, one would expect that the aqueous layer near a polystyrene-DVB surface (e.g., in the layer within 5 Å of the surface) would show properties reminiscent of both the anion exchangers and the activated carbons.

Within recent years, copolymers of this type with high surface areas per gram have become available from various manufacturers. One of these, an experimental product by Rohm and Haas, XAD-4, is started to have an area of 800 m^2/g. The material is presumed to be an agglomerate of very small copolymer beads and is the starting product for preparation for macroreticular resins. These essentially colorless materials have been introduced for use in certain organic separations.

We have carried out several series of acid adsorption and complex-ion adsorption experiments with these materials and showed that at least qualitatively their properties are very similar to those of the activated carbons. Thus, XAD-4 strongly adsorbs acids from concentrated LiCl solutions, and it strongly adsorbs complex ions of the MCl_4^- type from concentrated chloride solutions. Nitrate complexes of Th(IV) and U(VI) may also be adsorbed from concentrated nitrate solutions. A variety of separations are feasible which are reminiscent of equivalent anion exchange separations and activated carbon separations. A few typical illustrations are shown in Figs. 6.20 and 6.21.

The similarities in adsorptive behavior between anion exchangers, copolymers, and activated carbons are striking.

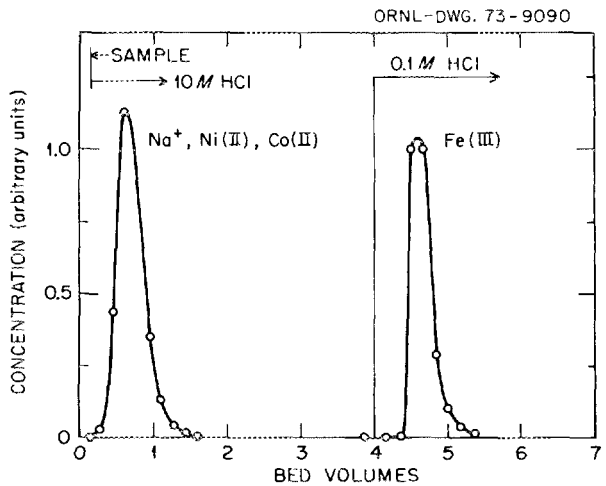

Fig. 6.20. Separation of Fe(III) from some weakly adsorbed elements. Conditions: polystyrene-DVB copolymer (Rohm & Haas XAD-4); sample – trace Na^+, Ni(II), and Co(II) and 5 × 10^{-4} *M* Fe(III) in 10 *M* HCl.

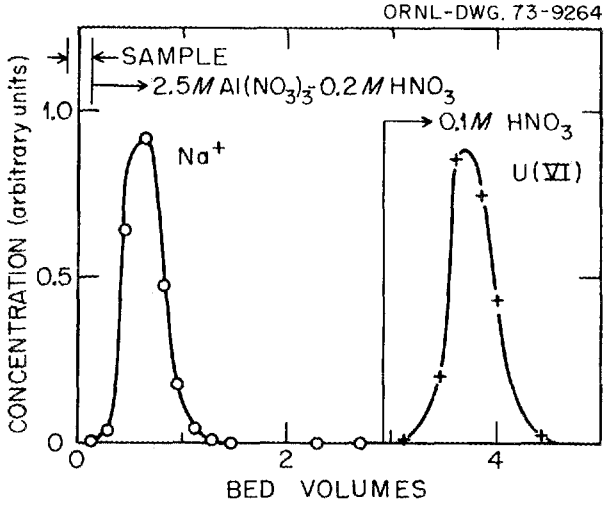

Fig. 6.21. Separation of U(VI) from Na^+ in concentrated $Al(NO_3)_3$ solution. Conditions: polystyrene-DVB copolymer (XAD-4), 25°C, 0.05 *M* U(VI), trace ^{22}Na in 2.5 *M* $Al(NO_3)_3$–0.2 *M* HNO_3.

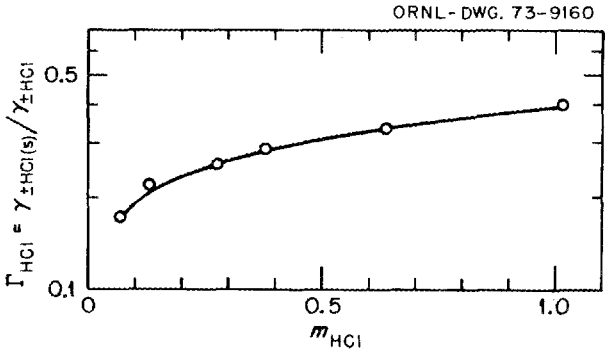

Fig. 6.22. Activity coefficient ratio of HCl in 12.7 *m* LiCl. Conditions: coconut charcoal, microporous volume 0.6 cc/g.

ADSORPTION OF INORGANIC MATERIALS ON ACTIVATED CARBON

F. Nelson K. A. Kraus

Last year we reported on the adsorption of a variety of inorganic materials on activated carbons and illustrated these adsorptions with a number of separations. These experiments dealt with cation exchange properties of activated carbons, which become dominant in basic solutions, with adsorption of certain salts from neutral and slightly acidic solutions, and with adsorption of negatively charged chloride complexes from concentrated chloride solutions. The studies have been extended, with particular emphasis on adsorption of metal complexes from concentrated electrolyte solutions, including adsorption and separations involving uranium(VI) in concentrated nitrate solutions. Much of this work has been written up and presented at the 29th Annual Purdue Industrial Waste Conference, May 1974.

In view of the formal similarity in the adsorption of metal complexes by activated carbons and by commerical ion exchange resins of the polystyrene-DVB type (e.g., Dowex 1), detailed studies of acid adsorption by activated carbons were carried out. Such acid adsorption has long been known for activated carbons,[1] but it was of interest to get a quantitative comparison on adsorption of acids from concentrated electrolyte solutions by these two types of materials. The studies were carried out with a coconut charcoal whose microporous volume was estimated from nitrogen and water adsorption isotherms to be about 0.6 cc per gram of dry carbon.[2]

In an extensive series of experiments, uptake of HCl and of LiCl from the two-component systems and from various HCl-LiCl mixtures was determined. From the uptake data, activity coefficient ratios $\Gamma = \gamma_{\pm J(r)}/\gamma_{\pm J}$ were calculated for the components *J* (subscript *r* designates the carbon phase, no subscript the solution phase; the carbon phase here is identified with the microporous volume). A typical set of results is shown in Fig. 6.22 for a series of HCl-LiCl mixtures with ionic strength 12.7 *m*. The activity coefficient ratio Γ_{HCl} is significantly less than unity and decreases with decreasing molality of HCl; Γ_{LiCl} is essentially constant and near unity in these mixtures. These results are both qualitatively and quantitatively similar to those which we have observed earlier[3] for anion exchange resins of the polystyrene-DVB type.

Preferential adsorption of acids from concentrated electrolyte solutions seems to be a general phenomenon for the activated carbons, as it was for anion exchangers. Because of this preferential adsorption, activated carbons can be used to remove acids from salt solutions. Use of small columns of activated carbon for deacidification HCl-NaCl, $HClO_4$-$NaClO_4$, and HNO_3-$LiNO_3$ solutions is illustrated in Fig. 6.23 and 6.24.

Many investigators have ascribed anion exchange properties to activated carbon (see, e.g., refs. 4 and 5). This anion exchange activity has been deduced from retention of certain anions by extensively washed carbons and has been attributed to carbonium ions incorporated in the carbon network. Although the existence of these fixed anion exchange sites is still controversial, there is no doubt that residual anions are difficult to remove by washing. The extent of possible anion exchange activity, as determined by such washing

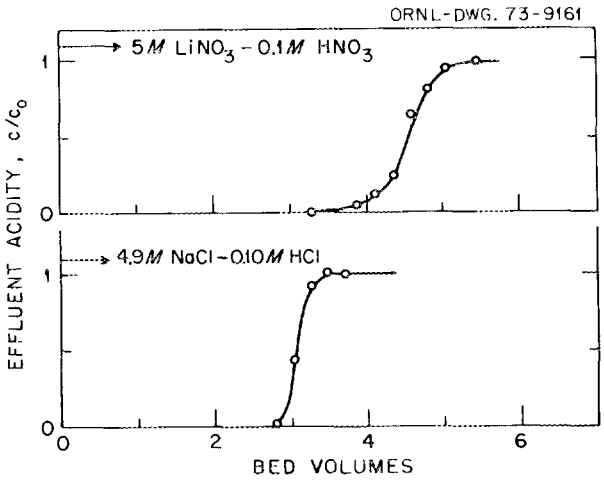

Fig. 6.23. Adsorption of acids from concentrated electrolyte solutions. Conditions: coconut charcoal, 100–200 mesh, 25°C.

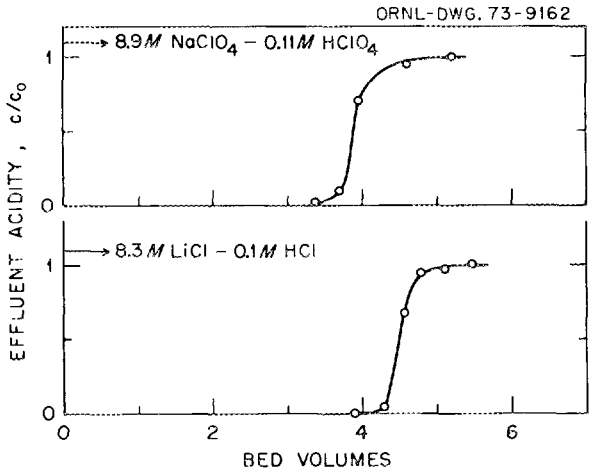

Fig. 6.24. Adsorption of acids from concentrated electrolyte solutions. Conditions: coconut charcoal, 100–200 mesh, 25°C.

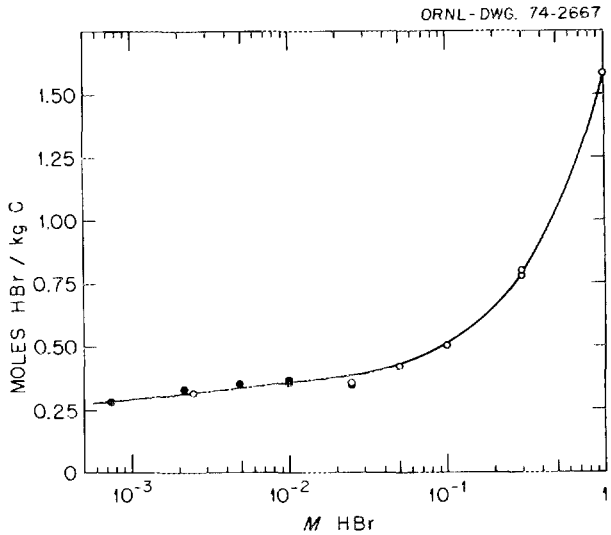

Fig. 6.25. Adsorption of HBr by activated carbon (coconut charcoal).

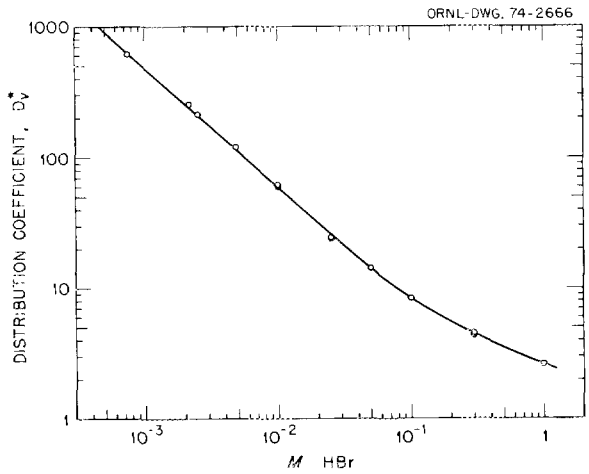

Fig. 6.26. Adsorption of HBr by activated carbon. Conditions: coconut charcoal, microporous volume 0.6 cc/g.

experiments, however, is quite small (of the order of a few tenths of a mole per kilogram of adsorbent) and thus is insufficient to be held responsible for the similarity between the organic ion exchange resins and the carbon.

We believe that anion retention by activated carbon is less due to carbonium ions in the network than to adsorption of acid by the carbon, with distribution coefficients of the acid increasing rapidly with decreasing ionic strength. A particularly convenient system to study is adsorption of HBr since the total bromide content can easily be determined by a radiometric self-exchange method with solutions containing the tracer ^{82}Br. The results of a series of experiments on bromide adsorption in the range 10^{-3} to 1 M HBr are shown in Fig. 6.25. While HBr adsorption decreases with decreasing HBr concentration and tends to level off at low HBr concentrations, there is no region in which HBr uptake becomes completely independent of concentration, as one would have expected from an anion exchanger of fixed capacity. A plot of distribution coefficients D vs molarity of HBr (Fig. 6.26) or of Γ vs molarity of HBr (note that in this case D is about equal to $1/\Gamma$) shows no "break" which would imply a significant change in the mechanism of adsorption of HBr.

As is well known, activated carbon contains macropores and pores of intermediate size, in addition to the micropores. One can conceive of filling the larger pores with some other adsorbents such as a hydrous oxide without affecting the microporous structure. The resulting material might then show the combined adsorptive properties of activated carbon and of the "filler" for which the activated carbon would be the carrier. Such arrangements might also be of advantage when the filler adsorbent cannot easily be prepared in a form permitting high-velocity column operation.

In this context we have prepared an activated carbon containing the hydrous oxide of Fe(III) by first adsorbing Fe(III) as the negatively charged chloride complex, treating the mixture with ammonia, and washing and drying the product. The resulting composite contained 3.5 moles of Fe(III) per kilogram of carbon.

The activated carbon containing the hydrous oxide showed some enhancement in adsorption of the copper-ammonia complex over the untreated material and significantly higher adsorption of strontium. Phenol adsorption was slightly less than for the untreated material.

Activated carbon containing the hydrous Fe(III) oxide becomes strongly ferromagnetic when heated a short time in a nitrogen atmosphere near 650°C. X-ray examination showed that 80 to 90% of the iron oxide in the carbon had the magnetite structure and presumably was Fe_3O_4.[6]

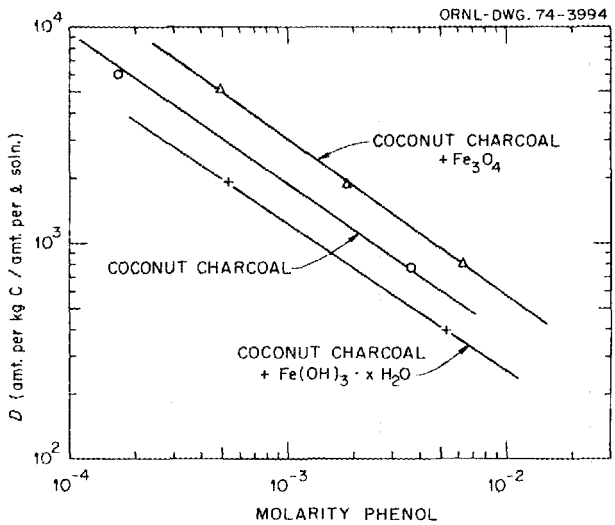

Fig. 6.27. Effect of iron oxides on adsorption of phenol by activated carbon. Conditions: 100–200 mesh coconut charcoal, 0.10 *M* $NaHCO_3$, 25°C.

These magnetically active carbons retain their capacity for adsorption of organic compounds. An illustration is given in Fig. 6.27, in which distribution coefficients for phenol are given for the original untreated coconut charcoal and one containing 21% Fe_3O_4 by weight. The distribution coefficients refer to the amount of phenol adsorbed per kilogram of carbon, not per kilogram of adsorbent. Corresponding data for the adsorption of phenol by the precursor material [carbon containing hydrous Fe(III) oxide] are also shown in the figure. While the Fe(III)-containing carbon shows somewhat lower adsorption for phenol than the untreated charcoal, the magnetic activated carbon shows higher distribution coefficients. It is not clear if this improvement results from additional activation during the heating process or from added adsorption of phenol by the magnetite in the carbon.

We believe that magnetic activated carbons may have special uses in a number of separations since removal of these carbons by magnetic methods could, under some conditions, be much more efficient and rapid than removal by conventional settling techniques.

---

1. V. R. Deitz, *Bibliography of Solid Adsorbents (1900–1942)*, Lancaster Press, Lancaster, Pa., 1944; *Bibliography of Solid Adsorbents (1943–1953)*, U.S. Department of Commerce, National Bureau of Standards Circular 566 (1956).
2. We are indebted to E. L. Fuller, Jr., for measurement of the adsorption isotherms.
3. F. Nelson and K. A. Kraus, *J. Amer. Chem. Soc.* **80**, 4154 (1958).
4. B. Steenberg, "Adsorption and Exchange of Ions on Activated Charcoal," Ph.D. thesis, Stockholm University, Almquist and Wiksells, Uppsala, 1944.
5. V. A. Garten and J. E. Weiss, *Rev. Pure Appl. Chem.* 7, 69 (1957).
6. We are indebted to L. D. Hulett of the Analytical Chemistry Division for the x-ray examinations.

EXTRACTION OF LITHIUM FROM NEUTRAL SALT SOLUTIONS WITH FLUORINATED β-DIKETONES[1]

F. G. Seeley[2] W. H. Baldwin

The quantitative and selective solvent extraction of lithium from aqueous solutions of alkali metal salts with β-diketones has been reported previously.[3,4] However, at pH values below 11, practicable extraction levels were not obtained, and it was reasoned that fluorinated β-diketones might be sufficiently acidic to allow efficient extraction of lithium from near-neutral salt solutions. The applicability of selective and quantitative extraction of lithium from neutral brines and seawater concentrates is obvious.

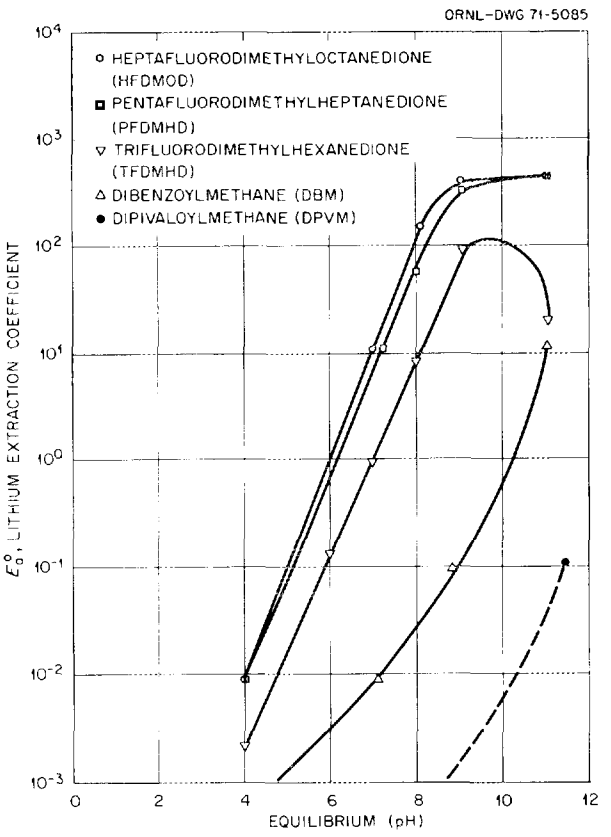

Fig. 6.28. Dependence of lithium extraction coefficients for various β-diketones on pH. Organic phase, 0.2 *M* β-diketone–0.1 *M* TOPO in benzene; aqueous phase, 1 *M* KCl and 0.01 *M* LiCl.

Figure 6.28 summarizes the lithium extraction with 0.2 *M* solutions of several β-diketones [in 0.1 *M* trioctylphosphine oxide (TOPO) in benzene] from 1 *M* KCl over the pH range 4 to 11. The efficiency of lithium extraction is seen in general to be orders of magnitude greater for the fluorinated β-diketones (HFDMOD, PFDMHD, and TFDMHD) than for the nonfluorinated analogs (DBM and DPVM) at the same pH.

Although with the compound 1,1,1,2,2,3,3-heptafluoro-7,7-dimethyl-4,6-octanedione (HFDMOD) the separation factors for lithium vs the other alkali metals are good (about 1300 from sodium, 2500 to 4000 from potassium, rubidium, and cesium), the selectivity over the alkaline earths is poor (in fact, magnesium and calcium are extracted more strongly than lithium, and strontium extraction is about equal to that of lithium). Additionally, the present cost of these fluorinated β-diketones makes impractical the large-scale recovery of lithium from brines in which the lithium concentration is low (less than 100 ppm). However, the process has been shown advantageous in the treatment of certain brine concentrates.[5]

1. Based on work carried out in the Chemical Technology Division: *Chem. Technol. Div. Annu. Progr. Rep. Mar. 31, 1971*, ORNL-4682, p. 168; F. G. Seeley and W. H. Baldwin, U.S. Pat. 3,793,433 (Feb. 19, 1974).
2. Chemical Technology Division.
3. T. V. Healy, *Chem. Div. Progr. Rep. November 1964–April 1965*, AERE PR/Chemistry 8, Harwell, Berks. (1965).
4. D. A. Lee, W. L. Taylor, W. J. McDowell, and J. S. Drury, *J. Inorg. Nucl. Chem.* **30**, 2807 (1968).
5. *Chem. Technol. Div. Annu. Progr. Rep. Mar. 31, 1972*, ORNL-4794, p. 57.

ELECTROCHEMISTRY

TWENTY-YEAR INHIBITION OF CORROSION BY THE PERTECHNETATE ION

G. H. Cartledge[1]

Over 20 years have elapsed since the discovery in our laboratory of the effectiveness of the pertechnetate ion in inhibiting the corrosion of iron and steel.[2–4] In the meantime, numerous studies bearing on the mechanism of the inhibiting action of the pertechnetate ion and other inorganic oxyanions have been carried out.[5] As an illustration of the long-term inhibiting action of the pertechnetate ion, a test specimen of carbon steel remains bright and unchanged in weight and beta activity after being exposed for 20 years in 5×10^{-4} *f* $KTcO_4$ containing 10 ppm of chloride ion at pH ~6, and with access of air. It may be concluded that the continuing passivity is maintained by the combined action of oxygen and the noncathodic effect of adsorbed pertechnetate ions, the stability of the film being enhanced by a very small amount (much less than monolayer) of $Tc(OH)_4$ contained in it. A summary of these studies has been published in *Corrosion*.[6]

1. Consultant.
2. G. H. Cartledge, *J. Amer. Chem. Soc.* 77, 2658 (1955).
3. G. H. Cartledge, *J. Phys. Chem.* 59, 979 (1955).
4. G. H. Cartledge, *Corrosion* **11**, 335t (1955).
5. G. H. Cartledge, *Brit. Corros. J.* **1**, 293 (1966).
6. G. H. Cartledge, *Corrosion* **29**, 361 (1973).

EFFECT OF Ti(IV) ON THE ELECTROCHEMICAL BEHAVIOR OF TITANIUM AND ITS RELEVANCE TO PITTING AND CREVICE CORROSION

E. J. Kelly

In recent years, several authors have reported that Ti(IV) ions inhibit the active-state dissolution of titanium.[1] The results summarized in this report show how

one might easily arrive at that conclusion, but also prove that the conclusion is incorrect. In fact, Ti(IV) ions have no effect on the constant-potential dissolution rate of titanium, and actually accelerate rather than inhibit the open-circuit corrosion rate of the metal. The importance of this finding, particularly in the areas of pitting and crevice corrosion, is discussed below.

The upper curve in Fig. 6.29 is a typical anodic polarization curve for titanium in deoxygenated 1 N H_2SO_4 in the absence of Ti(IV) ions. At any potential in the region scanned in Fig. 6.29 the net anodic current density, i, is given by the algebraic sum of the partial anodic current density corresponding to the oxidation of titanium to Ti(III) ions in solution, i_d, and the partial cathodic current density corresponding to the reduction of hydrogen ions, i_h; that is, $i = i_d + i_h$. [It should be noted that net and partial anodic (oxidation) currents are positive, while net and partial cathodic (reduction) currents are negative.] At the open-circuit corrosion potential, E_{corr}, $i = 0$ and $i_d = |i_h|$. As the potential becomes increasingly positive

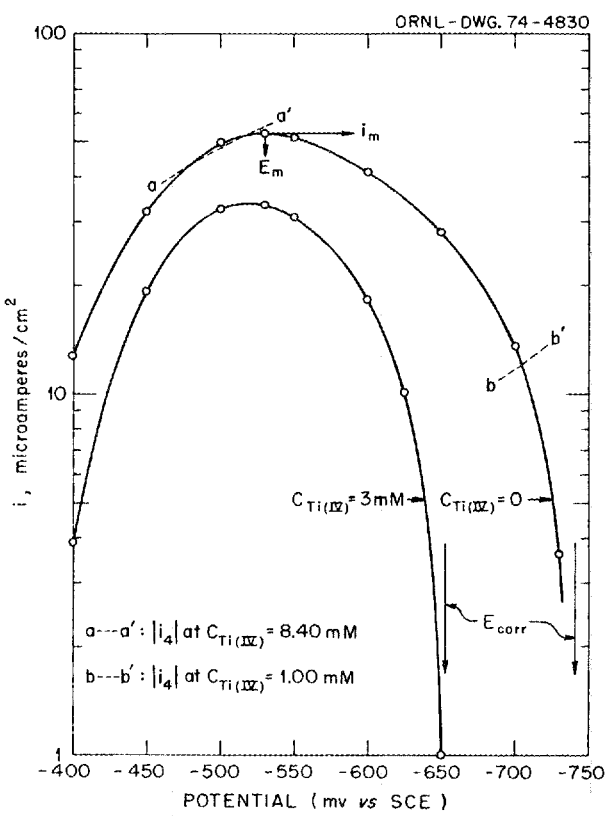

Fig. 6.29. Effect of Ti(IV) on the anodic polarization of titanium in deoxygenated 1 N H_2SO_4 at 30°C.

relative to E_{corr}, i_d increases and $|i_h|$ decreases. Coulometric weight-loss experiments have shown that at potentials as negative as E_m, $|i_h|$ is negligible compared with i_d ($|i_h| < 0.02 i_d$ at E_m). At potentials positive to E_m, i decreases as the metal is transformed from the active to the passive state. The detailed mechanistics and kinetics of the processes just described have been presented elsewhere.[2] Here, our interest lies in comparing the upper and lower curves of Fig. 6.29, the lower curve being the anodic polarization curve in the presence of Ti(IV) ions ($C_{Ti(IV)}$ = 3 mM). At first glance, it is easy to see how one might erroneously conclude that Ti(IV) ions inhibit the dissolution of titanium, since the entire anodic polarization curve is lowered by Ti(IV) ions. In a coulometric weight-loss experiment conducted at E_m, one might anticipate that, for $C_{Ti(IV)}$ = 3 mM, the current density calculated from the weight-loss data would be 33.3 $\mu A/cm^2$, just as the current density of 52.8 $\mu A/cm^2$ was calculated from the weight-loss data when $C_{Ti(IV)} = 0$. Actually, the experimentally observed weight loss corresponds to 52.8 $\mu A/cm^2$ (i.e., to i_m) in either case.

The effects of Ti(IV) ions on the polarization and corrosion behavior of titanium can be explained and completely quantified if one assumes that Ti(IV) ions are reduced to Ti(III) in the potential region under consideration and, second, that the Ti(IV) ions have no effect other than to contribute a partial cathodic current density corresponding to their reduction (i_4); thus neither i_d nor i_h is affected by the presence of Ti(IV) ions. Then the net anodic current density is given by

$$i = i_d + i_h + i_4 \ , \tag{1}$$

which becomes, in accordance with the second assumption above,

$$i = (i_d + i_h)_{C_{Ti(IV)}=0} + i_4 \ , \tag{2}$$

or

$$i = i_{C_{Ti(IV)}=0} + i_4 \ , \tag{3}$$

where $i_{C_{Ti(IV)}=0}$ is given by the upper curve in Fig. 6.29. The experiments described below prove the validity of these assumptions.

A titanium electrode was maintained at E_m in 1 N H_2SO_4. The steady-state value of i was 54.2 $\mu A/cm^2$. Then, known volumes of a standard solution of Ti(IV) in 1 N H_2SO_4 were added to the cell solution, and i was

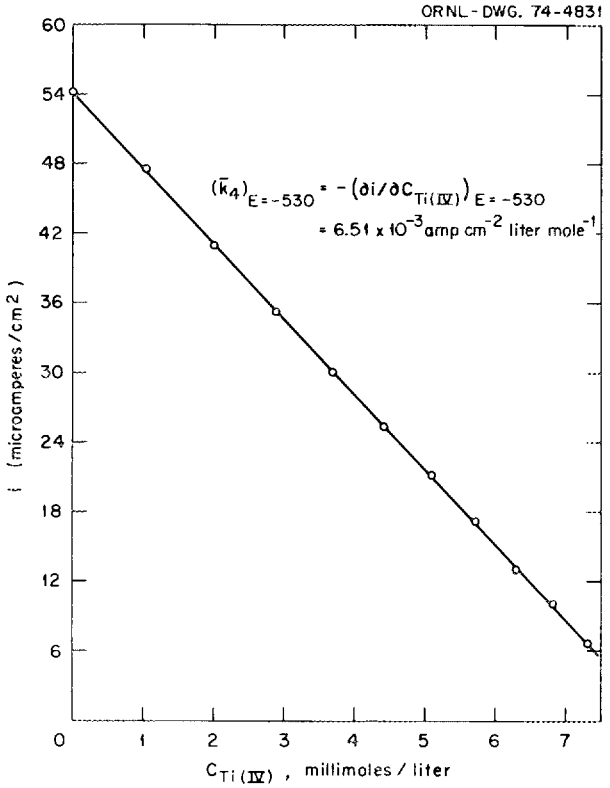

Fig. 6.30. Variation of i with $C_{Ti(IV)}$ at E = −530 mV vs S.C.E. Deoxygenated 1 N H_2SO_4 at 30°C.

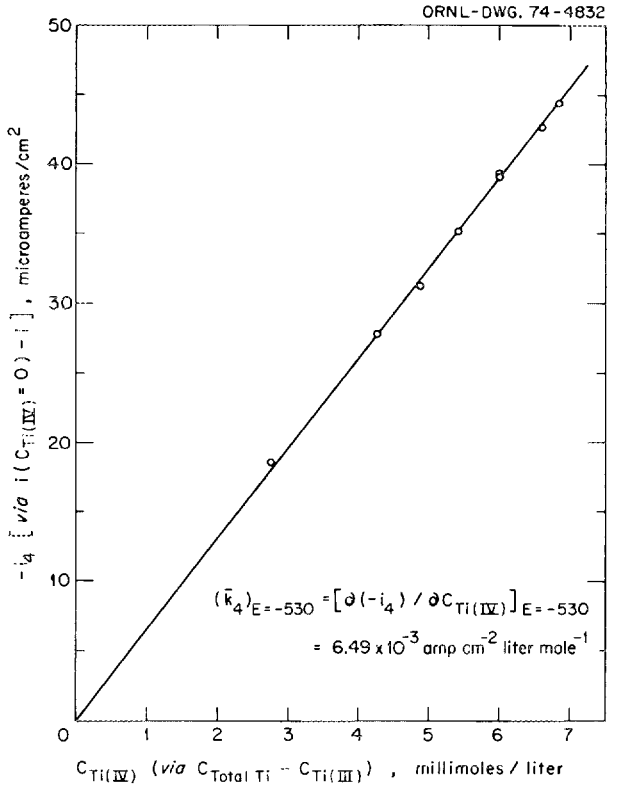

Fig. 6.31. Variation of i_4 with $C_{Ti(IV)}$ at E = −530 mV vs S.C.E. Deoxygenated 1 N H_2SO_4 at 30°C.

measured as a function of $C_{Ti(IV)}$. The results are shown in Fig. 6.30. According to Eq. (3), $(\partial i/\partial C_{Ti(IV)})_E = (\partial i_4/\partial C_{Ti(IV)})_E$, and it therefore follows from the results shown in Fig. 6.30 that

$$i_4 = -\bar{k}_4 C_{Ti(IV)} \,. \tag{4}$$

In other words, the reduction of Ti(IV) to Ti(III) is first order in $C_{Ti(IV)}$. The addition of Ti(IV) required 2.73 hr. Upon completion of the addition, the electrode was maintained at E_m for another 218.47 hr, during which time, samples were periodically removed from the cell and analyzed for Ti(III) via permanganate titration and for total Ti(III + IV) via the hydrogen peroxide spectrophotometric method. The concentration of Ti(IV) was calculated as the difference, $C_{Ti(IV)} = C_{total\ Ti} - C_{Ti(III)}$. In Fig. 6.31, $-i_4$ [calculated by use of Eq. (3)] is plotted against the concentration of Ti(IV) determined by the chemical analyses. The value of $\bar{k}_4$ is virtually identical to that determined by the addition experiment (cf. Fig. 6.30). During the 221.2 hr in which Ti(IV) was present, the titanium electrode exhibited a weight loss of 19.25 mg; this corresponds to a constant dissolution current density of 53.24 μA/cm^2. In the absence of Ti(IV), the dissolution current density values were 54.2 μA/cm^2 (cf. Fig. 6.30), 52.8 μA/cm^2 (cf. Fig. 6.29, i_m), and 51.6 μA/cm^2 (used in Fig. 6.31). These results show that Ti(IV) has no effect on the constant-potential dissolution rate of titanium, and they confirm the validity of Eqs. (1)–(4).

According to Eq. (3), at each potential the difference in the i values shown by the upper and lower curves in Fig. 6.29 is equal to $|i_4|$, and consequently the value of $\bar{k}_4$ may be determined by inserting i_4 and the specified concentration of Ti(IV) into Eq. (4). Then, having determined the potential dependence of $\bar{k}_4$, Eq. (4) may be used to construct $|i_4|$ vs potential curves (e.g., *a-a'* and *b-b'* in Fig. 6.29) for any value of $C_{Ti(IV)}$. At the open-circuit corrosion potential, $i = 0$, and according to Eq. (3), $|i_4| = i_{C_{Ti(IV)}=0}$; that is, the open-circuit corrosion potential in the presence of Ti(IV) is given by the intersection of the corresponding $|i_4|$ vs potential curve with the upper curve in Fig. 6.29. The corrosion potential vs $C_{Ti(IV)}$ curve calculated in this manner is shown by the dashed curve in Fig. 6.32.

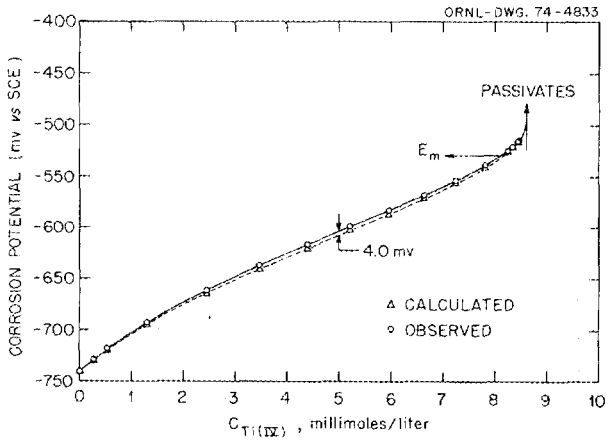

Fig. 6.32. Effect of Ti(IV) on the corrosion potential of titanium in deoxygenated 1 *N* H_2SO_4 at 30°C.

The solid curve in Fig. 6.32 shows the experimentally observed corrosion potential as a function of $C_{Ti(IV)}$. The data for the solid curve were obtained by an addition experiment in which known volumes of a standard Ti(IV) solution [Ti(IV) in 1 *N* H_2SO_4] were added to the cell, which initially contained a known volume of 1 *N* H_2SO_4. It is important to note that when $C_{Ti(IV)}$ reaches the level where the $|i_4|$ vs potential curve is tangent to the upper curve in Fig. 6.29, the titanium should passivate. This was observed to occur at $C_{Ti(IV)} = 8.6$ m*M*.

The open-circuit corrosion rate is given by the value of i_d existing at the intersection of the upper curve in Fig. 6.29 and the corrosion potential. With increasing $C_{Ti(IV)}$, the corrosion potential becomes increasingly positive (cf. Fig. 6.32) and consequently the corrosion rate increases. The corrosion rate reaches a maximum value corresponding to i_m (cf. Fig. 6.29) and then drops sharply when $C_{Ti(IV)}$ reaches the critical passivation concentration of 8.6 m*M*. Thus, although the constant-potential titanium dissolution rate is independent of Ti(IV), the corrosion rate is accelerated by Ti(IV) ions.

When titanium undergoes pitting (or crevice) corrosion, the metal at the base of the pit is in the active state; that is, the potential and pH conditions are such that active-state dissolution of the metal to form Ti(III) ions occurs. In moving from the base to the mouth of the pit or crevice, the interfacial potential difference and pH rise, and consequently the active state is transformed into the passive state. It was shown in earlier phases of this program that Ti(III) is oxidized at the passive titanium surface to Ti(IV).[3] In the present work, on the other hand, it was shown that Ti(IV) is reduced to Ti(III) at the active titanium surface and that the presence of Ti(IV) accelerates the corrosion rate of titanium. With regard to pitting or crevice corrosion, these facts suggest the following situation. As Ti(III) egresses from the base of the pit, it encounters conditions under which it is known to be oxidized to Ti(IV) (i.e., a passive surface). The resultant Ti(IV) diffuses back to the base of the pit, where it encounters conditions under which it is known to be reduced to Ti(III) (i.e., an active surface) and to accelerate the corrosion rate of the active base of the pit. Thus Ti(IV) would have a deleterious effect on pitting or crevice corrosion, but only if the concentration of Ti(IV) remained below the critical concentration required to passivate the active surface. If the critical concentration is attained, the metal passivates and pitting ceases. This phenomenon of spontaneous self-healing has long been recognized in pitting and crevice corrosion, but never adequately explained on a mechanistic basis.

1. N. T. Thomas and K. Nobe, *J. Electrochem. Soc.* **119**, 1450 (1972).

2. E. J. Kelly, *Proc. Fifth Int. Congress on Metallic Corrosion, Tokyo, Japan, May 22–26, 1972*, in press.

3. E. J. Kelly, *Chem. Div. Annu. Progr. Rep. May 20, 1973*, ORNL-4891, p. 87.

SEPARATION AND ANALYSIS OF IONS WITH A PACKED-BED ELECTRODE

R. E. Meyer F. A. Posey

Properties of a packed-bed silver electrode, for use in a device for the separation and analysis of iodide, bromide, and chloride ions, were described previously.[1] The electrode, as shown in Fig. 6.33, is composed of silver granules which are packed into a cylindrical bed; the potential of the electrode is controlled by use of a potentiostat. The sample solution is forced through the electrode with a positive-displacement tubing pump at a constant, known flow rate.

If the packed-bed silver electrode is maintained at a definite electrode potential, the silver ion concentration within the pores of the electrode will eventually attain the equilibrium concentration for that potential. Then, if a solution containing an ion which is capable of interacting with silver ion is pumped through the electrode, and if certain other conditions are fulfilled, reaction will proceed until equilibrium with respect to both ions is established. Thus, in the case of a precipitating ion such as the chloride ion, equilibrium with respect to both Ag^+ and Cl^- is achieved at flow rates that are sufficiently low. Similarly, if a complexing ion such as CN^- is pumped through the electrode, equilibrium with respect to Ag^+, CN^-, and $Ag(CN)_2^-$ is

ORNL-DWG. 73-3471

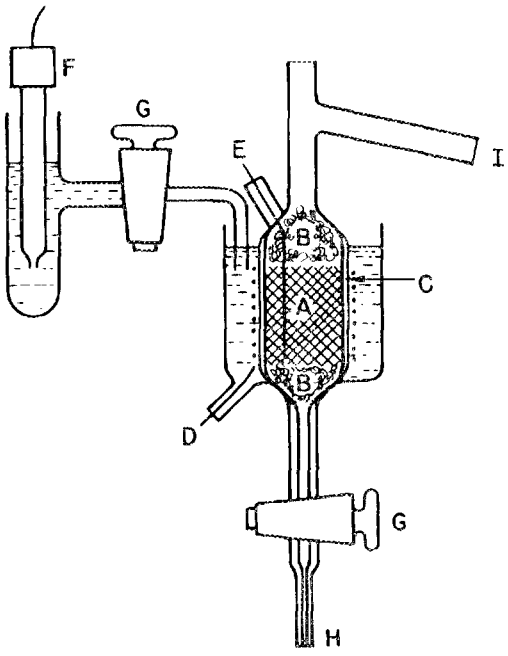

Fig. 6.33. Cross section of electrolytic cell for halide analysis. *A*, packed bed of silver granules; *B*, glass wool; *C*, section of filter tube; *D*, counterelectrode; *E*, silver wire to packed bed; *F*, reference electrode; *G*, stopcocks; *H*, solution inlet; *I*, solution outlet.

established under appropriate conditions. Further, if the potential of the electrode is set correctly, the reaction can be made to proceed essentially quantitatively; in this case the current needed to supply the silver ions is a measure of the concentration of the reacting ion in the sample solution. In the case of precipitation reactions, use of this device simultaneously separates the reacting ion from the solution and determines its concentration. By using a series of these cells set at appropriate potentials, an analyst may simultaneously separate and determine the concentrations of the halide ions with considerable precision. Some results of analyses of mixtures of halides are shown in Table 6.11. Detailed results of these studies have been published in the *Journal of Electroanalytical Chemistry and Interfacial Electrochemistry*.[2]

The cyanide ion interacts with the silver packed-bed electrode in two ways. Over the potential range from approximately 0 to +150 mV vs S.C.E., the complex ion $Ag(CN)_2^-$ is formed essentially quantitatively. Above +150 mV, precipitation of AgCN begins, and at potentials from ca. +225 to ca. +275 mV, the reaction is essentially quantitative. At potentials above ca. +300 mV, the current begins to increase excessively due to dissolution of silver from the packed-bed electrode. For analytical purposes the complexing reaction is preferable to the precipitation reaction, since precipitation of AgCN occurs at potentials only slightly less positive than the region of precipitation of AgCl for chloride-containing solutions. Thus chloride ion, which is a common constituent of aqueous streams, interferes with the determination at potentials suitable for complete precipitation of cyanide. However, cyanide ion can be removed quantitatively from an aqueous stream by precipitation in a silver packed-bed electrode, and this system therefore provides a good electrochemical method of removal as long as the chloride ion concentration is not excessive.

A calibration curve is shown in Fig. 6.34 for the potential region where the complexing reaction predominates. At low concentrations, the curve tends to bend upward because of interfering reactions; however, this bending is reasonably reproducible and does not seriously interfere with low-level analysis. At higher concentrations of cyanide ion (greater than 10^{-3} *M*), a slightly lower potential was used to avoid the region where precipitation of AgCN occurs. Equilibrium-type calculations show that the region of precipitation becomes less positive as the concentration of cyanide ion increases.

In principle, it should be possible to analyze solutions containing sulfide ion by this technique. Silver sulfide has an extremely low solubility (solubility product about 10^{-51}), and sulfide ion should be removed completely by a packed-bed silver electrode maintained at the appropriate electrode potential. We have carried out extensive measurements with sulfide solutions and have found that, in general, steady currents are not obtained. The problems may be associated with possible interferences but more probably are connected with certain aspects of the complicated chemistry of aqueous sulfide systems.

In the experiments described above, the procedure for analysis is simply to insert the input end of a tubing pump into the sample and turn on the pump, thus allowing the sample solution to flow through the packed-bed electrode. Comparisons between unknown and standard solutions are then made with the assumption that the flow rates are identical. The total amount of solution needed varies, but generally a 3- to 10-ml sample volume is required. Because tubing pumps ordinarily do not reproduce flow rates to better than about 1% over short periods of time (hours), there is always an error associated with irreproducibility of flow

Table 6.11. Analysis of solutions of mixed halides

All solutions 0.2 *M* KNO_3; nominal flow rate, 0.02 ml/sec.

Solution	Halides	Molarity	Mixture current (mA)	Standard current (mA)	Percent difference	Potential (mV vs S.C.E.)
1	I^-	10^{-4}	0.200	0.193	+3.6	0
	Br^-	10^{-3}	1.98	1.99	−0.5	+200
2	I^-	10^{-3}	1.93	1.93	0	+50
	Br^-	10^{-5}	0.0220	0.0210	+4.8	+200
3	I^-	10^{-3}	2.09	2.10	−0.5	0
	Cl^-	10^{-4}	0.220	0.218	+0.9	+275
4	I^-	10^{-3}	2.10	2.10	0	0
	Cl^-	2×10^{-4}	0.396	0.398	−0.5	+275
5	I^-	5×10^{-4}	1.04	1.05	−1.0	0
	Cl^-	5×10^{-4}	0.94	0.96	−2.0	+275
6	I^-	2×10^{-4}	0.416	0.420	−1.0	0
	Cl^-	10^{-3}	1.88	1.92	−2.1	+275
7	I^-	10^{-5}	0.0201	0.0207	−2.9	+50
	Cl^-	10^{-3}	2.01	2.08	−3.4	+275
8	Br^-	10^{-3}	2.21	2.21	0	+170
	Cl^-	2×10^{-4}	0.372	0.376	−1.1	+275
9	Br^-	5×10^{-4}	1.14	1.12	+1.8	+170
	Cl^-	5×10^{-4}	0.96	0.97	−1.0	+275
10	Br^-	2×10^{-4}	0.430	0.406	+6.4	+130
	Cl^-	10^{-3}	1.88	1.92	−2.1	+275
11	I^-	2×10^{-4}	0.392	0.392	0	0
	Br^-	5×10^{-4}	1.13	1.08	+4.6	+150
	Cl^-	10^{-3}	2.00	2.03	−1.5	+275

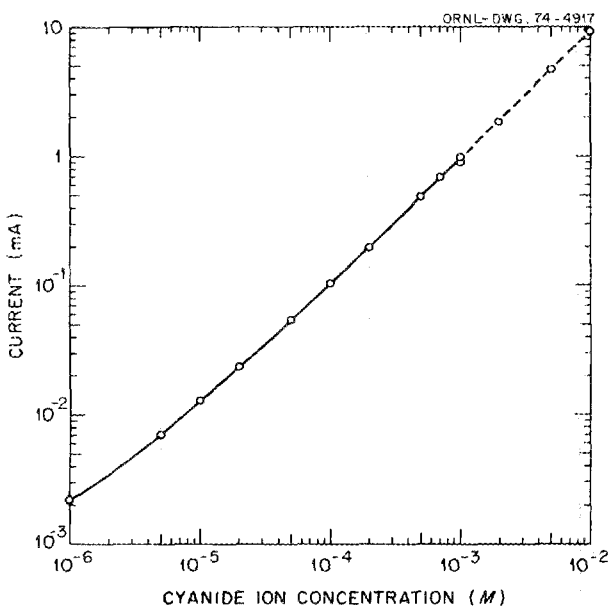

Fig. 6.34. Response of silver packed-bed electrode to cyanide ion. Flow rate, 0.022 ml/sec. Electrode potentials: solid line, +125 mV vs S.C.E.; dashed line, +100 mV vs S.C.E.

rate. However, this method of analysis does have the distinct advantage that volumetric glassware need not be used (except possibly for calibrating the flow rate of the pump). An alternative method of analysis is possible with only a slight modification of the basic apparatus. In this method a reservoir of inert electrolyte is provided, and solution from the reservoir is pumped through the cell at a rate which need not be known or precisely controlled. A steady, but usually quite small, background current is observed. A device is provided for introducing into the stream a known volume (typically 1 ml) of the unknown sample. As the unknown sample is pumped through the cell a current pulse is observed which corresponds to the electrochemical interaction of the unknown with the electrode system. The amount of the unknown is determined by integration of the current pulse. In an experiment carried out to assess the accuracy and convenience of this method, small volumes of various solutions containing silver ion were added to the cell in this manner. The results, which are shown in Table 6.12, show that reasonable accuracy may be obtained by this simple

Table 6.12. Determination of silver ion with a packed-bed silver electrode

Electrode potential: −700 mV vs S.C.E.

Sample No.	Sample volume (ml)	Concentration (*M*)	Equivalents in sample	Equivalents observed	Percent error
1	1.0	5.9×10^{-4}	5.9×10^{-7}	5.72×10^{-7}	−3.1
2	1.0	5.9×10^{-4}	5.9×10^{-7}	5.69×10^{-7}	−3.6
3	1.0	5.9×10^{-4}	5.9×10^{-7}	5.84×10^{-7}	−1.0
4	2.0	5.9×10^{-4}	1.18×10^{-6}	1.15×10^{-6}	−2.5
5	2.0	5.9×10^{-4}	1.18×10^{-6}	1.14×10^{-6}	−3.4
6	0.5	5.9×10^{-4}	2.95×10^{-7}	2.90×10^{-7}	−1.7
7	0.5	5.9×10^{-4}	2.95×10^{-7}	2.97×10^{-7}	+0.7
8	1.0	2.95×10^{-3}	2.95×10^{-6}	2.91×10^{-6}	−1.3
9	1.0	2.95×10^{-3}	2.95×10^{-6}	2.91×10^{-6}	−1.7
10	2.0	2.95×10^{-3}	5.9×10^{-6}	6.11×10^{-6}	+3.6
11	2.0	2.95×10^{-3}	5.9×10^{-6}	5.68×10^{-6}	−3.7

method. The results of Fig. 6.34 were obtained by graphical integration; more accurate results should be attainable by use of electronic integration.

1. R. E. Meyer and F. A. Posey, *Chem. Div. Annu. Progr. Rep. May 20, 1973*, ORNL-4891, p. 89.
2. R. E. Meyer and F. A. Posey, *J. Electroanal. Chem. Interfacial Electrochem.* 49, 377 (1974).

SENSOR FOR DISSOLVED OXYGEN

R. E. Meyer F. A. Posey

We have described in previous publications[1,2] an electrochemical device for the determination of dissolved oxygen at the part-per-billion level. A silicone rubber membrane was used in this device to separate the dissolved oxygen from possible interfering ions. At higher levels of dissolved oxygen (in the range of air saturation, ca. 8 ppm), conditions are not so stringent since, for most solutions, the interfering ion concentration is likely to be relatively small compared with the dissolved oxygen concentration. We have therefore tested essentially the same device as that used for halide analysis[3] as a sensor for oxygen analysis. The only change that was necessary was to set the potential at approximately −750 mV vs S.C.E. Some results are shown in Fig. 6.35. The sample stream was prepared by mixing air-saturated and helium-saturated streams at known flow rates. Errors average less than 3% and represent both the error of measurement and the errors associated with mixing and measurement of the flow rates of the two streams. We feel that the sensor may have application in a number of areas which require continuous monitoring of the dissolved oxygen content of flowing streams, particularly those where the concentration, rather than the activity, of dissolved oxygen is desired.

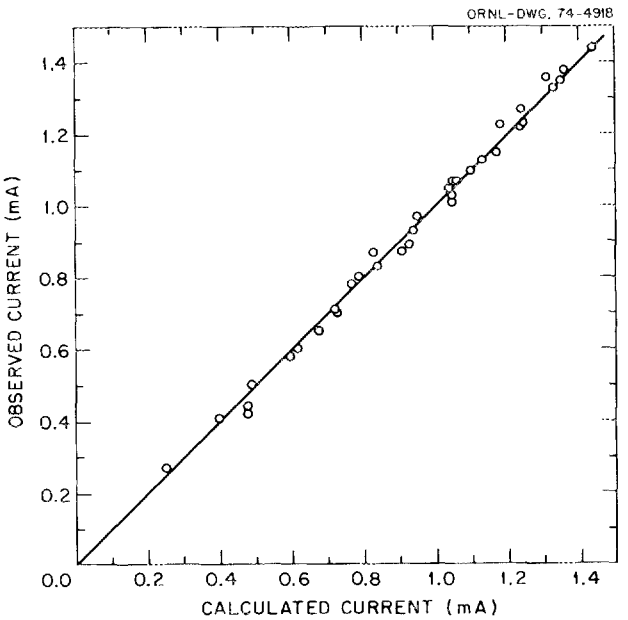

Fig. 6.35. Comparison of observed oxygen-reduction current with current calculated from mixing of air-saturated and helium-saturated streams. Packed-bed silver electrode; electrode potential: −750 mV vs S.C.E.

1. R. E. Meyer, F. A. Posey, and P. M. Lantz, *Desalination* 11, 329 (1972).
2. R. E. Meyer, F. A. Posey, and P. M. Lantz, *Chem. Div. Annu. Progr. Rep. May 20, 1973*, ORNL-4891, p. 91.
3. R. E. Meyer and F. A. Posey, "Separation and Analysis of Ions with a Packed-Bed Electrode," the preceding contribution, this report.

ELECTROANALYSIS OF SMALL SOLUTION VOLUMES WITH A PACKED-BED ELECTRODE USING LINEAR POTENTIAL-SWEEP COULOMETRY

H. R. Bronstein F. A. Posey

An apparatus was designed, constructed, and tested for investigation of the applicability of packed-bed electrodes to quantitative electroanalysis of trace amounts of oxidizable or reducible solutes in small sample volumes (1 ml or less) by linear-sweep voltammetry and/or coulometry. The packed-bed electrode is composed of nonporous glassy carbon spheres (about 100μ in diameter). Figure 6.36 is a photograph of the relatively simple cell. The central portion contains the cylindrical packed bed of glassy carbon spheres ($^7/_8$ in. in diameter; 1 in. in length). The side arm on the right in Fig. 6.36 contains a reference electrode (saturated calomel); the side arm on the left leads to a graphite rod counterelectrode. A length of Teflon tubing was sometimes used, as shown in Fig. 6.36, to prevent reaction products in the counterelectrode compartment from reaching the packed-bed electrode during an experiment. Electrical contact with the packed-bed electrode is made by an insulated carbon rod. Ports are provided in the Teflon cap assembly for introduction of samples, deaerated inert electrolyte, and an inert-gas stream which blankets the bed.

PHOTO 0770-74

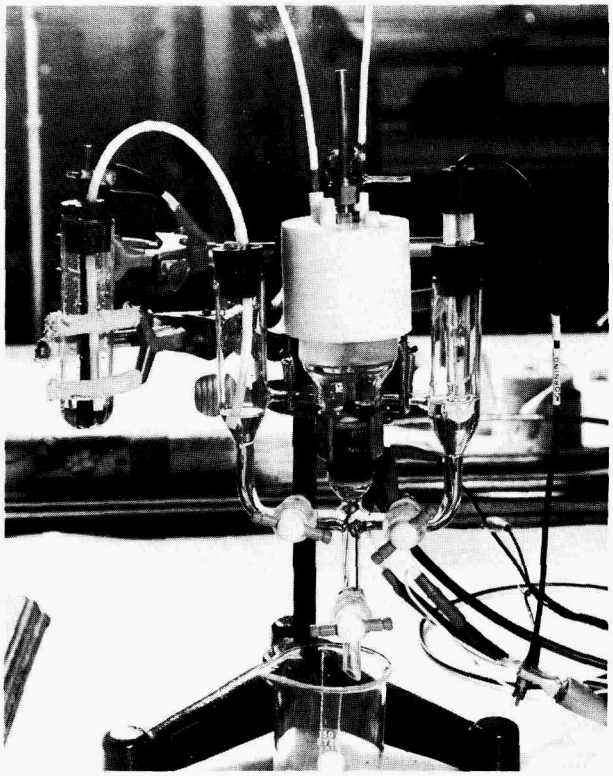

Fig. 6.36. Cell for electroanalysis of small solution volumes with a packed-bed electrode of glassy carbon spheres.

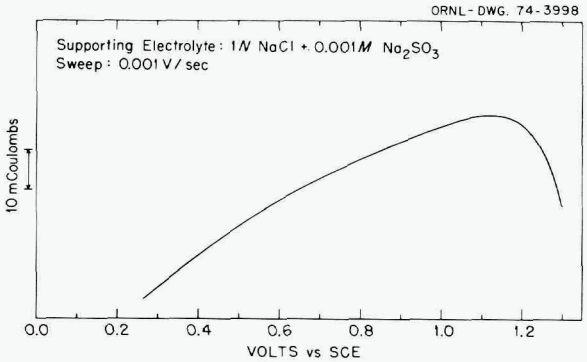

Fig. 6.37. Background anodic sweep on glassy carbon packed-bed electrode in the absence of electroactive substances.

A precisely measured volume of sample (as small as 10^{-2} ml) is passed into the packed-bed electrode using an electrochemically inert supporting electrolyte (NaCl, H_2SO_4, etc.). The potential of the packed-bed electrode is subsequently varied at a constant rate, and the amount of each oxidizable or reducible substance present is measured coulometrically at its appropriate potential range for reaction. Microgram quantities of lead, cadmium, and copper ions, and their mixtures, have been determined by this technique with an accuracy of better than ±1%.

A plot of charge accumulated during an anodic sweep, in the absence of oxidizable or reducible substances in the solution, is shown in Fig. 6.37. This curve is the "background" which is required for estimation of the quantity of electroactive species stripped from the packed-bed electrode for the inert electrolyte in question (1 *N* NaCl). Some experimental curves obtained for determination of cadmium by this method are shown in Fig. 6.38. The supporting electrolyte, 1 *N* NaCl, was deaerated by addition of a small amount of sodium sulfite. The plot of current as a function of electrode potential shows the current peak due to deposition of cadmium on the surface of the glassy carbon spheres (lower portion of current trace) during the cathodic part of the potential scan; the upper portion of the current trace shows the peak due to stripping of the cadmium from the bed during the subsequent anodic potential sweep. We find that, in general, more precise analytical results are obtained for reducible metal ions on the anodic half cycle (stripping) than on the

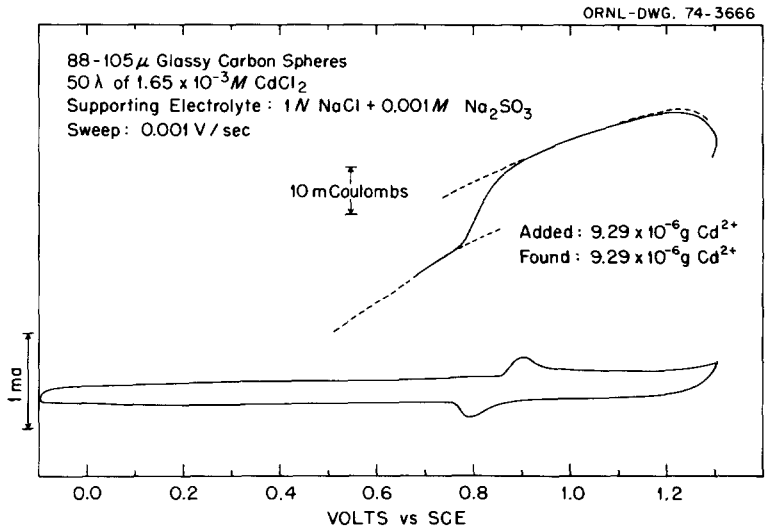

Fig. 6.38. Coulometric determination of cadmium with the packed-bed electrode of glassy carbon spheres.

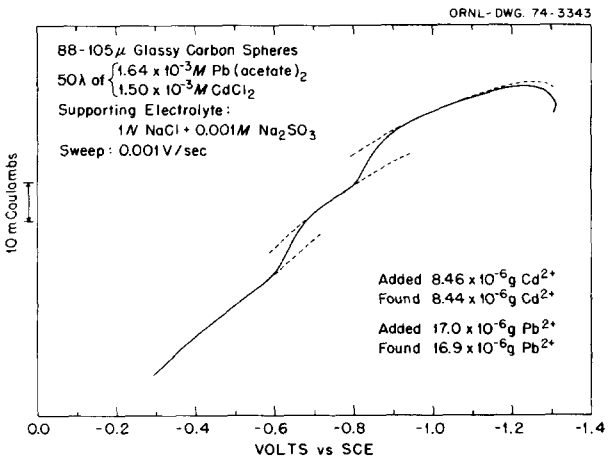

Fig. 6.39. Coulometric determination of a mixture of lead and cadmium with the packed-bed electrode of glassy carbon spheres.

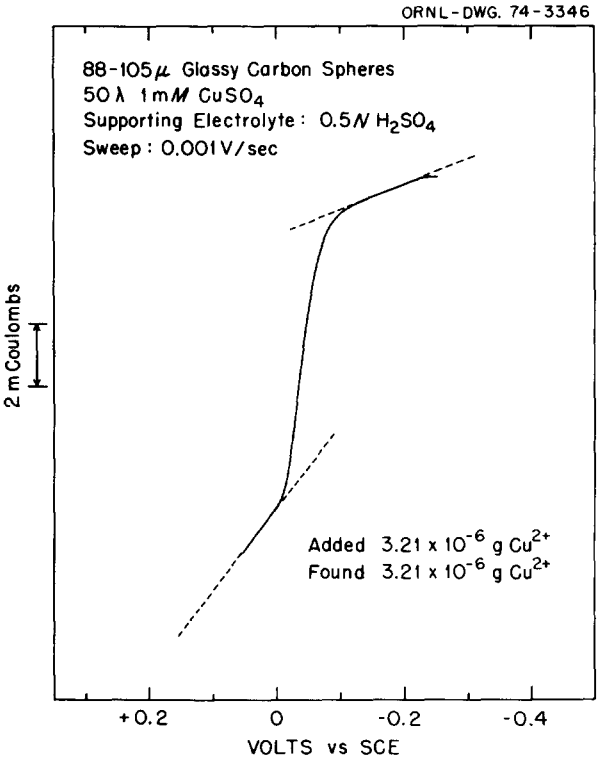

Fig. 6.40. Coulometric determination of copper with the packed-bed electrode of glassy carbon spheres using enhanced sensitivity.

cathodic half cycle (deposition). We also show in Fig. 6.38 the corresponding coulometric curve for anodic stripping, from which the amount of cadmium added may be obtained by noting the points at which significant deviations from the background curve occur (cf. dashed lines) and subtracting these values to give the total number of coulombs due to the stripping reaction. Results of coulometric analysis of a mixture of lead and cadmium ions are shown in Fig. 6.39. We find that use of a cathodic sweep for deposition prior to the anodic sweep in the case of analysis of mixtures leads to much more accurate results than simple deposition at a negative electrode potential followed by an anodic sweep. Sensitivity of the method could be further increased by adjustment of the current amplification factor and/or the coulometric constant. An example of a stripping curve run at increased sensitivity is shown in Fig. 6.40; in this case, copper was analyzed

with dilute sulfuric acid as inert electrolyte. It should be noted that a wide variety of supporting electrolytes may be used, depending upon the particular application and the ions to be analyzed.

These results not only have confirmed the theoretical computations which had suggested that the above method should be at least the equal of conventional polarography and some other electroanalytical methods[1–3] in sensitivity, but also have shown that the method permits the use of extremely small sample volumes with relatively simple experimental equipment and manipulations. The results of this investigation will be submitted for publication in the *Journal of Electroanalytical Chemistry and Interfacial Electrochemistry.*

1. D. M. Oglesby et al., *Anal. Chem.* 37, 1317 (1965).
2. A. T. Hubbard and F. C. Anson, p. 145 in *Electroanalytical Chemistry*, vol. 4, ed. A. J. Bard, Marcel Dekker, Inc., New York, 1970.
3. T. Fujinaga, *Pure Appl. Chem.* 25, 709 (1971).

POROUS ELECTRODE STUDIES IN MOLTEN SALTS[1]

H. R. Bronstein F. A. Posey

Work was initiated to investigate the feasibility of using a porous or packed-bed electrode as a continuous on-line monitor of the concentration of dissolved bismuth in molten reactor fuel salt. Fabrication of a prototype quartz cell and other accessories for the studies was largely completed. The necessary equipment for temperature control, a suitable furnace, and instrumentation for accurate monitoring of the temperature of the melt were acquired. A manifold for vacuum and inert pressure control over the melt was constructed. These components are now being assembled as a bench-scale test unit prior to initiation of experimental measurements.

1. Work carried out for the Molten-Salt Reactor Program.

ELECTROCHEMICAL RECOVERY OF REDUCIBLE INORGANIC POLLUTANTS FROM AQUEOUS STREAMS[1]

A. A. Palko F. A. Posey

Research continued on the development of efficient and economical methods for removal and recovery of reducible metal ions from flowing streams by porous and packed-bed electrolytic cells. This work is an extension of studies carried out earlier on recovery of copper from the brine blowdown of desalting plants.[2,3] Most of the effort during the first part of our studies[4] was devoted to recovery of dissolved mercury from simulated chlor-alkali plant brine by porous carbon electrodes. Data were obtained on the effect of solution composition, pH, temperature, etc., on mercury reduction from aqueous solutions onto carbon substrates. Tests were carried out on the removal efficiency of porous carbon electrodes as a function of electrode length, solution flow rate, electrode potential, etc., and on the mode of deposition of mercury onto carbon surfaces. The results had implications for the development of large-scale devices for removal of mercury from flowing streams.

More recently, most of our work has been concerned with study of the feasibility of removing dissolved lead from two different types of industrial effluents obtained from a lead–lead dioxide plating plant and from a major manufacturer of organolead compounds.[5] As in the case of the earlier studies on mercury recovery, a comprehensive series of measurements was carried out on the effect of solution composition, temperature, pH, and other factors on the rate of reduction of lead, copper, cadmium, and a number of other metals on a carbon substrate. It was observed that lead, copper, and cadmium could be reduced over a useful range of electrode potentials for all the solutions examined, so that efficient removal of these substances from flowing streams on porous and packed-bed electrodes is feasible. It was found that one effluent, a dilute rinse water from a continuous lead–lead dioxide strip plating operation, could not be treated efficiently because of limited solution conductivity. The other plant effluent, from the manufacture of lead antiknock compounds, was successfully treated electrolytically to remove dissolved inorganic and organic lead compounds under laboratory conditions.

Subsequent work has been concerned with the development of a practical prototype lead-recovery cell and with testing on both synthetic and actual plant effluent. Following successful completion of tests with the unit, we plan to design and construct a small fully instrumented demonstration unit, capable of treating perhaps 1000 to 5000 gal/day of effluent, which will be shipped to the manufacturing plant for extended on-site evaluation of technical and economic aspects of the process.

1. Research carried out under the ORNL-NSF Ecology and Analysis of Trace Contaminants program, sponsored by NSF/RANN under Union Carbide Corporation's contract with the Atomic Energy Commission.

2. F. A. Posey, *Chem. Div. Annu. Progr. Rep. May 20, 1972*, ORNL-4791, p. 113.

3. F. A. Posey, *Electrolytic Demonstration Unit for Copper Removal from Distillation Plant Blowdown* , ORNL-TM-4112 (March 1973).

4. F. A. Posey and A. A. Palko, "Electrochemical Removal of Reducible Inorganic Pollutants from Aqueous Streams," p. 367 in *Ecology and Analysis of Trace Contaminants*, ORNL-NSF-EATC-1 (March 1973).

5. F. A. Posey and A. A. Palko, "Electrochemical Recovery of Reducible Inorganic Pollutants from Aqueous Streams," p. 360 in *Ecology and Analysis of Trace Contaminants*, ORNL-NSF-EATC-6 (January 1974).

EFFECT OF SOLVENT ON THE ELECTROCHEMISTRY OF IRON[1]

A. L. Bacarella

A study has been made of the electrochemical behavior of the active iron electrode in acidic ethanol-water media. The purpose of the investigation was to determine the kinetic order with respect to water and protons in the corrosion mechanism. Solvent mixtures ranging from pure water to almost pure ethanol were investigated. The potential measurements in the investigation were made with respect to a saturated aqueous calomel electrode as the reference electrode. In order to interpret the results, values for the junction potentials, E_L^S, between the acidic ethanol-water solvent and the saturated aqueous KCl were needed. A first interpretation of the results was obtained using the junction potentials proposed by Gutbezahl and Grunwald.[2] These junction potentials were obtained from a correlation of the pK's of organic acids in ethanol-water solvents. The correlation was based on the validity of the "activity" postulate of Grunwald.[3] It was shown that a satisfactory interpretation of the results was obtained using a modification of a mechanism proposed by Kelly[4] for the iron dissolution and hydrogen evolution reactions on zone-refined iron in hydrogen-saturated sodium benzoate solutions, referred to as the inhibited system. The following equations were obtained using the above mechanism:[5]

$$\log i_+^S = 3.183 - E_{Pt}^S/0.06 + E_{Fe}^S/0.04 + 2\log\frac{1}{1+\lambda R}, \quad (1)$$

$$\log i_-^S = -5.810 + E_{Pt}^S/0.06 - E_{Fe}^S/0.120 + \log\frac{1}{1+\lambda R}, \quad (2)$$

$$\log i_{corr} - \frac{5}{4}\log\frac{1}{1+\lambda R} + 3.562 = \frac{1}{2}E_{Pt}^S/0.06 = -\frac{1}{2}pA, \quad (3)$$

$$E_{Fe(corr)}^S + 0.03\log\frac{1}{1+\lambda R} + 0.270 = E_{Pt}^S, \quad (4)$$

where $E_{Pt,Fe}^S = E_{cell\ Pt,Fe}^S + E_{SCE} + E_L^S$ is the potential of the platinum or iron electrode vs the standard hydrogen electrode in water, (S.H.E.)^w; $E_{cell\ Pt,Fe}^S$ is the experimentally measured cell potential; the constant λ is a ratio of rate constants; R = (wt % EtOH)/(wt % HOH); and pA = pH in pure water solvent.

Recently another set of liquid junction potentials, E_L^P, was evaluated for this system by Popovych.[6] Not only do these potentials differ in magnitude but they also differ in sign from those proposed by Gutbezahl and Grunwald. These junction potentials were based on the assumption of equal medium effects for ions of a reference electrolyte, the electrolyte being composed of large symmetrical ions as similar in size and structure as are available. If the proposed mechanism is accepted, then these junction potentials do not provide a satisfactory fit to the data. This is most readily shown by Fig. 6.41, which is a plot of the experimental vs the calculated open-circuit corrosion potential for the iron

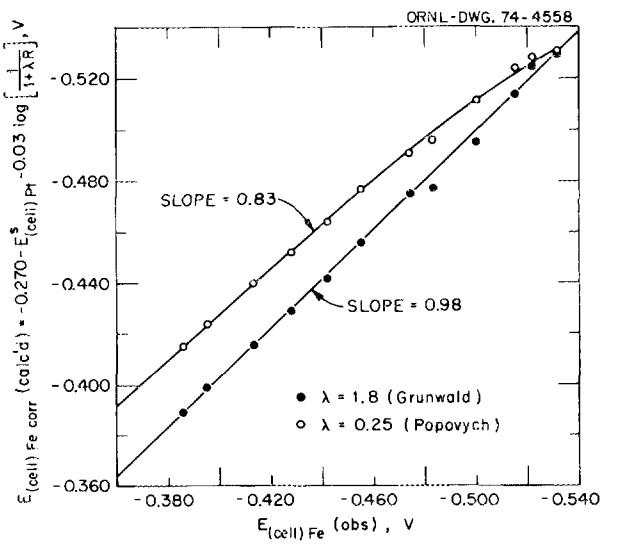

Fig. 6.41. The calculated vs the observed corrosion potential for iron in hydrogen-saturated 0.50 M H_2SO_4–EtOH–HOH at 30°C.

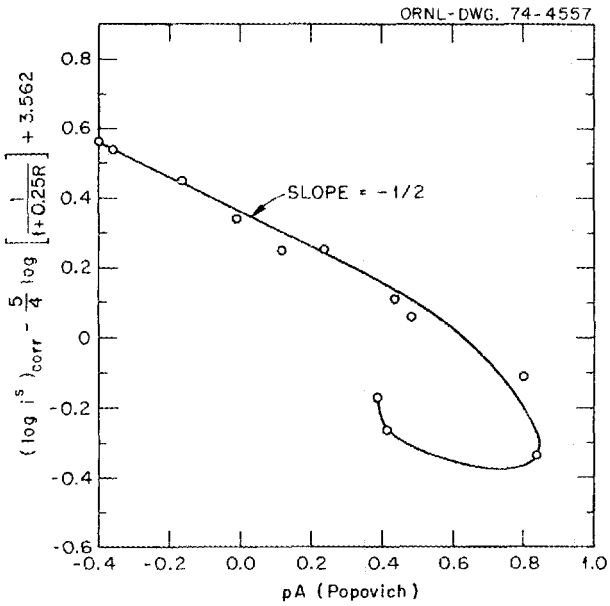

Fig. 6.42. The corrosion current for iron in hydrogen-saturated 0.50 M H_2SO_4–EtOH–HOH as a function of pA at 30°C, using Popovych's junction potentials.

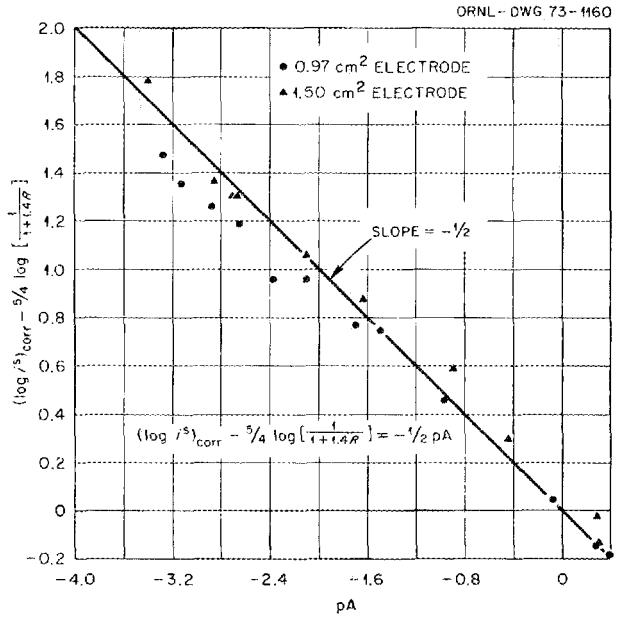

Fig. 6.43. The corrosion current for iron in hydrogen-saturated 0.50 M H_2SO_4–EtOH–HOH as a function of pA.

electrode according to Eq. (4). Since the corrosion potential is independent of E_L^S, the only unknown in Eq. (4) is λ. The two values for λ were obtained from Eq. (1). Here, the two sets of junction potentials E_L^G and E_L^P were used, and the best values for λ were determined. For Grunwald's junction potentials (E_L^G), λ = 1.8, and for Popovych's (E_L^P), λ = 0.25. For perfect agreement the slope of the line in Fig. 6.41 should be unity and the line should pass through the origin. Obviously, Grunwald's junction potentials provide a much better fit. Using these values for λ and the respective junction potentials, the corrosion currents as a function of pA are compared in Figs. 6.42 and 6.43. By definition:

$$pA = -\log a_+ = \frac{-E_{Pt}^S}{0.06} = -\frac{E_{cell\ Pt}^S + E_{S.C.E.} + E_L^S}{0.06} .$$

According to Eq. (3),

$$\frac{\partial\{(\log i^S)_{corr} - {}^5\!/_4 \log [1/(1+\lambda R)]\}}{\partial pA} = -1/2 ,$$

and again, better agreement is obtained using Grunwald's values for E_L^S.

Indeed, the above arguments can be reversed, and the best value for λ determined from Eq. (4) can be used to generate a set of experimental junction potentials. These potentials agree in sign and magnitude with those proposed by Gutbezahl and Grunwald.[2]

1. Work performed in the Reactor Chemistry Division.
2. B. Gutbezahl and E. Grunwald, *J. Amer. Chem. Soc.* **75**, 565 (1953).
3. E. Grunwald, *J. Phys. Colloid Chem.* **55**, 881 (1951).
4. E. J. Kelly, *J. Electrochem. Soc.* **115**, 1111 (1968).
5. A. L. Bacarella and A. L. Sutton, *Reactor Chem. Div. Annu. Progr. Rep. May 31, 1971*, ORNL-4717, p. 78.
6. O. Popovych, *Crit. Rev. Anal. Chem.* **1**, 73 (1970).

CALORIMETRY

HEAT OF IMMERSION OF THORIUM OXIDE AT ELEVATED TEMPERATURES[1]

H. F. Holmes

The surface properties of thorium oxide have been studied by infrared spectroscopy[2] at temperatures up to 800°C, by water vapor adsorption measurements[3] up to 500°C, and by extensive heat of immersion calorimetry[4] in liquid water at 25°C. The present study extends the calorimetric measurements to 200°C and provides basic information on the oxide-water interface in a temperature range where no previous calorimetric data are available.

Specific surface areas of the six samples used in the present study were 14.7, 35.5, 14.5, 6.60, 2.96, and 46.7 m^2/g for samples A, F, G, H, I, and BB-14 respectively. With the exception of sample BB-14, the samples were derived from the thermal decomposition of thorium oxalate, with the only real difference being the calcination temperature. Sample BB-14 is a sol-gel material. The heats of immersion (in liquid water) were measured with an adiabatic calorimeter capable of operating at temperatures up to 200°C.

Results for these six samples of thorium oxide are shown in Figs. 6.44 and 6.45. The specific surface areas (from nitrogen adsorption) have been used to reduce the data to a unit-area basis. It should be emphasized that all of the results in Figs. 6.44 and 6.45 are for samples which have been outgassed at 500°C for 24 hr and sealed, under high vacuum, in Pyrex bulbs. It is obvious from these results that the heat of immersion can increase, decrease, or remain constant as the immersion temperature increases. Although there is no quantitative relationship, samples having a high specific surface area (A, F, G, and BB-14) are more energetic than those with a relatively low specific surface area (H and I). This agrees with previous results[5] obtained at a constant immersion temperature of 25°C. In all cases the magnitude of the heat of immersion is clear evidence for a chemisorption process.

The heat of immersion of thorium oxide in liquid water at 25°C is very dependent on the temperature at which the samples are outgassed.[5] This is also true at elevated temperatures. Table 6.13 lists the heat of immersion of samples A, F, and BB-14 for samples which were outgassed at 500°C (h_i^{500}) and 200°C (h_i^{200}). If one assumes that all of the weight loss between 200 and 500°C is water, then one can calculate the average net heat of adsorption for this water. One simply divides the difference in the heat of immersion for samples outgassed at these two temperatures by the weight loss and converts to the proper units. The striking observation is that the difference in the heat of immersion for samples outgassed at 200 and 500°C is independent of immersion temperature over the range of 25 to 150°C. This is true for all three samples, each of which has a different dependence on immersion temperature. The quantities of water given in Table 6.13 are roughly equivalent to 0.8 of a chemisorbed monolayer in all three cases. It is known that, after outgassing at 500°C, a thorium oxide surface contains

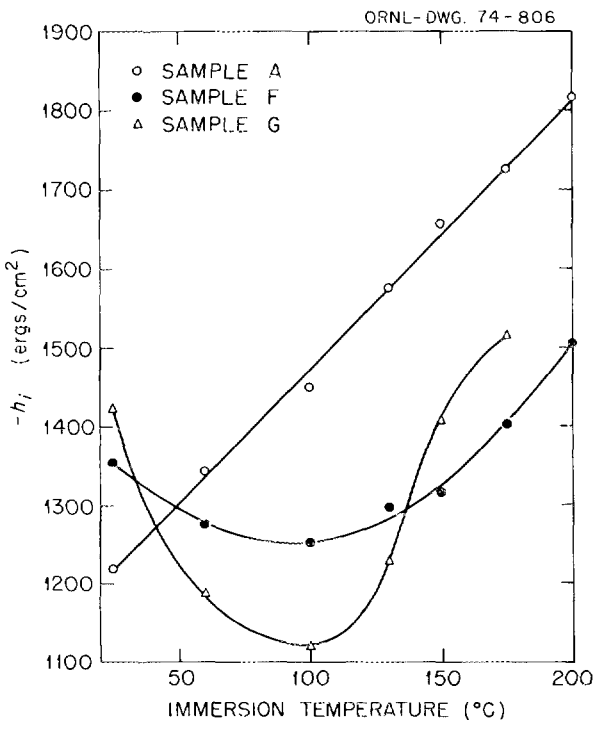

Fig. 6.44. Heat of immersion of ThO_2 in water. Samples outgassed at 500°C.

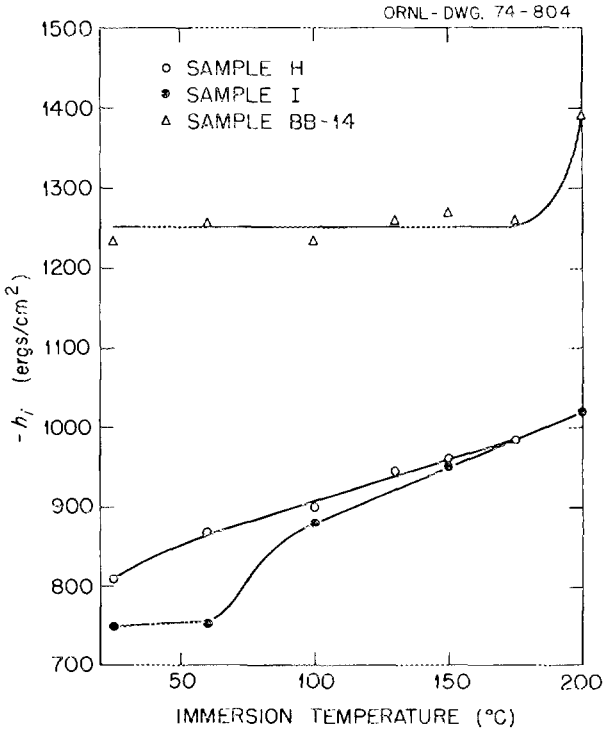

Fig. 6.45. Heat of immersion of ThO_2 in water. Samples outgassed at 500°C.

Table 6.13. Estimation of average net heat of adsorption

In ergs per square centimeter

Immersion temperature (°C)	Sample A			Sample F			Sample BB-14		
	h_i^{500}	h_i^{200}	h_i^{500}-h_i^{200}	h_i^{500}	h_i^{200}	h_i^{500}-h_i^{200}	h_i^{500}	h_i^{200}	h_i^{500}-h_i^{200}
25	1220	587	633	1355	855	500	1232	684	548
60	1342	685	657	1277	760	517	1256	679	577
100	1450	793	657	1254	723	531	1232	687	545
130	1575	926	649	1298	762	536	1258	693	565
150	1657	1003	654	1316	829	487	1269	690	579
Average			650 ± 7			514 ± 17	1253 ± 9	687 ± 4	563 ± 13
Weight loss between 200 and 500°C (mg/g)			2.60			6.4			11.2
Average ΔH_a (kcal/mole)			15.8			12.6			10.7

about one-half a monolayer of chemisorbed water in the form of surface hydroxyl groups.[5] This means that the average net heats of adsorption given in Table 6.13 are for completion of the chemisorbed layer plus a small amount of irreversibly adsorbed molecular water. It is clear that the complex dependence on immersion temperature is due to factors other than a chemisorbed layer of surface hydroxyl groups. From this, one concludes that the integral heat of immersion of thorium oxide contains contributions which reflect considerable interaction with several layers of water adjacent to the oxide surface. This observation agrees with the conclusion reached by Tyler et al.[6] in their study of the heat of immersion of silica over the relatively limited temperature range of 11.5 to 54.5°C.

1. Extended abstract of paper presented at the 167th National Meeting of the American Chemical Society, Los Angeles, Calif., Mar. 31–Apr. 5, 1974; abstract COLL-103. Work performed in the Reactor Chemistry Division.

2. E. L. Fuller, Jr., H. F. Holmes, and R. B. Gammage, *J. Colloid Interface Sci.* **33**, 623 (1970).

3. R. B. Gammage, E. L. Fuller, Jr., and H. F. Holmes, *J. Phys. Chem.* **74**, 4276 (1970).

4. H. F. Holmes, E. L. Fuller, Jr., and C. H. Secoy, *J. Phys. Chem.* **72**, 2095 (1968).

5. H. F. Holmes and C. H. Secoy, *J. Phys. Chem.* **69**, 151 (1965).

6. A. J. Tyler et al., *Trans. Faraday Soc.* **67**, 483 (1971).

INTERFACIAL PHENOMENA

THEORY OF THERMODIFFUSIOPHORESIS OF SPHERICAL AEROSOL PARTICLES[1,2]

B. K. Annis E. A. Mason[3]

An aerosol particle in a gas in which a temperature or concentration gradient is maintained will experience a force proportional to the appropriate gradient, and a steady-state motion will result such that the force is balanced by the fluid drag on the moving particle. The phenomena are then known respectively as thermo- and diffusiophoresis. In the case of a gas mixture that is nonuniform in both temperature and concentration a composite motion referred to as thermodiffusiophoresis may occur. Rigorous mathematical descriptions of the phoretic effects are available when the ratio of the particle radius to the mean free path of the gas is small (free-molecule regime) or large (continuum regime); however, in the intermediate range it is necessary to resort to approximate or semiempirical methods. Previous reports[4,5] have discussed the application of the so-called "dusty-gas" model to aerosol transport problems. The model has now been extended to provide expressions for the motions of spherical particles in gas mixtures having both temperature and composition gradients which cover the free-molecule to the continuum regime.

The model treats the aerosol particles as one component of a multicomponent mixture, and yields explicitly the complete pressure and composition dependence of thermodiffusiophoresis. Effects of molecular internal degrees of freedom are included, but not effects connected with the thermal conductivity of the particles. Thermophoresis and diffusiophoresis are found to interact in three ways with each other in thermodiffusiophoresis. Thermophoresis itself is enhanced in a mixture, diffusiophoresis itself is enhanced in the presence of a temperature gradient, and there is also a direct coupling term involving the translational thermal diffusion factor of the gas mixture. The model has been extended to include the effects of finite boundaries on the gas. The case of thermophoresis in a single gas in the so-called transition region with respect to both the particle diameter and boundary spacing has been worked out in detail. There is reasonable agreement of the present results with previous theoretical and experimental work where they overlap.

1. This research was supported in part by the National Science Foundation Grant GK-38196.

2. To be published in *J. Aerosol Sci.* 6 (1975).

3. Brown University, Providence, R.I.

4. B. K. Annis, A. P. Malinauskas, and E. A. Mason, *J. Aerosol Sci.* 3, 55 (1972).

5. B. K. Annis, A. P. Malinauskas, and E. A. Mason, *J. Aerosol Sci.* 4, 271 (1973).

ION MICROPROBE INVESTIGATION OF THE SURFACE MIGRATION OF MOLECULAR OXIDES ON NaCl[1,2]

B. K. Annis S. S. Cristy[3]

The meager amount of data for the migration of surface layers on solid substrates demonstrates that the magnitude of the diffusion coefficients can range from nearly gas-phase values to those of the slowest bulk processes. There is every indication that a considerable amount of additional data must be acquired before even crude estimates of the effect can be made. We report here what we believe to be the first results for the diffusion of molecular oxides over an ionic substrate.

Sodium chloride substrates were prepared from standard Harshaw Chemical Company optical-grade polished blanks of approximate dimensions 17 mm by 8 mm by 1.5 mm. On approximately one-half of the crystal a film of either La_2O_3 or SrO was laid down by an electron beam deposition technique. The purities of La_2O_3 and SrO were specified by the suppliers as 99.999 and 99.5% respectively. The thicknesses of the deposits were inferred from measurements of the surface density and were estimated to be 633 Å for La_2O_3 (corresponding to 40 $\mu g/cm^2$) and 1400 Å for SrO (corresponding to 66 $\mu g/cm^2$). The La_2O_3 samples were heated in air at 693°K for a period of 880 hr, and the SrO samples were heated in a helium stream for periods of 473 and 977 hr, also at 693°K. Some of the samples were not heat treated but were examined after deposition to ensure that the region of the diffusion source was well defined.

The detectability limits of the ion microprobe were estimated as 2×10^{-4} $\mu g/cm^2$ of La_2O_3 on the surface, which, for the 60- by 75-μm area typically sputtered, would correspond to about 1×10^{-14} g of La_2O_3. For strontium oxide the figure was 3×10^{-4} $\mu g/cm^2$, or, for a sputtered area of 30 by 38 μm, about 3×10^{-15} g SrO. The sputtering beam consisted of negative oxygen ions of a few keV energy and with intensity in the range 1.5 to 4.5 nA. The usual technique was to begin the sputtering pattern at some distance from the oxide coating and move inward to the boundary of the deposit. The location of the various sputtered areas was determined to within ±1 μm. Finally, due to the insulating nature of the NaCl substrate, it was necessary to carbon coat the surfaces.

Some of the data are shown in Figs. 6.46–6.48. The experimental concentration profiles were plotted with the logarithm of a quantity proportional to the amount of material per unit area as ordinate and the distance from the edge of the deposit as abscissa. The profiles in this form were then superposed on similar plots generated from the usual one-dimensional diffusion equation for a semi-infinite source,

$$C = \frac{C_0}{2} \operatorname{erfc} \frac{x}{2\sqrt{D_S t}}, \tag{1}$$

where t is the length of the heating period, x is a distance from the source of the diffusing material, C_0 is the initial surface concentration at $x = 0$, $t = 0$, and D_S is the surface diffusion coefficient. The curves computed for a representative range of D_S are shown in the plots. In general, it would be expected that a more complex model that would permit a loss of surface material in the bulk of the substrate should be applied. However, it can be demonstrated that for practical purposes the concentration profiles generated by more elaborate theory are indistinguishable from those of Eq. (1) when plotted in terms of reduced variables. Consequently, since information regarding volume diffusion is lacking, we have chosen the simplest approach.

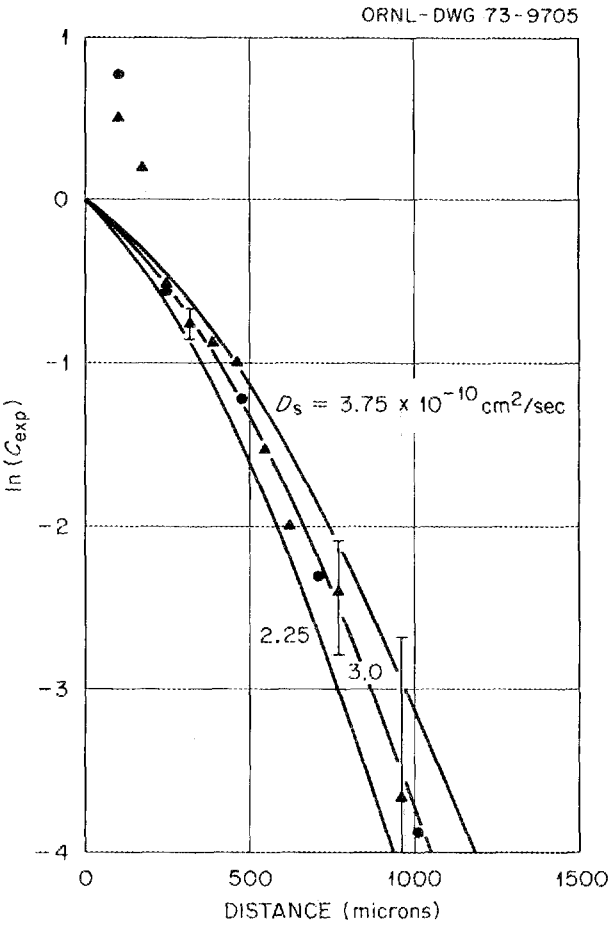

Fig. 6.46. Surface distribution of La_2O_3 for a heating period of 880 hr.

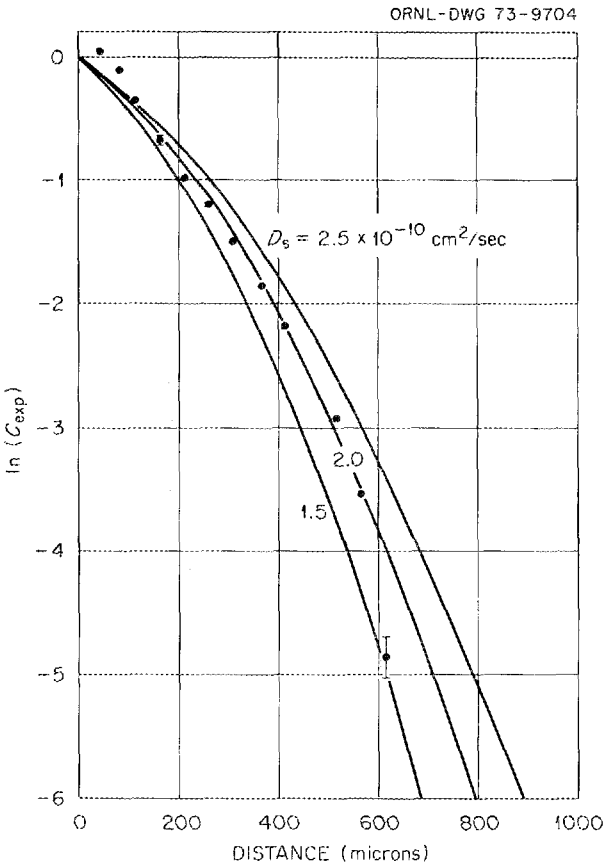

Fig. 6.47. Surface distribution of SrO for a heating period of 473 hr.

As is evident in Figs. 6.46–6.48, the behavior in the first 150 to 200 μ for both molecular species often differed from that predicted by the simple model. An obvious explanation would be that multilayer diffusion was occurring in this region. However, by scaling the concentrations to that obtained on the deposit, we found that for the La_2O_3 and the 473-hr SrO samples, the estimated film thicknesses were less than the 2-Å figure commonly used for a monolayer. On the other hand, one of the sets of 977-hr SrO data is in good agreement with the model even at 50 μ, where the film thickness is estimated to have been about 3 Å.

The SrO data also deviate from the elementary model by falling off more rapidly at the lower extreme of the curves. Similar behavior was not noted for La_2O_3 but could have been masked by the larger statistical uncertainties in these data. The rapid decrease could indicate a concentration dependence for the diffusion coefficient. However, plots based on the model of a diffusion coefficient that is directly proportional to the concentration were found to require greater curvature in the intermediate portion of the curve than was observed. In the intermediate range of distances, for which the concentration decreases by better than an order of magnitude, Eq. (1) can be seen to give an adequate fit. Although the figures display curves based on Eq. (1), the effect of the finite size of the sputtered patch was taken into account and found not to produce behavior significantly different from that shown. The value of the diffusion coefficient obtained from the intermediate part of the curve for La_2O_3 is 3.0 X 10^{-10} cm²/sec. The SrO data for heating periods differing by about a factor of 2 appear consistent and provide a value of the diffusion coefficient of 2.0 X 10^{-10} cm²/sec. The overall uncertainty in the diffusion coefficients is estimated at 30 to 50%.

1. Summary of published paper, *Scr. Met.* 8, 695 (1974). Work performed in the Reactor Chemistry Division.

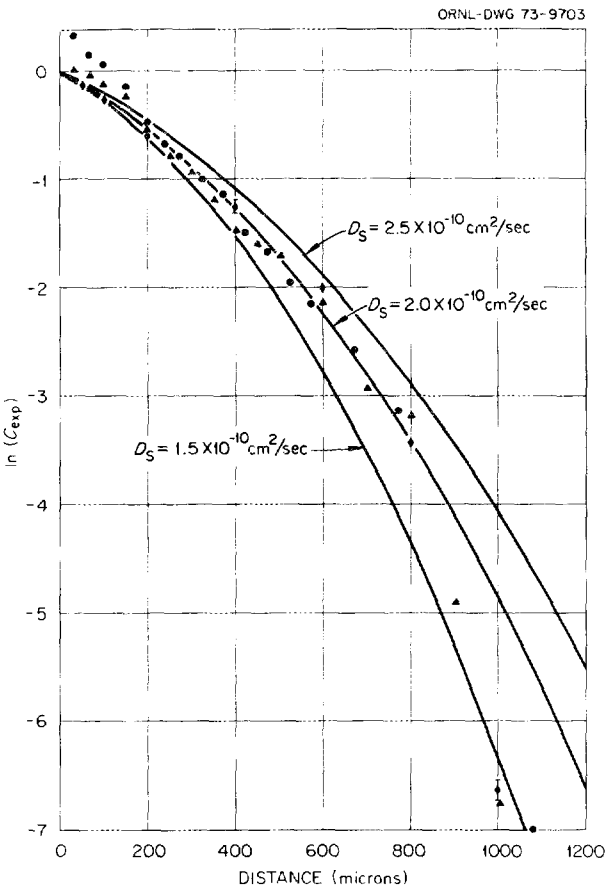

Fig. 6.48. Surface distribution of SrO for a heating period of 977 hr.

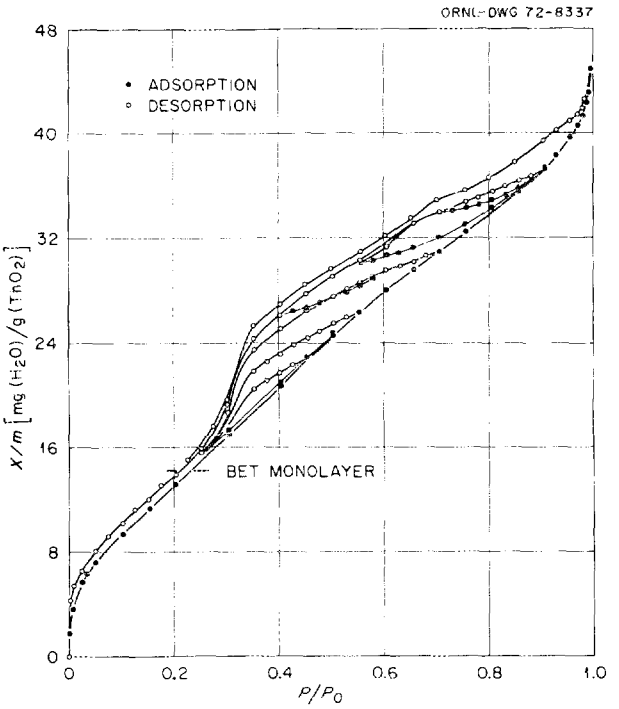

Fig. 6.49. Water vapor sorption by sol-gel thoria at 22.00°C.

2. We would like to thank Messrs. Kobisk, Adair, and Harmon for the film deposition work, and the late Dr. G. M. Watson for suggesting this study.

3. Y-12 Development Division.

SORPTION BY SOL-GEL THORIA[1]

E. L. Fuller, Jr.

The sorption properties of thoria have important implications in nuclear, catalytic, and ceramic applications. We have extended our studies to sol-gel thoria, which is a semirigid matrix of crystallites adhesively held together by a sheathing layer of sorbed water. This intercrystalline buffer is difficult to remove, but prolonged evacuation does lead to contractive extraction. The partial collapse of the matrix upon removal of the intercrystalline sheathing water closes micropores markedly to exclude nitrogen without grossly altering the amount and size of capillary avenues. Once the intercrystalline contact is formed, the stronger association resists direct prizing water penetration. However, scission (and water reentry) does occur as the matrix swells under the capillary forces of water in the larger voids. Considerable desorption hysteresis is noted as water is removed from three types of capillary avenues and the intercrystalline contact zones. In contrast, the matrix retains its integrity at −196°C under the weaker influence of the capillary forces of nitrogen, where a unimodal capillary hysteresis is noted.

Water vapor adsorbs on sol-gel thoria in a rather unique manner (Fig. 6.49). The adsorption isotherm is very nearly linear over an extended pressure region, so that BET analyses give erroneously high estimates of the monolayer capacity. Three ranges of hysteretic capillary retention are noted as desorption inflections at ca. $0.9P_0$, $0.7P_0$, and $0.35P_0$. The low-pressure retention between $0.001P_0$ and $0.3P_0$ prevails only if the adsorptive excursion exceeds $0.6P_0$ and is removed by prolonged exposure to dynamic vacuum (less than 10^{-6} P_0). The magnitude of each of these desorptive retentions is linearly related to the preceding adsorptive maximum. Hysteretic scanning is noted for the higher-pressure modes but is not present in the low-pressure retention. Note that the water adsorption described here is that observed over and above the appreciable chemisorbed component that cannot be removed at

22.00°C and 10^{-6} torr. As this chemisorbed component is removed at elevated temperatures the physical (reversible) water adsorption diminishes monotonically (Fig. 6.50). The nearly constant supercritical (above 374°C) sorption capacity prevails as the chemisorbed contingent still undergoes a monotonic decrease. Apparently the amount and pressure dependence of the reversible sorption are dictated by the pore geometry of the sorbent, with little or no variation due to the thermodynamics of the sorbate.

Nitrogen sorption (Fig. 6.51) aids in evaluating the nature of the surface. A single mode of hysteretic desorption is noted. The amount of the nitrogen capillary retention depends on the adsorptive maximum to a limited extent (up to but not beyond $0.97P_0$) and is independent of the amount of chemisorbed water and/or carbon dioxide. Conversely, the apparent nitrogen monolayer capacity is definitely inversely related to the amount of chemisorption, which in turn is inversely related to the outgassing temperature.

Throughout the cycling processes (20 to 500°C) to remove and replace chemisorbed species, the macroporous structure of the matrix is unaltered (as sensed by nitrogen capillary condensation and multilayer formation). The volume and shape of these larger capillary voids are unaffected by the chemisorption, sheathing, and/or the small amount of fusion at 500°C, all of which occur in the micro- or submicroporous regions of the matrix. However, extensive interparticulate fusion occurs at temperatures above 500°C. As the sample temperature is increased progressively, the matrix closes irreversibly until at 1000°C in vacuum the closure is essentially complete. The sorption activity is thence limited to the external surfaces of the matrix particles. Nitrogen is physically adsorbed on this surface reversibly without capillary condensation. Carbon dioxide is only weakly physically sorbed with little or no chemisorption. Water vapor is chemisorbed to hydroxyl-hydrate this external surface. No penetration can be effected as the physisorption of water is

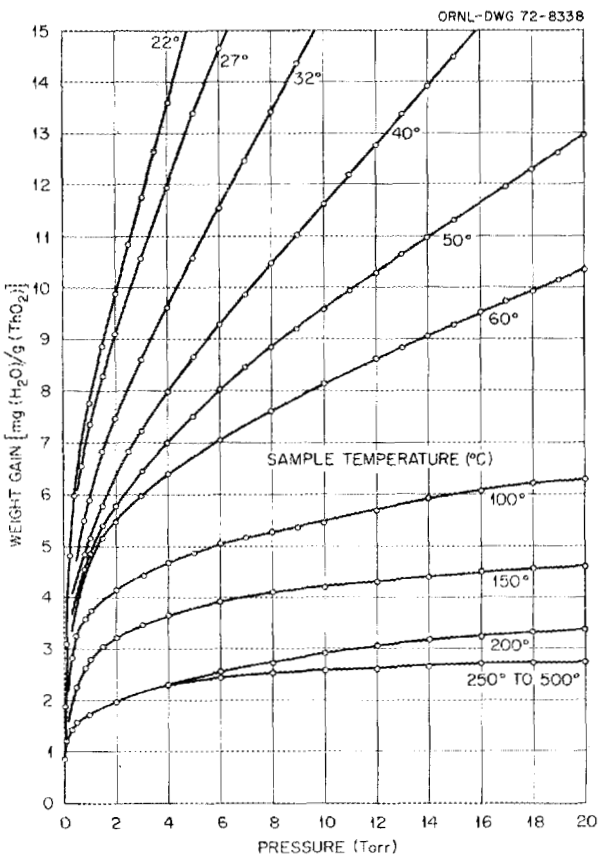

Fig. 6.50. Water vapor sorption by sol-gel thoria at elevated temperatures.

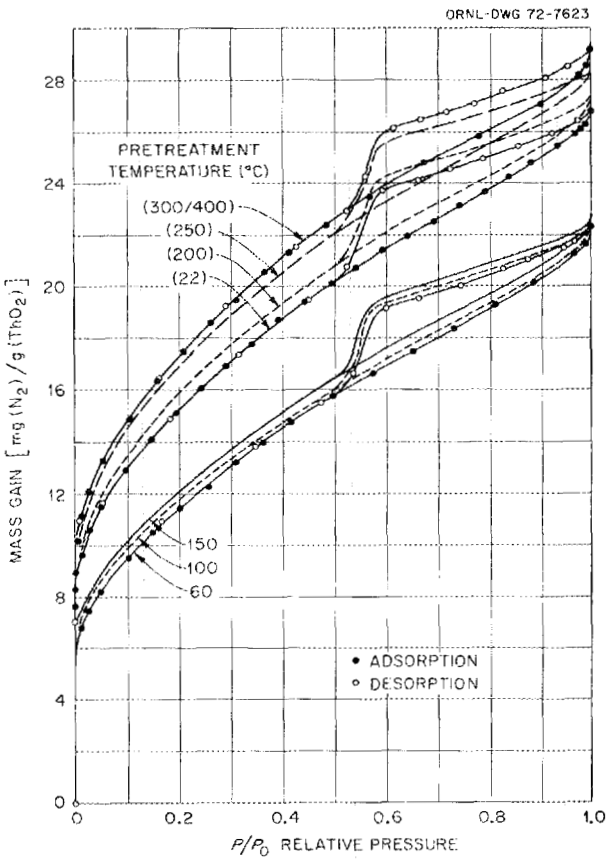

Fig. 6.51. Nitrogen sorption by sol-gel thoria at −196°C.

followed up to near saturation pressure. The sorptive capacity decreases 50-fold as the internal surfaces are "healed" by the cohesive sintering process.

Although the sorption behavior of sol-gel thoria is complex, most of the intricacies are readily understood in light of the juxtaposition of the crystallites in the gel matrix. The analyses are almost exclusively a study of the entire gamut of pore sizes. These range from the submicroporous (between the crystallite contacts per se), to the micropore size (interstitially accommodating single molecules), on to the large capillary pores where the bulk properties of the condensate are noted.

1. Presented at The 47th National Colloid Symposium, Ottawa, Canada, June 1973. Work performed in the Reactor Chemistry Division.

SOME SURFACE PROPERTIES OF APOLLO 17 SOILS[1,2]

H. F. Holmes E. L. Fuller, Jr.
R. B. Gammage[3]

This report is part of a continuing program which is designed to investigate some aspects of the interaction of gases with lunar materials. The present study concerns the surface chemistry of Apollo 17 lunar fines, samples 74220,35 (the orange soil) and 74241,42 (the gray control soil). Experimentally, the study consisted of measuring the adsorption of nitrogen, argon, and oxygen (all at 77°K) and also of water vapor (at 20°C).

There are general similarities and some contrasts between these fines and those from the Apollo 12, 14, and 16 missions.[4,5] Similarities include:

Table 6.14. Specific surface areas as obtained by application of the BET method for the adsorption of nitrogen on lunar samples at 77°K

Outgassing temperature (°C)	Specific surface area[a] (m^2/g)	
	Sample 74220,35	Sample 74241,42
25 (pre-H_2O)	0.35	0.36
300 (pre-H_2O)	0.42	0.37
25 (post-H_2O)	0.90	0.57
100 (post-H_2O)	1.02	0.64
200 (post-H_2O)	1.40	0.88
300 (post-H_2O)	1.38	1.01

[a]S. Brunauer, P. H. Emmett, and E. Teller, *J. Amer. Chem. Soc.* **60**, 309 (1938).

1. Initially (prior to water adsorption), both samples from Apollo 17 had a low specific surface area (Table 6.14).
2. There was no evidence for a pore system of the type that affects gas adsorption isotherms (i.e., gives rise to capillary condensation hysteresis loops and consists of pores less than a few hundred angstroms in size), as the initial nitrogen isotherms were completely reversible over the entire pressure range (Figs. 6.52 and 6.53).
3. Both samples were attacked by water vapor at high relative pressures.
4. The attack by water vapor increased the specific surface area and created a pore system which gave rise to a capillary condensation hysteresis loop in the isotherms (Figs. 6.52 and 6.53).

Specific surface areas obtained from the nitrogen adsorption data (by the BET method[6]) are given in Table 6.14. The value for sample 74220 after outgassing at 300°C (pre-H_2O) is in good agreement with that reported by Cadenhead (0.46 m^2/g).[7]

Although there is a general similarity of all the results obtained to date, there are significant specific differences, not only between 74220 and 74241, but also between these two and the previously studied fines.[4,5]

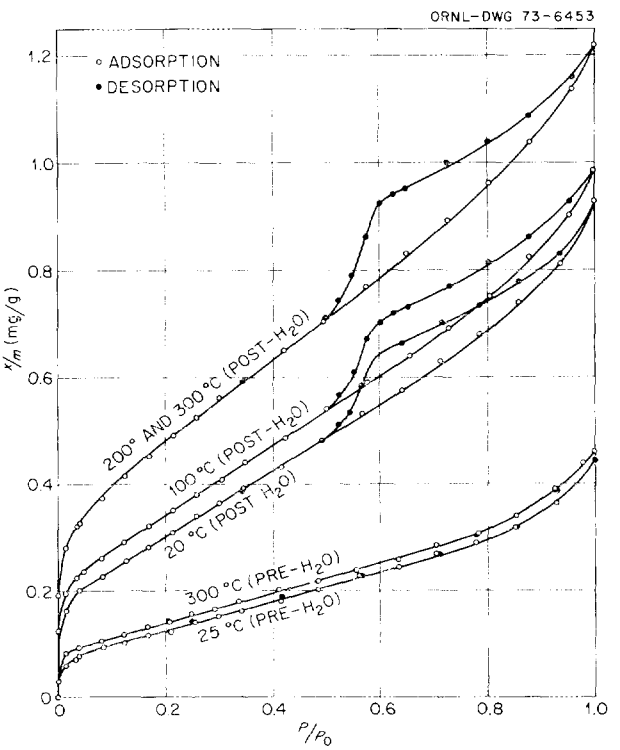

Fig. 6.52. Adsorption of N_2 on Apollo 17 lunar fine sample 74220,35 at 77°K. Sample outgassed at indicated temperature.

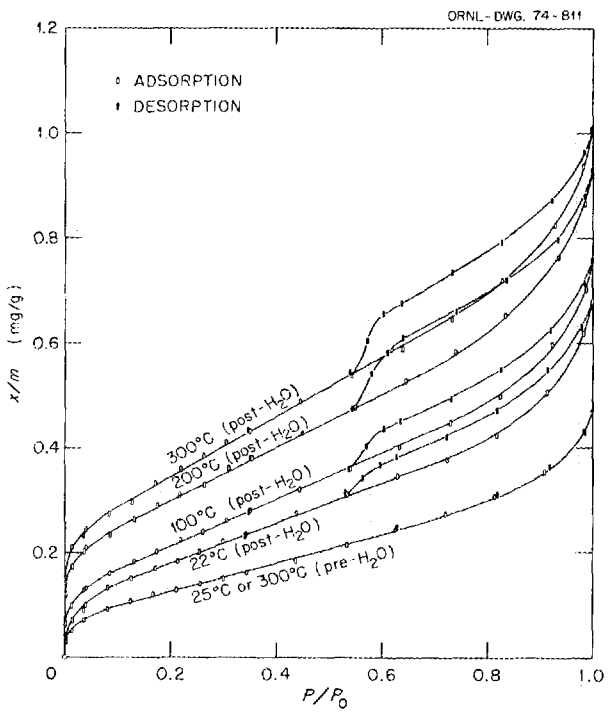

Fig. 6.53. Adsorption of N_2 on Apollo 17 lunar fine sample 74241,42 at 77°K. Sample outgassed at indicated temperature.

Both of the Apollo 17 samples were hydrophobic in their initial interaction with water vapor (water surface areas were about half of the nitrogen value). This can be contrasted with the hydrophilicity of the previous samples[4,5] and may be indirect evidence that the Apollo 17 samples have been heated to an elevated temperature (about 700°C or above). However, both of the Apollo 17 samples were strongly hydrophilic after the attack by water vapor at high relative pressures. The alteration of sample 74220 was completed with one cycle in water vapor to high relative pressures. This is a sharp contrast to Apollo 12, 14, and 16 samples, where the alteration process continued through several cycles.[4,5] This difference may be related to the very high glass content of sample 74220.[8] Another difference in sample characteristics may be seen in the blocking action of irreversibly adsorbed water (i.e., the dependence of nitrogen adsorption on the outgassing temperature). In the case of sample 74220 the effect of irreversibly adsorbed water on the specific surface area and hysteresis is much less than that observed with previously studied samples.[4,5] In this respect, sample 74241 is intermediate between 74220 and the previous samples. In the case of 74241 (and the previous samples) there is an increase in both the specific surface area and the size of the hysteresis loop when the outgassing temperature is increased from 200 to 300°C. Obviously this is not the case with sample 74220.

The general nature of the attack of lunar fines by adsorbed water at high relative pressures can be explained by the formation of a system of pores having wide bodies and narrow openings, with the narrow openings as the site where irreversibly adsorbed water blocks access of nitrogen to the pore system. The mechanism for the formation of this pore system has not been firmly established, but its generality leads us to believe that it is related to the radiation damage the samples have undergone.

Radionuclide investigations of Apollo 17 samples, also supported by NASA, are described in two contributions by G. D. O'Kelley and co-workers in Chapt. 1 of this report.

---

1. Research sponsored by the National Aeronautics and Space Administration through an interagency agreement with the U.S. Atomic Energy Commission. Work performed in part in the Reactor Chemistry Division.
2. Extended abstract of paper presented at the Fifth Lunar Science Conference, Houston, Tex., Mar. 18–22, 1974; also *Lunar Science V*, The Lunar Science Institute, Houston, 1974.
3. Health Physics Division.
4. H. F. Holmes, E. L. Fuller, Jr., and R. B. Gammage, *Earth Planet. Sci. Lett.* **19**, 90 (1973).
5. H. F. Holmes, E. L. Fuller, Jr., and R. B. Gammage, p. 2413 in *Proc. Fourth Lunar Sci. Conf., Geochim. Cosmochim. Acta*, Suppl. 4, vol. 3, Pergamon Press, New York, 1973.
6. S. Brunauer, P. H. Emmett, and E. Teller, *J. Amer. Chem. Soc.* **60**, 309 (1938).
7. D. A. Cadenhead, *Trans. Amer. Geophys. Union* **54**, 582 (1973).
8. Apollo 17 Preliminary Examination Team, *Science* **182**, 659 (1973).

MOLTEN SALTS

TEMPERATURE AND SOLVENT EFFECTS ON THE EQUILIBRIUM OF DILUTE URANIUM TRIFLUORIDE SOLUTIONS CONTAINED IN GRAPHITE[1]

L. M. Toth[2] L. O. Gilpatrick

The equilibrium of dilute UF_3-UF_4 molten fluoride solutions in contact with graphite and UC_2,

$$3UF_4(d) + UC_2(s) \rightleftharpoons 4UF_3(d) + 2C(\text{graphite}) ,$$

has been studied as a function of temperature (370° to 700°C) and melt composition. Equilibrium quotients, $Q = (UF_3)^4/(UF_4)^3$, for the reaction were determined by

measuring UF_3 and UF_4 concentrations spectrophotometrically. It was found that the equilibrium quotient is sensitive to both temperature and solvent changes, increasing as either the temperature increases or the alkali metal fluoride content of the solvent decreases.

The enthalpy of the above reaction in an $LiF\text{-}BeF_2$ (66-34 mole %) solution was calculated from the equilibrium quotient data using the van't Hoff equation. This value, 99.3 kcal, was compared with the change in enthalpy for the pure undissolved components (−12.90 kcal). Assuming that the cumulative effect of uncertainties in the thermodynamic data was not responsible for the above discrepancy in values, heats of solution for UF_3 and UF_4 in $LiF\text{-}BeF_2$ (66-34 mole %) can be determined. Using a value of 17 kcal/mole for UF_3 (ref. 3), the enthalpy of solution for UF_4 is found to be −15 kcal/mole. This value would suggest that UF_4 forms complexes of greater stability than does UF_3, in agreement with previous predictions.[4]

1. Expanded abstract of published paper, *J. Phys. Chem.* 77, 2799 (1973). Work performed in the Reactor Chemistry Division.
2. Metals and Ceramics Division.
3. This value was determined assuming that the enthalpy of solution for UF_3 is equivalent to that measured for CeF_3 by C. J. Barton et al., *Inorg. Chem.* 9, 307 (1970).
4. G. Long and F. F. Blankenship, *The Stability of UF_3*, ORNL-TM-2065 (1969).

EFFECT OF OXYGEN ON THE EQUILIBRIUM OF UF_3-UF_4 MOLTEN FLUORIDE SOLUTIONS CONTAINED IN GRAPHITE

L. O. Gilpatrick R. M. Waller
L. M. Toth[1]

With the reactivation of the Molten-Salt Reactor Program, an interest in those factors which affect the UF_3/UF_4 ratio in molten-salt reactor fuel solutions has returned. Some of the measurements made during the study of the UF_3-UF_4 solution equilibrium contained in graphite[2] indicated that contamination of the system by oxygen could cause a decrease in the equilibrium UF_3/UF_4 ratio through the formation of more stable oxycarbide phases.[3]

Recently an experimental program was established to verify these earlier observations and assess the seriousness of trace oxygen contamination on the UF_3-UF_4 equilibrium. Verification of the previous measurements has been achieved, and work to identify any additional solid phases which may form when oxygen is incorporated into the system will continue.

1. Metals and Ceramics Division.
2. L. M. Toth and L. O. Gilpatrick, "Temperature and Solvent Effects on the Equilibrium of Dilute Uranium Trifluoride Solutions Contained in Graphite," the preceding contribution, this report.
3. L. M. Toth and L. O. Gilpatrick, *The Equilibrium of Dilute UF_3 Solutions Contained in Graphite*, ORNL-TM-4056 (December 1972).

SYNTHESIS AND LIGAND-FIELD SPECTRUM OF POTASSIUM HEPTAFLUORONIOBATE(IV)[1]

L. O. Gilpatrick L. M. Toth[2]

For a study of the ligand-field spectrum of the Nb(IV) ion, inorganic ligands, especially the fluoride ion, provide an advantage over organic ligands because the weak Laporte forbidden transitions should be well removed from the lowest electronically allowed bands. The present description of the Nb(IV) absorption spectrum in a crystalline compound is a necessary precursor to explaining its absorption spectrum in fused-salt media.

The most satisfactory synthesis of the cubic compound K_3NbF_7 was found to be reduction of a molten $KF\text{-}NbF_5$ mixture with niobium metal at 850°C according to the relation:

$$15KF + 4NbF_5 + Nb \rightarrow 5K_3NbF_7 .$$

Debye-Scherrer x-ray analysis indicates that the compound is cubic with a unit cell equal to 8.93 Å and is isostructural with other disordered cubic compounds such as $(NH_4)_3ZrF_7$ and K_3NbOF_6 which belong to the space group O_h^5 ($Fm3m$). The transition-metal ion is coordinated to seven anions in a disordered pentagonal bipyramid having approximate D_{5h} symmetry.

The electronic spectrum of K_3NbF_7 was measured using a polished plate 1.5 mm thick for transmission, powdered samples for diffuse reflectance, and Kel-F mulled samples for a mull spectrum. The ligand-field spectrum extends from 1000 to 45,000 cm^{-1} (cf. Figs. 6.54 and 6.55) and consists of four weak bands which were assigned on the basis of a d^1 ion in a field of approximate D_{5h} symmetry. In a D_{5h} field, the five degenerate d orbitals split into three groups — a degenerate $e_1''[(yz), (zx)]$ ground state, a degenerate $e_2'[(x^2 - y^2), (xy)]$ excited state, and an $a_1'(z^2)$ excited state.[3] Distortions of the pentagonal bipyramidal structure as found in K_3NbF_7 cause the degeneracy of the e_1'' and e_2' states to be removed. The band at 28,570 cm^{-1} was assigned to the a_1' excited state, while the bands at 16,556 and 19,762 cm^{-1} were

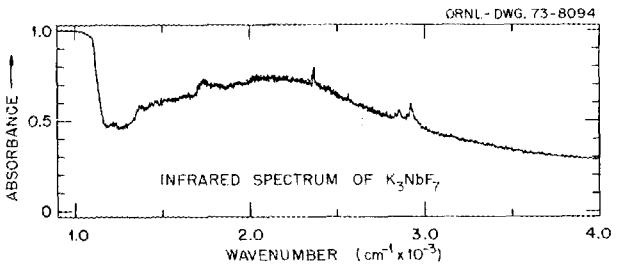

Fig. 6.54. The infrared absorption spectrum of K_3NbF_7 measured from a 1-mm-thick polished plate.

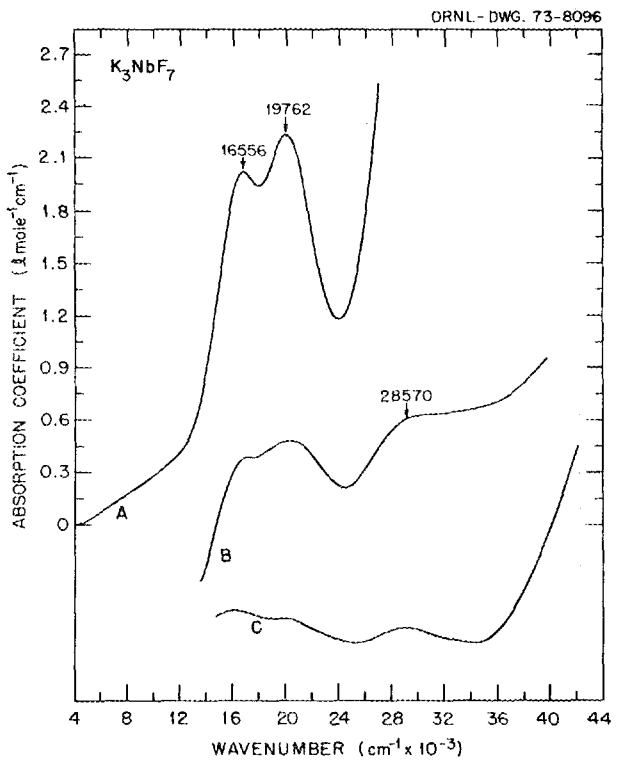

Fig. 6.55. Electronic spectrum of K_3NbF_7 at 25°C. *A*, absorption spectrum of polycrystalline plate with 1.5-mm path length; *B*, diffuse reflectance spectrum of a powdered sample against LiF reference; *C*, Kel-F mull spectrum against LiF mull reference. The molar absorption coefficient scale applies only to curve *A*.

assigned to the degenerate e_2' state, which is split by the distortion from perfect D_{5h} symmetry. If the e_2' state is split, then the e_1'' ground state is expected to be split also. However, the band arising from the split ground state should appear in the infrared region outside the range of the visible-ultraviolet absorption spectrometer. Using an infrared spectrometer, it was found at 2150 cm^{-1} beside the intense absorption caused by the NbF_7^{3-} vibrational modes which extend from 1100 cm^{-1} to lower energies.

The effect of higher temperatures on the absorption spectrum was examined by measuring absorption spectra up to 600°C. The splitting of the degenerate electronic states was observed to increase progressively with temperature because of increased vibrational disorder.

1. Expanded abstract of paper accepted for publication in *Inorganic Chemistry*.
2. Metals and Ceramics Division.
3. S. T. Spees, Jr., and J. R. Parumareddi, *J. Phys. Chem.* 72, 1822 (1968).

COORDINATION BEHAVIOR OF Nb(IV) IN MOLTEN LiF-BeF_2 MIXTURES

L. O. Gilpatrick L. M. Toth[1]

The redox chemistry of those second-row transition elements which are recognized in molten-salt reactors as fission products or proposed structural metals has been a subject of interest during the past year. When present as dilute species in molten salt solutions, these transition elements form ions which can vary extensively in oxidation number depending on the redox potential of the system. The main effort of this research is focused on relating the chemistry of these ions to their coordination behavior as observed through absorption spectroscopy.

The electronic absorption spectrum of Nb(IV), which obeys Beer's law for concentrations up to 0.30 mole/liter, has been measured in fluoride melts and is found to consist of four weak bands occurring at 5500, 13,300, 20,000, and 26,300 cm^{-1}. The spectrum is tentatively assigned on the basis of a d^1 ion in a seven-coordinated complex, NbF_7^{3-}, of very low symmetry, C_1, where the degeneracy of the *d* orbitals is completely removed. A maximum of four ligand-field bands are then possible, and they are identified with those which have been measured in the melt. These bands can be related directly to the four bands observed in crystalline K_3NbF_7 (ref. 2) and represent then the limit of splitting which could occur in the crystalline solid spectrum.

1. Metals and Ceramics Division.
2. L. O. Gilpatrick and L. M. Toth, "Synthesis and Ligand-Field Spectrum of Potassium Heptafluoroniobate(IV)," the preceding contribution, this report.

PHASE RELATIONS IN FLUOROBORATE SYSTEMS. THE SYSTEM RbF-$RbBF_4$[1]

L. O. Gilpatrick C. J. Barton[2]

This investigation of the system RbF-$RbBF_4$ represents an extension of studies we have made of the

systems $NaF\text{-}NaBF_4$ and $KF\text{-}KBF_4$ as well as the system $NaF\text{-}KF\text{-}BF_3$.[3,4] Differential thermal analysis (D.T.A.) was the chief technique used in this investigation, but a few compositions were examined by the gradient-quenching technique to identify the phases present. We believe the calibration procedures used assured a temperature reliability of ±2°C.

A simple eutectic was found in this system, with no compounds formed between the end members and no evidence of any solid solution present within the limits of the experimental procedures. All data points shown in Fig. 6.56 represent the mean of from two to nine D.T.A. heating-cooling cycle measurements.

The eutectic composition was estimated by graphical methods to be 68.5 mole % $RbBF_4$ and to have a melting point of 442° ± 2°C. All compositions other than pure RbF will show the presence of $RbBF_4$ as a pure phase coprecipitated with crystalline RbF at temperatures below the eutectic temperature. In support of this expectation, all compositions except pure RbF showed the characteristic polymorphic crystal transition of pure $RbBF_4$ upon heating at a constant mean temperature of 246° ± 2°C.

1. Summary of paper, *J. Inorg. Nucl. Chem.* **36**, 725 (1974). Work performed in the Reactor Chemistry Division.
2. Now of the Environmental Sciences Division.
3. C. J. Barton, L. O. Gilpatrick, J. A. Bornmann, H. H. Stone, T. N. McVay, and Herbert Insley, *J. Inorg. Nucl. Chem.* **33**, 337 (1971).
4. C. J. Barton, L. O. Gilpatrick, J. A. Bornmann, T. N. McVay, and H. Insley, *J. Inorg. Nucl. Chem.* **33**, 345 (1971).

PHASE EQUILIBRIA IN THE SYSTEMS $BeF_2\text{-}CeF_3$, $LiF\text{-}CeF_3$, AND $LiF\text{-}BeF_2\text{-}CeF_3$[1]

C. J. Barton[2] L. O. Gilpatrick
H. Insley[3]

A continuing interest in the application of the solvent $LiF\text{-}BeF_2$ to molten-salt breeder reactor technology[4] has stimulated the study of the behavior of CeF_3 in this solvent. Phase relations in the ternary system $LiF\text{-}BeF_2\text{-}CeF_3$ were examined because CeF_3 has been found to be quite similar to PuF_3 in its solubility in fluoride mixtures and in its phase relationships.[5] Therefore CeF_3 was chosen as an experimentally convenient guide to the fate of PuF_3 in this system, as well as a guide to typical rare-earth fission product behavior.

A tentative phase diagram for the system $BeF_2\text{-}CeF_3$ is presented in Fig. 6.57, which shows it to be a simple eutectic system with a eutectic composition of 4 ± 1 mole % CeF_3 and melting at 540 ± 3°C. Data were obtained for this very viscous system using differential thermal analysis (D.T.A.) and the gradient quenching technique.[6] These techniques were also used for the remainder of the study. Additional data from D.T.A. and visual observations are reported further to refine a previously published phase diagram (Fig. 6.58) for the system $LiF\text{-}CeF_3$.[7] The ternary system $LiF\text{-}BeF_2\text{-}CeF_3$

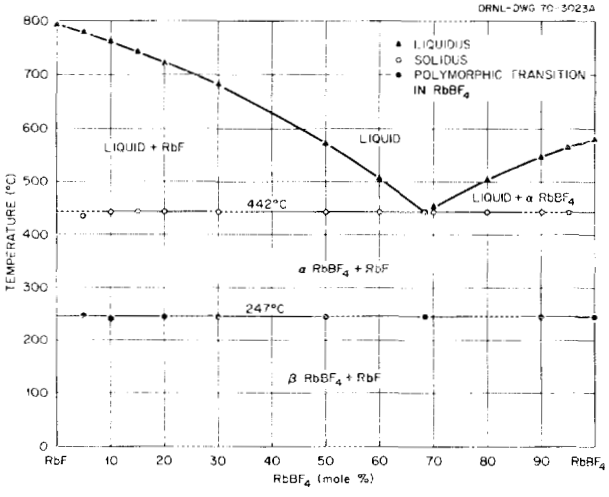

Fig. 6.56. The system $RbBF_4\text{-}RbF$.

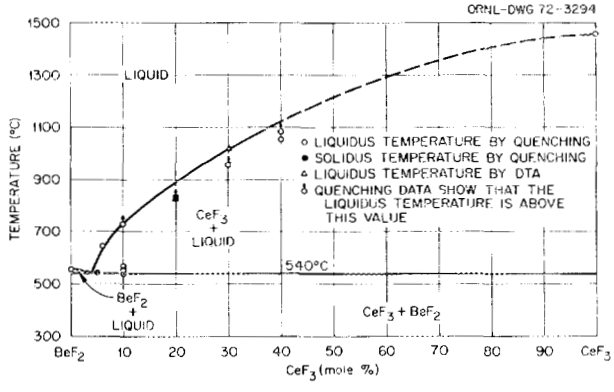

Fig. 6.57. Tentative phase diagram of the system $BeF_2\text{-}CeF_3$.

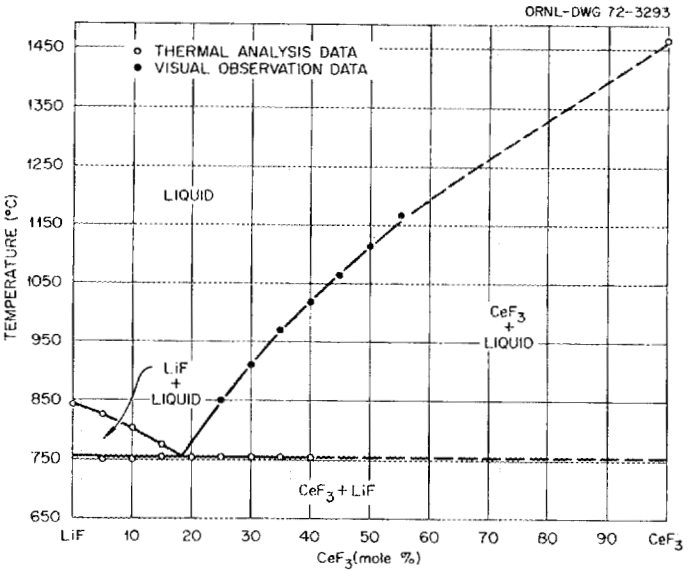

Fig. 6.58. The system LiF-CeF_3.

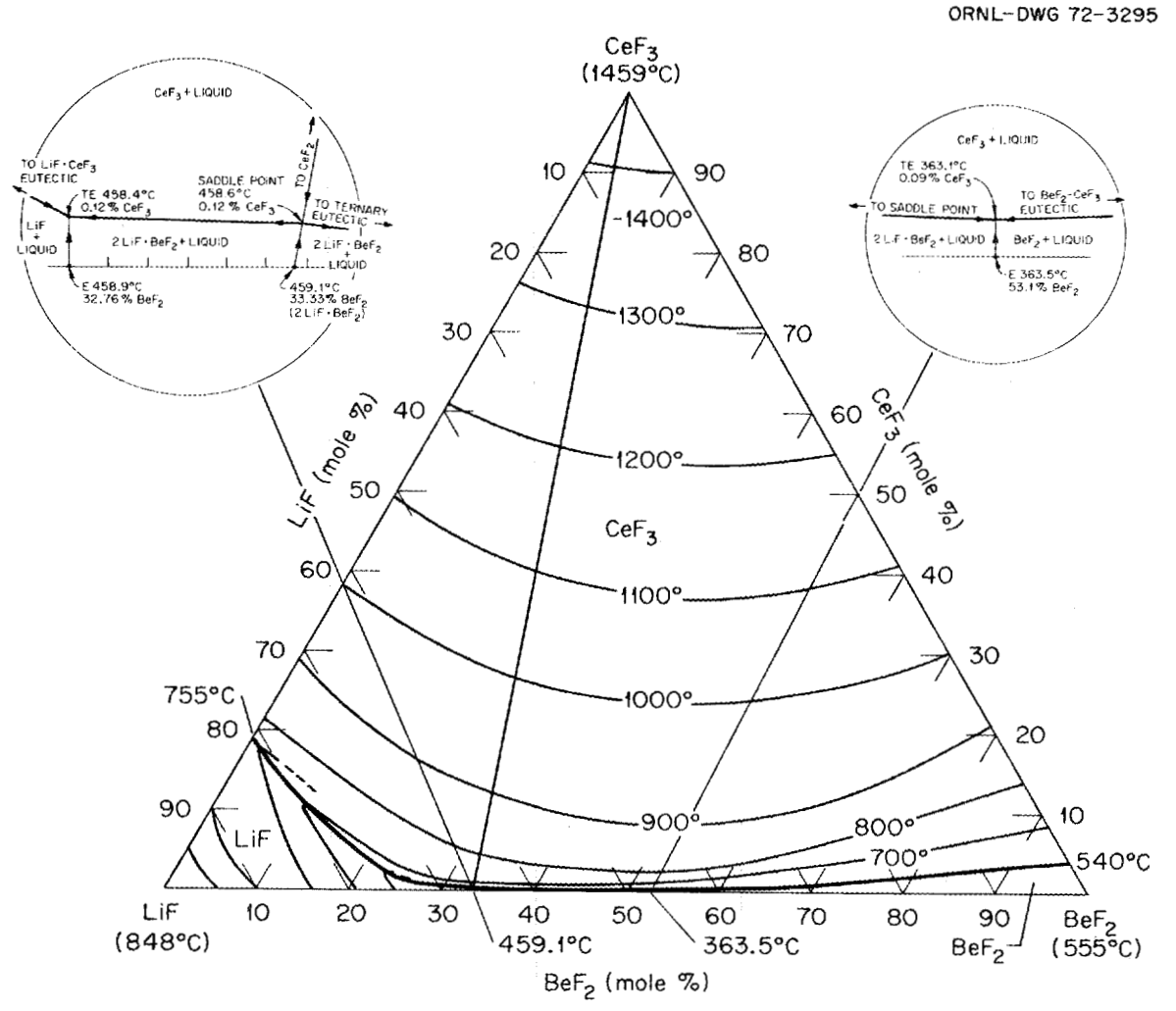

Fig. 6.59. The system LiF-BeF_2-CeF_3.

(Fig. 6.59) is dominated by the CeF_3 primary phase field. The three invariant points in the ternary are all estimated to contain approximately 0.1 mole % CeF_3. They have melting points about 0.5°C lower than the corresponding $LiF\text{-}BeF_2$ invariant points. These invariant points for the system $LiF\text{-}BeF_2$ were taken from the remaining binary component of this system, which has been extensively studied and previously reported in the literature.[8,9]

1. Expanded abstract of paper, *J. Inorg. Nucl. Chem.* 36, 1271 (1974). Work performed in the Reactor Chemistry Division.
2. Now of the Environmental Sciences Division.
3. Consultant.
4. W. R. Grimes, *Nucl. Appl. Technol.* 8, 137 (1970).
5. C. J. Barton et al., *Inorg. Chem.* 9, 307 (1970).
6. C. J. Barton et al., *J. Amer. Ceram. Soc.* 41, 63 (1958).
7. C. J. Barton, L. M. Bratcher, R. L. Shiel, and W. R. Grimes, p. 69 in *Phase Diagrams of Nuclear Materials,* ORNL-2548, ed. by R. E. Thoma (1959); see also E. M. Levin and H. F. McMurdil, *Phase Diagrams for Ceramists,* Part II, American Ceramic Society, Columbus, Ohio, 1959.
8. R. E. Thoma et al., *J. Nucl. Mater.* 27, 166 (1968).
9. K. A. Romberger, J. Braunstein, and R. E. Thoma, *J. Phys. Chem.* 76, 1154 (1972).

OXIDE CHEMISTRY OF NIOBIUM(V) IN MOLTEN $LiF\text{-}BeF_2$ MIXTURES[1]

Gann Ting[2] C. E. Bamberger[3]
C. F. Baes, Jr. G. Mamantov[4]

The chemistry of niobium in molten fluorides is relevant to the Molten-Salt Breeder Reactor Program for several reasons: (1) During the operation of the MSRE, the appearance of fission product ^{95}Nb in the fuel seemed to be a sensitive function of the state of oxidation (the U^{4+}/U^{3+} ratio) of the fuel.[5] This effect, which presumably involves the oxidation of the metal to a soluble species, might be a useful indicator of the state of oxidation of the fuel. (2) Niobium pentoxide (Nb_2O_5), like protactinium pentoxide (Pa_2O_5), is expected to be sparingly soluble in molten fluorides, and it has been proposed that Nb(V) might be used as a stand-in for Pa(V) in studies of fuel reprocessing methods involving oxide precipitation. However, the smaller size of Nb^{5+} ion (0.69 Å) compared with Pa^{5+} ion (0.89 Å) might produce oxyions of Nb(V), while none were found for Pa(V).[6] This would profoundly affect the chemistry of Nb(V) in molten fluorides containing oxide. (3) In the system $NiO\text{-}Nb_2O_5$, at least two intermediate compounds, $NiNb_2O_6$ and $Ni_4Nb_2O_9$, are known, and since NiO is also a sparingly soluble oxide, precipitation of these nickel niobates

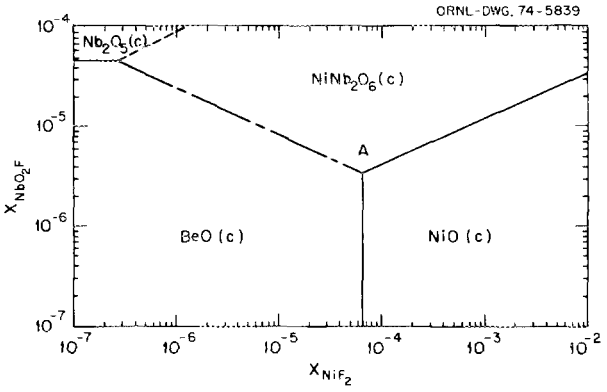

Fig. 6.60. Phase diagram representing the NbO_2F and NiF_2 concentrations in molten $LiF\text{-}BeF_2$ (67-33 mole %) at 600°C as a function of the oxide phases present at equilibrium.

may be expected further to complicate the chemistry of Nb(V) in an MSBR fuel contained in a nickel-base alloy.

The results of our equilibrations at 600°C involving the sparingly soluble oxides BeO, NiO, Nb_2O_5, and $NiNb_2O_6$ in molten $LiF\text{-}BeF_2$ (67-33 mole %) are represented by the solid boundaries shown in Fig. 6.60. The reactions corresponding to each of these three-phase equilibria (two oxide phases and the molten fluoride phase) are listed in Table 6.15, reactions (1), (4), and (5). The dashed boundaries can be constructed from the stoichiometries of the derived reactions (2) and (3). Contrary to reports in the literature,[7] the compound $Ni_4Nb_2O_9$ could not be established as a stable phase in this system.

The boundary between $NiNb_2O_6$ and NiO in Fig. 6.60 was of special interest since its slope gives direct evidence for the formation of an oxyion, NbO_2^+, in the molten fluoride phase. This can be seen from the following general reaction (d indicates dissolved species):

$$\frac{x}{2}NiNb_2O_6(c) + \frac{y}{2}NiF_2(d) \rightleftharpoons Nb_xO_{(5x-y)/2}F_y(d) + \frac{x+y}{2}NiO(c)$$

and its equilibrium quotient (X denotes mole fraction)

$$Q = X[Nb_xO_{(5x-y)/2}F_y]/[X(NiF_2)]^{y/2}$$

From the slope of ½ observed for the boundary in Fig. 6.60 corresponding to this reaction, the value of y is 1.[8] From this we conclude that Nb(V) forms the oxyion NbO_2^+ in solution. The alternative polynuclear ions

Table 6.15. Equilibria of Nb_2O_5, NiO, and BeO with LiF-BeF_2 (67-33 mole %) at 600°C

Reaction	Boundary	Equilibrium reaction	Q^a
(1)	$Nb_2O_5(c)/BeO(c)$	$\frac{1}{2}Nb_2O_5(c) + \frac{1}{2}BeF_2(d) \rightleftharpoons NbO_2F(d) + \frac{1}{2}BeO(c)$	$X(NbO_2F) = 10^{-4.34}$
(2)	$Nb_2O_5(c)/NiNb_2O_6(c)$	$Nb_2O_5(c) + \frac{1}{2}NiF_2(d) \rightleftharpoons NbO_2F(d) + \frac{1}{2}NiNb_2O_6(c)$	$X(NbO_2F)/[X(NiF_2)]^{1/2} = 10^{-1.06}$
(3)	$NiNb_2O_6(c)/BeO(c)$	$\frac{1}{2}NiNb_2O_6(c) + BeF_2(d) \rightleftharpoons NbO_2F(d) + \frac{1}{2}NiF_2(d) + BeO(c)$	$X(NbO_2F)\,X(NiF_2)^{1/2} = 10^{-6.50}$
(4)	$NiO(c)/BeO(c)$	$NiO(c) + BeF_2(d) \rightleftharpoons NiF_2(d) + BeO(c)$	$X(NiF_2) = 10^{-4.18}$
(5)	$NiNb_2O_6(c)/NiO(c)$	$\frac{1}{2}NiNb_2O_6(c) + \frac{1}{2}NiF_2(d) \rightleftharpoons NbO_2F(d) + NiO(c)$	$X(NbO_2F)/[X(NiF_2)]^{1/2} = 10^{-3.44}$

[a]In LiF-BeF_2 (67-33 mole %) the activity of $BeF_2(d)$ has been defined as unity.

which are possible ($Nb_3O_7^+$, $Nb_5O_{12}^+$, . . .) seem quite unlikely at the low concentrations of niobium involved.

The magnitude of the solubility of Nb_2O_5 (i.e., the height of the Nb_2O_5/BeO boundary in Fig. 6.60), which is much greater than originally expected, provides additional strong evidence that an oxyion of Nb(V) is formed in solution. The stability of Nb^{5+} otherwise required to explain this high solubility would be so great that the Nb^{4+} found by Weaver et al. to be formed by the reaction[9]

$$Nb^0(c) + 4HF(g) \rightleftharpoons NbF_4(d) + 2H_2(g) \qquad (1)$$

should have disproportionated almost completely:

$$NbF_4(d) \rightleftharpoons \frac{4}{5} NbF_5(d) + \frac{1}{5} Nb^0(c) . \qquad (2)$$

This was clearly not the case.

From the measured equilibrium quotients and the formation free energies of the other oxides and dissolved fluorides involved, we obtain the free energy of formation of NbO_2F in the mole fraction standard state in LiF-BeF_2 (67-33 mole %):

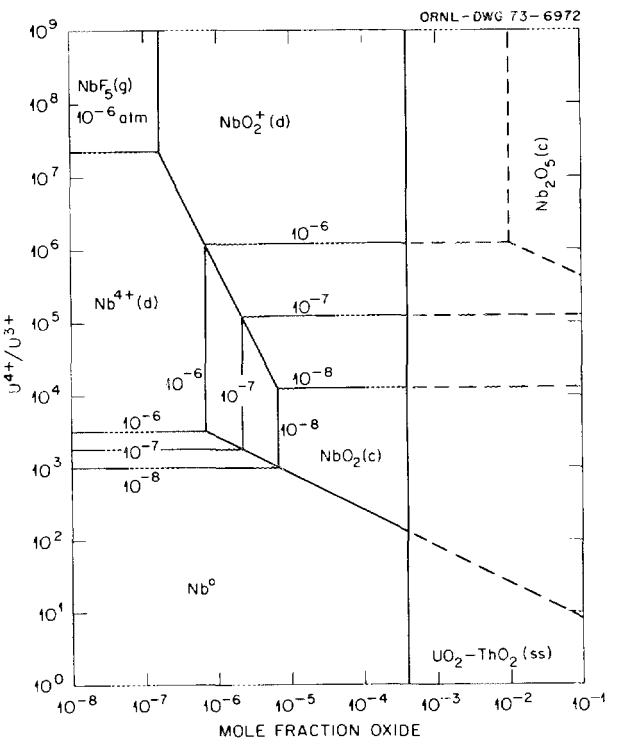

Fig. 6.61. Pourbaix diagram for niobium in LiF-BeF_2-ThF_4 (72-16-12 mole %) at 600°C.

$$\Delta G^f\ [NbO_2F(d)] = -250.7 + 45.9T/10^3 \text{ kcal/mole} ,$$

and of $NiNb_2O_6$:

$$\Delta G^f\ [NiNb_2O_6(c)] = -509.0 + 112.7T/10^4 \text{ kcal/mole} .$$

With the measurements of the equilibrium quotient for reaction (1),[9] we can also construct the Pourbaix diagram shown in Fig. 6.61, wherein the conditions of oxide concentration and redox potential are shown under which the various forms of niobium are stable in a molten-salt breeder reactor fuel.

1. Summary of paper now in preparation, based on portions of a Ph.D. thesis "Thermodynamic and Electrochemical Studies of Niobium in Molten Fluorides and Chloroaluminates," by Gann Ting, University of Tennessee, Knoxville, August 1973. Work performed in the Reactor Chemistry Division.
2. Guest scientist, Institute of Nuclear Energy Research, Republic of China. Present address: Institute of Nuclear Energy Research, Lung-Tan, Taiwan.
3. Now of the Chemical Technology Division.
4. Consultant to Analytical Chemistry Division, Department of Chemistry, University of Tennessee, Knoxville.
5. R. E. Thoma, *Chemical Aspects of MSRE Operation*, ORNL-4658 (December 1971), pp. 94–99.
6. R. G. Ross, C. E. Bamberger, and C. F. Baes, Jr., *J. Inorg. Nucl. Chem.* **35**, 433 (1973).
7. E. V. Tkatchenko, F. Abbattista, and A. Burdeze, *Izv. Akad. Nauk SSSR, Neorg. Mater.* **5**, 1671 (1969); F. Abbattista, E. V. Tkatchenko, and C. T. Chiantavetto, *Atti Accad. Sci. Torino, Cl. Sci. Fis., Mat. Natur.* **103**, 605 (1969).
8. In this reaction and in Table 6.15, for convenience we write the formulas of dissolved species as neutral components. The number of F^- ions thus shown is not intended to imply the number F^- ions actually present in a given species.
9. C. F. Weaver, H. A. Friedman, and J. S. Gill, *MSR Program Semiannu. Progr. Rep. Aug. 31, 1970*, ORNL-4622, p. 73.

THE CHEMISTRY AND THERMODYNAMICS OF MOLTEN-SALT REACTOR FUELS[1]

C. F. Baes, Jr.

The fuel of a molten-salt breeder reactor (MSBR), in which fissile ^{233}U is bred from ^{232}Th by thermal neutrons, will probably consist of the mixture LiF-BeF_2-ThF_4 (72-16-12 mole %) at about 600°C in which less than 1 mole % of fissile UF_4 or PuF_3 is dissolved. A fairly detailed knowledge of the chemistry of such a molten salt mixture has been gained from measurements of heterogeneous equilibria involving various gaseous (e.g., HF, H_2O) and solid (usually oxide) compounds combined with the thermochemical data which are available for the pure compounds.

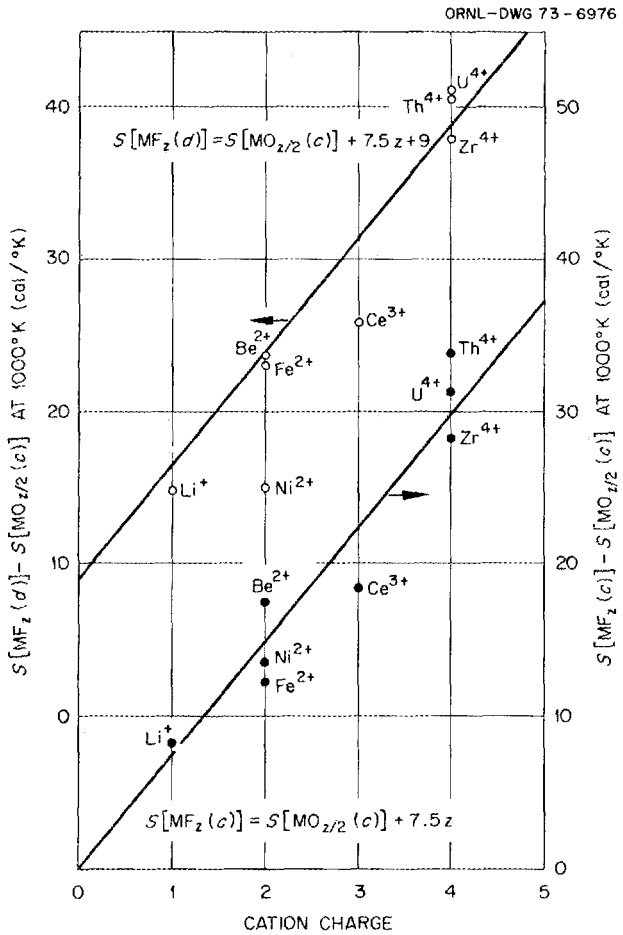

Fig. 6.62. Correlation of entropies of crystalline fluorides and of fluorides dissolved in molten LiF-BeF$_2$ (67-33 mole %) with entropies of crystalline oxides.

The entropy of a fluoride component in the fuel can be estimated with useful accuracy from the known entropy of the corresponding oxide and the charge on the cation (Fig. 6.62). The activity coefficients of BeF_2, ThF_4, and UF_4 decrease strongly as the mole percentage of LiF in an LiF-BeF_2-ThF_4 solvent is increased, but the variations do not exceed a factor of 10 from activity coefficient values in the reference composition LiF-BeF_2 (67-33 mole %). The activity coefficient changes for CeF_3, UF_3, PuF_3, and NiF_2 are less pronounced.

The solubility of oxides in such molten fluoride mixtures generally decreases with z_+^2/r_+ (the square of the charge of the cation divided by its radius) for the cation involved (Fig. 6.63). Thus BeO, ZrO_2, the actinide dioxides, and especially Pa_2O_5 show a low solubility in MSBR fuels. The actinide dioxides form solid solutions which can exchange tetravalent cations with the molten fluoride and could as a result prove useful in fuel reprocessing. The oxide Pa_2O_5 (or an addition compound of it) is so insoluble that it could be used selectively to remove ^{233}Pa bred in the fuel (Fig. 6.64).

The fuel of the MSBR will be maintained mildly reducing with the ratio U^{4+}/U^{3+} in the range 10 to 100. The other actinides then will be present as Th^{4+}, Pa^{4+}, and Pu^{3+}. Corrosion reactions with the metals of the nickel-base container alloy (Hastelloy N) will not be favored thermodynamically (Fig. 6.65). The noble-gas fission products are insoluble and can be removed by continuous stripping with an inert gas. Group VII, I, II, III, and IV fission products should appear as dissolved

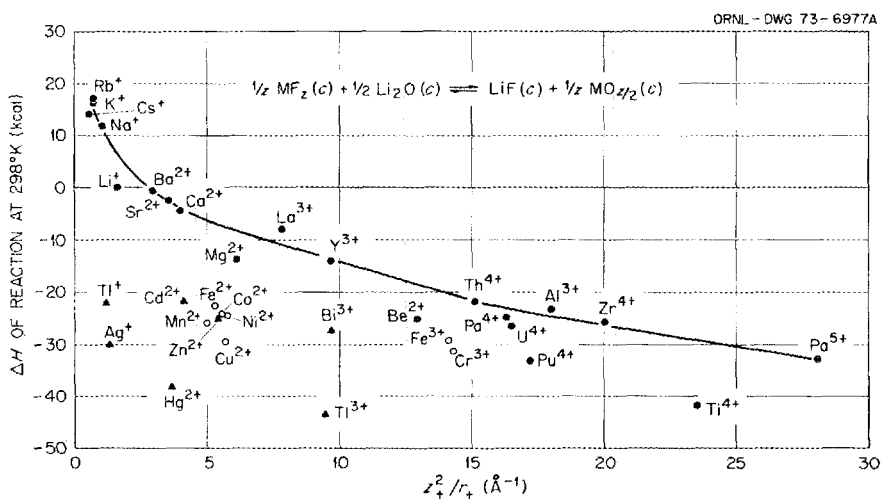

Fig. 6.63. Effect of cation charge and radius on the relative stability of oxides and fluorides. ●, pre-transition; ○, transition; and ▲, post-transition elements.

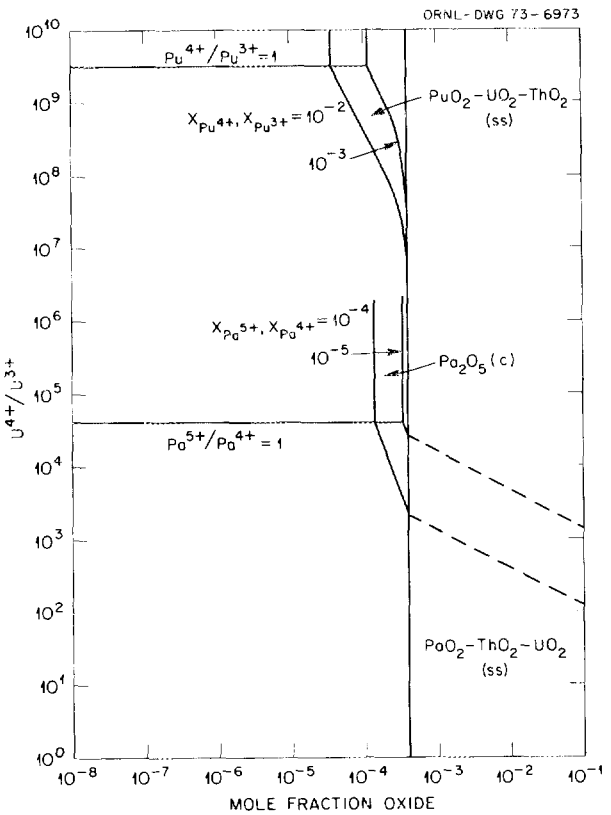

Fig. 6.64. Pourbaix diagram for the actinide elements in LiF-BeF_2-ThF_4 (72-16-12 mole %) at 600°C. *X* denotes mole fraction; ss, solid solution.

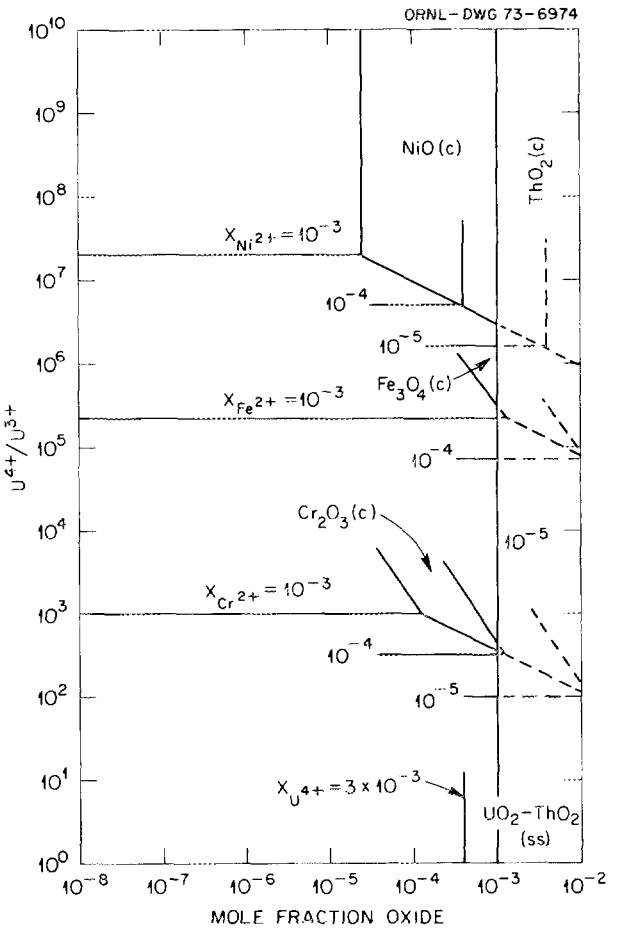

Fig. 6.65. Pourbaix diagram for structural metals in LiF-BeF_2-ThF_4 (72-16-12 mole%) at 600°C. The horizontal lines denote equilibrium between the indicated mole fraction of ions and the pure metal.

species in their normal valences. The remaining fission products (principally Nb, Mo, Te, and Ru) should be reduced to the metallic state.

1. Summary of invited paper presented at the U.S.-Japanese Conference on the Thermodynamics of Nuclear Materials, Ames, Iowa, July 1973, and included in the published proceedings, *J. Nucl. Mater.* 51, 149 (1974). Work performed in the Reactor Chemistry Division.

COMPETITIVE HYDRATION AND ASSOCIATION EQUILIBRIA IN HYDROUS MELTS[1]

H. Braunstein P. T. Hardesty[2]
J. Braunstein

We have reported previously[3] the effect of water on association equilibria of the dilute solute ions Cd^{2+} and Br^- in the solvent $Ca(NO_3)_2$. A quasi-lattice model of competing association and hydration,[4] which had been demonstrated to fit association equilibria in the solvents NH_4NO_3-H_2O and equimolar [$LiNO_3$-KNO_3]-H_2O over a wide range of water contents, could not account for the results in the solvent $Ca(NO_3)_2$-H_2O. One of the assumptions in the quasi-lattice model was that water, in the absence of an associating ion such as Cd^{2+}, follows Henry's law; that is, the quasi-lattice model had been developed as a limiting law for infinite dilution of water in molten salt. In the two solvents in which fit was observed, the Henry's law region was unexpectedly long, which is not the case for $Ca(NO_3)_2$-H_2O. The model was therefore modified to take account of the experimental variation of water activity in formulating the competing association and hydration equilibria. Although the modified equations seemed to fit the data, the range of water contents in $Ca(NO_3)_2$ was too small for a valid test. Accordingly, emf measurements of the association equilibrium $Cd^{2+} + Br^- \rightleftharpoons CdBr^+$ [$Ca(NO_3)_2 \cdot R_{H_2O}$] were extended over a wide range of

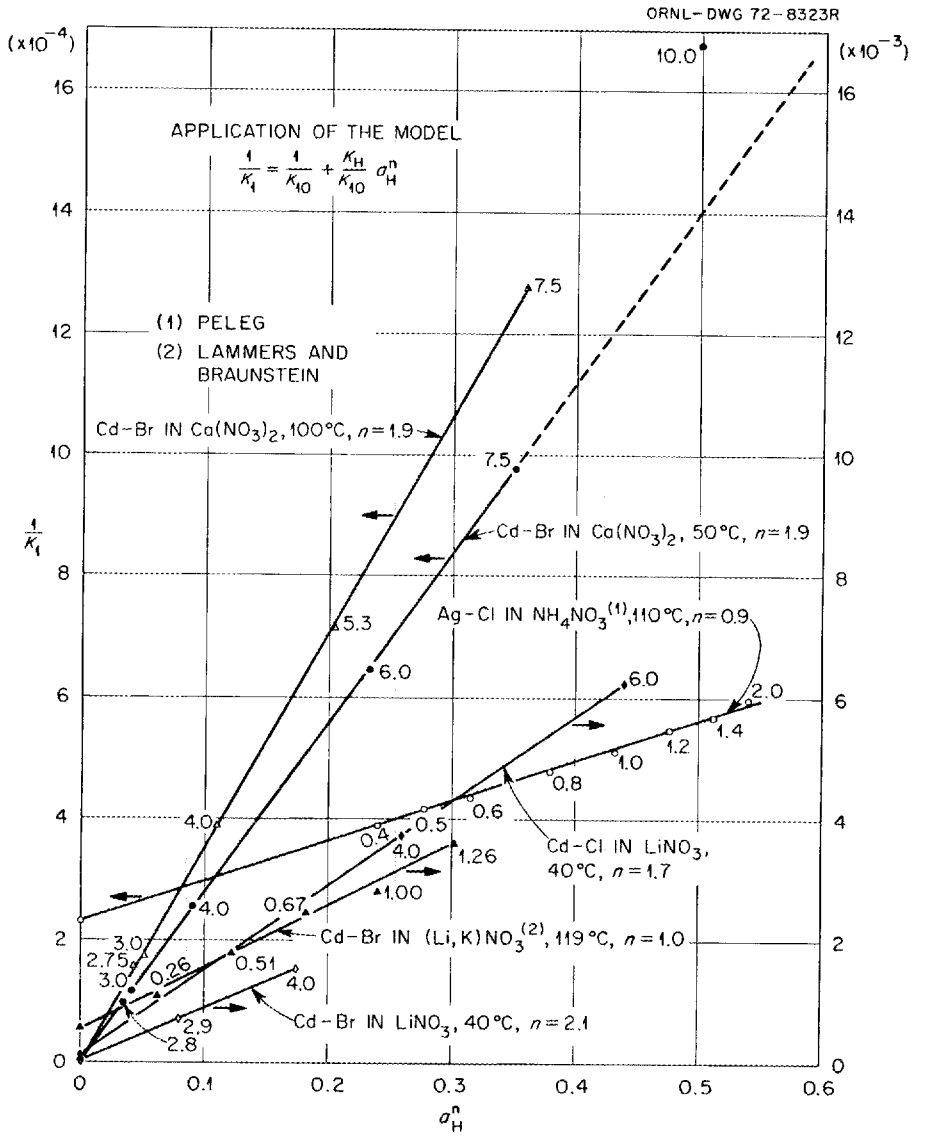

Fig. 6.66. The mass action model; dependence of association constants on water activity and water mole ratio. References: (1) M. Peleg, *J. Phys. Chem.* 75, 2060, 3711 (1971); (2) P. C. Lammers and J. Braunstein, *J. Phys. Chem.* 71, 2026 (1967).

water contents, $2.8 < R < 10.0$ moles of water per mole of $Ca(NO_3)_2$ at 50°C.[5] If the competing equilibria are

$$Cd^{2+} + Br^- \rightleftharpoons CdBr^+; \quad \Delta G^\circ_{CdBr} = -RT \ln K_{10} ,$$

$$Cd^{2+} + nH_2O \rightleftharpoons Cd(H_2O)_n^{2+}; \quad \Delta G^\circ_H = -RT \ln K_H ,$$

the experimentally determined association constant for the formation of $CdBr^+$ in the solvent $Ca(NO_3)_2 \cdot R_{H_2O}$, K_1, should be given by

$$\frac{1}{K_1} = \frac{1}{K_{10}} + \frac{K_H}{K_{10}} a_H{}^n ,$$

where a_H is the water activity in the solvent. Plots of experimental values of $1/K_1$ vs $a_H{}^n$ in Fig. 6.66 demonstrate the fit of the model for the new data in $Ca(NO_3)_2$-H_2O and for data available in the literature for other hydrous melts.[5] Preliminary results in the solvent $Mg(NO_3)_2$-H_2O also are fitted by the model. The relation between parameters of the quasi-lattice model and those of the modified model is given by

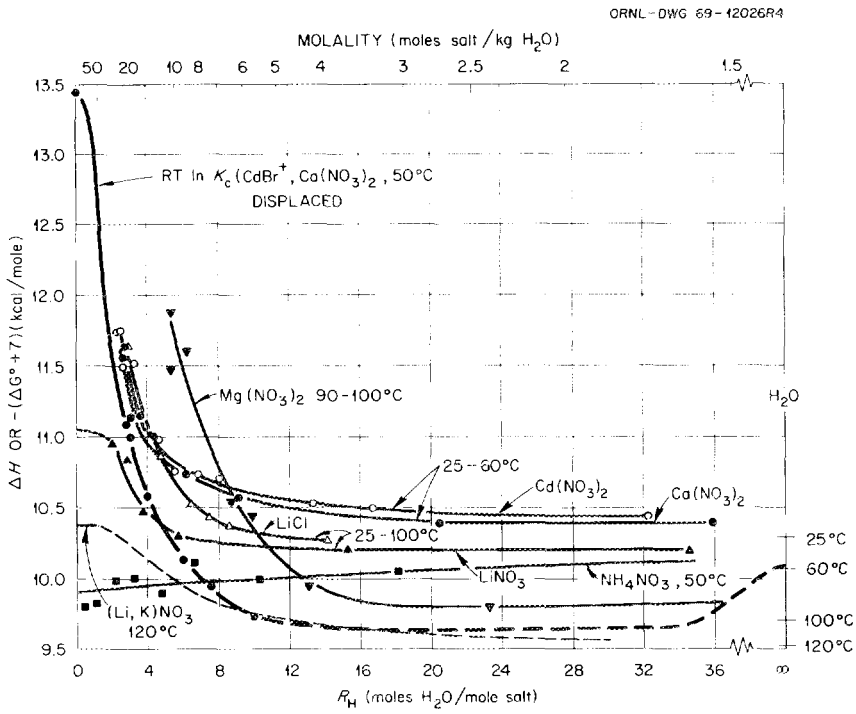

Fig. 6.67. Enthalpy of vaporization of water from melts as a function of the water content and free energy of solute association.

$$\frac{e^{-\Delta A_H}}{e^{-\Delta G^\circ_H}} = \frac{a_H{}^n}{R},$$

where ΔA_H is the Helmholtz free energy of association of associating cation with water in the quasi-lattice model. Thus either the quasi-lattice model or the modified model will fit when $n = 1$ and also Henry's law is valid.

As seen in Fig. 6.67, the free energy of association of dilute solute ions in salt-water solvents shows a dependence on water content similar to that of the enthalpy of vaporization of water in the hydrous melt region.

1. Work performed in the Reactor Chemistry Division.

2. Oak Ridge Associated Universities Summer Student Trainee from Brescia College, Owensboro, Ky.

3. H. Braunstein and J. Braunstein, *Reactor Chem. Div. Annu. Progr. Rep. May 31, 1972*, ORNL-4801, p. 60; H. Braunstein, J. Braunstein, A. S. Minano, and R. E. Hagman, *Inorg. Chem.* 12, 1407 (1973).

4. J. Braunstein, "Statistical Thermodynamics of Molten Salts and Concentrated Aqueous Electrolytes," in *Ionic Interactions*, S. Petrucci, ed., vol. I, Academic Press, New York, 1971, p. 179.

5. H. Braunstein, J. Braunstein, and P. T. Hardesty, *J. Phys. Chem.* 77, 1907 (1973).

TRANSPORT BEHAVIOR OF CONCENTRATED AQUEOUS ELECTROLYTE SOLUTIONS

A. L. Bacarella D. Brown[1]
J. Braunstein

Transport coefficients in molten salts and concentrated aqueous electrolyte solutions are of interest for practical and theoretical reasons, including studies of relations between thermodynamic and transport properties and in the evaluation of structural models of transport behavior.

Here, the diffusion coefficients, D, of dilute Cd^{2+} ion in concentrated aqueous $Ca(NO_3)_2$ solutions were determined from the Sand equation, $D = I^2\tau/\pi F^2 A^2 C^2$, using chronopotentiometric techniques. The Cd^{2+} ions, at concentrations C below 10^{-2} M, were reduced at a mercury pool electrode with area, A, of about 1 cm^2. The constant current, I, used to reduce the Cd^{2+} concentration to depletion at the mercury/solution interface was obtained from a circuit employing a field-effect transistor (FET) and powered by two 6-V Eveready lantern batteries in parallel.[2] The transition times, τ, ranging from 1 to 8 sec, were determined from chronopotentiograms recorded on a Hewlett-Packard 7100B strip chart recorder. Chart

Table 6.16. Diffusion coefficients of Cd^{2+} in concentrated solutions of $Ca(NO_3)_2$ at $T = 50°C$

D, cm^2/sec ($\times 10^{-5}$)	0.0043	0.0056	0.0074	0.0093	0.026	0.030	0.22	0.46	0.70	(1.75)
Mole ratio (moles H_2O/mole Ca^{2+})	2.90	2.99	3.13	3.25	3.76	3.88	6.67	10.0	14.3	(∞)
Molality (moles Ca^{2+}/kg H_2O)	19.1	18.6	17.7	17.1	14.8	14.3	8.32	5.55	3.88	(0)
Molarity (moles Ca^{2+}/liter)	8.52	8.40	8.25	8.11	7.58	7.47	5.53	4.19	3.18	(0)

speeds ranging from 0.5 to 2.0 in./sec were used. The applicability of the Sand equation was confirmed by proportionality of $I\tau^{1/2}$ to C and by the lack of dependence of $I\tau^{1/2}/C$ on I. The measurements were made at 50°C, and the $Ca(NO_3)_2$ concentration ranged from 6.4 to 17.1 N (equivalents per liter), or 14.3 to 2.9 moles of water per mole of salt. The diffusion coefficient decreased from 7.0×10^{-6} to 4.3×10^{-8} cm^2/sec as indicated in Table 6.16 with concentration scales mole ratio (R moles of H_2O per mole of salt), molality, and molarity. The decrease is most marked in the region with less than 6 to 10 moles of water per mole of salt, in a manner similar to the marked variation of thermodynamic properties in this concentration range.[3] It may be compared with the decrease of the equivalent conductance and fluidity of $Ca(NO_3)_2$-H_2O melts.[4] Transport data at low temperatures, in particular the increase in the Arrhenius activation energy with decreasing temperature, have been interpreted in terms of a "zero mobility" concept. As the temperature is decreased below the normal melting point (i.e., into the supercooled region), the particle mobilities become much smaller than values characteristic of liquids, and approach values expected for crystals or a rigid glass. The temperature dependence of a transport coefficient, w, may, at a given concentration, be expressed in the form of the semiempirical Fulcher equation

$$w = A \exp\ [-k/(T - T_0)] \tag{1}$$

rather than the Arrhenius equation, which applies at high temperatures.[4] A constant value of the parameter T_0 would imply that the mobility vanishes at a temperature $T = T_0$, which is near the glass transition temperature, rather than at $T = 0$. Equation (1) and the closeness of T_0 to the glass transition temperature have been partially justified in terms of the free-volume model, the configurational rearrangement model, and thermodynamic arguments. Recent work suggests that with decreasing temperature a second Arrhenius region is approached.[5] Nevertheless, Eq. (1) is useful in representing the departure of transport properties from high-temperature Arrhenius behavior. Angell has proposed and given an approximate derivation of an analogous semiempirical equation to represent the isothermal concentration dependence of transport properties into the supersaturated region:

$$w = A' \exp\ [-k'/(N_0 - N)]\ . \tag{2}$$

Here, the parameter N_0 would be interpreted as a "zero-mobility concentration" at which the solution is transformed, by packing, into a glass. The model, which is certainly oversimplified, would suggest similar values of N_0 for diffusivity, conductivity, and fluidity. Figure 6.68 shows a plot of log D vs $1/(N_0 - N)$, with different values for the parameter N_0. The opposite curvature of the plots for values of N_0 less than or greater than 24 equiv/liter suggests a value for N_0^D near 24 equiv/liter. Extrapolation of Angell's N_0 values from conductance measurements at $T = 0.35$ and 18°C to 50°C gives a value of N_0^Λ equal to 26.7 equiv/liter. Viscosity data at 20°, 40°, and 60°C give values for N_0^η of 24.2, 25.8, and 27.3 equiv/liter respectively. From the slope of the line in Fig. 6.68 corresponding to the value $N_0^D = 24$, the equation for D becomes

$$\log D = -3.688 - 25.64/(24 - N)\ . \tag{3}$$

Equation (3) is derived from data at relatively high $Ca(NO_3)_2$ concentrations and is not expected to apply in dilute solutions. It is surprising, and perhaps fortuitous, that an extrapolation of the data with Eq. (3) to infinite dilution, over nearly three orders of magnitude of the diffusion coefficient, should yield a reasonable value. Equation (3), at $N = 0$, gives $D = 1.75 \times 10^{-5}$ cm^2/sec at 50°C. With an assumed activation energy of 5 kcal/mole, a value for D of 8.8×10^{-6}

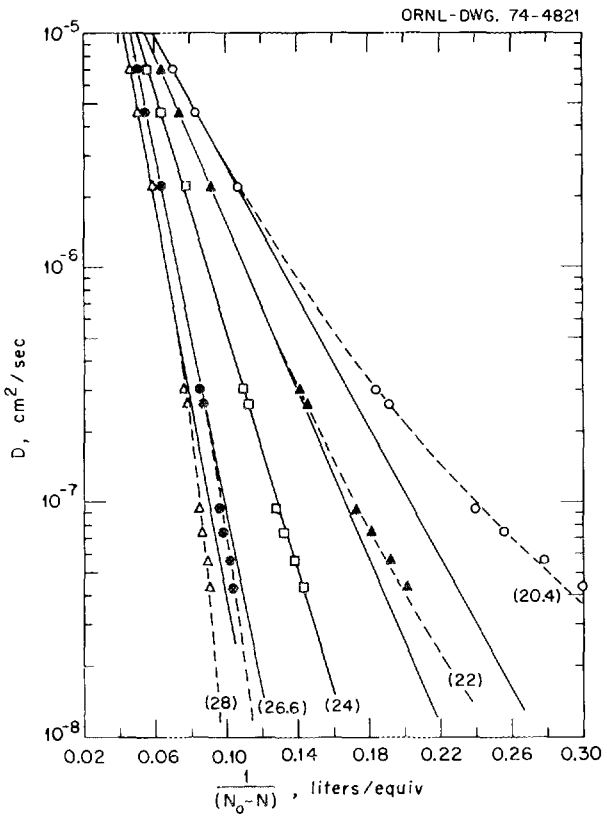

Fig. 6.68. The diffusion coefficient for Cd^{2+} in concentrated $Ca(NO_3)_2$ solution as a function of $1/(N_0 - N)$ at 50.0°C.

cm^2/sec at 25°C is obtained, compared with the experimental value $D = 7.2 \times 10^{-6}$ cm^2/sec.[6]

Further measurements will be performed at temperatures as low as 15°C (melting point of $Ca(NO_3)_2 \cdot 4H_2O$, about 43°C). At temperatures deep into the supercooled region the concept of "zero-mobility concentration" should be more sharply defined. Measurements in the solvent $LiNO_3$-H_2O are of interest since its thermodynamic properties vary much like those of $Ca(NO_3)_2$-H_2O although it is less viscous. Similarly, $CaCl_2$ solutions show viscosity behavior similar to $Ca(NO_3)_2$ solutions, but the interactions of the probe ions, Cd^{2+}, are much weaker with nitrate than with chloride ions.

1. Oak Ridge Associated Universities Summer Student Trainee from Kenyon College, Gambier, Ohio.

2. Designed by T. R. Mueller, Analytical Chemistry Division.

3. H. Braunstein, J. Braunstein, and P. T. Hardesty, *J. Phys. Chem.* 77, 1907 (1973).

4. C. A. Angell, *J. Phys. Chem.* 70, 3988 (1966); C. A. Angell, *J. Chem. Phys.* 46, 4673 (1967).

5. J. H. Ambrus, C. T. Moynihan, and P. B. Macedo, *J. Electrochem. Soc.* 119, 192 (1972).

6. R. Parsons, *Handbook of Electrochemical Constants*, Academic Press, New York, 1959, p. 79.

ANODIC CHRONOPOTENTIOMETRY OF BERYLLIUM ELECTRODES IN MOLTEN MIXTURES OF BERYLLIUM FLUORIDE WITH ALKALI FLUORIDES[1]

H. R. Bronstein J. Braunstein

Transport and thermodynamic properties of beryllium fluoride–alkali fluoride mixtures are of interest in connection with theories of ionic liquids and vitreous systems, and by virtue of structural relationships between fluoroberyllates and silicates. Previously,[2] we have reported that when a constant current is imposed at a beryllium anode immersed in a molten BeF_2-NaF mixture (75 mole % BeF_2), a sharp voltage rise is required after a period of time in order to sustain the constant current. Our initial interpretation of such a chronopotentiometric transition was that depletion of the anode region of alkali ions, the only electrically mobile cations in the system, resulted in formation of a nearly insulating layer of beryllium fluoride.[2] Clearly, however, enrichment of the anode region in BeF_2 must be partly compensated by back diffusion of alkali fluoride, driven by the diffusional gradient between the BeF_2-rich anode region and the bulk mixture. In the zeroth-order treatment of this diffusion problem, neglecting possible interaction between diffusion and electrical migration, the equation for the chronopotentiometric transition is considered idential with that for ordinary chronopotentiometry of extremely dilute solutes in a supporting electrolyte, with the exception of the physical interpretation of one of the boundary conditions,

$$I = \mathbf{F}\left[D\frac{\partial c_{Na^+}}{\partial x}\right]_{\text{electrode surface}}$$

where I is the current density, $\mathbf{F}$ the Faraday constant, D the mutual diffusion coefficient of Na^+ and Be^{2+}, c the concentration of Na^+ (moles/cm^3), and x the distance from the electrode surface.[3] This boundary condition results from depletion of an *electrically mobile, electrochemically inactive* ionic constituent, in distinction from ordinary chronopotentiometry, where a similar boundary condition results from depletion of an *electrically immobile electroactive* constituent. An experimental chronopotentiogram is given in Fig. 6.69 together with a calculated chronopotentiogram based on the above model with estimated values of the

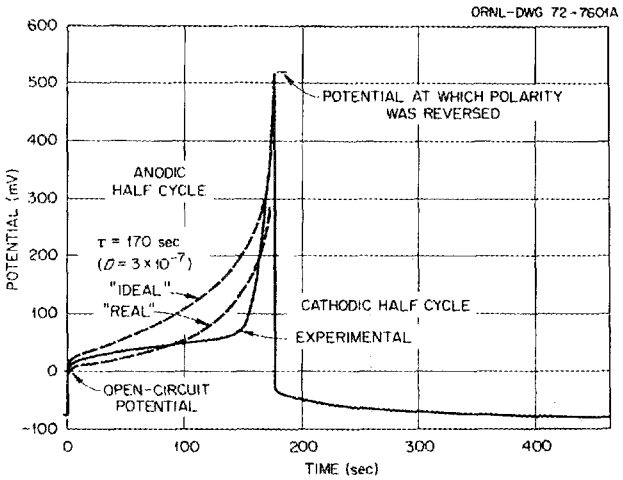

Fig. 6.69. Typical chronopotentiogram in molten NaF-BeF_2 (75 mole % BeF_2) at 520°C, current density about 40 mA/cm^2. Potential of beryllium working electrode, relative to a beryllium reference electrode, vs time.

activity coefficients in the melt, an uncertain electrode area,[3] and a graphically estimated transition time. These preliminary calculations also neglect the concentration dependence of the diffusion coefficient (hence D is a mean value) and possible variations of the transference number and IR drop. [The upper curve ("ideal") neglects deviations from thermodynamic ideality of the mixture in the calculation.] The low diffusion coefficient is consistent with the low electrical conductivity and the high viscosity of BeF_2-rich melts. The latter also accounts for the insensitivity to convection in spite of long transition times.

In order to provide more reproducible and accurate data to characterize this new phenomenon and refine the model, a new all-metal cell was designed and constructed as illustrated in Fig. 6.70. A new beryllium electrode assembly designed to provide a better-defined electrode area is illustrated in Fig. 6.71. New chronopotentiometric measurements were carried out in 90 mole % BeF_2–10 mole % LiF, where reliable activity coefficient data are available,[4] in order to test the apparatus. Although curvature of the chronopotentiograms at long times leads to difficulties in the usual graphical methods of estimating transition times, the new results demonstrated the reproducibility of the emf-time curves. An analysis of the emf-time curves to provide diffusion coefficients was initiated.

1. Work performed in the Reactor Chemistry Division.
2. H. R. Bronstein, J. Truitt, and J. Braunstein, *Reactor Chem. Div. Annu. Progr. Rep. May 31, 1972*, ORNL-4801, p. 5.
3. J. Braunstein, H. R. Bronstein, and J. Truitt, *J. Electroanal. Chem. Interfacial Electrochem.* 44, 463 (1973).
4. B. F. Hitch and C. F. Baes, Jr., *Inorg. Chem.* 8, 201 (1969).

IRREVERSIBLE THERMODYNAMICS OF ELECTROMIGRATIONAL DEPLETION CHRONOPOTENTIOMETRY[1]

C. E. Vallet[2] J. Braunstein

Previous work[3] has demonstrated the existence of chronopotentiometric transitions based on depletion of electrically mobile (but electrochemically inactive) constituents by migration (ED) in molten mixtures of BeF_2 with NaF or LiF. Prediction of this effect[3] in alkali chloroaluminate melts has been confirmed experimentally.[4] This electrochemical method is of potential value also for studies of mass transport in certain membranes and in some molten, crystalline, and vitreous electrolytes, including silicates. Since the equations employed in the previous zeroth-order evaluation of diffusion coefficients[3] were derived heuristically, a more rigorous analysis based on the thermodynamics of irreversible processes (TIP) has been initiated. A schematic representation of the processes occurring at the electrode and the melt is given in Fig. 6.72.

The proper flows for symmetric formulation of the TIP phenomenological equations for a binary system LF-BF (representing, e.g., LiF and $BeF_2/2$) may be derived from the dissipation function, Φ, in terms of the flows, J_i, of the ionic constituents L, B, and F. The conjugate forces, X_i, are the gradients of electrochemical potential $[\nabla\tilde{\mu}_i = \nabla(\mu_i + \mathbf{F}e_iZ_i\psi)]$; Z_ie_i is the signed charge of the constituent, and μ_i and ψ are the individually indeterminate chemical and electrical potentials:

$$\Phi = \sum_i J_iX_i = J_L\ \nabla\tilde{\mu}_L + J_B\ \nabla\tilde{\mu}_B + J_F\ \nabla\tilde{\mu}_F\ . \qquad (1)$$

In order to simplify the equations, the flows (J_i), concentrations (c_i), chemical potentials (μ_{ij}), and electrochemical potentials ($\tilde{\mu}_i$) refer to equivalents rather than moles. Noting that the sum of the flows is the current density,

$$J_L + J_B - J_F = I/\mathbf{F}\ , \qquad (2)$$

that the ionic electrochemical potentials may be combined to give the chemical potentials (per equivalent) of the neutral components,

$$\mu_{LF} = \tilde{\mu}_L + \tilde{\mu}_F;\ \ \mu_{BF} = \tilde{\mu}_B + \tilde{\mu}_F\ , \qquad (3)$$

ORNL-DWG. 74-314

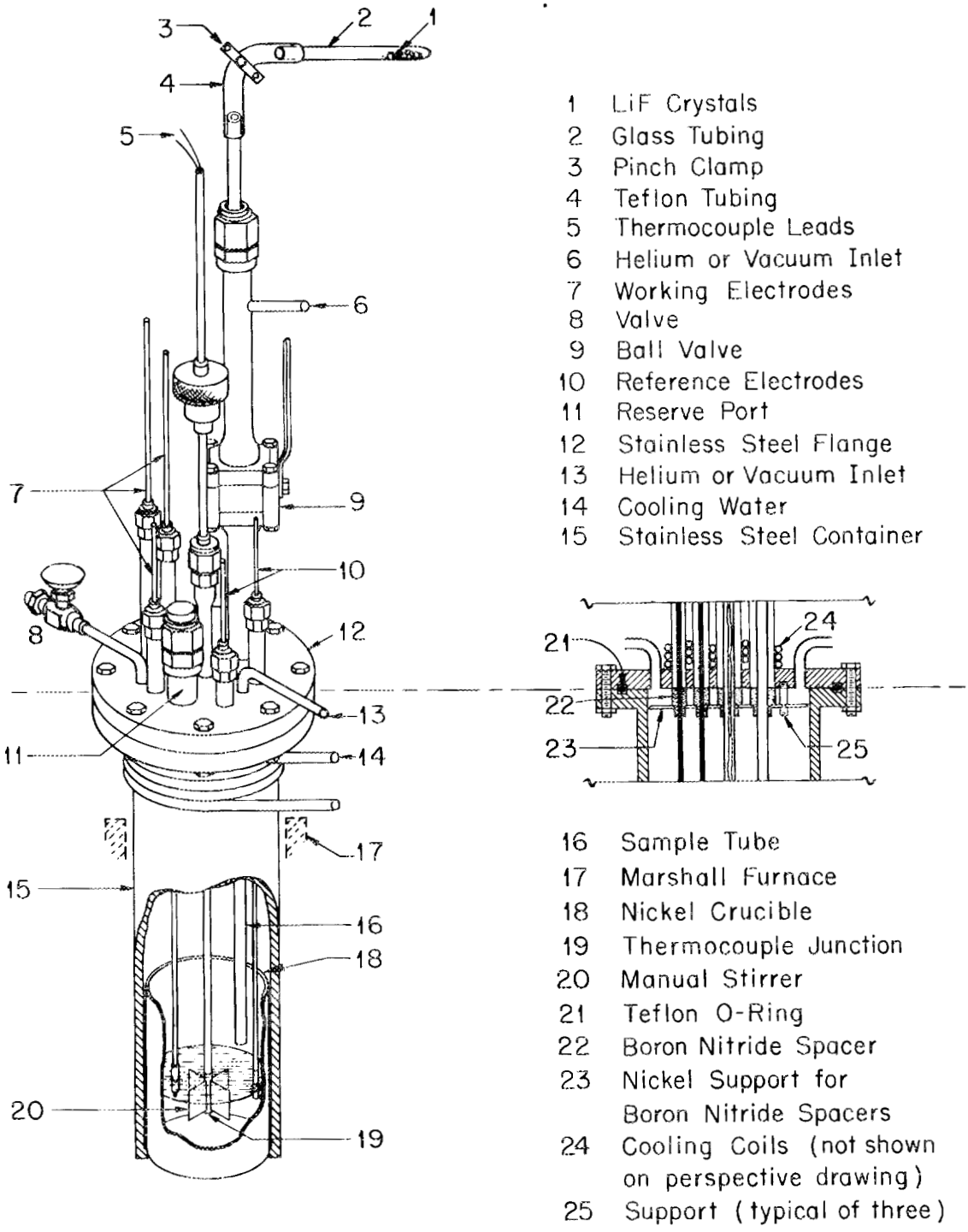

Fig. 6.70. All-metal cell and container assembly for chronopotentiometry in $LiF\text{-}BeF_2$.

ORNL-DWG. 73-8269

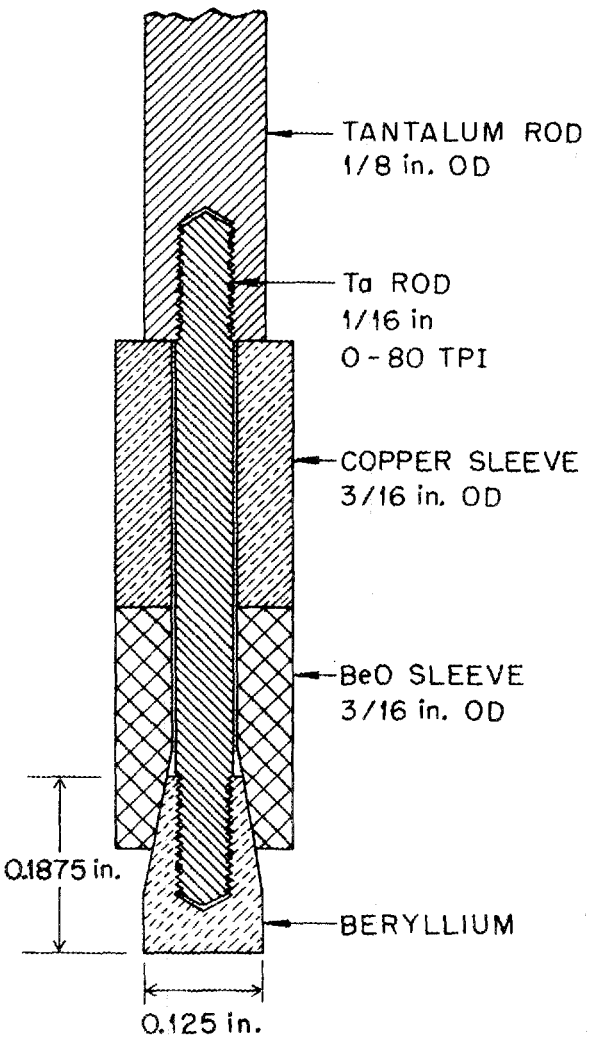

Fig. 6.71. Beryllium working electrode for chronopotentiometry of beryllium fluoride–alkali fluoride mixtures.

and applying the Gibbs-Duhem equation, the dissipation function, with ionic flows all referred to any common reference frame, becomes

$$\Phi = [J_B - (c_B/c_L)J_L - I/F]\ \nabla\mu_{BF} + (I/F)\nabla\tilde{\mu}_B\ . \quad (4)$$

The appropriate phenomenological equations, incorporating the Onsager reciprocal relation, thus are

$$-[J_B{}^F - (c_B/c_L)J_L{}^F - I/F] = D\ \nabla\mu_{BF} + L\ \nabla\tilde{\mu}_B\ , \quad (5a)$$

$$-I/F = L\ \nabla\mu_{BF} + K\ \nabla\tilde{\mu}_B\ , \quad (5b)$$

with flows now referred to fluoride ion constituent. Eliminating the gradient of electrochemical potential,

$$(1 + c_B/c_L)J_L{}^F = (D - L^2/K)\ \nabla\mu_{BF} - (L/K)I/F\ . \quad (6)$$

The phenomenological coefficients may be related to conventional transport coefficients by comparison of the above equations with Ohm's law, Fick's first law, and the definition of the Hittorf transference number, leading to the one-dimensional flux equation

$$J_L{}^F = -D\frac{\bar{V}_F}{\bar{V}_B}\frac{\partial c_L}{\partial x} + t_L{}^F I/F$$
$$= -D\frac{\partial c_L}{\partial \xi} + t_L{}^F I/F\ , \quad (7)$$

where D is the Fick's law mutual (or inter-) diffusion coefficient of the binary mixture,

$$D = -\frac{J_L{}^V}{\nabla c_L}\bigg|_{I=0}\ , \quad (8)$$

and ξ is a distance variable such that equal increments of ξ contain equal numbers of F, $d\xi = (\bar{V}_B/\bar{V}_F)\ dx$, $\bar{V}_B$ represents the partial equivalent volume of BeF_2, and $\bar{V}_F$ the equivalent volume of the mixture; $t_L{}^F$ is the fraction of the current carried by the ion constituent L (e.g., Li^+).

The emf of the concentration cell[5]

$$\underset{\mathrm{I}}{\mathrm{Be\,|\,LF\text{-}BF}}\ \vdots\ \underset{\mathrm{II}}{\mathrm{LF\text{-}BF\,|\,Be}}$$

resulting from electrolysis of an initially uniform electrolyte between beryllium electrodes follows from integration of Eq. (5*b*) from one electrode through the electrolyte into the other electrode:

$$\frac{2FE}{RT} = \frac{2F}{RT}[IR] + \overline{t_L{}^F}\ \ln\left(\frac{y(1-y_0)^2}{y_0(1-y)^2}\right) + \int_{y_0}^{y}\overline{t_L{}^F}\left(\frac{1+y}{1-y}\right)\frac{d\ln\gamma_{BeF_2}}{dy}\,dy\ , \quad (9)$$

where y is the BeF_2 mole fraction, γ_{BeF_2} is the activity coefficient, and $\overline{t_L{}^F}$ is a mean transference number.

In this first-order treatment, three simplifying assumptions are made that must subsequently be relaxed:

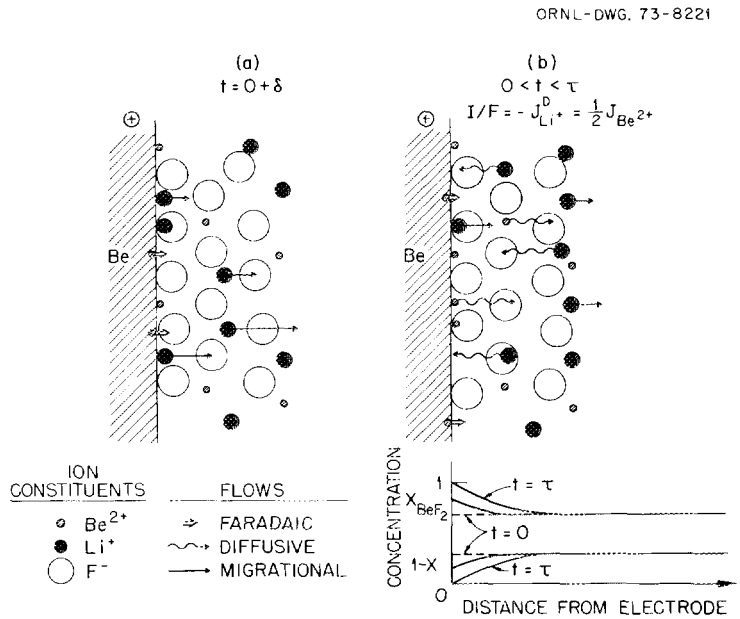

Fig. 6.72. Schematic representation of Faradaic, diffusive, and migrational flows in anodic ED chronopotentiometry of beryllium in BeF_2-LiF mixtures. (*a*) Initiation of electrolysis; (*b*) during electrolysis at times short relative to the transition time (τ). Ion constituents: ⊘ Be^{2+}; ● Li^+; ○ F^-.

(1) the *IR* drop during the course of the chronopotentiogram is assumed constant. (Experimental evidence from rapidly repeated and current-reversal chronopotentiograms suggests this to be at least restrictive of the three assumptions.) (2) The transference number of L (Li^+), which has been demonstrated to be unity between 20 and 70 mole % BeF_2,[5] is assumed to remain unity at compositions up to nearly pure BeF_2. (This is being tested experimentally. The slightly less severe restriction that $t_L{}^F$ is constant in the composition range of the chronopotentiogram also leads to more tractable equations.) (3) The diffusion coefficient is assumed independent of composition. This is clearly the most severe restriction, but the calculated diffusion coefficient may be treated as a mean value to serve as a starting point for evaluating the composition dependence.

If the transference number $t_L{}^F$ is independent of composition, differentiation of Eq. (7) with respect to the distance variable leads to Fick's second law:

$$\frac{\partial J_L{}^F}{\partial \xi} = \frac{\partial c_L}{\partial t} = \frac{\partial}{\partial \xi} D \frac{\partial c_L}{\partial \xi} . \tag{10}$$

Since the flux $J_L{}^F$ must vanish at the electrode surface, Eq. (7) provides one of the boundary conditions:

$$I = \frac{FD}{t_L{}^F} \frac{\partial c_L}{\partial \xi} \bigg|_{x=0} . \tag{11}$$

Applying assumption (3) to Eq. (10), Fick's second law with its two boundary conditions and initial condition are mathematically equivalent to those of ordinary chronopotentiometry,[6] with the concentration of L at the electrode surface given as a function of time by the Sand equation:

$$c_L = c_L{}^0 - \frac{2}{\sqrt{\pi}} \frac{I}{F\sqrt{D/t_L{}^F}} \sqrt{t} . \tag{12}$$

The composition at the electrode surface can be calculated by successive approximations[7] from the electromotive force along a chronopotentiogram[3] with assumption (1) and a knowledge of the activity coefficients.

Figure 6.73 demonstrates the observed time dependence of c_L in typical chronopotentiograms at two different current densities. The first-order equations are in general accord with the observed results, which show approximate linearity in the square root of time and transition times essentially independent of the current density, confirming the qualitative correctness of the

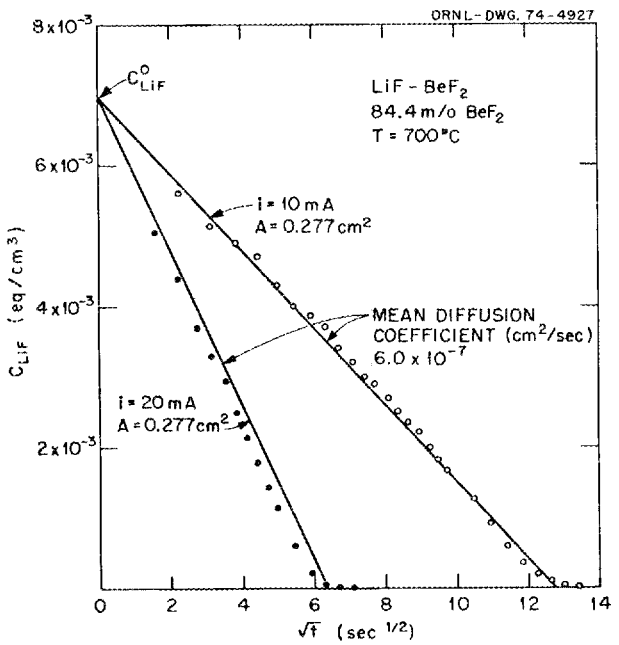

Fig. 6.73. LiF concentration at electrode surface as a function of time. Melt composition, 84.4 mole % BeF_2; temperature, 700°C.

model. It is clear, however, from the slightly sigmoid shape of the data and the upward curvature of the concentation at long times, that refinement of the mathematical treatment, guided by experimental results on the form of the composition dependence of the diffusion coefficient, is needed.

1. Work performed in part in the Reactor Chemistry Division.
2. Visiting scientist, Laboratoire de Thermodynamique, Associé au C.N.R.S., Université de Provence, Marseille, France.
3. J. Braunstein, H. R. Bronstein, and J. Truitt, *J. Electroanal. Chem. Interfacial Electrochem.* **44**, 463 (1973).
4. B. Gilbert, D. L. Brotherton, and G. Mamantov, *J. Electrochem. Soc.*, in press.
5. K. A. Romberger and J. Braunstein, *Inorg. Chem.* **9**, 1273 (1970); D. D. Sood and J. Braunstein, *J. Electrochem. Soc.* **121**, 247 (1974).
6. P. Delahay, *New Instrumental Methods in Electrochemistry*, Interscience, New York, 1954, p. 179.
7. C. E. Vallet, H. R. Bronstein, and J. Braunstein, *J. Electrochem. Soc.*, in press.

ELECTROCHEMICAL STUDY OF MASS TRANSPORT IN MOLTEN LiF-BeF_2 MIXTURES

C. E. Vallet[1] J. Braunstein

New electromigrational depletion chronopotentiometric measurements have been carried out in molten

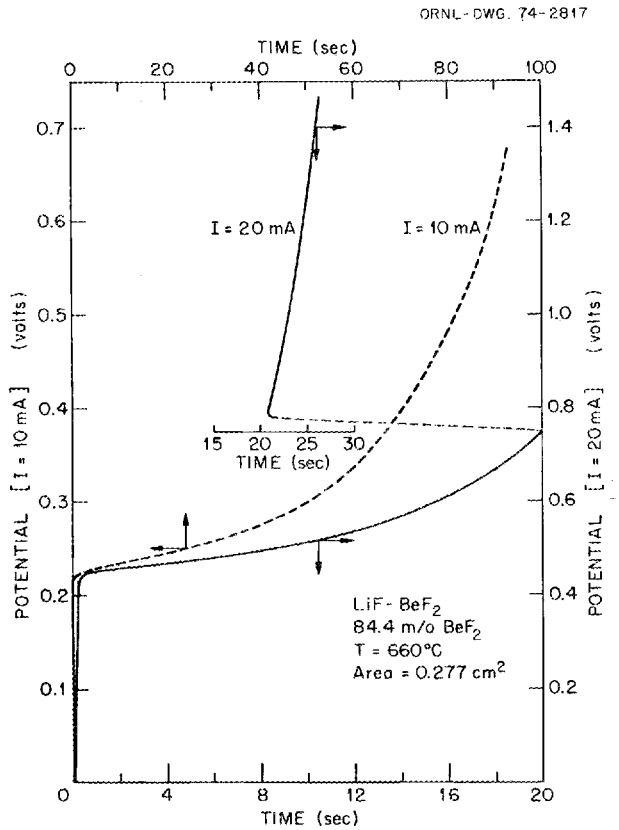

Fig. 6.74. Typical ED chronopotentiograms in molten LiF-BeF_2 at two different current densities.

mixtures containing 78, 84, and 95 mole % BeF_2 at five temperatures between 564° and 704°C, and analyzed in terms of the equations presented in the preceding contribution.[2] The apparatus described previously[3] was employed, and recorder traces of two chronopotentiograms are shown in Fig. 6.74. These emf-time curves, typical of those at other compositions and temperatures, illustrate the proportionality of the initial *IR* drop to the current density and the need to analyze the entire emf-time curve rather than attempt to determine a transition time by the usual graphical method.

The diffusion equations derived in the preceding contribution[2] were first solved with the assumption of a composition-independent diffusion coefficient, thus yielding mean values. The method of calculation[4] of the mean diffusion coefficients from the emf-time data of a chronopotentiogram is summarized in Fig. 6.75.

The calculated mean diffusion coefficients obtained from measurements in the 95 mole % BeF_2 mixtures are shown in Fig. 6.76 as a function of temperature and calculated LiF concentration at the electrode surface.

emf (e), time (t)
read from experimental recordings

$$\frac{2FE}{RT} = \frac{2F}{RT}[IR] + \overline{t_L{}^F} \ln\left(\frac{y(1-y_0)^2}{y_0(1-y)^2}\right) + \overline{t_L{}^F} \int_{y_0}^{y} \frac{1+y}{1-y} \frac{d \ln \gamma_{BeF_2}}{dy} dy$$

y = mole fraction of BeF_2; $\overline{t_L{}^F}$, transference number of $Li^+ = 1$; γ_{BeF_2}, activity coefficient [B. F. Hitch and C. F. Baes, Jr., *Inorg. Chem.* 8, 201 (1969)].

y, time

successive approximations

$$C_{LF} = (1-y)/[\overline{V}_{LF} + (\overline{V}_{BF} - \overline{V}_{LF})y]$$

C_{LF}: LiF concentration in equiv/cm^3; $\overline{V}$: partial equivalent volumes of LiF, $\frac{1}{2}BeF_2$.

C_{LF}, time

Sand equation

$\overline{D}$, mean diffusion coefficient over the concentration range between the bulk composition and the concentration at the electrode surface at time t.

Fig. 6.75. Method of calculation of mean diffusion coefficients.

At each temperature except 602°C, chronopotentiograms were run with at least two different current densities. The points at 660°C are from seven chronopotentiograms obtained at four different current densities; this illustrates the reproducibility of the results and is analogous to constancy of the product of the transition time and the square of the current density in ordinary chronopotentiometry. We initially focused on the nearly constant values of $\overline{D}$ obtained from the early part of the chronopotentiograms, but beyond the initial uncertainty of emf, in order to obtain values corresponding to melt composition as near 95 mole % BeF_2 as possible. Because of uncertainties in the composition dependence and weighting, this seemed more appropriate than a least-squares fit or extrapolation. These values of $\overline{D}$ are determined largely by the region of the chronopotentiogram near but generally before the inflection.

The diffusivity is expected to fall with increasing BeF_2 content in qualitatively the same manner as the electrical conductance and the fluidity. Hence the relatively small variation of $\overline{D}$ along the chronopotentiogram, with an increase indicated toward pure BeF_2, was not at first expected. It may reflect a value of $\overline{t_L{}^F}$ decreasing faster than the decrease of D, since $\overline{D} = \overline{D}/\overline{t_L{}^F}$, and indicates the need for transference number measurements at higher BeF_2 contents, which are in progress. Similar results were obtained from the meas-

ORNL-DWG. 74-812A

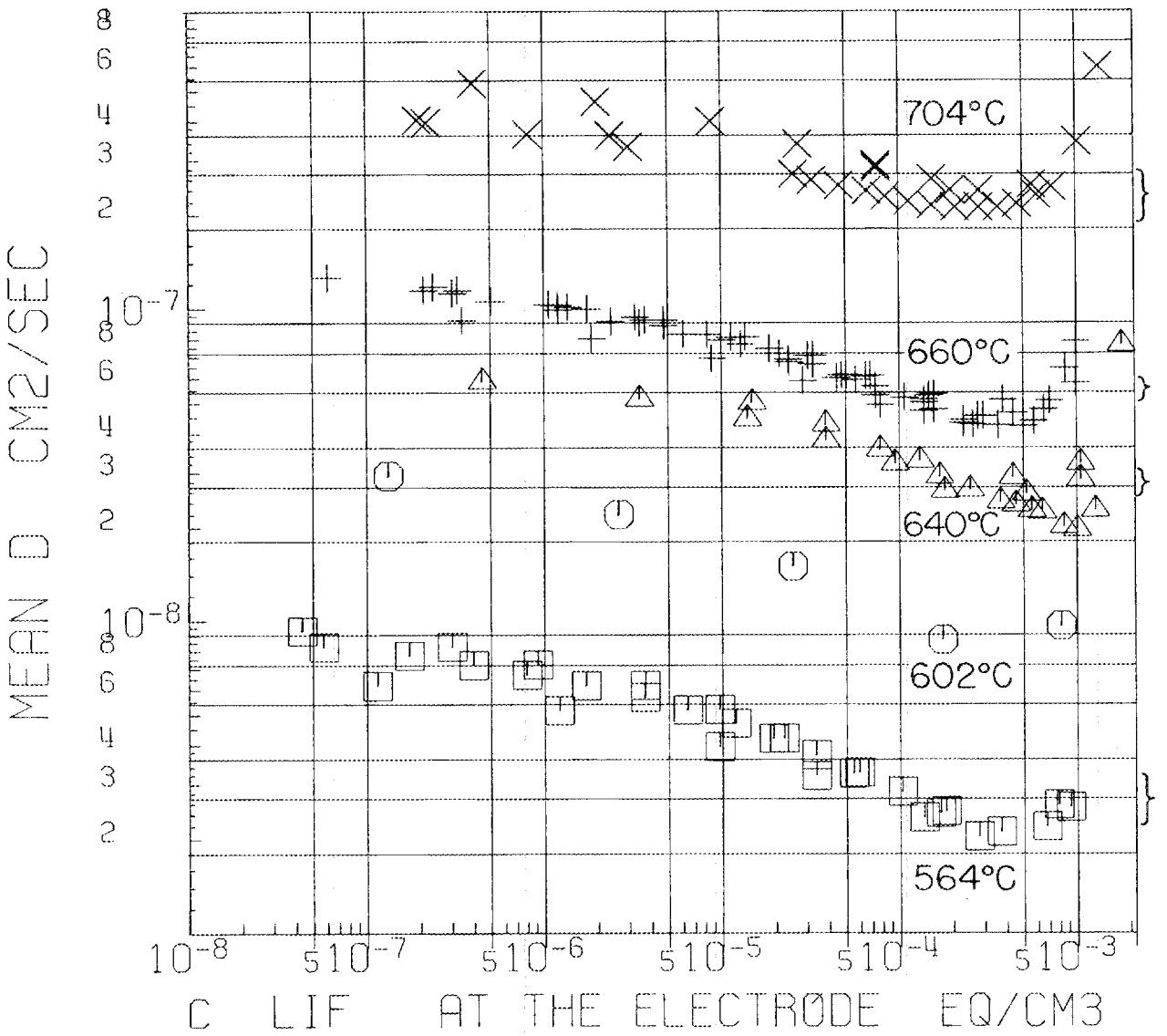

Fig. 6.76. Mean diffusion coefficients at different temperatures in molten LiF–95 mole % BeF_2 as a function of LiF concentration at the electrode surface.

urements in melts of bulk composition 84 and 78 mole % BeF_2, although the values of $\bar{D}$ were, as expected from the viscosity and conductance, higher than for the 95 mole % melt. Values of $\bar{D}$ as a function of bulk composition and temperature are summarized in Table 6.17. The temperature dependence of the results at 95% indicates a mean activation energy for diffusion of 50.5 (±~0.5) kcal/mole for compositions between 95 and 99 mole % BeF_2. Cantor et al.[5] report activation energies for viscous flow of 40 kcal/mole for 95 mole % BeF_2, 52 kcal/mole for 99 mole % BeF_2, and 59.6 kcal/mole for pure BeF_2. The activation energy for electrical conductance[6] in pure BeF_2 is 44 kcal/mole. A correct solution of the diffusion equations with composition-dependent diffusion coefficients and transference numbers should, of course, give identical dependence of $\bar{D}$ on composition whether calculated from chronopotentiograms of a melt at a single bulk composition or from the initial portions of chronopotentiograms obtained in melts with differing bulk compositions. An attempt was made to estimate $\bar{D}$ as a function of concentration from the mean $\bar{D}$ at 78, 84, and 95%

Table 6.17. Mean values of interdiffusion coefficient, $\bar{D}$, and Arrhenius energy, $\overline{\Delta H}$, in molten LiF-BeF_2, for melts of initial composition y_0

y_0 (mole % BeF_2)	$\bar{D}$ (cm^2/sec) 564°C	570°C	602°C	635°C	640°C	660°C	704°C	$\overline{\Delta H}$ (kcal/mole), 564–704°C
95	3.0×10^{-9}		1.0×10^{-8}		3.0×10^{-8}	6.0×10^{-8}	2.5×10^{-7}	50.5
84.4		3.2×10^{-8}	5.0×10^{-8}			2.8×10^{-7}	6.0×10^{-7}	37.8
77.8		8.0×10^{-8}	1.6×10^{-7}	3.5×10^{-7}		5.2×10^{-7}	1.2×10^{-6}	31.1

Table 6.18. Composition dependence of interdiffusion coefficients D and Arrhenius energy ΔH in molten LiF-BeF_2

Concentration (mole % BeF_2)	D (cm^2/sec) 570°C	660°C	700°C	ΔH (kcal/mole), 570–700°C
98	$\sim 1.0 \times 10^{-9}$	$\sim 1.8 \times 10^{-8}$	$\sim 1.3 \times 10^{-7}$	~58
95	1.0×10^{-8}	1.0×10^{-7}	3.5×10^{-7}	46
90	4.5×10^{-8}	2.4×10^{-7}	6.0×10^{-7}	33
84.4	7.6×10^{-8}	4.0×10^{-7}	7.0×10^{-7}	28.0
80	9.6×10^{-8}	6.0×10^{-7}	1.1×10^{-6}	27.6
77.8	1.3×10^{-7}	7.5×10^{-7}	1.2×10^{-6}	26.5

BeF_2 by the Crank-Park method.[7] In view of the fairly large spacing of the initial compositions, the unweighted mean employed in the Crank-Park method seems unrealistic. Either solution of the diffusion equation or measurements at more closely spaced bulk compositions, which are in progress, will be needed to indicate the proper weighting. It appears not unreasonable to assume that the results close to the initial bulk composition contributed highly to the mean D. In a preliminary test of the applicability of such a method, we therefore incorporated a weighting function proportional to the LiF concentration at the electrode surface. Table 6.18 shows the concentration and temperature dependence of the interdiffusion coefficients obtained thus, and illustrates the general agreement with the mean values over a range of composition listed in Table 6.17. The interdiffusion coefficients fall rapidly between 95 mole % BeF_2 and pure BeF_2. As the composition approaches pure BeF_2, the interdiffusion coefficient approaches the limiting self-diffusion coefficient of the solute ion (here Li). Our data, by extrapolation, lead to lower values than those predicted by molecular dynamics calculations.[8]

The temperature dependence of the initial IR drops for any composition (proportional to the current density for any temperature) leads to Arrhenius energies for conductance that are consistent with available direct measurements[6] in pure BeF_2 and in mixtures of lower BeF_2 content, as shown in Fig. 6.77. This figure also shows, for comparison, the composition dependence of the Arrhenius energies for mutual diffusion (calculated in this work) and for viscous flow.[5]

This study of ED chronopotentiometry was intended to show the possibilities of the method in highly viscous melts where direct measurements of diffusivity and conductance are very difficult. Refinements in the analysis will be possible when the transference numbers of Li^+ relative to fluoride have been determined in melts of high BeF_2 content, in addition to further chronopotentiometry on a wider range of more closely spaced compositions. Diffusivities, like the electrical conductance and viscosity in these melts, and in silicates, show very marked changes as the melt becomes more highly structured.

1. Visiting scientist, Laboratoire de Thermodynamique, Associé au C.N.R.S., Université de Provence, Marseille, France.

2. C. E. Vallet and J. Braunstein, "Irreversible Thermodynamics of Electromigrational Depletion Chronopotentiometry," the preceding contribution, this report.

3. H. R. Bronstein and J. Braunstein, "Anodic Chronopotentiometry of Beryllium Electrodes in Molten Mixtures of Beryllium Fluoride with Alkali Fluorides," a previous contribution in this chapter, this report.

4. C. E. Vallet, H. R. Bronstein, and J. Braunstein, *J. Electrochem. Soc.*, in press.

5. S. Cantor, W. T. Ward, and C. T. Moynihan, *J. Chem. Phys.* **50**, 2874 (1969).

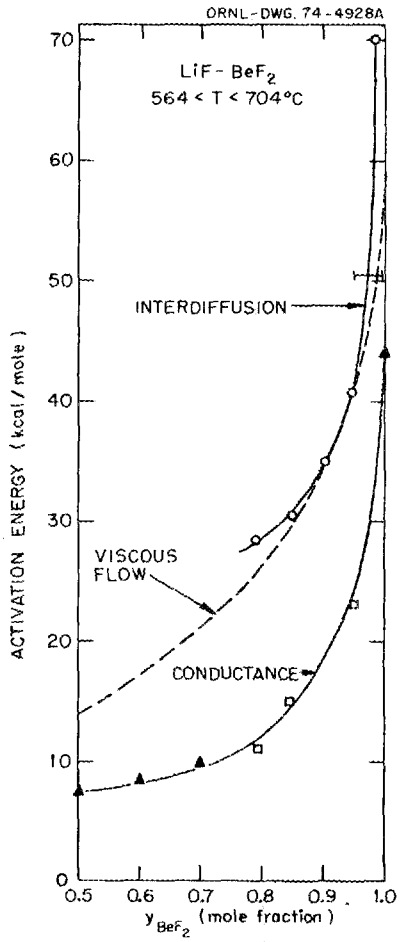

Fig. 6.77. Concentration dependence of activation energies. ○, interdiffusion, calculated from Crank-Park method with weighted mean assumption; |—|, activation energy calculated from mean interdiffusion coefficient in melt of bulk composition 95 mole % BeF_2; □, conductance (this work); ▲, conductance (ref. 6); ——, viscous flow (ref. 5).

6. G. D. Robbins and J. Braunstein, *MSR Program Semiannu. Progr. Rep. Feb. 28, 1969,* ORNL-4396, p. 184; G. D. Robbins and J. Braunstein, *MSR Program Semiannu. Progr. Rep. Feb. 28, 1970,* ORNL-4548, p. 156.

7. J. Crank and G. S. Park, *Trans. Faraday Soc.* **45,** 240 (1949).

8. H. A. Levy, A. H. Narten, and A. Rahman, *Chem. Div. Annu. Progr. Rep. May 20, 1973,* ORNL-4891, p. 120.

APPLICATION OF THE QUASI-LATTICE MODEL IN DILUTE RECIPROCAL MOLTEN SALT MIXTURES. THE SYSTEM SILVER SULFATE–POTASSIUM NITRATE[1]

C. E. Vallet[2] J. Braunstein

Association equilibria in dilute reciprocal molten salt mixtures (i.e., dilute solutions of at least one foreign cation and one foreign anion in a molten salt solvent) provide valuable tests of physical models such as the quasi-lattice model of molten salts.[3] The system silver sulfate–potassium nitrate remains of particular interest for a number of reasons, despite previous investigations by means of emf measurements[4,5] and phase diagrams.[6] First, it is one of few systems in which a temperature dependence of the association energy has been reported,[4] and this temperature dependence has been questioned in a more recent emf study.[5] Second, systems of mixed charge type offer problems connected with the Temkin activities of charged and neutral species associated with counting of sites on the quasi lattice.[7] Third, the phase-diagram investigation[6] (which provided confirmation of the applicability of conformal ionic solution theory[8] in the concentrated solution region of Ag_2SO_4 in molten KNO_3) indicated that in the dilute solution region, where a quasi-lattice correction term becomes important, the results appeared to be more consistent with a temperature-dependent association energy. Finally, the previous investigations were carried out over only a limited range of silver concentrations, making it impossible to analyze the data for higher-order associations than pairwise:

$$Ag^+ + SO_4^{2-} \rightleftharpoons AgSO_4^-; \qquad K_1 \qquad (\Delta A_1)$$

Here we report association equilibria and energies obtained from new emf measurements of the concentration cell

$$Ag \left| \begin{array}{c|c} AgNO_3 & AgNO_3 \\ KNO_3 & KNO_3 \\ & K_2SO_4 \end{array} \right| Ag$$

The silver concentrations were varied over a wide range (mole ratio 2×10^{-4} to 10^{-2}) in order to permit evaluation of K_{12} and the second association energy for the association of silver and sulfate:

$$AgSO_4^- + Ag^+ \rightleftharpoons Ag_2SO_4; \qquad K_{12} \qquad (\Delta A_{12})$$

Measurements were carried out in a series of silver concentrations at two temperatures, 622° and 663°K. Furthermore, a new technique was developed to resolve definitively the questioned temperature dependence of the association energy ΔA_1. In some of the experiments a cell with a given silver concentration was cycled in temperature before and after several sulfate additions, the difference of values of the emf's providing a more direct measure of the temperature dependence of ΔA_1.

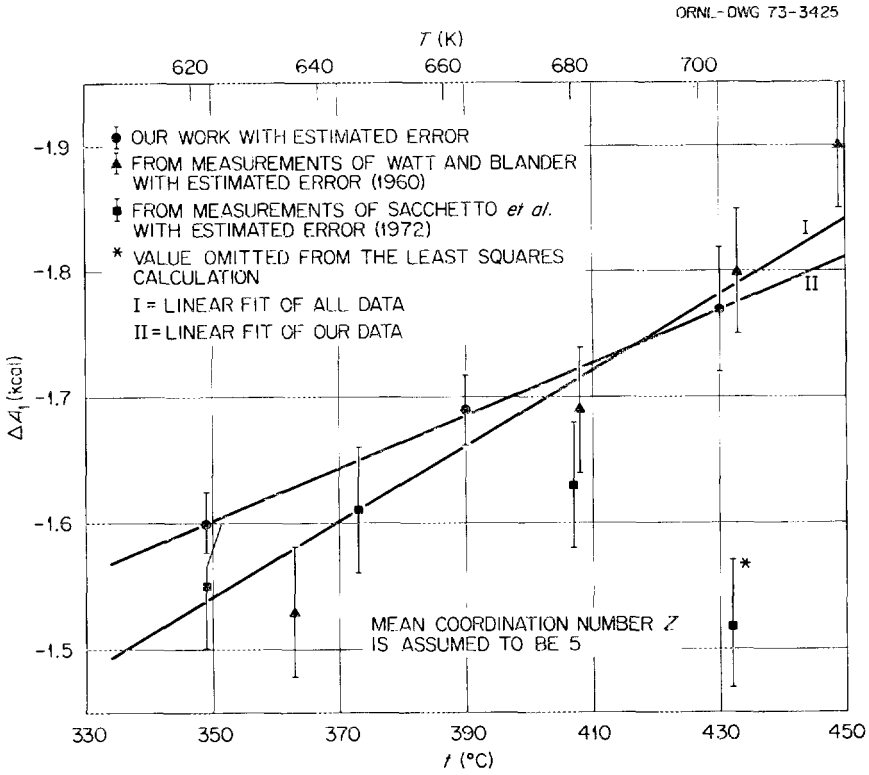

Fig. 6.78. Temperature dependence of $(Ag\text{-}SO_4)^-$ pair association energy.

This new technique was essential because of the very small emf change observed in this system and the very small magnitude of ΔA_1.

As shown in Fig. 6.78, our results[9] confirm the increased stability of $AgSO_4^-$ pairs with increasing temperature. This dependence is in the same direction as observed for AgCN pairs and for the charge-unsymmetric CdX^+ pairs ($X = Br^-$ or I^-). In the quasilattice calculations, only configurational entropy is taken into account; the variation of ΔA_1 with the temperature, $[-\partial\Delta A_1/\partial T] \sim 2.5 \times 10^{-3}$ kcal/deg, may be interpreted as the "specific entropy of association" characterizing a change in the internal degrees of freedom of the SO_4^{2-} ion. The association energy ΔA_{12} was calculated with the generalized quasi-lattice model, and the results are given in Table 6.19.

Table 6.19. $AgSO_4^-$ and Ag-SO_4-Ag association energies calculated assuming a mean coordination number of 5

T (°K)	ΔA_1 (kcal)	ΔA_{12} (kcal)
622	−1.599 ± 0.022	
663	−1.691 ± 0.026	−1.97 ± 0.29

Although the uncertainty of ΔA_{12} does not permit a determination of whether it too, like ΔA_1, is temperature dependent, it is clear that this second association is significant and may have a higher stability than the first association, as has been reported for AgI.

1. Work performed in the Reactor Chemistry Division.
2. Visiting scientist, Laboratoire de Thermodynamique, Associé au C.N.R.S., Université de Provence, Marseille, France, under a research grant from the Ministere des Affaires Etrangeres Francais (1972–1973).
3. M. Blander, *Molten Salt Chemistry*, M. Blander, ed., Interscience, New York, N.Y., 1964, p. 221; J. Braunstein, *Ionic Interactions*, vol. 1, S. Petrucci, ed., Academic Press, New York, N.Y., 1971, p. 179.
4. W. J. Watt and M. Blander, *J. Phys. Chem.* **64**, 729 (1960).
5. G. A. Sacchetto, C. Macca, and G. G. Bombi, *J. Electroanal. Chem. Interfacial Electrochem.* **36**, 319 (1972).
6. M. L. Saboungi, C. E. Vallet, and Y. Doucet, *J. Phys. Chem.* **77**, 1699 (1973).
7. J. Braunstein, H. Braunstein, R. E. Hagman, and A. S. Minano, *Inorg. Chem.* **12**, 1407 (1973).
8. M. Blander and S. Yosim, *J. Chem. Phys.* **39**, 2610 (1963); M. Blander and L. E. Topol, *Electrochim. Acta* **10**, 1161 (1965).
9. C. E. Vallet and J. Braunstein, *J. Phys. Chem.* **77**, 2672 (1973).

THERMODYNAMICS OF LITHIUM-BISMUTH ALLOYS FROM EMF MEASUREMENTS WITH MOLTEN LiF-BeF_2 MIXTURES[1]

D. D. Sood[2] J. Braunstein

The thermodynamic properties of lithium and its liquid alloys are of importance in the development of molten-salt reactor technology, controlled thermonuclear reactors, and molten-salt batteries. The limiting excess chemical potential of lithium at infinite dilution in bismuth has been reported previously[3-5] but was based on extrapolation into the Henry's law region of lithium in bismuth from measurements at higher lithium concentrations.[1] We have shown that the electromotive force of the cell

$$\mathrm{Be|LiF}(1-x),\mathrm{BeF_2}(x)|\mathrm{Li}(y),\mathrm{Bi}$$

where x is the mole fraction of beryllium fluoride in the molten salt and y is the mole fraction of lithium in the coulometrically generated bismuth electrode, follows the Nernst equation in the alloy concentration. These measurements in the Henry's law region, together with thermodynamic data[6] for pure LiF and pure BeF_2, phase data,[7] and activity coefficient data[8] for LiF-BeF_2 mixtures, thus permitted a needed independent reevaluation of the limiting excess chemical potential of lithium at infinite dilution in bismuth by means of the cycle indicated in Table 6.20. The result was $\mu^E(\mathrm{Li}, \infty\ \mathrm{Bi};\ T = 819°\mathrm{K}) = -16.8$ kcal/mole, confirming the value reported by Foster et al.[3] Measurements with this cell at varying salt composition also demonstrated its applicability to transference number determinations in LiF-BeF_2 mixtures.

1. Abstracted from D. D. Sood and J. Braunstein, *J. Electrochem. Soc.* **121**, 247 (1974). Work performed in the Reactor Chemistry Division.
2. Visiting scientist, Bhabha Atomic Research Centre, Bombay, India.
3. M. S. Foster, S. E. Wood, and C. E. Crouthamel, *Inorg. Chem.* **3**, 1428 (1964).
4. J. J. Egan and R. H. Wiswall, *Nucleonics* **15**, 104 (1957).
5. L. M. Ferris, J. C. Mailen, and F. J. Smith, *J. Inorg. Nucl. Chem.* **33**, 1325 (1971).
6. D. R. Stull, ed., *JANAF Thermochemical Tables,* report PB 168 370 (August 1965).
7. K. A. Romberger, J. Braunstein, and R. E. Thoma, *J. Phys. Chem.* **76**, 1143 (1972).
8. B. F. Hitch and C. F. Baes, *Inorg. Chem.* **8**, 201 (1969).

Table 6.20. Cycle for evaluation of excess chemical potential of lithium in bismuth

Reaction	Contribution, ΔG_i, to the cell free energy change	Description
$\mathrm{Be(c)} + 2\mathrm{LiF(c)} \rightarrow \mathrm{BeF_2(c)} + 2\mathrm{Li}(\ell)$	$\Delta G^\circ_f[\mathrm{BeF_2(c)}] - 2\Delta G^\circ_f[\mathrm{LiF(c)}]$	Exchange[a]
$2\mathrm{Li}(\ell) \rightarrow 2\ \mathrm{Li}(y)[\mathrm{Bi}]$	$2RT \ln y + 2\mu^E(\mathrm{Li})$	Dilution[b]
$2\mathrm{LiF}(x) \rightarrow 2\mathrm{LiF}(x')$	$2RT \ln \left[\left(\frac{1-x'}{1-x}\right)\left(\frac{\gamma'_{\mathrm{BeF_2}}}{\gamma_{\mathrm{LiF}}}\right)\right]$	Concentration[c]
$2\mathrm{LiF}(x') \rightarrow 2\mathrm{LiF(c)}$	$\Delta G = 0$	Crystallization
$\mathrm{BeF_2(c)} \rightarrow \mathrm{BeF_2}(x'')$	$\Delta G = 0$	Dissolution
$\mathrm{BeF_2}(x'') \rightarrow \mathrm{BeF_2}(x)$	$RT \ln \left[\left(\frac{x}{x''}\right)\left(\frac{\gamma_{\mathrm{BeF_2}}}{\gamma''_{\mathrm{BeF_2}}}\right)\right]$	Dilution[c]
$\mathrm{Be(c)} + 2\mathrm{LiF}(1-x) \rightarrow \mathrm{BeF_2}(x) + 2\mathrm{Li}(y)[\mathrm{Bi}]$	$\sum_i \Delta G_i = \Delta G = -2\mathrm{F}E$	Cell reaction[b]

Note: Unprimed x and γ refer to values at the experimental composition; singly primed quantities refer to the liquidus composition at LiF saturation at the same temperature; doubly primed values refer to the liquidus composition at BeF_2 saturation.

[a]D. R. Stull, ed., *JANAF Thermochemical Tables,* report PB 168 370 (August 1965).

[b]This work.

[c]K. A. Romberger, J. Braunstein, and R. E. Thoma, *J. Phys. Chem.* **76**, 1143 (1972); B. F. Hitch and C. F. Baes, *Inorg. Chem.* **8**, 201 (1969).

7. Chemical Physics

Under this heading are collected a set of research programs characterized by their somewhat more atomistic approach to problems than those covered in "Physical Chemistry." These include neutron and x-ray diffraction, infrared and Raman spectroscopy, ESR spectroscopy, electron spectroscopy, and atomic and molecular collisions. This year the work in neutron and x-ray diffraction continues to show the complementarity of these methods in crystal structure studies, and the associated development of theoretical methods have permitted many complex structural determinations to be made with relative ease. An example is the structure of the charge-transfer complexing agent TCNQ which is of great interest in connection with recent studies of highly conductive organic compounds (TTF-TCNQ). Techniques developed for the study of structure in liquids have now been used to determine the structure of amorphous ice. Electron spin resonance studies of liquids during photolysis have been extended to simple peptides and there is now hope that more complex systems may be amenable. In the work on collision dynamics advances have been made in the studies of chemical reactions of electronically excited mercury, and numerous experiments designed to better define the states of energetic ions penetrating solids have been carried out.

NEUTRON AND X-RAY DIFFRACTION

X-RAY AND NEUTRON CRYSTAL-STRUCTURE ANALYSIS OF PHOSPHOTUNGSTIC ACID HEXAHYDRATE, $H_3PW_{12}O_{40}\cdot 6H_2O$

M.-R. Noe-Spirlet[1] G. M. Brown
W. R. Busing H. A. Levy

Knowledge of the atomic configuration of the anion $PW_{12}O_{40}^{3-}$ of phosphotungstic acid is of central importance in relation to the structures of heteropoly acids, since the ion and analogs of it with other atoms replacing either phosphorus or tungsten or both are known to occur in at least 80 crystalline compounds (see review by Evans[2]). We have refined by x-ray and neutron single-crystal diffraction methods the structure of the so-called pentahydrate of phosphotungstic acid,[3] which we now find almost certainly to be the hexahydrate.

The space group is $Pn3m$, and there are two units $H_3PW_{12}O_{40}\cdot 6H_2O$ in the cubic cell with translation $a = b = c = 12.1506(5)$ Å. Refinement of the parameters of Keggin's roughly determined structure[3] (which was based on a few x-ray powder diffraction data) was first carried out using a set of 3373 Mo K_α intensity data (the reflections of one octant of reciprocal space to the limit of 60° in 2θ, representing 528 symmetry-independent reflections). The data were initially corrected for absorption and at an advanced stage of refinement were also corrected for anisotropic extinction.

In the process of refinement by standard least-squares and Fourier methods, the general correctness of the Keggin approximation to the structure of the ion $PW_{12}O_{40}^{3-}$ was confirmed, but the Keggin positions for the water oxygen atoms were found to be incorrect. He placed 6 water oxygen atoms at the positions $\frac{1}{4}, \frac{3}{4}, \frac{3}{4}$; $\frac{3}{4}, \frac{1}{4}, \frac{3}{4}$; etc. (positions $6d$-$\bar{4}2m$; see *International Tables*[4]) and 4 water oxygens at the positions 0, 0, 0; 0, $\frac{1}{2}, \frac{1}{2}$; etc. ($4c$-$\bar{3}m$), whereas we find 24 "half" oxygen atoms occupying the 24 positions $x, \frac{1}{4}, \frac{3}{4}$; $\bar{x}, \frac{1}{4}, \frac{3}{4}$; etc. ($24h$-2). The hydrogen atoms could not be found from the x-ray data, but they were included in the final least-squares cycles in fixed positions corresponding to

a sensible hydrogen bonding scheme and to the known geometry of the water molecule. The final value of the usual discrepancy factor R was 0.059 (including all 528 independent reflections); the final value of the standard deviation of an observation of unit weight, σ_1, was 1.29.

While the x-ray refinement was in progress, a crystal sufficiently large for recording neutron-diffraction data was grown, and subsequently a total of 2975 individual reflections were recorded to the 2θ limit 130° (λ = 1.254 Å), representing 575 symmetry-independent reflections. The data were corrected for absorption and extinction in the same way as the x-ray data had been corrected. Least-squares refinement using the neutron data was started with parameters from the x-ray refinement (including the calculated coordinates of the hydrogen atoms). Refinement proceeded smoothly with only small changes in the atomic coordinates. The results again indicate that the crystal is a hexahydrate. The discrepancy index R is now 0.046, and σ_1 is 2.35 (all independent observations included). These indicators of goodness of fit are not so satisfactory as those usually obtained in neutron refinements in this laboratory. The excursions of density in the final difference map are approximately 9 times their usual magnitude.

Although we know of no precedents in crystal-structure analysis that suggest that our present structure is seriously at fault, we are attempting to discover the cause of the relatively poor agreement, which is most likely a minor fault of the model in the least-squares calculation. Even with the somewhat unsatisfactory fit in the least-squares refinement, the neutron data furnish rather precise hydrogen coordinates, which were not available from the x-ray data, as well as more precise parameters for the oxygen atoms.

The structure of the ion $PW_{12}O_{40}^{3-}$ as determined from the neutron data is shown stereoscopically in Fig. 7.1. The bond lengths P–O and W–O are compared in Table 7.1 with those corresponding to Keggin's parameters for his "pentahydrate" and with the Bradley and Illingworth[5] parameters for the 29-hydrate. The P–O(1) bond length is distinctly shorter than the earlier work indicated; indeed, it is a normal value for a phosphate tetrahedron (cf. lengths from 1.515 to 1.5397 Å for the P–O bonds to oxygen atoms not bearing hydrogen atoms in $CaHPO_4$).[6] The W–O(4) distance is in agreement with a prediction of Evans[2] from his work on the compound $(NH_4)_7Na_2[H_2GaW_{11}O_{40}]\cdot 15H_2O$ rather than with the distance 1.42 Å suggested by Baker.[7]

The hydrogen bonding pattern (Fig. 7.2) in the crystal is remarkable. The 24 half oxygen atoms O(W) of the water molecules are arranged in six square arrays centered on the $6d$-$\bar{4}2m$ sites of the cell. Associated with the 24 half oxygen atoms are 48 half hydrogen

Table 7.1. Bond lengths (Å) in the phosphotungstic anion, $PW_{12}O_{40}^{3-}$

Bond	This work		Keggin	Bradley and Illingworth
	X-ray	Neutron		
P–O(1)	1.526	1.528	1.71	1.71
W–O(1)	2.436	2.437	2.34	2.29
W–O(2)	1.902	1.903	1.85	1.93
W–O(3)	1.908	1.909	2.00	1.97
W–O(4)	1.707	1.705	1.85	1.84

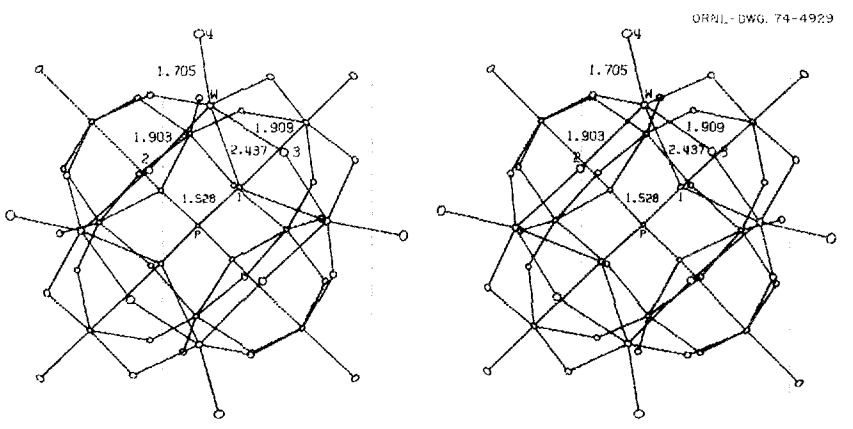

Fig. 7.1. Stereoscopic view of the $PW_{12}O_{40}^{-3}$ anion in the phosphotungstic acid hexahydrate crystal. View direction is along –c; a is along the horizontal from left to right. The symmetry-independent atoms are labeled, the numbers 1 through 4 indicating oxygen atoms O(1) through O(4). The bond lengths (Å) among these atoms are given.

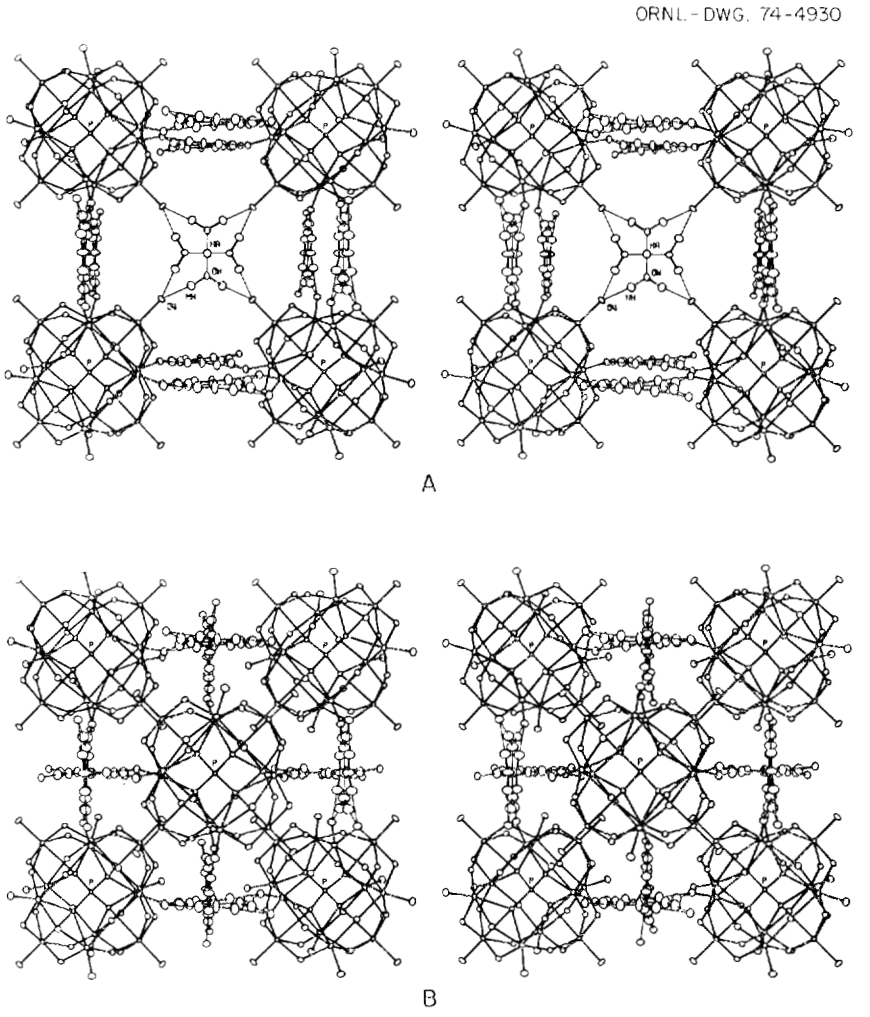

Fig. 7.2. Stereoscopic drawings showing the packing of anions $PW_{12}O_{40}^{-3}$ and dioxonium ions $H_5O_2^+$ in phosphotungstic acid hexahydrate. Orientation is same as in Fig. 7.1. See text for explanation.

atoms H(W) in general positions where they make good hydrogen bonds to 48 atoms O(4) at the unshared corners of the octahedra about the tungsten atoms. At the center of each square of half oxygen atoms is one of the protons H(A) from the ionization of the acid. The occupancy factor 0.5 found for the atoms O(W) and H(W) is the maximum above which there would have to be simultaneous occupancy of the neighboring oxygen sites on the squares which are only 1.665 Å apart. There is just one $H_5O_2^+$ ion at each $6d$-$\bar{4}2m$ site in the crystal; it may be oriented in either of two different ways. The two possible orientations are shown most clearly in the center of Fig. 7.2*a*. In either orientation the ion is hydrogen bonded to the same four atoms O(4).

The structure may be thought of as made up of two different arrangements of anions and disordered $H_5O_2^+$ ions with space-group symmetry $P\bar{4}3m$, the two arrangements having interpenetrating hydrogen bonding systems. A portion of one of the two cubic arrangements is shown in Fig. 7.2*a*. Figure 7.2*b* shows most of what is in Fig. 7.2*a*, plus one anion and four disordered $H_5O_2^+$ units of the second arrangement. The second arrangement may be thought of as derived from the first by inversion through a phosphorus atom followed by translation of the structure by $\frac{1}{2}, \frac{1}{2}, \frac{1}{2}$.

The linear, centered hydrogen bond

O(W)· · ·H(A)· · ·O(W)

of the $H_5O_2^+$ ion is only 2.355 Å long (uncorrected for thermal motion). Since the maximum theoretical correction (certainly a considerable overcorrection) to the bond length is 0.084 Å, this hydrogen bond is among

the shortest ever observed. The valence angle H(W)–O(W)–H(W) of the water molecule is 118.1°, markedly larger than the angle 104.52° in gaseous water[8] and larger than that usually found in crystalline hydrates. This enlarged valence angle and the unusually short O(W)· · ·H(A)· · ·O(W) hydrogen bond may be related to the fact that the whole dioxonium ion $H_5O_2^+$ is approximately planar, with the hydrogen bond direction as the bisector of the valence angle. The angle H(A)· · ·O(W)–H(W) is 120.9°.

The O(W)–H(W) bond length is 0.958 Å, the O(W)· · ·O(4) distance is 2.669 Å, the O(W)· · ·H(W) distance is 1.715 Å, and angle O(W)–H(W)· · ·O(4) is 173.2°. The O(W)–H(W)· · ·O(4) hydrogen bond is therefore a normal, nearly linear hydrogen bond.

1. Graduate student, Department of Chemistry, University of Liège, Belgium.

2. H. T. Evans, Jr., in *Perspectives in Structural Chemistry*, vol. 4, J. D. Dunitz and J. A. Ibers, eds., Wiley, New York, 1971.

3. J. F. Keggin, *Proc. Roy. Soc. London, Ser. A* **144**, 75 (1934).

4. *International Tables for X-Ray Crystallography*, vol. 1, N.F.M. Henry and K. Lonsdale eds., pp. 336–37, Kynoch Press, Birmingham, England, 1952.

5. A. J. Bradley and J. W. Illingworth, *Proc. Roy. Soc. London, Ser. A* **157** (1936).

6. B. Dickens, J. S. Bowen, and W. E. Brown, *Acta Crystallogr. Sect. B* **28**, 797 (1972).

7. L. C. W. Baker, *Advances in the Chemistry of Coordination Compounds*, pp. 604–12, Macmillan, New York, 1961.

8. W. S. Benedict, N. Gailar, and E. K. Plyler, *J. Chem. Phys.* **24**, 1139 (1956).

CRYSTAL STRUCTURE OF THE 1:1 ADDUCT BETWEEN CHLORPROMAZINE AND 7,7,8,8-TETRACYANOQUINODIMETHANE

W. E. Thiessen R. M. Metzger[1]

Interest in the chlorpromazine cation radical ($CP\dot{Z}^+$) springs from speculation[2] that it might be responsible for the psychotropic activity of the tranquilizer chlorpromazine. Ohnishi and McConnell[3] have carried out electron paramagnetic resonance (e.p.r.) studies of $CP\dot{Z}^+$ in flowing DNA solutions and report that "the observed spectra are readily interpreted in terms of Lerman's intercalation model[4] where the helix axis is perpendicular to the aromatic molecular plane of $CP\dot{Z}^+$." The reference to the "aromatic molecular plane" is in analogy to the mutagenic acridine dyes, which do in fact possess planar aromatic ring systems and are thought to intercalate into DNA. In contrast to the acridine systems, the phenothiazine ring system in neutral chlorpromazine is known to have a nonplanar "butterfly" shape.[5]

In order to study the molecular geometry of $CP\dot{Z}^+$, one of us (R.M.M.) prepared crystals of the charge-transfer complex between CPZ and the ubiquitous complexing agent 7,7,8,8-tetracyanoquinodimethane (TCNQ). Acetonitrile solutions of the two components were prepared and mixed in a nitrogen atmosphere to yield a few shiny black needles with a strong exchange-narrowed room-temperature e.p.r. signal ($g \cong 2.00$, line width <1 G). Crystal data and some details of the intensity data collection at Stanford University[6] are given in Table 7.2. It should be particularly noted that there are four crystallographically independent entities, two CPZs and two TCNQs, in the asymmetric unit.

To begin the structure solution at Oak Ridge, the observed structure factors were corrected for overall thermal motion and placed on an absolute scale using program ORESTES[7] to yield a set of normalized structure factors. It was noted immediately that the reflections with even values of index h were strong ($\langle|E|^2\rangle_{k,l} = 1.30$), while those with h odd were weak ($\langle|E|^2\rangle_{k,l} = 0.71$). After the $|E|$s were renormalized as suggested by Hauptman and Karle,[8] the structure solution using Main, Woolfson, and Germain's MULTAN program[9] was straightforward. The original $|E|$ map based on the MULTAN signs for 688 $|E|$s revealed 61 of the 74 nonhydrogen atoms. The rest of these atoms and, eventually, all the hydrogens as well were discovered by Fourier methods. At present, $R(F) = 0.078$ for the 7497 reflections with $|F|^2 > 2\sigma(|F|^2)$.[10]

A stereoscopic drawing of part of the contents of the unit cell viewed nearly along a is displayed in Fig. 7.3. The reason for the disparity in intensity between even-h and odd-h reflections is immediately clear: for each

Table 7.2. Crystal data of the charge-transfer complex between CPZ and TCNQ

56,143 intensity data were collected from a crystal of dimensions 3 × 0.12 × 0.10 mm using monochromated Mo and Cu radiation on a Hilger-Watts FA-128 computer-controlled four-circle diffractometer yielding 11,151 unique data to $(\sin\theta)/\lambda = 0.6337$ Å^{-1}.

a = 13.718(6) Å (needle axis)
b = 19.081(4) Å
c = 19.972(5) Å
$\beta = 90.79(3)°$
Space group $P2_1/c$
$Z = 8$ for $C_{29}H_{23}N_6SCl$
ρ (calc) = 1.329 g/cm^3
ρ (meas) = 1.332 g/cm^3

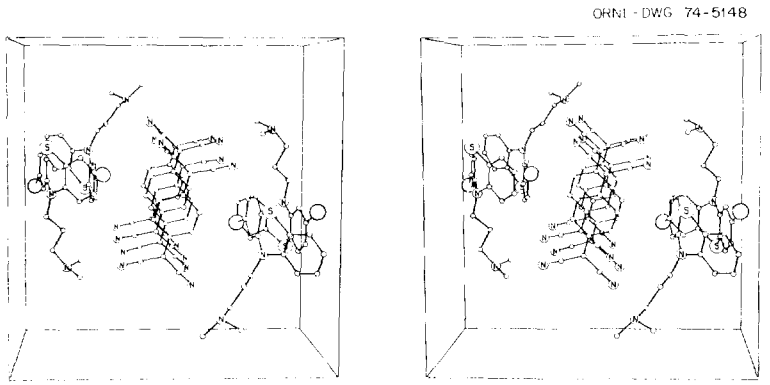

Fig. 7.3. The two independent CPZs, the two independent TCNQs, and their centrosymmetric mates. The outline of the unit cell is given; the view is approximately along **a**.

atom at x, y, z in the stack of TCNQs in the center of the drawing, there is a corresponding atom at approximately $(x + \frac{1}{2})$, y, z. The TCNQs therefore contribute very little to the reflections with h odd.

It is also apparent that the phenothiazine ring system of the CPZs is not planar; the angles between the planes of the benzene rings in the two independent molecules are 143.1 and 147.2°, somewhat larger than the angle of 139.4° in neutral CPZ.[4] That these entities really are cation radicals as indicated by the strong e.p.r. signal is borne out by the fact that the surroundings of the ring nitrogen atom are much less pyramidal than they are in neutral CPZ: the ring nitrogen departs from the plane of the three carbon atoms surrounding it by only 0.123 and 0.125 Å in the two independent cation radicals as opposed to a distance of 0.206 Å in neutral CPZ. This is the expected effect of removing an electron from the phenothiazine π-electron system.

Finally, the details of the TCNQ stacking are of interest. The very highly conducting TCNQ complexes which have attracted so much recent attention also possess stacks of TCNQ radical anions; in *N*-methylphenazinium-TCNQ[11] and 2,2′-bis-1,3-dithiole-TCNQ,[12] for example, there is a single interplanar spacing between the best planes through the TCNQs of 3.26 and 3.17 Å respectively. Because there are two TCNQs per asymmetric unit in CPZ·TCNQ which lie very nearly in parallel planes, there can be (and are) three different interplanar spacings. In this crystal the TCNQs seem to form definite "dimers" with a 3.09-Å spacing; the two neighboring molecules of each dimer are separated from their next nearest neighbors by spacings of 3.31 and 3.41 Å respectively. The 3.09-Å spacing is, as far as we know, the closest yet observed in any TCNQ complex at room temperature and is considerably shorter than the 3.16-Å spacing[13] found in the "dimers" in Rb^+TCNQ^- at −160°.

1. University of Mississippi.
2. L. H. Piette, G. Bulow, and I. Yamazaki, *Biochim. Biophys. Acta* **88**, 120 (1964).
3. S. Ohnishi and H. M. McConnell, *J. Amer. Chem. Soc.* **87**, 2293 (1965).
4. L. S. Lerman, *J. Mol. Biol.* **3**, 18 (1961); *Proc. Nat. Acad. Sci. U.S.* **49**, 94 (1963); *J. Mol. Biol.* **10**, 367 (1964).
5. J. J. H. McDowell, *Acta Crystallogr., Sect. B* **25**, 2175 (1969).
6. The data were collected in the Department of Chemistry, Stanford University. We gratefully acknowledge the guidance and assistance of P. G. Simpson and T. E. Hopkins to R.M.M. during this stage of the work.
7. Program ORESTES by W. E. Thiessen and H. A. Levy estimates overall scale and thermal parameters (isotropic or anisotropic) from single-crystal x-ray or neutron diffraction data, calculates and sorts a set of normalized structure factor magnitudes, and computes relevant statistics of the set. This program is available from the authors on request.
8. H. Hauptman and J. Karle, *Acta Crystallogr.* **12**, 846 (1959).
9. P. Main, M. M. Woolfson, and G. Germain, *MULTAN, a Computer Program for the Automatic Solution of Crystal Structures*, University of York, York, England (1971).
10. Because of the size of the problem, least-square refinement has been carried out by varying the positional and thermal parameters of the TCNQs and of the CPZs on alternate cycles.
11. C. J. Fritchie, Jr., *Acta Crystallogr.* **20**, 892 (1966).
12. T. J. Kistenmacher, T. E. Phillips, and D. O. Cowan, *Acta Crystallogr., Sect. B* **30**, 763 (1974).
13. H. Hoekstra, T. Spoelder, and A. Vos, *Acta Crystallogr., Sect. B* **28**, 14 (1972).

NUMERICAL EXPERIMENTS TO FACILITATE THE DIRECT SOLUTION OF THE CRYSTALLOGRAPHIC PHASE PROBLEM

W. R. Busing W. E. Thiessen

A crystal structure analysis begins with the measurement of reflection intensities and their reduction to normalized structure-factor magnitudes. If approxi-

mately correct phase angles can be assigned to the few hundred strongest reflections, then the structure can be obtained by Fourier synthesis.

Direct methods for phase determination make use of the fact that if the indices of three reflections add to zero, forming what we will call a triplet relationship, then the phase angles of these three reflections will also tend to add to zero. If phase angles are known or assumed for two reflections of a triplet, an estimate of the phase of the third reflection can be deduced. By assigning trial phases to several carefully chosen reflections (the starting set), the phases of the strong reflections can be found, and the corresponding Fourier map can be examined. Often the correct solution can be recognized among the results of the first few trials.

Strictly speaking, the phase of a reflection is given by the average of the phases derived from all the relationships in which it is involved; the phase determined from a single relationship may be grossly in error. Because an error in the early stages of phasing will usually cause the direct method to fail, it is important to use the most reliable relationships first.

In most routine crystallographic work the triplet relationships are of little interest once the correct structure solution is recognized. For the improvement of structure-solving techniques, however, it is desirable to analyze the triplet relationships for known crystal structures so that the effectiveness of different phasing strategies can be compared. We have prepared a computer program, RECAP, to generate these triplet relationships and to make this recapitulation.

Input to RECAP includes either the observed normalized structure factors or the structural information needed to compute them. The true phase angle for each reflection is calculated from the known structure. Using the few hundred reflections stronger than a specified minimum, the program generates the several thousand triplet relationships. For each of these relationships between three reflections the actual sum of the phase angles is readily obtained. Many will be nearly zero, but some will differ considerably from this value.

Program RECAP can also compute for each triplet relationship the Hauptman conditional average D (ref. 1) or the modified average $M(D - KS)$ (ref. 2). Large values of these quantities are theoretically associated with relationships most likely to have zero phase sums. The numbers of relationships in various categories of phase sum and of Hauptman average are tabulated by the program so that this hypothesis can be tested.

Thiessen and Busing have shown[3,4] that the phase sums of certain triplet relationships can be predicted if the orientations of most of the molecules or molecular fragments which make up the crystal are known. For some types of structures, such as those containing parallel benzenoid molecules, an appreciable number of the relationships will have phase sums near π rather than near zero. Program RECAP is also designed to compare the phase sums predicted on this structural basis with the correct values. For this purpose, information on the orientations of the fragments is taken from the output of program ORTRAN, which is described below.[5]

An experimental phase extension program, ORPHEX, has been prepared to compare various strategies for using the triplet relationships to develop the phases of the strong reflections. This program makes use of the Hauptman averages and the predictions based on structural information which are obtained from program RECAP. For known structures, the phases which are produced by ORPHEX are compared with the true phases so that difficulties which may arise can be diagnosed. These programs in their present form can also be used to solve unknown structures, and we hope that from them we will eventually develop a very fast and reliable program package for structure solution.

---

1. H. Hauptman, *Crystal Structure Determination. The Role of the Cosine Seminvariants,* Plenum Press, New York, pp. 159–62.
2. Ibid., pp. 192–97.
3. W. E. Thiessen and W. R. Busing, *Chem. Div. Annu. Progr. Rep. May 20, 1973,* ORNL-4891, p. 102.
4. W. E. Thiessen and W. R. Busing, *Acta Crystallogr.,* submitted for publication.
5. W. E. Thiessen and W. R. Busing, "ORTRAN: A Computer Program for Determining the Orientation of a Known Molecular Fragment in an Unknown Crystal Structure," the following contribution, this report.

ORTRAN: A COMPUTER PROGRAM FOR DETERMINING THE ORIENTATION OF A KNOWN MOLECULAR FRAGMENT IN AN UNKNOWN CRYSTAL STRUCTURE

W. E. Thiessen W. R. Busing

We have previously pointed out[1,2] that if the intensity pattern characteristic of the Fourier transform of a benzene ring can be recognized in the three-dimensional set of diffraction data from a crystal containing two centrosymmetrically related benzenoid molecules per unit cell, it is possible to predict phase-angle sums for triplets of strong reflections whose indices add to zero. Use of these predictions rendered possible the solution of a crystal structure for which standard methods of structure solution had failed.[3] We

now wish to describe a general routine for discovering the orientation or orientations of any known molecular fragment in a unit cell containing any combination of symmetry elements. A similarly general method for utilizing this information in the direct solution of crystal structures will be given in the following contribution.[4]

The computer program ORTRAN accepts as input the indices (h, k, l) and normalized structure-factor magnitudes ($|E|$) of those reflections with the largest $|E|$ values, the parameters and symmetry transformations of the unit cell, and the Cartesian coordinates of the suspected fragment in some standard orientation. The program performs a search for optimal orientations of the fragment using Lattman's[5] rotation angles in the way described by Williams.[6] The limits of the search are established according to the symmetry of the fragment and of the crystal using the methods of Hirshfeld.[7] For each orientation of the fragment, a figure of merit

$$S = \sum_i |E(\mathbf{h}_i)|^2 \, |T(\mathbf{h}_i)|^2$$

is computed,[8] where the summation is over an entire hemisphere of the reflection data and

$$T(\mathbf{h}_i) = \sum_j \exp\,(2\pi i \mathbf{h}_i \cdot \mathbf{x}'_j)$$

is the value of the Fourier transform of the oriented fragment at the reciprocal lattice point $\mathbf{h}_i$. Here $\mathbf{x}'_j$ is the position of an atom in the fragment after rotation.

A specified number of the orientations having the highest figure of merit are subjected to a finer rotational scan and finally refined to maximize S by adjusting the three orientation angles and a single scale factor that is applied to the atomic coordinates of the fragment. The program then produces a printer plot of the locations of the strong reflections in reciprocal space viewed along a specified axis of the oriented fragment. Such a plot for two benzenoid molecules related by an inversion center was displayed in a previous report.[1] As an illustration of a higher symmetry case, one in which there are two distinct but equivalent molecular orientations, a printer plot of reflections with $E \geqslant 1.5$ calculated from the positional parameters[9] for naphthalene, space group $P2_1/c$, with two molecules per unit cell is shown in Fig. 7.4. The view is along the columns corresponding to one of the orientations, and the characteristic benzenoid transform can be seen even though it is overlapped by the columns of the transform corresponding to the other orientation.

Finally, the program produces an output on punched cards or auxiliary storage for use in the phase-determination procedure outlined in the following contribution.[4] This output consists of the indices and normalized structure-factor magnitude for each strong reflection along with the transform values $T(\mathbf{h}_i)$ for each of the symmetry-related orientations of the fragment. These are signed real numbers if the fragment is centrosymmetric or complex quantities if it is noncentrosymmetric.

1. W. E. Thiessen and W. R. Busing, *Chem. Div. Annu. Progr. Rep. May 20, 1973*, ORNL-4891, p. 102.
2. W. E. Thiessen and W. R. Busing, *Acta Crystallogr.*, submitted for publication.
3. W. E. Thiessen and H. A. Levy, *Chem. Div. Annu. Progr. Rep. May 20, 1973*, ORNL-4891, p. 100.
4. W. R. Busing and W. E. Thiessen, "Utilizing Molecular Structure Information in Direct Methods of Crystal Structure Determination via a Modified Tangent Formula," the following contribution, this report.
5. E. E. Lattman, *Acta Crystallogr., Sect. B* **28**, 1065 (1972).
6. D. E. Williams, *Acta Crystallogr., Sect. A* **29**, 408 (1973).
7. F. L. Hirshfeld, *Acta Crystallogr., Sect. A* **24**, 301 (1968).
8. E. E. Lattman and W. E. Love, *Acta Crystallogr., Sect. B* **26**, 1854 (1970).
9. D. W. J. Cruickshank, *Acta Crystallogr.* **10**, 504 (1957).

UTILIZING MOLECULAR STRUCTURE INFORMATION IN DIRECT METHODS OF CRYSTAL STRUCTURE DETERMINATION VIA A MODIFIED TANGENT FORMULA

W. R. Busing W. E. Thiessen

Direct methods for solving the crystallographic phase problem are usually based on the assumption that if the indices of three reflections add to zero, then the sum of their phases will tend to be zero. In a previous report,[1] we showed that for a crystal composed of parallel centrosymmetrically related benzenoid molecules, certain of these triplet relationships can be predicted to have phase sums of π rather than zero. For the relationship $-\mathbf{h}, \mathbf{k}, \mathbf{h}-\mathbf{k}$ (where each vector represents the three indices of a reflection), the predicted phase sum is the phase of the complex product $T(-\mathbf{h})\,T(\mathbf{k})\,T(\mathbf{h}-\mathbf{k})$. Here $T(\mathbf{k})$ is the Fourier transform of a benzene ring in its correct orientation evaluated at the reciprocal lattice point $\mathbf{k}$. Program ORTRAN was originally devised to search the set of intensity data to establish this orientation and to evaluate the transform $T(\mathbf{k})$ for each reflection. We have now generalized this treatment to include crystals of higher symmetry.

In crystals of symmetry other than $P1$ or $P\bar{1}$, a fragment will occur in $n \geqslant 2$ symmetry-related orienta-

ORNL-DWG. 74-5568

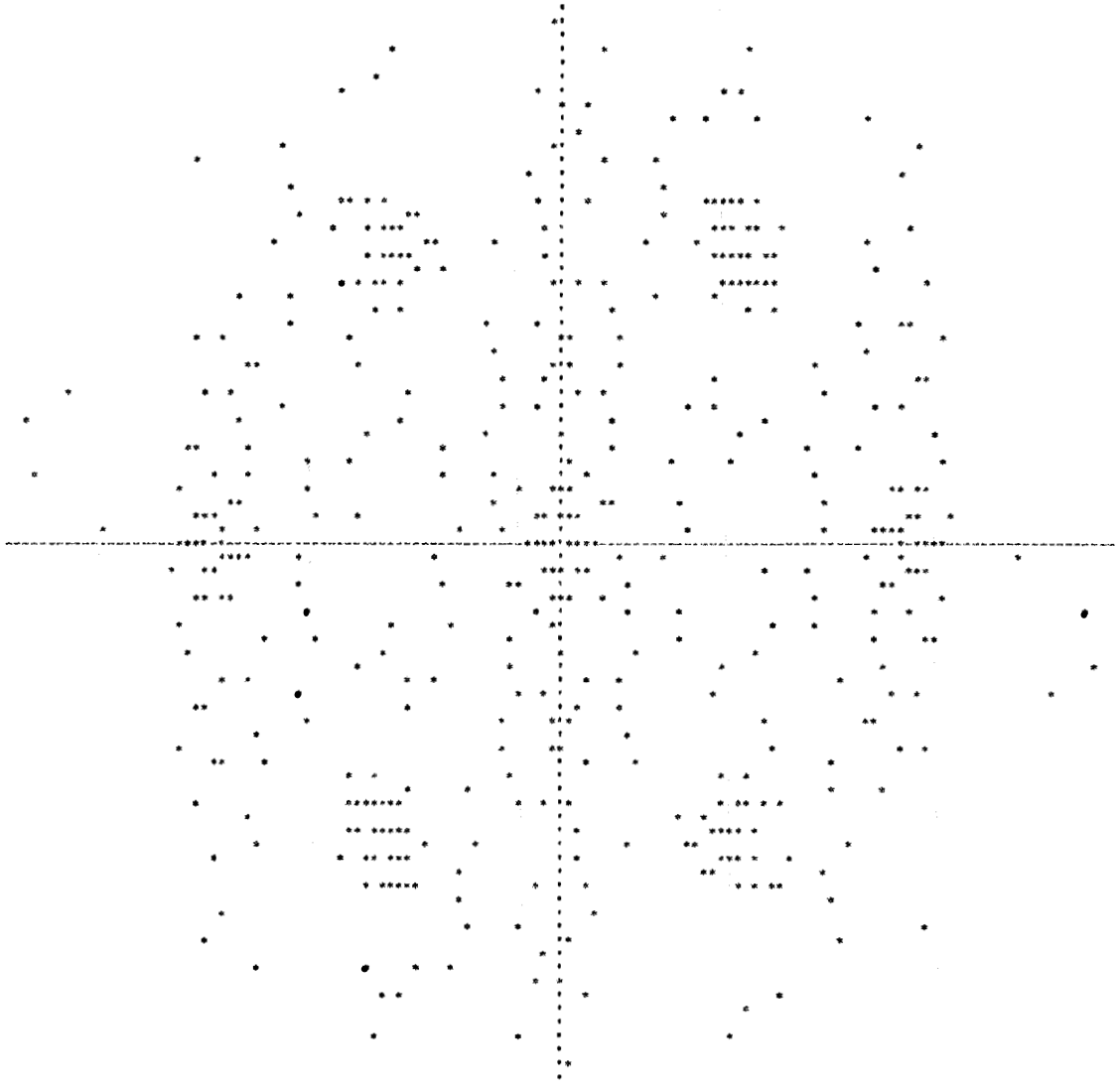

Fig. 7.4. A printer plot produced by program ORTRAN of the Bragg reflections from naphthalene having $|E| \geq 1.5$. The view is down the columns of one of the two overlapping transforms, and the hexagonal pattern typical of benzenoid molecules can be seen. The columns of the other transform, viewed from the side, appear approximately vertical in the figure.

tions. For any reflection **k**, there is a value of the transform $T_i(\mathbf{k})$, $i = 1, 2, \ldots, n$, calculated for each of these n orientations. These n quantities can be evaluated for each reflection by the program ORTRAN.[2]

We have recently shown[3] that, for these higher symmetries, the phase sum for a triplet relationship between three strong reflections is approximated by the phase of the quantity

$$\mathrm{P}(\mathbf{h}, \mathbf{k}) = \sum_{i=1}^{n} T_i(-\mathbf{h})\, T_i(\mathbf{k})\, T_i(\mathbf{h} - \mathbf{k}) .$$

The estimate of the phase of reflection **h** as derived from one triplet relationship is then

$$\phi(\mathbf{h}) = \phi(\mathbf{k}) + \phi(\mathbf{h} - \mathbf{k}) - \phi[\mathrm{P}(\mathbf{h}, \mathbf{k})] .$$

If reflection **h** is involved in several triplet relationships, its phase may be taken as that of the weighted average of complex numbers of unit magnitude, each with a phase calculated from one relationship. The average is expressed by the following modified tangent formula:

$$\tan \phi(\mathbf{h}) = \frac{\langle w(\mathbf{h}, \mathbf{k}) \sin \{\phi(\mathbf{k}) + \phi(\mathbf{h} - \mathbf{k}) - \phi[\mathrm{P}(\mathbf{h}, \mathbf{k})]\}\rangle_{\mathbf{k}}}{\langle w(\mathbf{h}, \mathbf{k}) \cos \{\phi(\mathbf{k}) + \phi(\mathbf{h} - \mathbf{k}) - \phi[\mathrm{P}(\mathbf{h}, \mathbf{k})]\}\rangle_{\mathbf{k}}} ,$$

where $w(\mathbf{h}, \mathbf{k})$ is the weight which reflects the precision with which $\phi[\mathrm{P}(\mathbf{h}, \mathbf{k})]$ represents the phase of each

relationship. We believe that this revised tangent formula will prove to be much more reliable than the tangent formula in current use,[4] which omits the phase of P and uses a different weighting scheme.

1. W. E. Thiessen and W. R. Busing, *Chem. Div. Annu. Progr. Rep. May 20, 1973*, ORNL-4891, p. 102.
2. W. E. Thiessen and W. R. Busing, "ORTRAN: A Computer Program for Determining the Orientation of a Known Molecular Fragment in an Unknown Crystal Structure," the preceding contribution, this report.
3. W. E. Thiessen and W. R. Busing, *Acta Crystallogr.*, submitted for publication.
4. J. Karle and I. L. Karle, *Acta Crystallogr.* **21**, 849 (1966).

CALCULATION OF ELECTROSTATIC CRYSTAL POTENTIALS FOR USE IN THE INTERPRETATION OF ESCA MEASUREMENTS

W. R. Busing

A computer program for calculating crystal lattice energies, which was described previously,[1] has been modified to provide the electrostatic site potentials needed for the interpretation of the results of electron spectroscopy for chemical analysis (ESCA). These ESCA experiments, which are being performed in the Physics Division,[2] have as one of their goals the comparison of the observed binding energy shifts for the nitrogen atom in morphine and morphine derivatives with the results of molecular orbital calculations. Because the samples are crystalline molecular solids, it is necessary to correct the observed electron energy for the electrostatic potential at the site from which it was emitted.[3,4] The program to be described calculates this potential by treating the atoms as point charges with fractional values provided by the molecular orbital computations. For molecular crystals with large unit cells the present program is more efficient and convenient to use than one available previously.[5]

The quantity which is needed is

$$\phi(\mathbf{x}_i) = \sum_{j \neq i} q_j r_{ij}^{-1} ,$$

the electrostatic potential at the site $\mathbf{x}_i$ arising from all other point charges q_j in the crystal. It is well known that this summation converges very slowly unless special procedures are adopted. A method pioneered by Ewald has been extended by Nijboer and DeWette,[6] and using their results we derive the following expression:

$$\phi(\mathbf{x}_i) = \sum_{r_{ij}>0}^{r_{ij}<r_{max}} q_j r_{ij}^{-1} \operatorname{erfc} a + \frac{1}{\pi V} \sum_{|\mathbf{h}|>0}^{|\mathbf{h}|<|\mathbf{h}|_{max}} c(\mathbf{h})|\mathbf{h}|^{-2} [A(\mathbf{h}) \cos 2\pi\mathbf{h}\cdot\mathbf{x}_i + B(\mathbf{h}) \sin 2\pi\mathbf{h}\cdot\mathbf{x}_i] \exp(-b^2) - 2Kq_i , \quad (1)$$

where

$$a^2 = \pi K^2 r_{ij}^2 ,$$
$$b^2 = \pi K^{-2} |\mathbf{h}|^2 .$$

The first term in Eq. (1) is simply a sum over the direct lattice vectors which lie in a sphere of radius r_{max} about point $\mathbf{x}_i$. Convergence of this sum is accelerated by the modification function erfc a, an error-function complement, which decreases from unity to zero as the distance r_{ij} (and thus the argument a) increases.

The amount lost from the direct lattice sum because of the modification function is compensated for exactly by a sum over reciprocal lattice points, which makes up the remainder of Eq. (1). These points are analogous to reflections with indices $\mathbf{h} = \{h, k, l\}$ in x-ray diffraction experiments. The quantities $A(\mathbf{h})$ and $B(\mathbf{h})$ are analogous to the real and imaginary parts of the structure factor, but with the charge q_k replacing the atomic scattering factor in the usual x-ray expressions. For noncentrosymmetric crystals

$$A(\mathbf{h}) = \sum_k^{\text{one cell}} q_k \cos 2\pi\mathbf{h}\cdot\mathbf{x}_k ,$$
$$B(\mathbf{h}) = \sum_k^{\text{one cell}} q_k \sin 2\pi\mathbf{h}\cdot\mathbf{x}_k , \quad (2)$$

or for centrosymmetric crystals

$$A(\mathbf{h}) = 2 \sum_k^{\text{half cell}} q_k \cos 2\pi\mathbf{h}\cdot\mathbf{x}_k ,$$
$$B = 0 . \quad (3)$$

The quantity $|\mathbf{h}|$ is the length of the reciprocal lattice vector, and V is the volume of the direct unit cell. Convergence of this sum is accelerated by the modification function $\exp(-b^2)$, which decreases from unity to zero as $|\mathbf{h}|$ (and therefore the argument b) increases.

Because the term for $-\mathbf{h}$ is the same as that for $\mathbf{h}$, only a hemisphere of the reciprocal lattice need be included. The multiplicity factor $c(\mathbf{h})$ has a value of 2 for all lattice points except those shared by the two hemispheres; for these its value is 1. The last term in Eq. (1) is the contribution to the reciprocal lattice sum for $\mathbf{h} = \mathbf{0}$.

The value of $\phi(\mathbf{x}_i)$ obtained from expression (1) is independent of the quantity K, which is known as the Ewald constant. This constant K does determine what parts of the result will be obtained from the direct and reciprocal lattice sums because it enters into a and b, the arguments of the modification functions. For $K = 0$, only the direct lattice sum contributes, but for larger values the reciprocal lattice sum becomes increasingly important.

Input to the program includes the lattice parameters, the coordinates of the atoms of one asymmetric unit, the symmetry information needed to generate the rest of the structure, and the effective atomic charges derived from molecular orbital calculations. The Ewald constant K and the limits r_{max} and $|\mathbf{h}|_{max}$ are also provided as input. Several values of these limits may be specified, and the program will use each set in succession so that an estimate of the convergence may be made.

Typical calculations with 42 atoms per molecule and four molecules per unit cell require 34 sec of computing time on the IBM 360/91 to obtain the electrostatic potentials at all the atom sites to four significant figures.

1. W. R. Busing, *Chem. Div. Annu. Progr. Rep. May 20, 1971*, ORNL-4706, p. 201.
2. T. A. Carlson, *Phys. Div. Annu. Progr. Rep. Dec. 31, 1973*, ORNL-4937, p. 239.
3. K. Siegbahn et al., *ESCA Applied to Free Molecules*, North-Holland Publishing Co., Amsterdam-London, 1969, p. 107.
4. L. E. Cox, J. J. Jack, and D. M. Hercules, *J. Amer. Chem. Soc.* **94**, 6575 (1972).
5. W. Van Gool and A. G. Piken, *J. Mater. Sci.* **4**, 95 (1969).
6. B. R. A. Nijboer and F. W. DeWette, *Physica* (Utrecht) **23**, 309 (1957).

NEUTRON DIFFRACTION STRUCTURAL STUDIES OF TWO TCNQ-COMPLEX CRYSTALS, A BIFLUORIDE CRYSTAL, AND A NORBORNANONE CRYSTAL

C. K. Johnson H. L. Reed II[1]
R. F. Hall[2]

Neutron crystallographic studies related to three different research projects are described here. The first project concerns the conduction of electricity in organic crystals, particularly those containing 7,7,8,8-tetracyanoquinodimethane (TCNQ). The second project is an investigation of the properties of very short hydrogen bonds, such as the one in the $(F{-}H{-}F)^-$ bifluoride ion, and the third project involves the stereochemical aspects of the 2-bicyclo[2.2.1]heptyl (norbornyl) cation.

One of the best known organic conductors is crystalline tetrathiofulvalene-TCNQ, and extensive research on this material is being done at ORNL and elsewhere. Unfortunately, the available crystals of TTF-TCNQ are much too small for neutron diffraction analysis. However, V. F. Raaen[3] succeeded in preparing large crystals of TCNQ-benzene (**I**) and TCNQ-hexamethylbenzene (**II**), and we analyzed these structures to see if the formation of π-molecular complexes with TCNQ has any pronounced influence on the molecular geometry of the hydrogen atoms in the conjugated hydrocarbons. The bond distances for **I**, as shown in Fig. 7.5, and the fact that the benzene molecule is planar within experimental error show that the induced perturbations of the benzene molecules are probably too small to be detected crystallographically. Because the best planes through the benzene and TCNQ molecules are not quite parallel (dihedral angle of 7°), it is impossible to give a unique interplanar spacing; however, close packing is indicated by the distance of 3.30 Å from the benzene plane to atoms C_2 and C_3 of TCNQ. The molecular packing is shown in Fig. 7.6. Our neutron diffraction analysis of **II** confirms the general features of the previously reported x-ray structure analysis;[4] however, we find that hexamethylbenzene (HMB) is disordered and must be described by two rotational isomers with occupancies of $^2/_3$ and $^1/_3$. The packing of TCNQ with the two different "rotamers" is shown in Figs. 7.7 and 7.8. We have no direct evidence that the disorder is dynamic, but the two HMB sites may be described as related by a 60° rigid-body rotation of HMB about an axis inclined 1.9° from the pseudo $\bar{3}$ molecular axis or by an intramolecular 60° "cogwheel" rotation of all methyl groups. The disorder complication prevents our obtaining high-precision parameters for HMB in **II**. A summary of the averaged distances from **I** and **II** is given in Table 7.3. The corrected distances were obtained by using segmented-body models[5] for thermal motion with added corrections for the large internal molecular motions of the hydrogen atoms.

The crystal structure of tetrathiourea tellurium di(hydrogen difluoride), $Te(Tu)_4(HF_2)_2$ (**III**), is of interest because the proton of the $(F{-}H{-}F)^-$ bifluoride ion is not on a crystallographic symmetry element. All

ORNL-DWG. 73-9268

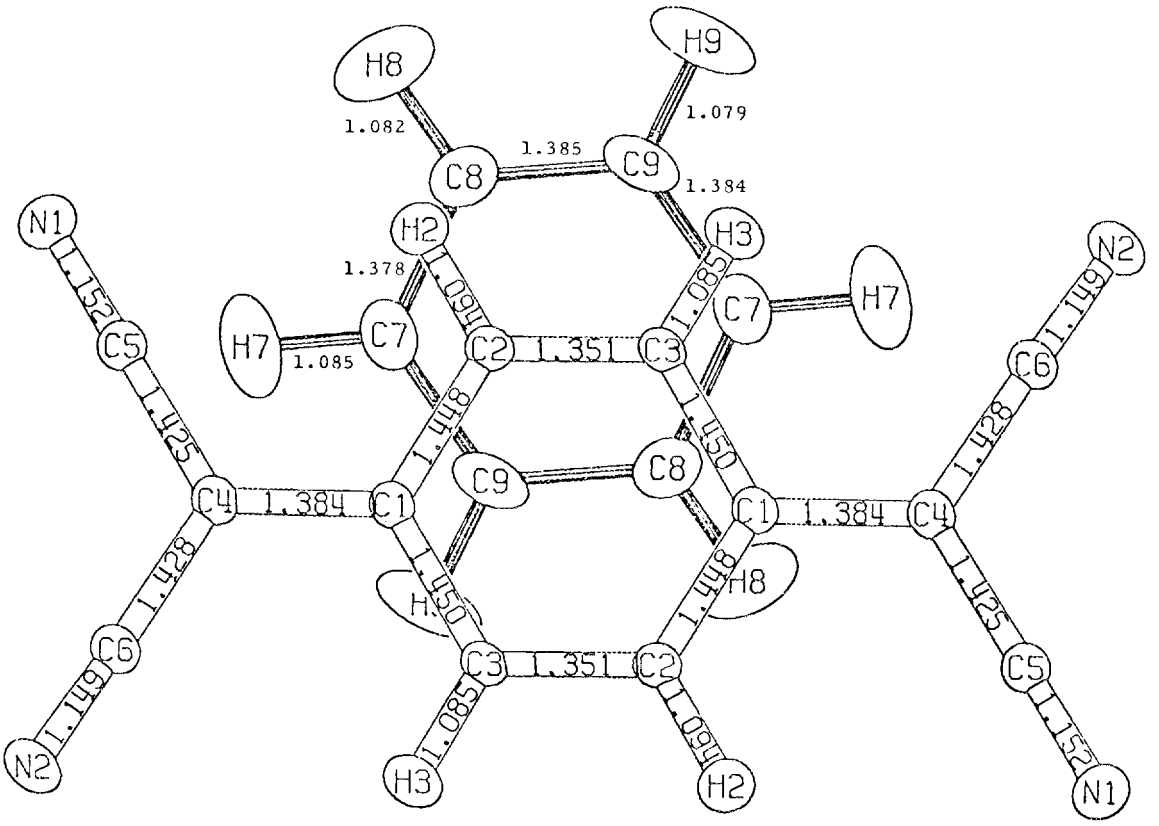

Fig. 7.5. TCNQ-benzene complex projected onto the benzene plane. Both molecules lie on centers of symmetry.

ORNL-DWG. 73-9273

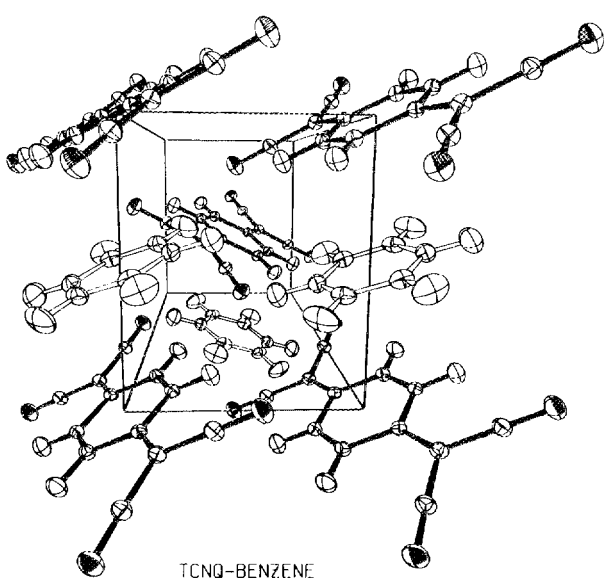

Fig. 7.6. Packing drawing of TCNQ-benzene.

structures reported previously, except one, have crystallographically centrosymmetric bifluoride ions. In the lone exception (*p*-toluidinium bifluoride)[6] the proton is 0.20 Å closer to one fluorine atom than it is to the other in the short 2.27-Å hydrogen bond, and this asymmetry was quite unexpected. Our bifluoride structure, on the other hand, has a nearly centered bifluoride proton, and Fig. 7.9 shows that the two fluorine atoms in **III** have very similar hydrogen-bonding environments, in contrast to the case in *p*-toluidinium bifluoride. This result supports the hypothesis that the potential function in a very short hydrogen bond is strongly dependent on the total hydrogen-bonding environment about the two fluorine atoms. The molecular packing of **III** is shown in Fig. 7.10. The crystals of **III** were grown by Jack Williams of Argonne National Laboratory.

The fourth structure, 5-*exo*-phenyl-5-*endo*-hydroxyl-2-norbornanone (**IV**), shown in Fig. 7.11, was selected for analysis because the [2.2.1]bicycloheptanone skeletal configuration should approximate that of the norbornyl carbocation if the carbocation has a classical structure. Ideally, we would like to have the actual

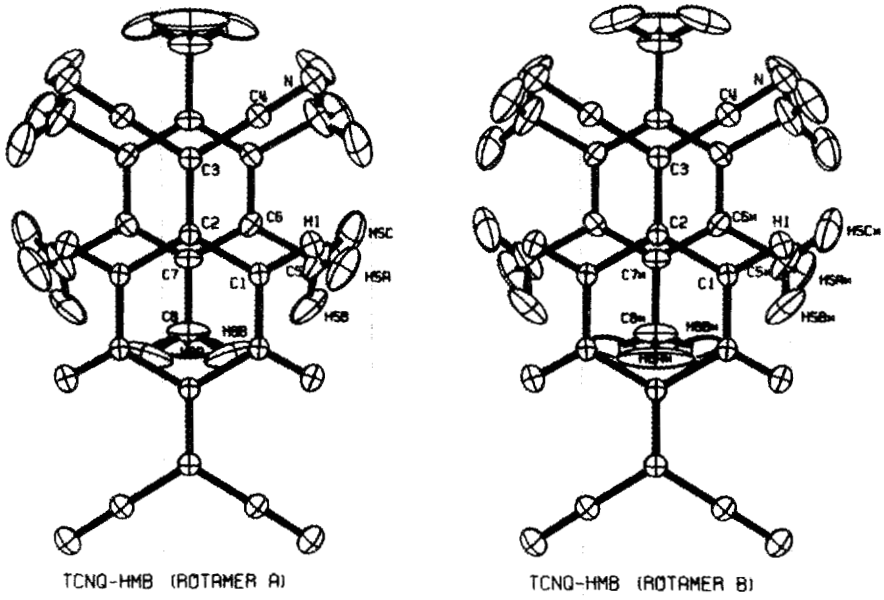

Fig. 7.7. TCNQ-hexamethylbenzene complex projected onto the hexamethylbenzene plane. The disordered structure is $^2/_3$ rotamer *A* and $^1/_3$ rotamer *B*.

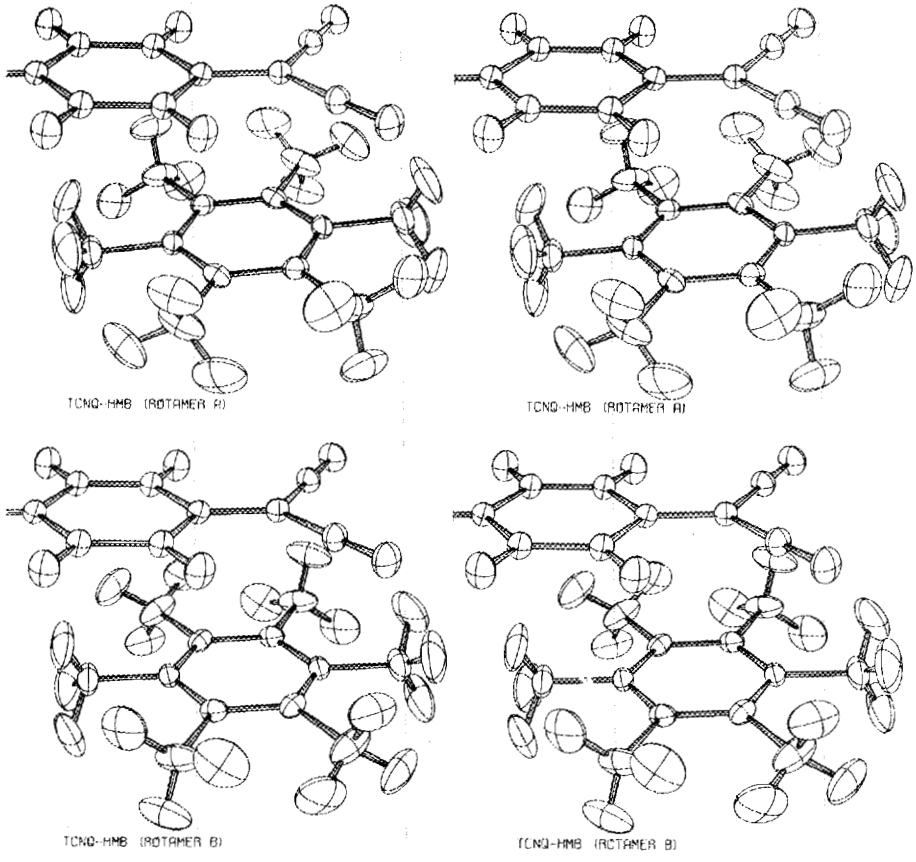

Fig. 7.8. Stereoscopic drawing showing how TCNQ packs with the two different rotamers of hexamethylbenzene.

ORNL-DWG 73-12495

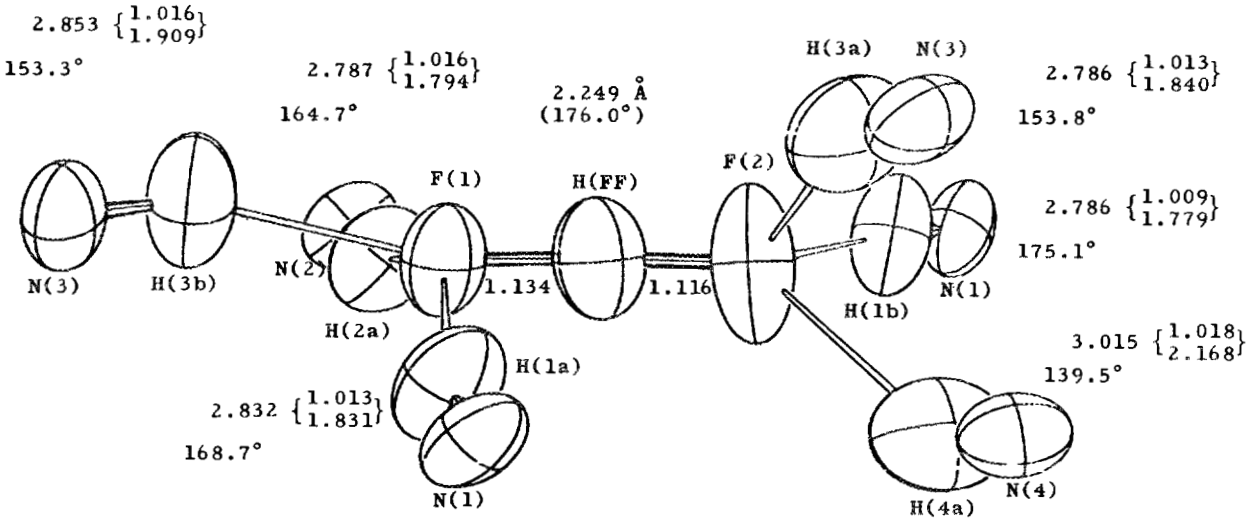

Fig. 7.9. Hydrogen bond distances in tetrathiourea tellurium di(hydrogen difluoride).

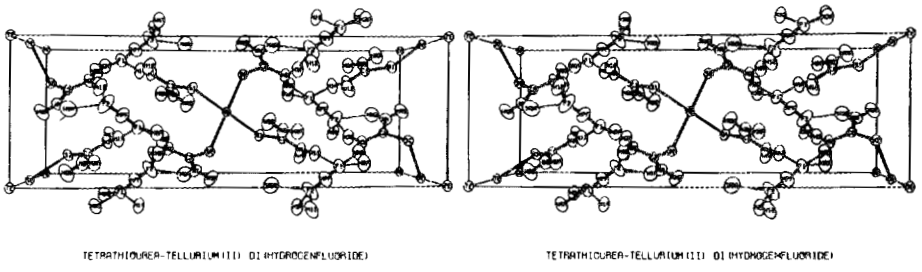

Fig. 7.10. Stereoscopic packing drawing for $Te(Tu)_4(HF_2)_2$.

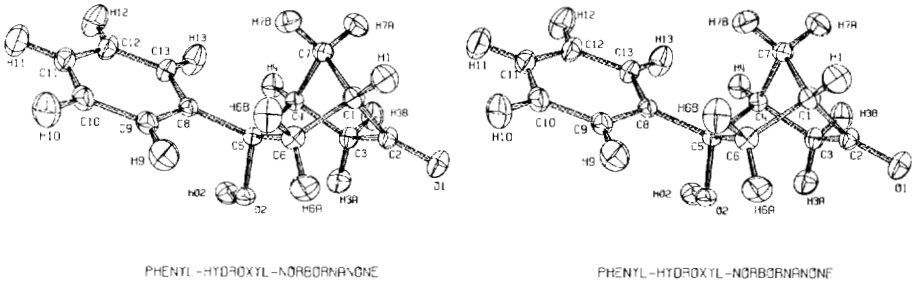

Fig. 7.11. Stereoscopic drawing of 5-*exo*-phenyl-5-*endo*-hydroxyl-2-norbornanone.

crystal structure of some norbornyl carbocation crystallized with a suitable counterion, but the reactivity of such materials makes this goal rather unrealistic except perhaps at low temperature. Crystals of **IV** were grown by B. M. Benjamin.

The unit-cell parameters, space group information, and statistics on data collection and least-squares refinement for the four structures are given in Table 7.4. The neutron data were collected at the HFIR reactor. Structure **I** was solved by model-building techniques, and structures **III** and **IV** were solved by the application of direct methods as implemented in the MULTAN program.[7] The ease with which the structures of **III** and **IV** were solved from the neutron data is

Table 7.3. Average distances from TCNQ-benzene and TCNQ-hexamethylbenzene

The d_{corr} values are based on the segmented-body model with special features noted in the right-hand column. The notation "normal coordinate" signifies that an estimate of internal molecular motion based on a normal-coordinate analysis was used.

Bond	d_0 (Å)	d_{corr} (Å)	Segmented-body model
			TCNQ
C–H	1.089	1.113	Normal coordinate
C=C	1.353	1.353	
C–C	1.448	1.450	
C=C	1.383	1.383	
C–C	1.427	1.434	C(–C≡N)$_2$ segment (torsion 4.5° and 5.0°, in-plane 3.0° and 3.0°)
C≡N	1.151	1.156	
			Benzene
C–C	1.382	1.401	
C–H	1.082	1.115	Normal coordinate
			Hexamethylbenzene (disordered)
C–C	1.400	1.415	
C–C$_m$	1.508	1.523	
C$_m$–H	1.042	1.090	Methyl segments (torsion 15.5° and 19.6°)

Table 7.4. Crystallographic data on the four structures

	I, TCNQ-benzene	II, TCNQ-HMB	III, Te(Tu)$_4$(HF$_2$)$_2$	IV, norbornanone
Space group	$P2_1/n$	$I2/m$	$I2/c$	$P2_1/n$
Z	2	2	4	4
a (Å)	15.82(2)	8.335(4)	22.35(1)	10.331(4)
b (Å)	6.170(6)	13.574(4)	7.914(4)	10.646(7)
c (Å)	7.485(3)	9.220(5)	10.151(4)	10.099(5)
β (deg)	91.10(4)	94.04(2)	90.72(3)	106.48(3)
Neutron data	1263	1734	2123	3421
$R(F^2)$	0.062	0.057	0.070	0.064

rather amazing since the theory of direct methods is based on the principle that all atoms are positive scatterers, whereas the hydrogen atoms are negative scatterers of neutrons relative to carbon, oxygen, and nitrogen atoms.

1. Student participant in the Great Lakes Colleges Association Science Semester, fall 1973, from DePauw University, Greencastle, Ind.

2. Oak Ridge Associated Universities Summer Student Trainee, from Rockhurst College, Kansas City, Mo.

3. See V. F. Raaen, Becky Wenzel, and C. R. Watson, Jr., "Preparation of Charge-Transfer Complexes," chap. 5, this report.

4. R. H. Cotton and D. E. Henn, *J. Chem. Soc. B* 1532 (1970).

5. C. K. Johnson, p. 132 in *Thermal Neutron Diffraction*, B. T. M. Willis, ed., Oxford University Press, London, 1970.

6. J. M. Williams and L. F. Schneemeyer, *J. Amer. Chem. Soc.* **95**, 5780 (1973).

7. P. Main, M. M. Woolfson, and G. Germain, *MULTAN, a Computer Program for the Automatic Solution of Crystal Structures*, University of York, York, England (1971).

THE REPRESENTATION PROBLEM IN COMBINATORIAL CHEMISTRY

C. K. Johnson

Chemistry and combinatorial mathematics are related in that chemistry is concerned with the arrangement of atoms into molecules and combinatorial theory concerns the arrangement of abstract elements into sets. As a consequence, some aspects of chemistry are basically combinatorial problems, and the term "combinatorial chemistry" seems to be a suitable name for the study of

problems in this domain. One of the classical problems in combinatorial chemistry is the enumeration of the molecules which satisfy a given empirical chemical formula, and work in this field extends back to the mathematician A. Cayley[1] in 1875.

The aspect of combinatorial chemistry with which we are concerned is the enumeration of permitted unimolecular rearrangement reactions which can transform a specific reactant to a specific product by the "best" (most probable) routes. This problem may be formulated algebraically using combinatorial group theory[2] with the rearrangement mechanisms, represented by permutations, serving as group generators. If the rearrangements are degenerate[3] (i.e., if the gross skeletal conformation is maintained but individual atoms and groups of atoms are interchanged), a permutation representation based on a set of characters with one letter for each atomic site may be used. The algebraic model[4-6] for the norbornyl system of carbonium ion rearrangements is based on such a representation, with the numbers 1–7 designating skeletal atom sites, the letters A–K designating substituent sites, and the symbols +, – denoting skeletal handedness. In a more general chemical system, such as adamantane,[7] the rearrangements can interconvert several skeletal conformations; thus the representation used must be capable of including the skeletal stereochemical information, and the sites on each different skeleton must be numbered by some deterministic scheme. In general, this requires an extended character set, but we have not found a satisfactory general algorithm which can handle all cases.

Another complication in representation arises when the skeleton has intrinsic three-dimensional symmetry such that the site labels may be positioned on the skeleton in several equivalent ways. This complication may be handled by the method of double cosets.[2,8,9] The basic principle of double cosets is most easily illustrated with graphs. For example, in the 4-homoadamantyl cation system of rearrangements[10] shown in Fig. 7.12, the skeleton has a mirror plane of symmetry. This mirror symmetry causes no complication except when a racemic mixture is represented, and for that case we need to form a union of the regular coset nodes for enantiomeric sites to form double-coset nodes as illustrated in Fig. 7.13. This situation did not arise in the norbornyl case because the norbornyl skeletal handedness designator (+, –) for right- and left-handed skeletons could simply be omitted from the representation for racemic mixtures.

The 4-homoadamantyl coset graphs shown in Fig. 7.13 may be extended to include carbonium-ion counterion complexes which may tend to inhibit certain rearrangements.[10] The location of the counterion is denoted by the added character R or S designating the right- or left-handed seven-atom face of the cation skeleton, and each generator is extended by the addition of an (RS) transposition.

Experimental studies on the 4-homoadamantyl system are currently being carried out by the organic chemistry group to test the chemical validity of the rearrangement networks given by the coset graphs.[11]

1. A. Cayley, *Ber. Deut. Chem. Ges.* 8, 1956 (1875).
2. W. Magnus, A. Karrass, and D. Solitar, *Combinatorial Group Theory: Presentations of Groups in Terms of Generators and Relations*, Interscience, New York, 1966.

ORNL-DWG. 74-4925

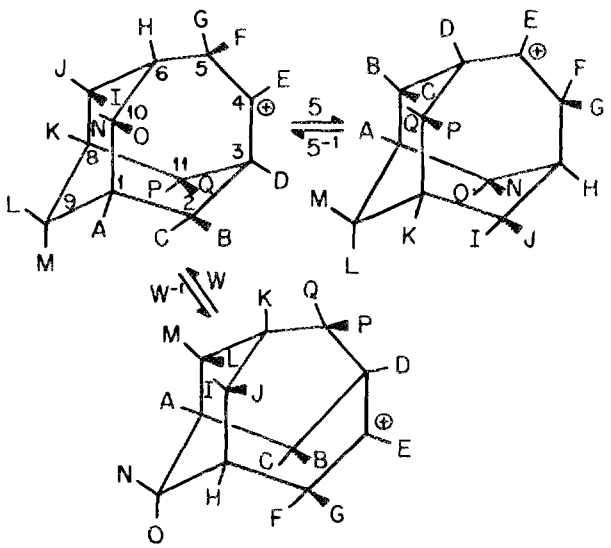

Fig. 7.12. Wagner-Meerwein (*W*) and 5,4-hydride shift (*5*) rearrangements of the 4-homoadamantyl cation. The permutation generators representing the rearrangements are

$$W = [(AKH)(BQG)(CPF)(INL)(JOM)(DE)] ,$$

$$5 = [(EGF)(AK)(BJ)(CI)(DH)(LM)(NQ)(OP)]$$

and are derived by direct inspection. A set of letters in parentheses describes a cyclic permutation; for example, (AKH) means that the atom on site A goes to site K, etc. (i.e., [A] → K, [K] → H, [H] → A). The rearrangements W and W^{-1} are not identical since $WW^{-1} = W^6 = I$; consequently, $W^5 = W^{-1}$. Similarly, $5^5 = 5^{-1}$; thus 5 and 5^{-1} are distinct rearrangements also.

ORNL - DWG. 74-4926

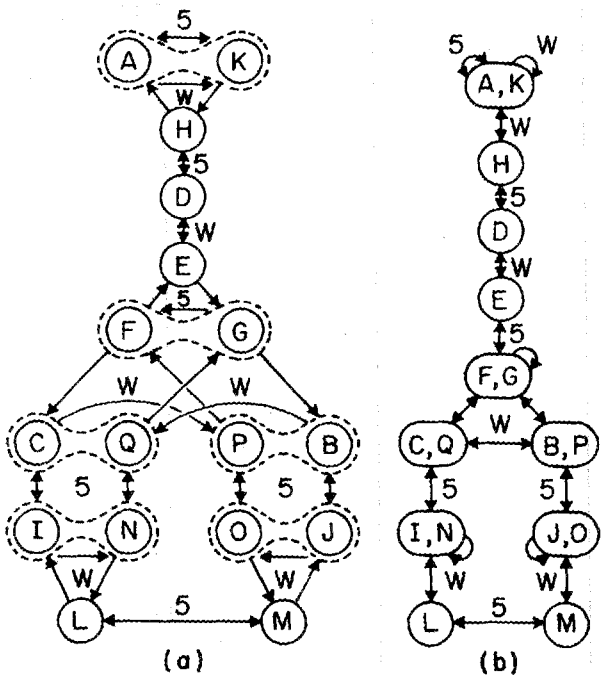

Fig. 7.13. Monosubstituent coset graphs for 4-homoadamantyl cations. The W^{-1} and 5^{-1} rearrangements are traced by inverting the directed edges for W and 5 respectively. The coset graphs are derived directly from the rearrangement generators given by Fig. 7.12. (*a*) Correspondence of regular-coset and double-coset graphs. The double-coset graph with 11 nodes is derived from the regular coset graph with 17 nodes by uniting the nodes for enantiomers as shown by the dashed lines. (*b*) Double-coset graph. This graph is used in the analysis of rearrangements carried out with racemic reactants.

3. P. von R. Schleyer, E. Funke, and S. H. Liggero, *J. Amer. Chem. Soc.* **91**, 3965 (1969).
4. C. K. Johnson and C. J. Collins, *J. Amer. Chem. Soc.* **96**, 2514 (1974).
5. C. J. Collins and C. K. Johnson, *J. Amer. Chem. Soc.* **95**, 4766 (1973).
6. C. J. Collins, C. K. Johnson, and V. F. Raaen, *J. Amer. Chem. Soc.* **96**, 2524 (1974).
7. H. W. Whitlock, Jr., and M. W. Siefken, *J. Amer. Chem. Soc.* **90**, 4929 (1968); E. M. Engler et al., *J. Amer. Chem. Soc.* **95**, 5769 (1973).
8. W. Hasselbarth and E. Ruch, *Theor. Chim. Acta* **29**, 259 (1973).
9. H. Brown, L. Hjelmeland, and L. Masinter, *Discrete Math.* **7**, 1 (1974).
10. J. E. Nordlander et al., *J. Amer. Chem. Soc.* **91**, 3962 (1969).
11. Also see C. J. Collins, C. K. Johnson, and W. W. Schmidt, "Combinatorial Chemistry," chap. 5, this report.

MEAN SPHERICAL MODEL FOR THE STRUCTURE OF LENNARD-JONES FLUIDS[1]

A. H. Narten L. Blum[2]
R. H. Fowler[3]

The equilibrium properties of simple fluids are described by the pair potential $v(r)$ and the pair correlation function $h(r)$. A third quantity of central importance in the theory of liquids is the direct correlation function $c(r)$, defined by the Ornstein-Zernike equation,[4]

$$h(r_{12}) = c(r_{12}) + \rho \int c(r_{13})\, h(r_{23})\, d\mathbf{r}_3 \,, \qquad (1)$$

with ρ the bulk number density. Most of the successful theories of fluids with spherical molecules provide closure relations for the Ornstein-Zernike equation.[5]

The mean spherical model (MSM) assumes that, outside a hard core radius r_c, the potential is linearly related to the direct correlation function

$$c(r) = -\beta\, v(r) \,, \qquad r \geqslant r_c \,, \qquad (2)$$

while inside r_c the exact relationship

$$h(r) = -1 \,, \qquad r < r_c \,, \qquad (3)$$

determines $c(r)$ through Eq. (1).

Substitution of (2) and (3) into (1) yields the MSM integral equation for the pair correlation function $h(r)$. The iterative numerical solution of integral equations often leads to difficulties,[6] and convergence of the iterated solutions to a final answer can be painfully slow. Andersen and Chandler[7] have derived a variational formulation of the MSM equation which greatly facilitates its solution and is expressed by the following set of equations:

$$\partial F/\partial c(r) = 0 \,, \qquad r < r_c \,, \qquad (4a)$$

where

$$F = \tfrac{1}{2}\rho^2\, \bar{c}(0) - (4\pi^2)^{-1} \int_0^\infty k^2 \{\rho\, \bar{c}(k) + \ln[1 - \rho\, \bar{c}(k)]\} dk \,, \qquad (4b)$$

and Eq. (2) for $r \geqslant r_c$. The function

$$\bar{c}(k) = 4\pi\rho \int_0^\infty r^2\, dr\, c(r) \sin(kr)/(kr)$$

is related to the liquid structure function

$$\bar{h}(k) = 4\pi\rho \int_0^\infty r^2\, dr\, h(r) \sin(kr)/(kr)$$

by the inverse of Eq. (1), namely,

$$\bar{h}(k) = \frac{\bar{c}(k)}{1 - \bar{c}(k)} .$$

In the variational formulation of Eqs. (4*a*) and (4*b*), the solution for $c(r)$ inside the core r_c is the set of functions which make the quantity F stationary with respect to changes of $c(r)$ inside the core.

We have solved the MSM for Lennard-Jones fluids in four different states, corresponding to those of neon, argon, krypton, and xenon at relatively high densities. Structure functions calculated for the model are shown in Fig. 7.14. The calculated functions $\bar{h}(k\sigma)$ for neon and argon can be compared with results derived from recent diffraction experiments[8,9] (Fig. 7.14, circles). The agreement is good, with root-mean-square deviation between experimental and calculated curves of value <0.02.

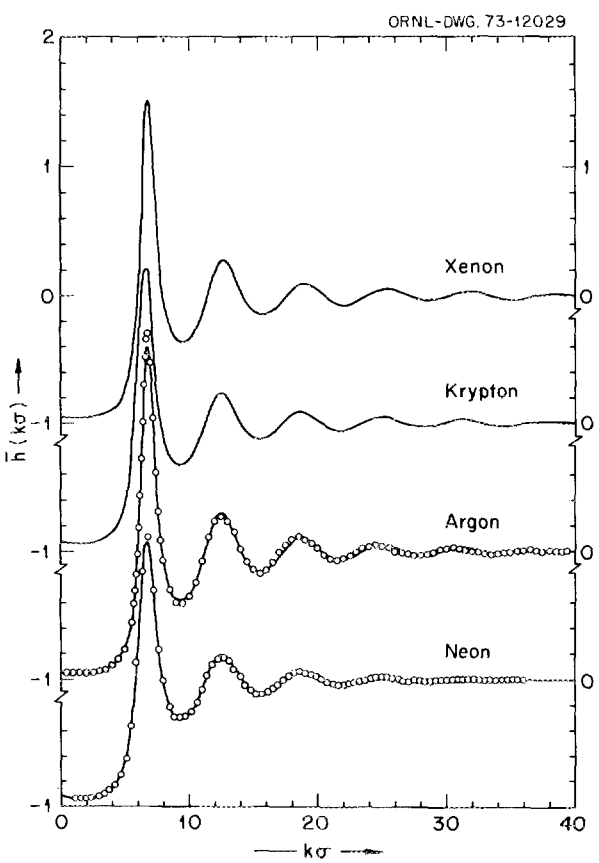

Fig. 7.14. Structure functions for Lennard-Jones fluids. Solid lines computed from potentials $v(r) = 4\epsilon[(\sigma/r)^{12} - (\sigma/r)^6]$ and MSM; circles derived from neutron diffraction. For the values of the potential parameters, see A. H. Narten, L. Blum, and R. H. Fowler, *J. Chem. Phys.* **60**, 3378 (1974).

We conclude that the MSM provides a good description of the structure of Lennard-Jones fluids of relatively high density. The computational convenience of the variational formulation of the MSM makes the model attractive for a description of multicomponent systems of spherical particles, such as molten salts. The model can also be extended to molecular fluids with only a moderate increase in computational effort.[10]

1. Expanded abstract of A. H. Narten, L. Blum, and R. H. Fowler, *J. Chem. Phys.* **60**, 3378 (1974).
2. Oak Ridge Associated Universities Research Participant from the University of Puerto Rico, Rio Piedras.
3. Mathematics Division.
4. L. S. Ornstein and F. Zernike, *Proc. Acad. Sci. (Amsterdam)* **17**, 793 (1914).
5. H. L. Frisch and J. L. Lebowitz, *The Equilibrium Theory of Classical Fluids*, Benjamin, New York, 1967.
6. A. A. Broyles, S. U. Chung, and H. L. Sahlin, *J. Chem. Phys.* **37**, 2462 (1962).
7. H. C. Andersen and D. Chandler, *J. Chem. Phys.* **57**, 1918 (1972).
8. L. A. DeGraaf and B. Mozer, *J. Chem. Phys.* **55**, 4967 (1971).
9. J. L. Yarnell et al., *Phys. Rev. A* **7**, 2130 (1973).
10. L. Blum, "Correlations in Molecular Liquids," the following contribution, this report.

CORRELATIONS IN MOLECULAR LIQUIDS

L. Blum[1]

The structure of a molecular liquid can be described by a pair distribution function $g(\mathbf{X}_1, \mathbf{X}_2)$, with $\mathbf{X}_i = (\mathbf{R}_i, \Omega_i)$, $\mathbf{R}_i$ the position of molecule i, and $\Omega_i = (\alpha_i, \beta_i, \gamma_i)$, the three Euler angles that define the orientation of molecule i. By means of group theoretical arguments, we have formulated[2] a unique decomposition of the pair correlation function $h(\mathbf{X}_1, \mathbf{X}_2) \equiv g(\mathbf{X}_1, \mathbf{X}_2) - 1$ in invariant terms, which are equivalent to the possible scalar products that can be formed with vectors attached to molecules 1 and 2. The expansion of the pair correlation function is of the form

$$h(\mathbf{X}_1, \mathbf{X}_2) = \sum_{\substack{mnl \\ \mu\nu}} h_{\mu\nu}^{mnl}(r)\, \Phi_{\mu\nu}^{mnl}(\Omega_1, \Omega_2, \mathbf{R}_{12}) . \qquad (1)$$

All orientational information is contained in the known coefficients $\Phi_{\mu\nu}^{mnl}(\Omega_1, \Omega_2, \mathbf{R}_{12})$, which are closely related[2] to Wigner's generalized spherical harmonic.[3] The quantities $h_{\mu\nu}^{mnl}(r)$ depend only on the separation

distance r and are accessible from scattering experiments.[4]

The expressions for some thermodynamic properties in terms of this expansion have also been obtained. All these expansions can be put into their irreducible representations, which have some interesting properties. In particular, they can be solved exactly in the so-called mean spherical approximation (MSA).[5]

We have studied numerically the MSA for simple liquids[5] and have found remarkably good agreement with computer simulations and diffraction experiments. We have solved exactly the MSA for systems of charged hard spheres,[6] for mixtures of charged hard spheres with different diameters,[7] and for mixtures of charged hard spheres and hard dipoles, all of equal diameter.[8] The last system simulates a real electrolyte solution with the solvent not treated as a continuum. We have also made progress toward the explicit solution of the MSA for systems of hard spheres with electric multipoles.

The outlook for these procedures as a viable theory for liquids like water has brightened considerably with the recent results of Verlet and Weis,[9] who showed that rather simple corrections to the MSA give remarkably good agreement with computer experiments in the case of dipolar liquids.

1. Oak Ridge Associated Universities research participant from the University of Puerto Rico, Rio Piedras.
2. L. Blum and A. J. Torruella, *J. Chem. Phys.* **56**, 303 (1972).
3. A. R. Edmonds, *Angular Momentum in Quantum Mechanics*, Princeton University Press, Princeton, N.J., 1957; M. Rotenberg, *The 3-j and 6-j Symbols*, Technology Press, MIT, Cambridge, Mass., 1959.
4. A. H. Narten, "Diffraction by Molecular Liquids," the following contribution, this report.
5. A. H. Narten, L. Blum, and R. H. Fowler, "Mean Spherical Model for the Structure of Lennard-Jones Fluids," the preceding contribution, this report.
6. L. Blum, *J. Chem. Phys.* **57**, 1862 (1972); **58**, 3295 (1973).
7. H. Tibavisco and L. Blum, unpublished.
8. L. Blum, *Chem. Phys. Lett.*, in press,
9. L. Verlet and J. J. Weis, to be published.

DIFFRACTION BY MOLECULAR LIQUIDS[1]

A. H. Narten

Molecular liquids were among the first to which the method of x-ray diffraction was applied, and a number of systems have been studied over the years. It was soon realized that the assumption of random orientation, made in the reduction of early diffraction data, was not tenable even for fluids with nearly spherical molecules.

The expansion method described in the preceding contribution[2] yields equations for the scattering of radiation by fluids in a form suitable for the treatment of nonspherical as well as spherical molecules. The static differential scattering cross section of a molecular liquid is of the form[3,4]

$$\frac{1}{N}\frac{d\sigma}{d\Omega} = \sum_{m\mu} |a_\mu^m(k)|^2 + |a_0^0(k)|^2 \bar{h}^{000}(k)$$

$$+ \sum_{mnl} \begin{pmatrix} mnl \\ 000 \end{pmatrix} \sum_{\mu\nu\neq 0} (-)^\nu a_\mu^m(k)[a_\nu^n(k)]^* \bar{h}_{\mu\nu}^{mnl}(k) , \quad (1)$$

with the standard notation[5] for Wigner's $3j$ symbols. The quantities $a_\mu^m(k)$ are the molecular form factors, discussed in the following contribution.[6] The quantities $\bar{h}_{\mu\nu}^{mnl}(k)$ are the generalized structure functions, closely related to the Fourier transform of the generalized correlation functions $h_{\mu\nu}^{mnl}(r)$ defined in the preceding contribution.[2] We note that for spherical molecules (m, $\mu = n$, $\nu = 0$), Eq. (1) reduces to the familiar form for the scattering from monatomic fluids.

The expansion (1) is convergent, and hence useful, only for molecules that are not too aspherical in the sense that their scattering density can be represented by a rapidly converging multipole expansion. Only in this case can there be hope of extracting the structure functions $\bar{h}_{\mu\nu}^{mnl}(k)$ from a small number of experiments involving different values of the scattering factors. Knowledge of these functions and their transforms is sufficient for the construction of the molecular correlation function $h(\mathbf{X}_1, \mathbf{X}_2)$, descriptive of the structure of molecular fluids, as discussed in the preceding contribution.[2]

The first application of the expansion method has been to the case of x-ray scattering from water.[7] We here discuss a preliminary analysis of results from x-ray and neutron scattering from liquid carbon tetrachloride.

X-ray and neutron scattering cross sections for liquid CCl_4 are shown in Fig. 7.15. The solid (neutron) and dashed (x ray) curves (a) represent the computed dilute gas scattering. Our first conclusion from the curves of Fig. 7.15 is that the scattering for values of the variable $k \gtrsim 6$ Å^{-1} is identical to that from independent molecules, and hence contains no information about the structure of the liquid. The solid and dashed curves (b) in Fig. 7.15 represent the spherical part, $|a_0^0|^2$, of the molecular scattering factors[6] for CCl_4. The large differences between curves a and b for values of $k \gtrsim 2$ Å^{-1} indicate that CCl_4 is "seen" by both x rays and neutrons as a highly nonspherical molecule. Hence,

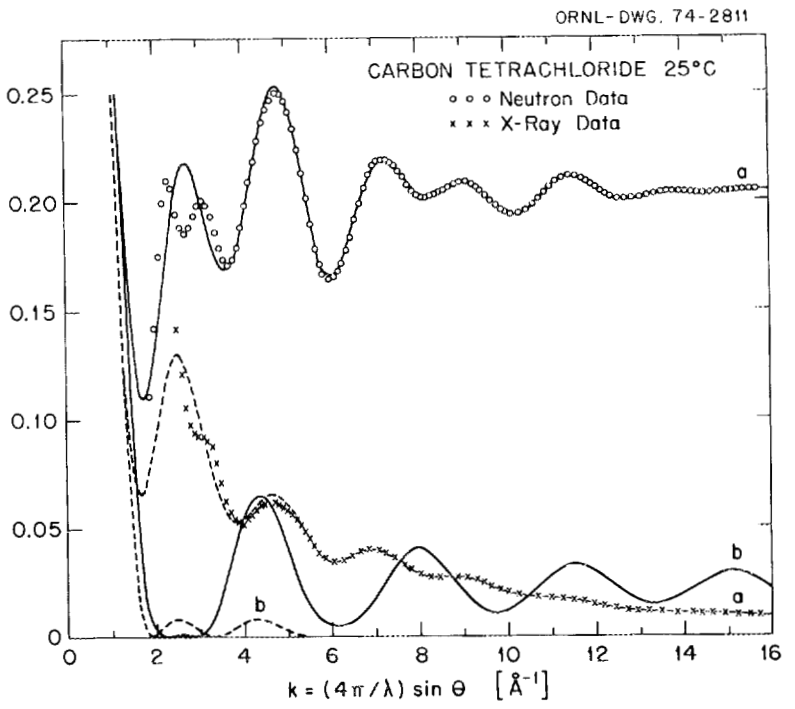

Fig. 7.15. Differential scattering cross sections. Computed gas scattering (*a*) and spherical part of the molecular scattering factors (*b*), normalized to unity at the origin. The measured data points (circles and crosses) are scaled to the computed gas scattering at values of $k \lesssim 6$ Å^{-1}.

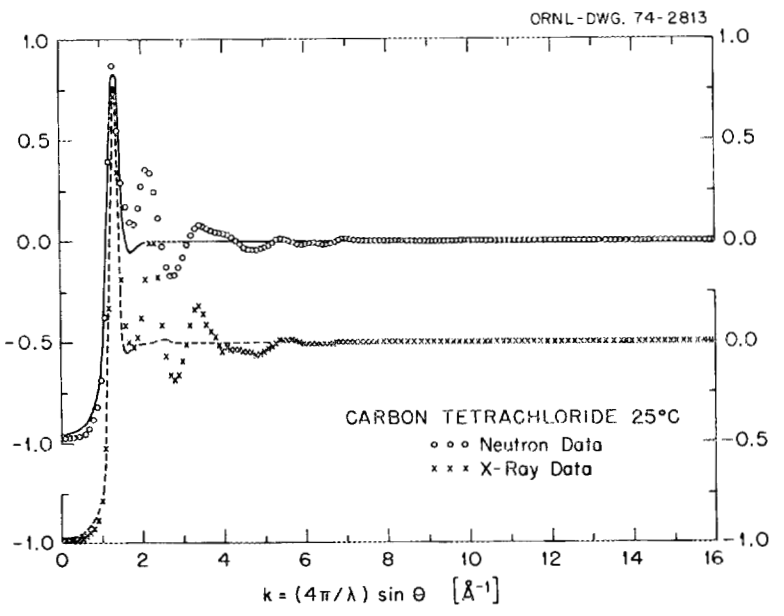

Fig. 7.16. Intermolecular part of the measured cross sections. Points are from experimental data, solid and broken lines computed for hard-sphere model.

nonspherical correlations in the liquid should be detectable by both diffraction methods. The very small differences between the sets of curves *a* and *b* below $k \sim 2$ Å^{-1} indicate that this part of the scattering curves, not shown in Fig. 7.15, is almost completely determined by the spherical part of the interactions between pairs of molecules.

Fig. 7.16 (points) shows the difference between the data points of Fig. 7.15 and the computed gas scattering, that is, the sum of the products of the molecular form factors and the generalized structure functions defined in Eq. (1). In order to test our assumption about the nature of the features below $k \sim 2$ Å^{-1} in the curves of Fig. 7.16, we have computed the spherical part of the scattering, $I^S = |a_0^0|^2 \bar{h}^{000}(k)$. The structure function $\bar{h}^{000}(k)$, descriptive of molecular centers, was calculated from a hard-sphere potential ($\sigma = 5.2$ Å), as discussed in a preceding contribution.[8] The result is shown in the solid (neutron) and dashed (x ray) curves of Fig. 7.16. The agreement between the data and the model is rather good below $k \sim 2$ Å^{-1}, indicating that this part of the scattering curves is insensitive to the detailed shape of the potential function (for van der Waals-type liquids such as CCl_4). We conclude that the nonspherical part of the correlation between pairs of CCl_4 molecules dominates the scattering curves (Fig. 7.16) in the region $2 \lesssim k \lesssim 6$ Å^{-1}.

It is instructive to calculate the Fourier transforms of the scattering curves of Fig. 7.16. The result is shown in Fig. 7.17. The points represent the total weighted sums of modified correlation functions for carbon tetrachloride. The solid lines represent the spherical part, and the dashed curves represent the sum of the nonspherical parts of the correlations.

We note (Fig. 7.17) that the nonspherical part of the intermolecular correlations in CCl_4 is of much shorter range than the spherical part and that it shows only two major maxima around 4 Å and around 6 Å. We therefore believe that the scattering cross section of liquid CCl_4 can be written, in good approximation, as the sum of only three terms. We are confident that the spherical part can be computed from a perturbational version of the hard-sphere model. The two nonspherical terms in the equation for the cross section can then be obtained uniquely from the two sets of diffraction data.

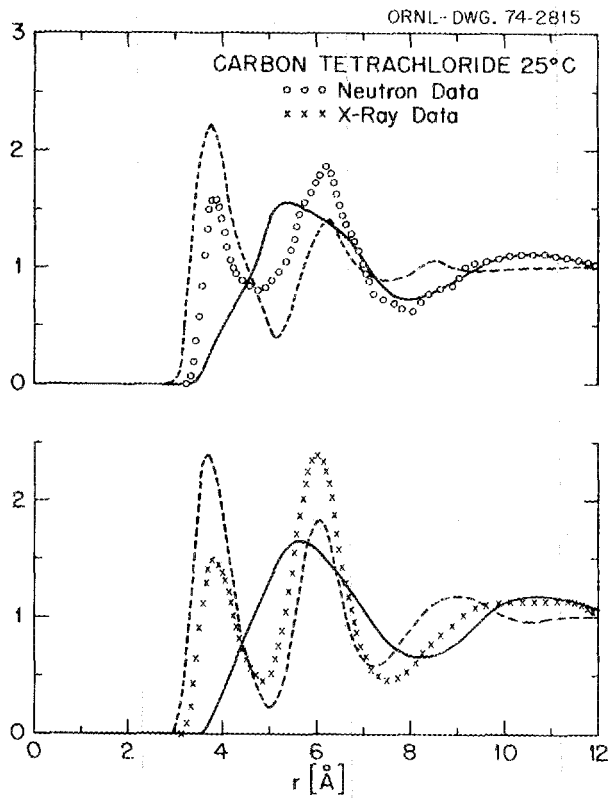

Fig. 7.17. Fourier transforms of the curves shown in Fig. 7.16. The curves derived from experiment (points) can be separated into contributions from positional correlation only (solid lines) and from nonspherical correlation (broken lines) in the liquid.

1. Expanded abstract of paper to be published in the *Proceedings of the American Crystallographic Association.*
2. L. Blum, "Correlations in Molecular Liquids," the preceding contribution, this report.
3. L. Blum, *J. Comput. Phys.* 7, 592 (1971).
4. L. Blum and A. J. Torruella, *J. Chem. Phys.* **56**, 303 (1972).
5. A. R. Edmonds, *Angular Momentum in Quantum Mechanics,* Princeton University Press, Princeton, N.J., 1957.
6. L. Blum, R. H. Fowler, and A. H. Narten, "Molecular Scattering Factors," the following contribution, this report.
7. A. H. Narten and H. A. Levy, *J. Chem. Phys.* **55**, 2263 (1971).
8. A. H. Narten, L. Blum, and R. H. Fowler, "Mean Spherical Model for the Structure of Lennard-Jones Fluids," a previous contribution in this section, this report.

MOLECULAR SCATTERING FACTORS

L. Blum[1] R. H. Fowler[2] A. H. Narten

Molecular scattering factors in x-ray analysis are often calculated from the isolated atom equation originally derived by Debye.[3] In this equation a polyatomic molecule is viewed as being composed of independent atoms located at the ends of interatomic vectors known primarily from spectroscopic and gas diffraction data. This approach ignores distortions in the electronic

density due to bonding. We here describe a simple method of computing the coefficients of the harmonic expansion of the molecular x-ray and neutron scattering factor as defined by Steele and Pecora.[4]

The x-ray scattering factors for free atoms can be expressed, in good approximation, by a sum of Gaussians,

$$f_\alpha(k) = \sum_n \alpha_{n,\alpha} e^{-\beta_{n,\alpha} k^2} + \gamma_{n,\alpha} , \quad (1)$$

and extensive tables of the constants α, β, and γ have been prepared.[5]

For rigid molecules, the scattering factor $a_\mu^m(k)$ is related to the atomic scattering scattering factor $f_\alpha(k)$ by the expression

$$a_\mu^m(k) = i^m (2m+1)^{-1/2} \times \sum_\alpha D_{\mu 0}^m(\hat{R}_\alpha) j_m(kR_\alpha) f_\alpha(k) , \quad (2)$$

if Eq. (1) holds for $f_\alpha(k)$. The summation is over the atoms α in the molecule. In Eq. (2), $D_{\mu 0}^m(\hat{R}_\alpha)$ is the generalized Wigner spherical harmonic for the angular coordinates of atom α, $\hat{R}_\alpha \equiv (\theta_\alpha, \phi_\alpha)$, $j_m(x)$ is the spherical Bessel function of order m, and R_α is the distance of atom α from the origin. For x rays, the atomic form factors are given by Eq. (1), while for neutrons the quantities f_α are constant with respect to k.

We have compared the results obtained from Eq. (2) with the more elaborate calculations of Morrison and Pings,[6] which are based on molecular wave functions. The agreement is excellent for N_2 and Cl_2 and becomes increasingly poorer for compounds such as HF, HLi, and H_2. We conclude that Eq. (2), exact for neutron scattering, yields x-ray scattering factors of good accuracy for all molecules not containing hydrogen or other very light atoms. Further studies to correct Eq. (2) for vibrational effects are in progress.

1. Oak Ridge Associated Universities research participant from the University of Puerto Rico, Rio Piedras.
2. Mathematics Division.
3. P. Debye, *Phys. Z.* **31**, 419 (1930).
4. W. Steele and R. Pecora, *J. Chem. Phys.* **42**, 1863 (1965).
5. D. T. Cromer and J. B. Mann, *Acta Crystallogr., Sect. A* **24**, 321 (1968).
6. P. F. Morrison and C. J. Pings, *J. Chem. Phys.* **56**, 280 (1972).

AMORPHOUS WATER

C. G. Venkatesh[1] S. A. Rice[2]
A. H. Narten

Amorphous water was first reported by Burton and Oliver[3] in 1935, and a number of studies of this material have been reported over the years. In most of these studies, water vapor was condensed on metal surfaces under vacuum, and the temperature range was 77 to 153°K (immediately above this temperature, cubic ice is always the dominant form). Ghormley[4] was the first to use temperatures of deposition below 77°K, and Olander and Rice[5] developed a method of preparation in the temperature range 20 to 55°K and demonstrated the complete absence of crystalline ice. It now appears that all deposits obtained at or above 77°K may have been contaminated with crystalline ice.

We here report the first x-ray diffraction study of pure amorphous water at 10°K. Water vapor was condensed at a very slow rate (about 4 mg/hr) on the horizontal surface of a copper single crystal attached to a liquid helium Dewar and mounted in an x-ray diffractometer designed for the study of noncrystalline materials. The surface (2 × 2 cm) of the copper crystal was carefully aligned to minimize Bragg scattering, and deposition was ended when the sample had reached a thickness of about 1 mm. The diffraction pattern was measured using a divergent beam of Mo K_α x rays, with a graphite monochromator mounted in the diffracted beam. The measurements were carried out over a period of 15 days, during which no systematic changes in the diffraction pattern were observed.

From the x-ray data, structure and correlation functions descriptive of molecular centers (oxygen atoms) have been derived.[6] The results are shown in Figs. 7.18 and 7.19, together with the corresponding curves for liquid water[7] near the melting point. The structure function, $\bar{h}_{OO}(k)$, for amorphous water (Fig. 7.18) shows no trace of the sharp Bragg peaks characteristic of crystalline materials.

Oxygen atom pair correlation functions, $h_{OO}(r)$, for amorphous and liquid water are compared in Fig. 7.19. Significant features of the curve for amorphous water may be summarized as follows:

1. Positional correlation between oxygen atoms extends over only a few molecular radii.
2. The first peak in $h_{OO}(r)$, characteristic of nearest neighbors, is completely resolved and can be described by a single Gaussian distance distribution centered at 2.76 Å with an rms variation of 0.1 Å.

The area under this peak corresponds to four oxygen atom pair interactions.

3. A sharp maximum at 3.3 Å, corresponding to about one oxygen atom pair interaction, is clearly resolved. Since, for tetrahedral coordination, interactions with second neighbors are centered around 4.5 Å (where a well-defined maximum is observed in Fig. 7.19), we conclude that this peak is part of a complex first coordination sphere.

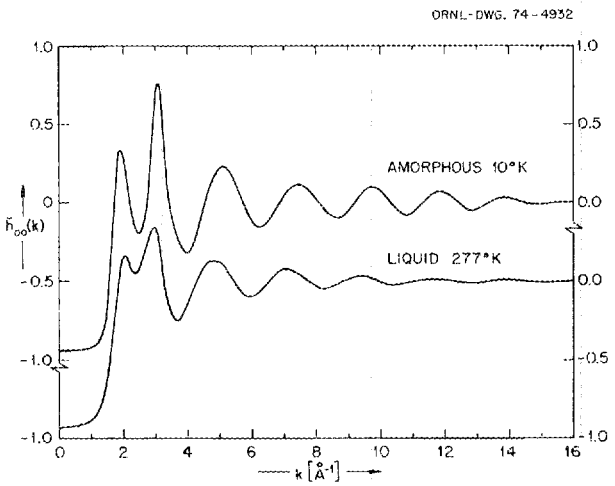

Fig. 7.18. Structure functions descriptive of oxygen atom pair interactions, derived from x-ray diffraction.

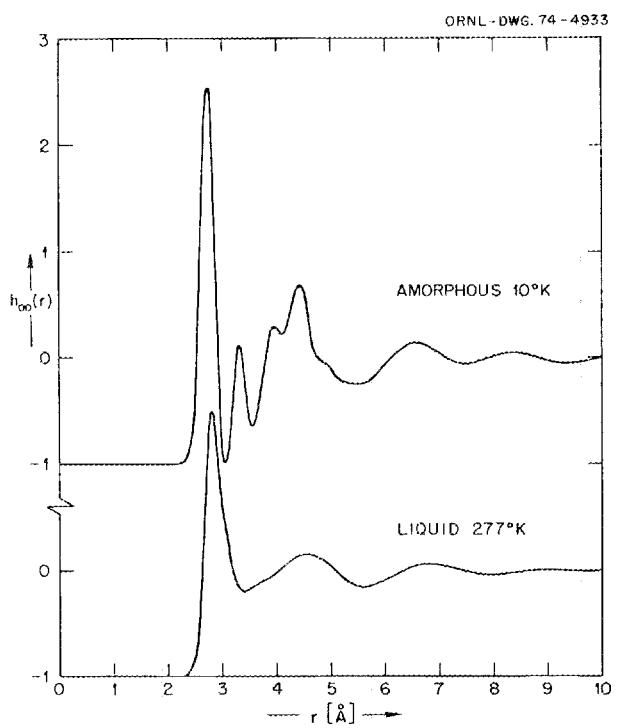

Fig. 7.19. Correlation functions for molecular centers (oxygen atoms). The peak near 3.3 Å is a unique feature of amorphous water.

Items 1 and 3 make the amorphous material distinctly different from the low-pressure ice phases I_H and I_C. Furthermore, these crystalline phases have densities near 0.93 g/cm^3, while we estimate [from the initial slope of $r\ h(r)$] that the microscopic density of the amorphous material is about 1.2 g/cm^3.

In the correlation function for liquid water, the upper bound of the first maximum is not well resolved, and it is not clear whether the barely resolved shoulder near 3.6 Å can be related to the peak of 3.3 Å in the curve for the amorphous material. Otherwise, the correlation functions for amorphous and liquid water (Fig. 7.19) show many similarities, the maxima in the curve for liquid water being shifted to slightly larger distances and very much broadened. We have shown[8] that in the liquid, as in the amorphous material, the first coordination shell of a water molecule is complex and cannot be described by tetrahedral coordination alone. Additional evidence for similarity between liquid and amorphous water has been obtained from current spectroscopic studies.[9]

1. Graduate student from the University of Chicago.
2. Chemistry Department, University of Chicago.
3. E. F. Burton and W. F. Oliver, *Proc. Roy. Soc. London, Ser. A.* **153**, 166 (1953).
4. J. A. Ghormley, *J. Chem. Phys.* **48**, 503 (1968).
5. D. S. Olander and S. A. Rice, *Proc. Nat. Acad. Sci. U.S.A.* **69**, 98 (1972).
6. A. H. Narten, "Diffraction by Molecular Liquids," a previous contribution in this section, this report.
7. ,A. H. Narten and H. A. Levy, *J. Chem. Phys.* **55**, 2263 (1971).
8. A. H. Narten and H. A. Levy, *Science* **165**, 447 (1969).
9. C. G. Venkatesh, S. A. Rice, and J. B. Bates, to be published.

DIFFRACTION PATTERN AND STRUCTURE OF IONIC SOLUTIONS

R. Triolo[1] A. H. Narten

The structure of molecular liquids such as water is, for many purposes, sufficiently described by probability functions of position and orientation,[2] and the main purpose of diffraction experiments is to provide a sensitive test of models and, eventually, a molecular theory of liquid water. The structure of aqueous solutions may be described in a similar manner. However, the correlation functions predicted by theoretical models are realistic only for very dilute solutions, for which the diffraction method may not be

sufficiently sensitive for testing. Hence the correlation functions obtainable from diffraction experiments at intermediate and high ionic concentration represent only the beginning of a description of the structure of aqueous solutions. The broader problem is to infer from the data something of the typical arrangement of ions and water molecules, insofar as this is nonrandom. The x-ray and neutron diffraction methods are complementary, and it is valuable that suitably chosen aqueous systems be studied by both methods over wide ranges of concentration. Such extensive studies reduce greatly the nonuniqueness of interpretation usually associated with diffraction data from liquids.

Ionic solutions were among the first liquids to which x-ray diffraction was applied. The neutron diffraction method has only recently been applied to solutions of LiCl in D_2O. [3] We here describe results obtained but not as yet analyzed for aqueous HCl and DCl solutions.

Fig. 7.20 shows weighted pair correlation functions derived from x-ray and neutron data, $G_X(r)$ and $G_N(r)$, for pure water and for various mole ratios H_2O/HCl and D_2O/DCl. The scattering factors ensure that interactions involving O dominate the x-ray curves while those involving D dominate the neutron curves. The curves for pure water have been previously presented and analyzed.[3] The variation of $G_X(r)$ and $G_N(r)$ with concentration yields directly some valuable information.

With increasing HCl concentration the peak at 2.84 Å, characteristic of O-O pairs, decreases in magnitude, while two new peaks appear. As in LiCl, the maximum at about 3.2 Å is ascribed to Cl-O interactions. The maximum at 2.52 Å is unique to HCl solutions, and we attribute this short O-O distance to the presence of excess protons. This feature in $G_X(r)$ is closely correlated with the increasing prominence in $G_N(r)$ of the second peak around 1.6 Å. This feature is understood as the intermolecular O ··· D distance in increasingly strong short hydrogen bonds in the concentrated acid solutions. The maximum around 2.2 Å in the functions $G_N(r)$, ascribed to Cl ··· DO hydrogen bonds, shows a more complex concentration dependence. The maxima

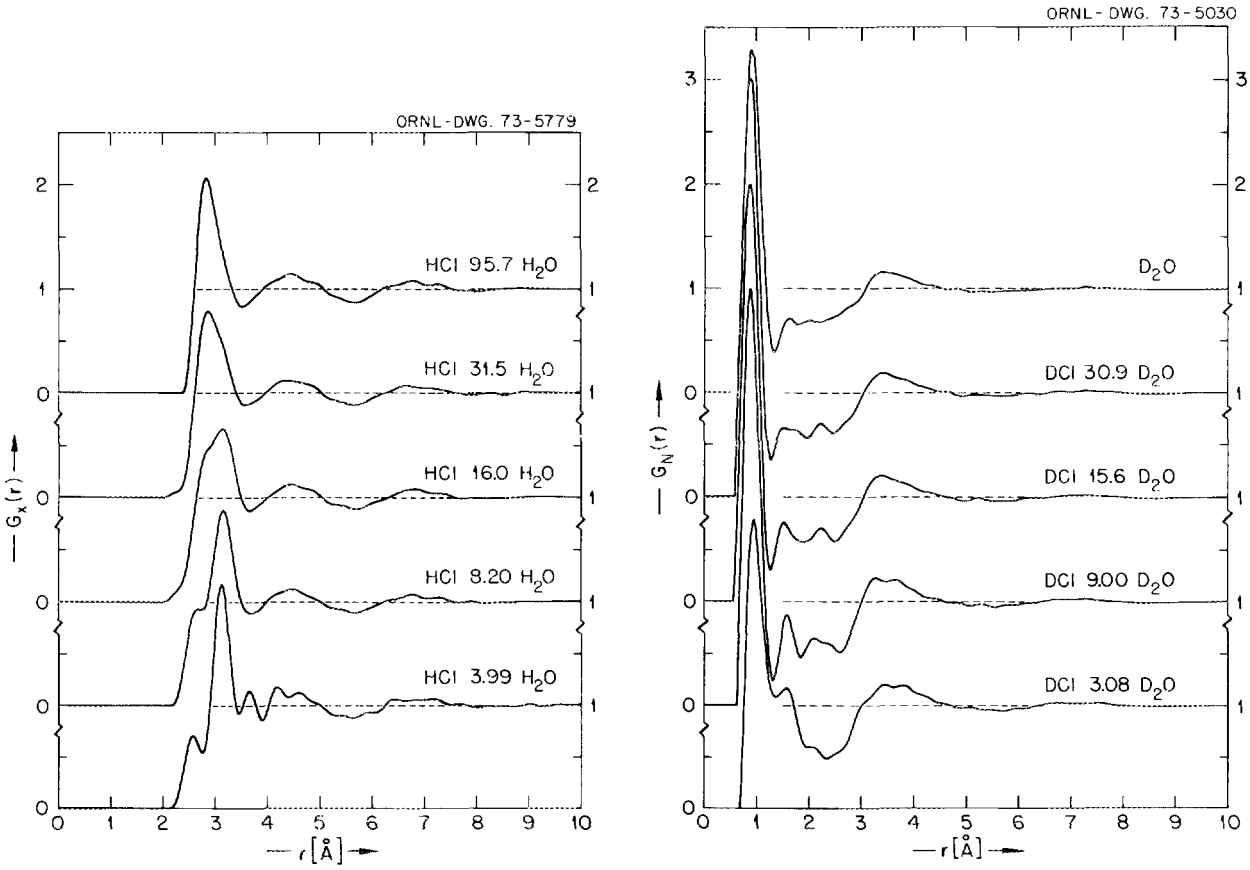

Fig. 7.20. Weighted correlation functions $G_X(r)$ from x-ray and $G_N(r)$ from neutron diffraction from water and HCl (DCl) solutions. In G_X, but not in G_N, the intramolecular O–H and H–H interactions have been removed.

around 4.5 Å and 7 Å in $G_X(r)$ show little change with concentration. We take this as an indication that the general tetrahedral environment, characteristic of water structure, does not undergo drastic qualitative changes when HCl is added to H_2O.

More detailed analysis of the neutron data, as yet incomplete, has clearly demonstrated the existence of D_3O^+ ions in the solutions. Analysis of the x-ray data has shown that these species are strongly hydrogen bonded to four water molecules, forming the "species" $H_9O_5^+$, with an O-O distance of 2.52 Å.

The advantage of complementary data from x-ray and neutron diffraction is again demonstrated, as is also the utility of data covering a wide range of concentration.

1. Visiting scientist from the University of Palermo, Palermo, Italy, 1972–73.
2. A. H. Narten, "Diffraction by Molecular Liquids," a previous contribution in this section, this report.
3. A. H. Narten, F. Vaslow, and H. A. Levy, *J. Chem. Phys.* 58, 5017 (1973).

DIBARIUM CHROMATE(IV), ISOTYPIC WITH RUBIDIUM CHROMATE(VI) AND DIBARIUM TITANATE(IV)

M. A. Bredig[1]

In connection with an investigation by C. Bamberger, Chemical Technology Division, of chromates of various chromium valencies, several x-ray films by H. Dunn, Analytical Chemistry Division, showing a powder pattern of unknown identity were submitted to me for interpretation. Through familiarity with several high-temperature crystal modifications of dicalcium (ortho) silicate, Ca_2SiO_4,[2] it was quickly possible to identify a compound A_2BO_4 of the very common structure type of which K_2SO_4 is usually taken as the prototype. The x-ray patterns thus confirmed the assumption, originally based on more or less indirect chemical considerations, that one of the reaction products obtained was one of the little-known chromates(IV), Ba_2CrO_4, with tetravalent chromium. Indexing of the unknown pattern in accordance with the NBS standard pattern of orthorhombic Rb_2CrO_4 (hexavalent chromium!), which is isotypic with α'-Ca_2SiO_4, or bredigite,[3] yielded the lattice constants of an orthorhombic unit cell containing four molecules Ba_2CrO_4; a = 7.58 ± 0.03 Å, b = 10.35 ± 0.05 Å, c = 5.86 ± 0.03 Å (calculated density: 5.65 ± 0.10 g/cm^3).

Until single crystals of Ba_2CrO_4 are available, the minor possibility remains that this compound actually belongs to the slightly distorted (monoclinic) variety of the same general structure type, of which the other, metastable high-temperature form of Ca_2SiO_4 (ref. 4) (β-Ca_2SiO_4 or larnite) and Ba_2TiO_4 (ref. 5) seem to be the only representatives known at present.

1. Consultant.
2. M. A. Bredig, *J. Phys. Chem.* 46, 747 (1942); 49, 537 (1945); *Amer. Ceram. Soc. J.* 33, 188 (1950).
3. C. E. Tilley and H. C. G. Vincent, *Mineral. Mag.* 28, 255 (1948); cf. also *Amer. Mineral.* 33, 786 (1948).
4. Mrs. C. M. Midgley, *Acta Crystallogr.* 5, 307 (1952).
5. J. A. Bland, *Acta Crystallogr.* 14, 875 (1961).

INFRARED AND RAMAN SPECTROSCOPY

MOLECULAR SPECTROSCOPY[1]

G. M. Begun

Molecular spectroscopy is basic to chemical isotope separation. A detailed knowledge of the vibrational-rotational structure of both infrared and visible-ultraviolet bands is essential to obtain photochemical isotopic effects with laser radiation.[2] Observations and calculations of the fundamental vibrational frequencies of isotopic molecules enable one to predict the equilibrium constants for the chemical exchange systems frequently used to separate the isotopes of the light elements. Molecular spectroscopy, especially Raman spectroscopy, is one of the most active regions of scientific investigation today. For these reasons we maintain a research effort in these fields which results in collaborative studies with other investigators.

For some years the technology of molten salts has been studied at ORNL, and Raman spectra have proven to be a powerful tool in revealing the species present in such mixtures. Recently we have obtained the laser Raman spectra of a number of halide melts at elevated temperatures. The spectra were taken as described previously.[3] Briefly, melted samples were illuminated with light from a helium-neon or an argon-ion laser, and spectra were recorded by means of a Cary model 81 Raman monochromator coupled with a photon counting system. Raman spectra were obtained for several group I-B halide mixtures with alkali halides. Spectra were obtained for CsCl-AgCl, KBr-AgBr, KI-AgI, CsCl-CuCl, and KCl-$AuCl_3$ mixtures. These spectra are shown in Figs. 7.21–7.23, and the data are summarized in Tables 7.5–7.7.

Since, in the case of the AgCl, AgBr, AgI, and CuCl melts only one broad polarized line was observed, interpretation of the results is not unambiguous. A paper is in preparation in which comparisons are made with solid and solution data for similar systems. The

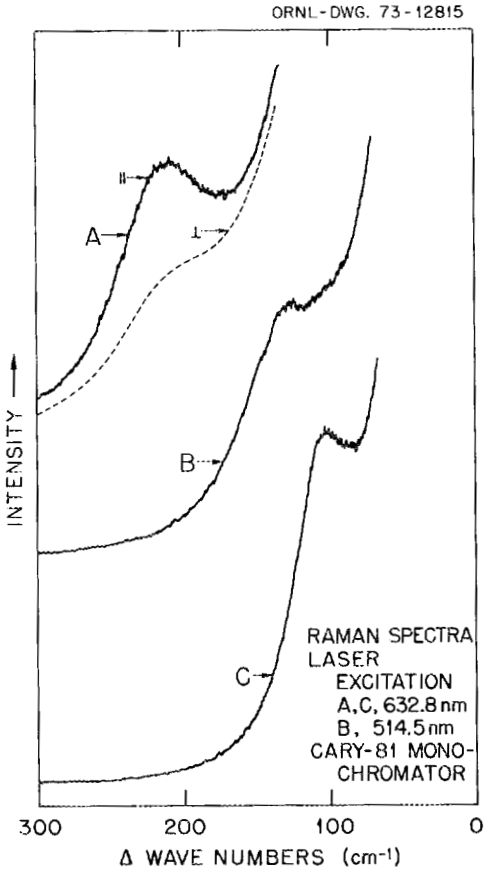

Fig. 7.21. Raman spectra of molten equimolar mixtures. *A*, CsCl-AgCl; *B*, KBr-AgBr; *C*, KI-AgI.

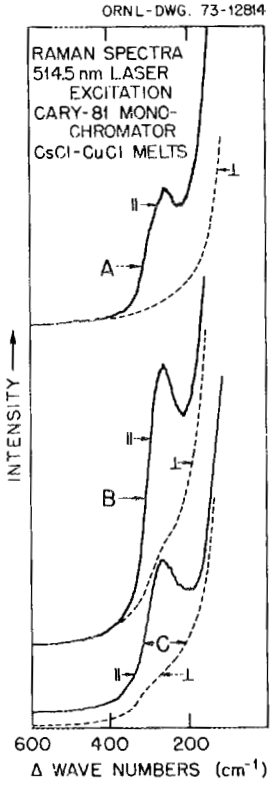

Fig. 7.22. Raman spectra of molten mixtures. *A*, 2CsCl-CuCl; *B*, CsCl-CuCl; *C*, CsCl-2CuCl.

spectrum of the $KCl\text{-}AuCl_3$ melt agrees well with that of the polycrystalline solid and that of the aqueous solution. The Raman pattern is that of a square planar $AuCl_4^-$ ion. This ion is clearly present in the $KCl\text{-}AuCl_3$ melt.

In order to examine the spectrum of highly corrosive fluoride melts at temperatures up to 900°C, a new Raman furnace was built consisting of an insulating firebrick, an outer quartz tube with small holes for the laser beam, an inner quartz tube wrapped with platinum heating wire, and finally a graphite "crucible" with four small holes at 90° to each other for the laser and Raman light. This type of windowless sample cell in which the sample is held by surface tension has been described elsewhere.[4] Initial Raman spectra of $LiF\text{-}NaF\text{-}AlF_3$ mixtures are shown in Figs. 7.24–7.26. These Raman spectra are by far the best obtained to date of these difficult-to-work-with materials. Our initial interpretation of these curves is that the peak near 626 cm^{-1} is characteristic of the tetrahedral AlF_4^-

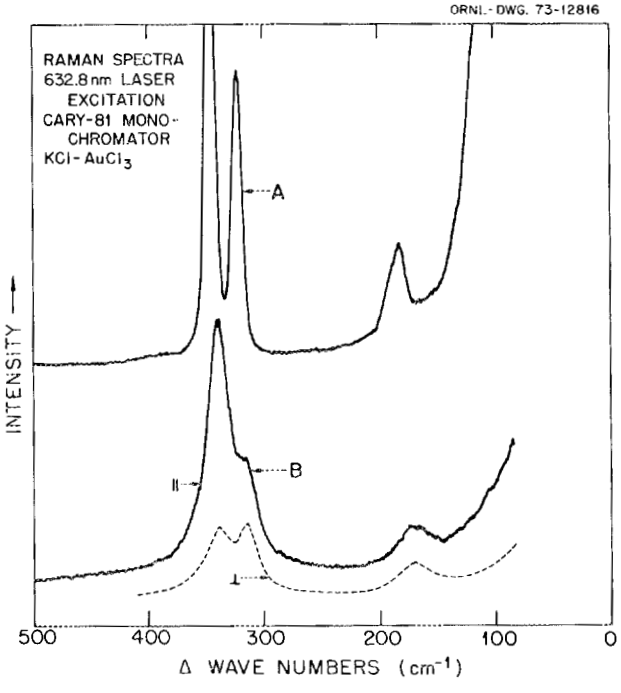

Fig. 7.23. Raman spectra of equimolar $KCl\text{-}AuCl_3$ mixtures. *A*, polycrystalline mixtures; *B*, melt.

Table 7.5. Raman frequencies of molten alkali halide–silver halide mixtures

p = polarized line

CsCl-AgCl		KBr-AgBr, 50-50 mole %	KI-AgI		
50-50 mole %	66.7-33.3 mole %		33.3-66.7 mole %	50-50 mole %	66.7-33.3 mole %
207 cm^{-1} (p)	211 cm^{-1} (p)	126 cm^{-1} (p)	100 cm^{-1} (p)	100 cm^{-1} (p)	100 cm^{-1} (p)

Table 7.6. Raman frequencies of molten CsCl-CuCl mixtures

sh = shoulder, p = polarized line

33.3-66.7 mole %	50-50 mole %	66.7-33.3 mole %
254 cm^{-1} (p)	255 cm^{-1} (p)	257 cm^{-1} (sh, p), 248 cm^{-1} (p)

Table 7.7. Raman frequencies of equimolar KCl-$AuCl_3$ Mixtures

s, strong; m, medium; sh, shoulder; w, weak; b, broad; p, polarized

Solid	Molten	Aqueous[a]	Assignment
348 cm^{-1} (s)	339 cm^{-1} (s, p)	347 cm^{-1} (s, p)	ν_1
322 cm^{-1} (m)	318 cm^{-1} (m, sh)	324 cm^{-1} (m)	ν_4
182 cm^{-1} (w, b)	171 cm^{-1} (m, b)	171 cm^{-1} (w, b)	ν_2

[a]Literature values.

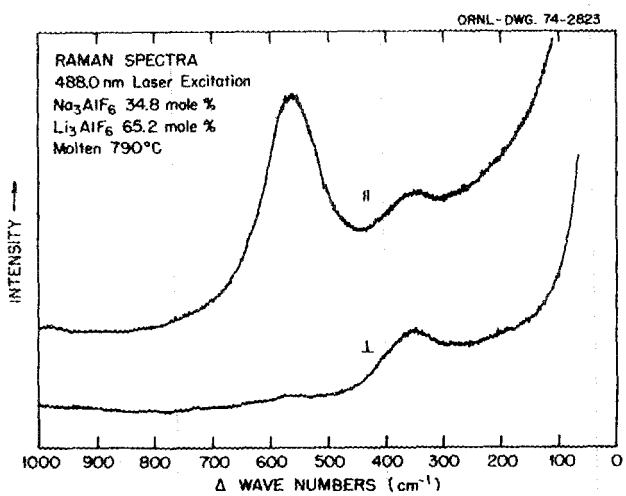

Fig. 7.24. Raman spectrum, molten Na_3AlF_6 (34.8 mole %) plus Li_3AlF_6 (65.2 mole %), 790°C.

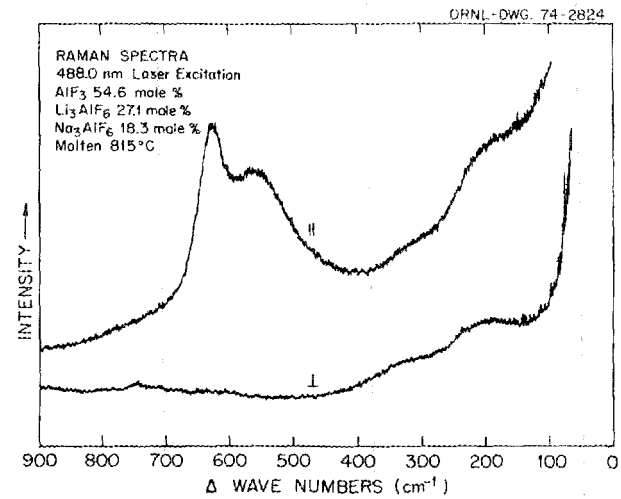

Fig. 7.25. Raman spectrum, molten AlF_3 (54.6 mole %) plus Li_3AlF_6 (27.1 mole %) plus Na_3AlF_6 (18.3 mole %), 815°C.

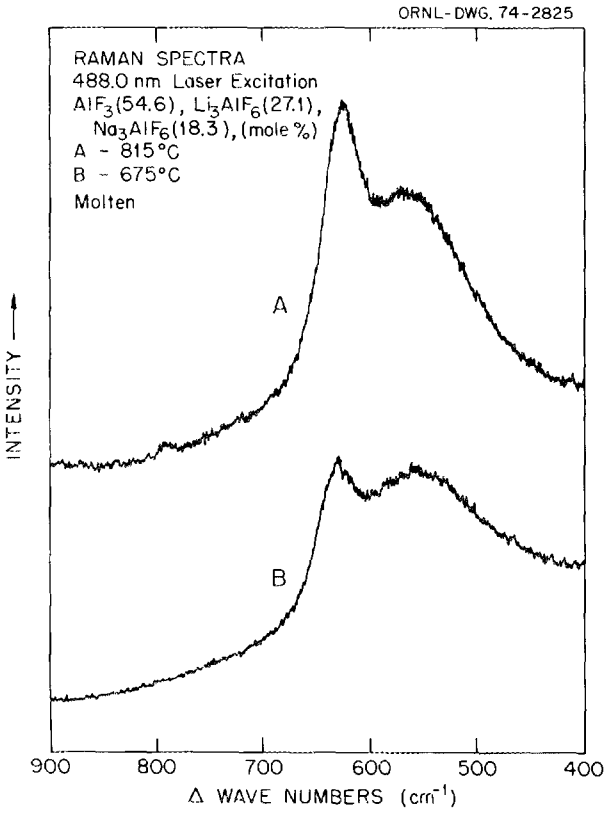

Fig. 7.26. Raman spectra, molten AlF_3 (54.6 mole %) plus Li_3AlF_6 (27.1 mole %) plus Na_3AlF_6 (18.3 mole %). *A*, 815°C; *B*, 675°C.

ion, while the peak near 550 cm^{-1} characterizes the octahedral AlF_6^{3-} ion. Especially interesting is the change in the relative intensities of the two peaks (Fig. 7.26) which takes place with variation of the sample temperature and indicates a shift in the equilibrium between AlF_6^{3-} and AlF_4^- with temperature. This work is continuing and we hope completely to characterize these ions spectroscopically.

1. B. Gilbert and G. Mamantov, Department of Chemistry, University of Tennessee, Knoxville, collaborated on some of this work.

2. G. M. Begun and W. H. Fletcher, "Laser Photochemical Isotope Separation," a contribution in chap. 3, this report.

3. G. M. Begun, *Chem. Div. Annu. Progr. Reps. May 20, 1970*, ORNL-4706, p. 92; *May 20, 1972*, ORNL-4791, p. 56; *May 20, 1973*, ORNL-4891, p. 55.

4. J. P. Young, *Inorg. Chem.* **6**, 1486 (1967).

INFRARED STUDY OF ADSORPTION SPECIES OF WATER ON MONOCLINIC AND TETRAGONAL ZIRCONIUM OXIDE AS A FUNCTION OF TEMPERATURE

P. A. Agron

The physical and chemical adsorption of several gaseous species on high-surface-area thorium and zirconium oxides has received extensive study here[1] because of their ceramic and catalytic properties. The infrared spectrum of the adsorption species of water vapor on thorium oxide has been reported[2] earlier. A double-beam Beckman IR-12 filter-grating spectrophotometer, modified to encompass high-temperature adsorption studies, was described in the latter study.[3]

The fluorite structure observed for thorium oxide is modified somewhat in the monoclinic[4] and tetragonal[5] forms of zirconium oxide. The pseudo fluorite packing of the monoclinic phase shows a packing of seven oxygen atoms about each cation, whereas the cation is coordinated to eight oxygen atoms in the tetragonal structure. A transformation to the fluorite structure occurs at elevated temperatures or on introduction of trace quantities of a larger cation. The spatial arrangement of the surface atoms of the zirconium oxides affects the observed spectra of adsorbed water molecules.

The monoclinic ZrO_2-G and the tetragonal ZrO_2-C samples, selected for the present infrared study, have been characterized by gravimetric adsorption studies[1] and by heat of water immersion measurements.[6] The BET surface areas for the respective monoclinic and tetragonal zirconium oxides are 23.7 and 52.7 m^2/g, corresponding to an estimated average particle size of 430 and 190 Å. Suitable self-supporting disks for transmission spectroscopic study were obtained by subjecting 300-mg samples of the oxides to 40,000 psi in a $^{13}/_{16}$-in die.

The adsorption-desorption cycling studies of water vapor at ambient temperatures of 40 to 500°C were followed with transmission spectra in the frequency region of 2400 to 4000 cm^{-1} for both polymorphs. The bending frequency spectrum of water molecules bound on the surface of the monoclinic ZrO_2-G disk was observed as a function of concentration. Repeated exposures of these high-surface-area oxides to a maximum vapor pressure of 4.6 torr of water at the elevated temperatures produced a partial resolution of vibrational frequency bands which may be associated with chemisorbed and physisorbed species.

Monoclinic ZrO_2-G

Exposure of the oxide to 4.6 torr of H_2O at 40°C results in a broad unresolved absorption band over the region from 2400 to 3800 cm^{-1}. This broad spectral band is attributed to the large extinction coefficient[7] of hydrogen-bonded water molecules adsorbed on the oxide surface. This absorption band is unresolved at 400°C and 4.6 torr of water vapor (Fig. 7.27*a*); however, the absorbance in the lower frequency region of this broad band is reduced to a large extent compared with that observed at 40°C. This is indicative of the presence of a lower concentration of multimeric hydrogen-bonded water molecules. On reducing the concentration of water adsorbed on the oxide by outgassing at 10^{-5} torr at elevated temperatures, a partial resolution of several underlying frequency bands emerges (Fig. 7.27).

The absorbance spectra of the higher frequency bands (Fig. 7.28) show an improved resolution on reducing the temperature from 500 to 100°C under vacuum conditions. The two higher frequency bands are assigned to chemisorbed O-H groups[8] (Table 7.8). Assuming that the extinction coefficient is similar for both these bands, the 3760-cm^{-1} band at the indicated lower concentration is assigned to O—H groups coordinated to a single cation, occupying an oxygen site at the corners and edges of crystallite faces. The 3660-cm^{-1} band is attributed to hydroxyl species on oxygen sites of low-index faces, which thus are shared by more than a single cation. The respective species are designated schematically in Table 7.8. The broader spectral subbands observed at 3580 and 3480 cm^{-1} are assigned to bound water species (Table 7.8).

Exchange studies with D_2O at 40°C are shown in Fig. 7.29. Corresponding spectral stretch frequency bands appear for the light and heavy adsorbed species. The correlation of these frequency bands is given in Table 7.8.

The bending frequency for the H_2O monomer isolated in low-temperature matrix studies has been assigned[6] values in the range of 1590 to 1600 cm^{-1}. At higher concentrations, the presence of hydrogen-bonded molecular water increases this bending frequency to 1650 cm^{-1}. In the present study, the shift of the bending frequency band on the zirconium oxide as a function of water concentration at 40°C is shown in Fig. 7.30.

Tetragonal ZrO_2-C

Analogous adsorption-desorption studies of water sorbed on the tetragonal ZrO_2-C disk were observed. Figure 7.31 shows the absorbance spectra of the outgassed oxide at successive elevated temperatures. The relatively narrow bands at 3725 and 3662 cm^{-1} are assigned to O—H species bound to cations at oxygen

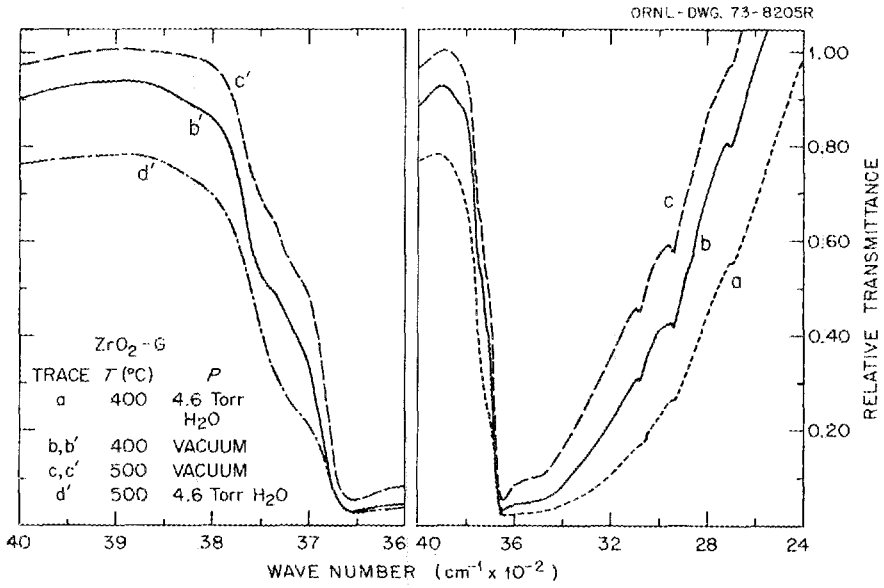

Fig. 7.27. Transmission spectra, 2400–4000 cm^{-1} region, adsorption-desorption of H_2O on ZrO_2-G at 400 and 500°C. *a*, Adsorption of H_2O at 4.6 torr and 400°C; *b*, outgassed sample at 400°C; *b′*, same on a fourfold expanded scale, 3600–4000 cm^{-1}; *c*, outgassed sample at 500°C; *c′*, same, on a fourfold expanded scale, 3600–4000 cm^{-1}; *d′*, adsorption of H_2O at 4.6 torr and 500°C.

lattice sites. The 3725-cm^{-1} band, with an estimated half-width of 70 cm^{-1} at 300°C, is attributed to O–H anions bound to a single cation at corners and edges of the irregularly stepped crystal faces. The 3662-cm^{-1} band, with a broader half-width, is assigned to hydroxyls coordinated to more than a single cation on low-index faces. These high-frequency bands are designated schematically in Table 7.9. The broader bands observed at 3595 and 3440 cm^{-1} wave numbers are assigned to bound water species (Table 7.9).

D_2O exchange at 300°C produced corresponding bands for both D_2O and H_2O species (Fig. 7.32). The

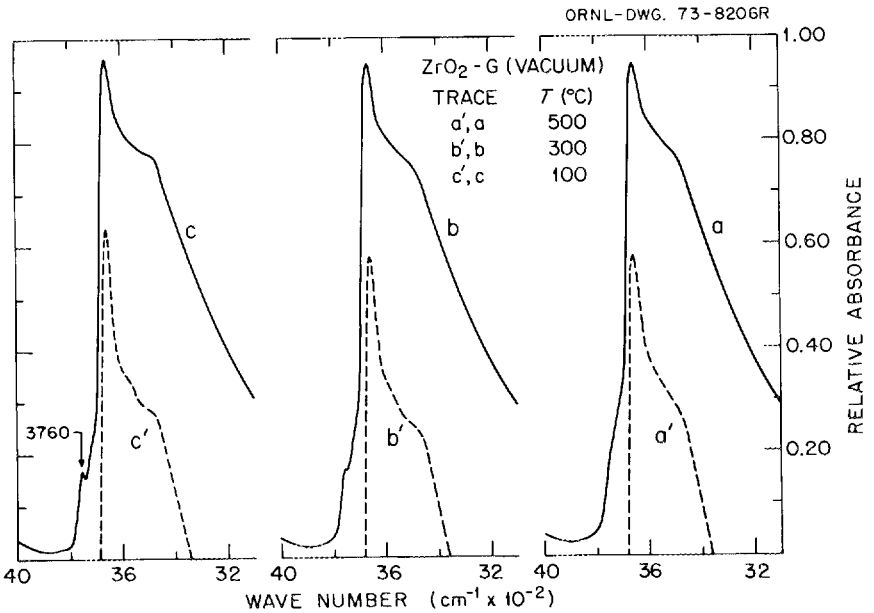

Fig. 7.28. Absorbance spectra, 3100–4000 cm^{-1} region, of H_2O on ZrO_2-G at 500, 300, and 100°C. *a*, outgassed sample at 500°C; *a′*, same, on a twofold expanded absorbance scale; *b*, sample cooled under vacuum to 300°C; *b′*, same, on a twofold expanded absorbance scale; *c*, sample cooled under vacuum to 100°C; *c′*, same, on a twofold expanded absorbance scale.

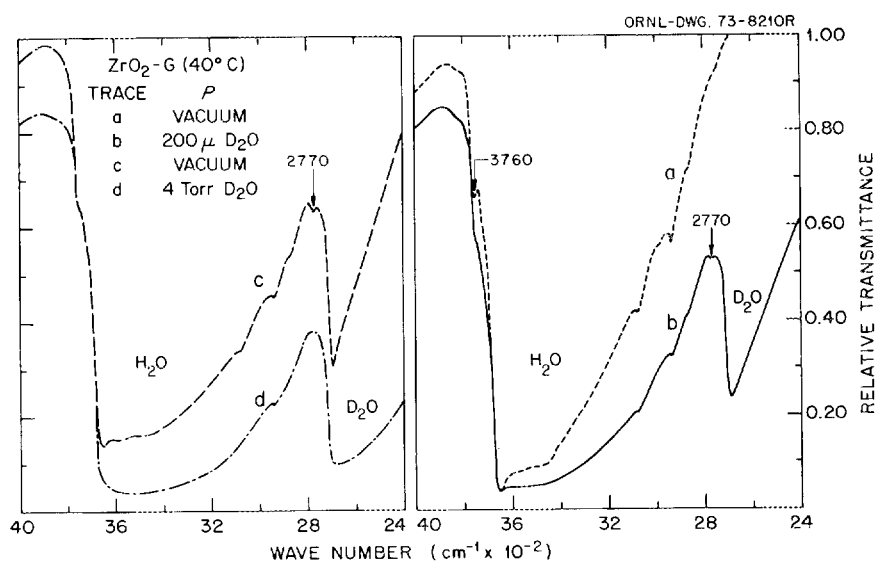

Fig. 7.29. Transmission spectra of D_2O exchange on ZrO_2-G, 2400–4000 cm^{-1} region, at 40°C. *a*, sample reduced to 40°C in vacuum, following extended desorption of H_2O at 500°C; *b*, exchange of D_2O at 200 μ; *c*, outgassed sample at 10^{-5} torr; *d*, exchange at 4 torr of D_2O.

correlations of the observed stretch frequency bands for both species are listed in Table 7.9. The ratio of the $\nu(O{-}H)/\nu(O{-}D)$ bands is in relatively good agreement with the expected values.

Summary

The difference observed for the stretch frequency of the singly bound hydroxyl anions (Tables 7.8 and 7.9) appears to be a function of the polarization of the anion in these two polymorphic structures. The analogous high-frequency stretch band reported[2] for ThO_2 falls at an intermediate value (3742 cm^{-1}). The stretch frequency for the multiply coordinated hydroxyl anions shows no apparent difference for these tetravalent oxides.

The acidity of the hydroxyl anions on high-surface-area oxides has a marked influence in promoting catalytic reactions. It would be informative to evaluate the catalytic capability of these tetravalent oxides in promoting specific organic reactions. Low-temperature matrix isolation[9] of the intermediates and reaction products[10] would provide a useful approach in understanding the governing mechanisms.

The spectroscopic study of the adsorbed species of water and carbon monoxide on high-surface-area titanium oxide is in progress.

7.8. Stretch vibration frequency bands obtained from sorption of water on monoclinic ZrO_2-G

Spectral species: Schematic representation	Spectral species: Band type	$\nu(O{-}H)$ (cm^{-1})	$\nu(O{-}D)$ (cm^{-1})
$[Zr{-}(O{-}H)]_M$	$\nu(O{-}H)_M$[a]	3760	2770
$\left[\begin{matrix}Zr\\Zr\end{matrix}\!>\!(O{-}H)\right]_M$	$\nu(O{-}H)_M$[b]	3660	2695
G_2	Bound H_2O	3580	2640
G_3	Bound H_2O	3480	2560

[a]Frequency contribution of surface O–H groups bound to a single cation of the monoclinic phase.
[b]Stretch frequency of bound O–H groups shared by two o three cations.

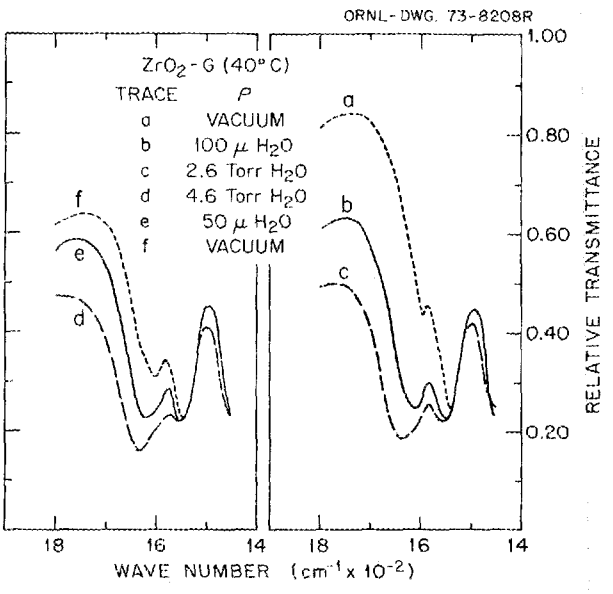

Fig. 7.30. Transmission spectra of the bending region of H_2O adsorbed on ZrO_2-G, 1450–1800 cm^{-1} region, at 40°C. *a*, temperature reduced to 40°C, under vacuum, after outgassing at 500°C; *b*, adsorption of H_2O at 100 μ pressure; *c*, adsorption of molecular water at 2.6 torr of H_2O; *d*, adsorption of molecular water at 4.6 torr of H_2O; *e*, spectral trace on reduction of water pressure to 50 μ; *f*, outgassed sample at 10^{-5} torr.

Table 7.9. Stretch vibration frequency bands obtained from sorption of water on tetragonal ZrO_2-C

Spectral species: Schematic representation	Spectral species: Band type	$\nu(O{-}H)$ (cm^{-1})	$\nu(O{-}D)$ (cm^{-1})
$[Zr{-}(O{-}H)]_T$	$\nu(O{-}H)_T$[a]	3725	2740
$\left[\begin{matrix}Zr\\Zr\end{matrix}\!>\!(O{-}H)\right]_T$	$\nu(O{-}H)_T$[b]	3662	2690
C_2	Bound H_2O	3595	2650
C_3	Bound H_2O	3440	2540

[a]Frequency contribution of surface O–H groups bound to a single cation of the tetragonal oxide.
[b]Stretch frequency of bound O–H groups shared by two or three cations.

1. R. B. Gammage, E. L. Fuller, Jr., and H. F. Holmes, *J. Phys. Chem.* **74**, 4276 (1970); H. F. Holmes, E. L. Fuller, Jr., and R. A. Beh, *J. Colloid Interface Sci.* (in press).
2. E. L. Fuller, Jr., H. F. Holmes, and R. B. Gammage, *J. Colloid Interface Sci.* **33**, 623 (1970).
3. E. L. Fuller, Jr., H. F. Holmes, and R. B. Gammage, *Infrared Studies of Thorium Oxide Surfaces*, ORNL-4378 (March 1969).
4. J. D. McCulloch and K. M. Trueblood, *Acta Crystallogr.* **12**, 507 (1959); D. K. Smith and H. W. Newkirk, *Acta Crystallogr.* **18**, 983 (1965).
5. G. Teufer, *Acta Crystallogr.* **15**, 1187 (1962).
6. H. F. Holmes, E. L. Fuller, Jr., and R. B. Gammage, *J. Phys. Chem.* **76**, 1497 (1972).
7. G. C. Pimentel, p. 107 in *Hydrogen Bonding*, D. Hadži, ed., Pergamon Press, New York, 1959.
8. L. H. Little, *Infrared Spectra of Adsorbed Species*, Academic Press, New York, 1966; M. L. Hair, *Infrared Spectroscopy in Surface Chemistry*, Marcel Dekker, New York, 1967.

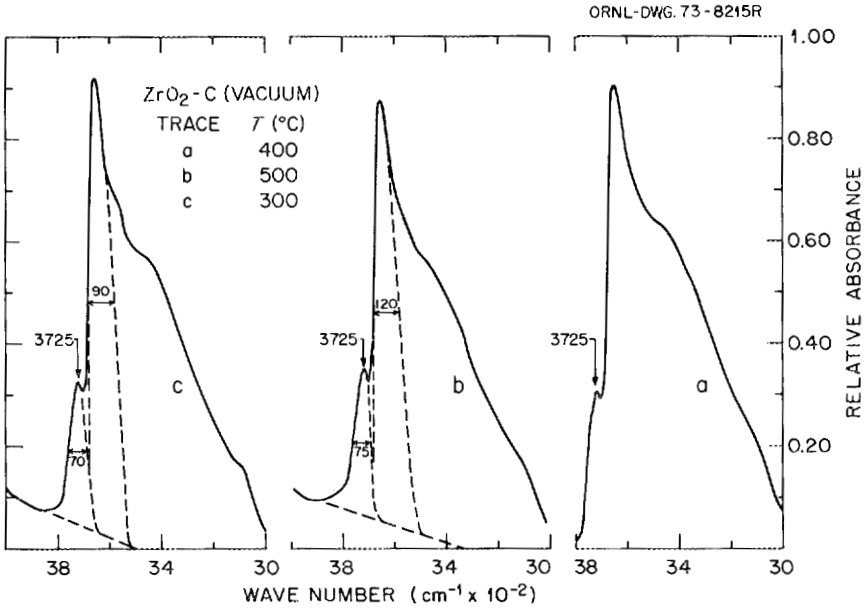

Fig. 7.31. Absorbance spectra, 3000–4000 cm^{-1} region, of ZrO_2-C at 400, 500, and 300°C (first cycle). *a*, absorbance spectra of sample desorbed at 400°C at 6 X 10^{-6} torr; *b*, desorption temperature raised to 500°C at 3 X 10^{-5} torr; *c*, desorption temperature reduced to 300°C at 2.5 X 10^{-6} torr.

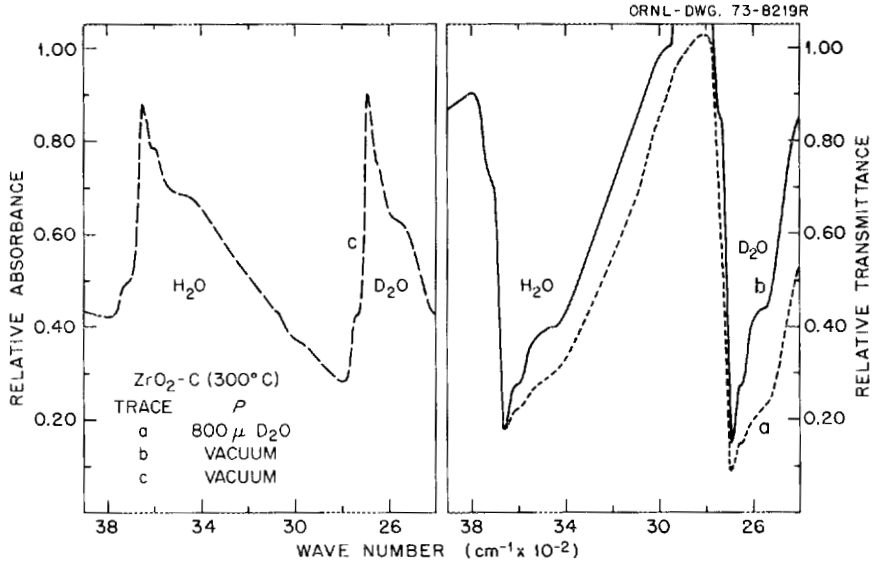

Fig. 7.32. Transmission and absorbance spectra of D_2O exchange on ZrO_2-C, 2400–4000 cm^{-1} region, at 300°C. *a*, transmission spectra of sample exposed to 800 μ of D_2O at 300°C; *b*, desorption of above-treated sample, *c*, absorbance spectral trace of *b* using a twofold reduced scale factor.

9. H. E. Hallam, ed., *Vibrational Spectroscopy of Trapped Species*, Wiley, New York, 1973.
10. M. M. Rochkind, *Anal. Chem.* **40**, 762 (1968).

MICROWAVE AND RADIO-FREQUENCY SPECTROSCOPY

ELECTRON SPIN RESONANCE STUDIES OF LIQUIDS DURING PHOTOLYSIS: PEPTIDES

Ralph Livingston David Doherty[1] Henry Zeldes

During the year a few Bence-Jones proteins obtained from Alan Solomon of the University of Tennessee Memorial Research Center were photolyzed in aqueous solution. Broad ESR signals were obtained, and even though the intensities of the signals were quite different for the two proteins studied, which might serve as the basis of an empirical study, it was apparent that very little could be said about the nature of the radicals from a direct analysis of the spectra. This work, however, was part of the impetus to study simple peptides in the hope that the spectra could be analyzed in detail and that any systematic trends might carry over to more complex systems. The study is a cooperative venture with the Biology Division.

Glycylglycine was initially studied, but unlike the proteins, signals were not obtained upon photolysis in aqueous solution. The addition of a small amount of hydrogen peroxide (about 1%), however, did give an excellent, well-resolved spectrum from a single radical. Under these conditions, photolysis of the peroxide gives ·OH, and the observed radical is the product of ·OH attack on the peptide, a process of great importance in radiation biology. The glycylglycine was present as the zwitterion. Upon adding acid the spectrum broadened and became weaker. No spectrum was obtained from the hydrochloride. In all of the work described here the peptides were in nearly neutral aqueous solutions containing about 1% hydrogen peroxide.

The finding of only a single radical from glycylglycine was of great interest. The peptide and also the resulting radical may exist in cis and trans forms. It is well known that there is a lack of free rotation about the peptide bond, and the trans isomer is presumably the more stable form. Each of the radicals described here is a single isomer, and presumably it is the trans configuration. There are two likely positions in glycylglycine, either CH_2 group, from which ·OH might abstract hydrogen, but it was clear from the spectrum that attack is selective for only one of these positions. There is ambiguity for glycylglycine, but there is no ambiguity for assignments of the radicals from β-alanylglycine, L-alanylglycine, and glycyl-L-alanine (Fig. 7.33), where here too only a single radical was formed. The assignment for glycylglycine was taken by comparison with these peptides. In each case the hydrogen that is abstracted comes from the carbon adjacent to the nitrogen of the peptide link. There is also ambiguity in the assignment of the radical studied from glycyl-β-alanine (Fig. 7.33), the two possible choices being abstraction from either of the adjacent CH_2 groups. (This peptide gave spectra from more than one radical.) The choice illustrated was made by comparison with the other peptides.

This study is in its initial stages but already illustrates systematics in the nature of ·OH attack and in the values of hyperfine couplings and g values. It is planned to extend the work to other dipeptides and then to more complex peptides.

1. Biology Division.

ORNL-DWG. 74-4550

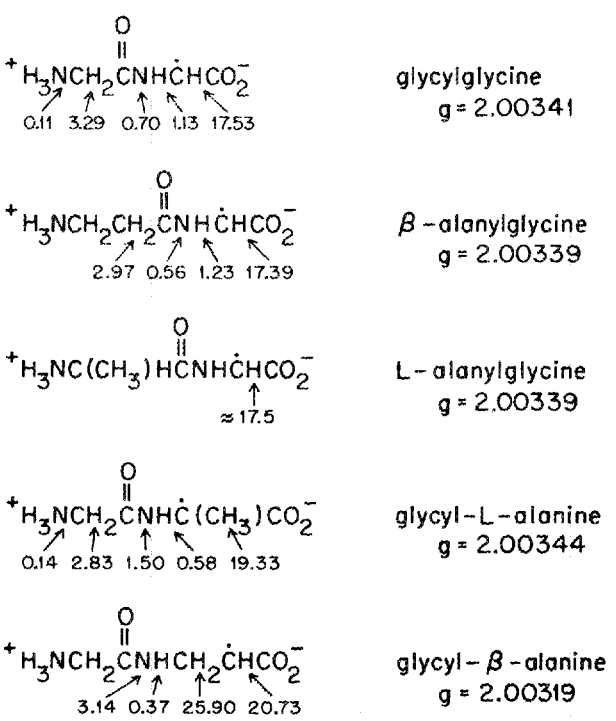

Fig. 7.33. The formulas show the radical formed by ·OH attack in aqueous solution of the indicated dipeptide. Hyperfine couplings given under each formula are in gauss.

ORNL-DWG. 73-6072A

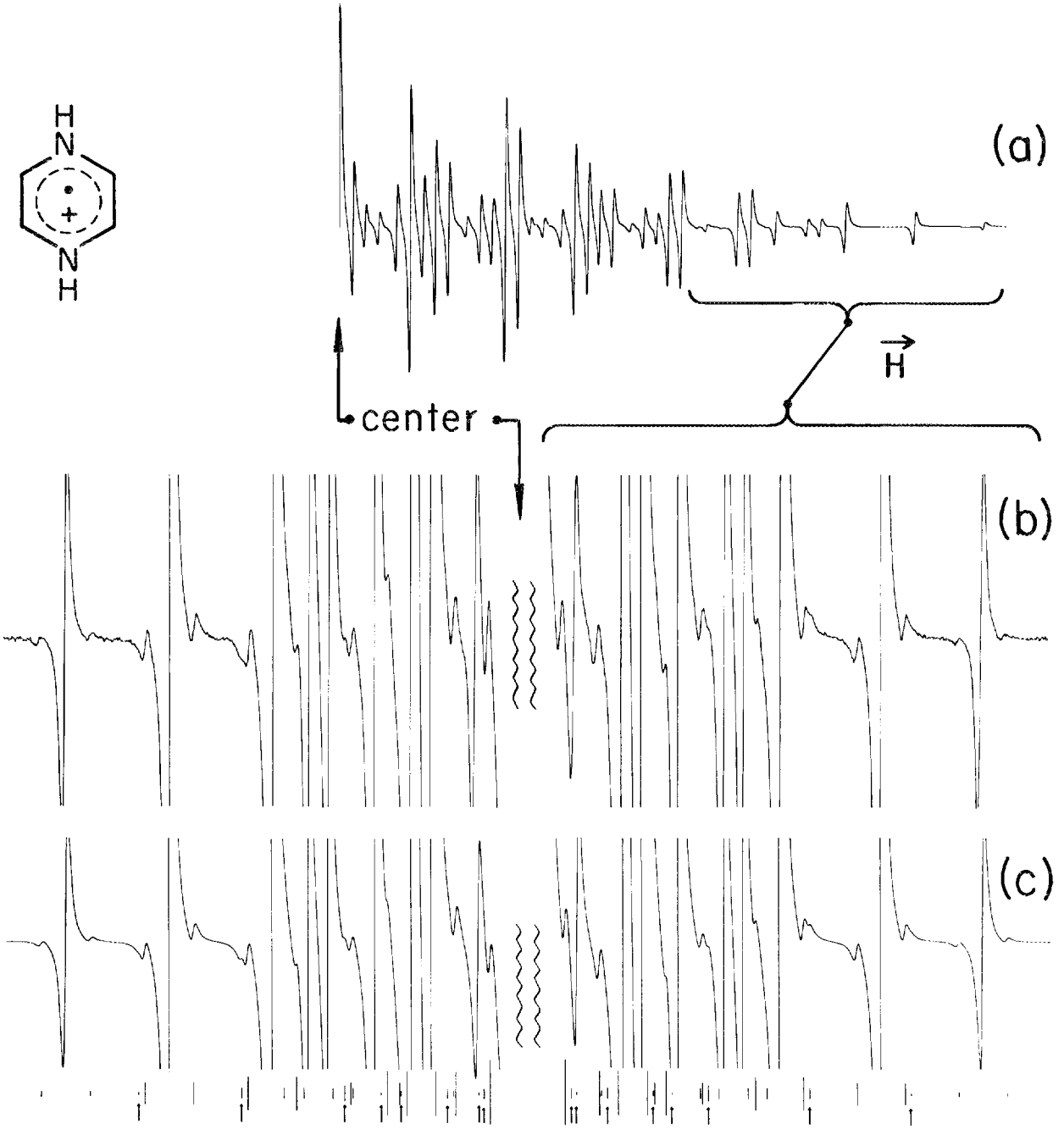

Fig. 7.34. Electron spin resonance spectra of 1,4-dihydropyrazine cation in aqueous solution near room temperature. *a*, recorded with low gain; *b*, some of the outermost lines recorded with high gain; *c*, a simulation of the outermost lines. The stick spectrum locates lines of ^{15}N (identified by arrows) and of ^{13}C.

ELECTRON SPIN RESONANCE STUDIES OF LIQUIDS DURING PHOTOLYSIS: HETEROCYCLIC COMPOUNDS CONTAINING NITROGEN[1]

Henry Zeldes Ralph Livingston

π-Electron heterocyclic radicals containing nitrogen which are present during photolysis of solutions near room temperature have been under study by electron spin resonance with the aims of identifying the radicals, determining the mechanisms of their formation and subsequent reactions, and determining improved relationships between the hyperfine couplings and π-electron spin density. The radicals studied result from the reduction of parent conjugated heterocyclic compounds. In some cases the parent compound is photolyzed in a solution containing isopropyl alcohol. The heterocycle becomes excited, probably to a triplet state, and abstracts a hydrogen atom from the alcohol to form a radical. The abstracted hydrogen usually attaches to nitrogen. In other cases, acetone as well as isopropyl alcohol is incorporated in the solutions. An excited acetone molecule abstracts a hydrogen atom from isopropyl alcohol to form the hydroxyisopropyl radical, which in turn donates an electron to the heterocyclic compound. Electron capture is followed by protonation of the ring nitrogen, and in those cases where there are two ring nitrogens, both readily protonate.

In the case of pyrazine a very intense spectrum (Fig. 7.34) of the diprotonated radical was produced in aqueous solution, making it possible to analyze the ^{13}C hyperfine structure with normal isotopic abundances. The spectrum of the monoprotonated radical was analyzed in a basic solution containing mostly isopropyl alcohol. This yielded the g value and the couplings for all of the nitrogen and hydrogen atoms.

A study has been completed on four radicals present during photolysis of solutions of 3,5-pyridinedicarboxylic acid and its anions. Radicals **I**, **II**, and **III**, respectively, result from hydrogen atom attachment to the nitrogen atom of the dicarboxylic acid, its monoanion, and its dianion. The pK values for the ionization of **I** and of **II** in aqueous solution have been measured. The spectrum of **II** strongly suggests that the carboxylic acid proton switches between the two equivalent positions for this proton is such a way that the radical is nearly always in one of the two equivalent conformations; the switching does not occur by way of ionization. A fourth radical has been made by the attachment of hydrogen to a carbon adjacent to the nitrogen of the excited parent dianion. Hyperfine couplings and g values have been deduced for all four radicals.

1. This is an expanded abstract of a paper appearing in *Mol. Phys.* 27, 261 (1974) and a paper in press with *Radiation Research.*

ELECTRON SPIN RESONANCE STUDY OF THE HYDROXYL RADICAL IN SINGLE CRYSTALS OF POTASSIUM HYDROXYLAMINE DISULFONATE

R. W. Holmberg

The formation of the hydroxyl radical (·OH) at low temperatures with ionizing radiation has been reported in ice and in a number of single crystals which contained water of hydration. It has been suggested[1] that the ·OH is produced by the transfer of a proton from H_2O^+ formed transiently during the radiolysis. Kinetic studies reported here indicate that ·OH may also be formed by the transfer of a hydrogen atom from a water molecule.

In a recent ESR investigation[2,3] of the free radicals in gamma-irradiated potassium hydroxylamine disulfonate $[K_2(SO_3)_2\ NOH{\cdot}2H_2O]$, it was observed that the hydroxyl radical is formed and another radical destroyed when the irradiated crystal is photolyzed with incandescent light at 77°K. The destroyed radical, exhibiting large hyperfine splittings from one nitrogen and one hydrogen, was tentatively identified[2] as $\dot{H}ON(SO_3)_2^-$. This identification is now open to serious question;[3] it will be designated as ·AH for the purposes of this discussion.

Studies have been carried out with crystals containing hydrogen, deuterium, and mixed hydrogen and deuterium. Rates of growth and decay of the ESR lines from ·OH and ·AH and their deuterated forms have been monitored. These results indicate that the reaction involves the reversible transfer of a hydrogen atom between H_2O and ·AH pairs fixed in the lattice:

$$\cdot AH \text{ --- } H_2O \underset{k}{\overset{h\nu}{\rightleftarrows}} AH_2 \text{ --- } \cdot OH\,.$$

Hydrogen and deuterium are transferred with roughly the same efficiency on photolytic excitation. The decay of ·OH and the regrowth of ·AH are both first order with the same rate and are very strongly isotope dependent. The rate constant for the transfer of hydrogen from AH_2 is 0.046 min^{-1} at 77°K and 0.0081 min^{-1} at 63°K, from which an activation energy of 1.2 kcal/mole is calculated. In a deuterated crystal,

no decay of ·OD was observed at 77°K in five days; the rate constant for deuterium transfer is estimated to be less than that for hydrogen by a factor of at least 1500. The transfer of hydrogen from ADH is first order with a rate constant about one-half of that from AH_2. This suggests that hydrogen and deuterium are exchanging positions in ADH rapidly at 77°K.

1. M. Iwaski et al., *J. Chem. Phys.* **57**, 3187 (1972).
2. R. W. Holmberg and B. J. Wilson, *Chem. Div. Annu. Progr. Rep. May 20, 1973*, ORNL-4891, p. 141.
3. R. W. Holmberg and B. J. Wilson, *J. Chem. Phys.* (in press).

ELECTRON SPECTROSCOPY

PHOTOIONIZATION OF NEON BETWEEN 100 AND 2000 eV; SINGLE AND MULTIPLE PROCESSES, ANGULAR DISTRIBUTIONS, AND SUBSHELL CROSS SECTIONS[1]

F. Wuilleumier[2] M. O. Krause

A complete partition of the photoionization cross section into its partial cross sections, with differentiation according to single and multiple processes, is much needed if we are to deepen our understanding of the photon-atom interaction and improve the reliability of total and partial cross-section values. Experimental data are especially needed in the ultrasoft x-ray range, $h\nu \lesssim 2$ keV, where the photon interacts with electrons in the outer regions of the atom. In these regions, electron-electron correlation may play an important role, and subshell cross sections may show irregular patterns. Reliable subshell cross sections are essential to quantitative chemical analysis by photoelectron spectrometry, whether applied in its conventional ESCA mode or the new x-ray (PAX) mode, and by fluorescence x-ray and Auger-electron spectrometry. Furthermore, the fate and the effects of radiation in matter can be predicted with greater confidence and accuracy if cross sections and interaction processes are well known. To the present time a partition of the total photoionization cross section, which is obtained from standard absorption and ionization-chamber measurements, has not been realized.

In this study, we used the technique of photoelectron spectrometry to delineate all aspects of photoionization in the soft x-ray region and obtain accurate *absolute* cross sections for the various single- and multiple-electron processes in the subshells of a free atom. We selected the neon atom for this investigation, covering the range $100 \lesssim h\nu \lesssim 2000$ eV. The results show that the conventional theories, which are based on the single-particle, frozen-structure model employing the Herman-Skillman potential, overestimate the subshell cross sections by 15 to 35% even for a relatively simple atom such as neon. One might expect larger errors in these theoretical predictions for the heavier elements when shells with high principal quantum numbers are involved for which neither the simple Herman-Skillman potential nor the single-particle approximation are adequate. However, the results show also that a recent calculation of great refinement, the random phase approximation with exchange (RPAE), by Amusia and co-workers, agrees excellently with experimental data in the small range where a comparison could be made. We have reason to believe that the RPAE model, which has not been applied extensively so far, is capable of predicting partial and total photoionization cross sections dependably. By contrast, the simple conventional model, used exclusively and extensively up to now, provides predictions accurate only within a factor of about 2.

1. Expanded abstract of paper accepted for publication in *Physical Review A*.
2. Visiting scientist from Laboratoire de Chimie Physique de la Faculté des Sciences de Paris. Present address: L.U.R.E., Orsay, France.

TOTAL AND PARTIAL ATOMIC LEVEL WIDTHS[1]

O. Keski-Rahkonen[2] M. O. Krause

Total natural level widths are directly related to the lifetime of a hole in that level against decay by radiative and nonradiative processes, and partial widths are proportional to the emission rates of these processes, namely, the radiative, Auger, and Coster-Kronig transitions. These quantities are of special interest in photoelectron, Auger-electron, and x-ray spectrometry, and of general interest in diverse areas of applied and fundamental research. Except for the K and L shells, experimental data of level widths are virtually nonexistent. However, a number of theoretical calculations, covering the K, L, M, and N shells throughout the periodic table, have been made since 1970. These calculations, with a few exceptions, utilize the Herman-Skillman atomic potential, relativistic and nonrelativistic, and in several instances refer only to one or the other of the partial widths or related quantities, as, for example, the radiative rates.

In this contribution we present in a unified manner the data that we have extracted from some 20 theoretical papers. The graphs, Figs. 7.35 and 7.36,

display the total level width Γ, the radiative width Γ_R, the Auger width Γ_A, and the Coster-Kronig width Γ_C for the *K, L, M,* and *N* shells throughout the periodic table and, in several cases, for the region $102 \leqslant Z \leqslant 120$. These graphs are intended to provide a quick survey of magnitude and trends of the level widths and related quantities. Besides the total width Γ, a measurable quantity, the following quantities can be readily obtained from the graphs:

1. lifetime of a single hole, $\tau = \hbar/\Gamma$;
2. total rates S of radiative, Auger, and Coster-Kronig transitions, $S_R = \Gamma_R/\hbar$, etc.;
3. yields of radiative (fluorescence), Auger, and Coster-Kronig transitions: $\omega = \Gamma_R/\Gamma$, $a = \Gamma_A/\Gamma$, and $f = \Gamma_C/\Gamma$ with the condition $\omega + a + f = 1$ since $\Gamma = \Gamma_R + \Gamma_A + \Gamma_C$;
4. widths of x-ray lines: $\Gamma(X \rightarrow Y) = \Gamma(X) + \Gamma(Y)$, where X and Y are the levels involved in the transition; and
5. widths of Auger and Coster-Kronig lines: $\Gamma(X - YZ) \approx \Gamma(X) + \Gamma(Y) + \Gamma(Z)$, where X, Y, and Z are the levels involved.

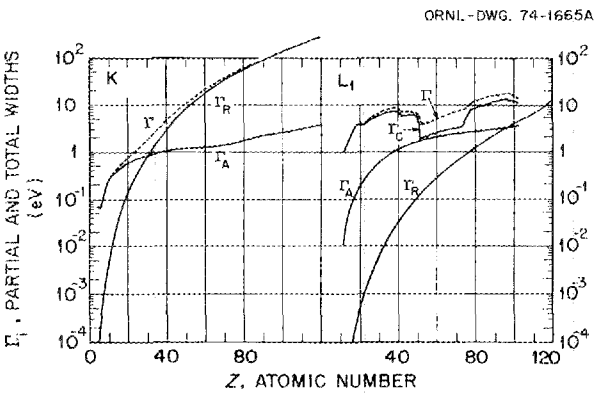

Fig. 7.35. Total and partial atomic level widths in eV, full width at half maximum (FWHM), for *K, L,* and *M* subshells of the elements. Γ = total width; Γ_R = radiative, Γ_A = Auger, and Γ_C = Coster-Kronig widths.

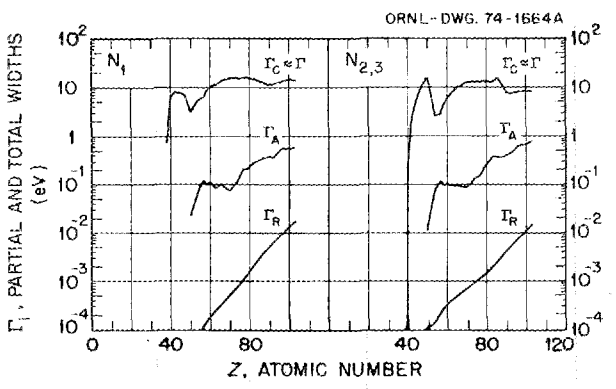

Fig. 7.36. Total and partial atomic level widths for the *N* shell of the elements. Notations same as in Fig. 7.35.

1. Expanded abstract of paper submitted to *Atomic Data and Nuclear Data Tables.*

2. Graduate student from Helsinki University of Technology, Finland, and the University of Tennessee, Knoxville.

ATOMIC AND MOLECULAR COLLISIONS

CROSSED-MOLECULAR-BEAM STUDY OF EXCITED-ATOM REACTIONS: $Hg(6^3P_2)$ WITH CHLORINE AND CHLORINATED METHANE MOLECULES

H. F. Krause S. Datz
S. G. Johnson[1] F. K. Schmidt-Bleek[2]

Numerous experimental methods have been employed to study neutral-neutral chemical reactions produced by metastable atoms,[3] but there have been few reports of single-collision molecular-beam experiments in which the chemical product is detected directly. We have investigated chemiluminescent reactions of metastable mercury atoms with halogenated molecules using molecular-beam techniques, and we report results for the reactant species Cl_2, CCl_4, $CHCl_3$, CH_2Cl_2, and CH_3Cl.

The metastable states of primary interest in these studies were the 6^3P_2 (5.460 eV) and 6^3P_0 (4.667 eV) states. The excited-atom beam was formed by passing an $Hg(6^1S_0)$ beam (120°C) through an intersecting electron beam (current regulated) whose energy was variable ($\Delta E \lesssim 0.25$ eV FWHM for $E \gtrsim 4.0$ eV). The fractionally excited beam was cleansed of secondary electrons and excited states having lifetimes shorter than 10^{-4} sec before it collided with the crossed beam (room temperature). Photons emitted from the beam intersection volume were dispersed by a grating monochromator and detected as pulses by a photomultiplier. The optical system operated in the region from 2400 to 6500 Å and was optimized for single-photon counting.[4]

The major results of these studies are summarized below:

1. $Hg(6^3P_2)$ produces chemiluminescence with Cl_2, CCl_4, and $CHCl_3$ via reaction (1):

$$Hg(6^3P_2) + ACl \rightarrow HgCl(B^2\Sigma^+) + A$$
$$\hookrightarrow HgCl(X^2\Sigma^+) + h\nu\,, \qquad (1)$$

where A = Cl, CCl_3, $CHCl_2$. The same reaction involving $Hg(6^3P_0)$ is exoergic only with Cl_2, and the cross section for it is less than 0.5 times that for $Hg(6^3P_2) + Cl_2$.

2. No chemiluminescence is observed with either CH_2Cl_2 or CH_3Cl on $Hg(6^3P_2)$.

3. Cross sections for the production of 2537-Å emission via intermultiplet relaxation, reaction (2), are much smaller for reactant species that show chemiluminescence than they are for species that do not chemiluminesce:

$$Hg(6^3P_2) + M \rightarrow Hg(6^3P_1) + M^{\dagger}$$
$$\hookrightarrow Hg(6^1S_0) + 2537\ \text{Å}, \qquad (2)$$

$$M = N_2, Cl_2, CCl_4, CHCl_3, CH_2Cl_2, CH_3Cl.$$

4. More highly excited states of mercury having electronic configuration $5d^9 6s^2 6p$ undergo inelastic collisions of the type noted in reaction (3), yielding mercury atomic radiation, but these states do not appear to produce any chemiluminescence with any of the molecular reactants investigated, even though additional final states of HgCl are energetically accessible (i.e., $C^2\Pi_{1/2}, D^2\Pi_{3/2}$):

$$Hg^{**}(5d^9 6s^2 6p) + Cl_2 \rightarrow Hg^*(5d^{10} 6s^1 nl) + Cl_2^{\ddagger}, \qquad (3)$$

where $nl = 6d$, $7s$, or $6p$.

The measured radiation arising from the reactive and inelastic phenomena, reactions (1) and (2) respectively, are shown in Fig. 7.37. For each reactant gas, signal plus noise and noise counts were accumulated at each wavelength, λ, for electron energy fixed at 6.0 eV (where the 6^3P_2 state is optimized). The spectra in Fig. 7.37 were obtained by dividing the accumulated signal counts at each wavelength by the measured monochromator-detector efficiency factors. An optical beam

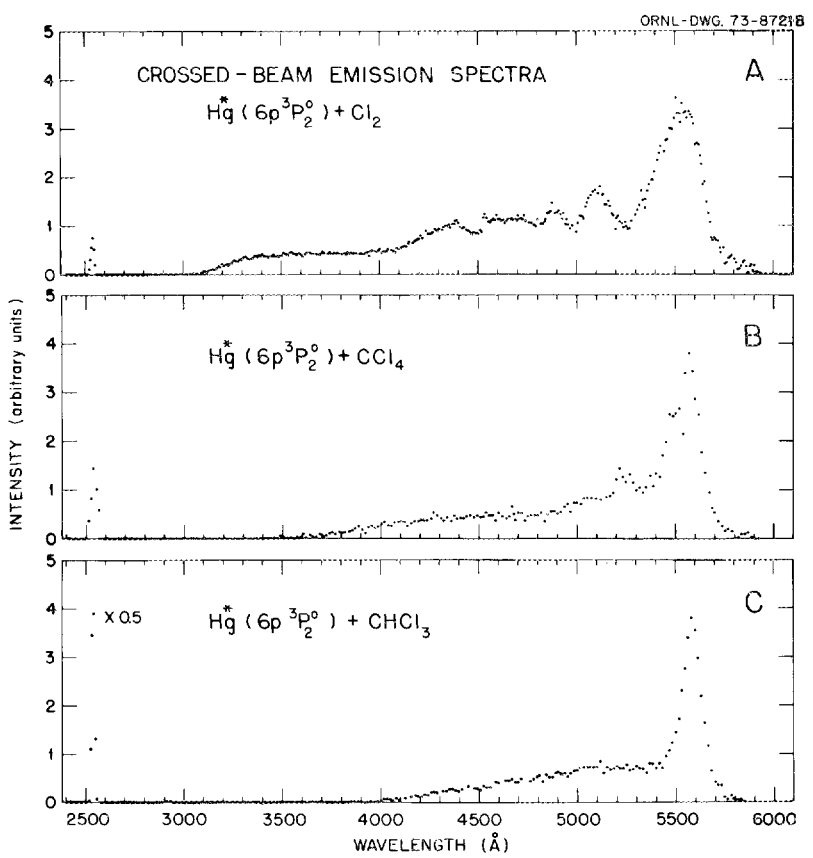

Fig. 7.37. Emission spectra produced by collisions of metastable $Hg(6^3P_2)$ atoms with chlorine and chlorinated methane molecules. (*A*) Chlorine molecules (Δλ = 10 Å FWHM), (*B*) carbon tetrachloride (Δλ = 35 Å), and (*C*) chloroform (Δλ = 35 Å). Radiation in the region from 3000 to 5900 Å corresponds to emission spectra of $HgCl(B^2\Sigma^+ \rightarrow X^2\Sigma^+)$. The 2537-Å radiation corresponds to decaying $Hg(6^3P_1)$ atoms produced in inelastic collisions.

monitor set to record the intensity at 5460 Å ensured that the intensity of both beams was constant throughout the entire wavelength scan of the monochromator. The radiating reaction product was identified using known emission spectra for excited states of the reactant molecules and all possible reaction products.[5] The similarity of the main spectral features displayed in Fig. 7.37 verifies the $HgCl(B^2\Sigma^+)$ identification. The possibility of interfering radiation from excited states of the reactant molecule can only arise in the case of Cl_2. The most intense emission from this source would be expected in the range from 4400 to 5200 Å.

Comparison of the chemiluminescent spectra indicates general patterns of energy disposal in reaction (1). Similarity of the spectra in the region from 5400 to 5700 Å demonstrates that $HgCl(B^2\Sigma^+, v' = 0 \rightarrow 5)$ occurs for Cl_2, CCl_4, and $CHCl_3$. A major difference in the spectra is the location of the short-wavelength emission edge, λ_{min}, which depends on the highest vibrational state of the product created in the reactive collision. The reaction exoergicity, ΔE_B, for formation of $HgCl(B^2\Sigma^+)$ is listed in Table 7.10 for each reactant molecule with $Hg(6^3P_2)$. If all of this energy excess were transferred into vibronic excitation of $HgCl(B^2\Sigma^+)$, the highest vibrational state excited would be v_{max}. The shortest-wavelength emission possible for that degree of excitation is compared with the observed emission edge in Table 7.10.

Table 7.10. The reaction exoergicity, ΔE_B, for formation of $HgCl(B^2\Sigma^+)$ for each reactant molecule with $Hg(6^3P_2)$

If all of this energy excess were transferred into vibronic excitation of $HgCl(B^2\Sigma^+)$, the highest vibrational state excited would be v_{max}. The shortest-wavelength emission possible for that degree of excitation, λ_{min}, is compared with the observed emission edge.

$$Hg(6^3P_2) + ACl \rightarrow HgCl(B) + A + \Delta E_B$$

$$\Delta E_B = E(Hg^3P_2) - D_0^0(ACl) + D_0^0 HgCl(X) - h\nu_{00}(HgCl(B \rightarrow x))$$

ACl	ΔE_B[a] (eV)	Approximate v_{max}	λ_{min} (Å) Calculated	λ_{min} (Å) Observed
Cl_2	1.08	60	3100	3100
CCl_4	0.61	26	3550	3550
$CHCl_3$	0.68	30	3420	~4000
CH_2Cl_2	0.38	17	~4000	
CH_3Cl	0.07	4	~4700	

[a]For $^3P_0$ subtract 0.8 eV.

For Cl_2 and CCl_4, the calculated and observed emission edges coincide using available Cl bond energies (2.475 eV and 2.949 eV respectively[5,6]). The emission edge for $CHCl_3$ differs from that obtained with CCl_4 even though the Cl bond strengths for these species are almost identical.[7] For $CHCl_3$, a maximum of about 50% of the reaction energy is observed in $HgCl(B)$ vibronic excitation, implying a lower effective vibrational temperature of $HgCl(B^2\Sigma^+)$ for the reaction with $CHCl_3$ than for the reaction with CCl_4. Structural differences in the range from 5200 to 5800 Å are consistent with this suggestion.

As noted in Table 7.10, the reaction $Hg(6^3P_0) + Cl_2 \rightarrow HgCl^*(B^2\Sigma^+) + Cl$ is exoergic by 0.28 eV, and photon emission from this reaction is possible in the range from 4000 to 5900 Å. Since $Hg(6^3P_0)$ production is also large at an electron energy of 6.0 eV, it became necessary to establish whether the spectra obtained from Cl_2 shown in Fig. 7.37 could be partially attributed to chemiluminescence produced by $Hg(6^3P_0)$. A test for evaluating the reactivity of $Hg(6^3P_2)$ vs that of $Hg(6^3P_0)$ is to observe crossed-beam photon emission as a function of the electron energy at wavelengths (1) where chemiluminescence can be due only to $Hg(6^3P_2)$ (i.e., 3000 → 4000 Å) and (2) where chemiluminescence can be due to both the 6^3P_2 and 6^3P_0 states (i.e., 4000 → 5900 Å). Since the excitation functions for electron-impact excitation of $Hg(6^3P_2)$ and $Hg(6^3P_0)$ are different,[4,8,9] the excitation function for chemiluminescence should also differ in wavelength regions 1 and 2 above if reactions involving the 6^3P_0 are significant compared with those of 6^3P_2.

Studies of crossed-beam photon emission vs electron energy were performed in the case of Cl_2 not only throughout the range 3000 → 5900 Å but also at 2537 Å [reaction (2)]. Typical results for chemiluminescent emission are shown in Fig. 7.38*A*. The electron energy was calibrated absolutely by extrapolating the data of Fig. 7.38*B* to 5.46 eV assuming a linear threshold law for the 6^3P_2 excitation function. Excitation functions identical to Fig. 7.38*A* were measured throughout the entire wavelength range 3000 → 5900 Å. Between 5.4 and 8.5 eV, the data are in close agreement with previous measurements[8] of the electron excitation function for the 6^3P_2 state. The spectrum shown in Fig. 7.37*A* is, therefore, predominantly due to reactions involving the 6^3P_2 state.

The observed predominance of the chemiluminscent reaction involving the 6^3P_2 state over that due to 6^3P_0 implies either (1) that the electron excitation cross section for 6^3P_0 production is much smaller than that

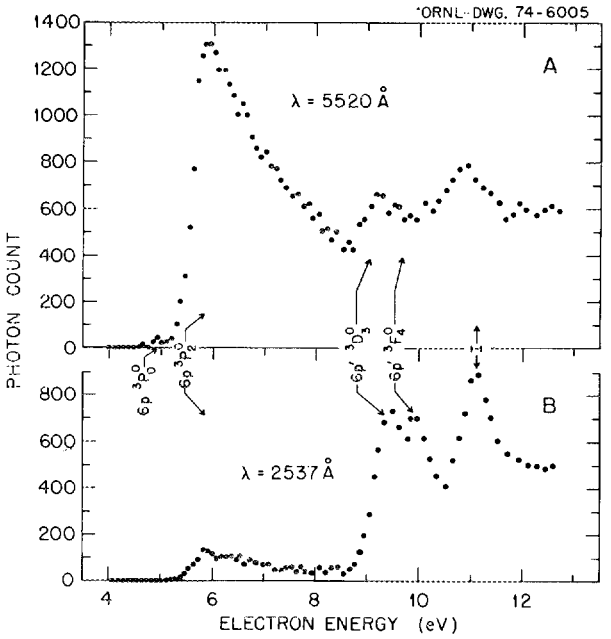

Fig. 7.38. Photon intensity ($\Delta\lambda = 80$ Å FWHM) produced by collisions of metastable mercury atoms with chlorine molecules vs electron energy of the Hg exciter. (*A*) $HgCl(B^2\Sigma^+ \rightarrow X^2\Sigma^+)$ emission, (*B*) $Hg(6^3P_1 \rightarrow 6^1S_0)$ emission. Some excited states of Hg that contribute to these electron excitation functions are known from their appearance potential and resonant structure.

for 6^3P_2 and/or (2) that the Cl_2 reaction cross section for 6^3P_0 is much smaller than that for the 6^3P_2 state. By measuring the ratio of the electron-impact excitation functions for the 6^3P metastable states using an optical-excitation–fluorescence technique[4] we were able to establish that the ratio of reactive cross sections, $\sigma_r(6^3P_0)/\sigma_r(6^3P_2)$, is less than 0.5.

Two comments about the structure above 8.5 eV in Fig. 7.38 are appropriate. First, the structure in Fig. 7.38*B* indicates that several states of the $5d^9 6s^2 6p$ electronic configuration are being excited at the higher electron energies. These states, which must have lifetimes $\gtrsim 10^{-4}$ sec, undergo inelastic collisions [reaction (3)]. These collisions occur with species other than Cl_2 and will be discussed in detail elsewhere.[4] Second, the structure that appears above 8.5 eV in Fig. 7.38*A* is not due to reaction (1) produced by these more highly excited states. This was proved by showing that the electron-impact excitation function for 6^3P_2 is identical to that shown in Fig. 7.38*A* (presumed due to cascade contributions from higher-lying states). Also, no additional chemiluminescent reactions were observed.

1. Graduate student, Department of Chemistry, University of Tennessee, Knoxville.

2. Associate Professor, Department of Chemistry, University of Tennessee, Knoxville.

3. D. H. Stedman and D. W. Setser, *Reactions in Chemical Kinetics*, vol. 6, part 4, Pergamon Press, New York, 1971, p. 193.

4. S. G. Johnson, H. F. Krause, S. Datz, and F. K. Schmidt-Bleek, to be published.

5. Gerhard Herzberg, *Spectra of Diatomic Molecules*, vol. I, Van Nostrand, New York, 1950.

6. J. B. Farmer et al., *J. Chem. Phys.* **24**, 348 (1956).

7. R. I. Reed and Walter Snedden, *Trans. Faraday Soc.* **55**, 876 (1959).

8. (*a*) W. L. Borst, *Phys. Rev.* **181**, 257 (1969); (*b*) A. I. Korotkov and N. A. Prilezhaeva, *Sov. Phys. J.* **13**, 1625 (1970).

9. (*a*) J. C. McConnell and B. L. Moiseiwitsch, *J. Phys. B* **1**, 406 (1968); (*b*) A. I. Korotkov, *Opt. Spectrosc. USSR* **28**, 347 (1970); (*c*) I. P. Bogdanova and V. D. Marvsin, *Eighth International Conference on the Physics of Electronic and Atomic Collisions*, B. C. Čobić and M. V. Kurepa, eds., vol. 2, Institute of Physics, Belgrad, Yugoslavia, 1973, p. 875.

CROSSED-MOLECULAR-BEAM STUDY OF ELECTRON TRANSFER REACTIONS AT THERMAL COLLISION ENERGIES

B. K. Annis H. F. Krause
S. Datz

Study of the interactions of alkali atoms with halogenated molecules at thermal energies has been extensive for a wide range of reaction energetics.[1] Reactions have not been investigated for cases where the electron affinity of the reactant molecule exceeds the ionization potential of the atom. We have initiated a program to explore this situation.

The thermal-energy reaction

$$M + UF_6 \rightarrow M^+ + UF_6^- ,$$

where M is Li, Na, K, Rb, or Cs, is now under investigation. A lower limit for the electron affinity of UF_6 has been predicted to be 5.5 eV;[2] therefore the reaction is exoergic for all alkali species (maximum ionization potential for M is $\lesssim 5.4$ v). We have established that the reaction occurs on surfaces of the vacuum system with potassium and cesium. If the gas-phase reaction occurs for either of these species, the total cross section is smaller than 10^{-18} cm^2.

Crossed-beam geometry was used, and a Channeltron detector, which rotated about the scattering center, was employed to detect either positive or negative ions. The possibility of gas-phase ionization with other alkali species and the detailed nature of the surface-catalyzed reaction will be investigated in the near future.

1. D. R. Herschbach, *Advan. Chem. Phys.* **10**, 319 (1966).

2. R. N. Compton, Health Physics Division, private communication.

INFLUENCE OF IONIC CHARGE STATE ON THE STOPPING POWER OF 27.8- AND 40-MeV OXYGEN IONS IN THE [011] CHANNEL OF SILVER[1]

S. Datz
B. R. Appleton[2]
J. A. Biggerstaff[3]
M. D. Brown[4]
H. F. Krause
C. D. Moak[3]
T. S. Noggle[2]

In many cases, it has been assumed that the stopping power of an ion is not strongly influenced by its ionic charge because screening electrons would largely mask the effect of charge-state differences. Usually it is difficult to tell whether an ion moving through a solid is highly stripped but highly screened or less highly stripped and screened. Earlier experiments had demonstrated that fast prestripped oxygen ions are able to survive passage through crystal channels of about 1 μm length and more without electron capture or loss. An experiment to detect slight differences in screening which would cause small differences in the stopping powers of O^{8+}, O^{7+}, and O^{6+} ions has been performed with 27.8- and 40-MeV oxygen ions in the [011] channel of a silver crystal with 0.8 μm path length. The differences are not small. The stopping powers follow the simple relation $S = kq^2$, where q is the ion charge. The result in this case indicates that dynamic screening by conduction electrons plays no significant role in equalizing stopping powers. The results appear to contradict the conclusion of Brandt et al.[5] that dynamic screening by conduction electrons occurs within a very short distance (0.04 μm) compared with our crystal thickness.

The experimental arrangement is shown in Fig. 7.39. Input ion charge states were selected by means of a deflecting magnet, and emerging ion charge states were selected by means of an electrostatic analyzer. Stopping powers were measured for various combinations of input and output charge. Part of the data is shown in Fig. 7.40. Clearly the stopping powers are different, and thus it can be said that conduction electrons do not dynamically screen out the differences in charge and stopping power. As shown in Fig. 7.41, the stopping

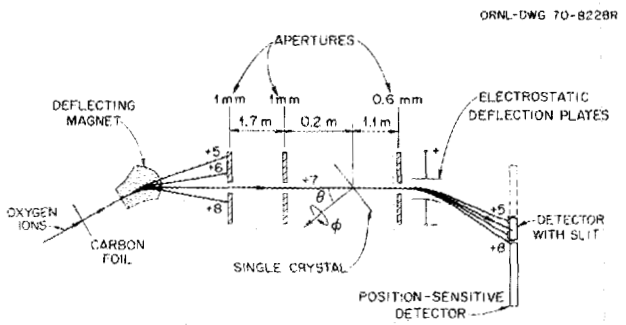

Fig. 7.39. Experimental arrangement.

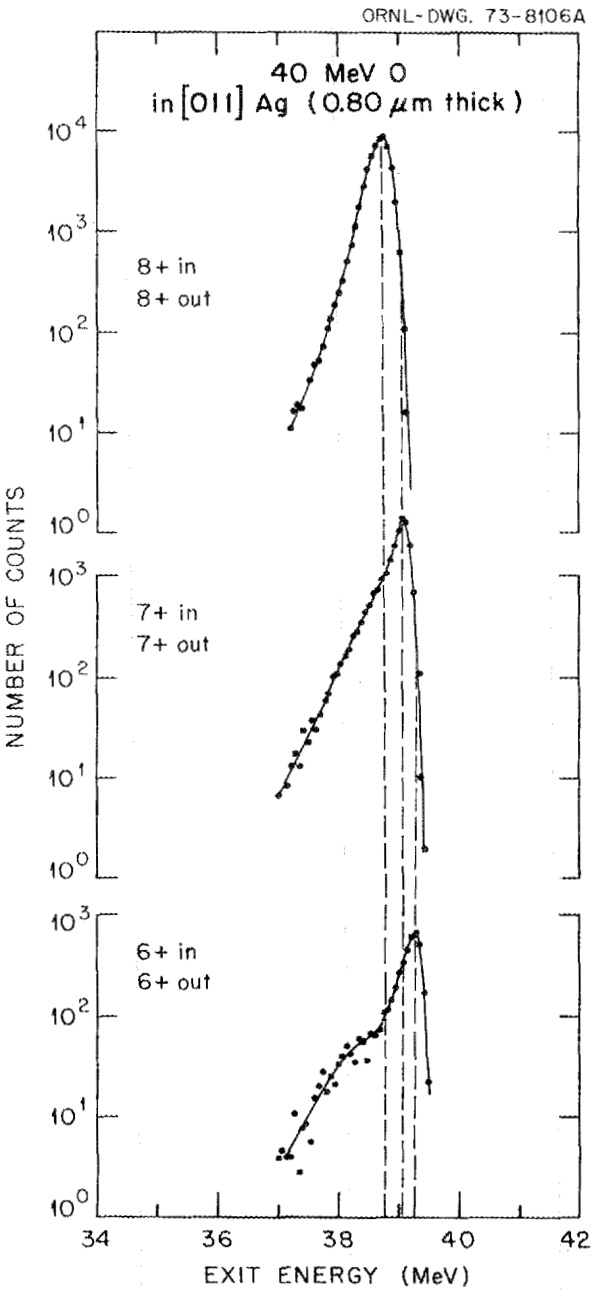

Fig. 7.40. Emergent energy spectra. 40-MeV oxygen ions, 0.8 μm path length in [011] channel in silver. $\Delta q = 0$.

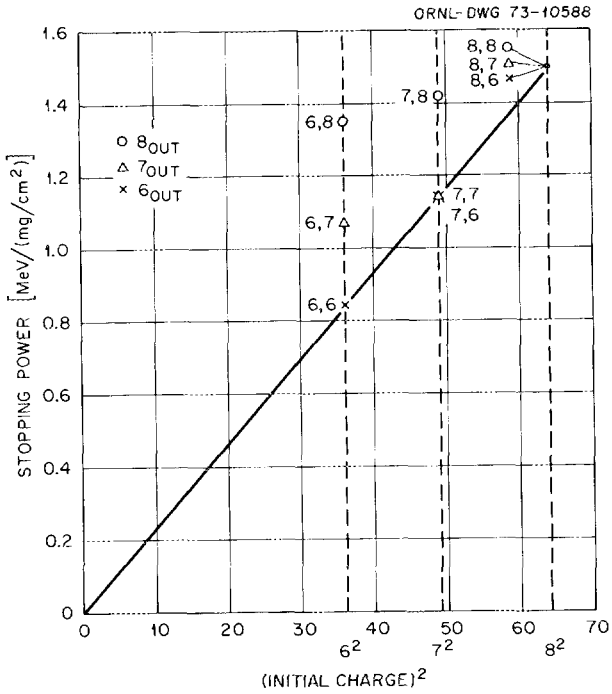

Fig. 7.41. Stopping powers of 40-MeV oxygen ions, [011] axis in silver, for various charge-state combinations, q_{in} and q_{out}.

powers of those ions which did not change charge are proportional to the square of the ion charge. A complete analysis of all the data is being prepared for publication.

1. A similar report appeared in *Phys. Div. Annu. Progr. Rep. Dec. 31, 1973*, ORNL-4937, p. 152.
2. Solid State Division.
3. Physics Division.
4. Visiting scientist, Kansas State University, Manhattan.
5. W. Brandt et al., *Phys. Rev. Lett.* **30**, 358 (1973).

VELOCITY DEPENDENCE OF THE STOPPING POWER OF CHANNELED IODINE IONS[1]

Sheldon Datz J. A. Biggerstaff[3]
B. R. Appleton[2] C. D. Moak[3]
T. S. Noggle[2]

Recent measurements of some uranium ion stopping powers in the energy range 30 to 90 MeV in polycrystalline targets,[4] together with earlier data for beryllium and iodine ions, have shown that $S_e = a + bE^{1/2}$ in the energy region where the theories of Lindhard, Scharff, and Schiøtt[5] and of Firsov[6] predict that electronic stopping should obey the relation $S_e = KE^{1/2}$. The heavier the ion, the larger the value of a. The important point is that the data cannot be reconciled with theory by a simple change of the value of K.

It was expected that ions moving in crystal channels and having no close collisions with atoms might show the $S_e = KE^{1/2}$ behavior. Some data taken by Eriksson, Davies, and Jespersgaard[7] with very-low-energy xenon ions in tungsten crystals do appear to follow this relationship. At higher energy, 21.6 to 32.5 MeV, iodine ion stopping powers have been measured for particles hyperchanneled[8] in the ⟨100⟩ axis of a crystal of silver. The results are shown in Fig. 7.42. Polycrystalline stopping powers measured by Moak and Brown[9] are shown as measured and, slightly below, after they were adjusted to remove the estimated contribution of nuclear stopping.[10] Channeling data generally have not been adjusted to remove the estimated contribution of nuclear stopping,[10] because there is strong evidence for the conclusion that nuclear stopping is negligible for channeled ions. The energy loss pattern for iodine ions hyperchanneled in the [100] axis in silver is shown schematically in Fig. 7.42. Beginning with particles showing the least energy loss (and running nearest the center of the channel), including particles which fall in the class of ordinary axially channeled particles, and finally including particles which run in the (100) planar channels, the behavior of the stopping power does not obey the relation $S = KE^{1/2}$. The data given by Eriksson, Davies, and Jespersgaard[7] have been included in the figure, even though both the ion and the stopping medium are different. At higher energies, where the iodine measurements were made, the stopping powers do follow the relation $S_e = a + bE^{1/2}$. The data suggest

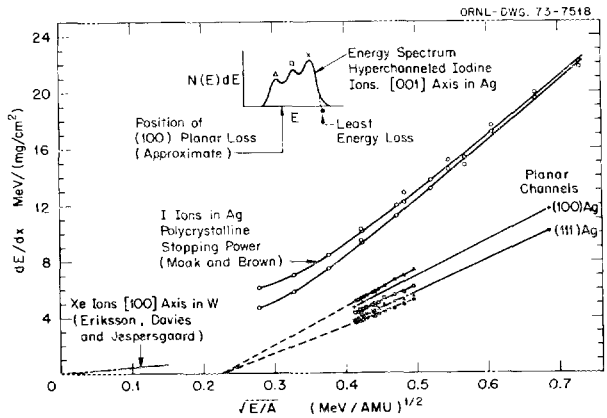

Fig. 7.42. Measured energy loss vs velocity ($\sqrt{E/A}$) for iodine ions in silver. Data include energy loss for polycrystalline silver, for iodine ions randomly directed in a silver single crystal, best channeled along the (100) and (111) planar channels, and hyperchanneled along the [001].

that below 21.6 MeV (or $\sqrt{E/A} = 0.41$ in Fig. 7.42) there is a velocity region where the stopping-power curve is more complicated and that some additions must be made to the theory for this velocity range. The importance of these conclusions extends beyond improvement of the stopping-power theory in this region. Extensive use is made of these theories in radiation damage calculations, for example, in calculating the damage distributions resulting from knock-on atoms; in cases where large amounts of damage are expected, such as a controlled thermonuclear reactor, these differences can be important.

1. A similar report appeared in *Solid State Div. Annu. Progr. Rep. Dec. 31, 1973,* ORNL-4952, p. 50.
2. Solid State Division.
3. Physics Division.
4. M. D. Brown and C. D. Moak, *Phys. Rev. B* **6**, 90 (1972).
5. J. Lindhard, M. Scharff, and H. E. Schiøtt, *Kgl. Dan. Vidensk. Selsk., Mat.-Fys. Medd.* **33**, No. 14 (1963).
6. O. B. Firsov, *Zh. Eksp. Teor. Fiz.* **36**, 1517 (1959) [*Sov. Phys. JETP* **9**, 1076 (1959)].
7. L. Eriksson, J. A. Davies, and P. Jespersgaard, *Phys. Rev.* **161**, 219 (1967).
8. B. R. Appleton, C. D. Moak, T. S. Noggle, and J. H. Barrett, *Phys. Rev. Lett.* **28**, 1307 (1972).
9. C. D. Moak and M. D. Brown, *Phys. Rev.* **149**, 224 (1966).
10. J. Lindhard, V. Nielson, and M. Scharff, *Kgl. Dan. Vidensk. Selsk., Mat.-Fys. Medd.* **36**, No. 10 (1969).

HYPERCHANNELING: INVESTIGATIONS FOR HIGH-ENERGY HEAVY IONS IN SILVER[1]

B. R. Appleton[2] C. D. Moak[3]
J. H. Barrett[2] S. Datz
J. A. Biggerstaff[3] T. S. Noggle[2]

When a beam of energetic ions enters a single crystal parallel to an axial direction, those which enter most nearly the center of the channel receive the smallest deflections. Some small fraction will acquire trajectories which remain within the confines of one particular axis (i.e., the open region surrounded by nearest neighbor rows), while a larger fraction will be axially channeled, but wander from one particular axis to another. Those ions confined to a particular axial channel will have two distinguishing characteristics: (1) they will be populated over a much smaller range of angles than regular axial channeling and (2) they will have a much lower rate of energy loss. It is this particular axial channeling phenomenon which we call hyperchanneling. Although this effect was recognized to exist in the 1963 paper by Robinson and Oen[4] which initiated present-day channeling studies, it was not until 1966 that the first experimental observation was reported by Eisen.[5] He attributed a high-energy tail for 375-keV protons transmitted through 2.2-μm silicon crystals along the [110] direction to protons which remained within a single axial channel (hyperchanneling) in traversing the crystals. The effect was not, however, sufficiently prominent to investigate in detail. No further investigations of this phenomenon were reported until 1972, when Appleton, Moak, Noggle, and Barrett[6,7] observed hyperchanneling for high-energy heavy ions. For 21.6-MeV iodine ions transmitted through thin silver single crystals near the [011] axis, they observed a distinct hyperchanneled group of ions with much lower energy loss rates than regular axial channeling and with a characteristic critical angle well within the axial critical angle. Because of the prominence of this effect for high-energy heavy ions, it was possible to study the details of hyperchanneling phenomena.

Recently the investigations for high-energy heavy ions were extended to include measurements for the [001] directions as well as the [011], and these results were compared with model calculations. Although the main features of the hyperchanneling measurements could be understood in terms of the model, several new and unexpected features appeared. Perhaps the most interesting of these can be understood with the aid of Fig. 7.43. The two sets of data shown in this figure were obtained by measuring the transmitted energy spectra of 21.6-MeV iodine ions incident at various angles, $\Delta\psi$, relative to the [001] (left-hand figure) and [011] (right-hand figure). The spectra were measured by an energy-sensitive detector in line with the incident beams, but with an acceptance angle of only ±0.012°. Consider first the data for the [011] axis. The features in these spectra are well understood in terms of the hyperchanneling model. The intense peak at lowest energy loss, near $\Delta\psi = 0$, results from hyperchanneled ions; the smaller peak at lower dE/dx which grows as $|\Delta\psi|$ increases can be identified as axially channeled ions which are wandering from one particular axis to another. These same two peaks can be identified in the spectra for the [001] axis, but in addition, group structure which cannot be understood in terms of the model calculations at all appears at intermediate energy loss values. Although more work is required to identify the nature of this structure, it appears likely that it results from discrete oscillations supported within a [001] hyperchannel. It clearly is a fine-structure effect which will be valuable in studying the ion-solid interaction potential.

1. A similar report appeared in *Phys. Div. Annu. Progr. Rep. Dec. 31, 1973,* ORNL-4937, p. 155.

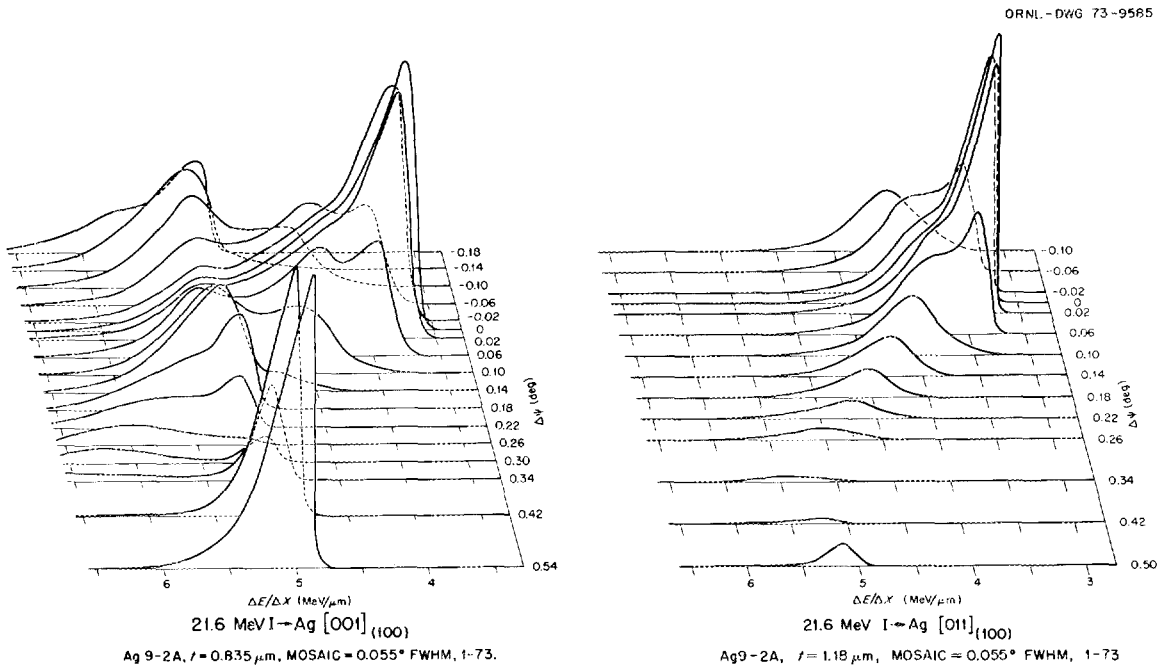

Fig. 7.43. Comparison of normalized transmitted energy loss distributions for 21.6-MeV iodine ions incident at various angles to [001] in (100) (path length, 0.835 μm; mosaic spread, 0.055°FWHM) and to [011] in (100) (path length, 1.18 μm; mosaic spread, 0.055°).

2. Solid State Division.
3. Physics Division.
4. M. T. Robinson and O. S. Oen, *Phys. Rev.* **132**, 2385 (1963).
5. F. H. Eisen, *Phys. Lett.* **23**, 401 (1966).
6. B. R. Appleton, C. D. Moak, T. S. Noggle, and J. H. Barrett, *Phys. Rev. Lett.* **28**, 1307 (1972).
7. B. R. Appleton, J. H. Barrett, T. S. Noggle, and C. D. Moak, *Radiat. Eff.* **13**, 171 (1972).

CHARACTERIZATION OF CHARGE STATES OF ENERGETIC IONS IN SOLIDS[1]

Sheldon Datz — Roman Laubert[3]
B. R. Appleton[2] — R. S. Peterson[3]
J. R. Mowat[3] — R. S. Thoe[3]
I. A. Sellin[3]

The states of energetic ions penetrating solids have been a subject of considerable study in the past few years. The matter goes back to the observations of Lassen[4] in 1951 that the charge states of heavy ions emerging from solids were considerably higher than those emerging from gaseous targets. However, it is also found that the electronic stopping powers in solid media are essentially the same as those measured in gaseous media, and the "effective charge" derived from stopping powers in solids is that which is observed for ions in gases.[5,6] Two solutions to this disparity have been proposed. The first suggested that dynamical screening by electrons in the solid tends to neutralize the excess charge on the ions moving in the solid.[7,8] However, at velocities $v \gg v_0$ the effect of screening should be small, and recent experiments with channeled oxygen ions indicate that screening electrons are ineffective in altering the stopping power of an ion in a given charge state. An alternative explanation was proposed by Betz and Grodzins,[9] who suggested that the actual charge state in the solid is essentially the same as that in the gas but that many of the bound electrons are present in highly excited states which are lost by autoionizing and/or Auger events after emergence from the solid. Hence, comparison of effective charge states inside the solid with charge states measured after emergence provides an experimental test of these theories.

In this work, we utilize the observation that x-ray production cross sections for high-velocity (1 to 4 MeV per nucleon) ions are highly sensitive to the charge state of the projectile ion. For example, Mowat et al.[10] found that the cross section for neon K x-ray production by bombardment with 80-MeV argon ions varied by a factor of 60 depending on the argon charge state (6+ to 17+). We reasoned that comparing the x-ray

production cross sections in solid and gaseous targets containing the same target element would provide a measure of the charge state of the penetrating ion. The results of these experiments are also critical to interpretation of measured heavy-ion-induced x-ray cross sections in which solid targets are used.

Beams of 86-MeV Ar^{6+} from the Oak Ridge Isochronous Cyclotron and 40-MeV O^{6+} from the Oak Ridge Tandem Van de Graaff were passed through a thin carbon foil for further charge stripping. A beam of a given charge state was then selected by magnetic deflection and entered a differentially pumped windowless gas cell. The cell could be filled with SiH_4 gas at pressures of about 20 millitorr, and x rays generated by ion-beam collision were counted by a Si(Li) detector which viewed the collision region at 90° from the beam direction. At this low pressure, maximum estimated charge exchange in the gas was always $\lesssim 5\%$ so that single-collision conditions with ions of a known charge state were obtained. The solid targets consisted of thin silicon films (7 to 50 $\mu g/cm^2$) deposited on a 150-$\mu g/cm^2$ plastic backing which could be positioned at the center of the evacuated gas cell. The silicon surface faced the beam and was tilted at an angle of 36° to the beam direction so that the Si(Li) detector could view the silicon surface directly. In the argon experiments an additional silicon foil could be inserted about 30 cm upstream of the cell. In this way an entrant charge-state distribution characteristic of that emerging from solid silicon could be prepared. The particle current was monitored in the case of the oxygen experiment by counting protons which were Rutherford-scattered from a gold foil placed behind the cell. For the argon experiments a separately pumped, electrically and magnetically guarded Faraday cup was used as a beam monitor.

Charge-state distributions for the oxygen ions emerging from silicon were measured using electrostatic analysis and a position-sensitive surface-barrier detector. The charge fractions F_i were 0.2, 0.7, and 0.1 for 6+, 7+, and 8+ respectively. The charge-state distributions for argon ions emerging from a silicon target were obtained by measuring the current at the focus of a magnetic analyzer following a silicon stripper foil. The principal charge fractions F_i found were 0.11 (13+), 0.27 (14+), 0.34 (15+), and 0.20 (16+). In no case did the estimated error in charge-state fraction exceed 0.03.

The x-ray results for oxygen ions are shown in Fig. 7.44. With the gas (SiH_4) target the cross section for silicon K x-ray production is seen to vary by a factor of about 2.5 as the incident ion charge is changed from 6+ to 8+. The origin of this strong charge-state effect is still incompletely known. A smaller variation (about 60%) is observed when a solid target is used. This effect of incident charge state in thin solid targets has been recently reported by Brandt et al.[8] for oxygen ions in aluminum. They found that the effect diminished as the foil thickness was increased, and they attributed this charge-state effect to dynamic screening, that is, the time required for the plasma to respond to the disturbance introduced by the penetrating ion. An alternative explanation could lie in the nonequilibrium of the ion charge state. Capture and loss cross sections for 40-MeV oxygen ions in argon, for example, are on the order of 2×10^{-17} cm^2. Thus the silicon target thickness (about 2×10^{17} atoms/cm^2) should be insufficient to attain equilibrium.

The observed charge-state dependence is expected to evolve gradually with increasing target thickness from the rising straight line observed for thin (gaseous) targets to a horizontal straight line at equilibrium thickness. The two lines representing the extremes in density should intersect at the projectile charge corresponding to the effective equilibrium charge in the solid. The equilibrium charge-state distribution of 40-MeV oxygen emerging from silicon is strongly peaked at 7+. At equilibrium, the input charge dependence of the x-ray cross section would be a horizontal line intersecting the SiH_4 line at charge 7+, if the effective charge in the solid were equal to the most

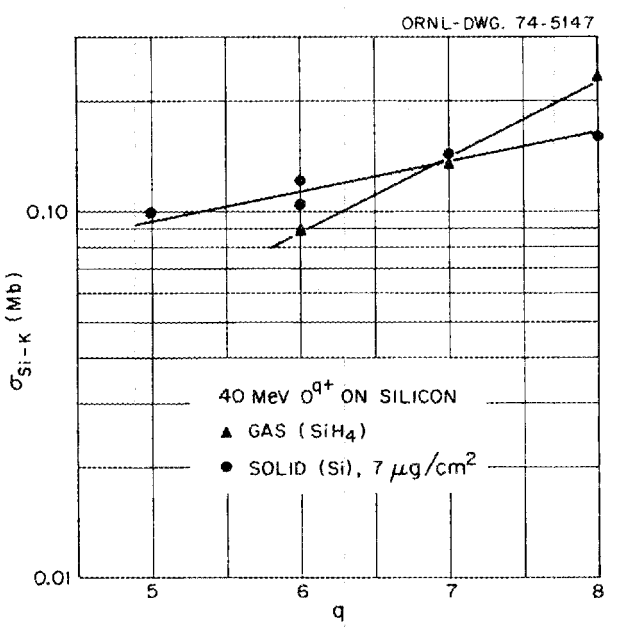

Fig. 7.44. Silicon K x-ray production cross section in megabarns (Mb) produced by 40-MeV oxygen ion bombardment of SiH_4 and solid silicon as a function of incident ion charge state.

probable emergent charge. Moreover, since the cross sections for leaving charge state 7+ ($\sigma_{7,5}$ and $\sigma_{7,8}$) should be lower at this energy than those for attaining charge 7+ ($\sigma_{8,7}$ and $\sigma_{6,7}$), one would expect near coincidence with the 7+ value of the gas target for incident 7+ ions even before charge-state equilibrium is obtained. Arguments based on dynamic screening in which the bound electrons are not considered lead to almost the same expected effective charge state. Here

$$q_{\mathrm{scr}} \cong Z(1 - v_0/v) = 7.2$$

for 40-MeV oxygen ions.[8]

For relatively low-Z ions such as oxygen, only slight dependence of emergent charge state on medium (solid or gas) is expected. The semiempirical calculations of Dmitriev and Nikolaev[11] give 7.4 and 7.6 for the expected charge (Table 7.11). From our charge distribution measurements we obtain $\bar{q} = 6.9$, and the effective charge state (q_{eff}) indicated by the measured x-ray cross section is 7 ± 0.25. Hence the oxygen results are satisfyingly consistent with all expectations and tend to demonstrate the validity of our method.

The situation for argon ions, where the theoretical predictions differ, are shown in Fig. 7.45. The cross sections for silicon K x-ray emission vary by a factor of about 7 for argon charges ranging from 6+ to 16+. The cross section for silicon K x-ray emission from solid silicon was found to be 0.095 ± 0.005 Mb and was essentially independent of input charge and target thickness. This cross section corresponds to an effective charge state of 11.5 ± 1 and is to be compared with our measured emergent mean charge of 14.8. The corresponding predictions of Dmitriev and Nikolaev[11] are 13.7 for solids and 12.5 for gases.

A useful check on the validity of these procedures was made by preparing an equilibrium-distribution beam in the upstream silicon foil referred to above. This equilibrated beam yielded a mean cross section σ_m in SiH_4 approximately equal to that anticipated on the basis of a combination of the fractional single-charge-state cross sections σ_i, that is,

$$\sigma_m = \Sigma F_i \sigma_i \ .$$

When the equilibrated beam was passed through a solid silicon target, no difference was observed in the cross section derived from the single-charge-component beam results. From this prefoil experiment alone it can be seen that the cross section in a solid target is a factor of

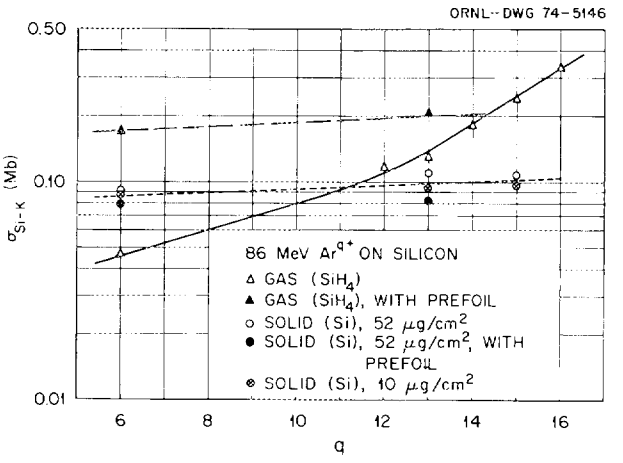

Fig. 7.45. Silicon K x-ray production cross section produced by 86-MeV argon ion bombardment of SiH_4 and solid silicon as a function of incident ion charge state. The "prefoil" points denote experiments in which the beam passed through a silicon foil before entering the target.

Table 7.11. Summary of the data

Bracketed values are for 40-MeV oxygen; unbracketed values are for 86-MeV argon

	X-ray data	Measured distribution	Semiempirical theory[a]
Mean charge emerging from solid	14 ± 0.5	14.8 [6.9]	13.7 [7.6]
Mean charge emerging from gas			12.5 [7.4]
Effective charge state in solid	11.5 ± 1 [7.0 ± 0.25]		

[a]I. S. Dmitriev and V. S. Nikolaev, *Sov. Phys. JETP* **20**, 409 (1965).

about 2 lower than that anticipated on the basis of the measured emergent charge.

The results for oxygen ions, being in agreement with all expectations, indicate that other possible solid-state effects on the silicon K x-ray yield are small. Hence the results for argon at the same MeV per nucleon clearly indicate a lower effective charge for the ion while in the solid than is observed in the emergent beam. The effects of screening at this velocity (about 10 v_0) are expected to be small. Hence the argon data are in accord with arguments of Betz and Grodzins[9] and strongly indicate that the ion passes through the solid with at least three more electrons accompanying it than remain bound to it shortly after emergence. These additional electrons must be in close enough proximity (i.e., L-shell radius) to act in reducing the silicon atom's K ionization cross section. Moreover, in order to liberate these electrons by autoionizing or Auger processes, additional electrons in excited states must also be present and associated with the emerging ion.

1. Research supported in part by ONR, NSF, and NASA; and by the U.S. Atomic Energy Commission under Union Carbide Corporation's contract with the U.S. Atomic Energy Commission.

2. Solid State Division.

3. University of Tennessee, Knoxville.

4. N. O. Lassen, *Kgl. Dan. Vidensk. Selsk., Mat.-Fys. Medd.* **26**, No. 5 and No. 12 (1951).

5. P. E. Pierce and M. Blann, *Phys. Rev.* **173**, 390 (1968).

6. M. D. Brown and C. D. Moak, *Phys. Rev. B* **6**, 90 (1972).

7. N. Bohr and J. Lindhard, *Kgl. Dan. Vidensk. Selsk., Mat.-Fys. Medd.* **28**, No. 7 (1954).

8. W. Brandt et al., *Phys. Rev. Lett.* **30**, 358 (1973).

9. H. D. Betz and L. Grodzins, *Phys. Rev. Lett.* **25**, 211 (1970).

10. J. R. Mowat, I. A. Sellin, D. J. Pegg, R. S. Peterson, M. D. Brown, and J. R. Macdonald, *Phys. Rev. A* **9**, 1974 (in press).

11. I. S. Dmitriev and V. S. Nikolaev, *Sov. Phys. JETP* **20**, 409 (1965).

Publications

NUCLEAR CHEMISTRY

M. H. Lietzke and R. W. Stoughton, "Electrons," "Elements," "Isotopes," "Radioisotopes," "Neutrons," "Polonium," "Protons," "X-rays," in *The Encyclopedia of Chemistry*, C. A. Hampel and G. C. Hawley, eds., Van Nostrand-Reinhold, New York, 1973.

E. Roeckl,[1] P. F. Dittner, R. Klapisch,[2] C. Thibault,[2] C. Rigaud,[2] and R. Prieels,[3] "Delayed Neutron Emission from the Decay of Neutron-Rich Rb and Cs Isotopes," *Nucl. Phys. A* **222**, 621 (1974).

S. C. Pancholi,[4] J. J. Pinajian,[5] N. R. Johnson, A. Kumar,[4] S. K. Soni,[4] M. M. Bajaj,[4] S. L. Gupta,[4] and N. K. Saha,[4] "Decay of ^{59}Fe to Levels of ^{59}Co," *Phys. Rev. C* **8**, 2277 (1973).

G. Garcia-Bermudez,[6] S. L. Gupta,[6] N. C. Singhal,[6] A. V. Ramayya,[6] J. Lange,[6] J. H. Hamilton,[6] and N. R. Johnson, "Search for Closed-Shell Effects on the $E2/M1$ Mixing of Transitions in ^{116}Sn," *Phys. Rev. C* **9**, 1060 (1973).

S. L. Gupta,[6] G. Garcia-Bermudez,[6] J. Lange,[6] J. H. Hamilton,[6] A. V. Ramayya,[6] N. C. Singhal,[6] K. R. Baker,[6] and N. R. Johnson, "Spin of the 1082.8 keV Level in ^{152}Sm," *Nucl. Phys. A* **221**, 541 (1974).

R. O. Sayer,[7] E. Eichler, N. R. Johnson, D. C. Hensley,[7] and L. L. Riedinger,[8] "Coulomb Excitation of Ground Bands in ^{160,162,164}Dy with ^{20}Ne and ^{35}Cl Ions," *Phys. Rev. C* **9**, 1103 (1973).

P. H. Stelson,[7] C. E. Bemis, Jr., F. K. McGowan,[7] W. T. Milner,[7] J. L. C. Ford, Jr.,[7] R. L. Robinson,[7] and W. Tuttle,[9] "Coulomb Nuclear Interference for α-Particles on Rare Earth Nuclei," p. 378 in *Proc. Int. Conf. Nucl. Phys.* J. de Boer and H. J. Mang, eds., vol. 1, North-Holland, Amsterdam, 1973.

C. E. Bemis, Jr., P. H. Stelson,[7] F. K. McGowan,[7] W. T. Milner,[7] J. L. C. Ford, Jr.,[7] R. L. Robinson,[7] and W. Tuttle,[9] "On the Interference between Direct Nuclear and Coulomb Excitation with Alpha Particles of ^{154}Sm, ^{166}Er, and ^{182}W," *Phys. Rev. C* **8**, 1934 (1973).

R. Bimbot,[10] D. Gardes,[10] R. L. Hahn, Y. de Moras,[10] and M. F. Rivet,[10] "Recoil Study of Incomplete Fusion Reactions Involving the Exchange of Many Nucleons (>10) between Ar Projectiles and Rare-Earth Targets," p. 613 in *Proc. Int. Conf. Nucl. Phys.*, J. de Boer and H. J. Mang, eds., vol. 1, North-Holland, Amsterdam, 1973.

H. Gauvin,[10] R. L. Hahn, B. Lagarde,[10] Y. LeBeyec,[10] and M. Lefort,[10] "Excitation Functions and Alpha Decay from Compound Nuclei in Ar Induced Reactions on ^{144}Sm and ^{166}Er," *Nucl. Phys. A* **220**, 84 (1974).

H. Gauvin,[10] R. L. Hahn, B. Lagarde,[10] Y. LeBeyec,[10] and M. Lefort,[10] "Détermination Directe de la Probabilité de Transition ^{149}Dy $\rightarrow$ ^{149f}Tb par Capture Électronique," *C. R. Acad. Sci. Ser. B* **277**, 107 (1973).

---

1. Gesellschaft für Schwerionenforschung mbH., Darmstadt, Germany.
2. Laboratoire René-Bernas du Centre de Spectrométrie Nucléaire et de Spectrométrie de Masse, Orsay, France.
3. Institut de Physique Corpusculaire, Louvain-la-Neuve, Belgium.
4. University of Delhi, India.
5. Isotopes Division.
6. Vanderbilt University, Nashville, Tenn.
7. Physics Division.
8. University of Tennessee, Knoxville.
9. Graduate student, University of Tennessee, Knoxville.
10. Institut de Physique Nucléaire, Orsay, France.

C. R. Bingham,[8] D. U. O'Kain,[8] K. S. Toth,[7] and R. L. Hahn, "Measurement of α-Decay Branching Ratios for ^{150,151}Dy and ^{149m}Tb," *Phys. Rev. C* **7**, 2575 (1973).

K. S. Toth,[7] R. L. Hahn, C. R. Bingham,[8] M. A. Ijaz,[11] and R. F. Walker, Jr.,[12] "Study of Hafnium α Emitters: New Isotopes ^{159}Hf, ^{160}Hf, and ^{161}Hf," *Phys. Rev. C* **7**, 2010 (1973).

H. Gauvin,[10] R. L. Hahn, Y. LeBeyec,[10] M. Lefort,[10] and J. Livet,[10] "Reactions of ^{40}Ar with ^{159}Tb, ^{142}Nd, and ^{144}Sm; New α-Activities from ^{189}Bi, ^{173}Pt, and ^{177}Au," *Nucl. Phys. A* **208**, 360 (1973).

R. L. Ferguson, F. Plasil,[7] F. Pleasonton,[7] S. C. Burnett,[13] and H. W. Schmitt,[7] "Systematics of Fragment Mass and Energy Distributions for Proton-Induced Fission of ^{233}U, ^{235}U, and ^{238}U," *Phys. Rev. C* **7**, 2510 (1973).

J. S. Eldridge,[14] G. D. O'Kelley, K. J. Northcutt,[14] and E. Schonfeld,[15] "Nondestructive Determination of Radionuclides in Lunar Samples Using a Large, Low-Background Gamma-Ray Spectrometer and a Novel Application of Least-Squares Fitting," *Nucl. Instrum. Methods* **112**, 319 (1973).

J. S. Eldridge,[14] G. D. O'Kelley, and K. J. Northcutt,[14] "Radionuclide Concentrations in Apollo 16 Lunar Samples Determined by Nondestructive Gamma-Ray Spectrometry," p. 2115 in *Geochim. Cosmochim. Acta, Suppl. 4,* vol. 2, Pergamon, New York, 1973.

J. S. Eldridge,[14] G. D. O'Kelley, and K. J. Northcutt,[14] "Primordial Radioelement Concentrations in Rocks and Soils from Taurus-Littrow," p. 206 in *Lunar Science V,* The Lunar Science Institute, Houston, Tex., 1974.

Lunar Sample Preliminary Examination Team (including G. D. O'Kelley), "The Apollo 17 Lunar Samples: Chemical and Petrographic Description," *Science* **182**, 659 (1973).

Lunar Sample Preliminary Examination Team (including G. D. O'Kelley), "Lunar Sample Information Catalog — Apollo 17," NASA Johnson Space Center, Houston, Tex., Report MSC-03211, April 1973.

Lunar Sample Preliminary Examination Team (including G. D. O'Kelley), "A Petrographic and Chemical Description of Samples from the Lunar Highlands," Chap. 7, Part A in *Apollo 16 Preliminary Science Report,* R. Brett and A. W. England, eds., NASA Report SP-315, Washington, D.C., 1973.

Lunar Sample Preliminary Examination Team (including G. D. O'Kelley), "Preliminary Examination of Lunar Samples from Apollo 17," Chap. 6 in *Apollo 17 Preliminary Science Report,* NASA Johnson Space Center, Report SP-330, Washington, D.C., 1973.

CHEMISTRY AND PHYSICS OF TRANSURANIUM ELEMENTS

J. S. Boyno,[16] J. R. Huizenga,[17] Th. W. Elze,[18] and C. E. Bemis, Jr., "Levels of ^{234}U and ^{236}U Excited by the (d,d') Reaction," *Nucl. Phys. A* **209**, 125 (1973).

W. T. Milner,[7] F. K. McGowan,[7] C. E. Bemis, Jr., J. L. C. Ford, Jr.,[7] R. L. Robinson,[7] and P. H. Stelson,[7] "Equilibrium Quadrupole and Hexadecapole Deformations in Actinide Nuclei," *J. Phys. (Paris), Colloq.* No. 5, 112 (1972).

C. E. Bemis, Jr., F. K. McGowan,[7] J. L. C. Ford, Jr.,[7] W. T. Milner,[7] P. H. Stelson,[7] and R. L. Robinson,[7] "$E2$ and $E4$ Transition Moments and Equilibrium Deformation in the Actinide Nuclei," *Phys. Rev. C* **8**, 1466 (1973).

F. Pleasonton,[7] R. L. Ferguson, F. Plasil,[7] and C. E. Bemis, Jr., "Fragment-Mass and Kinetic-Energy Distributions from the Spontaneous Fission of ^{246}Cm," *Phys. Rev. C* **8**, 1018 (1973).

---

11. Virginia Polytechnic Institute and State University, Blacksburg.
12. Centenary College, Shreveport, La.
13. Oak Ridge Graduate Fellow from University of Tennessee, Knoxville, under appointment with Oak Ridge Associated Universities. Present address: U.S. Atomic Energy Commission, Washington, D.C.
14. Analytical Chemistry Division.
15. NASA Johnson Space Center, Houston, Tex.
16. Michigan State University, East Lansing.
17. University of Rochester, Rochester, N.Y.
18. Universität Frankfurt/Main, West Germany.

R. L. Ferguson, F. Plasil,[7] H. Freiesleben,[19] C. E. Bemis, Jr., and H. W. Schmitt,[7] "Fragment Kinetic Energy in ^{18}O-Induced Fission of ^{232}Th and ^{246}Cm," *Phys. Rev. C* **8**, 1104 (1973).

J. R. Stokely,[14] C. E. Bemis, Jr., R. D. Baybarz,[20] and R. Eby,[14] "The Absolute Specific Activity and Half Life for ^{249}Cf," *J. Inorg. Nucl. Chem.* **35**, 3369 (1973).

Twenty-nine authors including C. E. Bemis, Jr., "The Unisor Project," p. 318 in *Proc. 8th Int. Conf. Low Energy Ion Accelerators and Mass Separators,* G. Andersson and G. Holm, eds., Goteborg, Sweden, 1973.

R. J. Silva, P. F. Dittner, M. L. Mallory, O. L. Keller, Jr., K. Eskola,[21] P. Eskola,[21] M. Nurmia,[21] and A. Ghiorso,[21] "The New Nuclide Nobelium-259," *Nucl. Phys. A* **216**, 97 (1973).

C. E. Bemis, Jr., R. J. Silva, D. C. Hensley,[7] O. L. Keller, Jr., J. R. Tarrant, L. D. Hunt, P. F. Dittner, R. L. Hahn, and C. D. Goodman,[7] "An X-Ray Identification of Element 104," *Phys. Rev. Lett.* **31**, 647 (1973).

O. L. Keller, Jr., C. W. Nestor, Jr.,[22] T. A. Carlson,[23] and Burkhard Fricke,[1] "Predicted Properties of the Superheavy Elements. II. Element 111, Eka-Gold," *J. Phys. Chem.* **77**, 1806 (1973).

R. W. Stoughton, J. Halperin, J. S. Drury, F. G. Perey,[24] R. L. Macklin,[7] R. V. Gentry,[25] C. B. Moore,[26] J. E. Noakes,[27] R. M. Milton,[28] J. H. McCarthy,[29] and D. W. Sherwood,[30] "A Search for Naturally Occurring Superheavy Elements," *Nature (London) Phys. Sci.* **246**, 26 (1973).

R. V. Gentry,[25] S. S. Cristy,[31] J. F. McLaughlin,[31] and J. A. McHugh,[32] "Ion Microprobe Confirmation of Pb Isotope Ratios and Search for Isomer Precursors in Polonium Radiohalos," *Nature (London)* **244**, 282 (1973).

R. V. Gentry,[25] "Radioactive Halos," *Annu. Rev. Nucl. Sci.* **23**, 347 (1973).

R. V. Gentry,[25] "Radiohalos in a Radiochronological and Cosmological Perspective," *Science* **184**, 62 (1974).

J. H. Burns, "Structure of Tetracyclopentadienyluranium(IV)," *J. Amer. Chem. Soc.* **95**, 3815 (1973).

J. H. Burns, "Structural Studies on Organometallic Compounds of Lanthanides and Actinides," p. 846 in *Proc. 10th Rare Earth Res. Conf.*, CONF-730402-P2, 1973.

J. H. Burns, book review, *The Actinide Elements,* by K. W. Bagnall, *Science* **180**, 1357 (1973).

J. H. Burns, "The Molecular and Crystal Structure of Tetracyclopentadienyluranium(IV)," *J. Organometal. Chem.* **69**, 225 (1974).

J. N. Stevenson,[33] "The Microchemical Preparations of Metallic Curium-248 and Californium-249 by the Reduction of Their Trifluorides, and Related Structural Studies," Ph.D. thesis, University of Tennessee, Knoxville, August 1973; also, TID-26453.

J. R. Peterson,[34] "Compounds of Divalent Lanthanides and Actinides," *Proc. Tenth Rare Earth Res. Conf.* **1**, 4 (1973).

J. N. Stevenson[33] and J. R. Peterson,[34] "The Trigonal and Orthorhombic Crystal Structures of CfF_3 and Their Temperature Relationship," *J. Inorg. Nucl. Chem.* **35**, 3481 (1973).

---

19. University of Rochester, Rochester, N.Y. Present address: Universität Marburg, Germany.
20. Chemical Technology Division.
21. Lawrence Berkeley Laboratory, University of California, Berkeley.
22. Mathematics Division.
23. Now of the Physics Division.
24. Neutron Physics Division.
25. Visiting scientist from the Institute of Planetary Science, Columbia Union College, Takoma Park, Md.
26. Center for Meteorite Studies, Arizona State University, Tempe.
27. Geochronology Laboratory, University of Georgia, Athens.
28. Linde Division, Union Carbide Corporation, Tarrytown, N.Y.
29. Geological Survey, U.S. Department of the Interior, Denver, Colo.
30. U.S. Atomic Energy Commission Headquarters, Germantown, Md.
31. Laboratory Development Department, Y-12 Plant.
32. Knolls Atomic Power Laboratory, Schenectady, N.Y.
33. Graduate student, University of Tennessee, Knoxville. Present address: Nuclear Power School, U.S. Navy, Bainbridge, Md.
34. Consultant, Department of Chemistry, University of Tennessee, Knoxville.

J. R. Peterson,[34] "Table of Nuclides," p. 3–12 in *Lange's Handbook of Chemistry,* 11th ed., J. A. Dean, ed. McGraw-Hill, New York, 1973.

ISOTOPE CHEMISTRY

L. L. Brown and J. S. Drury, "Fractionation of Carbon Isotopes. The CYANEX System: A Liquid-Liquid Chemical Exchange Process," *J. Inorg. Nucl. Chem.* **35**, 2897 (1973).

RADIATION CHEMISTRY

J. A. Ghormley, R. L. Ellsworth,[35] and C. J. Hochanadel, "Reaction of Excited Oxygen Atoms with Nitrous Oxide. Rate Constants for Reaction of Ozone with Nitric Oxide and with Nitrogen Dioxide," *J. Phys. Chem.* **77**, 1341 (1973).

ORGANIC CHEMISTRY

B. M. Benjamin and C. J. Collins, "^{14}C Isotope Effects in the 1,3-Dipolar Addition of N,α-Diphenylnitrone and Styrene. A Concerted Cyclic Process," *J. Amer. Chem. Soc.* **95**, 6145 (1973).

C. J. Collins and M. H. Lietzke, "An Analysis of the Acid-Catalyzed Racemization of (–)-Camphene-^{13}C. Is *endo*-Methyl Migration Necessary?," *J. Amer. Chem. Soc.* **95**, 6842 (1973).

C. J. Collins and C. K. Johnson, "A Computer-Assisted Analysis of the Camphor-^{14}C Sulfuric Acid Reaction. Is 3,2-Endo Hydroxyl Shift Necessary?," *J. Amer. Chem. Soc.* **95**, 4766 (1973).

C. K. Johnson and C. J. Collins, "An Algebraic Model for the Rearrangements of 2-Bicyclo[2.2.1]heptyl Cations," *J. Amer. Chem. Soc.* **96**, 2514 (1974).

C. J. Collins, C. K. Johnson, and V. F. Raaen, "Molecular Rearrangements. XXX. Applications of an Algebraic-Graphical Model for Analyzing Rearrangements of Bicyclo[2.2.1]heptyl Cations," *J. Amer. Chem. Soc.* **96**, 2524 (1974).

C. E. Klots,[36] R. N. Compton,[36] and V. F. Raaen, "Electronic and Ionic Properties of Molecular TTF and TCNQ," *J. Chem. Phys.* **60**, 1177 (1974).

PHYSICAL CHEMISTRY

T. J. Lemmonds,[9] "The Standard Potential of the Ag, AgBr Electrode in DBr Solutions," M.S. thesis, University of Tennessee, Knoxville, March 1974.

R. E. Mesmer and A. C. Rutenberg,[37] "Fluorine-19 Nuclear Magnetic Resonance Studies on Fluoroborate Species in Aqueous Solution,"[38] *Inorg. Chem.* **12**, 699 (1973).

F. H. Sweeton,[39] R. E. Mesmer, and C. F. Baes, Jr., "A High-Temperature Flowing EMF Cell,"[38] *J. Phys. E* **6**, 165 (1973).

C. F. Baes, Jr., and R. E. Mesmer, "The Hydrolysis of Cations. A Critical Review of Hydrolytic Species and Their Stability Constants in Aqueous Solution,"[38] ORNL-NSF-EATC-3, Part I (January 1974).

F. H. Sweeton,[39] R. E. Mesmer, and C. F. Baes, Jr., "Acidity Measurements at Elevated Temperatures. VII. Dissociation of Water,"[38] *J. Solution Chem.* **3**, 191 (1974).

---

35. Student participant in the Great Lakes Colleges Association Science Semester, fall 1971, from the College of Wooster, Wooster, Ohio.
36. Health Physics Division.
37. Now of the Product Certification Division, Y-12 Plant.
38. Work performed in the Reactor Chemistry Division.
39. Now of the Environmental Sciences Division.

W. L. Marshall and Ruth Slusher,[40] "Debye-Hückel Correlated Solubilities of Calcium Sulfate in Water and in Aqueous Sodium Nitrate and Lithium Nitrate Solutions of Molality 0 to 6 Mol kg^{-1} and at Temperatures from 398 to 623 K,"[38] *J. Chem. Thermodyn.* **5**, 189 (1973).

R. Kalyanaraman,[41] L. B. Yeatts,[42] and W. L. Marshall, "High Temperature Debye-Hückel Correlated Solubilities of Calcium Sulfate in Aqueous Sodium Perchlorate Solutions,"[38] *J. Chem. Thermodyn.* **5**, 891 (1973).

R. Kalyanaraman,[41] L. B. Yeatts,[42] and W. L. Marshall, "Solubility of Calcium Sulfate in $CaSO_4$ + Na_2SO_4 + $NaClO_4$ + H_2O at 273 to 623 K,"[38] *J. Chem. Thermodyn.* **5**, 899 (1973).

L. B. Yeatts,[42] P. M. Lantz,[43] and W. L. Marshall, "Solubilities of Calcium Sulfate Dihydrate at 25°C in Brackish Waters and Their Concentrates; Effect of Calgon Additive and Predictions for Reverse Osmosis Processes,"[38,44] ORNL-4914 (September 1973).

F. G. Seeley[20] and W. H. Baldwin, "Extraction of Lithium from Neutral Brines Using a Beta Diketone and Trioctylphosphine Oxide," U.S. Pat. 3,793,433 (Feb. 19, 1974).

C. E. Higgins[42] and W. H. Baldwin, "Interactions of Poly(Hydroxypropyl Acrylate-co-Tetraethylene Glycol Dimethacrylate) with Aqueous Electrolytes," *J. Appl. Polym. Sci.* **17**, 3815 (1973).

L. Dresner, V. R. Cain,[45] and W. Davis, Jr.,[20] "INTAKE: A Numerical Program to Calculate Fluid Velocity Profiles Near a Rectangular Inlet in a Stream with Cross Flow,"[46] ORNL-TM-4185 (July 1973).

K. A. Kraus and H. A. Mahlman, "Cross-Flow Filtration Process for Removal of Total Organic Carbon and Phosphates from Aqueous Sewage Effluents." U.S. Pat. 3,733,265 (May 15, 1973).

K. A. Kraus, "Process for Treatment of Aqueous Suspensions," U.S. Pat. 3,778,366 (Dec. 11, 1973).

C. P. Wedig,[47] A. D. Schwope,[47] and P. H. Dhargalkar,[47] "Adsorption and Filtration of Trace Contaminants in Aqueous Effluents," ORNL-MIT-147 (document date April 26, 1972; issued November 1973).

R. J. Raridon[48] and G. E. Moore, compilers, "Water Research Program Biennial Progress Report for Period March 15, 1968 to March 15, 1970, Properties of Solutions,"[44] ORNL-TM-4212 (August 1973).

R. E. Minturn, compiler, "Water Research Program Final Report for Period March 15, 1970 to October 31, 1972, Separations Processes,"[44] ORNL-TM-4236 (1973); identical with OSW R&D Report 903.

R. E. Minturn, "Calcium Sulfate Scaling in Reverse Osmosis (Hyperfiltration) of Brackish Waters by Hollow-Fiber and Spiral-Wound Modules,"[44] Final Report to the Office of Saline Water, ORNL-TM-4330 (July 1973); identical with OSW R&D Report 897.

J. S. Johnson, "Dual-Layer Hyperfiltration Membrane and Process for Using Same," U.S. Pat. 3,743,595 (July 3, 1973).

T. W. Bush,[49] E. M. Suuberg,[49] J. J. Toman,[49] and M. Yonezawa,[49] "Performance Characteristics of Dynamically Formed Hydrous Zr(IV) Oxide-Polyacrylic Acid Membranes in Treating Textile Dyeing Effluents," ORNL-MIT-182 (1973).

---

40. Now of the Computer Sciences Division.
41. International Atomic Energy Agency Fellow (1971), Bhabha Atomic Research Centre, Trombay, Bombay, India.
42. Now of the Analytical Chemistry Division.
43. A member of the Chemistry Division when work was performed; now of the Health Physics Division.
44. Research sponsored by the Office of Saline Water, U.S. Department of the Interior, under Union Carbide Corporation's contract with the U.S. Atomic Energy Commission.
45. Reactor Division.
46. Work performed in the Reactor Division.
47. Graduate student, Massachusetts Institute of Technology, School of Chemical Engineering Practice, Oak Ridge Station, J. T. Day, Director; Fred Nelson and H. O. Phillips, consultants to project.
48. Now of the Mathematics Division.
49. Graduate student, Massachusetts Institute of Technology, School of Chemical Engineering Practice, Oak Ridge Station, J. W. Tester, Director; J. S. Johnson, Jr., and R. E. Minturn, consultants to project.

C. A. Brandon,[50] J. S. Johnson, R. E. Minturn, and J. J. Porter,[50] "Complete Reuse of Textile Dyeing Wastes Processed with Dynamic Membrane Hyperfiltration,"[51] *Text. Chem. Color.* **5**, 35 (1973).

J. S. Johnson, Jr., R. E. Minturn, and G. E. Moore, "Filtration Techniques for Purification of Kraft Pulp Mill and Bleach Plant Wastes,"[52] *Tappi* **57**, 134 (1974).

G. H. Cartledge,[53] "Twenty-Year Inhibition of Corrosion by the Pertechnetate Ion," *Corrosion* **29**, 361 (1973).

M. C. Banta,[54] R. E. Meyer, and F. A. Posey, "Chronopotentiometry of the Silver-Silver Sulfide System,"[55] *J. Electroanal. Chem. Inter-facial Electrochem.* **47**, 223 (1973).

R. E. Meyer and F. A. Posey, "Separation and Analysis of Iodide, Bromide, and Chloride Ions with the Packed-Bed Silver Electrode," *J. Electroanal. Chem. Inter-facial Electrochem.* **49**, 377 (1974).

A. L. Bacarella and J. C. Griess, Jr.,[56] "The Anodic Dissolution of Copper in Flowing Sodium Chloride Solutions Between 25° and 175°C,"[38,57] *J. Electrochem. Soc.* **120**, 459 (1973).

L. D. Hulett,[14] A. L. Bacarella,[58] L. LiDonnici,[59] and J. C. Griess,[56,58] "Analysis of Protective Oxide Films on Copper-Nickel Alloys by Photoelectron Spectroscopy,"[57] *J. Electron Spectrosc. Relat. Phenomena* **1**, 169 (1972/73).

J. C. Griess, Jr.,[56] A. L. Bacarella, and E. G. Bohlmann, "Water Research Program Final Report for Period March 15, 1966 to October 31, 1972, Corrosion Studies,"[38,44] ORNL-TM-4340 (October 1973).

A. Y. Herrell,[60] "The Enthalpies of Formation of Tc_2O_7 (c) and TcO_4^- (aq) by Solution Calorimetry," Ph.D. thesis, Wayne State University, Detroit, Mich. (1973).

H. F. Holmes, E. L. Fuller, Jr., and R. B. Gammage,[36] "Alteration of an Apollo 12 Sample by Adsorption of Water Vapor,"[38] *Earth Planet. Sci. Lett.* **19**, 90 (1973).

H. F. Holmes, E. L. Fuller, Jr., and R. B. Gammage,[36] "Interaction of Gases with Lunar Materials: Apollo 12, 14, and 16 Samples,"[38] p. 2413 in *Proc. Fourth Lunar Sci. Conf., Geochim. Cosmochim. Acta, Suppl. 4*, vol. 3, Pergamon, New York, 1973.

H. F. Holmes, E. L. Fuller, Jr., and R. B. Gammage,[36] "Some Surface Properties of Apollo 17 Soils,"[38] p. 347 in *Lunar Science V*, The Lunar Science Institute, Houston, Tex., 1974.

---

50. Clemson University, Clemson, S.C.

51. Work at ORNL supported by the ORNL-NSF Environmental Program under Union Carbide Corporation's contract with the U.S. Atomic Energy Commission.

52. Research sponsored by the National Science Foundation/RANN under Union Carbide Corporation's contract with the U.S. Atomic Energy Commission.

53. Consultant.

54. Department of Chemistry, Sam Houston State University, Huntsville, Tex.

55. Research jointly sponsored by the Office of Saline Water, U.S. Department of the Interior, and the U.S. Atomic Energy Commission under contract with the Union Carbide Corporation and by the Office of Research and Grants of Sam Houston State University.

56. Now of the Metals and Ceramics Division.

57. Research jointly sponsored by the Office of Saline Water, U.S. Department of the Interior, and the U.S. Atomic Energy Commission under contract with the Union Carbide Corporation.

58. Work performed while a member of the Reactor Chemistry Division.

59. Oak Ridge Associated Universities Summer Student Trainee from Barnard College, New York.

60. National Science Foundation Science Faculty Fellow, Wayne State University, Detroit, Mich.

H. Braunstein, J. Braunstein, and P. T. Hardesty,[61] "Hydration and Association Equilibria in Molten Salts Containing Water. III. The Association of Cadmium Ion with Bromide in the Solvent Calcium Nitrate–Water,"[38] *J. Phys. Chem.* 77(15), 1907 (1973).

H. Braunstein, J. Braunstein, A. S. Minano,[62] and R. E. Hagman,[62] "Association of Cadmium (II) and Bromide in Anhydrous Molten Mixtures of Calcium Nitrate with Sodium Nitrate or Potassium Nitrate and the Effect of Water,"[38] *Inorg. Chem.* **12**, 1407 (1973).

J. Braunstein, H. R. Bronstein, and J. Truitt,[58] "Chronopotentiometry Based on Diffusion of Mobile Nonelectroactive Species,"[38] *J. Electroanal. Chem. Inter-facial Electrochem.* **44**, 463 (1973).

J. Braunstein, Gleb Mamantov,[8] and G. P. Smith,[63] eds., *Advances in Molten Salt Chemistry,* vol. 2, Plenum Press, New York, 1973.

C. E. Vallet[64] and J. Braunstein, "Application of the Quasilattice Model to Association in Dilute Reciprocal Molten Salt Mixtures. The System Silver Sulfate–Potassium Nitrate,"[38] *J. Phys. Chem.* 77, 2672 (1973).

D. D. Sood[65] and J. Braunstein, "Lithium-Bismuth Alloy Electrodes for Thermodynamic Investigation of Molten LiF-BeF_2 Mixtures,"[38] *J. Electrochem. Soc.* **121**, 247 (1974).

L. M. Toth[56] and L. O. Gilpatrick, "Temperature and Solvent Effects on the Equilibrium of Dilute Uranium Trifluoride Solutions Contained in Graphite,"[38] *J. Phys. Chem.* 77, 2799 (1973).

R. E. Mesmer, K. M. Palen, and C. F. Baes, Jr., "Fluoroborate Equilibria in Aqueous Solutions,"[38] *Inorg. Chem.* **12**, 89 (1973).

R. G. Ross,[20] C. E. Bamberger,[20] and C. F. Baes, Jr., "The Oxide Chemistry of Protactinium in Molten Fluorides,"[38] *J. Inorg. Nucl. Chem.* **35**, 433 (1973).

C. F. Baes, Jr., C. E. Bamberger,[20] and R. G. Ross,[20] "Recovery of Protactinium from Molten Fluoride Nuclear Fuel Compositions,"[38] U.S. Pat. 3,781,403 (Dec. 25, 1973).

C. E. Bamberger,[20] B. F. Hitch,[20] and C. F. Baes, Jr., "Determination of the Free Energies of Formation of $NaNiF_3$ and $NaFeF_3$,"[38] *J. Inorg. Nucl. Chem.* **36**, 543 (1974).

CHEMICAL PHYSICS

G. M. Brown and H. A. Levy, "Further Refinement of the Structure of Sucrose Based on Neutron-Diffraction Data," *Acta Crystallogr., Sect. B* **29**, 790 (1973).

G. M. Brown and R. Chidambaram,[65] "Dinuclear Copper(II) Acetate Monohydrate: A Redetermination of the Structure by Neutron-Diffraction Analysis," *Acta Crystallogr., Sect. B* **29**, 2393 (1973).

R. Chidambaram[65] and G. M. Brown, "A Model for a Torsional Oscillator in Crystallographic Least-Squares Refinements, *Acta Crystallogr., Sect. B* **29**, 2388 (1973).

G. M. Brown and O. A. W. Strydom,[66] "Hexachlorobenzene, C_6Cl_6: The Crystal and Molecular Structure from Least-Squares Refinement with New X-Ray Data," *Acta Crystallogr., Sect. B* **30**, 801 (1974).

J. B. Bates[67] and W. R. Busing, "Intermolecular Potential Function Model for Crystalline Hexachlorobenzene," *J. Chem. Phys.* **60**, 2414 (1974).

---

61. Oak Ridge Associated Universities Summer Student Trainee from Brescia College, Owensboro, Ky.
62. Graduate student, University of Maine at Orono.
63. Metals and Ceramics Division.
64. Visiting scientist from University of Provence, Marseille, France; French Foreign Office Postdoctoral Fellow 1972–1973; Foreign Assignment from C.N.R.S., 1973–1974.
65. Visiting scientist from Bhabha Atomic Research Centre, Trombay, Bombay India.
66. Visiting scientist (1972–73) from Atomic Energy Board, Pretoria, South Africa.
67. Solid State Division.

F. Vaslow[68] and A. H. Narten, "Diffraction Pattern and Structure of Molten BeF_2-LiF Solutions," *J. Chem. Phys.* **59**, 4949 (1973).

A. H. Narten, F. Vaslow,[68] and H. A. Levy, "Diffraction Pattern and Structure of Aqueous Lithium Chloride Solutions," *J. Chem. Phys.* **58**, 5017 (1973).

L. Blum,[69] "Invariant Expansion III: The General Solution of the Mean Spherical Model for Neutral Spheres with Electrostatic Interactions," *J. Chem. Phys.* **58**, 3295 (1973).

H. Zeldes and R. Livingston, "Electron Spin Resonance Study of Liquids during Photolysis. XV. Substituted Pyridines," *J. Phys. Chem.* 77, 2076 (1973).

R. Livingston and H. Zeldes, "Electron Spin Resonance Study of Liquids during Photolysis. XVI. Kinetics of Radicals Showing Emission from Tartaric Acid," *J. Chem. Phys.* **59**, 4891 (1973).

H. Zeldes and R. Livingston, "Electron Spin Resonance of Photolytically Reduced Pyrazine," *Mol. Phys.* **27**, 261 (1974).

S. Datz, B. R. Appleton,[67] and C. D. Moak,[7] "Detailed Studies of Ion Trajectories and Associated Channeling Potentials and Stopping Powers," p. 153 in *Channeling*, D. V. Morgan, ed., Wiley, New York, 1973.

S. Datz, J. L. Duggan,[70] L. C. Feldman,[71] E. Laegsgaard,[72] and J. U. Andersen,[72] "Cross Sections for *L*-Subshell Ionization in Au by the Collision of Protons and Helium Ions," *Phys. Rev. A* **9**, 192 (1974).

---

68. Present address: Argonne National Laboratory, Argonne, Ill.
69. Oak Ridge Associated Universities Research Participant from the University of Puerto Rico, Rio Piedras, summer 1970.
70. Oak Ridge Associated Universities.
71. Bell Telephone Laboratories and Physics Institute, University of Aarhus, Denmark.
72. Physics Institute, University of Aarhus, Denmark.

Papers Presented at Scientific and Technical Meetings

NUCLEAR CHEMISTRY

F. Plasil,*[1] R. L. Ferguson, and F. Pleasonton,[1] "Heavy-Ion-Induced Fission of Nuclei in the Region of Silver," Third Symposium on the Physics and Chemistry of Fission, Rochester, N.Y., Aug. 13–17, 1973.

R. L. Ferguson,* F. Plasil,[1] and F. Pleasonton,[1] "Angular Momentum Effects in the Fission of the ^{153}Tb Compound Nucleus," 1974 Spring Meeting, American Physical Society, Washington, D.C., Apr. 22–25, 1974; *Bull. Amer. Phys. Soc.* **19**, 428 (1974).

J. H. Hamilton*[2] et al. (including N. R. Johnson), "Properties of $K^{\pi} = 2^{+}$ and 0^{+} Bands in ^{156,158}Gd and ^{176,178,180}Hf," International Nuclear Physics Conference, Munich, Germany, Aug. 25, 1973.

N. R. Johnson,* R. J. Sturm,[3] M. W. Guidry,[4] E. Eichler, R. O. Sayer,[1] N. C. Singhal,[5] G. D. O'Kelley and D. C. Hensley,[1] "Lifetimes of Rotational States in ^{232}Th," 1973 Fall Meeting, American Physical Society, Bloomington, Ind., Nov. 1–3, 1973; *Bull. Amer. Phys. Soc.* **18**, 1405 (1973).

M. W. Guidry,*[4] R. J. Sturm,[3] N. R. Johnson, E. Eichler, G. D. O'Kelley, G. B. Hagemann,[6] and D. C. Hensley,[1] "Multiple Coulomb Excitation of ^{236}U," 1973 Fall Meeting, American Physical Society, Bloomington, Ind., Nov. 1–3, 1973; *Bull. Amer. Phys. Soc.* **18**, 1405 (1973).

R. J. Sturm,*[3] N. R. Johnson, M. W. Guidry,[4] R. O. Sayer,[1] E. Eichler, N. C. Singhal,[5] and D. C. Hensley,[1] "Lifetimes of the 10^{+} State in ^{154}Sm," 1973 Fall Meeting, American Physical Society, Bloomington, Ind., Nov. 1–3, 1973; *Bull. Amer. Phys. Soc.* **18**, 1405 (1973).

K. S. R. Sastry,*[7] A. V. Ramayya,[2] R. S. Lee,[2] J. H. Hamilton,[2] R. Mlekodaj,[8] and N. R. Johnson, "Precession of Gamma-Gamma Correlation in ^{126}Xe," 1973 Fall Meeting, American Physical Society, Bloomington, Ind. Nov. 1–3, 1973; *Bull. Amer. Phys. Soc.* **18**, 1425 (1973).

N. R. Johnson, "Lifetime Measurements of Rotational States by the Doppler-Shift Recoil-Distance Technique," Southeastern Section, American Physical Society, Winston-Salem, N.C., Nov. 8–10, 1973 (invited).

E. H. Spejewski*[8] and the UNISOR Consortium (including N. R. Johnson), "Initial UNISOR Research: New Isotopes ^{186}Tl, ^{188}Tl, ^{116}I; Decays of ^{189,190}Tl, ^{117}Xe and ^{117}I; and Off-Line Atomic and Nuclear Studies," XXIV Annual National Conference of the Academy of Sciences, USSR, Nuclear Spectroscopy and Structure of the Atomic Nucleus, Kharkov, Russia, January 1974 (invited).

---

*Speaker.

1. Physics Division.
2. Vanderbilt University, Nashville, Tenn.
3. Max Kade Foundation Fellow from University of Marburg, Germany.
4. Oak Ridge Graduate Fellow from University of Tennessee, Knoxville, under appointment with Oak Ridge Associated Universities.
5. Postdoctoral Fellow, Vanderbilt University, Nashville, Tenn., assigned to ORNL.
6. Physics Division. Permanent address: Niels Bohr Institute, Copenhagen, Denmark.
7. University of Massachusetts, Amherst.
8. UNISOR Consortium.

L. L. Riedinger,*[9] P. H. Stelson,[1] G. B. Hagemann,[6] D. C. Hensley,[1] N. R. Johnson, R. L. Robinson,[1] and R. O. Sayer,[1] "Decoupled Rotational Bands in ^{163,165}Yb," 1974 Spring Meeting, American Physical Society, Washington, D.C., Apr. 22–25, 1974; *Bull. Amer. Phys. Soc.* **19**, 524 (1974).

R. O. Sayer,*[1] R. J. Sturm,[3] N. R. Johnson, E. Eichler, N. C. Singhal,[5] M. W. Guidry,[4] and G. D. O'Kelley, "Recoil-Distance Lifetimes of Levels in ^{164}Dy," 1974 Spring Meeting, American Physical Society, Washington, D.C., Apr. 22–25, 1974; *Bull. Amer. Phys. Soc.* **19**, 524 (1974).

P. H. Stelson,*[1] L. L. Riedinger,[9] E. Eichler, D. C. Hensley,[1] N. R. Johnson, R. L. Robinson,[1] R. O. Sayer,[1] and G. J. Smith,[1] "Ground-State Rotational Bands in ^{170}W and ^{176}Os," 1974 Spring Meeting, American Physical Society, Washington, D.C., Apr. 22–25, 1974; *Bull. Amer. Phys. Soc.* **19**, 525 (1974).

M. W. Guidry,*[4] R. Sturm,[3] G. D. O'Kelley, N. R. Johnson, E. Eichler, R. O. Sayer,[1] and N. C. Singhal,[5] "Doppler-Plunger Lifetimes in ^{236}U," 1974 Spring Meeting, American Physical Society, Washington, D.C., Apr. 22–25, 1974; *Bull. Amer. Phys. Soc.* **19**, 599 (1974).

R. Bimbot,*[10] D. Gardes,[10] R. L. Hahn, Y. de Moras,[10] and M. F. Rivet,[10] "Incomplete Fusion of Ar and Rare-Earth Nuclei," XII International Meeting on Nuclear Physics, Villars, France, 1974.

G. D. O'Kelley,* J. S. Eldridge,[11] and K. J. Northcutt,[11] "Concentrations of Cosmogenic Radionuclides in Apollo 17 Samples: Effects of the Solar Flare of August, 1972," Fifth Lunar Science Conference, Houston, Tex., Mar. 18–22, 1974; p. 577 in *Lunar Science V,* Lunar Science Institute, Houston, Tex., 1974.

CHEMISTRY AND PHYSICS OF TRANSURANIUM ELEMENTS

R. L. Hahn,* P. F. Dittner, K. S. Toth,[1] and O. L. Keller, Jr., "Transfer and Compound-Nucleus Reactions in the Interactions of ^{12}C with ^{239}Pu and ^{238}U," 1974 Spring Meeting, American Physical Society, Washington, D.C., Apr. 22–25, 1974; *Bull. Amer. Phys. Soc.* **19**, 428 (1974).

J. W. T. Dabbs,*[1] C. E. Bemis, G. D. James,[12] N. W. Hill,[13] M. S. Moore,[14] and A. N. Ellis,[14] "Neutron Fission Cross Sections of ^{249}Cf," 1974 Spring Meeting, American Physical Society, Washington, D.C., Apr. 22–25, 1974; *Bull. Amer. Phys. Soc.* **19**, 596 (1974).

R. J. Silva, W. J. McDowell,[15] O. L. Keller, Jr.,* and J. R. Tarrant, "Nobelium: Comparative Chemistry to Other Divalent Elements," 25th Southeastern Regional Meeting, American Chemical Society, Charleston, S.C., Nov. 7–9, 1973.

O. L. Keller, Jr., "Predictions of Chemical and Physical Properties of Superheavy Elements," 140th Meeting, American Association for the Advancement of Science, San Francisco, Calif., Feb. 25–Mar. 1, 1974 (invited).

J. R. Peterson*[16] and J. H. Burns, "Single-Crystal X-Ray Diffraction Studies of Compounds of the Transuranium Elements," XXIVth International Union of Pure and Applied Chemistry Congress, Hamburg, Germany, Sept. 2–8, 1973.

J. H. Burns,* W. H. Baldwin, and P. G. Laubereau,[17] "The Crystal and Molecular Structure of the Cyclohexylisonitrile Adduct of Praseodymium Tricyclopentadienide," American Crystallographic Association, University of California, Berkeley, Mar. 24–28, 1974.

---

9. Department of Physics, University of Tennessee, Knoxville.
10. Institut de Physique Nucléaire, Orsay, France.
11. Analytical Chemistry Division.
12. Present address: Atomic Energy Research Establishment, Harwell, England.
13. Instrumentation and Controls Division.
14. Los Alamos Scientific Laboratory, Los Alamos, N.M.
15. Chemical Technology Division.
16. Consultant, Department of Chemistry, University of Tennessee, Knoxville.
17. Visiting scientist from Federal Republic of Germany, Bonn.

J. R. Peterson*[16] and J. N. Stevenson,[18] "Microchemical Techniques Used in Solid-State Studies of Transplutonium Elements and Compounds," International Symposium on Microchemical Techniques – 1973, Pennsylvania State University, University Park, Aug. 19–24, 1973.

J. R. Peterson,[16] J. N. Stevenson,[18] R. G. Haire,[15] and J. Fuger,[19] "The Preparation of Berkelium Metal for Determination of Its Heat of Solution," 167th National Meeting, American Chemical Society, Los Angeles, Calif., Mar. 31–Apr. 5, 1974; abstract NUCL-60.

PHYSICAL CHEMISTRY

J. S. Johnson, Jr., "Dynamically Formed Membranes in Aqueous Separations," Gordon Research Conference on Separation and Purification, Colby College, New London, N.H., Aug. 20–24, 1973 (invited).

R. E. Minturn, "Dynamic Membranes in Ultrafiltration and Hyperfiltration of Industrial Effluents," Symposium on Chemistry and the Environment, 25th Southeastern Regional Meeting, American Chemical Society, Charleston, S.C., Nov. 7–9, 1973 (invited).

W. L. Marshall* and J. S. Gill,[20] "Effect of Pressure on Liquid-Liquid Immiscibility of High Temperature Aqueous Solution Mixtures of Uranyl Sulfate and Sulfuric Acid, 285–450°C, 75–1800 Bars,"[21] 167th National Meeting, American Chemical Society, Los Angeles, Calif., Mar. 30–Apr. 5, 1974; abstract PHYS-49.

K. A. Kraus, "Cross-Flow Filtration and Axial Filtration," 29th Annual Purdue Industrial Waste Conference, Lafayette, Ind., May 7–9, 1974 (invited).

F. Nelson* and K. A. Kraus, "Adsorption of Inorganic Materials by Activated Carbon," 29th Annual Purdue Industrial Waste Conference, Lafayette, Ind., May 7–9, 1974 (invited).

E. J. Kelly, "Anodic Dissolution of Titanium in Acidic Sulfate Solutions," Symposium on Kinetics and Mechanisms of Metallic Dissolution, 144th Meeting, Electrochemical Society, Boston, Mass., Oct. 7–13, 1973 (invited).

A. L. Bacarella* and A. L. Sutton,[22] "The Effect of Solvent on the Electrochemistry of Iron,"[21] 144th Meeting, Electrochemical Society, Boston, Mass., Oct. 11, 1973.

H. F. Holmes, "The Heat of Immersion of Thorium Oxide at Elevated Temperatures,"[21] 167th National Meeting, American Chemical Society, Los Angeles, Calif., Mar. 31–Apr. 5, 1974; abstract COLL-103.

H. F. Holmes,* E. L. Fuller, Jr., and R. A. Beh,[23] "Adsorption of Argon, Nitrogen, and Water Vapor on Zirconium Oxide,"[21] 47th National Colloid Symposium, Carleton University, Ottawa, Ontario, Canada, June 18–20, 1973.

R. B. Gammage,[24] H. F. Holmes,* E. L. Fuller, Jr., and D. R. Glasson,[25] "Pore Structures Induced by Water Vapor Adsorbed on Non-Porous Lunar Fines and Ground Calcite,"[21] 47th National Colloid Symposium, Carleton University, Ottawa, Ontario, Canada, June 18–20, 1973.

---

18. Graduate student and postdoctoral research associate, University of Tennessee, Knoxville. Present address: Nuclear Power School, U.S. Navy, Bainbridge, Md.
19. Institute of Radiochemistry, University of Liège, Liège, Belgium.
20. Present address: Department of Public Health, State of Tennessee, Nashville.
21. Work performed in the Reactor Chemistry Division.
22. Now of the Chemical Technology Division.
23. Oak Ridge Associated Universities Summer Student Trainee from St. Ambrose College, Davenport, Iowa.
24. Health Physics Division.
25. John Graymore Chemistry Laboratories, Plymouth Polytechnic, Plymouth, England.

E. L. Fuller, Jr.,* and H. F. Holmes, "Adsorption on Sol-Gel Thorium Oxide,"[21] 47th National Colloid Symposium, Carleton University, Ottawa, Ontario, Canada, June 18–20, 1973.

E. L. Fuller, Jr.,* H. F. Holmes, and R. B. Gammage,[24] "Interaction of Gases with Lunar Materials: Textural Changes Induced by Sorbed Water,"[21] 166th National Meeting, American Chemical Society, Chicago, Ill., Aug. 26–31, 1973; abstract COLL-12.

R. B. Gammage,*[24] H. F. Holmes, and E. L. Fuller, Jr., "Pore Structures Induced in Lunar Fines by Adsorbed Water,"[21] RILEM/IUPAC International Symposium on Pore Structure and Properties of Materials, Prague, Czechoslovakia, Sept. 18–21, 1973.

H. F. Holmes,* E. L. Fuller, Jr., and R. B. Gammage,[24] "Some Surface Properties of Apollo 17 Soils,"[21] Fifth Lunar Science Conference, Houston, Tex., Mar. 18–22, 1974.

J. Braunstein,* H. Braunstein, and P. T. Hardesty,[26] "Competitive Hydration and Association Equilibria in Hydrous Melts,"[21] 15th International Conference on Coordination Chemistry, Moscow, June 25–30, 1973.

J. Braunstein,* H. R. Bronstein, and C. E. Vallet,[27] "Chronopotentiometry Based on Diffusion of Mobile Non-Electroactive Species,"[21] Gordon Research Conference on Molten Salts, Brewster Academy, Wolfeboro, N.H., Aug. 27–31, 1973 (invited).

C. E. Vallet*[27] and J. Braunstein, "Application of the Quasilattice Model to Association in Dilute Reciprocal Molten Salt Mixtures. The System Silver Sulfate–Potassium Nitrate,"[21] Gordon Research Conference on Molten Salts, Brewster Academy, Wolfeboro, N.H., Aug. 27–31, 1973.

C. F. Baes, Jr., "The Chemistry and Thermodynamics of Molten-Salt Reactor Fuels,"[21] U.S.-Japanese Seminar on Thermodynamics and Phase Relations of Nuclear Materials, Ames, Iowa, July 9–12, 1973 (invited).

CHEMICAL PHYSICS

J. B. Bates*[28] and W. R. Busing, "Intermolecular Potential Function Models of Crystalline Hexachlorobenzene and Solid Chlorine," Paper M2, Symposium on Molecular Structure and Spectroscopy, Ohio State University, Columbus, June 12, 1973.

G. M. Brown* and O. A. W. Strydom,[29] "Hexachlorobenzene, C_6Cl_6: Crystal and Molecular Structure from Refinement on New Three-Dimensional X-ray Data," American Crystallographic Association, Storrs, Conn., June 17–22, 1973.

L. H. Hall*[30] and G. M. Brown, "Crystal Structure of Ferrocenylmethylpyridinium Iodide, $(C_5H_5)Fe(C_5H_4)$-$CH_2(NC_5H_5)^+I^-$," American Crystallographic Association, Storrs, Conn., June 17–22, 1973.

R. M. Metzger,*[31] W. E. Thiessen, T. E. Hopkins,[32] and P. G. Simpson,[33] "The Crystal Structure of the (1:1) Adduct Between Chlorpromazine and 7,7,8,8-Tetracyanoquinodimethane," American Crystallographic Association, University of California, Berkeley, Mar. 24–28, 1974.

C. K. Johnson,* H. L. Reed II,[34] R. F. Hall,[35] and V. F. Raaen, "Physical and Molecular Properties of TCNQ-Benzene and TCNQ-Hexamethylbenzene Crystals," American Crystallographic Association, University of California, Berkeley, Mar. 24–28, 1974.

---

26. Oak Ridge Associated Universities Summer Student Trainee from Brescia College, Owensboro, Ky.
27. Visiting scientist from University of Provence, Marseille, France; French Foreign Office Postdoctoral fellow, 1972–73; Foreign Assignment from C.N.R.S., 1973–74.
28. Solid State Division.
29. Visiting scientist (1972–73) from Atomic Energy Board, Pretoria, South Africa.
30. Department of Chemistry, Eastern Nazarene College, Wollaston, Mass.
31. Department of Chemistry, University of Mississippi, University.
32. Department of Chemistry, Oregon State University, Corvallis.
33. Monsanto Corporation, Pensacola, Fla.
34. Student participant in the Great Lakes Colleges Association Science Semester, fall 1973, from DePauw University, Greencastle, Ind.
35. Oak Ridge Associated Universities Summer Student Trainee from Rockhurst College, Kansas City, Mo.

C. K. Johnson, "Critical Evaluation of Protein Crystallographic Results," NAS Conference on Critical Evaluation of Chemical and Physical Structural Information, Dartmouth College, Hanover, N.H., June 24–29, 1973 (invited).

W. E. Thiessen* and W. R. Busing, "Identification of Systematically Aberrant Phase Relationships Arising from Structural Regularity," American Crystallographic Association, Storrs, Conn., June 17–22, 1973.

W. R. Busing* and W. E. Thiessen, "ORTRAN, A Computer Program to Search a Data Set for the Transform of a Molecular Fragment," American Crystallographic Association, University of California, Berkeley, Mar. 24–28, 1974.

A. H. Narten, "X-Ray and Neutron Diffraction from Water and Aqueous Solutions," International Symposium on the Structure of Water and Aqueous Solutions, Marburg, Germany, July 19–28, 1973 (invited).

A. H. Narten, "Diffraction by Molecular Liquids," American Crystallographic Association, University of California, Berkeley, Mar. 24–28, 1974 (invited).

R. Livingston* and H. Zeldes, "ESR Studies of Radicals in Photolyzed Liquids," Fourth International Conference on Atomic Spectroscopy and the Twentieth Canadian Spectroscopy Symposium, Toronto, Canada, Nov. 2, 1973 (invited).

F. Wuilleumier*[36] and M. O. Krause, "Experimental Determination of Absolute Subshell Photoionization Cross Sections in Neon," 8th International Conference on the Physics of Electronic and Atomic Collisions, Beograd, Yugoslavia, July 16–24, 1973.

S. Datz,* B. R. Appleton,[28] J. A. Biggerstaff,[1] M. D. Brown,[37] H. F. Krause, C. D. Moak,[1] and T. S. Noggle,[28] "Charge State Dependence of Stopping Power for Oxygen Ions Channeled in Silver," Fifth International Conference on Atomic Collisions in Solids, Gatlinburg, Tenn., Sept. 24–29, 1973.

J. R. Mowat,*[9] B. R. Appleton,[28] J. A. Biggerstaff,[1] S. Datz, C. D. Moak,[1] and I. A. Sellin,[9] "Charge State Dependence of Si *K* X-Ray Production in Solid and Gaseous Targets by 40 MeV Oxygen Ion Impact," Fifth International Conference on Atomic Collisions in Solids, Gatlinburg, Tenn., Sept. 24–29, 1973.

J. H. Barrett,[28] B. R. Appleton,*[28] J. A. Biggerstaff,[1] S. Datz, C. D. Moak,[1] and T. S. Noggle,[28] "Hyperchanneling," Fifth International Conference on Atomic Collisions in Solids, Gatlinburg, Tenn., Sept. 24–29, 1973.

C. D. Moak,*[1] B. R. Appleton,[28] J. A. Biggerstaff,[1] S. Datz, and T. S. Noggle,[28] "Velocity Dependence of the Stopping Power of Channeled Iodine Ions," Fifth International Conference on Atomic Collisions in Solids, Gatlinburg, Tenn., Sept. 24–29, 1973.

B. R. Appleton,*[28] S. Datz, J. A. Biggerstaff,[1] T. S. Noggle,[28] C. D, Moak,[1] M. D. Brown,[37] H. F. Krause, R. H. Ritchie,[24] and V. N. Neelavathi,[24] "Radiative Electron Capture by Channeled Oxygen Ions," Fifth International Conference on Atomic Collisions in Solids, Gatlinburg, Tenn., Sept. 24–29, 1973.

S. Datz,* J. R. Mowat,[9] I. A. Sellin,[9] B. R. Appleton,[28] J. A. Biggerstaff,[1] and C. D. Moak,[1] "Effective Charge State of Heavy Ions Penetrating Solids Deduced from Comparing X-Ray Yields in Gases and Solids," *Bull. Amer. Phys. Soc.* **18**, 1508 (1973).

B. R. Appleton,*[28] J. H. Barrett,[28] T. S. Noggle,[28] C. D. Moak,[1] S. Datz, H. F. Krause, and J. A. Biggerstaff,[1] "Group Structure of Hyperchanneled Heavy Ions," *Bull. Amer. Phys. Soc.* **19**, 209 (1974).

B. R. Appleton,*[28] J. A. Biggerstaff,[1] T. S. Noggle,[28] S. Datz, C. D. Moak,[1] M. D. Brown,[37] and H. F. Krause, "Radiative Electron Capture by Chaneled Oxygen Ions," *Bull. Amer. Phys. Soc.* **19**, 210 (1974).

---

36. Visiting scientist from Laboratoire de Chimie Physique de la Faculté des Sciences de Paris.
37. Department of Physics, Kansas State University, Manhattan.

Lectures

NUCLEAR CHEMISTRY

N. R. Johnson, "Lifetimes of High-Spin States in Actinide Nuclei by the Doppler-Shift Recoil-Distance Technique," Seminar, Physics Department, Vanderbilt University, Nashville, Tenn., Nov. 15, 1973 (ORAU Traveling Lecture).

N. R. Johnson, "Lifetimes of Rotational States in Deformed Nuclei by the Doppler-Shift Recoil-Distance Technique," Chemistry Department, Texas A & M University, College Station, Dec. 11, 1973 (ORAU Traveling Lecture).

G. D. O'Kelley, "Radioactivity Measurements on Returned Lunar Samples," Chemistry Department, Brookhaven National Laboratory, Upton, N.Y., May 30, 1973.

G. D. O'Kelley, "The New Moon – Scientific Results from the Apollo and Luna Sampling Missions," Chemistry Department, University of Tennessee, Knoxville, Feb. 26, 1974.

G. D. O'Kelley, "Radioactivity of Lunar Samples," Seminar, ORNL Chemistry Division, May 3, 1974.

CHEMISTRY AND PHYSICS OF TRANSURANIUM ELEMENTS

R. L. Hahn, "Recoil Nuclei from Heavy-Ion Reactions at Oak Ridge and Orsay," Seminar, Institut für Kernchemie, Johannes Gutenberg Universität, Mainz, Germany, March 1973; Seminar, Institut des Sciences Nucléaire, Grenoble, April 1973.

E. H. Taylor, "Research Genesis," 1973–74 Lectureship Program, The Robert A. Welch Foundation, Texas Wesleyan College, Ft. Worth, Jan. 28, 1974; Austin College, Sherman, Tex., Jan. 29, 1974; Midwestern University, Wichita Falls, Tex., Jan. 30, 1974.

R. L. Hahn, "Les Noyaux de Recul Produits avec les Ions Lourds en Amérique et en France," Seminar, Institut de Physique Nucléaire, Orsay, May 1973; Seminar, Centre d'Études Nucléaire, Bordeaux, June 1973.

R. L. Hahn, "The Last Tango: Experiences with ALICE in Orsay," Seminar, ORNL Chemistry Division, January 1974; Joint Physics-Chemistry Colloquium, Virginia Polytechnic Institute and State University, Blacksburg, March 1974.

P. F. Dittner, "Heavy Ion Experiments at ORNL," Colloquium of the Laboratoire René Bernas du Centre de Spectrométrie Nucléaire et de Spectrométrie de Masse, Orsay, France, June 6, 1973.

C. E. Bemis, Jr., "Element 104 and Beyond — An Unequivocal Identification Using Characteristic X Rays," Physics Department, Indiana University, Bloomington, Oct. 5, 1973; Physics Department Colloquium, University of Tennessee, Knoxville, Oct. 17, 1973; Physics Department Colloquium, University of Pennsylvania, Philadelphia, Nov. 7, 1973.

J. R. Peterson,[1] "Recent Progress in the Characterization of Curium, Berkelium, and Californium Metals and Their Compounds," Seminar, Institute of Radiochemistry, Kernforschungszentrum, Karlsruhe, Germany, July 13, 1973.

---

1. Consultant, Department of Chemistry, University of Tennessee, Knoxville.

J. R. Peterson,[1] "Preparation and Characterization of Curium, Berkelium, and Californium Metals and Some of Their Compounds," Seminar, Materials Science Division, Argonne National Laboratory, Argonne, Ill., Feb. 13, 1974.

R. L. Fellows,[2] "The Influence of Ligand Coordination on the Hypersensitive Electronic Transitions of Rare Earth Ions," Seminar, ORNL Chemistry Division, Feb. 15, 1974.

ORGANIC CHEMISTRY

C. J. Collins, "Memory Effects, Coset Graphs and Combinatorial Games in Organic Chemistry," E. I. Dupont de Nemours, Experimental Station, Wilmington, Del., Mar. 22, 1974.

PHYSICAL CHEMISTRY

R. E. Mesmer, "The Hydrolysis Behavior of Toxic Metal Ions," Southeast Environmental Research Laboratory, Environmental Protection Agency, Athens, Ga., May 29, 1973.

J. S. Johnson, Jr., "The Future of Dynamic Membranes," Union Carbide Corporation, South Charleston, W.Va., Feb. 26, 1974.

R. E. Minturn, "Hyperfiltration and Cross-Flow Filtration in Desalination and Pollution Control," Vanderbilt University, Nashville, Tenn., Apr. 15, 1974.

J. Braunstein, "Thermodynamics of Electrolyte Solutions with Water as a Solute," State University College of New York at Fredonia; University of Maine at Orono; University of Maine at Presque Isle, May 1973.

J. Braunstein, "Electrochemical Studies of Transport and Thermodynamics in Molten Fluorides Containing Beryllium Fluoride," Colloquium, Institute of Physical Chemistry and Electrochemistry, University of Karlsruhe, Germany, June 1973.

J. Braunstein, "Ionic Solution Chemistry: Bridging the Gap from Dilute Solutions to Molten Salts," Western Michigan University, Kalamazoo, November 1973; University of Mississippi, University, March 15, 1974 (ORAU Traveling Lecture).

C. E. Vallet,[3] "Electromigrational Depletion Chronopotentiometry, "Seminar, Chemical Engineering Division, Argonne National Laboratory, Argonne, Ill., Feb. 18, 1974.

C. F. Baes, Jr., "The Hydrolysis of Cations," seminar, Department of Analytical Chemistry, University of Florida, Gainesville, March 1973.

CHEMICAL PHYSICS

A. H. Narten, "Ionic Hydration in Lithium Chloride and Hydrogen Chloride Solutions," Swiss Federal Institute of Technology, Zurich, Switzerland, July 7, 1973.

A. H. Narten, "Structure and Orientation of Water Molecules from Neutron Diffraction," KFA, Jülich, Germany, July 17, 1973.

C. K. Johnson, "Algebraic and Crystallographic Analyses of Norbornyl Cation Rearrangements," Brookhaven National Laboratory, Upton, Long Island, N.Y., July 11, 1973.

---

2. Postdoctoral research associate from the University of Tennessee, Knoxville.

3. Visiting scientist from University of Provence, Marseille, France; French Foreign Office Postdoctoral Fellow, 1972–73; Foreign Assignment from C.N.R.S., 1973–74.

R. Livingston, "ESR Studies of Radicals in Photolyzed Liquids," Seminars, Chemistry Department, University of Waterloo, Waterloo, Canada, Nov. 1, 1973; Chemistry Department, Bryn Mawr College, Bryn Mawr, Pa., Feb. 1, 1974; Chemistry Department, Washington University, St. Louis, Mo., Feb. 14, 1974; School of Pharmacy, University of Southern California, Los Angeles, Apr. 25, 1974.

M. O. Krause, "PAX, the X-Ray Mode of Photoelectron Spectrometry," Physical Science Colloquium, Thomas J. Watson Research Center, IBM, Yorktown Heights, N.Y., Nov. 15, 1973.

S. Datz, "On the States of Ions Penetrating Solids," Lecture Series, NATO Summer School On Radiation Damage in Materials, Porto Vecchio, Corsica, France, Aug. 28–Sept. 7, 1973; Department of Physics, University of North Carolina, Chapel Hill, Apr. 17, 1974.

S. Datz, "Collisions of Fast Heavy Ions in Dense Media," Physics Institute, University of Munich, Munich, Germany, Aug. 23, 1973.

S. Datz, "Inelastic and Reactive Scattering of Metastable Mercury," Department of Chemistry, University of Texas, Austin, Feb. 27, 1974; Texas Academy of Science, Denton, Mar. 1, 1974.

Supplementary Activities

STAFF

PROFESSIONAL AND EDUCATIONAL ACTIVITIES

C. F. Baes, Jr.	Visiting Professor of Chemistry, College of William and Mary, Williamsburg, Va., September 1972–June 1973.
C. E. Bemis, Jr.	Member, Organizing Committee, International Conference on Reactions between Complex Nuclei, Nashville, Tenn., June 1974.
J. Braunstein	Editor, *Advances in Molten Salt Chemistry,* 1970–present.
W. R. Busing	Secretary-Treasurer, U.S.A. National Committee for Crystallography, National Academy of Sciences–National Research Council, Jan. 1, 1974–Dec. 31, 1976.
C. J. Collins	Professor of Chemistry, part time, University of Tennessee, Knoxville, January 1964–present. Member, Executive Committee, Organic Division, American Chemical Society, Jan. 1, 1973–Dec. 31, 1974. Member, Editorial Board, *Isotopes in Organic Chemistry,* Elsevier Publishing Co., Amsterdam, 1972–present. President, Committee for the Southeastern Regional Meeting, American Chemical Society, Gatlinburg, Tenn., 1976.
S. Datz	Chairman, V International Conference on Atomic Collisions in Solids, 1972–73. Member, National Academy of Sciences–National Research Council Committee on Atomic and Molecular Physics. Associate Editor, *Atomic Data and Nuclear Data Tables,* 1969–present. Advisory Editor, *Case Studies in Atomic Physics,* 1970–present.
L. Dresner	Lecturer in Chemical Engineering, University of Tennessee, Knoxville, 1963–present.
E. Eichler	Chairman, Gordon Research Conference on Nuclear Chemistry, 1973. Membership Committee, Division of Nuclear Chemistry and Technology, American Chemical Society, 1972–73.
J. A. Ghormley	Editorial Board, *Radiation Research,* 1972–75.
R. L. Hahn	Member, Ph.D. thesis examining juries, University of Paris and University of Bordeaux, June 1973.
C. K. Johnson	Member, U.S.A. National Committee for Crystallography, National Academy of Sciences–National Research Council, Jan. 1, 1972–Dec. 31, 1974. Member, National Research Council Committee on Chemical Crystallography, to June 30, 1976. Cochairman, Organizing Committee for NAS Conference on Critical Evaluation of Chemical and Physical Structural Information, Dartmouth College, Hanover, N.H., June 24–29, 1973.
J. S. Johnson, Jr.	Symposium organizer, "Chemistry and the Environment," 25th Southeastern Regional Meeting, American Chemical Society, Charleston, S.C., Nov. 8, 1973.
O. L. Keller, Jr.	Member, USAEC Transplutonium Program Committee, 1966–present. Alternate Councilor and Member of Executive Committee, Division of Nuclear Chemistry and Technology, American Chemical Society, 1971–present.
K. A. Kraus	Editorial Board, *Journal of Chromatography,* 1958–present. Editorial Advisory Board, *Journal of Inorganic and Nuclear Chemistry,* 1958–present. Editorial Board, *Desalination,* 1966–present. Member, University of Tennessee Water Resources Research Center Advisory Council. Judge, Southern Appalachian Science and Engineering Fair, Knoxville, Tenn., Apr. 4, 1974. Session Chairman, "Chemistry and the Environment," 25th Southeastern Regional Meeting, American Chemical Society, Charleston, S.C., November 1973.
H. A. Levy	Editor and reporter, Discussions on Theoretical Chemistry, NAS Conference on Critical Evaluation of Chemical and Physical Structural Information, Dartmouth College, Hanover, N.H., June 24–29, 1973.

M. H. Lietzke	Professor of Chemistry, part time, University of Tennessee, Knoxville, January 1964–present.
Ralph Livingston	Professor of Chemistry, part time, University of Tennessee, Knoxville, January 1964–present. ORNL liaison officer for ORNL–University of Tennessee part-time teaching programs, 1968–present. Editorial Board, *The Journal of Magnetic Resonance*, January 1971–present. Editorial Board, *Magnetic Resonance Review*, September 1971–present. Judge, Southern Appalachian Science and Engineering Fair, Knoxville, Tenn., Apr. 4, 1974.
W. L. Marshall	Member, National Council, American Chemical Society, 1969–present; Committee on Chemical Education, 1970–present; Chairman, Subcommittee on High School Chemistry, 1971–present; Subcommittee on Organizational Structure, 1972–present. Member, Ph.D. examination committee (oceanography), Dalhousie University, Halifax, Nova Scotia, Canada, 1973. Vice-President, Oak Ridge Chapter of Sigma Xi – The Research Society of America, 1974–75.
G. D. O'Kelley	Professor of Chemistry, part time, University of Tennessee, Knoxville, January 1964–present. Member, Nominating Committee, Division of Nuclear Chemistry and Technology, American Chemical Society, 1973–74. Member, Subcommittee on Radiochemistry, Committee on Nuclear Science, National Research Council, 1962–73. Associate Editor, *Proceedings of the Fifth Lunar Science Conference, Geochimica et Cosmochimica Acta.*
R. W. Stoughton	Editorial Advisory Board, *Journal of Inorganic and Nuclear Chemistry*, 1958–present. Consulting Editor, *Inorganic and Nuclear Chemistry Letters*, 1965–present.
E. H. Taylor	Board of Directors, Institute of Catalysis. Advisory Board, American Chemical Society and U.S. Atomic Energy Commission Monographs on Chemistry and Chemical Engineering in Nuclear Technology.

FOREIGN MEETINGS AND ACTIVITIES

Meeting and/or Activity	Location	Staff Member(s)
Visiting scientist, Institut de Physique Nucléaire, July 1972–Aug. 1973, and Nov. 1973	Orsay, France	R. L. Hahn
Alexander von Humboldt, Awardee for Senior U.S. Scientists, Sept. 1972–Sept. 1973	Darmstadt and Mainz, Federal Republic of Germany	P. F. Dittner
Fulbright-Hays Grant, July 1973–July 1974	Weizmann Institute of Science, Rehovot, Israel	L. Dresner
International Symposium on the Structure of Water and Aqueous Solutions, July 19–28, 1973	Marburg, Germany	A. H. Narten
Guest professor, Sept. 1973–Sept. 1974	Johannes Gutenberg-Universität Mainz, Germany	R. J. Silva
XXIVth International Union of Pure and Applied Chemistry Congress, Sept. 2–8, 1973	Hamburg, Germany	J. R. Peterson[1]

COLLABORATIVE RESEARCH

Institution	Collaborator(s)	Subject	Staff Member(s)
Argonne National Laboratory	R. Sjobloom J. P. Unik K. L. Wolf	Search for superheavy elements in accelerator targets	J. Halperin R. W. Stoughton
	S. Fried	Search for superheavy elements in nature	J. Halperin R. W. Stoughton
Arizona State University, Center for Meteorite Studies	C. B. Moore	Search for superheavy elements in nature	J. Halperin R. W. Stoughton
Atomic Energy Research Establishment, Harwell	G. D. James	Analysis of neutron fission cross sections for ^{249}Cf	C. E. Bemis, Jr.

1. Consultant, Department of Chemistry, University of Tennessee, Knoxville.

Institution	Collaborator(s)	Subject	Staff Member(s)
Canton Textile Mills, Inc.	J. C. Gray	Hyperfiltration of indigo dye wastes	R. E. Minturn
The Catholic University of America, Washington, D.C.	C. T. Moynihan	Transport and thermodynamics in vitreous electrolytes	J. Braunstein
Central College, Pella, Iowa	P. J. Ogren	Absorption spectrum and reaction kinetics of methylperoxy radical	C. J. Hochanadel J. A. Ghormley J. W. Boyle
University of Chicago	S. A. Rice	Structure of water	A. H. Narten
Clemson University and LaFrance Industries	C. A. Brandon J. J. Porter	Textile dye wastes	J. S. Johnson, Jr. R. E. Minturn
Cornell University	J. M. Bird	Search for superheavy elements in nature	J. Halperin R. W. Stoughton
University of Delft, Netherlands	B. van Nooijen	Decay properties of ^{84}Y	N. R. Johnson
University of Delhi, India	S. C. Pancholi	Level structure of ^{59}Co	N. R. Johnson
		Gamma-gamma angular correlation measurements in ^{127}I	N. R. Johnson
Eastern Nazarene College	L. H. Hall	X-ray diffraction	G. M. Brown
Environmental Protection Agency, Southeast Water Laboratory	R. R. Swank T. Culbertson	Cross-flow filtration of herbicide wash waters	A. J. Shor J. S. Johnson, Jr.
Florida State University	R. K. Sheline	Levels in ^{161}Tb excited by (^{3}He,d) reaction and by decay of 3.7-min ^{161}Gd	N. R. Johnson G. D. O'Kelley
Furman University	R. O. Sayer	Coulomb excitation of rare-earth and actinide nuclei	E. Eichler N. R. Johnson G. D. O'Kelley
	R. O. Sayer D. L. Vassy	Decay of ^{136}Cs	G. D. O'Kelley
University of Georgia, Geochronology Laboratory	J. E. Noakes	Search for superheavy elements in nature	J. Halperin R. W. Stoughton
Gesellschaft für Schwerionenforschung, Darmstadt, Germany	H. H. Gutbrod	Heavy-ion fission and fusion experiments at the Lawrence Berkeley Laboratory Super-Hilac	R. L. Ferguson
	Burkhard Fricke	Prediction of properties of element 115	O. L. Keller, Jr.
Institute of Nuclear Research, Amsterdam, Netherlands	J. Konijn	Decay properties of ^{84}Y	N. R. Johnson
Institut de Physique Nucléaire, Orsay, France	M. Lefort	Study of nuclear reactions and products formed with Ar- and Kr-ion beams	R. L Hahn
	J. Malý	Search for superheavy elements in nature and in accelerator targets	J. Halperin R. J. Silva R. W. Stoughton
International Paper Co.	L. J. Breithaupt	Kraft pulp and paper wastes	J. S. Johnson, Jr. R. E. Minturn
Knoxville College	D. D. Gibler	Low temperature matrix isolation Raman spectroscopy	G. M. Begun
Lawrence Berkeley Laboratory	R. M. Diamond F. S. Stephens	Lifetime measurements of high-spin states in ^{232}Th following Coulomb excitation with ^{84}Kr	N. R. Johnson E. Eichler
	E. Cheifetz R. C. Jared E. R. Guisti S. G. Thompson	Search for superheavy elements in nature	J. S. Drury J. Halperin R. J. Silva R. W. Stoughton
	R. E. Eppley A. Ghiorso	Search for superheavy elements in accelerator targets	J. Halperin R. W. Stoughton

Institution	Collaborator(s)	Subject	Staff Member(s)
Lawrence Radiation Laboratory, Livermore	R. G. Lanier R. A. Meyer	Levels in ^{161}Tb excited by (^{3}He,*d*) reaction and by decay of 3.7-min ^{161}Gd	N. R. Johnson G. D. O'Kelley
University of Liège, Belgium	J. Fuger	Experimental determination of the heat of solution of Bk metal	J. R. Peterson[1] R. G. Haire[2]
Los Alamos Scientific Laboratory	M. S. Moore A. N. Ellis	Analysis of neutron fission cross sections for ^{249}Cf	C. E. Bemis, Jr.
	H. C. Britt R. H. Stokes B. H. Erkkila	Heavy-ion fission and fusion experiments at the Lawrence Berkeley Laboratory Super-Hilac	R. L. Ferguson
University of Maine at Presque Isle	T. B. Tripp	Thermodynamics of concentrated aqueous electrolytes	J. Braunstein
Massachusetts Institute of Technology, School of Chemical Engineering Practice, Oak Ridge Station	J. W. Tester R. M. Mayer T. W. Bush E. M. Suuberg J. J. Toman M. Yonezawa	Hyperfiltration of textile dye wastes	J. S. Johnson, Jr. R. E. Minturn
	J. W. Tester R. M. Mayer S. A. Murtha R. Filiba J. S. Newman R. D. Orlandi	Cross-flow filtration of sanitary sewage	J. S. Johnson, Jr.
University of Mississippi	R. M. Metzger	Chlorpromazine-TCNQ complex	W. E. Thiessen
Nagoya University, Japan	F. Katoh	Determination of monopole matrix elements in ^{156}Gd	N. R. Johnson
National Accelerator Laboratory	D. Theriot	Search for superheavy elements in accelerator targets	J. Halperin R. W. Stoughton
University of Palermo, Italy	R. Triolo	Diffraction studies of electrolyte solutions	A. H. Narten
University of Puerto Rico	L. Blum	Theory of liquid structure	A. H. Narten
University of Rochester	H. Freiesleben	Fragment kinetic energy in ^{18}O-induced fission of ^{232}Th and ^{246}Cm	R. L. Ferguson C. E. Bemis, Jr.
Scripps Institute of Oceanography	T. R. Folsom	Search for superheavy elements in nature	J. Halperin R. W. Stoughton
Stanford Linear Accelerator Center	D. Busick D. Walz	Search for superheavy elements in accelerator targets	J. Halperin R. W. Stoughton
University of Tennessee, Knoxville	B. Gilbert G. Mamantov	Raman spectral studies of fused salt systems	G. M. Begun
	F. K. Schmidt-Bleek	Collision chemistry	S. Datz H. F. Krause
	L. L. Riedinger	Coulomb excitation of rare-earth and actinide nuclei	E. Eichler N. R. Johnson G. D. O'Kelley
	L. L. Riedinger	High-spin states in nuclei from compound-nucleus reactions	N. R. Johnson E. Eichler
Union Carbide Corp., Linde Laboratories	G. J. Nihart	Search for superheavy elements in nature	J. Halperin R. W. Stoughton
UNISOR Consortium	K. S. R. Sastry et al.	Precession of gamma-gamma correlation in ^{126}Xe	N. R. Johnson

2. Chemical Technology Division.

Institution	Collaborator(s)	Subject	Staff Member(s)
UNISOR Project	A. C. Rester R. Mlekodaj	Development of data-acquisition system	E. Eichler N. R. Johnson G. D. O'Kelley
U.S. Geological Survey	J. H. McCarthy	Search for superheavy elements in nature	J. Halperin R. W. Stoughton
Vanderbilt University	J. H. Hamilton N. C. Singhal	Studies of high-spin states in ^{232}Th by the Doppler-shift recoil-distance technique	N. R. Johnson E. Eichler G. D. O'Kelley
	G. D. Benson R. G. Albridge A. V. Ramayya	Decay of ^{192}Au to levels in ^{192}Pt	G. D. O'Kelley

ANNUAL INFORMATION MEETING AND ADVISORY COMMITTEE

The Annual Information Meeting of the Chemistry Division was held September 10 and 11, 1973, in the Central Auditorium, Building 4500N. Reports presented at the Meeting were:

Monday, September 10, 1973

E. H. Taylor	Introduction
C. E. Bemis, Jr.	Element 104: An X-Ray Identification Using the Isotope ^{257}104
O. L. Keller, Jr.	Nobelium: Comparative Chemistry to Other Divalent Elements
N. R. Johnson	Lifetimes of Rotational States in Deformed Nuclei by the Doppler-Shift Recoil-Distance Method
R. L. Ferguson	Heavy-Ion Induced Fission of Medium-Weight Elements
G. D. O'Kelley	A Look Back at Apollo: Studies of Returned Lunar Samples by Gamma-Ray Spectrometry
H. F. Holmes	Adsorption of Gases on Lunar Soils

Tuesday, September 11, 1973

W. H. Baldwin	Organic Scintillators and Heat Exchangers
V. F. Raaen	Synthesis of Organic Conductors
G. M. Brown	Intramural and Extramural Cooperative Crystallography
H. F. Krause	Chemical Reactions of Metastable Mercury
R. E. Mesmer	The Dissociation of Weak Acids and Bases in Aqueous Solutions to 300°C
R. E. Meyer	Separation and Analysis with Porous Electrodes
K. A. Kraus	Activated Carbon in Inorganic Systems

Members of the Advisory Committee were:

Prof. George S. Hammond
Vice Chancellor – Sciences
University of California, Santa Cruz
Santa Cruz, California 95060

Dr. Joseph J. Katz
Argonne National Laboratory
9700 South Cass Avenue
Argonne, Illinois 60493

Dr. Edward A. Mason
Chemistry Department
Brown University
Providence, Rhode Island 02912

Dr. John O. Rasmussen
Lawrence Berkeley Laboratory
University of California
Berkeley, California 94720

Prof. Henry Taube
Department of Chemistry
Stanford University
Stanford, California 94305

On March 19, 1974, the Chemistry Division programs in Molecular Sciences were discussed with members of the Division of Physical Research, U.S. Atomic Energy Commission. Reports presented at this meeting were:

C. J. Collins	Combinatorial Chemistry: A New Aid in Understanding Molecular Rearrangements
D. A. Lee	Chromatographic Separation of Cobalt and Calcium Isotopes
C. F. Baes	EMF Studies of Hydrolytic and Other Ionic Equilibria in Aqueous Solutions to 300°C
W. L. Marshall	High-Temperature Electrical Conductance and Solubility Studies of Aqueous Electrolytes
M. H. Lietzke	Predictions of Thermodynamic Properties of Aqueous Electrolyte Mixtures over Wide Ranges of Temperature and Composition
K. A. Kraus	Activated Carbon
E. H. Taylor	Miscellaneous Topics
T. J. Sworski	Photooxidation and Fluorescence of Cerium(III) in Aqueous Sulfuric Acid Solutions
C. J. Hochanadel	Pulse Radiolysis and Flash Photolysis of Small Molecules in the Gas Phase
R. Livingston	ESR Studies of Radicals in Photolyzed Liquids
S. Datz	Reactive and Inelastic Scattering of Metastable Mercury

VISITING SCIENTISTS

Name	Affiliation	ORNL Research Program	Sponsor
R. L. Fellows	University of Tennessee	Transuranium Research Laboratory	University of Tennessee Research Grant
W. H. Fletcher	University of Tennessee	Isotope Chemistry	Consultant
R. V. Gentry	Columbia Union College	Transuranium Research Laboratory	Columbia Union College
J. F. Gomes Ferreira	University of Lisbon, Portugal	Transuranium Research Laboratory	NATO and Portuguese Government
M. C. Noé	University of Tennessee	Transuranium Research Laboratory	University of Tennessee Research Grant
J. R. Peterson	University of Tennessee	Transuranium Research Laboratory	Consultant
F. K. Schmidt-Bleek	University of Tennessee	Molecular Beam	Consultant
N. C. Singhal	Vanderbilt University	Nuclear Chemistry	Vanderbilt University
R. Sturm	University of Marburg, Marburg, Germany	Nuclear Chemistry	Max Kade Foundation Senior Fellowship
C. E. Vallet	University of Provence, Marseilles, France	Molten Salts	French Foreign Office Postdoctoral Fellow and C. N. R. S.

STUDENTS

GRADUATE

Name	Major Professor and/or Institution	Staff Advisor	Field of Research	Sponsor
L. L. Collins, Jr.	G. D. O'Kelley, University of Tennessee	G. D. O'Kelley E. Eichler	Nuclear decay scheme spectroscopy	University of Tennessee

Name	Major Professor and/or Institution	Staff Advisor	Field of Research	Sponsor
M. W. Guidry	G. D. O'Kelley, University of Tennessee	G. D. O'Kelley E. Eichler N. R. Johnson	Heavy-ion Coulomb excitation of actinide nuclei	Oak Ridge Graduate Fellowship Program
A. Y. Herrell	Karl H. Gayer, Wayne State University	R. H. Busey	Enthalpies of Formation of $Tc_2O_7(c)$ and $TcO_4^-(aq)$ by Solution Calorimetry (Ph.D. thesis, 1973)	National Science Foundation Science Faculty Fellowship
F. D. Hwang	F. K. Schmidt-Bleek, University of Tennessee	S. Datz H. F. Krause	Hot-atom collisions using molecular beams	
S. G. Johnson	F. K. Schmidt-Bleek, University of Tennessee	S. Datz H. F. Krause	Excited atom-molecule reactions	Oak Ridge Graduate Fellowship Program
Olavi Keski-Rahkonen	J. R. Peterson, University of Tennessee	M. O. Krause	Photoelectron and x-ray spectrometry of actinide elements and compounds	ASLA/Fulbright-Hays and Univerversity of Tennessee Research Grant
T. J. Lemmonds	M. H. Lietzke, University of Tennessee	M. H. Lietzke	The Standard Potential of the Ag, AgBr Electrode in DBr Solutions (M.S. thesis, March 1974)	
M.-R. Noé-Spirlet	H. Brasseur, University of Liège, Belgium	G. M. Brown H. A. Levy	Structure of heteropoly acids	University of Liège
G. Ostrom	F. K. Schmidt-Bleek, University of Tennessee	S. Datz	Low energy electron-induced sputtering of alkali halides	
W. W. Schmidt	C. J. Collins, University of Tennessee	C. J. Collins	Organic cations and trace analysis	University of Tennessee
J. N. Stevenson	J. R. Peterson, University of Tennessee	O. L. Keller, Jr. L. J. Nugent	Solid-State Studies of Some Actinide Elements and Compounds (Ph.D. thesis, August 1973)	University of Tennessee Research Grant
C. G. Venkatesh	S. A. Rice, University of Chicago	A. H. Narten	Amorphous water	University of Chicago

UNDERGRADUATE

Name	Institution	ORNL Research Program	Sponsor
J. S. Bernstein	Centenary College	Microwave and Radio-Frequency Spectroscopy	Southern College University Union
D. H. Brown	Kenyon College	Physical Chemistry	ORAU Summer Student Trainee Program
J. C. Foster	University of the South	Organic Chemistry	Southern College University Union
R. F. Hall	Rockhurst College	Neutron and X-Ray Diffraction	ORAU Summer Student Trainee Program
D. L. Herting	University of South Dakota	Physical Chemistry	ORAU Summer Student Trainee Program
H. L. Reed II	DePauw University	Neutron and X-Ray Diffraction	Great Lakes Colleges Association
B. J. Wenzel	University of Northern Iowa	Organic Chemistry	ORAU Summer Student Trainee Program
M. S. Wolfe	Earlham College	Radiation Chemistry	Great Lakes Colleges Association
J. M. Zeigler	Wabash College	Organic Chemistry	Great Lakes Colleges Association

ORNL-4976
UC-4 – Chemistry

INTERNAL DISTRIBUTION

1. Biology Library
2–4. Central Research Library
5. Laboratory Shift Supervisor
6. MIT Practice School
7. ORNL–Y-12 Technical Library Document Reference Section
8–22. Laboratory Records Department
23. Laboratory Records, ORNL R.C.
24. H. J. Adler
25. P. A. Agron
26. B. K. Annis
27. S. I. Auerbach
28. J. A. Auxier
29. A. L. Bacarella
30. C. F. Baes
31. W. H. Baldwin
32. S. E. Beall
33. G. M. Begun
34. C. E. Bemis, Jr.
35. D. S. Billington
36. E. G. Bohlmann
37. C. J. Borkowski
38. J. Braunstein
39. M. A. Bredig
40. H. R. Bronstein
41. A. R. Brosi
42. G. M. Brown
43. J. H. Burns
44. R. H. Busey
45. W. R. Busing
46. T. A. Carlson
47. H. P. Carter
48. G. H. Cartledge
49. C. J. Collins
50. F. L. Culler
51. S. Datz
52. L. Dresner
53. J. S. Drury
54. A. S. Dworkin
55. E. Eichler
56. G. G. Fee
57. D. E. Ferguson
58. R. L. Ferguson
59. J. L. C. Ford
60. W. Fulkerson
61. E. L. Fuller
62. R. V. Gentry
63. J. A. Ghormley
64. J. H. Gillette
65. L. O. Gilpatrick
66. C. D. Goodman
67. W. R. Grimes
68. R. L. Hahn
69. J. Halperin
70. R. F. Hibbs
71. C. J. Hochanadel
72. H. F. Holmes
73. C. K. Johnson
74. J. S. Johnson, Jr.
75. N. R. Johnson
76. O. L. Keller, Jr.
77. E. J. Kelly
78. B. H. Ketelle
79. K. A. Kraus
80. M. O. Krause
81. W. C. Kuykendall
82. E. Lamb
83. H. A. Levy
84. M. H. Lietzke
85. R. Livingston
86. R. S. Livingston
87. B. K. Lyon
88. R. N. Lyon
89. W. L. Marshall
90. Peter Mazur
91. H. F. McDuffie
92. J. R. McNally, Jr.
93. L. E. McNeese
94. R. E. Mesmer
95. R. E. Meyer
96. R. E. Minturn
97–100. G. E. Moore
101. A. H. Narten
102. L. J. Nugent
103. G. D. O'Kelley
104–105. R. B. Parker
106. F. Plasil
107. J. J. Pinajian
108. F. A. Posey
109. H. Postma
110. A. S. Quist
111. R. J. Raridon
112. S. A. Reynolds
113. C. R. Richmond

114. M. W. Rosenthal
115. R. M. Rush
116. H. W. Schmitt
117. W. D. Shults
118. S. Siegel
119. M. J. Skinner
120. H. G. Smith
121. A. H. Snell
122. P. H. Stelson
123. J. N. Stevenson
124. R. W. Stoughton
125. D. A. Sundberg
126. T. J. Sworski
127–186. E. H. Taylor
187. W. E. Thiessen
188. R. E. Thoma
189. J. R. Totter
190. K. S. Toth
191. L. M. Toth
192. D. B. Trauger
193. J. R. Weir, Jr.
194. J. C. White
195. M. K. Wilkinson
196. A. Zucker
197. George S. Hammond (Advisory Committee)
198. Edward A. Mason (Advisory Committee)
199. John O. Rasmussen (Advisory Committee)
200. Stuart A. Rice (Advisory Committee)

EXTERNAL DISTRIBUTION

201. D. A. Bromley, Department of Physics, Yale University, New Haven, Conn. 06520
202. Prof. Georges Duyckaerts, Institut de Chimie, Université de Liège, Sart Tilman, 4000 Liège Belgium
203. M. Froment, President Section 05, Centre Nationale de la Recherche Scientifique, 15 Quai Anatole France, 75700 Paris, France
204. J. H. Hamilton, Physics Department, Vanderbilt University, Nashville, Tenn. 37203
205. Prof. G. Herrmann, Institut für Anorganische Chemie und Kernchemie, Universität Mainz, 6500 Mainz, Postfach 3980, Germany.
206. G. W. Johnson, Director, Division of Applied Technology, USAEC, Washington, D. C. 20545
207. Prof. M. Lefort, Institut de Physique Nucléaire, B. P. No. 1, 91406 Orsay, France.
208. J. L. Liverman, Director, Biomedical & Environmental Research, USAEC, Washington, D.C. 20545
209. H. G. MacPherson, Institute for Energy Analysis, P.O. Box 117, Oak Ridge, Tenn. 37830
210. L. G. Mayfield, Deputy Director, Division of Advanced Technology Application, National Science Foundation-RANN, 1800 G Street N.W., Washington, D.C. 20550
211. D. R. Miller, Division of Physical Research, USAEC, Washington, D.C. 20545
212. J. R. Peterson, Department of Chemistry, University of Tennessee, Knoxville, Tenn. 37916
213. E. S. Pierce, Assistant Director for Molecular Sciences & Energy Research, Division of Physical Research, USAEC, Washington, D.C. 20545
214. P. L. Johnson, Executive Director, Oak Ridge Associated Universities, P.O. Box 117, Oak Ridge, Tenn. 37830
215. Robert Rabin, Division of Environmental Systems and Resources, National Science Foundation, 1800 G Street, N.W., Washington, D.C. 20550
216. G. L. Rogosa, Acting Assistant Director for Nuclear Sciences, Division of Physical Research, USAEC, Washington, D.C. 20545
217. R. H. Schuler, Radiation Research Laboratories, Mellon Institute of Science, Carnegie-Mellon University, 4400 Fifth Ave., Pittsburgh, Pa. 15213.
218. D. K. Stevens, Assistant Director for Materials Sciences, Division of Physical Research, USAEC, Washington, D.C. 20545
219. J. M. Teem, Director, Division of Physical Research, USAEC, Washington, D.C. 20545
220. A. M. Weinberg, Director, New Energy R & D Office (FEO), Office of Energy R & D, 145 Old Executive Office Building, Washington, D.C. 20500
221. Research and Technical Support Division, AEC-ORO
222. Technion, Israel Institute of Technology, Department of Nuclear Science, Haifa, Israel
223. Union Carbide Corporation, Chemicals Division, P.O. Box 8361, South Charleston, W. Va. 25303.
224–394. Given distribution as shown in TID-4500 under Chemistry Category (25 copies – NTIS)